IPPJ-AM-50

PROCEEDINGS
OF
THE JAPAN-U.S. WORKSHOP P-92
ON
PLASMA MATERIAL INTERACTION/HIGH HEAT FLUX DATA NEEDS FOR THE NEXT STEP IGNITION AND STEADY STATE DEVICES

JANUARY 26-30, 1987

EDITED BY A. MIYAHARA AND K.L. WILSON

INSTITUTE OF PLASMA PHYSICS
NAGOYA UNIVERSITY

NAGOYA, JAPAN

IPPJ-AM-50

PROCEEDINGS
OF
THE JAPAN-U.S. WORKSHOP P-92
ON
PLASMA MATERIAL INTERACTION/HIGH HEAT FLUX DATA NEEDS FOR THE NEXT STEP IGNITION AND STEADY STATE DEVICES

JANUARY 26 – 30, 1987

Edited by
A. MIYAHARA AND K. L. WILSON

Institute of Plasma Physics, Nagoya University
Chikusa-ku, Nagoya 464, Japan

May 1987

TABLE OF CONTENTS

ISSUES OF EACH TOPIC

PREFACE

to the Japan-U.S. Workshop on Plasma Material Interaction/High Heat Flux Data Needs for the Nest Step Ignition and Steady State Devices

I am gratified that this important and very timely workshop has proven to fulfill our expectations concerning highlighting the state of the in-vessel materials data base, including both isotropic and non-isotropic graphite and post-graphite materials, as well as the engineering problems associated with in-vessel component design and fabrication for existing and future confinement devices around the world.

In particular, one of the important measurements of the success of such a conference is how well the information exchanged by all countries involved is utilized by each to streamline its own programs, cut development costs and time and, in general, increase the efficiency with which it proceeds toward the completion of the data base required for its individual needs.

The inclusion of both European and Canadian participants has added immeasurably to the usefulness of this conference. This conference has produced the exchange of large amounts of information relevant to the needs of each participant country. This broad base of participants, each of whose home program is in a different stage of development relevant to divergent national goals and timetables has highlighted many areas of existing

complementarity of technical programs. I hope that this exchange will serve to streamline the future programs of each country and that a report of how effective this information sharing has been will be presented at next year's conference.

The engineering design and materials required to satisfy even normal (as opposed to disruptive) operation of a plasma with high edge temperatures are formidable. Historically, the satisfaction of these requirements has evolved as the job of the engineering technologist. An important aspect of this conference has been to emphasize, once again, the need for a plasma physics program to find ways to lower edge temperatures. In addition, this conference highlights the immediate need to establish an international data base on graphite materials for the next generation device. I hope that an international working group to this end will be part of the next workshop.

I give my heartfelt thanks to the Institute of Plasma Physics in Nagoya University for hosting this conference and to the co-chairmen Prof. A. Miyahara and Dr. Kenneth Wilson, whose detailed planning and foresight provided us with an excellent framework for success. The conference participants have worked long hours and diligently to insure this success. We gratefully acknowledge the fine assistance of the secretaries of Institute who provided the necessary and very efficient support required to compile the large amounts of data exchanged.

I look forward to the effective utilization of the results of this year's workshop and to next year's exchange in the US.

M.M. Cohen
Office of Fusion Energy
U.S. Dept. of Energy

EXECUTIVE SUMMARY

A. INTRODUCTION

The Japan-US workshop on "Plasma Material Interaction/High Heat Flux Data Needs for the Next Step Ignition and Steady State Devices", was held at Institute of Plasma Physics, Nagoya University, on January 26-30, 1987. This is the second workshop in this series of US-Japan workshops after the first, which was held at Sandia National Laboratories Livermore on June 24-27, 1985, under the title of "Plasma-Wall Interaction Data Needs Critical to Burning Core Experiment (BCX)". Among the 65 participants at the present workshop, six were from the U.S., four from the EC and one scientist attended from Canada.

The primary objective of this workshop was to answer the question, "Are existing carbon materials (graphites and carbon-carbon composites) feasible for the CIT-experiment or not? " The approach to this question needs a definition of how reference materials for CIT are to be selected out of existing materials.

In this course, many physics and engineering investigations are necessary. Whether the background is rigid enough to answer this problem has also to be determined. Besides near term questions related to CIT, the workshop was also aimed at defining the problem area and surveying the present efforts concerning ETR which can be regarded as the international reference machine to the next generation projects like FER, TIBER-II, NET and OTR.

In order to discuss these problems, the workshop was organized in four sessions: The first plenary session attempted to give an overview on present activities and to outline new issues to be anticipated from future machines. The second session followed with presentations on subgroup topics which are considered critical both to CIT and ETR. Session 3 was sub-group meetings to discuss and summarize the present status, immediate data needs for CIT, and extended efforts for ETR studies. In Session 4, summaries were presented by each sub-group leader and discussed in plenary format. After four days of intensive discussion, we concluded (1) existing isographite is a very good candidate for CIT as plasma facing material although some date are still needed to meet the serious requirements from the plasma environment; (2) carbon-carbon composites seem to be a better candidate than isographite, with respect to the high heat flux issues; (3) For ETR studies, experiences from CIT and long pulse non-ignition machines are necessary, especially in the area of compatibility with active cooling and radiation damage.

The organization of this proceeding includes executive summary and detailed summaries from each sub-group. The manuscript or viewgraphs submitted by speakers of plenary and sub-group topics sessions follow the workshop agenda, are appended to this report. We believe these attachments, although preliminary, are beneficial to understand the physics and engineering background of the performed discussions.

B. TNS-TNG OPTIONS

The categorization of TNS(The Next Step)- TNG(The Next Generation) options are:

1. CIT family - CIT(TFTR, JET)
2. Long pulse non-ignition family - TORE SUPRA, ASDEX-U, LHS (Large Helical System)
3. ETR family - TIBER-II, FER, NET, OTR, INTOR

The requirements for plasma facing materials of the present CIT design option (R=1.22m, r_p=0.45m) are not very different from the figures given in last workshop at SNLL 1985, except that it has adopted a double null divertor configuration. The fluence of 14 MeV neutrons after 3000 full DT shots of 3.2 sec discharge time will be $<5\times10^{22}n/m^2$. Heat loads to the carbon first wall are expected up to 9.5 MW/m^2 for normal operation. The disruption regime features heat loads of $9MJ/m^2$ in a time of about 1 msec on the limiters. While Japan and the European Comunity(EC) do not currently have an option on a CIT family machine in their strategy, they have long pulse non-ignition machine options to prepare the database for the next generation machine of the ETR family. These machines [TORE SUPRA(EC), ASDEX-U(EC) and LHS(Japan, under conceptual design)] are planned to operate with pulse lengths of 30s to steady state. Quasi-steady state heat loads of up to $40MW/m^2$ have to be removed by active cooling in case of leading edge of the TORE SUPRA pump limiter. Thus these projects are expected to greatly foster the development of highly efficient actively cooled first wall components. Investigations of this

family will also generate a database on active impurity and particle control issues. Compared to the prior workshop, presently it is rather easier to discuss and assess PMI/HHF studies because the material requirements for the ETR family have become more clear and better defined. Expected neutron fluences are 5×10^{25}-3×20^{26}n/m^2. The main issues to be solved for ETR will be the evaluation of the feasibility of first wall materials under these fluences and the development of actively cooled structures which are capable of heat removal under long pulse (>200s) operation. In these concepts, first wall components of utmost reliability are needed due to the limited abilities of remote handling devices. Whether candidate materials for CIT and long pulse no-ignition machines can also be adopted for ETR or not, will be the serious problem area for the PMI/HHF community. Extensive investigations to evaluate the feasibility under given conditions are extremely necessary, as otherwise further progress in fusion research will be blocked.

It is also necessary to mention that through operational experiences of the present day's machines like TFTR, JET, and JT-60, we must learn the feasibility of graphite in divertor operation, conditions of off-normal operations, and special recycling behavior of graphite walls as indicated in supershots and wall pumping.

C. MATERIAL DATA NEEDS AND STRATEGY

Based on the consensus of the last workshop and the operational experiences of large tokamaks, isographite was considered as the primary candidate for CIT. Compared to the last workshop, more emphasis has been put on C-C composite materials during the discussions, although the database is still insufficient. Beryllium was not discussed in detail because we concentrated on establishing reference candidate carbon materials. For this reason, materials discussed belong to four categories:

1. Isotropic graphite
2. Anisotropic graphite
3. Carbon/Carbon composite
4. Dense carbon films by carbonization

The comprehensive evaluation of various candidate for PMI/HHF materials was undertaken through presentation and discussions of each subgroup. Items that have been discussed are as follows:

(1) Characterization

(2) Outgassing properties

(3) High heat flux experiments

(4) Sputtering, synergisms and erosion/redeposition processes

(5) Recycling and tritium inventory

(6) Radiation damage

(7) Modelling

(8) Engineering and design aspects

(9) Advanced carbon based materials

The outcome of the presentations and discussions of each topic was summarized under the aspect of present status and future data needs:

(1) and (6) Characterization and radiation damage

Radiation damage of isographite is not expected to be serious for CIT use, however, for ETR level irradiation, experiments using fission reactors are at least necessary to estimate feasibility. Radiation damage of C-C composite materials must be investigated, especially for ETR level of irradiation. Pyrolytic graphite will not be feasible from the standpoint of neutron irradiation even under low fluences like in CIT as the thermal conductivity rapidly decreases. For the physical and chemical properties of each graphite, as a function of temperature, sufficient data are not available. It is necessary to complete this work in order to do optimized design for ETR.

(2) Outgassing properties

After pretreatment in high vacuum and bake-out at high temperatures, the outgassing of almost all isographites and C-C composites are small enough for CIT use. These items are based on operational experience so that a more systematic database is necessary to evaluate which pretreatment is the best before installation in the tokamak and which in-situ

conditioning procedure is necessarry afterwards. The database for graphites were reviewed, and no large discrepancies were found. In partial pressure measurements, remarkable differences are recognized at three specific temperature regions of approximately below 200°C, between 200-800°C, and higher than 800°C. Although well pretreated before installation, readsorption of environmental gas is to be expected in graphite during installation. Elevation of the wall temperature to at least 350°C for baking procedure is recommended through experiences of large machine operation.

(3) High heat flux experiments

Through laboratory experiments, it was found that standard isographite with small thermal expansion coefficient shows good thermal shock behavior compared to graphites with high thermal expansion coefficient. For C-C composites, even better characteristics are expected. More intensive and systematic studies with reference to high temperature material properties up to 3000°C are neccessary to obtain a rigid design base.

Damages caused by runaway electrons must be considered in conjunction with engineering aspects, especially for energy deposition on cooling tubes of long pulse machines. However, for CIT use, isographites and C-C composites are feasible.

(4) Sputtering, synergisms and erosion/redeposition processes

Temperature excursions of CIT tiles during one shot are expected from room temperature to above 2000°C. After the discharge, the temperature drops once more to nearly room temperature. Three different mechanisms for erosion must be considered: physical sputtering, chemical sputtering, and enhanced sublimation. Although some database is available for these processes, more data are needed for lower incident ion energy (< 50eV) and higher fluxes to simulate real edge conditions. Redeposition processes must be investigated to evaluate the life time of tiles.

(5) Recycling and tritium inventory.

One of the critical questions is the maximum tritium inventory in the graphite tiles of TFTR, JET, and CIT. While several preliminary studies have been performed in various laboratories, the estimation of the inventory is still ambiguous because of the various retention processes that occur during tokamak operation. Data with higher accuracy are needed for tritium solubility, diffusion, permeation, recombination and trapping.

Besides the estimation of wall inventory, knowledge on the recycling properties of the wall will become very important to achieve H-mode like operation in tokamaks. Supershots in TFTR and wall pumping in JET are typical examples of graphite's recycling properties. A detailed and systematic approach is necessary.

(6) Described in (1)

(7) Modelling

Two types of modelling are needed. One is mainly the plasma physicist's responsibility to define edge properties and incident particle fluxes and energies to the plasma facing material. The other is the modelling of PMI and material behaviour itself. More intensive efforts and better communication between material scientists and plasma physicists are necessary to perform reasonable experiments with CIT, long pulse devices and ETR. A review of existing codes on an international scale is warranted.

(8) Engineering aspects

This topic included communication of machine operation experiences as well as those of designers and manufactures. Many considerations are needed regarding the way plasma-interactive components are fabricated, pretreated, installed, baked, discharge cleaned, and operated. It is concluded from past experience and laboratory experiments, that isographite is feasible for CIT. For ETR, more investigation is necessary in the next few years to establish operation with active cooling and to check on the resistance against higher ($>10^{25}n/m^2$) neutron fluences. Cost of components were discussed from the standpoint of necessary energy and capital cost.

(9) Advanced carbon based materials

Investigation of coatings was one of the main fields of research during the past two years, but from the standpoint of CIT and ETR issues,it is not a baseline concept. However, it could still play an important role in pretreatment sealing the graphites and covering large areas of vessels with dense carbon films. Naturally occuring carbonization through redeposition processes are also related to this investigation.

Much data are needed to establish a reasonable design for CIT and ETR. Accuracy of the database also has to be discussed through design procedures. With concern to CIT issues, the database for graphite materials is fairly complete except the fields of recycling and very high heat flux behaviors, whereas the database on C-C composites is still insufficient. ETR adds the aditional requirements of active cooling in a high neutron flux enviroment.

D. UTILIZATION OF EXISTING FACILITIES

The utilization of existing fusion devices to contribute to the database for CIT, long pulse non-ignition machines and ETRs is very important. Although they have issued large amounts of data, more systematic research and better defined PMI/HHF investigations are necessary.

HHF testing for off normal operation using NBI test stands have been performed at several laboratories. In this field of large area, high power ($>20kW/cm^2$), short pulse ($<0.1sec$) irradiation, facilities must be used in collaborative efforts in order to obtain a sufficient database.

Runaway electron simulation experiments using linac facilities in combination with numerical evaluation by Monte Carlo codes have to be organized for the ETR database.

Plasma devices, such as PISCES and the Tritium Plasma Experiment, are effective for PMI investigations. Other fcilities, such as outgassing measurement devices, are also important for improving the database. Cross checking of the database among various facilities is necessary to prove the reliability of the data.

E. FUTURE COLLABORATIONS

It is recognized that isographite will be feasible as a CIT tile material. More detailed PMI/HHF investigations are necessary to obtain a rigid database for CIT and to explore the extention to ETR use. The needs for further data can be extracted from the following summary papers.

Investigation of active cooling compatible to candidate materials is the most important item for long pulse non-ignition machines and ETRs. Utilization of fission reactors

to investigate graphite radiation damage is also an important issue for future collaborations.

To establish the common and standard database for CIT, ETR and long pulse non-ignition machines, it is recommended that a data center for each participating country be nominated to promote further collaborations.

Japan-US Workshop on Plasma Material Interaction/High Heat Flux Data Needs for the Next Step Ignition and Steady State Devices

January 26 - 30, 1987
Institute of Plasma Physics, Nagoya University
Co-chairmen: K.L. Wilson (SNLL)
A. Miyahara (IPP Nagoya)

Workshop Program

1st Day, January 26 (Mon.)

0. Opening Session

0.1. Opening talk M.M. Cohen(DOE)

1. Plenary Session

1.1 Plasma Surface Interactions in Compact Ignition Devices
M.A. Ulrickson (PPPL)

1.2 Some Considerations on Plasma Facing Materials in Tokamak Fusion Devices Y. Murakami (JAERI)

1.3 Experience with Graphite in JET K.J. Dietz (JET)

1.4 U.S. efforts on graphite and carbon related material studies
K.L. Wilson (SNLL)

1.5 Japanese efforts on graphite and carbon related material studies
T. Yamashina (Hokkaido Univ.)

1.6 Carbon erosion processes for CIT and ETR applications
A.A. Haasz (Univ. of Tronto)

1.7 Semi-empirical equation for modelling of chemical erosion of graphite N. Itoh (Nagoya Univ.)

1.8 Comment on plasma facing material studies on ETR
A. Miyahara (IPP Nagoya)

1.9 Application of graphite materials to the next generation machine
M. Seki (JAERI)

Coffee break

2. Presentation of each subgroup

2.1. Characterization of graphites and C-C composites

2.1.1 Some brief remarks on several critical aspects of graphite database for fusion energy applications W.P. Eartherly (ORNL)

2.1.2 Characterization of graphites and C-C composites T. Oku (JAERI)

2.2. Outgassing properties

2.2.1 Sandia Livermore conditioning studies K.L. Wilson (SNLL)

2.2.2 Thermal outgassing of various kinds of graphite Y. Kubota (IPP)

2.2.3 1) On gas uptake of coated and bare graphite during exposure
2) Hydrogen and deuterium retention in wall samples of JET
W. Eckstein (MPI)

2.2.4 Absorption and desorption of D_2 on graphite
H. Atsumi and M. Miyake (Osaka Univ.)

2.3. HHF-experiments on carbon related materials

2.3.1 High heat flux tests on C-materials J. Linke (KFA)

2.3.2 1) Disruption simulation experiments on graphite by H^+-beam at the 10 MW neutral beam injection test stand of the IPP Nagoya
2) Runaway-electron linear accelerator experiments
H. Bolt (IPP Nagoya)

2.3.3 Thermal Shock and Fracture Toughness Considerations for Graphite in Tokamak Fusion Reactors, R.T. McGrath

<u>2nd Day, January 27 (Tues.)</u>

2.4. Sputtering, synergisms and erosion processes

2.4.1 High flux plasma bombardment of graphite Y. Hirooka (UCLA)

2.4.2 Assessment of graphite for limiter/divertor and first wall tiles in CIT and ETR-type machines A.A. Haasz (Univ. of Toronto)

2.4.3 Ion-induced sputterng and interfacial reaction of metals or metal-carbides deposited on graphite at high temperatures
K. Morita (Nagoya Univ.)

2.4.4 Chemical erosion of graphite and diamond materials due to low energy hydrogen bombardment R. Yamada (JAERI)

2.4.5 Comments on erosion of graphite V. Philipps (KFA)

2.4.6 Thermal desorption process and surface roughness of POCO graphite irradiated by hydrogen ion beam T. Hino (Hokkaido Univ.)

2.5. Recycling properties and tritium inventory

2.5.1 Estimation retention, permeation and recycling
T. Tanabe (Osaka Univ.)

2.5.2 Tritium inventory K.L. Wilson (SNLL)

2.5.3 Trapping-release behaviours of hydrogen isotopes in/from graphite
--- Modification by the presence Fe impurity ---
K. Ichimura (Toyama Univ.)

2.5.4 Hydrogen permeation through graphite M. Yamawaki (Tokyo Univ.)

2.5.5 Comments on recycling and hydrogen inventory V. Philipps (KFA)

2.6. Activation and radiation damage

2.6.1 Some consideration on selection criteria for graphite as fusion reactor materials Y. Oku (JAERI)

2.6.2 Presentation on graphite technology W.P. Eartherly (ORNL)

2.6.3 Neutron irradiation tests for graphite and low-Z-ceramics
J. Linke (KFA)

2.7. Modelling and physics back ground

2.7.1 Runaway electron analysis for Tore Supra R.T. McGrath (SNLA)

2.8. Engineering and design aspects

2.8.1 Fusion application of C-C composites T. Uchikawa (MHI)

2.8.2 Problems with criteria for material selection and failure assessment M. Shibui (Toshiba)

2.8.3 Active cooling with swirl tube enhancement with application to the Tore Supra modulas design R.T. McGrath (SNLA)

2.8.4 CO_2 laser beam test of an actively cooled first wall element with graphite-clad SiC tile Y. Gotoh (Hitachi)

2.8.5 Limiter heat loads in TFTR due to disruptions
M.A. Ulrickson (PPPL)

2.8.6 Design aspects of in vessel components K.J. Dietz (JET)

2.9. Advanced carbon based materials

2.9.1 Experiment on first wall carbon coating Y. Sakamoto (RIKEN)

2.9.2 Properties of carbon coating films produced by glow, RF and ECR discharges T. Hino (Hokkaido Univ.)

3rd Day, January 28 (Wed.)

Summary presentations by 9 subgroups

4th Day, January 29 (Thurs.)

Preparation of manuscripts

5th Day, Jan. 30 (Fri.)

Conclusion summary

JAPAN-US WORKSHOP ON PLASMA MATERIAL INTERACTION/HIGH HEAT FLUX DATA NEEDS
FOR THE NEXT STEP IGNITION AND STEADY STATE DEVICES
JANUARY 26-30, 1987

INSTITUTE OF PLASMA PHYSICS, NAGOYA UNIVERSITY

PARTICIPANTS LISTS

COHEN, M.M.	USDOE
EARTHERLY, W.P.	ORNL
HIROOKA, Y.	UCLA
McGRATH, R.T.	SNLA
ULRICKSON, M.A.	PPPL
WILSON, K.L.	SNLL
DIETZ, K.J.	JET
ECKSTEIN, W.	MPI
HAASZ, A.A.	Univ. of Toronto
LINKE, J.	IRW/KFA
PHILIPPS, V.	IFC/KFA
AKAISHI, Kenya	Plasma Physics Laboratory, Kyoto University
BOLT, Harald	IPP Nagoya University
GOTOH, Yasutaka	Hitachi Ltd.
HINO, Tomoaki	Faculty of Engineering, Hokkaido University
ICHIMURA, Kenji	Toyama University
ITOH, Noriaki	Faculty of Science, Nagoya University
KAWAMURA, Takaichi	IPP Nagoya University
KUSAKI	Nippon Carbon Co.Ltd.
KUROYANAGI	Tokai carbon Co. Ltd.
KUBOTA, Yusuke	IPP Nagoya University

MARUYAMA	Toyo Carbon Co. Ltd.
MIYAHARA, Akira	IPP Nagoya University
MIYAKE, Masanori	Faculty of Engineering, Osaka University
MORITA, Kenji	Faculty of Engineering, Nagoya University
MURAKAMI, Yoshio	JAERI Naka Fusion Research Establishment
NAMBA, Chusei	IPP Nagoya University
NATSUME	Toyo Carbon Co. Ltd.
OHBAYASHI, Haruo	IPP Nagoya University
OKADA, Masatoshi	National Research institute for Metals
OKAMOTO, Kousuke	ULVAC Corporation,
OKU, Tatsuo	JAERI Tokai Fusion Research Establishment
SAGARA, Akio	IPP Nagoya University
SAKAGAMI	Sumitomo Electric Industries, Ltd.
SAKAMOTO, Yuichi	Plasma Physics Laboratory, RIKEN
SAKASHITA	Toyo Tanso Co. Ltd.
SEKI, Masahiro	JAERI Tokai Fusion Research Establishment
SHIBUI, Masanao	Toshiba corporation
SHIKAMA, Tatsuo	National Research Institute for Metals
SHIMIZU, Hajime	Electro Technical Laboratory
SUGIZAKI, Masakazu	Faculty of Engineering, Kyushu University
TAKEKAWA	Nippon Kokan K. K.
TANABE, Tetsuro	Faculty of Engineering, Osaka University
TSUJIMURA, Seiichi	Mitsubishi Heavy Industries Ltd.
UCHIKAWA, Takashi	Mitsubishi Heavy Industries Ltd.
URITANI, Akira	IPP Nagoya University
YAMADA, Reiji	JAERI Tokai Fusion Research Establishment
YAMADA	Toyo Tanso Co. Ltd.
YAMAMOTO	Toyo Carbon Co. Ltd.
YAMASHINA, Toshiro	Faculty of Engineering, Hokkaido University

YAMAWAKI, Michio	Faculty of Engineering The University of Tokyo,
YAMAZAKI, Seiichiro	Kawasaki Heavy Industries Ltd.
YASUDA, Shigeo	Ibiden Co. Ltd.

SUMMARY OF EACH GROUP

2.1: Characterization of Graphite and C/C Composites

2.6: Radiation Damage

W.P. Eatherly, ORNL T. Oku, JAERI J. Sako JAERI

T. Takekawa, Nippon Kokan K.K.

N. Yamamoto, Toyo Carbon Co., Ltd.

Introduction

The working group was asked by the Workshop Co-Chairmen to address not only the general problems given in the title above, but specifically consider the viability of graphite for use in the CIT and TIBER II/ ETR machines and the data base requirements to assure the viability.

Members of the working group were:

Carbon/Carbon Composites

The apparent advantages of carbon-fiber carbon-matrix structures for fusion energy applications are obvious: fabrication to shape, high strength, high thermal shock resistance, and non-catastrophic failure. High cost may not be a serious objection in view of those advantages. The serious problem remains one of ability to withstand particle damage, most specifically that from 14 Mev neutrons. The group has reached a concensus opinion as follows:

1. Applicability to the CIT and TIBER II/ETR: The present state-of-the-art can probably yield c/c materials satisfactory for the anticipated neutron fluence in the CIT. This statement is made not on the basis of existing information but on the considered experience of the group. It is counter to the observed data on neutron damage in early (ca. 1965) composites (see section 2 below) . The decision to consider use of C/C structures in CIT will require the immediate start of an irradiation program of candidate materials followed by establishment of data bases for successful candidates assuming such exist. To assure futher success at the present time, the program should be laid out to provide at least one iteration of materials from experience in the first irradiation experiments.

In the absence of any data on C/C at fluences hear the extreme for bulk graphites, one can consider their use in the ETR to be extremely doubtful. Any intent to use such structures here also demands the initiation of an immediate

radiation damage program to the high fluences required (the order of 10^{22} n/cm^2). Several generations of material development must be planned for in addition to the final accumulation of data bases for successful candidate composites.

2. Irradiation Damage Studies: The decision to investigate C/C composites for use in either CIT or ETR requires an immediate decision to perform neutron irradiation studies. For the low fluences required in the CIT, such studies can be performed quickly in a variety of reactors, and the presently planned Japanese and German irradiation programs including C/C's should be strongly encouraged. The use of HFIR in the United States would be desirable for the CIT studies but essential for the high-fluence requirements ($<10^{27}$ n/m^2) of the ETR. Because of the fact that the weave patterns will be sensitive to both the end application and to radiation damage, at least proof-test type reactor irradiation will be required.

In order to accomodate the wide variety of potential fiber choices, weave and lay-up types, and the several methods of densification, as well as the eventual development of a multi-temperature data base, this group feels an international effort should be developed in the interests of both efficiency and cost benefits. Clearly such an effort will require interchange of specimens between the three countries and a carefully laid out plan of candidate materials and reactor irradiation temperatures and fluences. For the CIT, particular attention will have to be paid to the change in thermal conductance, thermal expansion, and mechanical failure

mechanism. The early formation of a group familar 1) with C/C structure, 2) irradiation damage, and 3) reactor facilities should be formed as soon as possible to provide a coherant experimental plan on an international scale.

3.Data Base Requirements: The data base we discuss here applies to the general physical and chemical properties and not to the specific and concomitant requirement of hydrogen recycle and inventory. We do include out-gassing behaviour as a "chemical property" because the degassing is so closely tied to the raw materials and manufacturing methods.

The data base for fiber-reinforced composites is necessarily more complex than that for a single phase material. Since the fiber orientations are directed during fabrication in response to a prelimimary stress analysis of the final conponent, and the actual stresses then respond to the local structure of the composite, the data base must also cover the variability of various fiber lay-up and weave patterns. In addition to the normal acquisition of thermo-mechanical data used in design, a number of other special problems arise with C/C composites. One of the obvious differences is the decoupling of thermal diffusivity from thermal conductance: the fact that the fibers directed along the axis of heat transmission "short-circuit" the heat flow, transmission and steady-state behavior is obviously different and both types of information are needed.

A second strong difference is the multi-staged mechanism of failure, i.e., matrix cracking, fiber breakage, and fiber pullout in succession. Thus failure exhibits a "yield" in that large changes in strain take place at very little change

in stress. The mechanism of failure must be determined in part to determine the yarn lay-up patterns required. Closely associated with these phenomena is the weak interlaminar shear strength even in multi-dimensional weaves. Clearly these characteristics also require direct measurement of thermal shock failure since model studies cannot take into account the detailed morphology of the structure.

To sum up, considerable more effort will be expended on date base acquisition, with or without neutrons, than is required for a bulk graphite.

4. Data Requirements from the Mannfacturer: A significant amount of information, available from the manufacturer, is required to estimate the probable behavior of a C/C grade and to ensure the data then obtained can be imbedded in data from other composite structures to determine trends and directions for optimization. Thus correlated measurements of a number of properties on relatively few carefully selected types of composite materials is considerably more useful than an equivalent amount of isolated information over a number of grades. The following information is pertinent to a correlated development program and is usually readily obtained from the manufactures:

a. Fiber (monofilament) type,i.e., PAN, pitch, or other, including source and grade where pertinent.

b. Yarn characteristics: Filament diameter, number of filaments per yarn, yarn denier.

c. Weave and layup: pre-fab (tape or cloth) if used, multi-dimensional or multiweave patterns, and cell size.

d. Densification method: high or low pressure impregnation, CVD, or combinations thereof. Details on use of thermo-setting or thermoplastic impregnants if possible.

e. Final heat-treatment temperature.

It is suggested that a pre-selected set of grades be used by all investigators in the fusion energy program out of the almost infinite possible combinations of manufacturing techniques that can literally be imagined.

5. Specific Area Deserving Research Attention: The present weakest link in C/C composites, unlike the polymer matrix materials, is the interfacial strength between fiber and matrix. Quite outside the range of the normal sizing materials, other innovative techniques have and are being proposed. Since the fusion energy program requirements are severe in both thermal loads and, eventually, neutron damage, this work-shop group strongly recommends the several government funding agencies be alert to and sponsor exploratory work in improving the interfacial strengths.

6. Designer Interaction: The composite structures game is quite different from that of the bulk graphites. For the bulk graphites it is sufficient for the materials scientist to know the physical and mechanical properties required, including possible trade-offs, and he can go into the development

laboratory and plant and produce (if possible) such a grade of material. This is in strong contra-distinction to the composites, where the material is configured and structured around the actual design, geometry, and accompanying stress analyses of the component to be fabricated. Thus throughout all stages of a C/C development and data acquisition program an intimate relationship between designer, materials scientist, and fabricator is essential.

Bulk graphite

1. Materials for CIT and ETR

There are many graphites which meet the requirement of neutron fluency in CIT. In the case of ETR, however, some severe problems may occur when the bulk graphite is to be used to be the first wall towards the plasma. The first problem would be the difference in neutron spectrum between ETR and the fission reactors. There are lots of data on the critical properties of graphites irradiated in the fission reactors. They will not be able directly to be used for the ETR. A 14-Mev neutron from the ETR will make more severe damage for graphites than that from the fission reactors. The ETR is expected to be operated in a cyclic mode condition. This operating condition will create thermal cycle and fatigue problems. The first wall of the ETR will be subjected to thermal and mechanical loading up to 5×10^5 cycles per year. In contrast to the ETR, the fission reactors are normally operated in a steady state condition. The dimensional changes due to neutron irradiation are known to depend on the irradiation temperature. The maximum life is expected to be dependent upon the fluency and the temperature. As the operating temperature decreases, the maximum life may be increased unless the Wigner energy release problem occurs. The minimum temperature will be 250-300 C from the viewpoint of the Wigner energy release problem.

In addition, the neutron flux in the ETR is expected to be larger than that of the fission reactor. At the present time fission fluxes are available over a range of a factor of at

least 100, with the HFIR reactor providing the largest ($\sim 10^{15}$ $n \cdot cm^{-2} \cdot sec$). The ETR will have peak fluxes at a somewhat higher level. The fact that there is or is not a damage rate effect at these very high fluxes must be established, probably by simulation from beam-type devices.

2. Irradiation Data

Key properties in applying the bulk graphite to CIT and ETR are understood to be thermal conductivity, thermal expansion coefficient, degassing, and strengths and fracture toughness. The irradiation effects data on these properties of some graphites (POCO, ATJ, IG-110, etc.) are available for CIT condition. However, the data obtained so far will not be always to applicable to the case of ETR because of the reason stated above. In this connection, some facilities which simulate the operating condition of ETR are recommended to be developed to obtain the needed data. International cooperative studies will be helpful for obtaining the necessary data set. The US, German and Japanese reactors will be able to be used for irradiation tests.

3. Data Base

The general properties data needed are available, except for irradiation data, for both the CIT and ETR facilities. It is understood that what kinds of data should be intensively obtained should be made clear from the designers viewpoint.

Each country should continue an effort to obtain the data base for CIT and ETR.

4. Manufacturing Information

Since it is understood that there exist some bulk graphites which are available for CIT, some information on manufacturing bulk graphite should be given to the Workshop members to make clear the correlation between the properties and the manufacturing parameters. The parameters regarding the production process are listed in the Table 1. These parameters are critical to the radiation damage problem.

Concerning ETR these are understood to be important for improving the existing bulk graphites.

Table 1: Manufacturing parameters needed

	Items	Information Desired
1	Filler	Type, size, calcination temp.
		Primary & Secondary
2	Binder	Thermoplastic or Thermosetting
3	Pretreatment	Purification of filler and binder
4	Forming	Mould (JAR, CIP, MIP etc.) or Extrusion
5	Baking	Normal or Pressurized conditions
6	Densification	Thermosetting or Thermoplastics
		Number of cycles
7	Graphitization	Temperature
		Furnace (Atcheson furnace or Induction furnace)
8	Purification	Halogen (gas or salt) or Freon

5. Encourage Research

It is required for establishing systematic research work in order to attain the long range improvement of the conventional production technology of bulk graphite by new modification technologies, such as surface treatment and graded structure which should also be developed.

It is necessary to establish close relationships among manufactures, designers and institutes which are engaged in the assessment.

Highly Oriented Pyrolytic Graphite

A special purpose application of graphite being considered in fusion devices in the use of cooled pyrolytic graphite in regions of very high thermal loading. The highly oriented graphite (hot-worked pyrolytic) is geometrically arranged to intercept the plasma and transmit the heat in the a-b plane direction to the tube containing the cooling water.

The fluence conditions envisaged in the CIT machine are sufficient to cause concern in the radiation damage incurred by the pyrolytic. Even at these relatively low fluencies a severe loss of thermal conductivity can be expected depending in part on the temperature of the pyrolytic graphite at which the damage occurs. The working group confirms the necessity to obtain data on thermal conductivity at the expected fluency and operating temperatures.

Certainly there is a further concern in that at this or slightly greater fluencies, severe dimensional changes will occur (a-b contraction, c-expansion) along with concommitant development of severe internal stresses. It is the working group's conclusion that the use of highly-oriented pyrolytic graphite as a heat transfer agent must be limited to small neutron fluencies.

2.2 Outgassing properties

K.Akaishi, Y.Kubota, A.Uritani (IPP-Nagoya)
K.L.Wilson (SNLL)
W.Eckstein (MPI)

1.INTRODUCTION

The evaluation of the outgassing properties and an establishment of handling recommendations for graphites(include isographite, anisographite, and C-C composite) are very important tasks for the application of graphite to the first walls in fusion devices. The outgassing significantly depends not only on the graphite grade but also on pretreatment, heating parameters, storage periods, and storage method of graphite at manufacturer and user sides.

In this section, the outgassing experiments on graphites, which were performed in different laboratories to clarify the correlation between the outgassing and conditions, is summarized and evaluated for use in CIT.

2.CONDITIONS OF INVESTIGATION

Main experimental facilities and maximum heating temperature adopted are as follows:

a)SNLL : TDS, BET method(1600℃),
b)IPP-N : TDS, minute balance(1400℃),
c)ORNL : TDS(2000℃),
d)MPI : pressure difference, microbalance(RT,150℃,750℃)

The kinds of samples used to investigate the outgassing are isographite, anisographite, and C-C composites of 2D,3D and 4D weaves with weight of 0.3-20g. The initial conditions of samples before outgassing are classified into as-received, ultrasonic cleaned, and annealed states. However, there are several samples already pretreated and vacuum packed at manufacturer side among the as-received samples tested at user side. A definition of the

terminology or concept for "as-received" sample is necessary. As heating ramp rates of TDS measurement, 10, 25, and 60℃/min were adopted.

3.CONCLUSIONS OF OUTGASSING MEASUREMENTS

Outgassing of various kinds of graphites performed at four different laboratories are summerized as follows:
There is a large difference, more than one figure, in desorbed gas amount between not only as-received samples but also samples exposed to air after annealing at 1000-1400℃. The Desorbed gas amounts from C-C composites of 2D weaves, especially K-KARB, are greater than that of the other graphites. On the other hand, the desorbed gas amounts of pyrolytic carbon grades and C-C composites of 3D, 4D are relatively less than that of the other samples. However, no essential difference in TDS spectra or desorbed gas species between various kinds of graphites were observed.

A remarkable difference(1-2 figures) in the desorbed gas amount between the 1st and the following 2nd degassing is observed. After annealing in high vacuum and high temperature range of 1000-2000℃, the desorbed gas amount of most isographites, anisographites, and C-C composites is small enough for use in CIT. However, the absorbed gas amount in graphites during exposure to air,which was measured by TDS or balance, increases with exposure time and reaches a level close to the gas amount desorbed by as-received samples after 50 days. This means that although graphite is well annealed before installation, readsorption of environmental gas is to be expected during the installation period of the first wall. For gas redesorption after installation, the elevation of the wall temperature to at least 350℃ for baking procedure is recommended through experiences of large machine operation.

In partial pressure measurement by QMF, remarkable differences

are recognized at two specific temperature regions. The main gas species desorbed from samples are H_2O and hydrocarbons in the range below 800℃ and H_2 and CO in the range above 800℃ for both as-received sample and sample exposed to air after annealing. However, no gas was found for samples just after annealing up to 1000-2000℃ except gases due to background.

No clear correlation between outgassing and practical surface area of sample measured by BET method was found although there is little correlation between outgassing and apparent surface area of graphite under constant volume. Moreover,there is no apparent relation between the outgassing and density of graphites

Outgassings properties of various kinds of graphite were investigated in different laboratories. However, it is difficult to compare the results with each other and derive universal conclusions from the results because there are large difference in the experimental conditions(e.g., sample weight, pretreatment, or heating parameters) of the outgassing among the laboratories.

To establish better comparability of the experimental conditions and to investigate in-situ outgassing after installation of graphite to fusion test devices are necessary for the establishment of a complete database.

4.DATA NEEDS

For fusion application, the following data are required:

- in-situ outgassing behaviour after installation of graphites in fusion devices.
- outgassing rate at room temperature q(Torr l/s cm^2 or Torr l/sq) of graphites,
- data for readsorption and desorption of hydrogen isotopes during plasma graphite interaction related to H recycling and T inventory.
- data for evaluation of discharge cleaning effect on the graphite with H, D and He plasmas.
- methods to reduce absorption of environmented gas by graphites during storage.

Subgroup 2.3: High Heat Flux Experiments

J. Linke (KFA), M. Seki (JAERI), T. Shikama (NRIM),
H. Bolt (IPP Nagoya)

1. Introduction

To improve the data base on candidate materials for the first wall and high heat flux (HHF) components which directly face the plasma a variety of tests were performed at different laboratories. Beside the commonly used electron beam devices also neutral/ion beam bombardment and laser tests were used to simulate the heat load conditions of individual plasma discharges (single shot experiment) and the integrated damage due to cyclic exposure (thermal cycling). During short single shot experiments off-normal plasma conditions (disruptions) were simulated. In addition the failure during runaway-accidents was investigated by means of a 30 MeV electron linear accelerator.

A variety of candidate materials were tested, namely:
- isotropic and anisotropic fine grain graphites
- pyrolytic graphite
- C-C composites
- beryllium
- sandwich structures (carbon materials brazed to metallic substrates)

After the exposure to HHF-conditions different failure modes were observed; main defects were:
- evaporation/sublimation
- particle emission
- cracking
- melting (Be, braze, metallic substrates)

Besides methods to improve the thermomechanical behaviour of the plasma facing materials also engineering aspects should be taken into account which will reduce temperatures at critical

components, e. g. at the leading edge. With concern to the plasma behaviour under the aspect of plasma-wall interaction the development of means to better control plasma discharges and especially to avoid disruptive plasma behaviour is highly desirable.

2. Candidate Materials and Testing Facilities

The material candidates tested so far are shown in Table 1 together with the main characteristics, the major experimental observations, and the machines where these materials have been in use or will be installed in the near future.

The high heat flux test facilities used so far, or foreseen for future experiments, resp., are listed in table 2. Here also the major data of these devices are given.

3. Normal Operation

Experiments:

SNLA:
- erosion of fine grain graphites, pyrocarbon and C-C composites (e^--beam), Figure 1
- thermal cycling of graphites and C-C composites (cycle number n = 1,10,100,540): no damage detectable by SEM after 540 e^--beam pulses of 2kW/cm^2 power density and 10s duration, Figure 2.
- thermal cycling on water cooled divertor elements (graphite brazed to Mo) for ASDEX (e^--beam)
  - o no visible damages after 3000 cycles with 700w/cm^2 surface heat load, 20s pulse length
  - o intense erosion of the surface (emission of particles after 2.0kW/cm^2 electron beam pulses of 20s duration. Erosion depth approx. 5mm after 200 cycles

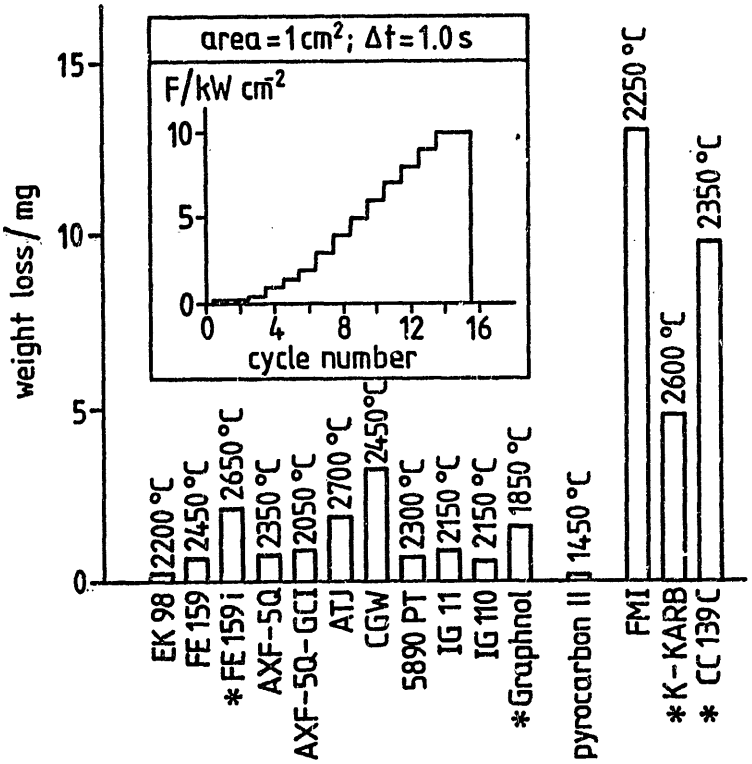

* sample geometry other than 25mm × 25mm × 10mm

Fig. 1: Weight loss of different C-materials (heat load conditions are shown in the insert). The indicated temperature values correspond to the maximum surface temperature in the 10 kW/cm^2 cycle.

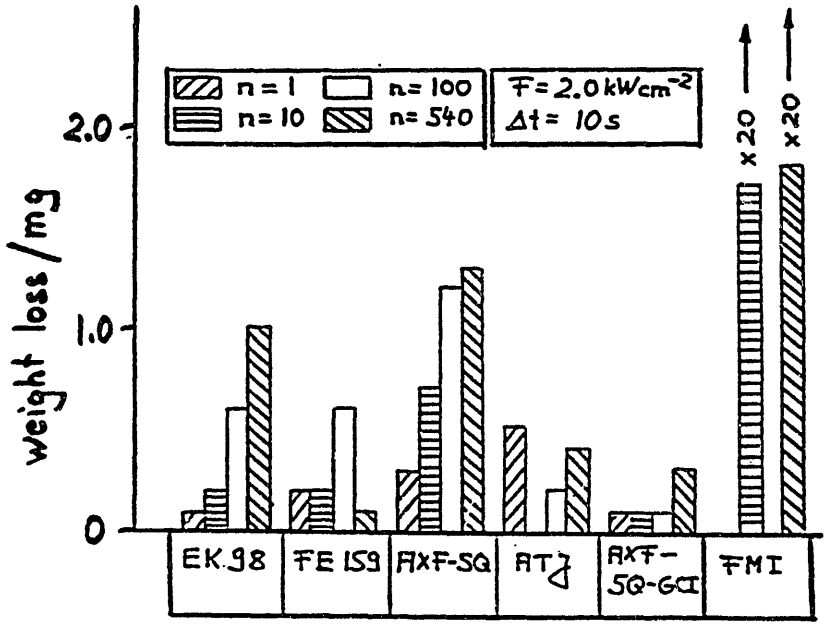

Fig. 2: Weight loss of different C-materials due to thermal cycling

- high heat fluxes on actively cooled Tore-Supra components (e^--beam):
  up to 4.4kW/cm^2, 30s pulse length, coolant flow up to 1l/s; twisted tape roughly doubles critical heat flux (CHF)
- thermal cycling on beryllium (e^--beam), 4000 cycles, 450 W/cm^2, 10s pulses;
  extensive cracking and surface damage; slotting of the tile surface decreases thermal stress concentration and leads to an acceptable design

KFA: - erosion of graphites and a C-C composite (e^--beam);

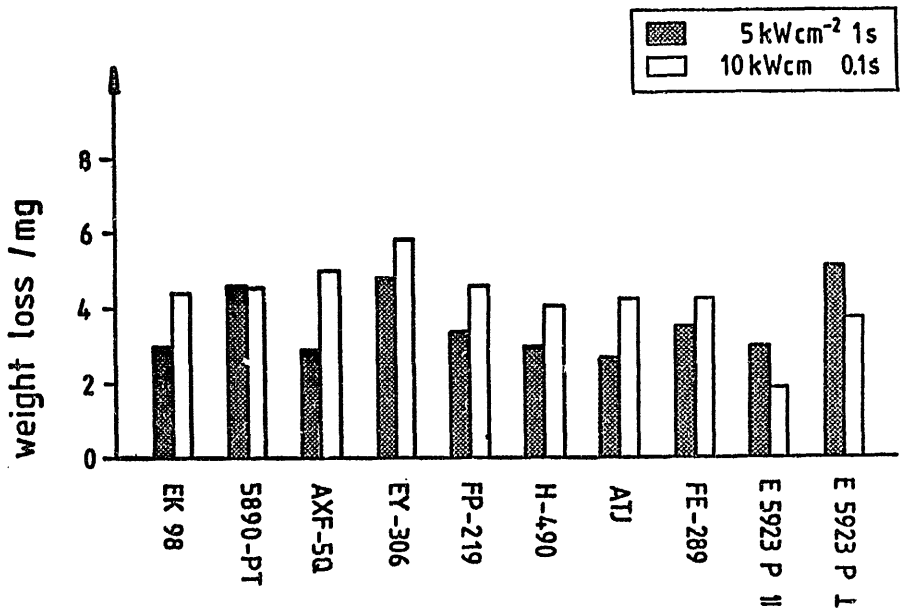

Fig. 3: Weight loss of different graphites and C-C composite (E 5923 P) after single shot e^--beam bombardment

Hitachi: - high heat flux test (Laser beam) on water cooled graphite/SiC/Cu-sandwich structures;
  10 cycles with pulses of 40s duration with maximum power densities of 1.7kW/cm^2; no cracking but evaporation of carbon occured

4. Off-normal operation

4.1 Disruptions

Experiments:

SNLA (e^--beam):
- high strength graphites (3 grades)
- isotropic and slightly anisotropic fine grain graphites (8 grades)
- C-C composites (3 grades)
- pyrolytic carbon (1 grade)

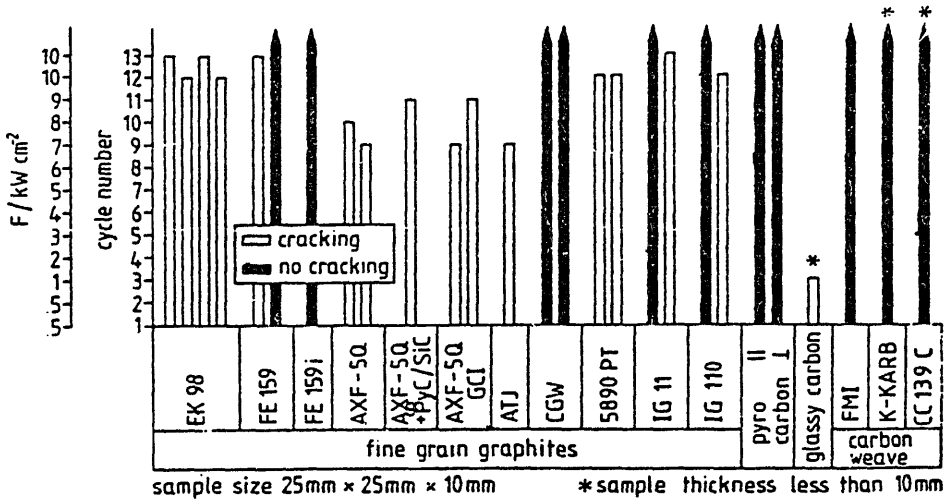

Fig. 4: Results of the cracking behaviour of different graphitic materials after successive electron beam pulses with increasing power density F

KFA (e^--beam):
- high strength graphite (1 grade)
- isotropic and slightly anisotropic fine grain graphites (7 grades)
- C-C composite (1 grade)

(see Figure 5)

JAERI/KHI: (electron beam experiments)
- 1 isotropic fine grain graphite

(see Figure 6)

IPP Nagoya: (ion beam experiments with Neutral Beam Injection test stand)

- high strength graphites (4 grades)
- isotropic and slightly anisotropic fine grain graphites (5 grades)
- anisotropic graphite (1 grade)

(see Figure 7)

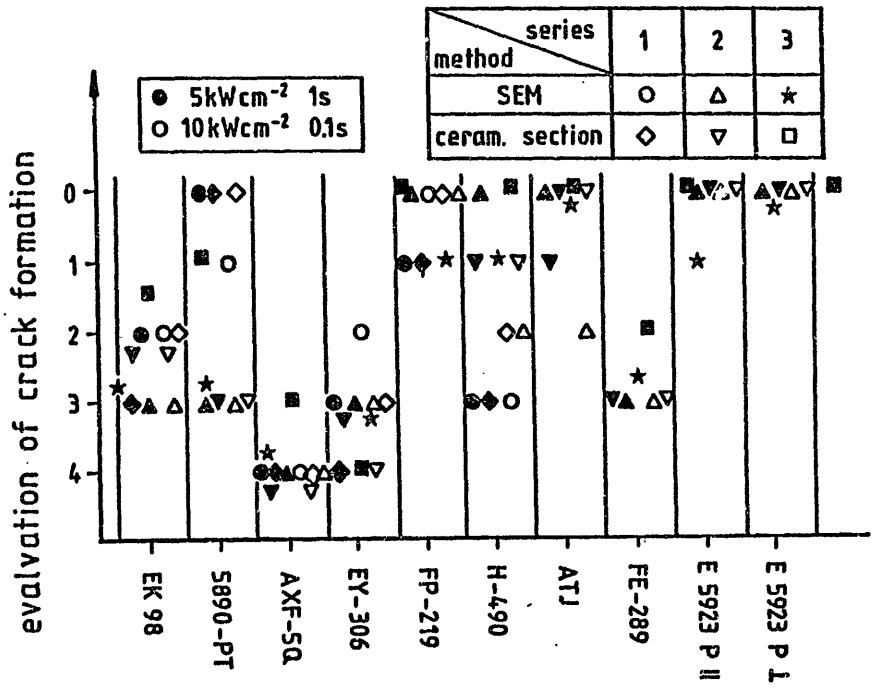

Fig. 5: Evaluation of the crack formation after 5kW/cm^2, 1s pulses (filled symbols) and 10kW/cm^2, 100ms pulses (open symbols) for the experimental series 1, 3, and 4. The effect of crack formation was evaluated separately on SEM-images and ceramographic cross sections. 0: optimum thermal shock behaviour, no cracks detectable; 4: worst thermal shock behaviour, severe cracking

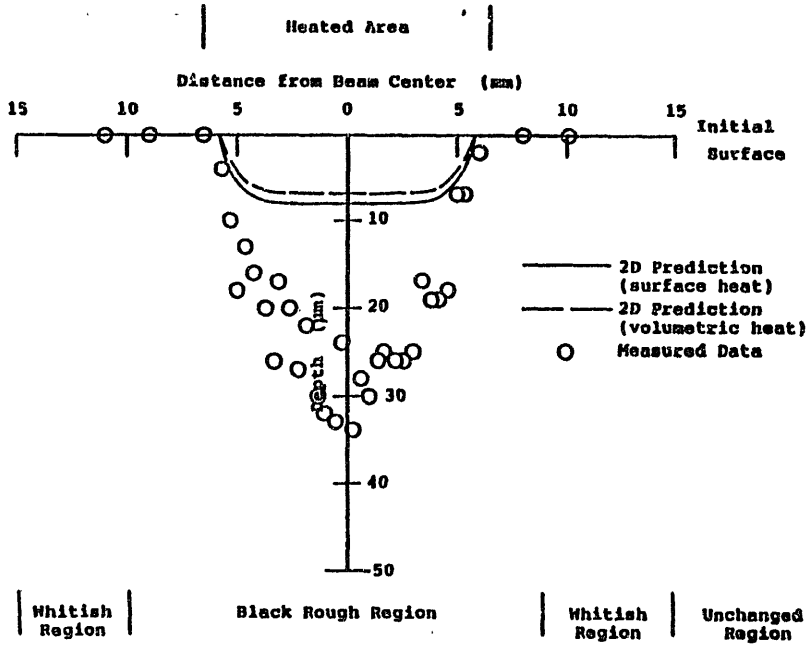

Fig. 6: Erosion on IG 11 graphite surface with 11.6MJ/m^2 energy deposited for 0.1s.

graphite	no. of samples tested	cracking (brackets: no. of samples)	erosion
AXF 5Q	3	netlike crack formation (2)	homogeneous erosion structure
ISO 880	2	netlike crack formation (2)	homogeneous erosion structure
T6-P	1	microcrack (SEM) (1)	loosening of surface structure
MT 200 K	1	microcrack (SEM) (1)	loosening of surface structure
CL 5890	3	---	loosening of surface structure
EK 98	3	crack (1), microcrack (1)	loosening of surface structure
ETP-10	2	---	long voids (∿200μm) (preexistent?)
IG 110	3	---	loosening of surface structure
ATJ (CGW)	3,1	---	
YPD	3	complete fracture (1)	little erosion

Fig. 7: Summary of results of disruption simulation tests. H^+-beam pulses with power densities of 9...10kW/cm^2 at pulse lengths of 157ms to 353ms; high strength

graphites are AXF 5Q, ISO 880, T6-P, MT-200 K. CL 58 PT, EK 98, ETP-10, IG 110, ATJ, and CGW are isotropi or slightly anisotropic fine grain grades. YPD is highly anisotropic.

Summary on disruption simulation experiments:
Thresholds for crack formation are:

- high strength graphites: P/A about 7kW/cm^2, t_H about 200
- isotropic and slightly anisotropic graphites: P/A above 10kW/cm^2, t_H above 200ms
- C-C composites: P/A above 10kW/cm^2, t_H above 1s
- pyrolytic carbon: P/A above 10kW/cm^2, t_H above 1s (bulk material)

4.2 Runaway-electrons

Experiment:

place	: Radiation Lab., Inst. of Scientific and Industrial Research, Osaka University
apparatus	: Electron Linear Accelerator
beam energies and pulse currents	: E = 20 MeV, I_p = 300 mA E = 25 MeV, I_p = 280 mA E = 30 MeV, I_p = 240 mA
pulse width	: t_p = 1.5 µs
repetition rate	: f = 120 pps (pulses per sec.)
input power	: P ≤ 1.30 kW
beam diameter	: d = 4 mm
irradiation times	: t_{irr} = 10...60 s

Fig. 8: Irradiation facility and runaway-electron simulation parameters

- bulk graphites are far more resistant against runaway-electro impact than bulk metals

- metal cooling tubes of actively cooled carbon-metal components may suffer serious damage

Numerical simulation (SNLA):
Monte Carlo Code TIGER for high energy electron-materials interaction in multidimensional mode.

- design with large graphite volumes needed to prevent excessive heating of metal cooling tubes of actively cooled components

5. Failure modes

I. erosion: vaporization (normal operation and disruptions)
hydrocarbon formation (normal operation and disruptions)
particle emission (disruptions)
splashing of melt from metal walls (disruption, runaway-electrons)

II. cracks: - cracks in self-supporting tiles:
graphite component failure
C-C composites crack propagation resistance?
- cracks in carbon materials brazed to metal substrates:
crack formation can be tolerated under certain circumstances:
Cracks have to propagate parallel to the thermal gradient and have to be stopped in the interface to the metal substrate.

III. failure of actively cooled structures:
- melting of the coolant tube walls
- failure of the interface under
o steady state operation: heat loads above the capacity of the component (e.g. above 4400W/cm^2 for the Tore Supra leading edge (SNLA), "CHF" limit

- o disruptions: heat loads onto components operating with very small safety margin (near "CHF" limit)
- o runaway-electrons: heating of metal tubes

6. HHF-data needs

- data base on erosion and damage thresholds (cracking)
  for:
  - C-C composites
  - pyrolytic carbon
  - coated systems
  - actively and radiatively cooled structures (tests of full size components; tests of structural integrity and performance in operation after a disruption; heat transfer behaviour of actively cooled components)

- crack propagation modes in carbon materials

- physical background of particle emission

- theoretical estimation of material behaviour under HHF-conditions:
  - o temperature dependent physical and mechanical data in the very high temperature regime needed (up to 3000°C)
  - o technical information on manufacturing processes of more complicated structures and properties (physical and mechanical) of brazes, substrates, etc.

Candidate Materials			
Materials	Main Characteristics	Experimental Observation	Machines
Iso Graphite	low cost, well established manuf. process	°high cracking threshold HF	TFTR(POCO AXF-5Q), JET(PT 5890, EK 89) JT-60(ETP-10, to be used) TEXTOR(IG-110; pump limiter blade, EK 98)
Aniso Graphite (Pyro Carbon)	°high thermal conductivity		Tore Spra(Pyro-C/Cu) TEXTOR ALT-II-Neutralizer Plate
Fiber Composite (2 directions)	high fracture toughness high thermal conductivity °high cost, °size?	high resistance to thermal cycling	TFTR(RF-limiter, scheduled to be used, June 87), JET(Dunlop DMS 678; NBI Shine though protection),TEXTOR(limiter blade)
Fiber (larger than 3 direction)	°same as 2D-Fiber °isotropic properties	°same as 2D-Fiber °loads 30MW/m^2 sustained for 3s	JET(Aerolor; examined as a condidate)
Be			JET(limiter as an alternative choice to graphite)
High Z refractories	°excellent thermal conductivity	surviving required thermal cycles, 10^4 cycles)	ETR family(W/Cu; divertor plate)

Table 1; Candidate materials for the 1st wall of confinement experiments

Location	NRIM	IPP Nagoya	JAERI	KHI	MHI	Hitachi	SNLA	SNLA	KFA	KFA*2
Type of Load	e^-	H^+, H^0	H^+, H^0	e^-	e^-	Laser	e^-	H^+, D^+	e^-	H^+, H^0
Particle energy	50eV, 2keV (150A/cm²) (50A/cal.)	<120keV		100keV	<120keV	λ=10.6μm	30keV	40keV	150keV	20... ...50keV
Power density	7.5KW/cm² ∿100KW/cm²	<20 KW/cm²	20KW/cm²	17KW/cm² for 13mm×13mm	∿100KW/cm²	up to 1.7KW/cm⁻²	up to 100KW/cm⁻²	>4KW/cm²	up to 50KW/cm⁻²	8-15KW/cm⁻²
Pulse length	1s ∿10mS 0.5s	< 1s	...10s	1ms..∞	50ms ∿ ∞	100ms...∞	few ms ...∞	10-30s	1ms... ∞	100ms... ...10s
Rise time	100ms, 5ms	10ms	50ms	less than 0.2ms	< 50ms	100ms		1ms		5..,10ms
Loaded area	1cm × 1cm, up to 2cm × 2cm	<150mm × 400mm	up to 60 × 80cm	4cm × 4cm*1 40cm × 40cm*2	up to 60cm × 60cm	6cm²	1...100cm²	>100cm²	up to 25cm²	150cm²
Total power	10KW, ∿200KW (pulse)	9MW	8MW	60KW	120KW	5KW	30KW	800KW	30KW	4MW
Thermal cycling	Yes, yes	No	No	Yes	Yes	Yes	Yes	Yes	Yes	Yes RR = 5min.

Table 2: High heat flux test facilities and major technical data.

*2 = available 07/87

*1 = high frequency rastering mode

*2 = low frequency rastering mode

RR = repetition rate

2.4. SPUTTERING, SYNERGISMS AND EROSION PROCESSES

Y. Hirooka, A. A. Haasz, K. Morita, R. Yamada, V. Philipps, N. Itoh, W. Eckstein

2.4.1 Operating Environment for Graphite

(1) Temperature of graphite

Based on experience with JET and TFTR and estimated thermal loads for CIT (6.5-9.5 MW/m^2), the limiter/divertor temperature under normal operating conditions is not expected to exceed ~2000 K. Wall graphite tiles under normal conditions are expected to remain below ~1000 K.

(2) Plasma particle fluxes and energies

(i) Limiters/divertor

- energetic H^+ ions : 10's eV - 100's eV
  $\sim 10^{18} - 10^{20}$ H^+/cm^2s
- Franck-Condon neutrals : few eV energy
  $\sim 10^{18} - 10^{20}$ H^o/cm^2s

(ii) Wall tiles

- charge exchange neutrals : up to keV's energy
  $\sim 10^{15} - 10^{16}/cm^2s$
- energetic H^+ ions : 10's eV - 100's eV
  $\sim 10^{16}$ H^+/cm^2s
- Franck-Condon neutals : few eV energy
  $\sim 10^{16}$ H^o/cm^2s

(3) Neutron irradiation

Neutron fluences for CIT are expected to remain low (leading to ~1 dpa). Considerably higher neutron fluences are expected for ETR-type machines. Although no database exists for the erosion of neutron-irradiated graphite, no significant influence on erosion is expected.

2.4.2 Erosion Data for Graphite

(1) Low Energy/high flux H^+ bombardment

Graphite erosion processes can be considered from the viewpoint of (i) physical sputtering, (ii) chemical erosion, and (iii) radiation-enhanced sublimation. Each of these processes dominates in a reasonably well-defined temperature range.

(i) Physical sputteriing (T<500 K)

Physical sputtering data have been well established. For example, physical sputtering for 100 eV H^+ and D^+ is ~7×10^{-3} C/H^+ and ~1.5×10^{-2} C/D^+, respectively. Missing data for energies below 100 eV can be reasonably well extrapolated with available sputtering models.

(ii) Chemical erosion (500 K<T<1200 K)

Chemical erosion, via the formation of CH_4 and heavier hydrocarbons dominates the erosion process in this temperature range. The erosion rate depends on substrate temperature, ion energy, and ion flux. An extensive database exists for H^+ energies down to ~50 eV and fluxes up to ~10^{16} H^+/cm^2s. While only limited data are available at fluxes >10^{16} H^+/cm^2s (PISCES and DITE carbon probe experiment), reasonably reliable extrapolation to CIT and ETR-relevant conditions could be

attempted. For 100 eV H^+, at ~10^{16} H^+/cm^2s the total erosion is about 10^{-1} C/H^+ at the temperature of maximum erosion. For fluxes in the 10^{16} - $10^{18}/cm^2s$ a decrease in the erosion yield has been observed.

(iii) Radiation-enhanced sublimation (RES) (T>1200 K)

At temperatues $\gtrsim$ 1200 K, a significant increase in the erosion of carbon occurs due to energetic ion impact. The released carbon is monatomic, with a thermal energy distribution. For 1 keV H^+ impact on graphite, the erosion yield reaches ~$3x10^{-1}$ C/H^+ at 2000 K. A decrease is expected for lower energies. Based on a C-interstitial formation model, a decrease in the yield is predicted for higher fluxes.

(2) Erosion due to oxygen impurities

Erosion yields for O^+ impacting on graphite are of order unity, mainly due to chemical formation of CO and CO_2. Therefore, erosion by oxygen (O being a main impurity in tokamaks) must be considered for the total erosion estimates of graphite.

(3) High Energy H and He bombardment

Sputtering data for energetic charge exchange neutrals and alphas impacting on carbon are availabe for energies up to ~10 keV from a combination of laboratory and calculated data. Calculations for higher energies could be readily performed.

2.4.3. Effect of impurities on erosion

Metallic impurity contamination of graphite surfaces as well as doping of the graphite lattice with impurity atoms have been demonstrated to reduce the chemical erosion of graphite. However, doping with high Z atoms also increases the high Z impurity

production which is not desirable. Effects of low Z doping of graphite to reduce chemical erosion should be investigated.

2.4.4 Erosion-redeposition processes with graphite

(i) Physical sputtering dominated regime

Substrate temperatures : (T_s<500 K; 1200 K<T_s<1400 K)

Due to its high velocity, physically sputtered carbon is not likely to be reionized to trigger redeposition unless the edge plasma temperature and density are very high.

(ii) Chemical-erosion dominated regime

Substrate temperature : 500 K<T_s<1200 K

The energy of the desorbing methane molecules is expected to be equal to the surface temperature. Therefore, the velocity of desorbing hydrocarbon molecules is significantly smaller than that of physically sputtered carbon. Redeposition of hydrocarbons is thus expected to occur. Redeposition of hydrocarbons was found to reduce the erosion yield by a factor of 2-3 in the 350-1200 K temperature range (PISCES experiment).

(iii) Sublimation-enhanced sputtering (T_s>1200 K)

The velocity distribution of the released carbon-atoms due to radiation-enhanced sublimation process was found experimentally to be Maxwellian. These carbon atoms can thus be treated in a similar manner as thermally evaporated atoms with respect to the ionization mean free path. Experimental confirmation of the effect of this mechanism on redeposition is required.

2.4.5 Caron/Carbon composites and carbon films

(i) Carbon/carbon composites

First results on the erosion of C/C composites show a

reduction of erosion yield compared with graphite during plasma exposure in PISCES.

(ii) Diamond-like carbon films

First results with diamond-like cabon films, produced by CVD at 1200 K, show lower erosion rates than pyrolytic graphite.

(iii) Hydrogenated amorphous carbon films (a-c:H)

Under energetic H^+ impact, the chemical erosion rate of a-c:H is similar to that of graphite. Under thermal H^o impact, however, the erosion of a-c:H films is considerably higher than the graphite case; in fact, it is almost as high as the erosion due to H^+ impact.

2.4.6 Outstanding data-needs

(i) Chemical erosion

- need $H^+ \rightarrow C$ erosion data for <50eV energies and fluxes $>10^{16}/cm^2s$
- need data for synergistic erosion (energetic H^+ and thermal H^o) in presence of surface impurities
- need further $O^+ \rightarrow C$ erosion data; need flux dependence and influence of surface impurities
- need controlled experiments to investigate erosion rates due to combined H^+ and O^+ impact on carbon

(ii) Radiation-enhanced sublimation (RES)

- need H^+ (and He^+) flux dependence data for graphite temperatures 1200 K<T<2000 K
- need data for <50eV (threshold for interstitial C-formation)

(iii) Erosion data with tritium impact on carbon

- need erosion data for T → C to confirm extrapolation of H, D data to tritium

(iv) Carbon/Carbon composites and carbon film

- need erosion data for C/C composites
- properties of dense carbon films need to be further investigated
- need erosion data for redeposited/codeposited films produced in tokamaks

(v) Erosion modelling

- further development of carbon erosion models, especially for tokamak-relevant fluxes, is recommended

2.4.7 Erosion data from current tokamaks

Available data on the different erosion processes (physical, chemical, RES) contributing to the observed C-erosion in current tokamaks are inconsistent. Different results reported for TEXTOR, JET and DITE may be due to different edge conditions (mainly ion temperatures). Under higher edge temperatures, as in JET, it is likely that physical sputtering dominates the carbon erosion for limiters, whereas at low ion edge temperatures (TEXTOR) chemical erosion might be predominant.

Chemical formation of thermal hydrocarbons is likely to result in a high redeposition rate of eroded molecules. Strong redeposition of carbon in the form of hydrogenated carbon films (a-C:H) has been observed in tokamaks. This behaviour strongly influences estimates of net erosion rates of carbon structures.

Carbon impurity radiation is expected to affect edge plasma

behaviour.

2.4.8 Conclusions

(i) Normal operation (limiters/divertor)

Under normal operating conditions, with ~10^{19} H^+/cm^2s at the limiters/divertor (with temperature rising to ~2000 K), an erosion rate of about 1 cm/10^4 shots (of ~4 s duration each) is estimated, based on maximum chemical erosion yields. Under more realistic temperatures, however, the erosion is more likely to be about an order of magnitude lower, i.e., ~1 mm/10^4 shots for CIT. Net erosion, will also be strongly influenced by redeposition.

(ii) Off-normal conditions (limiters/divertor)

The net erosion yield, however, is expected to be controlled by erosion during off-normal conditions.

(iii) Wall tiles

Wall erosion at anticipated fluxes of ~10^{16} H^+/cm^2s and tile temperature of ~800-900K (where maximum chemical erosion occurs) is expected to be negligibly small.

2.5 RECYCLING AND TRITIUM INVENTORY

K. Ichimura
T. Tanabe
K. Wilson
M. Yamawaki

1. INTRODUCTION

The interaction of hydrogen with graphite is important to fuel recycling between the plasma and limiter in today's Tokamaks such as JET and TFTR. It will also determine the in-vessel tritium inventory in these devices as well as in future carbon-based machines such as CIT and ETR. While much has been learned about hydrogen-graphite interactions from laboratory studies and device observations, a lack of several fundamental hydrogen transport parameters greatly hampers our modelling efforts. In this workshop summary, the database on hydrogen-graphite interactions is reviewed in section 2. In section 3, supershot conditioning in TFTR and wall pumping in JET are discussed, Finally in section 4 the status of tritium inventory estimates is critiqued. For more detailed discussions, there are several recent review papers such as those of Wilson (SNL) and Dylla (PPPL), as well as many topical reports in the 7th PSI Proceedings, 1986 AVS Proceedings, etc.

2.RETENTION MECHANISMS

Three mechanisms have been identified for hydrogen retention in graphite. Hydrogen implanted into graphite can become trapped within a saturated layer that extends to a depth equal to the ion range; it can diffuse along interconnected porosity; or it can undergo true lattice diffusion and trapping. In addition plasma interaction with graphite surfaces can lead to hydrogen trapping by means of a Co-deposition mechanism where eroded carbon combines with plasma hydrogen and is deposited on nearby surfaces

as a hydrogenated carbon film. The status of our understanding of each of these mechanisms will be discussed in the following sections.

2.1 The saturated layer

The formation of the saturated layer during hydrogen bombardment of graphite has received much study over the last 15 years. An extensive database exists for the saturated layer behavior, and phenomenological models exist to predict its recycling and isotope exchange behavior. Some information also exists on the physics and chemistry of the saturated layer. At room temperature, the saturated layer has a hydrogen to carbon ratio of 0.4. This layer is observed to thermally decompose at temperatures below 1000 K. Hence the saturated layer will form only in cooler regions of a Tokamak, such as the inner bumper limiter of TFTR. In CIT where graphite temperatures are expected to rise in many locations to 2200°C by the end of a discharge the saturated layer will only be a transient phenomenon, which forms at the start of a discharge, but decomposes as the surface temperature increases. Little further work is recommended for studv of the saturated layer, except for research on the chemistry of the microstructure.

2.2 Porosity diffusion

Graphite is essentially a porous material so that gaseous diffusion through pores and atomic diffusion on pore surfaces are intrinsically important to evaluate the hydrogen retention of graphite. Gaseous diffusion is principally Poisseul's (or molecular flow), so there is resistance against flow which has to be considered in evaluating the retention in graphite.

As for gaseous diffusion through pores, the data base is

quite poor at present. Yamawaki has recently initiated gaseous permeation in graphites, and the data appear to be incompatible with existing models. New data or new research are needed in the following items.

(1) Relation between permeability and porosity (pore size distribution, shape of pores, tortuosity factor etc.)

(2) Pressure dependence of permeability or relative contributions from viscous and slip flows to the total permeability.

(3) Temperature dependence of permeability; is there any discrepancy from the prediction by Carman's eq. ?

(4) Impurity and implantation effects

As for surface diffusion of pores, fundamental measurements have to be made in conjunction with those of lattice diffusion for various grades of graphite. Surface diffusion of atomic tritium has also been observed to occur on the porosity of nuclear grade graphites. Causey has reported a tritium surface diffusivity on the order of 10^{-5} cm^2/s at 500°C during tritium plasma exposure of POCO AXF-5Q. The surface diffusion of atoms as well as the dissociation of molecules on pore surfaces provides a short circuit pathway for tritium to reach the interior graphite grains. The database on these effects is small, and the impact of this mechanism on fuel recycling and tritium inventory is unknown.

2.3 Lattice diffusion solubility and molecular recombination

At elevated temperatures (~ 1000°C) hydrogen is observed to migrate in the graphite lattice. Knowledge of fundamental hydrogen transport parameters (e.g. diffusivity, solubility, and molecular recombination) are key to our understanding and successful modelling of hydrogen recycling and tritium inventory

for Tokamaks with graphite as the plasma facing material.

A few data are available at rather high temperatures. But the data scattering is very large and critically depends on the model employed for the experimental data analysis, because of the lack in the knowledge of the interaction of hydrogen and graphite.

2.3.1 Lattice diffusion

There are only a limited number of often contradictory datasets available. Recent measurement by Atsumi et al. give the values of around 10^{-12} cm^2/s at 1100 K which is in a fair agreement with the magnitude of diffusivity given by Causey. However, the values of diffusivity are often scattered because of trapping in intrinsic and/or extrinsic defects, and the apparent activation energy for diffusion becomes very large (as much as 5 eV) because of trap delayed diffusion. Below 500 K, absorption of hydrogen at the very large inner surface or pores make the lattice diffusion measurements very difficult.

2.3.2 Lattice solubility

Two opposite temperature dependences have been reported for hydrogen solubility at elevated temperature. Causey reported exothermic solution which means a higher solubility at lower temperatures, where as Atsumi et al. showed the opposite. The latter authors also reported a maximum solubility at about 1100 K with the value of around 10^{-2} STP cc/g. $atm^{1/2}$ and attributed the decrease of the solubility at higher temperatures to diffusional release during the quenching procedure for the measurements.

2.3.3 Recombination factor: Recycling - Inventory

Graphites, having different structures, are modified with

ion bombardment above fluence of 10^{18} $10^{19}/cm^2$, and show the steady-state (reproducible) trapping-release behaviors. Trapping-release behaviors consist of three mechanisms: that is, three peaks appear in thermal desorption spectra of hydrogen isotopes after ion implantation. On the basis of kinetic measurements and analyses, the desorption of Peak I, which appear in the lowest temperatures among the three, obeys the second order kinetics: namely, the rate-determining step is the association reaction of hydrogen isotope atoms on the surface. The rate-determining step of the second desorption (Peak II) is the same as the peak I. The third desorption (Peak III), which appears at the highest temperatures among the three, occurs with the diffusion-limit. The rate constants k_d of Peak I and II for desorption are determined.

From the observed rate constants for desorption. the recombination factors and/or surface recombination factors for Peak I and II are evaluated. These surface recombination factors k_sK^2 of Peak I show good agreement with the data obtained by Balooch and Olander. The evaluated recombination factors k_r of Peak I are about 10~11 order of magnitude smaller than those for the stainless steel at 500°C.

On the basis of temperature dependences of recombination factors, the dominant factor is different with operating temperatures of graphite: below 600°C, the recombination factor I (association reaction-limited) is dominant; Peak II (association reaction-limited) dominates in the temperature region from 600°C to 1000°C; and that of Peak III (diffusion-limited) is dominant above 1000°C.

To obtain the solution of dynamics for recycling and inventory, it is important to compile the data on 1) fluence rate

and energy of particles such as T^0, T_2^0, T^+, etc., 2) operating temperature of graphite, 3) effect of re-deposited hydrocarbon film on graphite, and so on.

Until a coherent and reproducible picture of hydrogen transport in graphite at elevated temperatures energies from the laboratory studies, no accurate modelling of hydrogen recycling and tritium inventory can be made.

2.4 Co-deposition

Co-deposition romoval of hydrogen in laboratory experiments has recently been demonstrated by Hsu (SNL), Clausing (ORNL) and Langley (ORNL). In all cases removal of hydrogen is observed to be unsaturable, since the eroded carbon and hydrogen atoms are Co-deposited on surfaces that are not in contact with the plasma. Evidence of Co-deposition has been seen in a number of tokamaks that have graphite plasma-interactive components. Co-deposited layers with 10^{17}-10^{18} D/cm^2 are observed on the walls and limiters of both TFTR and JET. While the exact mechanism of Co-deposition is not understood, our understanding is sufficient to identify Co-deposition as a potentially important source of tritium retention in devices like TFTR and JET. Its impact on CIT and ETR can not be determined without a better definition of the operating scenarios.

3. MODELLING

Applying DIFFUSE code, based on the diffusion and trapping theory which describes the hydrogen behavior in metals well, to estimate the tritium inventory in the graphite in TFTR has met with only limited success. Therefore we have to think about two issues, that is (1) Adequacy of the model and (2) Selection of material parameters.

1. Adequacy of the model

Because of its porous nature, graphite has a very large inner surface area which show a quite different physical properties compared with that of the metal. In the metal, hydrogen behavior is generally well described by solution, diffusion and trapping with consideration of surface recombination. Because the mathematical analysis based on the one dimensional Fick's diffusion equation is well established, it seems reasonable to start with this model available as DIFFUSE code. However, the problem arises as to what way shall we introduce the porous nature of the graphite? We can not use a simple one dimensional equation when we have to take into account the morphology of the graphite. At present there are no adequate models. The present recycling model also lacks any co-deposition mechanism. Co-deposition can remove hydrogen and thus reduce recycling. The co-deposited layer also is potentially a main source of tritium inventory in a D-T device. The effects of metallic deposits and surface roughness must also be addressed.

2. Selection of Material Parameters

As described in the previous section, the available data for solution, diffusion, permeation, recombination and trapping are very poor and show large scattering. Because of the critical importance for the estimation of tritium inventory and recycling, data production is highly desired.

4. RECYCLING IN FUSION DEVICES

4.1 Supershots in TFTR

The present high ion temperatures achieved in TFTR have resulted from a number of factors, including conditioning of the graphite limiters. Supershots require approximately ten

conditioning discharges of low density helium or deuterium. Due to sputtering of the limiter these discharges become carbon dominated, with Z_{eff} equal to six. These conditioning discharges reduce the global recycling coefficient from 1.0 to 0.5 for a limited number of shots. A gas input of 100 torr liter will reload the graphite and degrade per formance. Dylla (PPPL) has concluded that the depletion of the hydrogen saturated layer by ion induced desorption during the conditioning shots is responsible for the reduced recycling. The 100 torr liter pumping reservoir is equivalent to the amount of hydrogen stored in a 10 nm saturated layer over the 20 m^2 graphite bumper limiter. Ion induced desorption is a well-researched phenomenon. Recently Clausing and Langley (ORNL) have demonstrated outgassing of the saturated layer in a helium discharge, and Doyle (SNL) has recently shown that carbon ions have an even high ion induced cross section for release of hydrogen from a saturated layer than helium. Supershot conditioning therefore can be explained by the simple "bathtub" behavior of the saturated layer and does not need additional study.

4.2 Wall pumping in JET

Recently the interaction of plasmas with graphite limiters has led to a "wall pumping" phenomenon in JET and other tokamak devices. This is distinct from supershot conditioning in TFTR which requires plasma conditioning to achieve a limited pumping effect. In JET when the plasma is moved onto the inner graphite bumper limiter (which is at 350°C), a particle removal rate of up to 100 torr liter/sec has been observed. While the pumping effect may show some deterioration in a given discharge, the effect continues without evidence of saturation from discharge to discharge. (It should be noted that no similar wall pumping is

observed in TFTR, where the bumper limiter is 50°C.) The source of this large wall pumping is not well understood. It has been proposed that wall pumping might result from:

(1) Inward diffusion of hydrogen into the graphite.

(2) A transient pumping where the hydrogen super-saturation develops, and is released when the plasma is removed.

(3) Co-deposition of eroded carbon and hydrogen.

Understanding wall pumping is critical since it has such a strong effect on recycling, and it can potentially dominate tritium inventory if the pumped hydrogen is retained in the graphite or in a co-deposited layer. However, the database is insufficient to identify the mechanism responsible for wall pumping. Detailed particle balance accounting must be conducted in Tokamaks exhibiting wall pumping, and efforts must be made in the laboratory to simulate and model the phenomenon.

5. TRITIUM INVENTORY

Our current understanding of hydrogen-graphite interactions is too limited to make detailed theoretical calculations of tritium inventory in CIT or an ETR-device. Instead tritium inventory estimates are made using empirical observations from experience in operating Tokamaks and laboratory experiments. Study of graphite tiles and wall coupons removed from TFTR provide estimates of Co-deposition rates on surfaces and bulk uptake in graphite tiles. Measurements made on TFTR's moveable limiter tiles are relevant to CIT since temperatures well in excess of 2000°C were achieved during TFTR operation. Using these empirical observations from TFTR, coupled with surface areas and graphite volumes in CIT, a crude tritium inventory estimate can be made. It must be stressed that this estimate

does not include kinetic (i.e. time-dependent) effects nor does it allow for extrapolation to CIT operating scenarios that differ extensively from TFTR procedures. Tritium inventory and permeation estimates for graphite plasma-interactive components in a steady-state ETR device are beyond the scope of our present understanding of tritium-graphite interactions. Improvements in tritium inventory and permeation estimates can only come from increased knowledge of fundamental mechanisms plus extensive benchmarking of models and predictions with observations in operating devices such as JET and TFTR.

6. SUMMARY AND CONCLUSIONS

Four mechanisms dominate the retention and release behavior of hydrogen in graphite: (1) Saturated layer; (2) Diffusion on porosity; (3) Transgranular diffusion and molecular recombination; (4) Co-deposition. The lack of understanding of hydrogen transport in the graphite lattice at elevated temperature (i.e. mechanism (3)) severely hampers modelling of hydrogen recycling and tritium inventory in graphite. The models themselves need to be improved in the areas of graphite microstructure and in the co-deposition mechanism. While supershot conditioning in TFTR is well understood, wall pumping in JET remains a puzzling phenomenon. Tritium inventory estimates are forced to use empirical approaches because of the lack of reliable theoretical modelling.

The immediated needs in the area of recycling and inventory are:

(1) Data for hydrogen transport (diffusion, solubility, trapping, recombination) in graphite at elevated temperatures.

(2) Improved modelling, especially in the area of porosity effects and co-deposition of eroded carbon and hydrogen.

(3) Detailed particle accounting in devices exhibiting wall pumping.

Subgroup: 2.7 Modelling

T. Uchikawa, M. Shibui, R. McGrath, S. Gotoh, W. Ulickson,
K. Deetz, M. Seki, S. Sako, T. Kawamura

A better knowledge of the plasma edge is required for the design of CIT and future machines to be successful. These issues are plasma physics related and out of the scope of this workshop. This will require additional effort on the part of the plasma physics community.

Other issues such as modelling of sputtering, tritium retention, and runaway electrons are discussed in other sections.

Subgroup 2.8: Engineering and Design Aspects

T. Uchikawa, M.Shibui, R.Mcgrath, S. Gotoh, W. Ulrickson, K. Dietz, M. Seki, S. Sako, and T. Kawamura

Several critical issues have been identified for three groups of machines. They are near term machines (JET, JT-60, TFTR, D-III D, CIT), long pulse (Tore Supra, NET, FER), and ETR type devices having large neutron fluences. The first two categories have no significant radiation damage issues. The topics considered are heat fluxes, design aspects, cooling, fabrication, remote handling, and cost.

2.8.1 Heat Fluxes

a) Existing large Tokamaks

The power loads on in-vessel components such as inner wall, limiters, divertor plate are reasonably well known for normal operation conditions. They range from 0.2 MW/m^2 for walls up to 5 MW/m^2 for limiters or dump plates. These loads can comfortably be handled by inertia cooling for times below 10s.

This picture changes completely as soon as either abnormal operating conditions(runaways or disruptions) are concerned or components are subjected to loads for which they are not designed.

For disruptions it is agreed now that the thermal energy is lost within a short time (typical hundreds of μs) to the limiters, whereas the magnetically stored energy is dumped onto limiter and wall. The time scale is typically 2 - 20 ms for machines like TFTR or JET. It can be assumed that about 50% of the magnetic energy is dissipated in the limiter.

There are only a few detailed measurements during disruptions and the above assumptions are based on the scarce data available.

The knowledge on runaway behavior is even more sketchy. In JET for example runaways are mostly observed in conjunction with disruptions, but they generally do not present problems with the

graphite protection of the inner wall. As JET operates routinely at 5 MA (design value 4.8 MA) there are no major problems expected even when JET will be operated at 7 MA during 1987. To date it is not clear which role the runaways will play for the future machines.

In the existing Tokamaks graphite is the preferred material for wall armour and limiters. The operating experience so far has been good. Abnormal operating conditions could be handled without resulting in excessive damage.

b) Short term development

The next generation of machines will show the transition from inertia cooling (CIT) to active cooling (NET) and problems of radiation compatibility (insulators, expoxy resins, superconductors) will have to be solved. Disruptions will be the main hazard for in vessel components.

c) Long term

For machines like INTOR, ETR, FER there will be two main problems:

- radiation damage of material
- disruptions

The former will influence the heat loading limits of inner wall components, whereas the second will introduce the highest stresses and the highest erosion. Radiation is intrinsic to the fusion process and as such its consequences must be minimized by proper choice of materials and size of machine. It seems, however, necessary to develop means to control frequency of disruptions. In case that this cannot be achieved during the next 20 years, it is difficult to solve the engineering problems inherent to fusion.

2.8.2 Design Issues

After the heat load and its distribution are specified for a particular machine then the design of the limiter or first wall component can begin. The first calculation that is typically

done is a thermal response model. The calculation of the temperature of the component requires knowledge of the thermal properties of the material e.g. thermal conductivity (k), specific heat (C_p), and density. These properties are known as a function of temperature for a large number of graphites and several carbon/carbon composites. Data on the change of properties due to radiation damage is known for several graphites but not for any c/c composites. The materials properties data base needs to be expanded before ETR design can proceed without unnecessarily restricting the range of material choices. The thermal calculation requires specification of the cooling method, see section 2.8.3.

Temperature limits for components are determined by the erosion rate of carbon and the transport of the eroded carbon in the plasma as well as stress considerations as discussed below. The transport of impurities in a plasma is very poorly understood at this time. There is also evidence that the transport is influenced by things like pellet injection and/or the confinement mode(H-mode). This makes for a large uncertainty in the allowed maximum temperature. This is not a materials issue however since the solution rests in the plasma physics area. Better estimates of transport would allow for a smaller margin of safety in the engineering design.

The thermal calculations are followed by stress calculations. The required material properties are in general known, e.g. elastic modulus (E), Poisons Ratio (γ), and the thermal expansion coefficient (α). Again the radiation damage effects on these properties are much less well known. This information will be required for ETR. Since all of the machines are not steady state devices, thermal cycle fatigue must be considered in evaluating the allowable stress. Fatigue allowables (both flexural and tensile) are quite well known for structural graphites at room temperature. There is very little data for carbon/carbon composites. There is also very little data on the fatigue behavior of carbon or graphite materials at elevated temperatures. This is a serious need even in the short

term. Radiation damage effects on fatigue are largely unknown. This is a longer term need. Cyclic thermal fatigue data would be very useful because the stress distribution is unique in surface heated materials, i.e. there is no good mechanical analog.

Any of the low Z materials, including graphite, carbon/carbon composites, and beryllium are considered viable candidates for components. There are fairly strong plasma physics reservations concerning the use of high Z materials. The bonding technique chosen for long pulse machines will restrict the choice of materials compared to near term passively cooled components e.g. the use of pyrolytic graphite in Tore Supra. The choice of a bonding technique is critical for long pulse and ETR type machines.

2.8.3 Cooling of Plasma Interactive Components - Near Term Devices with Short Pulse Lengths (CIT)

In the near term for short pulse length operation, it is advantageous to keep the design of plasma interactive components as simple as possible. For a machine such as CIT, pulse length=3.6s, inertia and radiative cooling is probably sufficient for normal operation. Our major concern in this mode of operation is the surface temperature maximum of the plasma facing material. From this point of view graphite is well suited for this application. Surface temperatures in excess of 2000°C have been observed on TFTR graphite tiles with no significant increase in plasma contamination. Even for longer pulse lengths, inertia cooling is a viable option if it is supplemented with base plate cooling in between shots. This cooling method is in use in TFTR(water cooling) and JT-60 where nitrogen gas is used to cool the molybdenum divertor plates, and will be used on JET where water cooling of base plate mounting system cools large blocks of graphite or beryllium. Each of these machines has a pulse length of 2 - 10 seconds.

For cooling in between shots, the base plate holding the plasma facing material (assumed to be graphite in this discussion) has coolant lines brazed onto it or machined as an

integral part of the support structure. Sufficient thermal contact between the graphite tiles and the base plate for passive cooling can be achieved by bolting or clamping. Brazing is capable of providing better thermal contact but complicates the design and increases the cost. For short pulse length operation (CIT) design simplicity and low cost are to be emphasized.

There are a number of concerns associated with operation of the plasma interactive components in a machine such as CIT. Many of these are discussed in other sections of this report. Those specifically associated with cooling of the plasma contacting material are outgassing, sputter and chemical erosion and isotope exchange, all of which have strong dependence on the graphite temperature. Temperature of graphite surfaces contacting the plasma must be controlled with these items in mind. From an engineering point of view, reliability of the entire coolant system is important.

Near term-Long Pulse Operation

When pulse lengths extend beyond 10 seconds, active cooling of the plasma contacting surface during the pulse is required. Thermal gradients across graphite surfaces are large and good thermal contact with the coolant line is essential. For these applications, pyrolitic graphite has the advantage of excellent thermal conductivity in the a-b plane. Its use allows one to maximize the graphite armor thickness for a given surface temperature limit. This is highly desirable since it optimizes disruption protection. Good thermal contact implies that brazing or diffusion bonding of the graphite to the coolant line is required. The incorporation of brazes or bonds into the design generally produces additional design constraints, such as limits on braze temperature and increased thermal stresses.

All operational concerns listed in the table for short pulse operation are again concerns for long pulse lengths. Active cooling produces several serious additional problems. Thus attention must be paid to limits on peak heat fluxes for water or for gas coolants in order to avoid coolant line melting or braze

failure. Operationally this implies close monitoring of heat flux loads on PICs. Global monitoring of coolant temperature rise provides a measure of the integrated power loading. However, burn out generally ocurs in localized hot spots and monitoring of all activity cooled PIC surface is difficult. Additional concerns for water cooling are header effects such as flow stagnation, vibration of complex coolant assemblies and channel erosion at very high flow velocities. Gas coolants are an alternative to water but their high temperature and high pressure operation and cost are concerns.

ETR Type Devices

All of the issues discussed above are concerns for an ETR type device. The extended pulse length may actually reduce some earlier restrictions imposed by cyclic failures. The extended duty cycle and increased complexity in design make reliability an even more important issue. For fusion reactor operation, compatibility of the first wall and PIC coolant with that used in the tritium breeding blanket is a serious consideration. While this is not an absolute requirement for an ETR it is certainly desirable to begin to address this problem. Compatibility of blanket and PIC coolant stimulates interest in liquid metal coolants. One leading candidate is liquid lithium. The use of liquid metal coolants brings in a variety of MHD effects such as enhanced corrosion and large pressure drops.

A great deal of testing must be done to fully understand all of the complexities in PIC designs imposed by liquid metal cooling. If liquid metals are to be considered for PICs in an ETR design this testing must begin within the next few years.

2.8.4

(1) Know/Needs/Priority

KNOW	NEED	PRIORITY		
		short term	long pulse	ETR
*Design Criteria	1. QA/QC Criteria			
*Material properties	2. Allowable	3	2	5
*Analytical method	flow size	5	1	1
*Product examination	temperature	2	4	2
method	stress	4	5	4
*Possibility of damage	strain rate	1	3	3
tolerant design.	swelling			
	3. Pretreatment			
	baking			
	cleaning			
	packing			
	4. Finishing / Dimension			
	5. Properties			
	Thermal			
	Mechanical			
	˜Fatigue / creep			
	˙Radiation			
	(14 MeV Fusion)			

(2) Topics

(a) Inspection methods

The following inspection methods are available, but the first two seem to be promising.

X-CT....Relevant to detection of isolated flow/void.

UT .... Void density or cluster of flows.

MT ... Sensitivity problem

RT ... Sensitivity problem

(b) How should we assure products?

Three methods can be considered:

1. Assurance by analysis
2. Assurance by product inspection based on regulation or data base
3. Assurance by laboratory verification i.e. simulation

At least two items should be covered:

* failure against heat loadings
* neutron irradiation effects

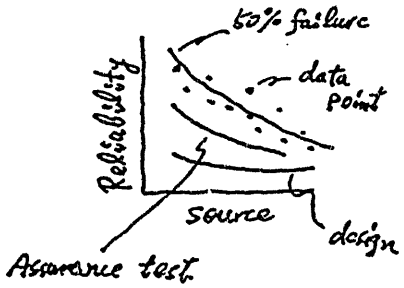

(c) Feasibility assessment

For long term machine, feasibility studies will be important.

Feasibility includes:

availability, fabricability, compatibility with machine, maintainability and ISI.

For long term machines, maintainability will be top priority for design components within damage tolerant regime. For next term availability and fabricability will be top.

2.8.5 Remote Handling

Remote installation of a component into the torus is required if the component is ever to be remotely maintained or repaired. This is because a remote handling machine will not have the same capability as a person for a long time. A remote alignment capability is necessary if the design heat loads are to be realized. This is due to the motion of the machine due to vacuum loads and thermal expansion at operating conditions. Any remote work will require a good inspection system. The remote handling requirements do not change significantly for machines beyond CIT because the radiation levels of even TFTR require remote maintenance after DT Q=1 experiments. Experience gained from TFTR and JET will be very valuable for CIT, ETR, NET and FER.

2.8.6 Costs

A few general remarks can be made concerning costs from an engineering standpoint. In general a complex material is more expensive than a simple one. Thus graphite is cheaper than carbon/carbon composites or beryllium or high Z materials which are cheaper than pyrolytic graphite. The complexity of the cooling method is also a strong cost driver, e.g. active cooling is more expensive than passive cooling. A mitigating factor for cost is that a highly reliable design may be initially more costly but cheaper in the long run. In general the costs are very design dependant.

2.9: Advanced Carbon Based Material

T. Hino Y. Sakamoto(RIKEN)

In the subgroup meeting, it is emphasized to establish the method to make carbon films with desirable properties:

(1) low hydrogen content for reduction of recycling, and

(2) hard and dense film for enhancement of the life time.

Since the plasma condition depends on the type of the plasma discharge, both glow and ECR discharge should be more carefully studied for the carbonization. We so far found that the ECR plasma can produce the carbon film with hard/dense structure and low hydrogen content. However, the relation between the film properties and the plasma condition has not been clearly obtained. So the further investigation is needed.

It has been demonstrated in TEXTOR that a-C:H films deported by glow discharge (RF-assisted) on the whole inner wall improve the plasma performance. Their isotopic ratio can be handled and they can be removed by glow discharge cleaning. Details can be found in review articles given at the 7th PSI as well as at the AVS conference (Baltimore). From the TEXTOR experiences temperature control of the walls to at least 350° should be highly descriable when applying the a-C:H films. The carbonization experiments performed in ECR-II(RIKEN) and Heliotron E(Kyoto University) are summarized in the following.

(1) Carbonization Experiments in ECR-II (Electron Cyclotron Resonance Plasma)

For carbon coating films produced by electron cyclotron resonance plasma in ECR-2 (RIKEN), the depth composition profiles were analyzed by Auger electron spectroscopy (AES). In the AES

analysis, the sputter-etching rate was two or more lower than that produced by a RF assisted glow discharge plasma in TEXTOR tokamak. This result indicates that a hard or dense carbon fil was produced by the ECR-plasma. The hydrogen concentration of the film was determined by thermal desorption spectroscopy (TDS The hydrogen content was approximately (20 - 30)%.

The carbon films produced by the ECR-plasma with different operation parameters were examined. As the increase of the gas pressure, the hydrogen concentration was increased. For the substrate negatively biased, impurities from the substrate were observed in the film. When the substrate was heated, no carbon film was formed.

(2) Carbonization Experiments in Heliotron E (Glow Discharge Plasma)

In Heliotron-E device, carbonization experiments were successfully performed by using a DC glow discharge with mixtur gas of hydrogen and methane. The properties of carbon films produced on surface probes of the surface analysis station were analyzed by Auger electron spectroscopy(AES). The film thickne was 40-50 nm, and almost no impurities were found in the film layer. The radial distribution of the film thickness was also analyzed. After the carbonization, the radiation loss of iron from the plasma of a main discharge was remarkably reduced.

From the depth profile analysis, it was found that D_2 or H discharge cleaning effectively removed the film. In addition, the formation of TiC in the film region was observed, after mai discharges with Ti-flashing in the carbonized chamber.

PLENARY SESSION

Opening Talk

M.M. Cohen

DEVELOPMENT AND TECHNOLOGY FY87 BUDGET DISTRIBUTION ($52.4M)

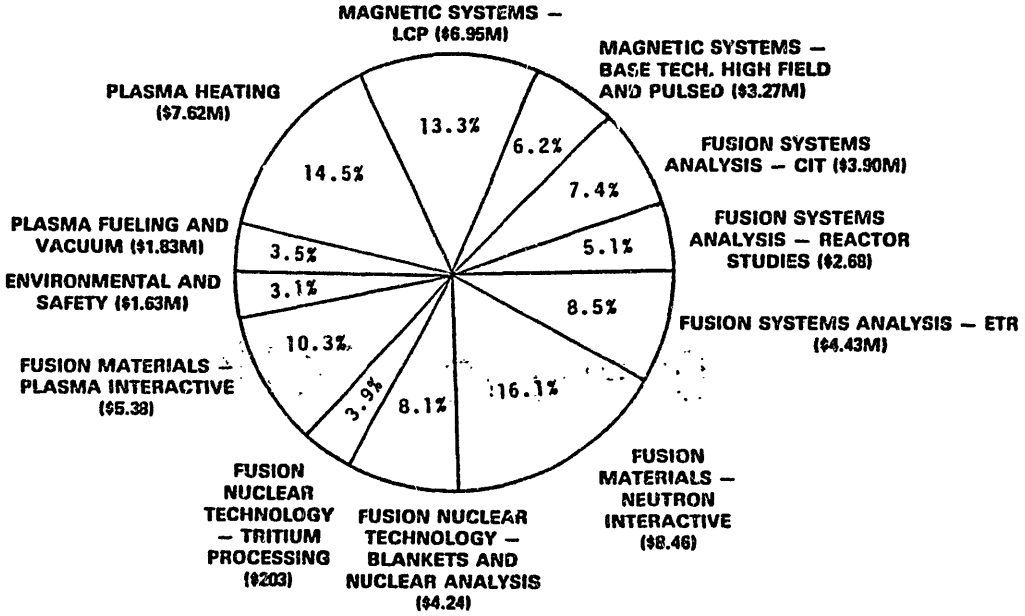

NEAR-AND INTERMEDIATE-TERM APPLICATIONS

LONG-TERM APPLICATIONS

THE
U.S. DOE
OFFICE OF FUSION ENERGY
DIVISION OF DEVELOPMENT & TECHNOLOGY
PROGRAM
IN

PLASMA/MATERIALS INTERACTIONS
AND
HIGH HEAT FLUX MATERIALS &
COMPONENTS

REACTOR TECHNOLOGIES BRANCH
PLASMA/MATERIALS INTERACTION, HIGH HEAT FLUX MATERIALS AND COMPONENT DEVELOPMENT TASK GROUPS

CHARTER

(A) PROVIDE TECHNICAL ASSESSMENTS OF THE STATE OF PMI/HHFMCD TECHNOLOGIES AND ADEQUACY OF THE DATA BASE AS RELATED TO FUSION POWER TECHNOLOGY GOALS AND SCHEDULED U.S. AND INTERNATIONAL FACILITIES.

(B) ASSESS TECHNICAL WORK, RELEVANCE AND ACCOMPLISHMENTS OF THE D&T PMI/HHFMCD PROGRAMS AND RECOMMEND CHANGES WHEN INDICATED.

(C) RECOMMEND DETAILED TECHNICAL OBJECTIVES, GOALS, MILESTONES, WORK TASKS, ESTIMATES OF MANPOWER AND FACILITIES REQUIREMENTS, AND ESTABLISH THE SUBGROUP STRUCTURE WITH WHICH TO ADDRESS THEM.

(D) COORDINATE THE REPORTING OF D&T FUNDED WORK WITHIN THE PMI/HHFMCD AREAS.

FUSION TECHNOLOGIES BRANCH
HIGH HEAT FLUX MATERIALS AND COMPONENT DEVELOPMENT AND PLASMA/MATERIALS AND INTERACTION TASK AREAS

OBJECTIVES

- TO INSURE THAT OFE TECHNOLOGY PROGRAMS, FACILITIES, AND INTERNATIONAL COLLABORATIVE EFFORTS HAVE THE REQUIRED MATERIALS, COMPONENTS, AND A TIMELY HIGH HEAT FLUX AND PLASMA/MATERIALS INTERACTION DATA BASE WHICH IS ADEQUATE FOR SUCCESSFUL DESIGN AND FABRICATION OF ALL IN-VESSEL COMPONENT NEEDS.

REACTOR TECHNOLOGIES BRANCH
HIGH HEAT FLUX MATERIALS & COMPONENT DEVELOPMENT TASK GROUP

MARVIN COHEN (DOE) – SPONSOR
MARK DAVIS (SNLA) – CHAIRMAN
BOB WATSON (SNLA) – SECRETARY
MOHAMMED ABDOU (UCLA)
MIKE ULRICKSON (PPPL)
JIM DOWNING (LANL)
SOL FIXLER (GRUMMAN)
JIM GORDON (TRW)
BRUCE LIPSCHULTZ (MIT)
RICH MATTAS (ANL)
PETER MIODUSZEWSKI (ORNL)
RALPH MOIR (LLNL)
LEIGH SEVIER (GA)
DAVE MORGAN (MDAC)

REACTOR TECHNOLOGIES BRANCH
PLASMA/MATERIALS INTERACTION TASK GROUP

M. M. COHEN – OFE COUNTERPART
W. BAUER (SNLL) – CHAIRMAN
K. WILSON (SNLL) – SECRETARY
R. CONN (UCLA)
S. ALLEN (LLNL)
K. BURRELL (GA)
S. COHEN (PPPL)
R. CONN (UCLA)
W. GAUSTER (SNLA)
P. MIODUSZEWSKI (ORNL)
B. LIPSCHULZ (MIT)
J. BROOKS (ANL)

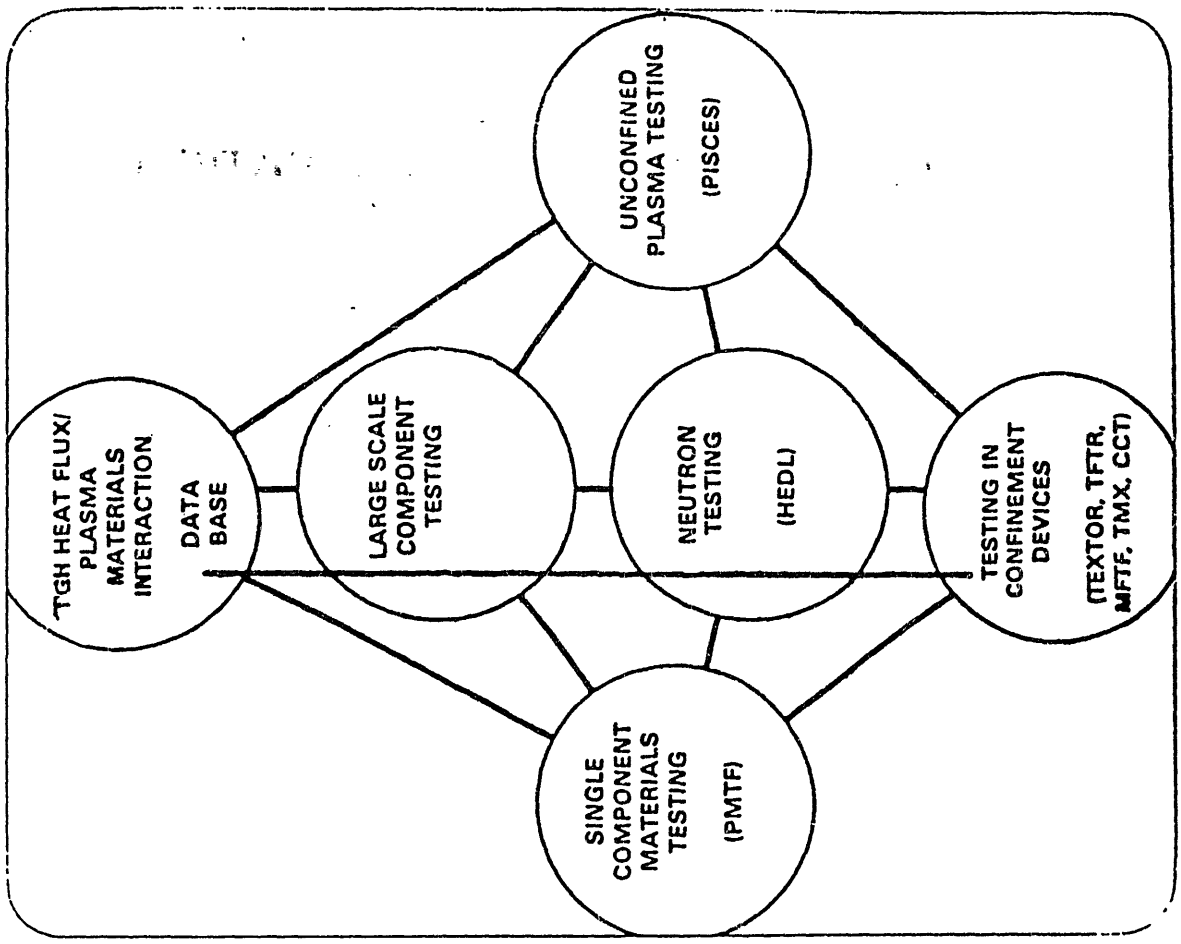

STRATEGY

- TO DEVELOP AND UTILIZE HIGH HEAT FLUX DIAGNOSTIC TOOLS AND SIMULATION TECHNIQUES.
- TO DEVELOP PLASMA COMPATIBLE MATERIALS, COATINGS, AND IN-VESSEL COMPONENTS WHICH ARE CAPABLE OF WITHSTANDING THE HIGH HEAT LOAD, PARTICLE, AND NEUTRONIC ENVIRONMENTS EXPECTED IN A FUSION REACTOR.
- TO DEVELOP MATERIALS AND COATINGS FOR IMPURITY, EROSION, AND DISRUPTION CONTROL, SURFACE CONDITIONING AND RECYCLING.
- TO DEVELOP PLASMA/EDGE DIAGNOSTIC TOOLS AND MODELS.

TO FUNCTION AS A SERVICE ORGANIZATION, UTILIZING THESE TOOLS, MODELS, MATERIALS AND COMPONENTS IN SUPPORT OF PRESENT AND FUTURE OFE PROGRAMS AND FACILITIES AND INTERNATIONAL NEEDS.

INTERNATIONAL COLLABORATION IS AN IMPORTANT ELEMENT NECESSARY FOR THE SUCCESS OF THE U.S. PLASMA/MATERIALS INTERACTION AND HIGH HEAT FLUX MATERIALS AND COMPONENT DEVELOPMENT PROGRAMS

- INTERNATIONAL COLLABORATION STRATEGY DOCUMENT

PMI/HHFMCD STRATEGY EVOLUTION

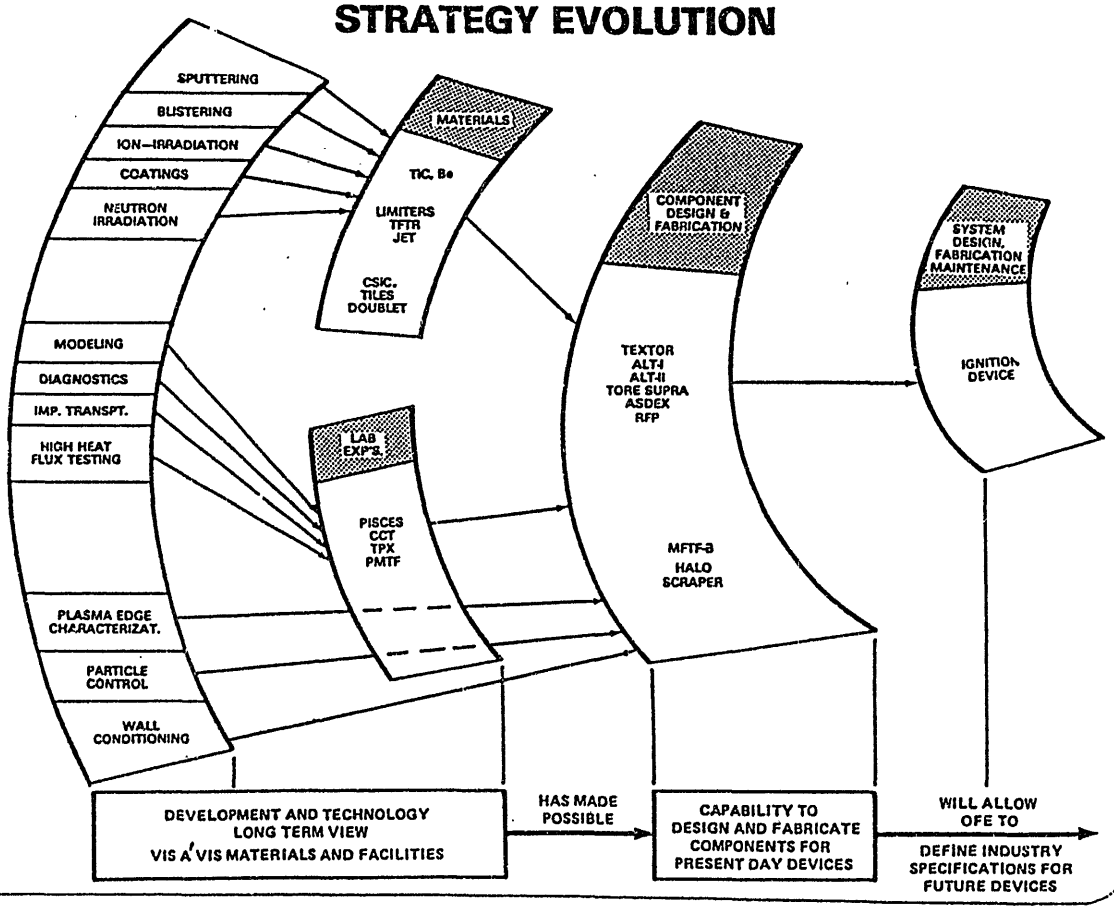

U.S.-INTERNATIONAL COOPERATIVE PMI/HHF ACTIVITIES

Program	Participants			Features/Objectives
ALT-I Pump Limiter in TEXTOR		U.S. Sandia & UCLA	Europe IP/KFA-Juelich	Module Pump Limiter with Several Head Designs and Several Materials (graphites, TIC, Inconel) Status: Final Year
Beryllium Limiter Experiment in ISX-B		U.S. ORNL & Sandia	Europe JET	Test use of Beryllium Limiters in a Tokamak and in PMTF Status: Completed
Pump Limiters/Fueling in TORE SUPRA		U.S. ORNL & Sandia	Europe F. aux Roses and Gadarche; C.E.A.	One Modular Pump Limiter with active cooling. Pellet Fueling. Status: Active; Design Phase
ALT-II Toroidal Belt Pump Limiter in TEXTOR	U.S. UCLA Sandia ORNL	Europe KFA-Juelich	Japan IPP-Nagoya	Complete Toroidal Belt Pump Limiter: Graphite Tiles and Radiative Cooling Status: Active; Construction
Divertor Materials Tests for ASDEX-UG		U.S. Sandia & UCLA	Europe MPI-Garching	Test materials (graphite) for ASDEX-UG Divertor Status: Active; Experiments in PMTF/PISCES/Diagnostic Facilities

Plasma Surface Interactions in Compact Ignition Devices

M. Ulrickson
Princeton University
Princeton, New Jersey USA

Abstract

Conditioning of the TFTR Bumper Limiter with Helium discharges has resulted in a substantial reduction of the recycling coefficient during deuterium operation. Values of $\tau_p^* = \tau_p/(1-R)$ as small as 150ms have been observed. Using absolute H_d measurements a recycling coefficient of o.5 is inferced.The effect is not well understood but may be due to ion induced desorption. Anticipated heat Loads in CIT are also presented.

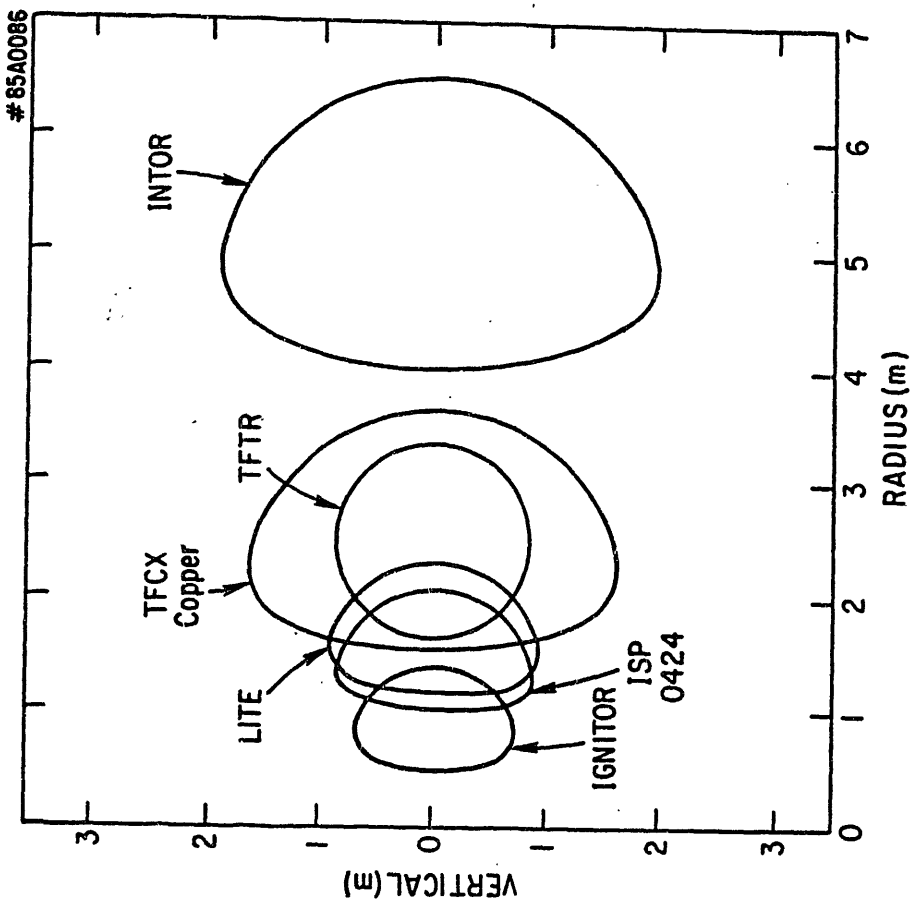

I. A brief description of CIT

II. Heat and particle loads to the limiter and divertor

III. Disruption effects

IV. Impurity generation and particle handling

V. Conclusions

Table I

TYPICAL PARAMETERS OF THE COMPACT IGNITION TORUS

Parameter	Units	Limiter	Divertor
Major radius	m	1.324	1.339
Minor radius	m	0.427	0.412
Elongation		2.00	2.45
Triangularity		0.41	0.58
Plasma current	MA	10.	9.
q (edge)		2.8	2.8
Field on axis	T	10.39	10.27
Beta limit	%	6.8	6.4
Density limit	$10^{20}/m^3$	6.6	6.4
Plasma temp.	keV	11.9	11.4
Fusion power	MW	300	300

Divertor Heat Loads

Charged particle power 36 MW

Radiated power in the divertor 12 MW

Effective area of the divertor plates

Inner plates = 2.6 m^2

Outer plates = 6.0 m^2

Limiter heat loads

Power to the limiter 42 MW

Limiter area is 6 m^2

Average limiter heat flux is 7.0 MW/m^2

A peaking factor of 1.4 is used for the limiter
Peak heat flux is then 9.5 MW/m^2

In/out asymmetries are 1:2 inner and 1:4 outer

An additional factor of 1.5 is taken for
misalignments and up/down asymmetries

The heat flux to the plates is then
inner plates = 8.0 MW/m^2
outer plates = 8.5 MW/m^2

Disruptions on Compact Devices

Stored energy
Thermal energy = 36 MJ
Magnetic energy = 42 MJ

Peak heat flux in 100 μsec thermal dump = 45 GW/m^2

Peak heat flux in 10 msec current decay = 470 MW/m^2

Total energy deposited 920 J/cm^2

DISRUPTIONS

D–III results showed about 50% of the stored energy lost in about 100 μsec

PDX found 20 to 30% of the magnetic energy dissipated in the plasma with a <200 μsec rate of rise

PDX found the disruption heat load peaked at the mid–plane on the inner bumper limiter

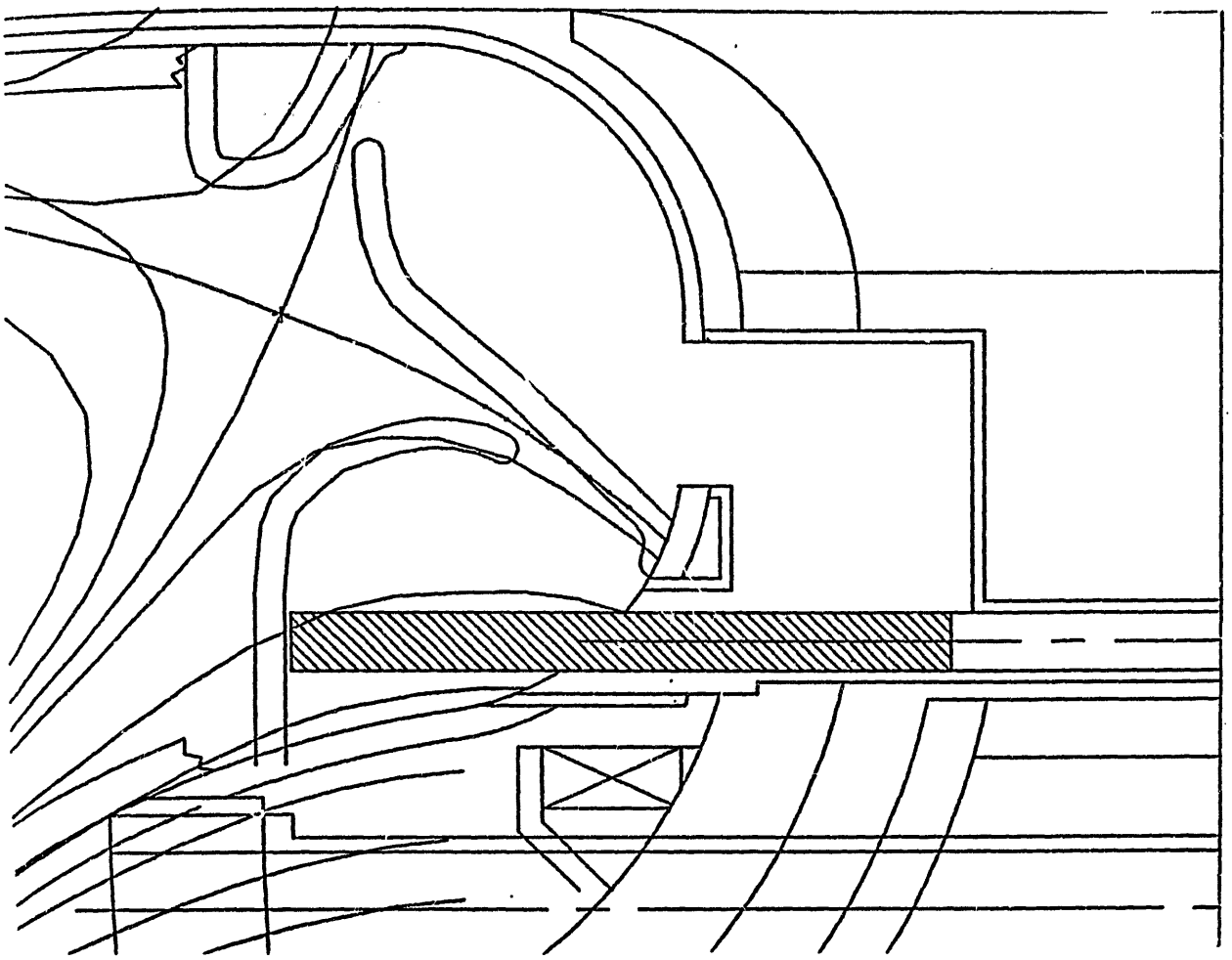

CONCLUSIONS

I. The high heat fluxes during normal operation leave a small margin for error in the scrape–off length, separatrix location, and plasma shape.

II. The impact of disruptions is very severe with large amounts of material being eroded.

III. There is a strong preference for graphite as the limiter/divertor plate material.

IV. The use of Zr/Al getter pumps in the divertor chamber should be considered.

Some Considerations on Plasma Facing Materials in Tokamak Fusion Devices

Yoshio Murakami

Japan Atomic Energy Research Institute,
Naka Fusion Research Establishment

Abstract

In order to assess the materials problems for the next step ignition and steady state fusion devices, the author discusses the critical issues of plasma facing materials, the comparison between low-Z materials and high-Z materials, and the future prospects of plasma facing materials development.

1. Introduction

Plasma-interactive components include first wall, limiter blades, divertor plates, protection armor, rf antenna, and so forth. The functional requirements and operating environment for these components are mainly determined by the plasma.

The major elements to be considered for the materials and processes are: (a) impurity release and surface modification, (b) hydrogen isotope recycling, retention and permeation, (c) high heat flux removal and thermomechanical response, and (d) the effects of run-away electrons and plasma disruptions.

The materials choice influences to a large extent the

- time consumed for wall conditioning,
- plasma confinement and heating characteristics,
- reproducibility of the plasma parameters, and
- wall integrity or lifetime of the components.

2. Critical Issues of Plasma Facing Materials

Concerning the impurity release and surface modification, a particular concern is the sputtering erosion caused by the energetic scrape-off plasma particles when they bombard the surface. We understand that the sputtered particles will enter the scrape-off plasma and possibly the main plasma, will be recycled and eventually will redeposit on other exposed surfaces. The redeposition process and the material integrity of the redeposited layer are considered important issues from the material view point.

Impurities in a fusion plasma not only decrease the fuel density but also increase radiation losses and degrade the confinement of the plasma. The radiation loss per atom from a given impurity element increases with its atomic number Z, namely almost in proportion to the third power of Z.

The need of low-Z materials for the plasma-interactive components will depend on how low the plasma edge temperature drops and how well the magnetic divertor works. At low edge temperatures, high-Z metals are feasible because sputtering is a minor concern and they have good thermomechanical properties. At medium edge temperatures, sputtering is a major concern and the only suitable candidate materials are those with low-Z. However, the erosion rate of low-Z materials is, in general, higher than that of high-Z materials.

Here, we reaches an important question: <u>Will it be possible to use a high-Z material for the plasma-interactive components of fusion reactors?</u>

The phenomena of hydrogen isotopes recycling, retention and permeation are also associated with plasma-wall interaction. Recent experiments on large tokamaks show that trapping and subsequent re-emission of hydrogen isotopes particles dominate the density and profile of the plasma. In future fusion reactors, the extent of tritium retention in and permeation through plasma-interactive components is an important question in assessing the safety and tritium handling requirements.

Concerning the high heat flux problems, knowledge on the thermal fatigue behavior of the materials often seems to be critical to the successful prediction of the component lifetime. In many cases, the stresses generated at the surface and interfaces exceed the yield strength of the material. The key issues for these components are, thus, the structural integrity of various candidate materials including composite materials and complex structures fabricated by coating, cladding or bonding.

Recent experiments on large tokamaks have shown that plasma

disruptions and accompanying run-away electrons can produce localized melting, splashing and vaporization of the surface of plasma-interactive components, and can also produce cracking in the structures below the melt layers.

The plasma disruption is characterized by a rapid decrease in the plasma current accompanied by a large heat deposition in a very short time on a localized area of wall surface. For instance, Fig. 1 indicates a distribution of the current decay rate of major disruptions which has been obtained in the JT-60 experiments. The current decay time is shorter than 10 ms, and the current decay rate reaches 200 MA/s at the maximum. Uncertainties exist in the magnitude of the heat fluxes.

Figure 2 shows the inside of the JT-60 vacuum vessel after five months Joule-heating experiment and succeeding three months supplementary heating experiment. The total number of the tokamak discharges during this period was 1354 and about 16% of the discharges was counted to be disruptive. Some of the inward limiters were damaged by melting of molybdenum maybe due to disruptions, run-away electrons or arcing. The photograph indicates the most severely damaged limiter which has been located at the mid-plane of the vacuum vessel. Surface melting was also occured on other components including the liner and divertor plate. From the visual inspection, it was found that all the damaged tiles were several milimeter protruded from the average level of the component. If we count the damaged tiles including those having very small damage at the edge, we can say that about 3% of the tiles have been damaged in total.

Here, another important question arises: Will it be possible to suppress the plasma disruptions in the future? The priority in the materials data needs will change markedly if the major disruptions could be suppressed completely.

In addition to these four elements, we also have to consider the effects of neutron irradiation. Neutron irradiation will generally degrade the performance of plasma-interactive components, and a thorough understanding of the effects of the irradiation on materials properties will be necessary for the successful prediction of the component lifetime. It seems that the effects of radiation damage on the mechanical and thermal properties of heat receiving materials, structural materials and their interfaces are of particular concern.

3. Low-Z Materials versus High-Z Materials

Historically, high-Z refractory metals such as tungsten and molybdenum were used for the limiter in early plasma confinement experiments. The initial experiments of graphite limiters were carried out in several tokamak devices such as TFR in France, JFT-2a in Japan and ISX-A in the US by replacing the traditional high-Z limiters. However, the results showed no clear differences between the low-Z and high-Z material limiters. The PLT experiment at PPPL first demonstrated the merit of graphite limiters in 1978. It showed a considerable reduction in radiation loss from the core plasma and a 50% increase in plasma temperature after the installation of graphite limiters instead of tungsten limiters (see Fig. 3).

The first carbon wall experiment was planned and carried out at JAERI by using JFT-2a in 1979. Carbon coating was applied on almost all the surface of the inner wall by methane discharge and magnetron sputtering. In this case, most radiation loss occured in the boundary plasma region, which resulted in the formation of a hotter peripheral plasma with cold boundary (see Fig. 4).

The development of low-Z coatings for JT-60 was initiated in 1980.

The development work included the selection of coating materials and coating methods, the evaluation of the integrity of the low-Z coated tiles, and the development of mass-production methods of coating with quality control.

For the initial experiments of JT-60, molybdenum was chosen as the structural and heat sink material of limiter, armor plate and divertor plate because it was noticed that this metal shows the most excellent thermal properties under high heat flux conditions. Besides molybdenum, Inconel was used as the structural material of liner plate.

On the basis of performance tests of different coating materials and methods, TiC was chosen as the coating material and decided to use the plasma-assisted CVD method for molybdenum substrate and the activated reactive evaporation method for Inconel substrate. The thickness of the coatings is about 0.02 mm.

Figure 5 shows the inside of the JT-60 vacuum vessel. The inner surface of the vessel is almost completely covered with the coated tiles, the number of which is nearly 10,000; about 7,500 pieces of TiC-coated molybdenum tiles and 2,500 pieces of TiC-coated Inconel tiles.

We measured the outgassing rate of these coated tiles at various temperatures, and found that the rate is comparable to that of uncoated molybdenum or Inconel tiles in a wide range of temperature (see Fig. 6). Two bakeout tests at temperatures up to 350 C were carried out after the installation of the tiles on site. The ultimate pressure obtained in the vacuum vessel was about 5×10^{-7} Pa.

The first plasma of April 8, 1985 was preceded by about 10 hrs of discharge cleaning. After brief studies were made on the effectiveness of the discharge cleaning, a discharge cleaning procedure keeping the vacuum vessel temperature at 200 C was established. After 30 hrs of the discharge cleaning a 1 MA tokamak discharge was obtained on May 24 of that year. Figure 7 shows the residual gas analyzer output during the 200 C and the succeeding room temperature discharge cleaning. We are very interested in the fact that the relative output level of mass number of 18 is much lower than those observed in usual tokamak devices with metallic first walls.

Figure 8 shows the radiated powers from the main plasma and from the divertor plasma as a function of the plasma current for both divertor and limiter discharges. In the divertor discharges, the radiated power from the main plasma was kept at 20-30% of the ohmic input. The radiated power from the main plasma was reduced from about 50% to about 25% by changing the operation mode from limiter discharge to divertor discharge. It was also found that the 'Z-effective' is between 1 and 2 in the divertor discharges when the electron density exceeds $3 \times 10^{19} m^{-3}$ (see Fig. 9).

As mentioned before, the need of low-Z materials for the plasma-interactive components of future fusion devices is an important question when the device is operated with magnetic divertor while it is essential when the device is operated with pump limiter.

If the plasma temperature near the divertor plate can be reduced to 20-30 eV, high-Z refractory metals are feasible because the incident ion energy is lower than the threshold energy for sputtering. From the sheath theory the edge temperature is determined by the ratio of the heat flux to the particle flux at the edge. One method for lowering the plasma edge temperature is the use of large impurity radiation losses from the plasma edge. Experimental and modelling studies indicate that the production of a very cool edge plasma by impurity radiation requires significant levels of impurities at the plasma edge. If these impurities were presented in the plasma center, they would cause significant energy losses, and are thus unacceptable. In addition, a significant portion of the plasma volume

would be required for the radiation region.

A second way of producing a low temperature plasma is to increase the particle flux by increasing the local recycling rate near the divertor plate or pump limiter. Both modelling calculations and experiments on ASDEX, Doublet-III, and PDX indicate that this can be accomplished by the use of a suitably designed poloidal divertor. A cool, dense plasma can be produced near the divertor plate by intense localized recycling of the plasma and neutral gas. The low temperature of the diverted plasma minimizes the erosion, and the high density of the plasma provides a high neutral density which eases the helium pumping requirement. This type of recycling has not been demonstrated for limiter discharge.

Table 1 shows the sputtering threshold energy for various low-Z and high-Z materials. It is clear that the threshold energy of high-Z materials such as tungsten and molybdenum is much higher than that of low-Z materials.

Based on these findings, the current divertor designs for the near-term fusion devices such as NET, FER and INTOR envisage the use of tungsten or tungsten alloy for the divertor plates which will be brazed to a heat sink material.

4. Future Prospects of Plasma Facing Materials Development

It is very difficult to mention the future prospects of plasma facing materials development for long pulse or continuous operation.

In most current tokamaks, graphite tiles are used or planned to use for the limiter blades, divertor plates and protection armor against plasma disruptions. I understand that the main purpose of this workshop is to assess the applicability of graphite and similar carbon materials to these components. Although the commercial isotropic graphites have many good properties such as low atomic number and high melting point, they have some shortcomings such as high erosion rate and high outgassing rate under service condition.

The pulse duration of the present plasma confinement devices including JT-60 is around 10 sec at the longest. These devices do not always need active steady-state heat removal of the components. On the other hand, active cooling of the components is essential to the near-term fusion devices such as NET, FER and INTOR, in which long pulse or continuous operation is an absolutely necessary condition.

As stated in the previous section, the current divertor designs for the near-term fusion devices envisage the use of low sputtering yield tungsten or tungsten alloy for the divertor plates. However, if it is essential to use low-Z materials for the plasma facing surface of the components, the major technical issues will be to improve thermal and mechanical properties of low-Z ceramic materials including carbon materials and to develop ceramic-metal bondings which will meet the severe fusion conditions.

Table 2 lists the characteristics and properties which have to be established for selecting the optimum materials and estimating the component performance and endurance.

In considering these requirements, I think it is important to distinguish between short and long-term effects on plasma-interactive component materials in the course of development. For these reasons, the impurity and high heat flux problems require immediate attention, while erosion and redeposition, tritium retention and permeation, and the effects of fusion neutrons will remain secondary issues until long operating times and large neutron fluences can be realized.

References will be added later.

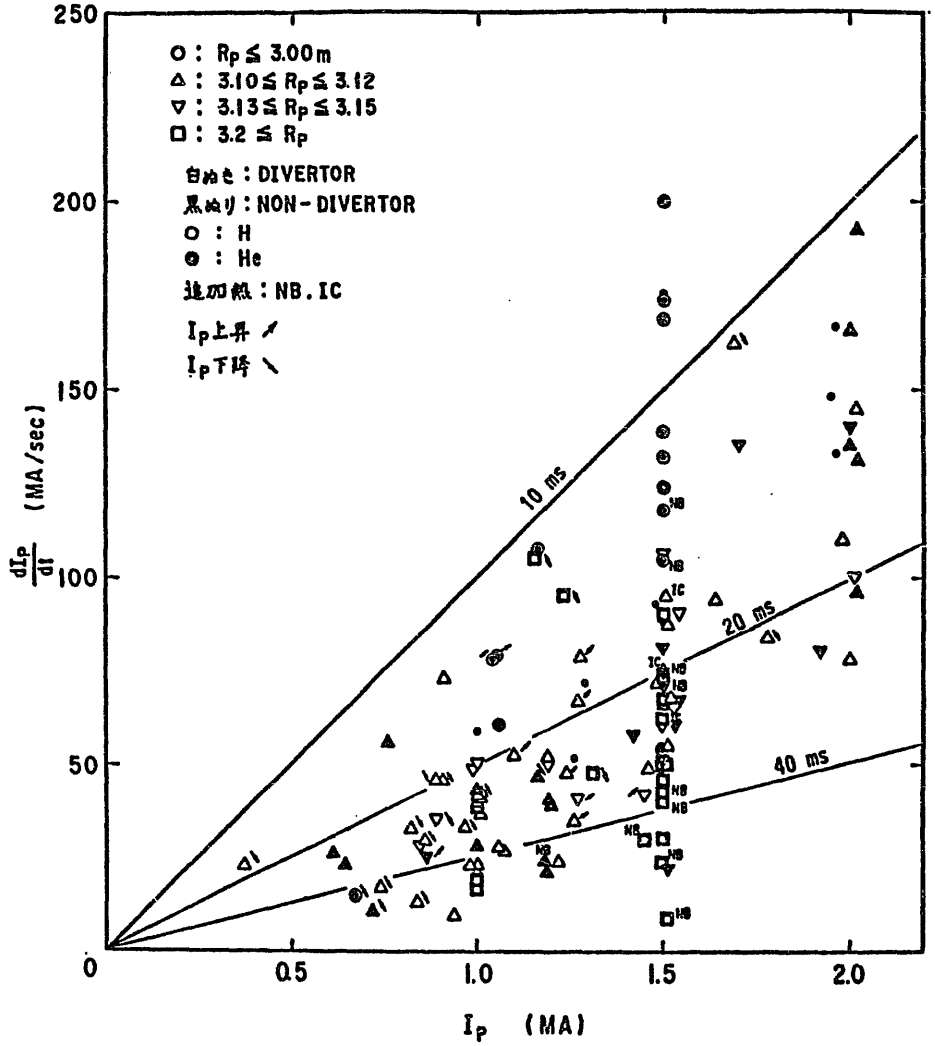

Fig. 1 Distribution of current decay rate of major disruptions which was obtained from the JT-60 experiment.

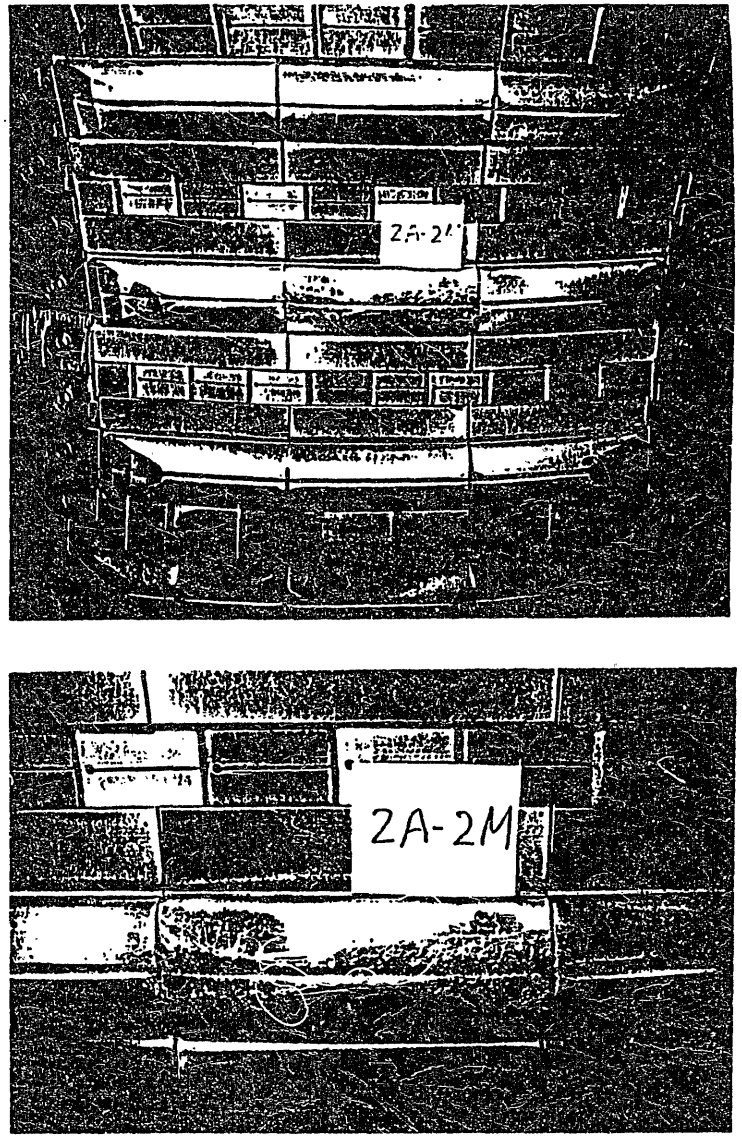

Fig. 2 Damaged limiters in the JT-60 vacuum vessel observed after five months Joule-heating experiment and succeeding three months supplementary heating experiment.

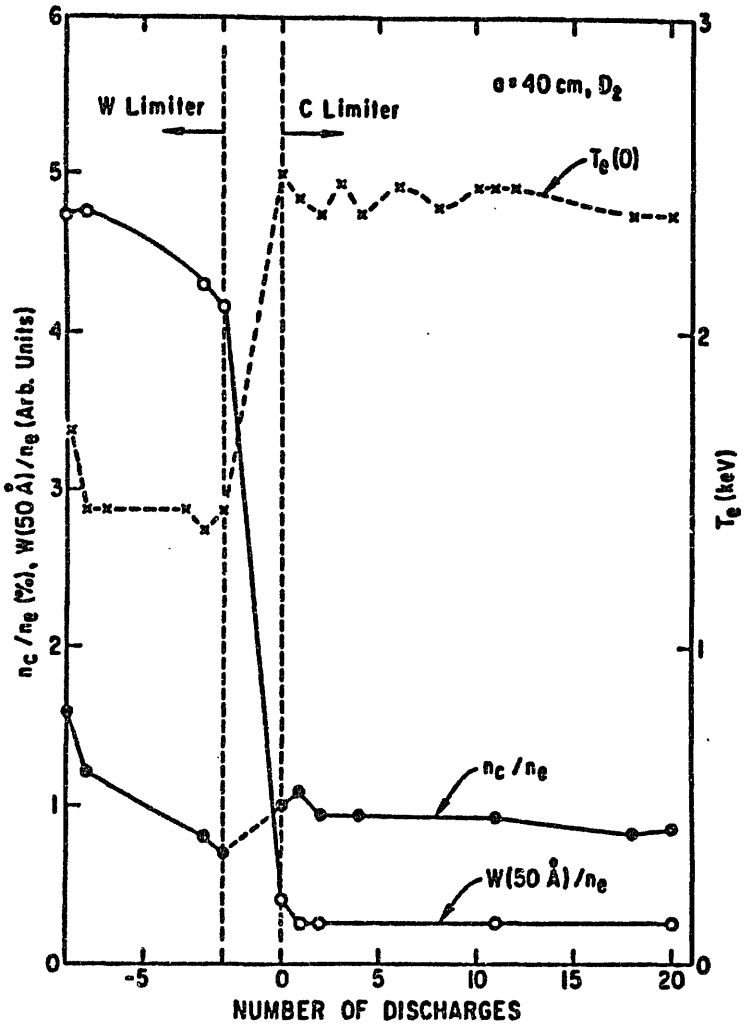

Fig. 3 *Changes in concentrations of tungsten and carbon when graphite limiter is substituted for tungsten limiter. Indicated tungsten level after change is spectroscopic background level.*

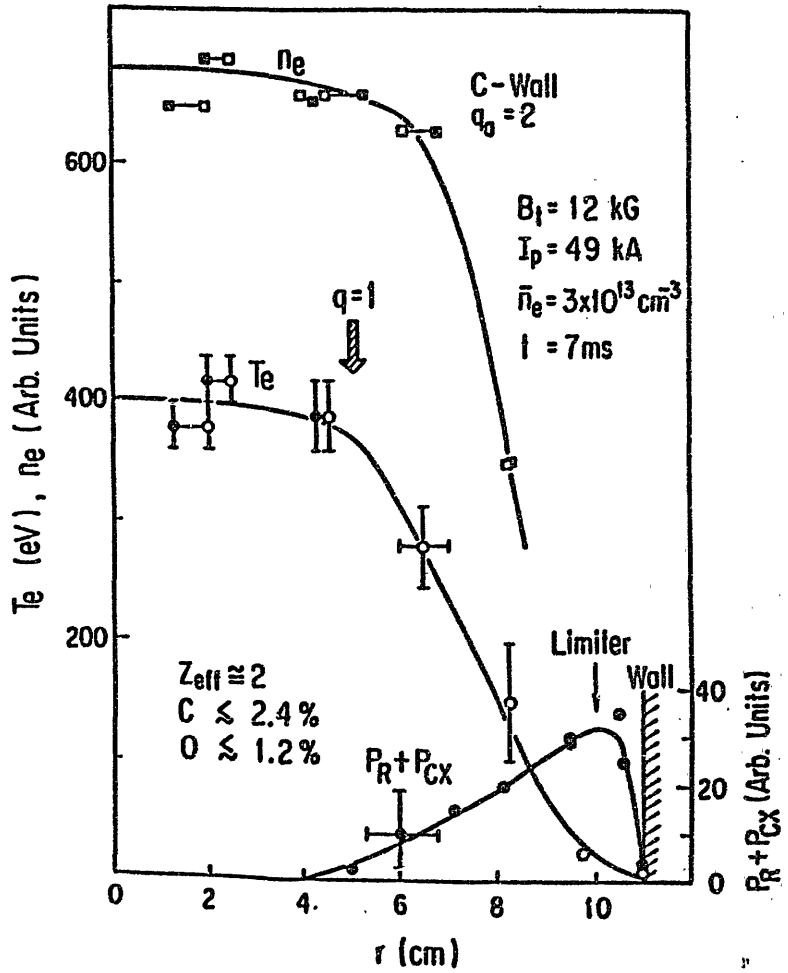

Fig. 4 Typical profiles of T_e, n_e and $P_R + P_{cx}$ in the case of low-q, C-wall experiments.

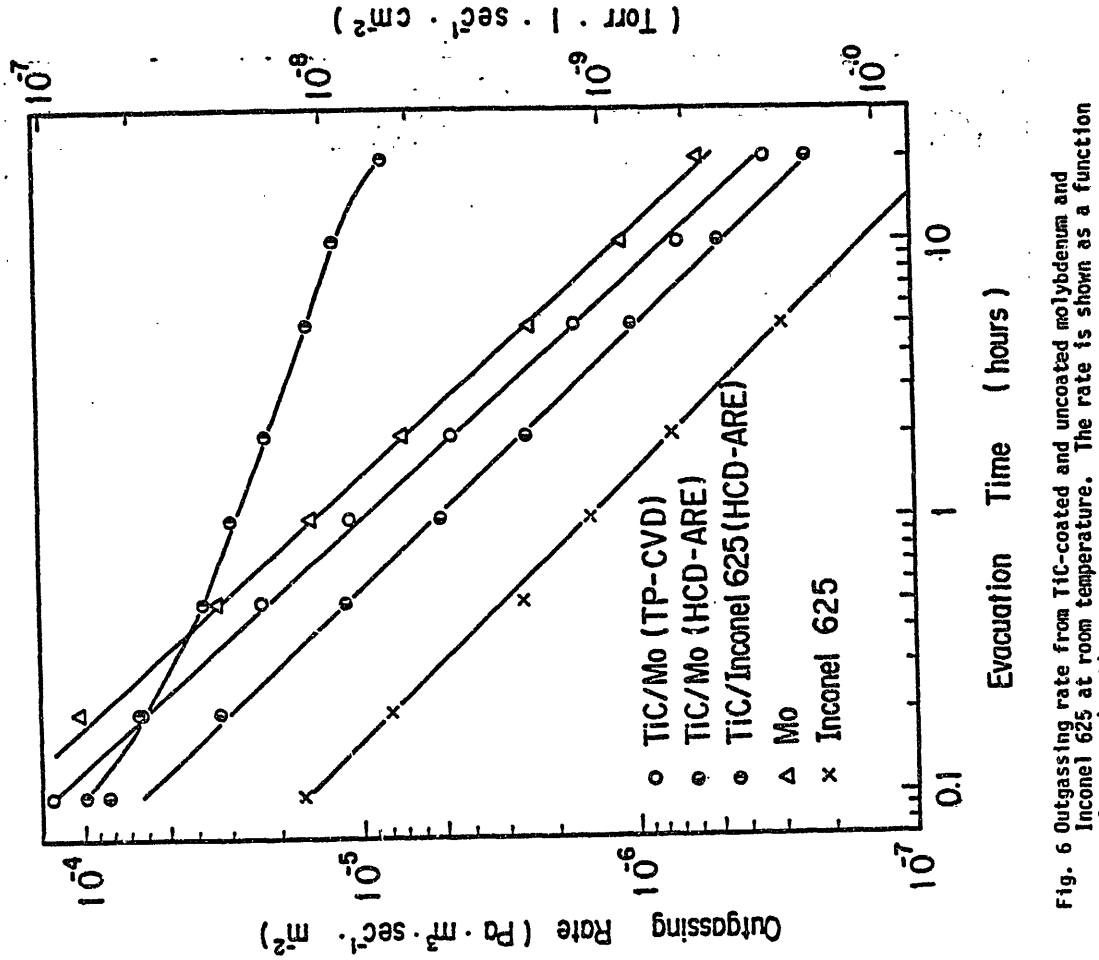

Fig. 6 Outgassing rate from TiC-coated and uncoated molybdenum and Inconel 625 at room temperature. The rate is shown as a function of evacuation time.

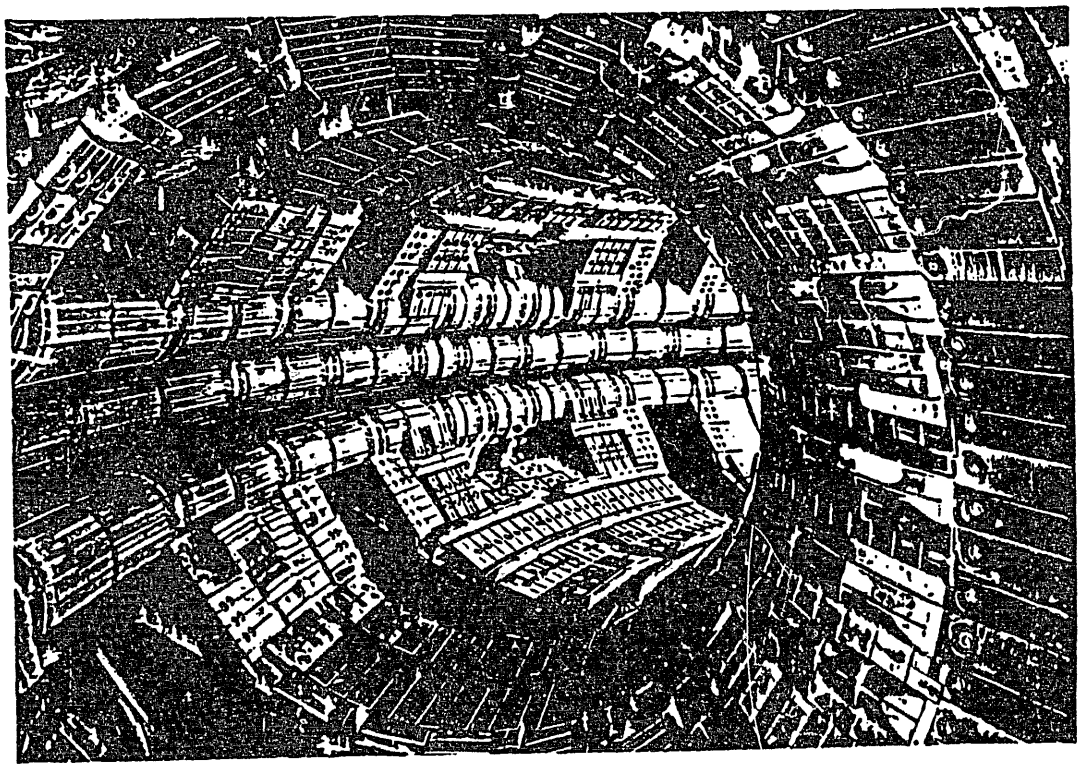

Fig. 5 Inside view of the JT-60 vacuum vessel.

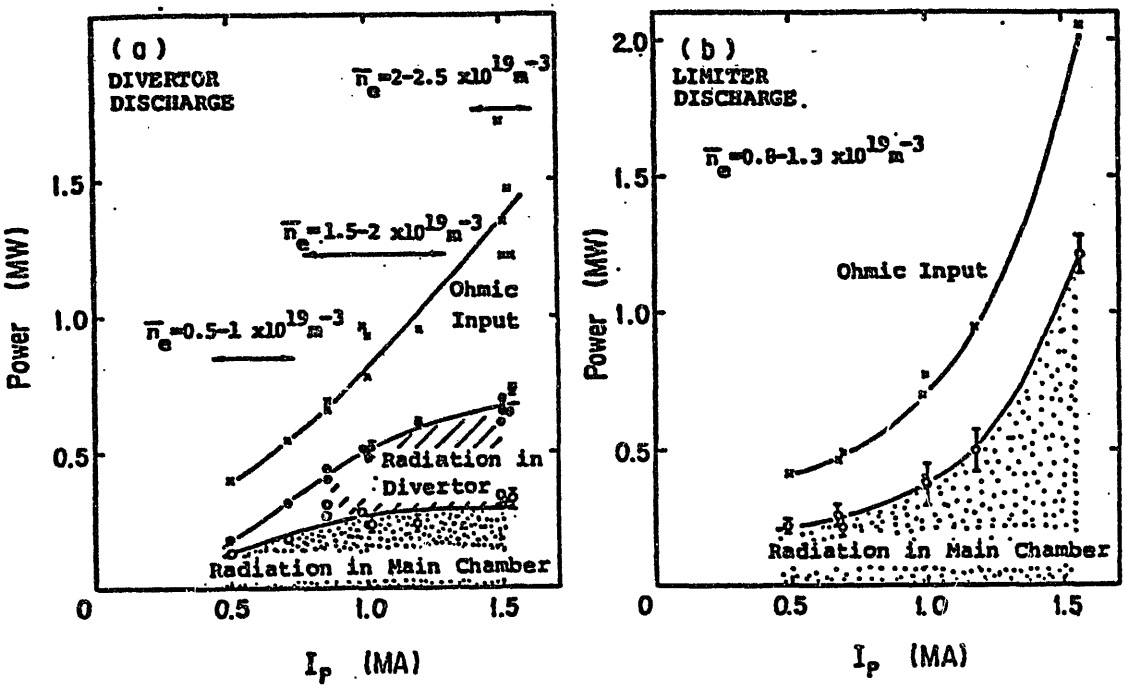

Fig. 8 Radiated power from main plasma compared to ohmic input power for (a) divertor and (b) limiter discharges. The radiated power from the main plasma is reduced by the divertor.

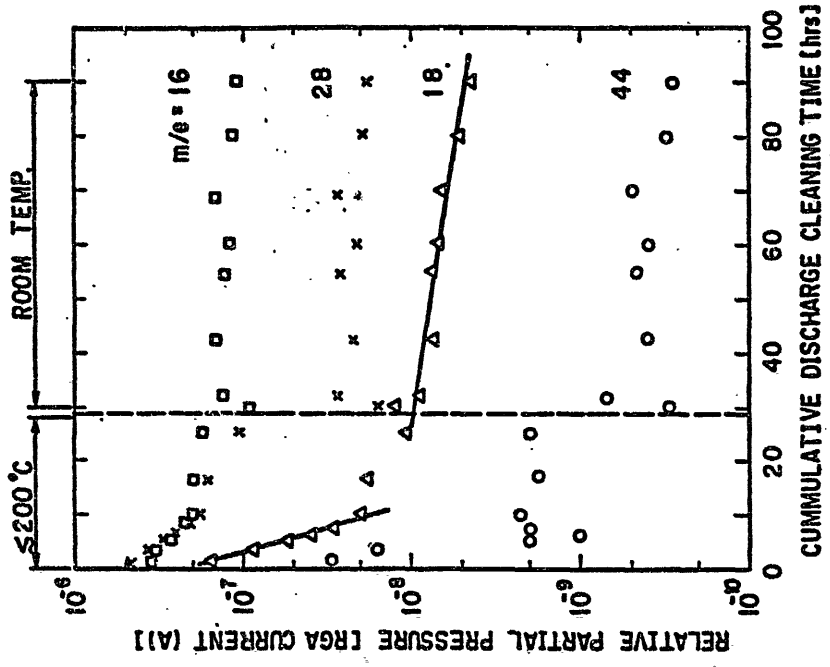

Fig. 7 Variation of RGA signal during discharge cleaning. A 30 hr high temperature discharge cleaning after the first plasma shot was followed by a room temperature discharge cleaning which was done alternately with several tokamak discharge phases.

Table 1 Sputtering threshold energy for different materials

TARGET \ ION	H	D	T	^{4}He	C	Self
Be	27,5	24	28*	33		
Graphite	9,9	10	13*	16	30	30
Ti	43,5	36*	28*	22	22*	41*
TiC	64	45	36*	30	30*	60*
Fe	64	40	37*	35	26*	35*
SS	64	40	37*	35	26*	35*
Mo	164	86	50*	39	30,6*	54*
W	400	175	140*	100	56*	70*

Unit is eV
* estimated value

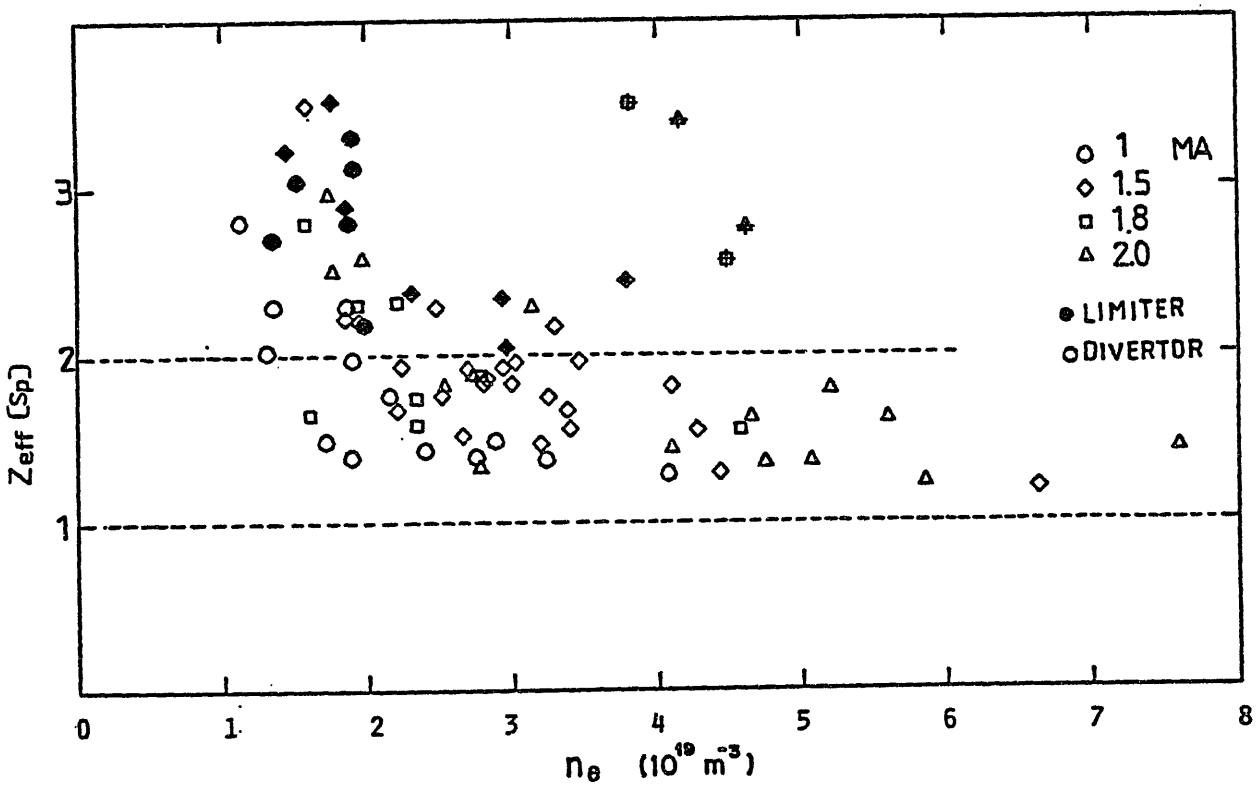

Fig. 9 Z_{eff} as a function of plasma density

Table 2 Characteristics and properties which must be established for selecting the optimum materials and estimating the component performance and endurance.

1. Fabrication
   a. Resources
   b. Industry existing
   c. Fabricability
   d. Joining (Brazing, Welding)
   e. Cost
   f. Control methods for base materials and joints

2. Physical Properties
   a. Specific heat
   b. Melting point
   c. Heat for melting
   d. Heat for vaporization
   e. Vapor pressure
   f. Thermal conductivity
   g. Thermal expansion coefficient
   h. Electrical resistivity
   i. Magnetic properties
   j. Phase transitions

3. Mechanical Properties
   a. Tensile
   b. Creep rate
   c. Creep-rupture life and ductility
   d. Low cycle fatigue
   e. Thermal fatigue
   f. Creep-fatigue interaction
   g. Fracture toughneees
   h. Fatigue crack growth
   i. Hydrogen isotope effects on the deformation, structure and properties
   j. Maximum allowable stress
   k. Thermal stress factor

4. Compatibility
   a. Coolant
      General corrosion
      Localized corrosion (stress, pitting and caustic)
      Impurity pick-up from the coolant and effects on the mechanical properties
   b. Hydrogen
      Solubility
      Diffusion
      Permeation

(continued)

5. Irradiation Effects
   a. Tensile properties
   b. Creep rate
   c. Creep rupture time
   d. Low cycle fatigue
   e. Thermal fatigue
   f. Creep-fatigue interaction
   g. Fracture toughness
   h. Fatigue crack growth
   i. Hydrogen isotope, diffusion, permeation and embrittlement
   j. Swelling and dimensional stability
   k. Helium embrittlement
   l. Coolant compatibility

6. Surface Effects
   a. Physical and chemical sputtering coefficient, effects of plasma impurities
   b. Recycling and properties of redeposited materials
   c. Plasma disruptions, run-away electron and arcing effects
   d. Surface conditioning and cleaning
   e. Hydrogen isotope recycling

7. Neutronics
   a. Neutron cross-section
   b. Activation and waste generation
   c. After heat
   d. Helium, hydrogen and solid transmutation products
   e. Displacement damage production
   f. Effect on tritium breeding

Experience with graphite in JET

K.J. Dietz

J E T

Abstract

A summary of in vessel components employing graphite as the materials facing the plasma is given.

This relate in particular to inner wall protection, belt limiter and separatrix dump plates.

The experience faired with graphite components shos on the one hand that graphite does not show damage as long as it is operated within the design limits and on the after hand exhibits high fluence against overloading conditions.

SUMMARY

- FINE GRAIN GRAPHITE
  (500W/cm^2 for 10s)
- CARBON FIBRE COMPOSITE
  (2 - 4kW/cm^2 for 10s)
- PYROLYTIC GRAPHITE
  (4kW/cm^2 for 10s)

- Heat transfer
- Hydrogen Retention - Release
- Maximum permitted surface temperature
- Cleaning - Outgassing

Z
3

83 661c

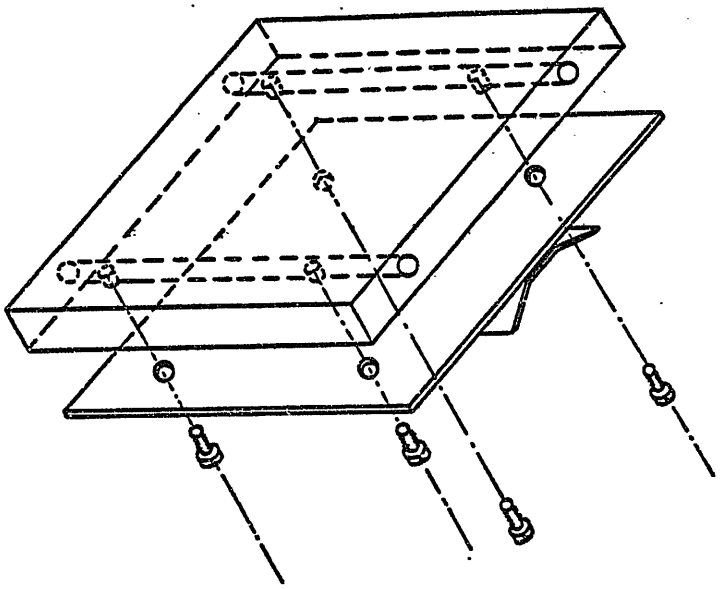

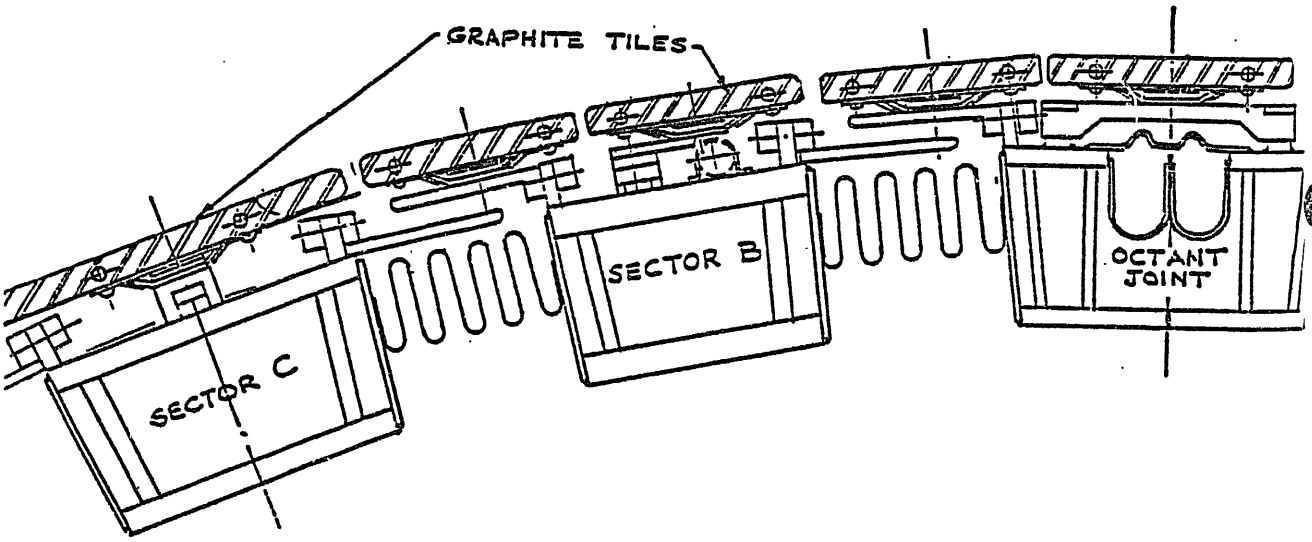
GRAPHITE TILES
SECTOR C
SECTOR B
OCTANT JOINT

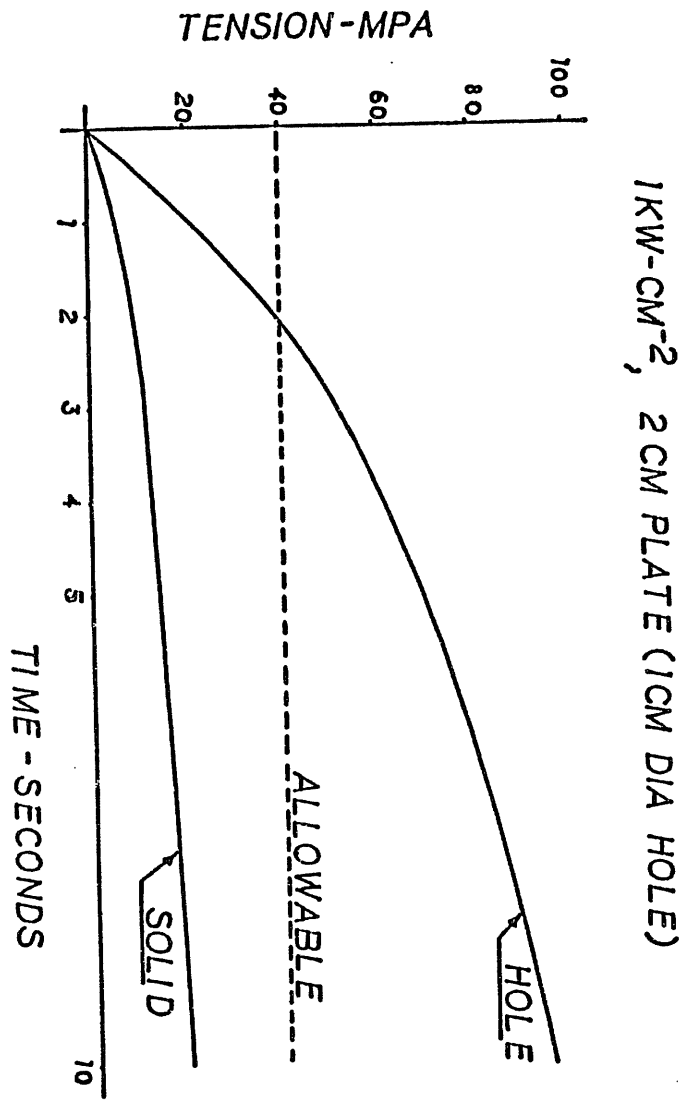

Graphite Protection

DESIGN PARAMETERS

- normal operation 30 W/cm² 10 s
- disruptions 30 kW/cm² 10 ms
- beam shine through 500 W/cm² 10 s
- unattenuated beam 2.0 kW/cm² 2 s

Tests:

1 kW/cm²	for 10 s	o.k.
1.5 kW/cm²	failed after 3 s	
10 kW/cm²	for 0.1 s	o.k.

Heat load and stresses (calculated)

2.5 kW/cm² safe for 0.2 s

supports increase stress by ~ 2.8

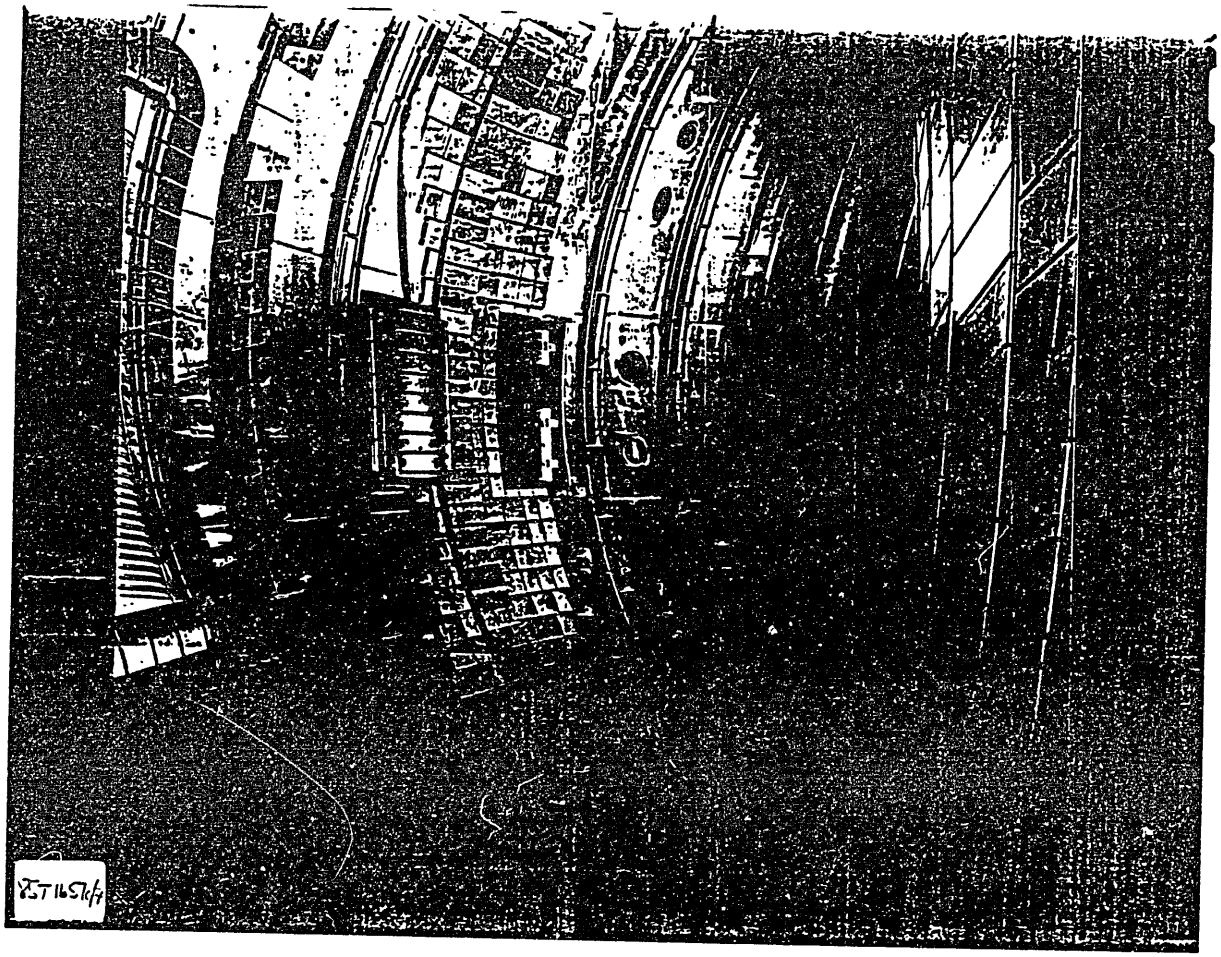
85 1651 f/1

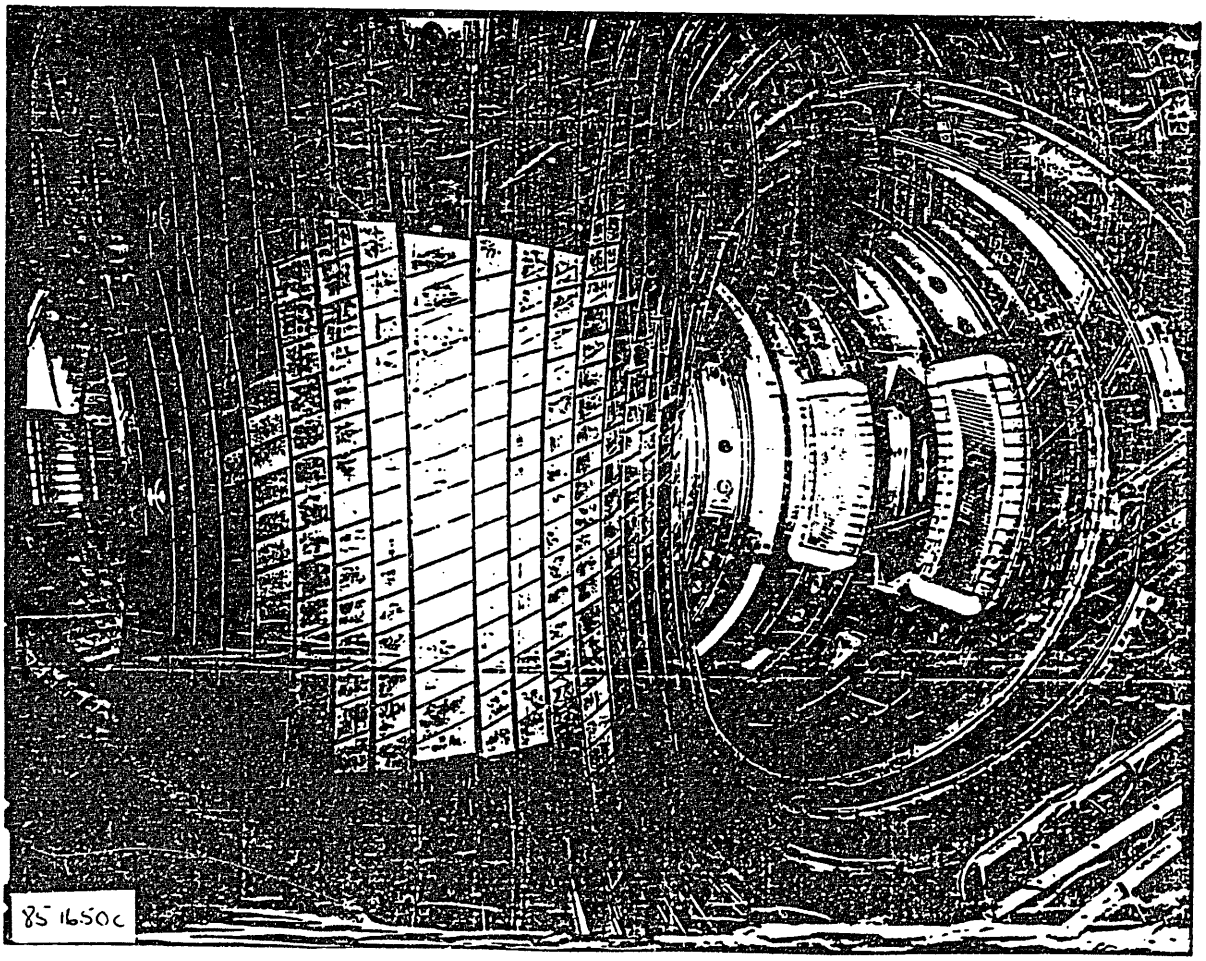
85 1650c

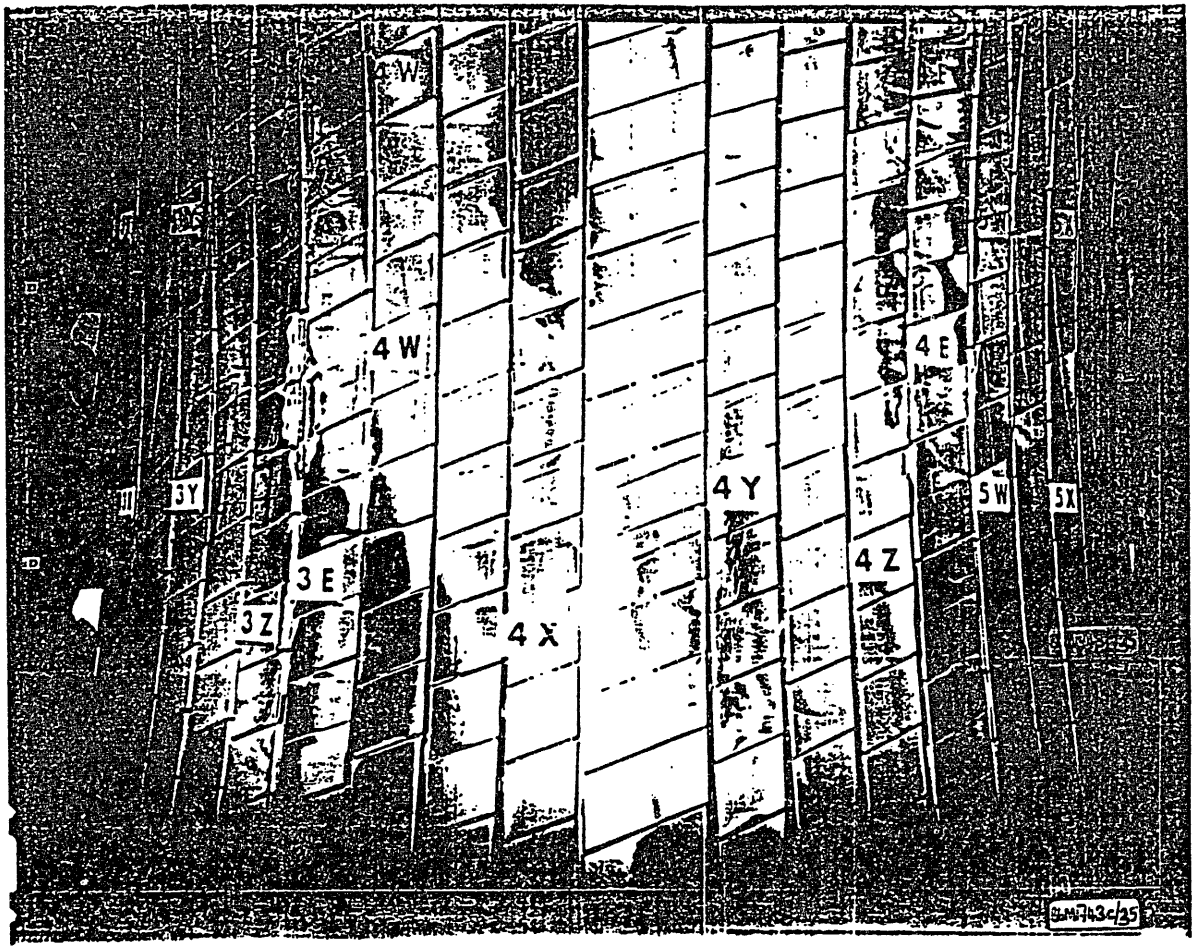
4W
4W
4E
3Y
4Y
5W
5X
3E
4Z
3Z
4X

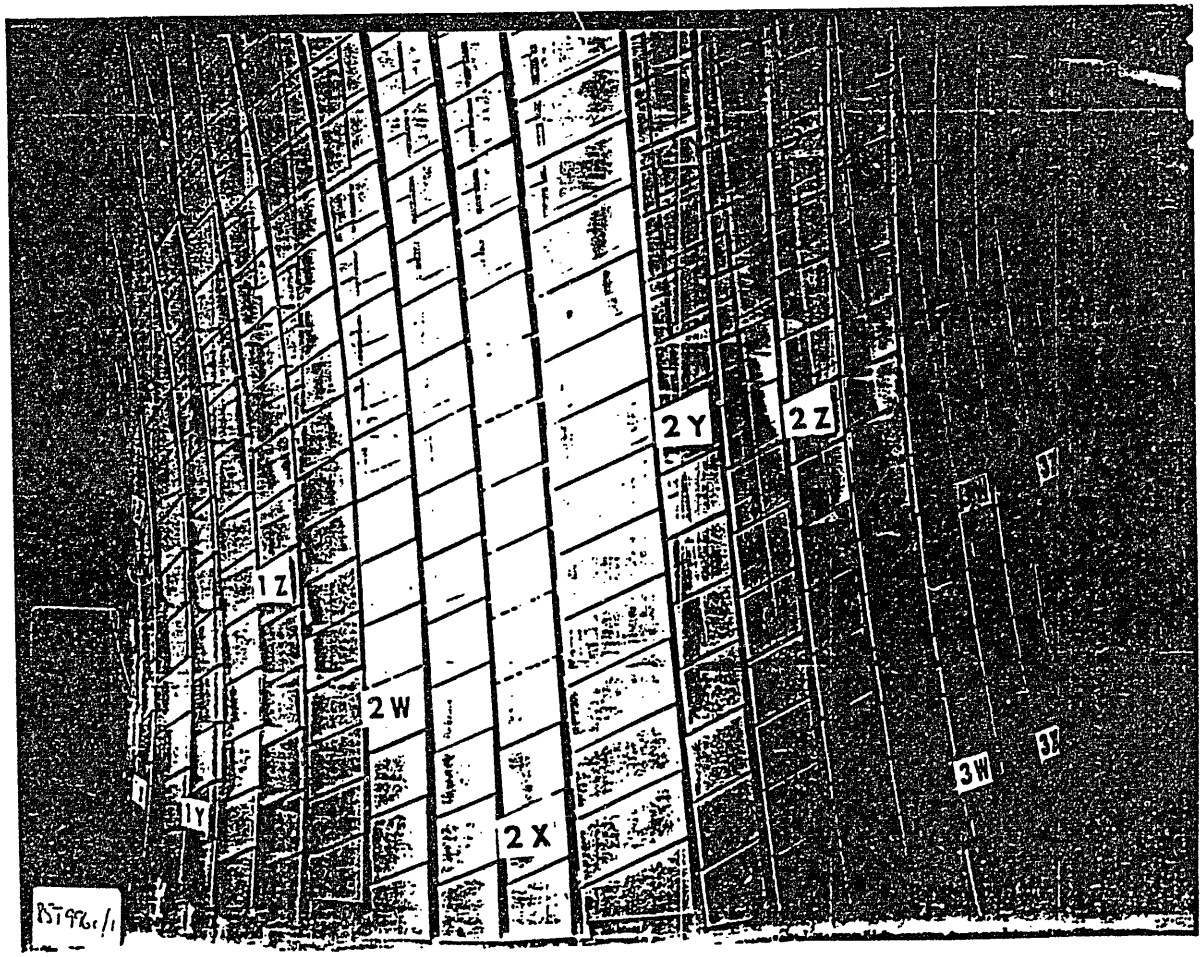
2Y
2Z
1Z
2W
1Y
2X
3W

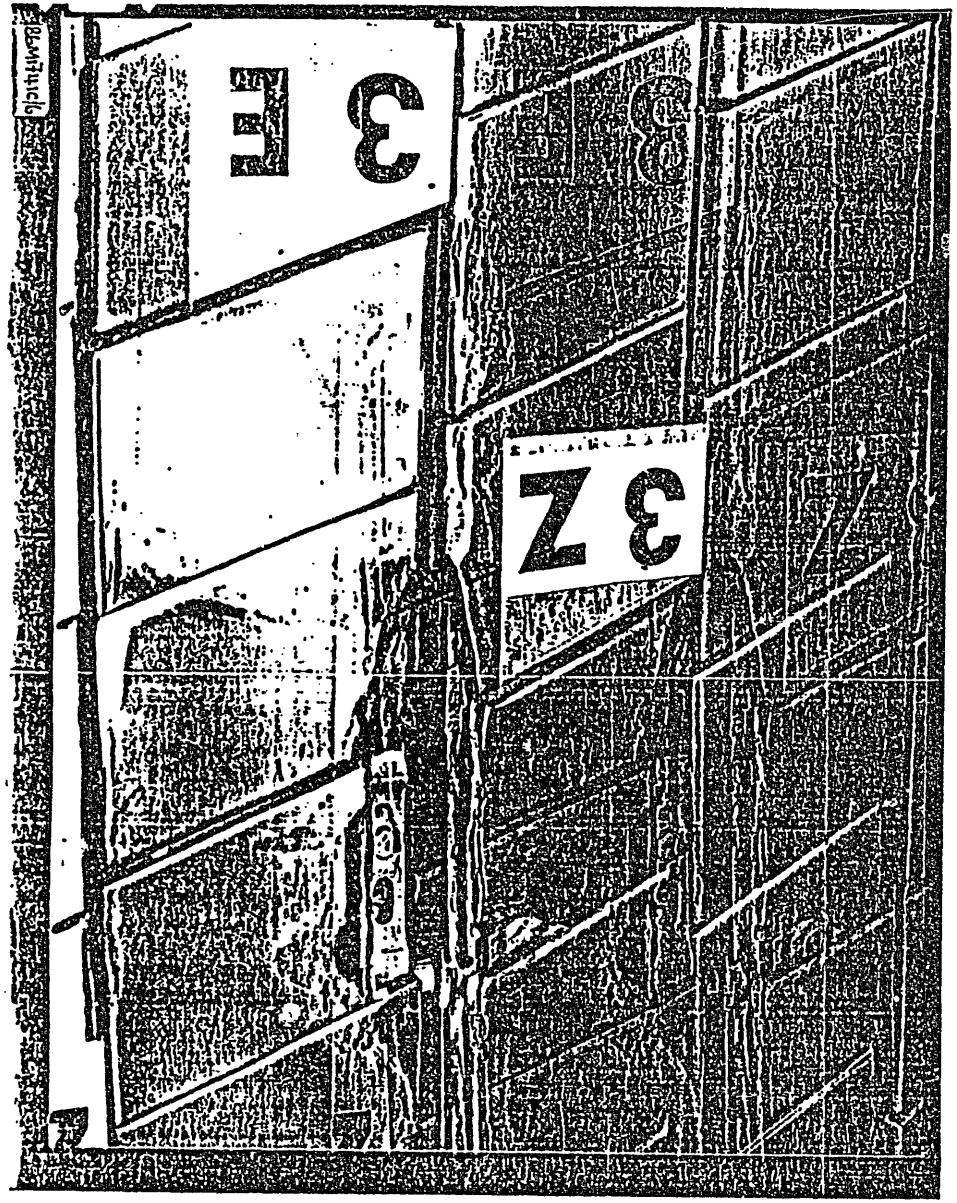

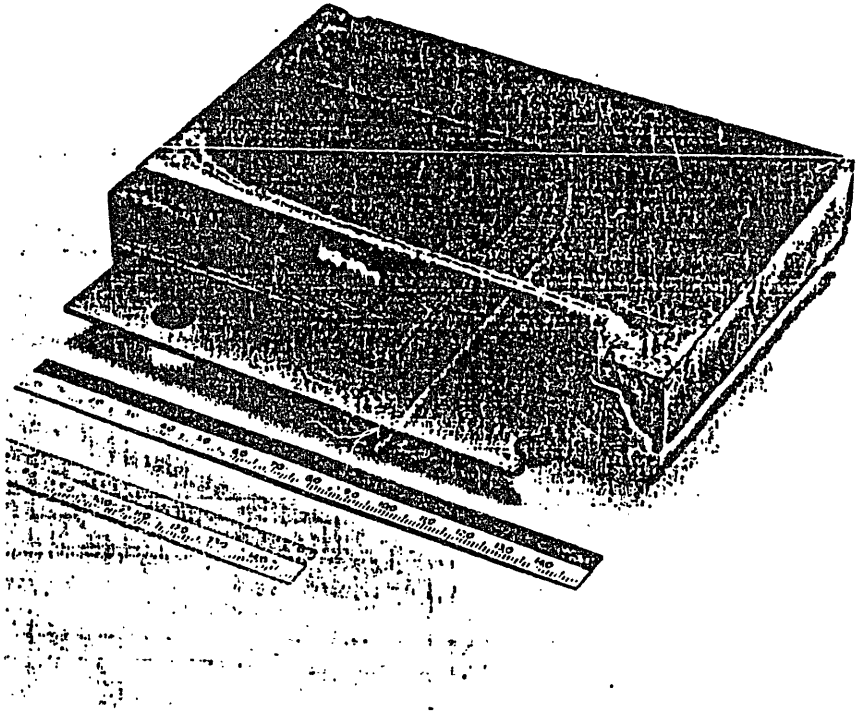

567380/2

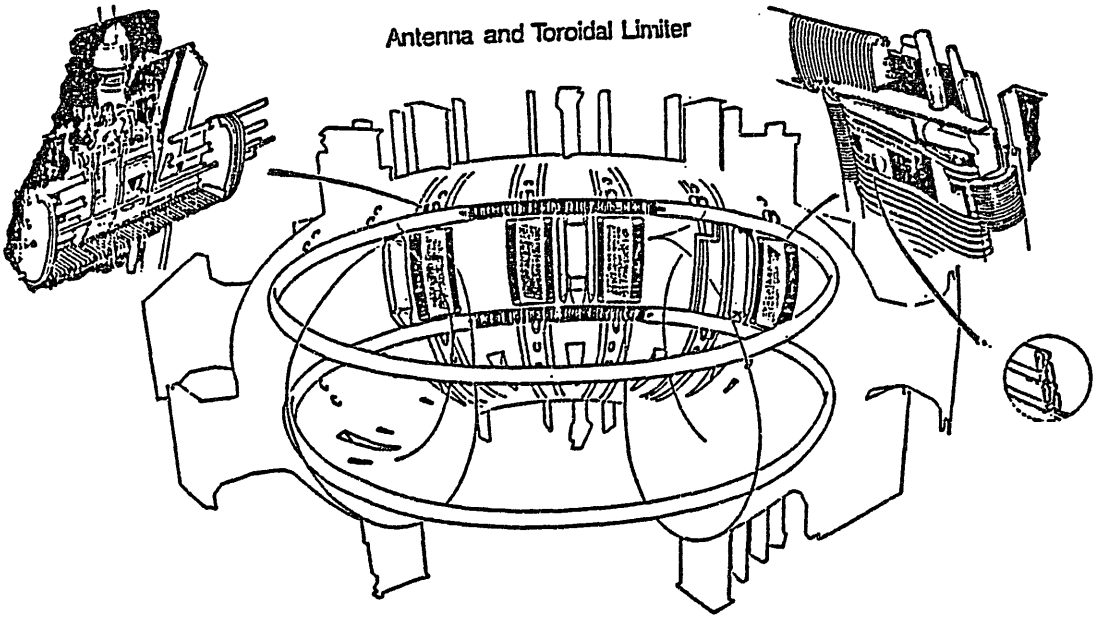
Antenna and Toroidal Limiter

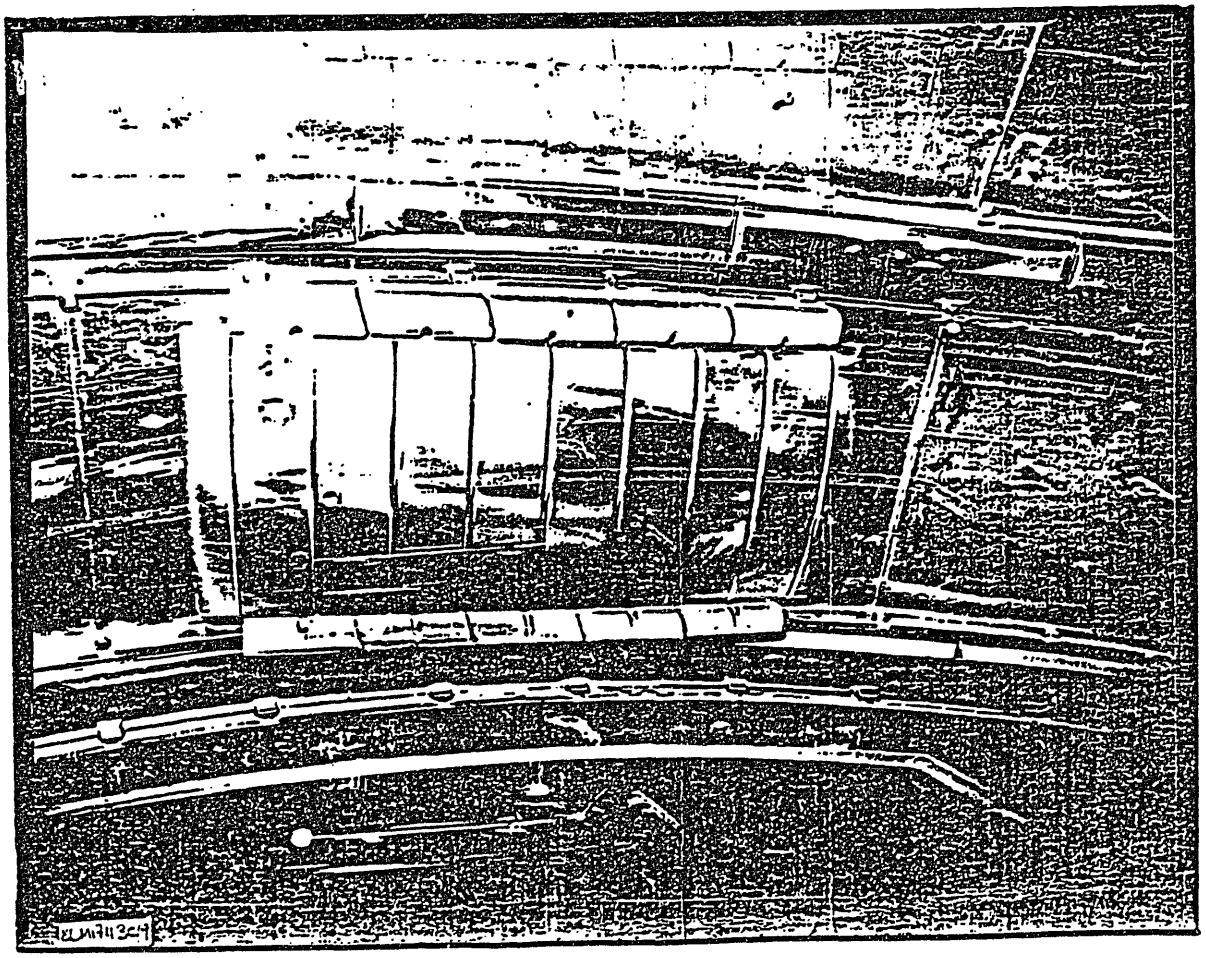

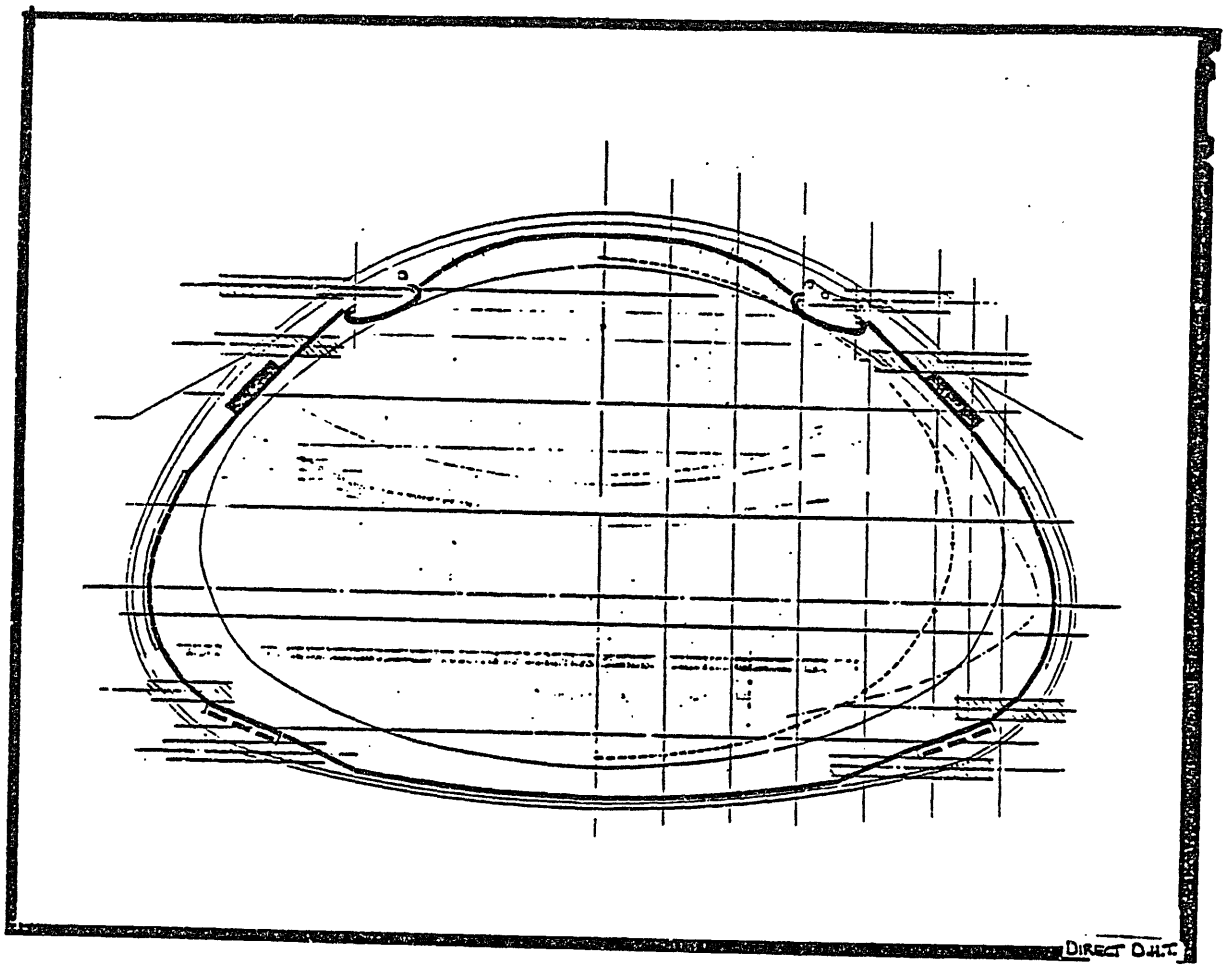

I: GRAPHITE COMPONENTS IN JET :

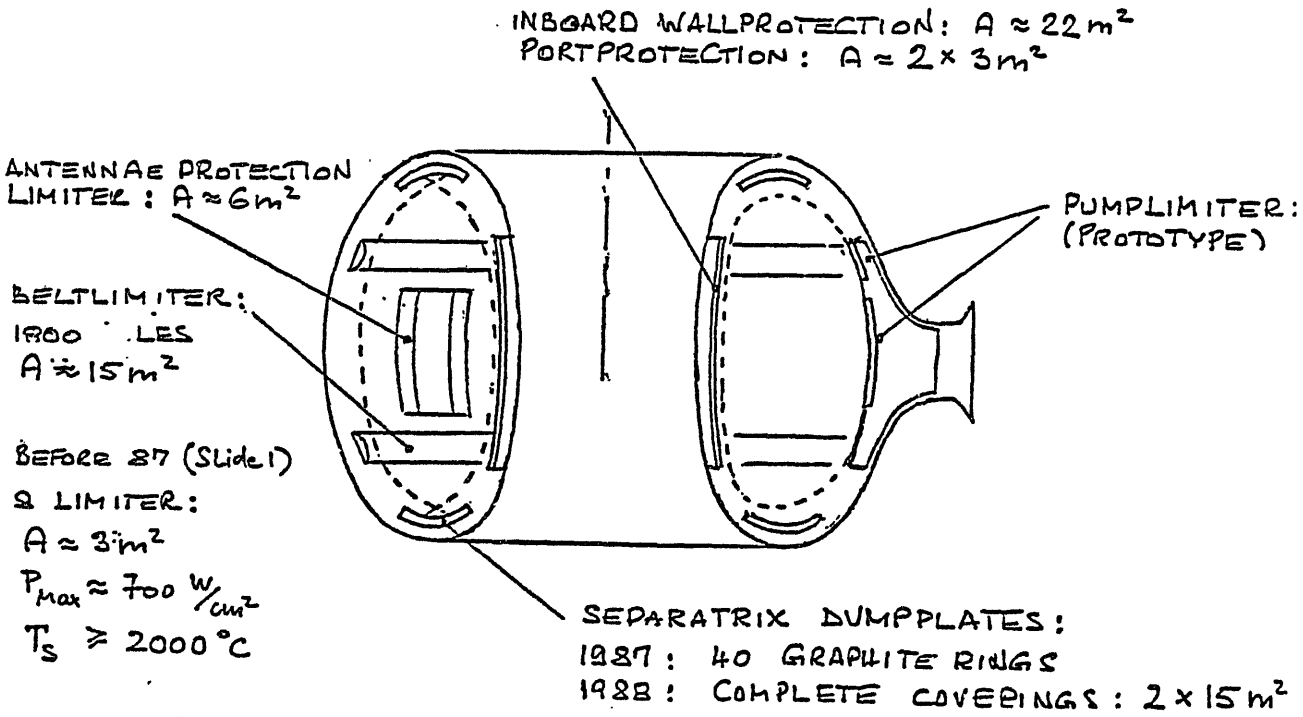

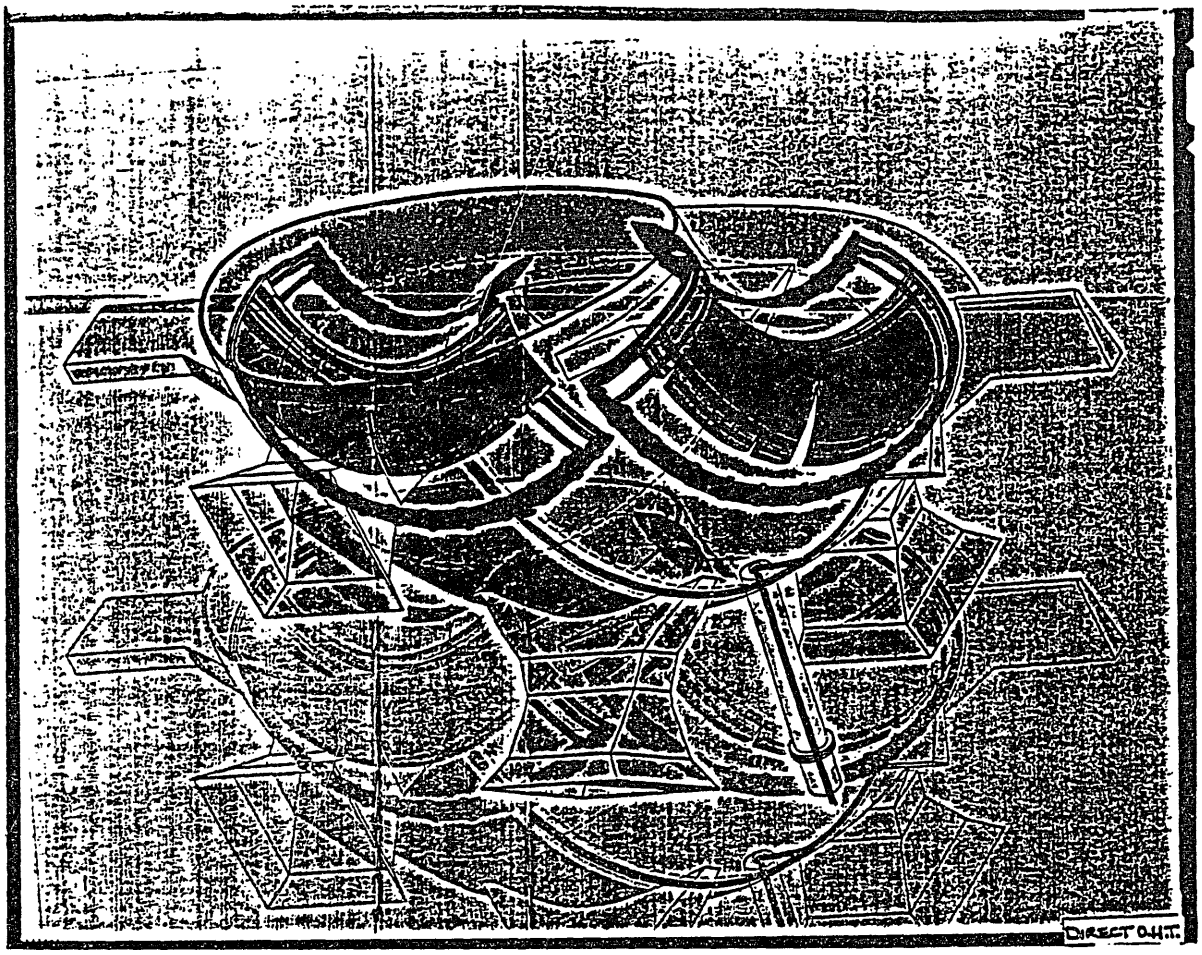
DIRECT O.H.T.

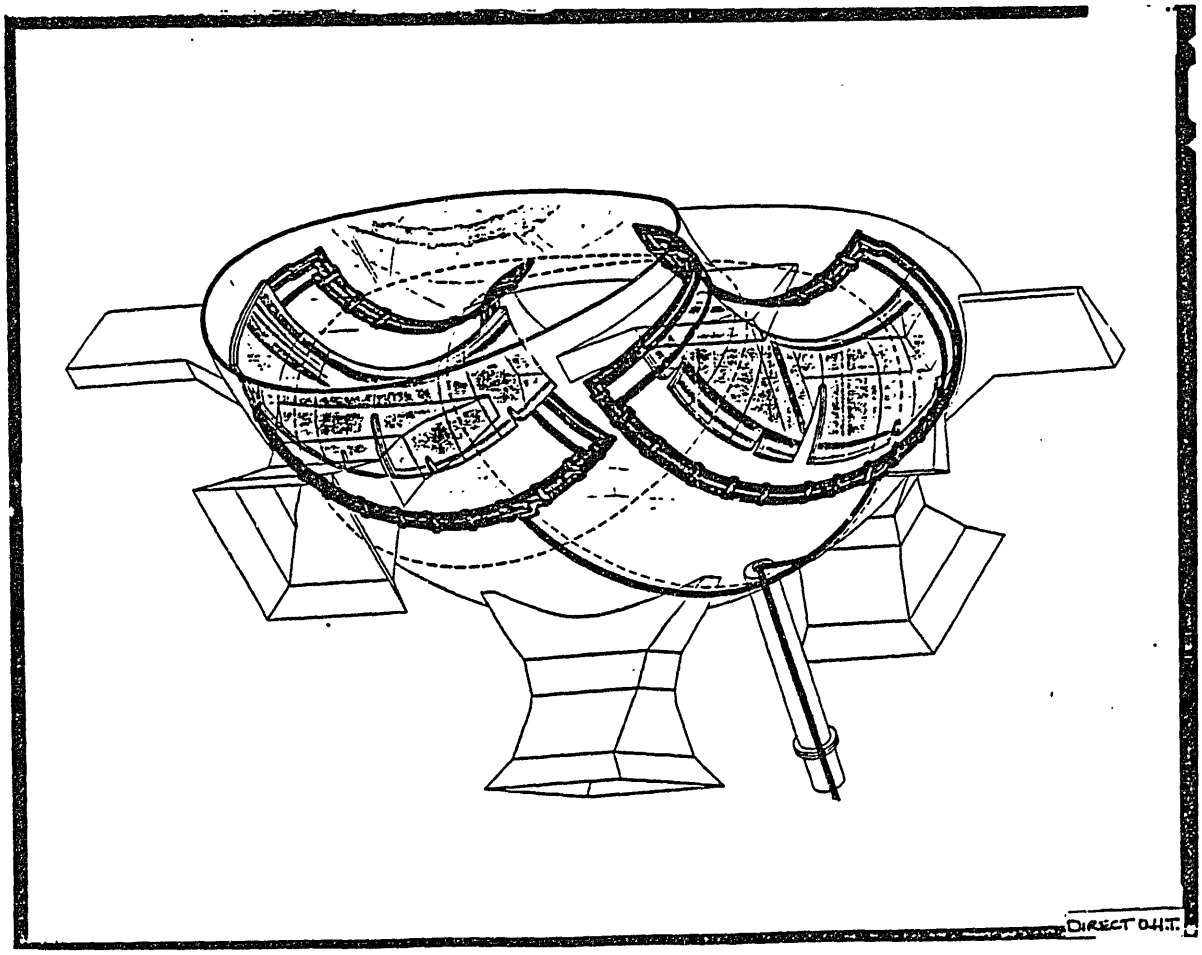
DIRECT O.H.T.

a) BELTLIMITER

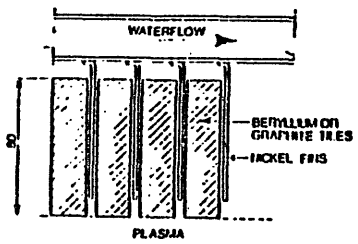

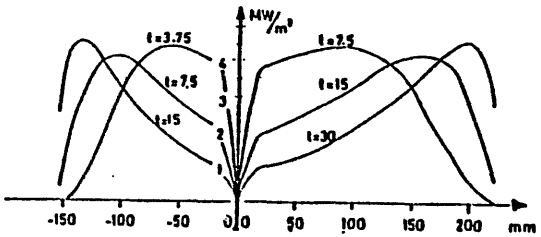

POWERLOAD !

$P_{Max} \approx 400\ W/cm^2$

THERMAL RESPONSE : $T_B \approx 300°C$

$T_S^{MAX} \approx 1250°C$

COOLINGTIME : $\approx$ 20 min. for 40 MW

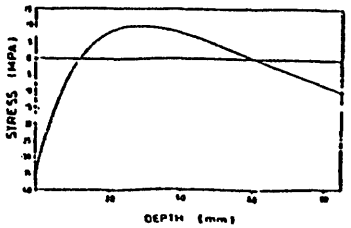

THERMAL STRESS

ABNORMAL LIMITERLOADING :

- RUNAWAYS (RARE EVENT) : SLIDE 2
- DISRUPTIONS : ENERGY QUENCH ($2 \cdot 10^{-4}$ s) $\approx$ 20 MJ onto LIMITER (1-10 μm EROSION)

b) INBOARD WALL PROTECTION: INERTIA-RADIATION COOLED (SLIDE)

- FOR PROTECTION AGAINST RUNAWAYS (PROBLEMS WITH INCONEL, GRAPHITE MORE TRANSPARENT)

- FOR PROTECTION AGAINST DISRUPTION: MAGNETIC ENERGY (≈50MJ) DURING CURRENT QUENCH ($\gtrsim 10^{-2}$ s). DISTRIBUTION OF POWER TO VACUUMVESSEL (EDDYCURRENT) AND WALL PROTECTION NOT CLEAR. (50 MJ / 20 m² → < 1 μm EROSION)

- FOR PROTECTION AGAINST NB-SHINE THROUGH:
  WITH PLASMA: $\lesssim 500$ W/cm² → $T_S \approx 1400$ °C AFTER 10 s
  WITHOUT " : 2 kW/cm²
  AFTER 0.1 (NORMAL INTERLOCK → ΔT ≈ 500 °C
  AFTER 1-2 s (INTERLOCK FAIL → FRACTURE BY THERMAL STRESSES

Ek 98
Pr 5890

⟹ AREAS WITH NB-SHINE THROUGH COVERED WITH CF-MATERIAL

DUNLOP DHS 678: 2D WOVEN, $\lambda_{\parallel} \geq 150 \frac{W}{mK}$
$\lambda_{\perp} \geq 30$ W/mK; $\sigma_{\parallel}$ (TENSILE) = 70 MN/m²);

HEATLOAD TESTS IN NB-TESTBED:
> 3 kW/cm² for a total of ≈ 30 s
(heavy erosion, no cracks)

- AS BUMPERLIMITER (MAINLY DURING PULSETERMINATION): see Wallpumping
  t ≈ FEW SECONDS; p = ?; NO T-MEASURE
  (SLIDE 3)

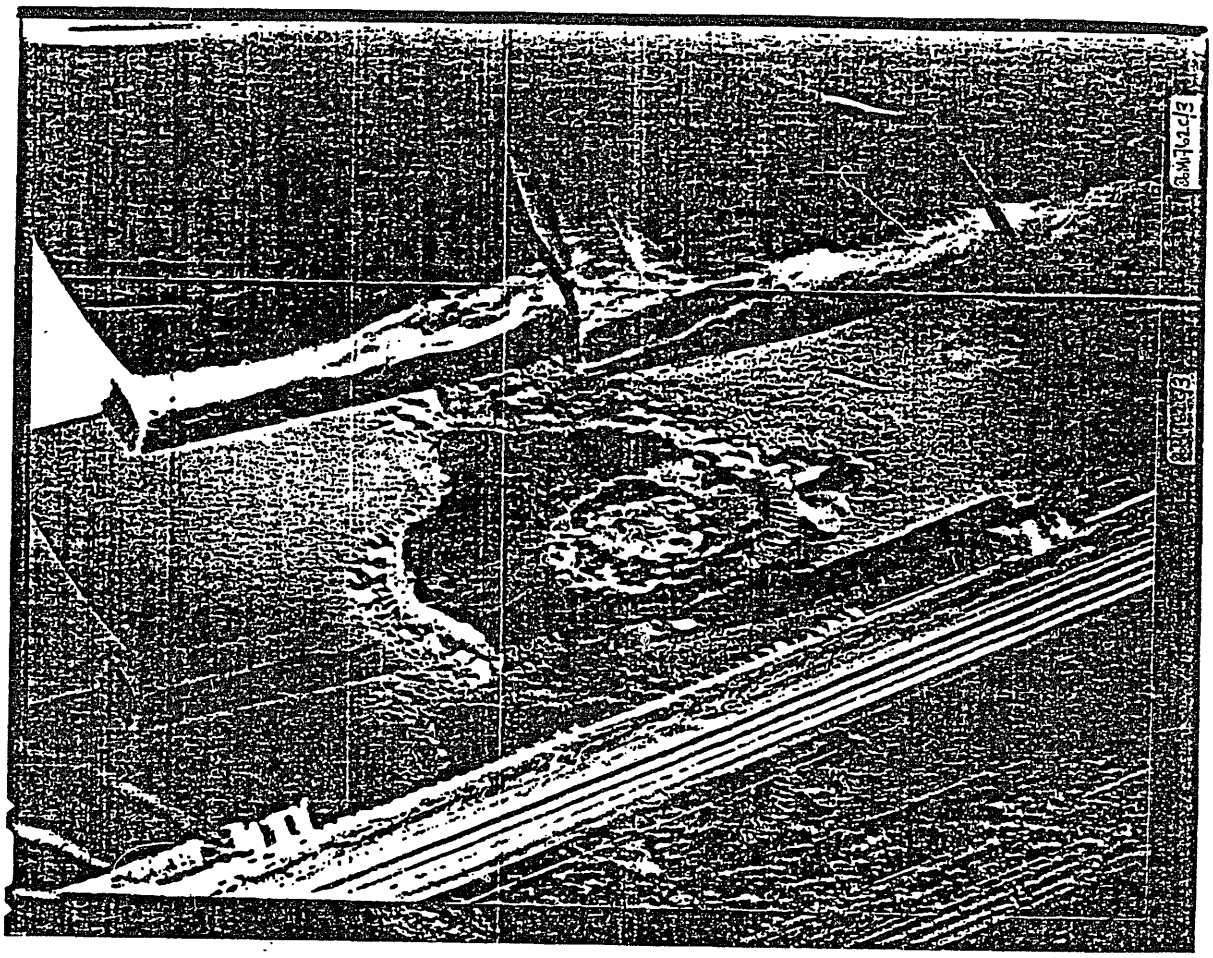

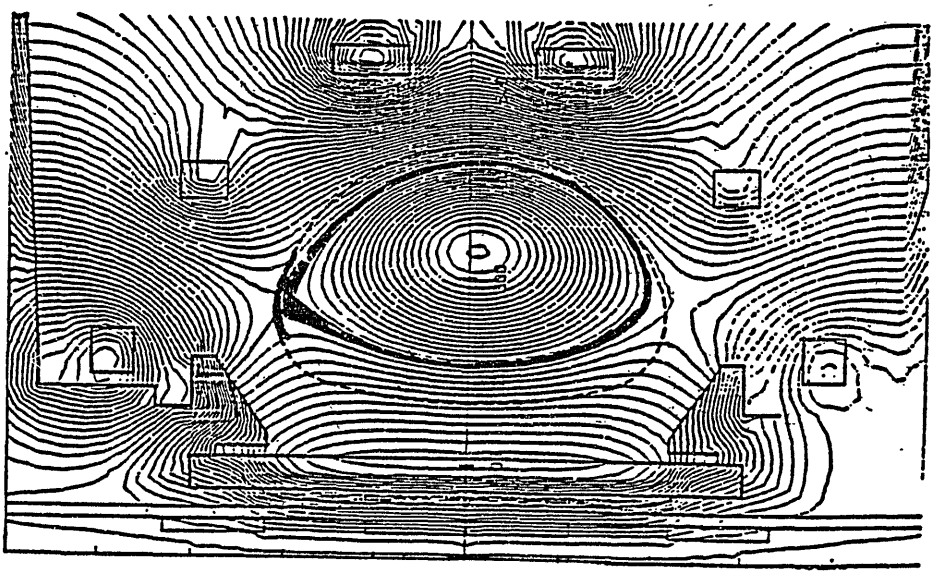

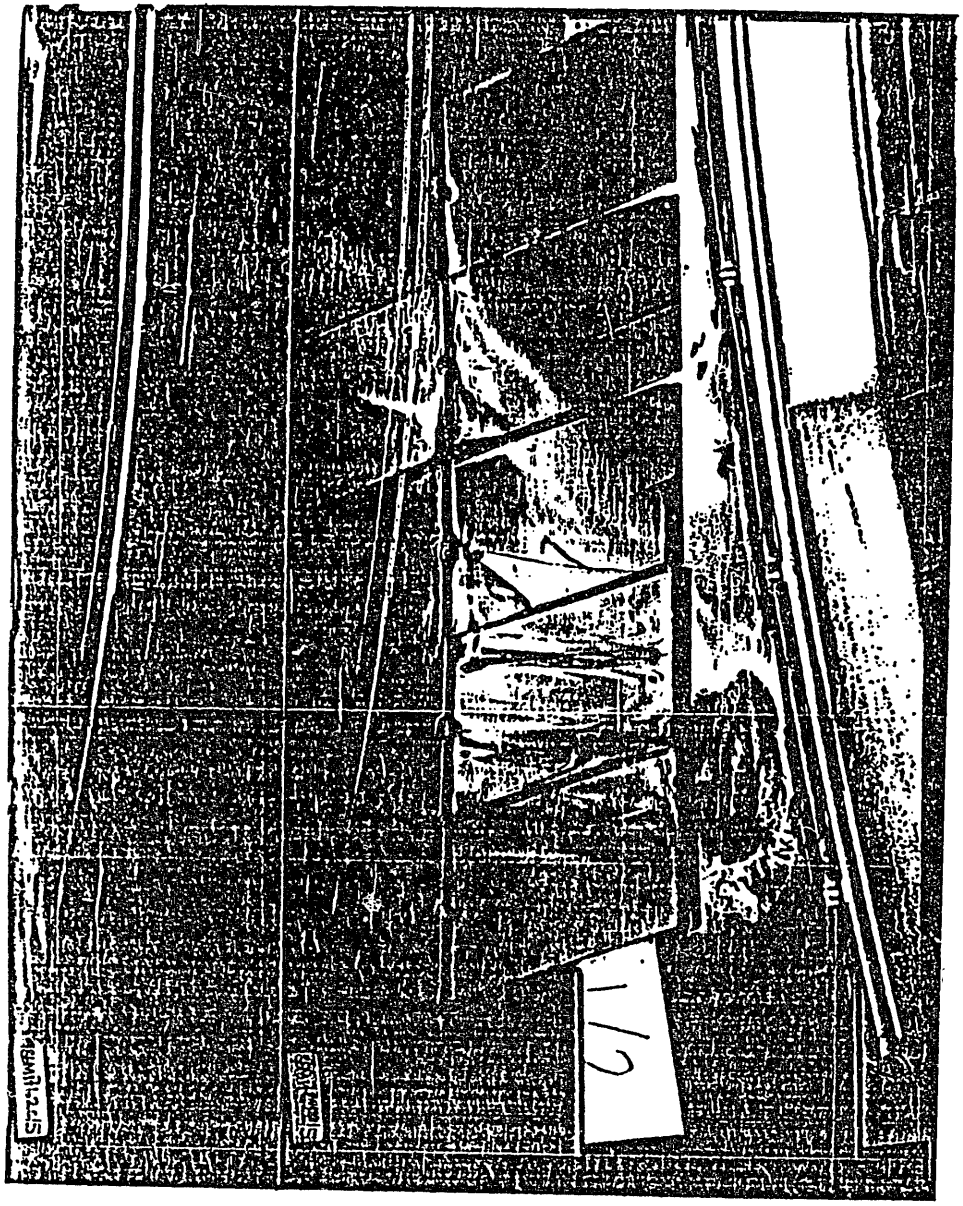

C) SEPARATRIX DUMPPLATES

- CURRENTLY 8 GRAPHITERINGS ; SINGLE NULL
  15 MW for 1-2 s (SLIDE)
  ⟹ CF-GRAPHITE IN LONG TERM
- MAXIMAL POWER LOADS ESTIMATED

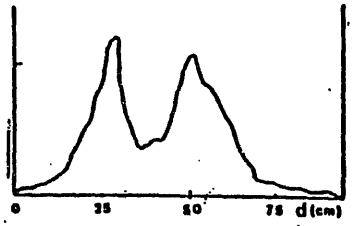

QUALITATIVE POWER DIST.
(INFRARED EMISSION;
NO T-MEAS.)

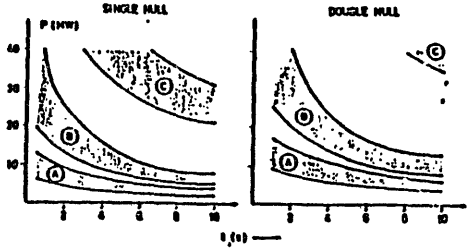

Fig. 5 Total power as a function of the pulse length to reach a surface temperature of the dump plates 2200°
Curve A: status in September 1986
Curve B: 40 graphite rings
Curve C: complete coverage with protection tiles.
The hatched areas are limited by curves representing different powers dissipated by radiation (upper limit 50%, lower limit 0% radiation).

$T_s \approx 2200°C$ → TOLERABLE THERMAL STRESSES (EVEN FOR NORMAL GRAPHITE) AND EROSIONRATES

• FINAL DESIGN : HEATTRANSFER THROUGH PRESSCONTACTS TO WATER-COOLED INCONE BASE PLATE:

COOLING TIME ≈ 10 min.

(HEATTRANSFER TEST NEEDED)

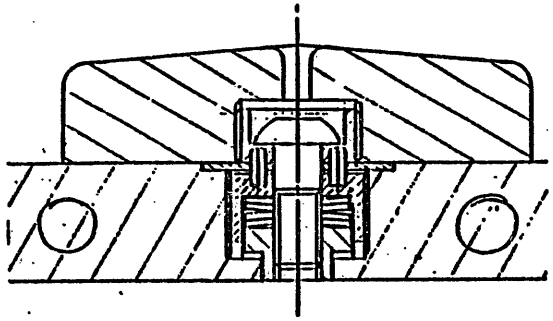

PROTOTYPE PUMPLIMITER

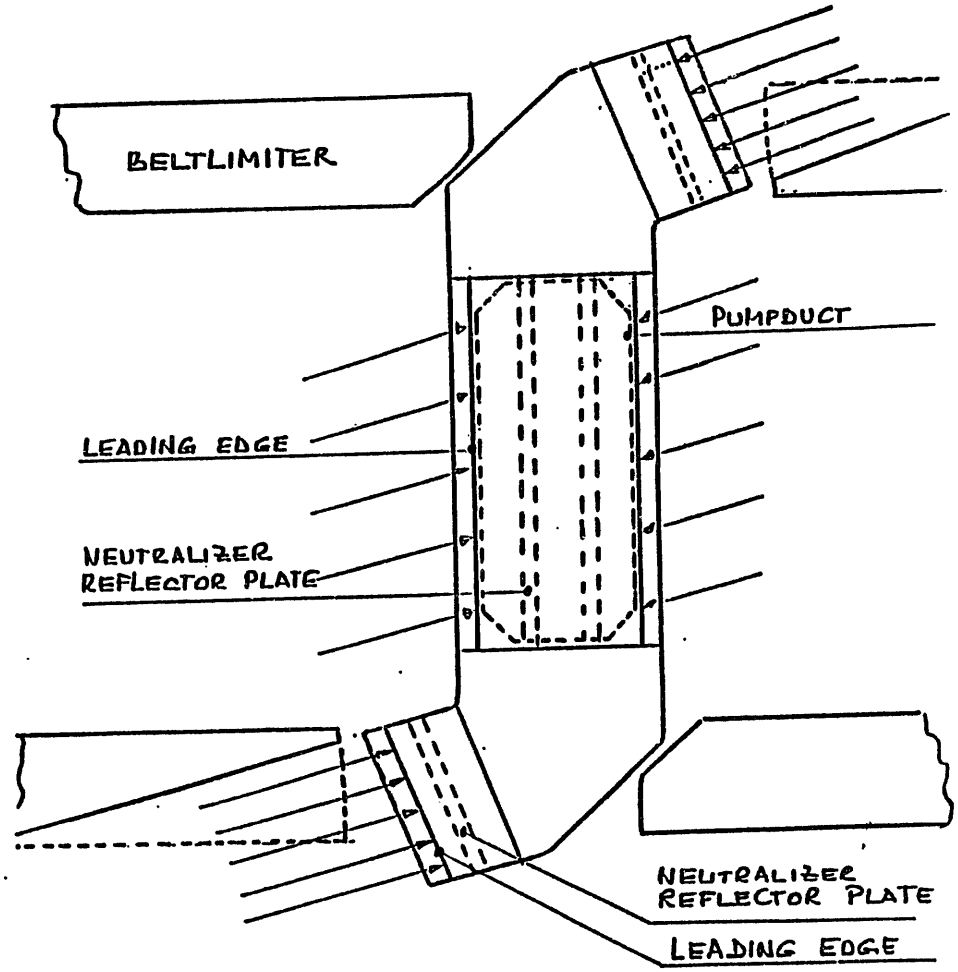

d) PUMPLIMITER

- PROTOTYPE
  - INERTIA COOLED GRAPHITE BLADE
    (2nd STAGE : ACTIVELY COOLED LIM.)
  - 2 - 3 kW/cm² ON LEADING EDGE REQUIRED FOR EFFIC. PUMPING

    (i) CF-MATERIAL : 1-2 s
    → MOVABLE BLADE

    (ii) PYROLITIC GRAPHITE : 10 s

    $\lambda_{RT} = 1600$ W/mK } FOR COMPRESSION ANNEALED GRAPHITE
    $\lambda_{2000°C} = 250$ W/mK

    BONDINGTECHNOLOGY ?
    RADIATIONRESISTANCE ?

- CONCEPTUAL DESIGN (SLIDE)

II. JET EXPERIENCE WITH CARBON WALL

- CURRENTLY 45 m² COVERED WITH GRAPH.
  (AFTER SHUTDOWN ≈ 30 m²)
  REST IS 'CARBONIZED'

- HEATRESISTANCE
  - DISRUPTIONS, RUNAWAYS, NORMAL COND. (WITHIN DESIGN LOAD) } NO PROBLEM
  - UNCONTROLLED LOADING : e.g. INBOARD WALL (BUMPER LIMITER), SEPARATRIX DUMPPLATES SLIDE) → CF-MATERIAL

TYPICAL IMPURITY CONC.

Carbon	2–4% (% of n_e)
Oxygen	1–2%
Chlorine	0.05–0.15%
Metals (Ni, Fe, Cr)	0.001–0.3%

$\bar{n}_e$	$1.9\times10^{19}\,m^{-3}$
(C)	1.9%
(O)	1.5%
(Cl)	0.05%
(Ni)	0.005%
Z_{eff}^{calc}	2.58
Z_{eff}^{brems}	2.71

IMPURITY CONC. INCREASES WITH ADDITIONAL POWER (WITHIN LIMITS GIVEN ABOVE). (SLIDE)
Z_{eff} REMAINS ABOUT CONSTANT WITH ADD. HEATING, SINCE D-CONC. INCREASES TOO.

FUEL DILUTION : ABOVE IMPURITY CONC. WOULD RESULT IN $\simeq 50\%$ REDUCTION IN α-PARTICLE PRODUCTION

– IMPURITIES SITUATION

- METALS (Ni) : FROM METAL-CONTAMINATED LIMITER AND FROM Ni-ANTENNA SCREEN (SLIDE

TEMPORARY METALSUPPRESSION BY CARBONISATION

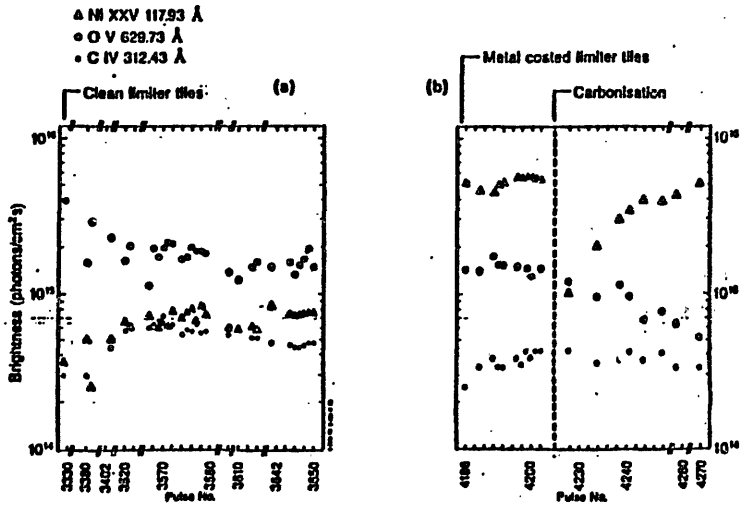

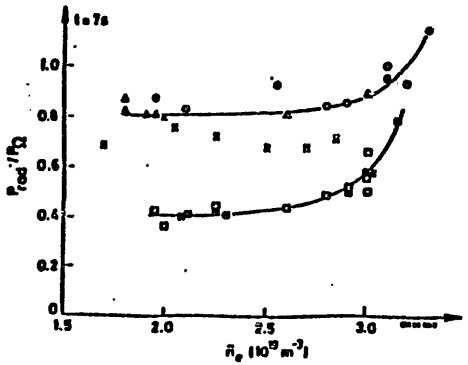

- RADIATION REDUCED FOR LOW DENSITIES
- NEGLIGIBLE INCREAS OF DENSITY LIMIT

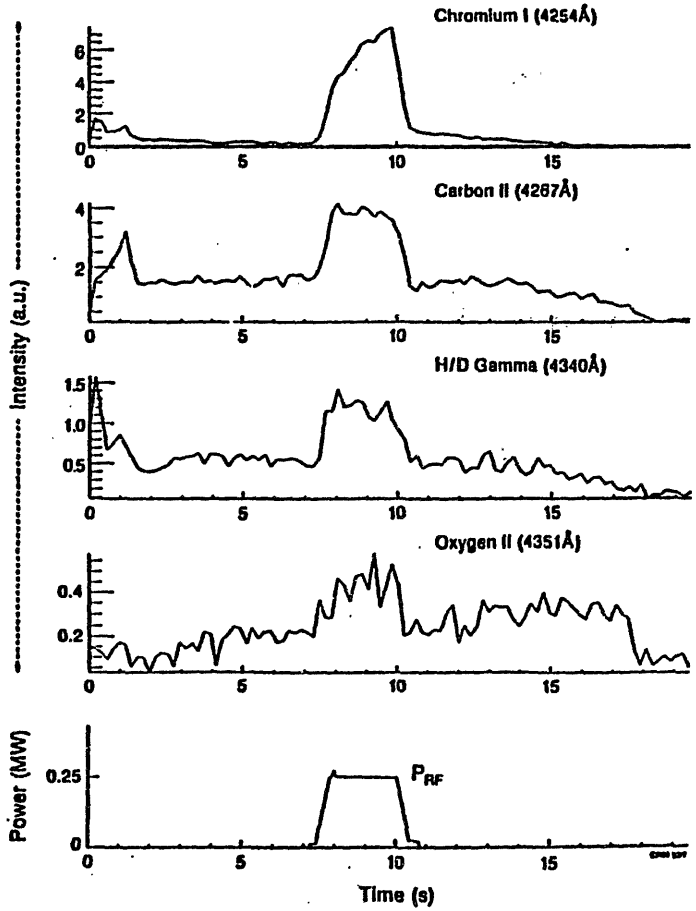

Fig. 12 Increase of various line intensities emitted in front of an antenna, when RF power is switched on.

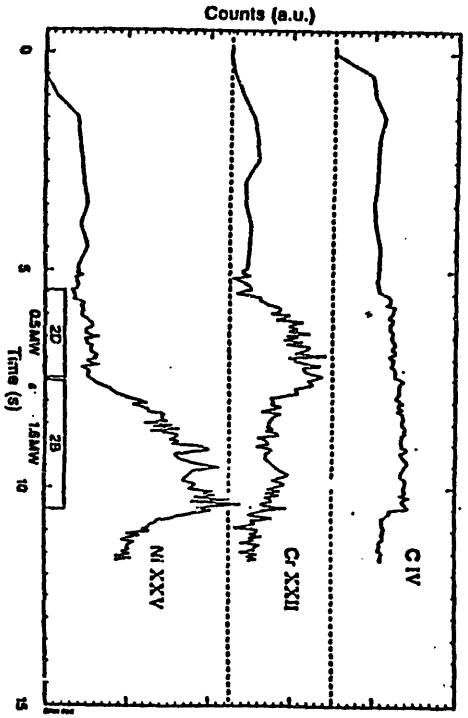

Fig. 13 Time evolution of chromium and nickel in the plasma, when antennae with different screen material are activated (antenna 2D: Cr, antenna 2B: Ni).

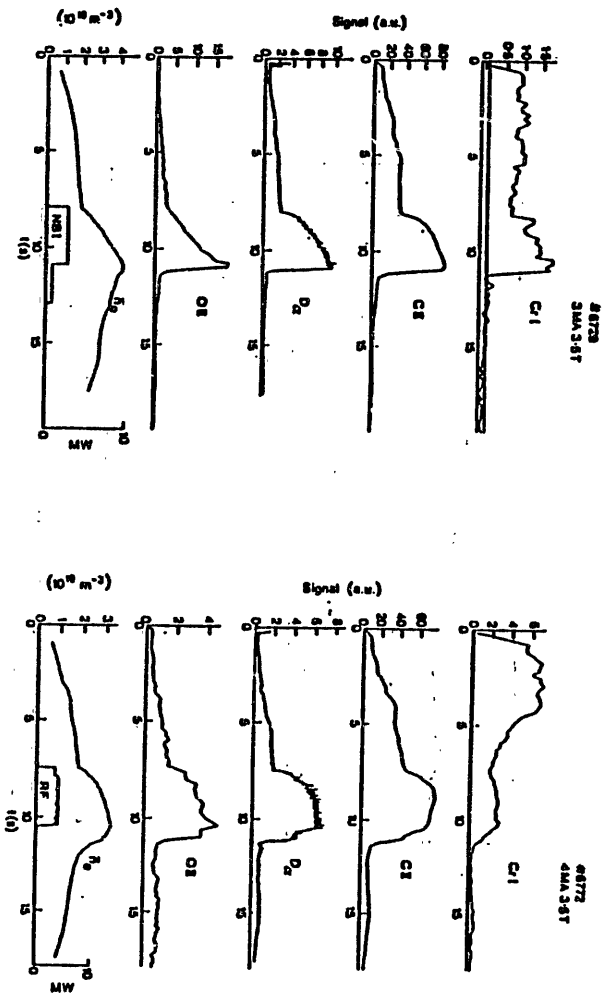

Fig.3 Increase of emission lines from various low ionization stages when auxiliary heating is switched in. a) neutral injection b) Radiofrequency

→ WALLPUMPING

- OBSERVED WHEN PLASMA IS SHIFTED TO INBOARD WALLPROTECTION OR X-POINT DUMPPLATES
- EMPLOYED FOR HIGH DENSITY PULSETERMINATION

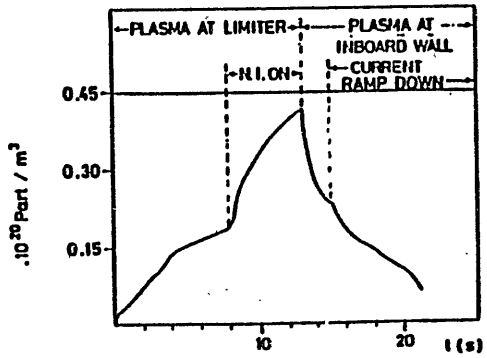

- $\pm\ 4 \cdot 10^{21}$ PARTICLES/S !
- STRONGPUMPING ONLY FOR 1-2S BUT REPEATABLE

  (SLIDE)
- ONLY SMALL PUMPING EFFECT IF PLASMA REMAINS ATTACHED TO LIMITER

  (SLIDE)
- POSSIBLE MECHANISMS:
  - a) PHYSICAL AND CHEMICAL SPUTTERING + C_1H - CO' AND CH - REDEPOSITION (SEE LIVERMORE RESULTS
  - b) H - TRAPPING
  - c) TRANSIENT PUMPING OF CARBON

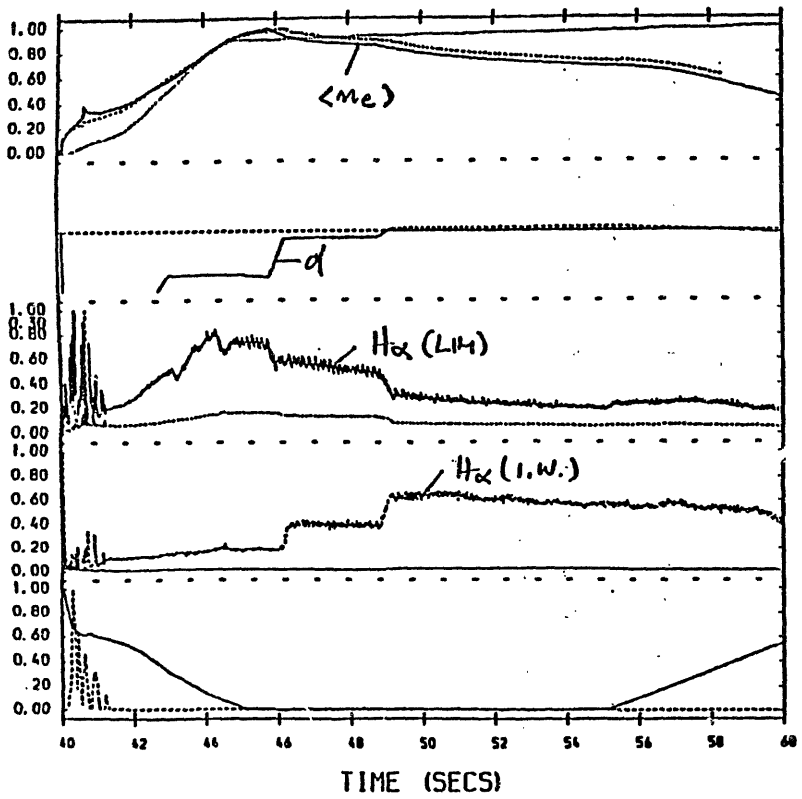
<ne>
d
Hα (LIM)
Hα (I.W.)
TIME (SECS)

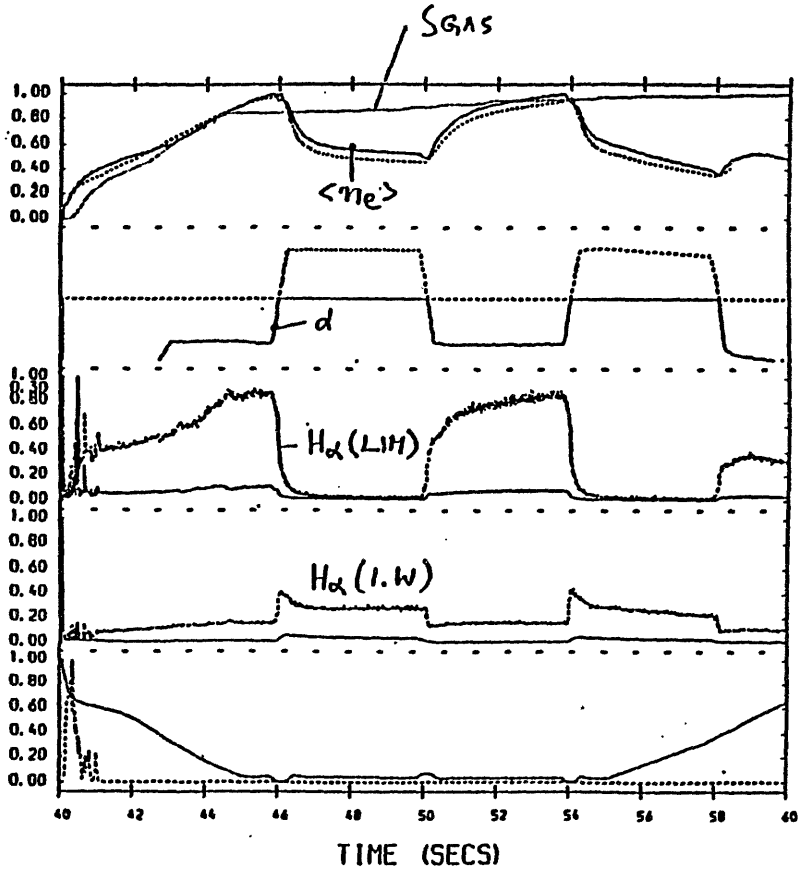
SGAS
<ne>
d
Hα (LIM)
Hα (I.W)
TIME (SECS)

U.S. Efforts on Graphite and Carbon Related Material Studies

K.L. Wilson

Sandia National Laboratories
Livermore, California USA

Abstract

The U.S. Plasma- Material interaction and high heat flux programs on graphite and carbon-based materials is reviewed. Highlights of research at Sandia, Oak Ridge, and UCLA are included.

SANDIA HAS A COMPREHENSIVE RESEARCH PROGRAM FOR CARBON APPLICATIONS IN MAGNETIC FUSION ENERGY

- CHARACTERIZATION
- PLASMA MATERIAL INTERACTIONS
  - EROSION-REDEPOSITION
  - HYDROGEN RECYCLING/TRITIUM INVENTORY
  - CONDITIONING
- HIGH HEAT FLUX TESTING
- ADVANCED MATERIALS DEVELOPMENT
- COMPONENT DEVELOPMENT

SANDIA

PMI RESEARCH ON GRAPHITE AT SANDIA

CONDITIONING

- OUTGASSING STUDIES
- BET POROSITY MEASUREMENTS
- CARBONIZATION

EROSION/REDEPOSITION

- LIMITER CHARACTERIZATION (TFTR, ETC.)
- LABORATORY EROSION STUDIES
- C-C COMPOSITE TESTS (TEXTOR, PLT)

HYDROGEN RECYCLE

- TRITIUM RETENTION (TFTR, CIT)
- RECYCLE MODEL (PPPL)
- WALL PUMPING (JET)

SANDIA OUTGASSING FACILITY

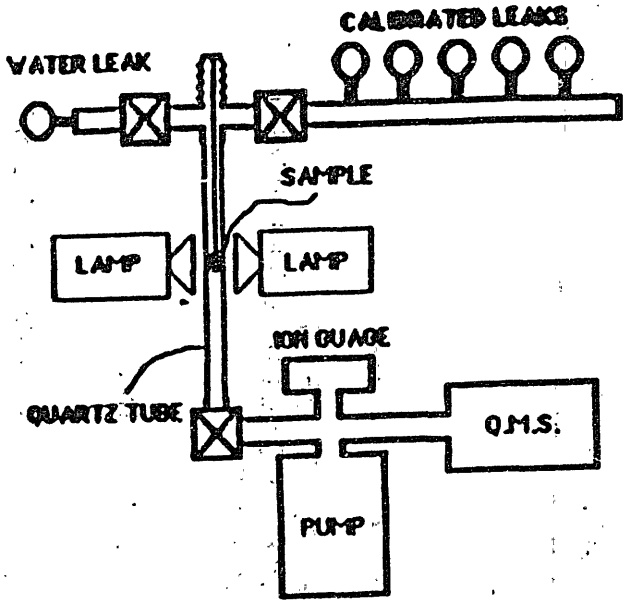

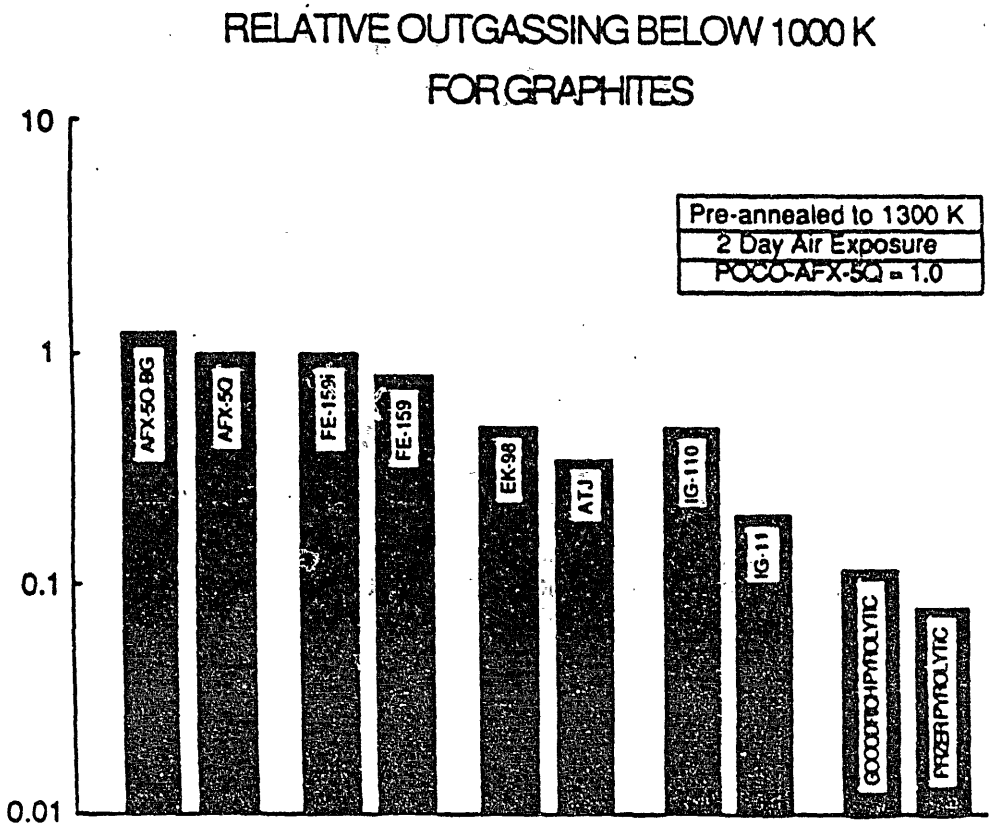
RELATIVE OUTGASSING BELOW 1000 K
FOR GRAPHITES
10
1
0.1
0.01
Pre-annealed to 1300 K
2 Day Air Exposure
POCO-AFX-5Q = 1.0
AFX-5Q BG
AFX-5Q
FE-159
FE-159
EK-98
ATJ
IG-110
IG-11
GOODFRICH PYROLYTIC
FRIZER PYROLYTIC

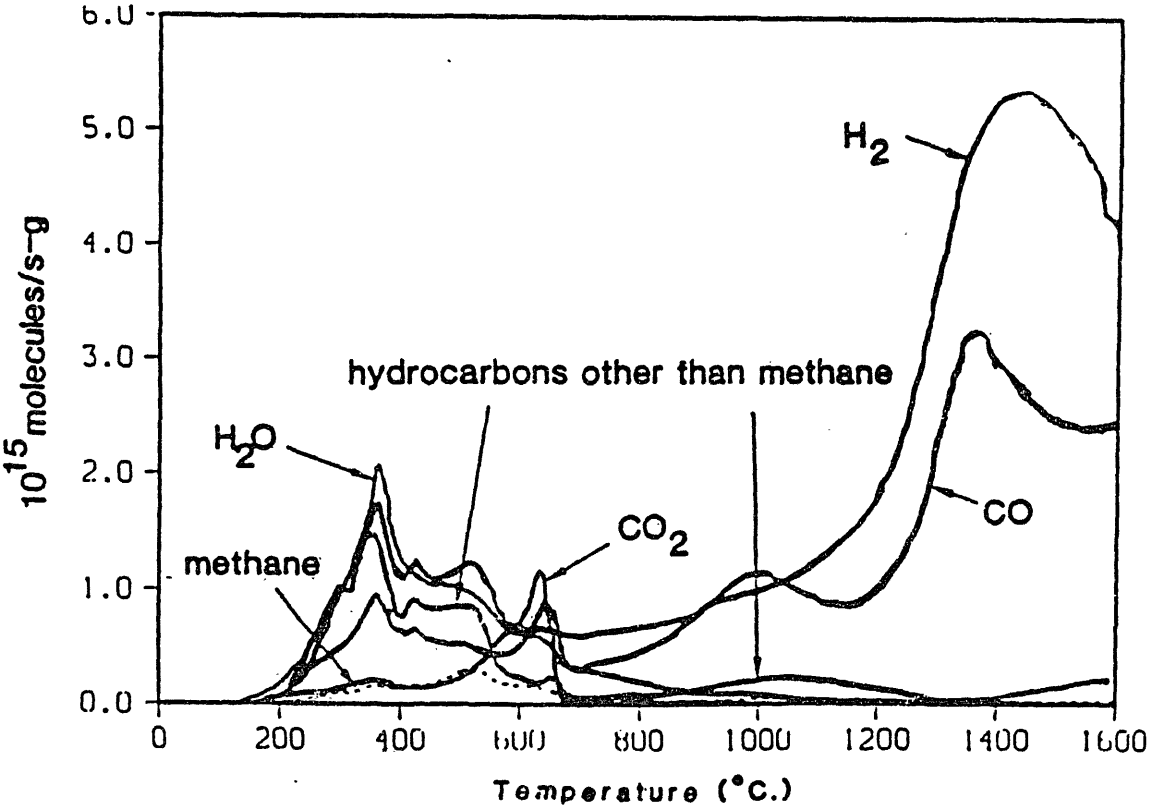
6.0
5.0
4.0
3.0
2.0
1.0
0.0
10^{15} molecules/s-g
H_2
hydrocarbons other than methane
H_2O
CO_2
CO
methane
0
200
400
600
800
1000
1200
1400
1600
Temperature (°C.)

Hydrogen Pumping With POCO-AXF5Q Graphite Electrodes

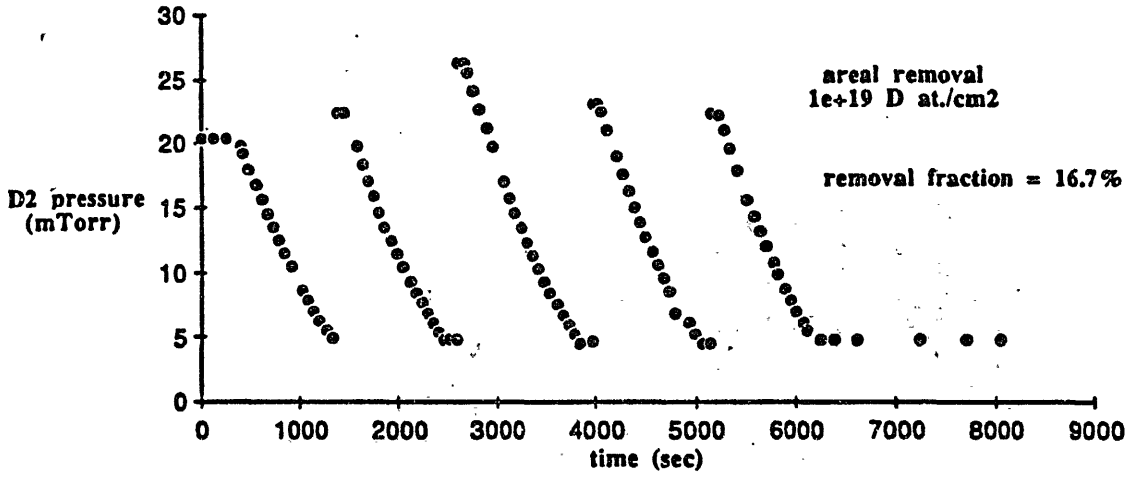

HSU

LAMPE FACILITY

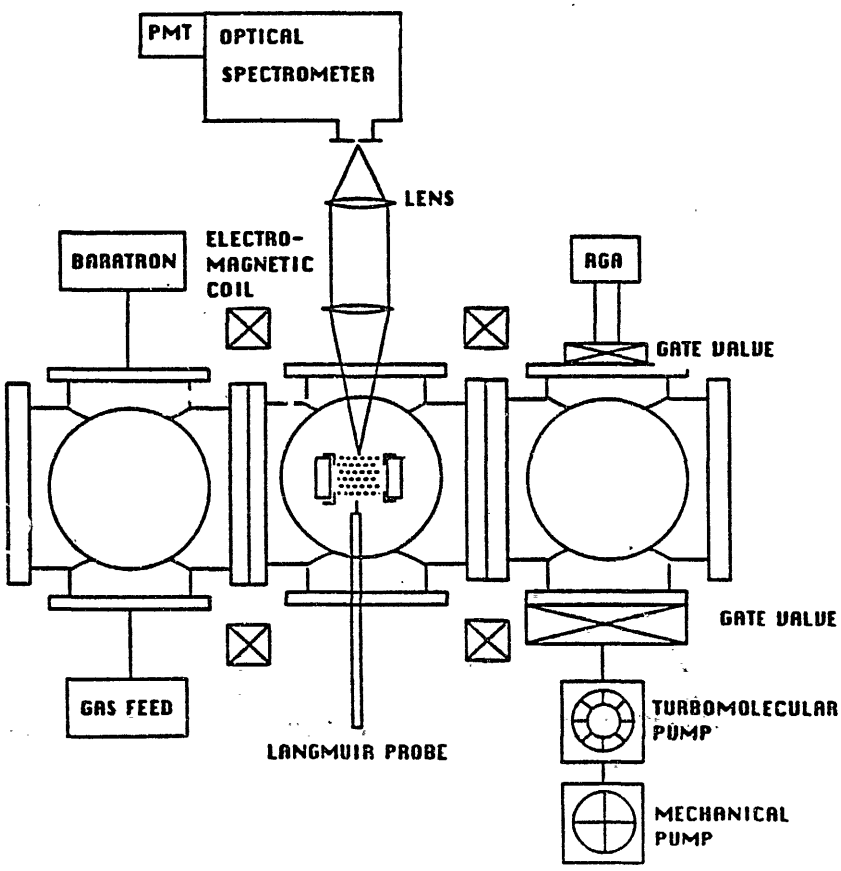

TRITIUM PLASMA EXPERIMENT

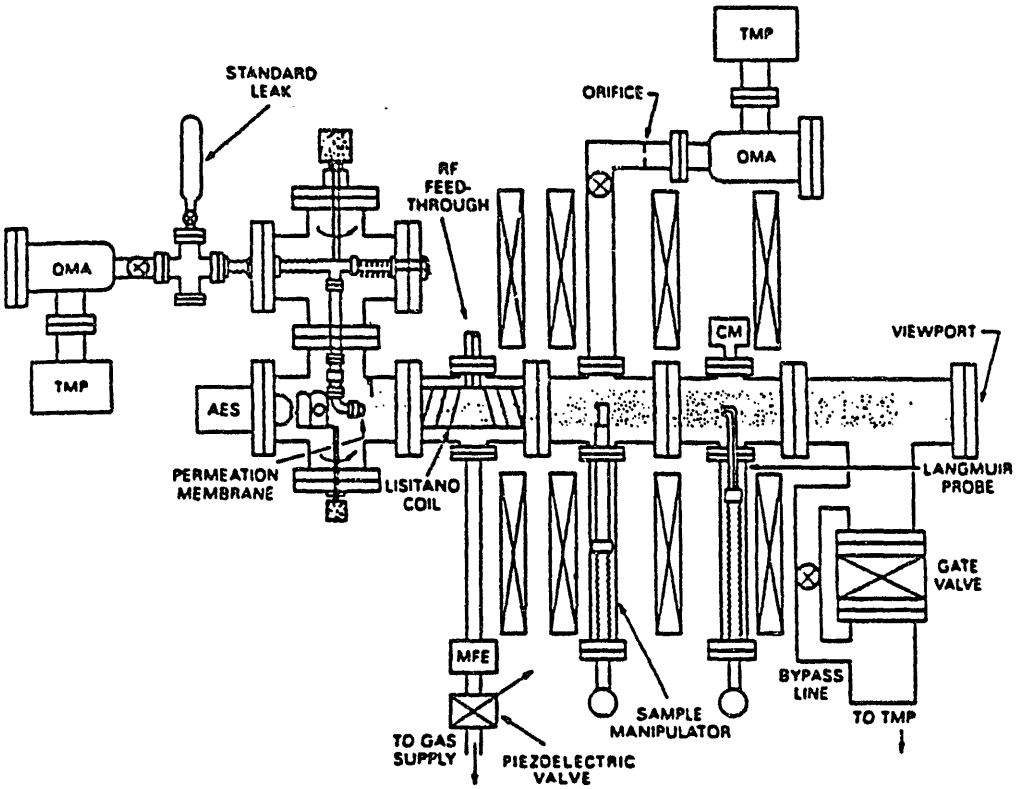

Schematic diagram of Tritium Plasma Experiment. AES = Auger electron spectrometer, QMA = quadrupole mass analyzer, TMP = turbomolecular pump, MFE = molecular flow element, CM = capacitance manometer.

Sandia National Laboratories

CO-DEPOSITION IS THE DOMINANT HYDROGEN REMOVAL MECHANISM

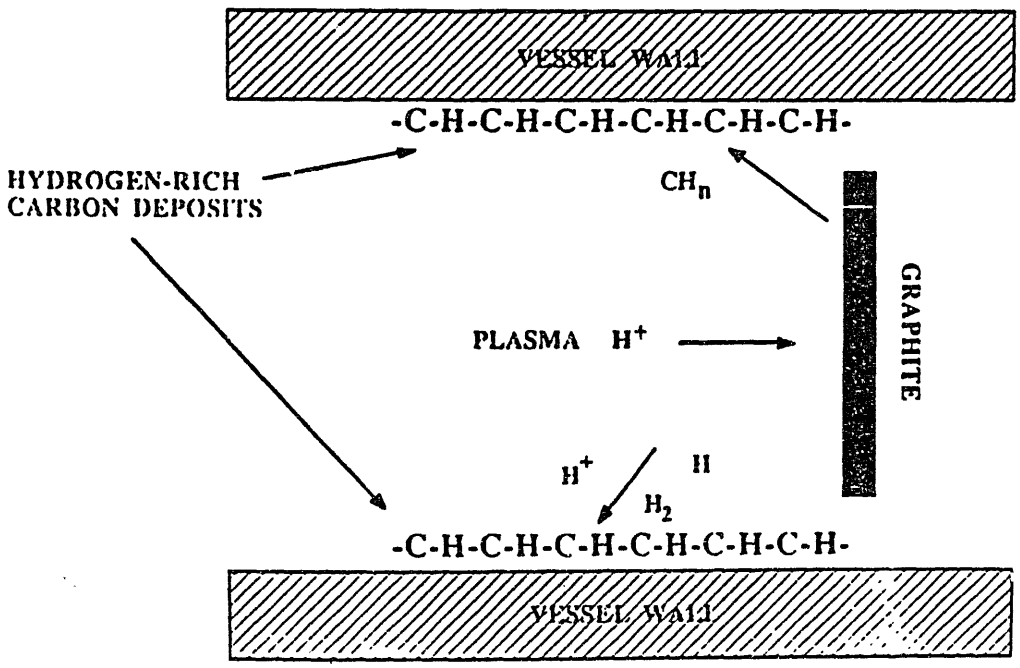

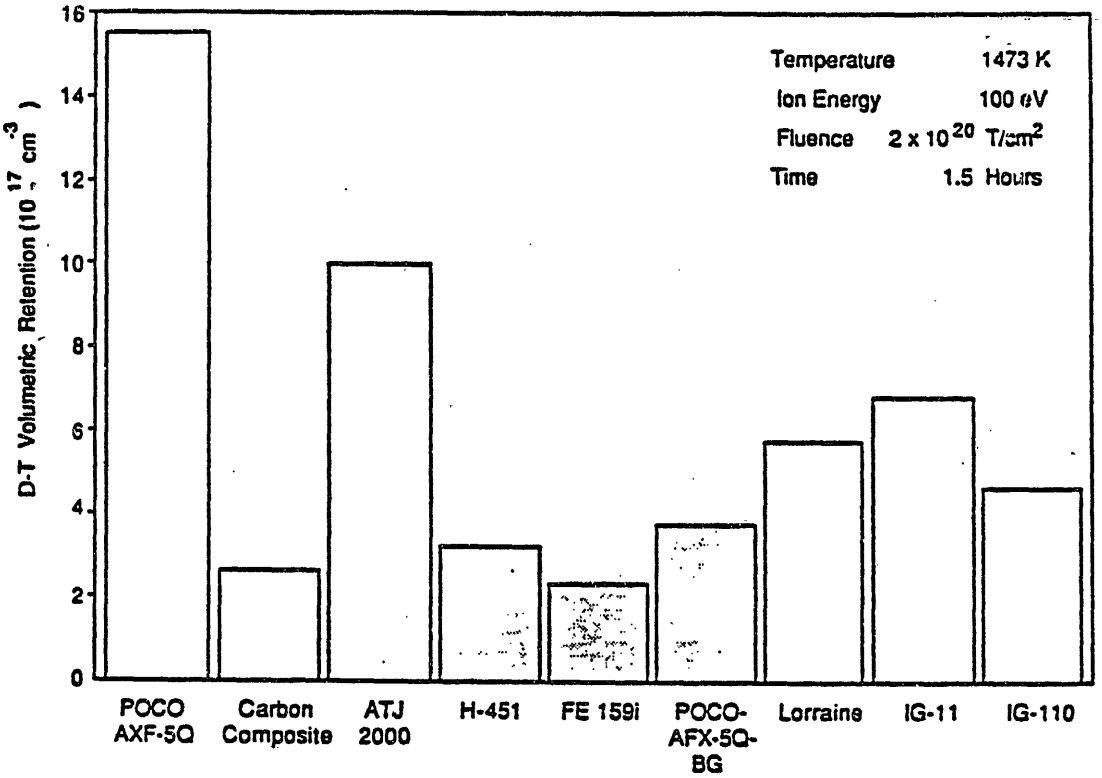

TRITIUM RETENTION IN GRAPHITE IS TEMPERATURE DEPENDENT

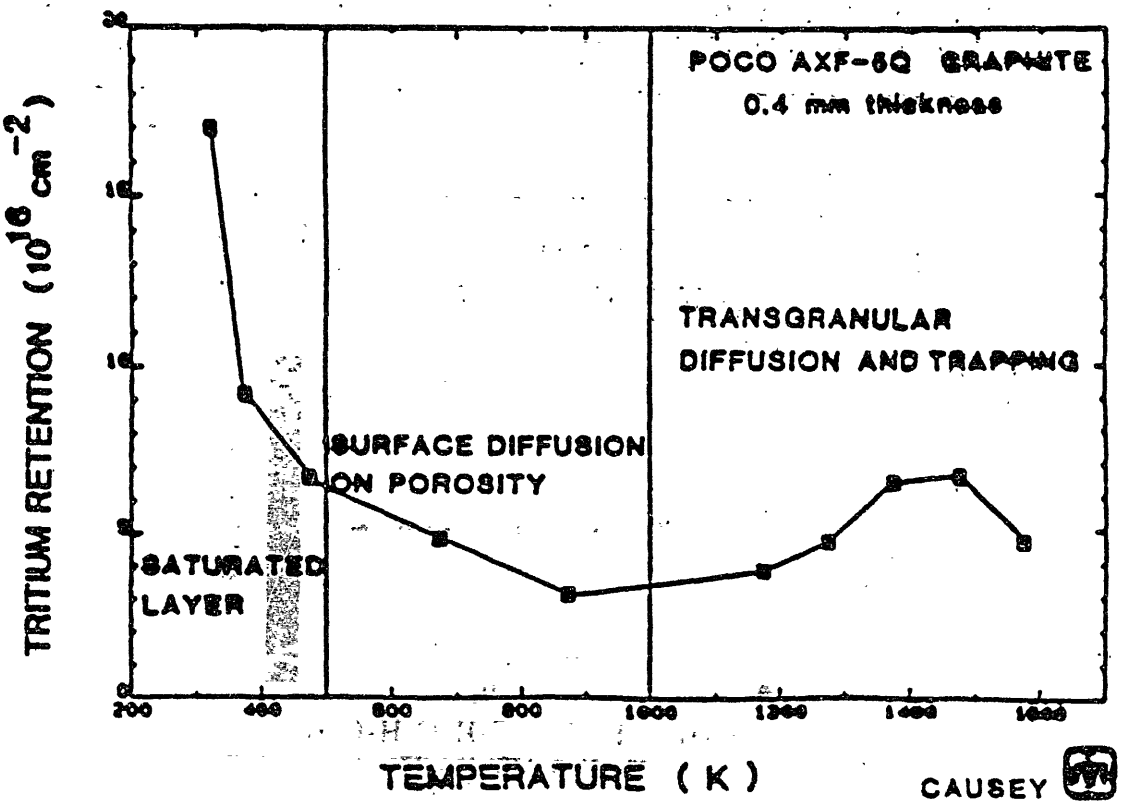

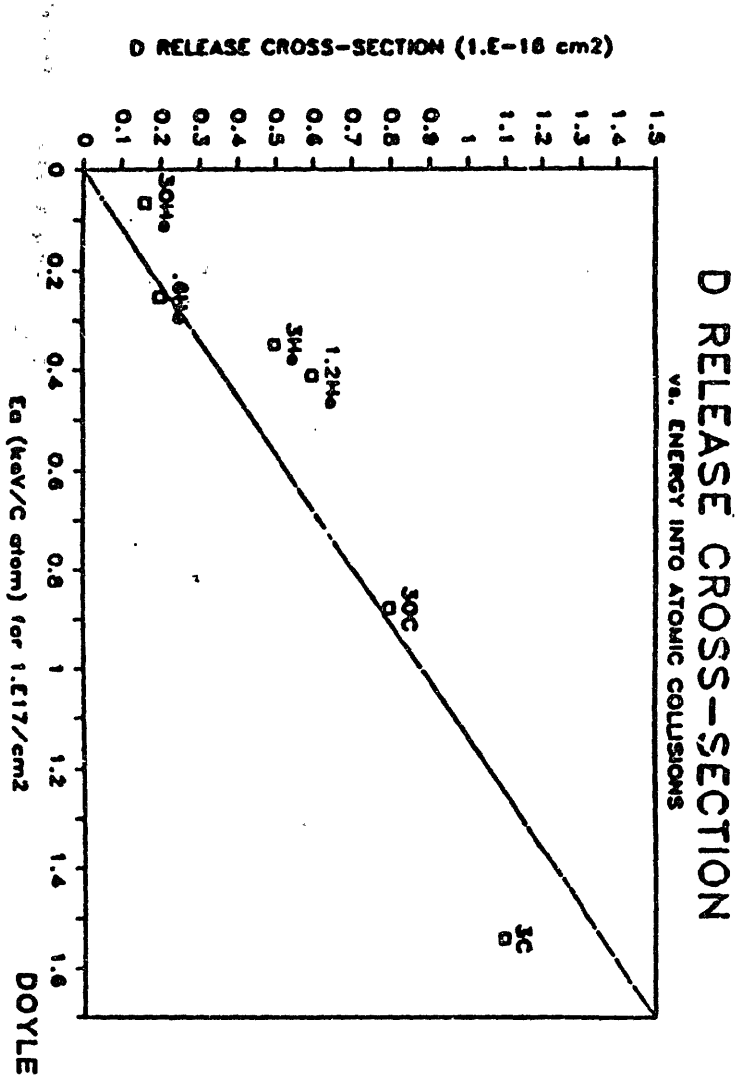

RECENT HIGHLIGHTS OF SANDIA'S GRAPHITE TECHNOLOGY PROGRAM

- TRITIUM UPTAKE IN POCO AXF-5Q
- CHARACTERIZATION OF TFTR LIMITERS
- SANDIA-PPPL LIMITER RECYCLING CODE
- SCOPING STUDY OF TRITIUM UPTAKE IN GRAPHITES AND C-C COMPOSITES
- OUTGASSING MEASUREMENTS FOR GRAPHITES AND C-C COMPOSITES
- C-C COMPOSITE TESTING IN TEXTOR
- CIT AND TFTR TRITIUM INVENTORY ESTIMATES
- WALL PUMPING BY GRAPHITE-PLASMA INTERACTION FOR JET

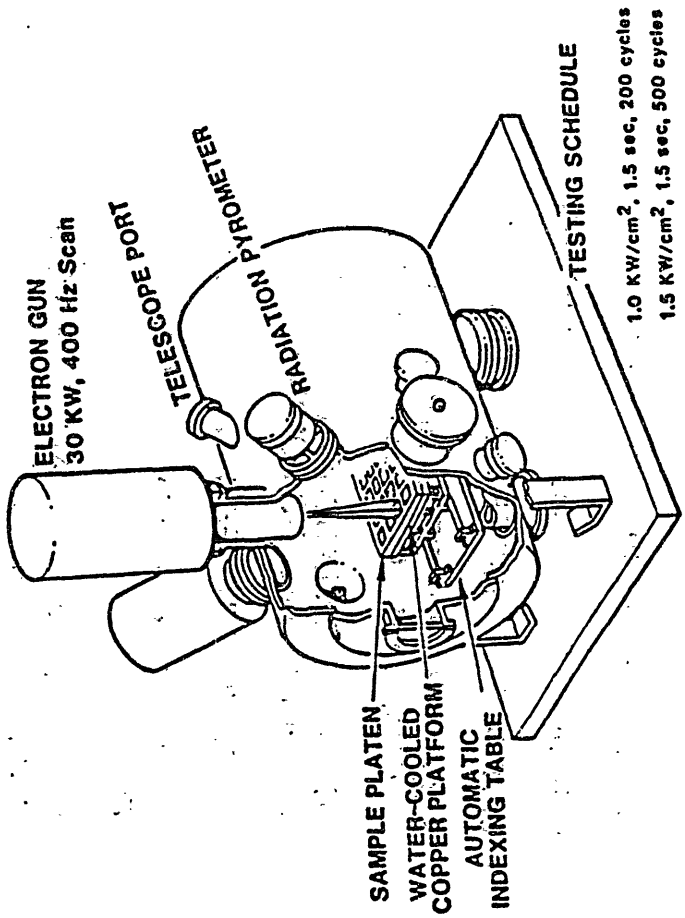

PLASMA MATERIALS TEST FACILITY (PMTF)

- DEDICATED TO THE DEVELOPMENT AND TESTING OF HIGH HEAT FLUX COMPONENTS

- FACILITY CONSISTS OF:
  - ELECTRON BEAM TEST SYSTEM (EBTS)
  - MULTIPLE BEAM TEST SYSTEM (MBTS)

Sandia National Laboratories

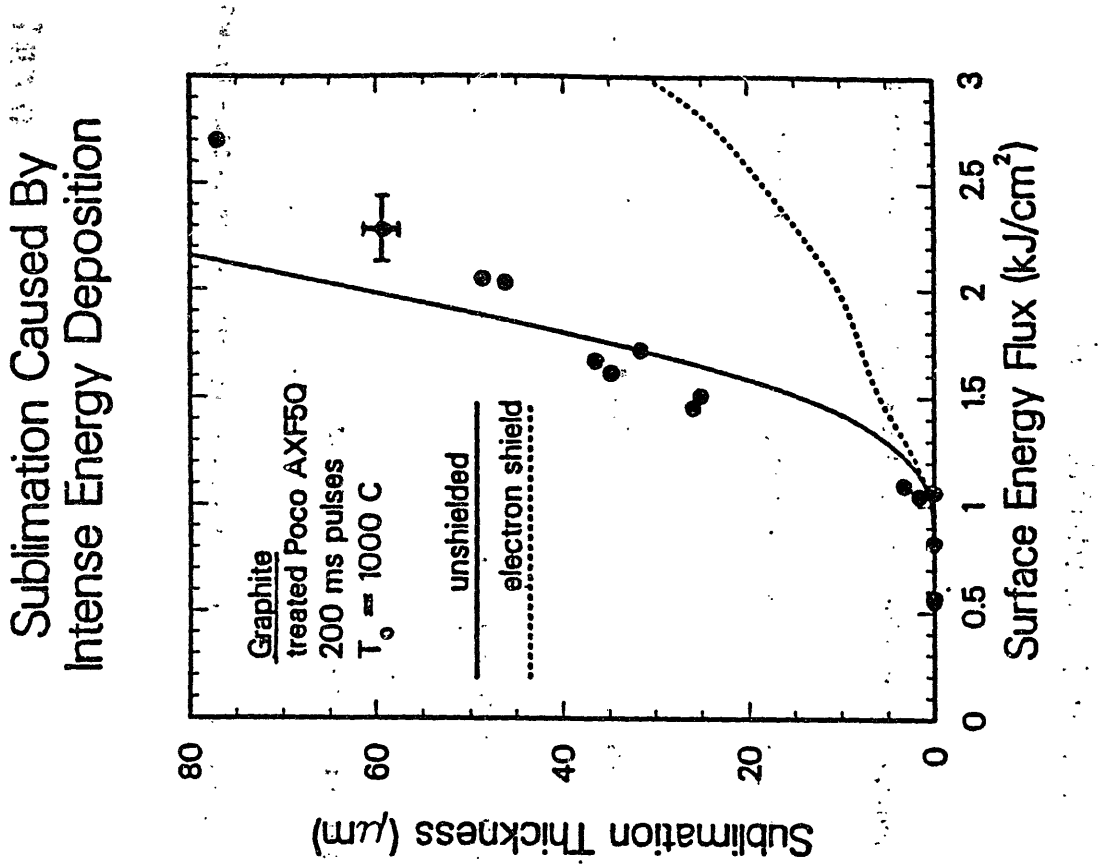

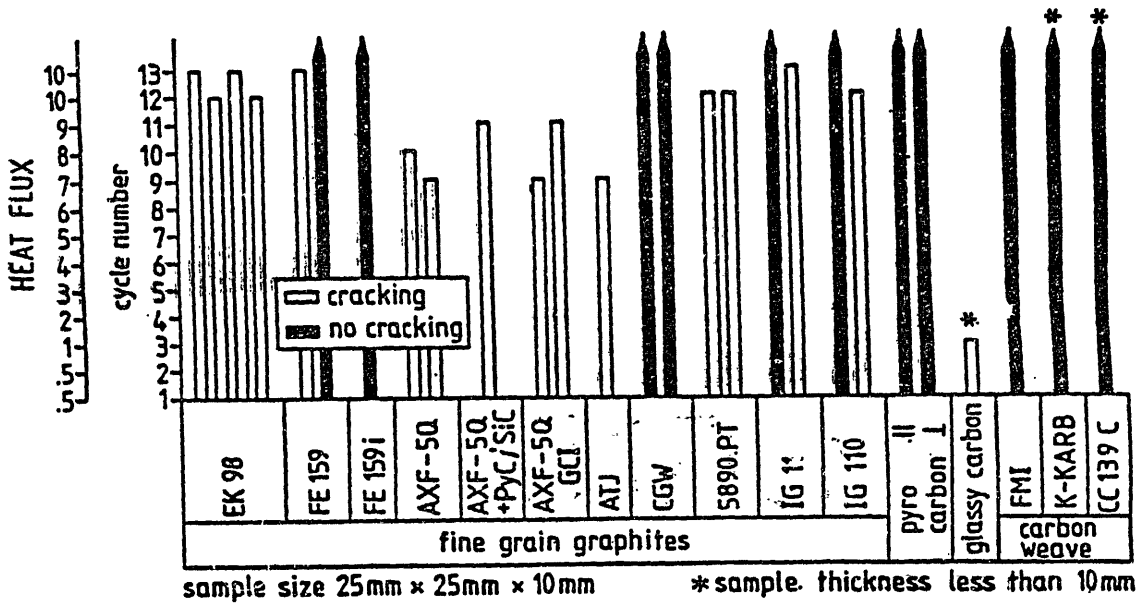

Thermomechanical behavior of different graphite materials.

ORNL

GRAPHITE STUDIES AT ORNL

- DECOMPOSITION AND REFORMATION OF SURFACE COMPLEXES
- CONDITIONING TECHNIQUES FOR PLASMA-SIDE MATERIALS
- RECYCLING AND RETENTION OF HYDROGEN ISOTOPES
- ION-INDUCED DETRAPPING
- PROPERTIES OF DOPED GRAPHITES
- CARBONIZATION TECHNIQUES AND PROPERTIES OF CARBON FILMS

ornl

ORNL OUTGASSING FACILITY

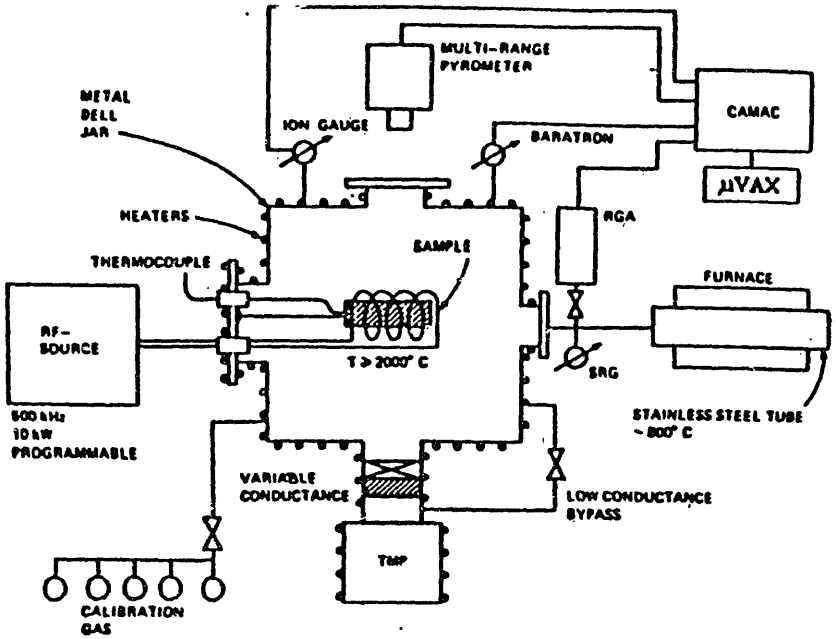

- APPARATUS:
  - -RF-POWER 10 kW
  - -SAMPLE SIZE 10 - 20g
  - -SAMPLE TEMPERATURE UP TO 2000 °C
  - -MICROPROCESSOR-CONTROLLED TEMPERATURE
  - -WALL TEMPERATURE CONTROLLED AT 100 °C
- OBJECTIVES:
  - -DECOMPOSITION AND REFORMATION OF SURFACES COMPLEXES
  - -CONDITIONING TECHNIQUES OF GRAPHITE COMPONENTS

ornl

OUTGASSING DATA

ornl

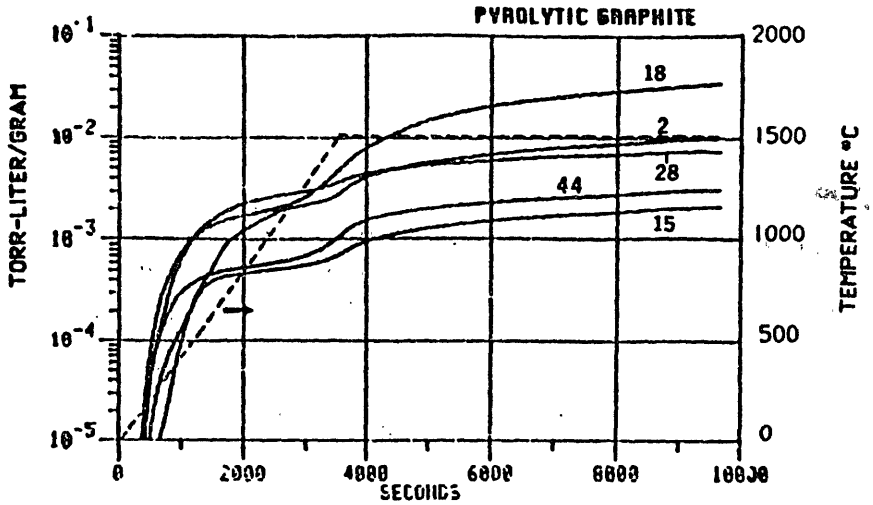

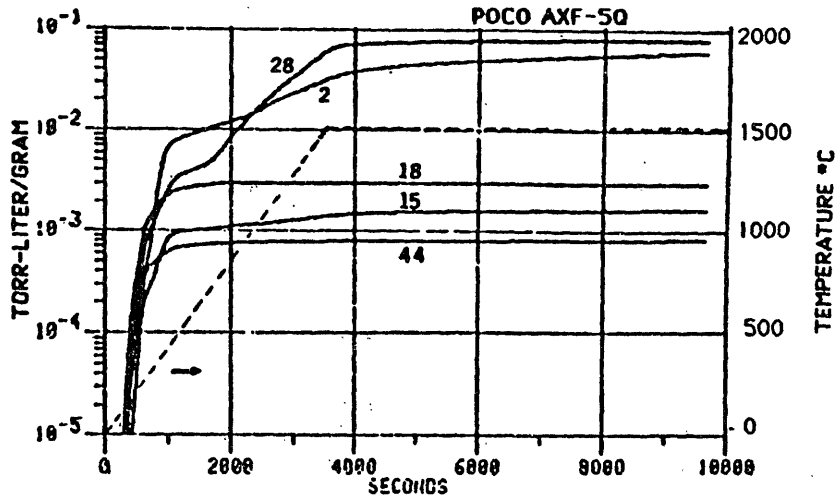

- ROOM-TEMPERATURE TO 1500 °C IN 3600 SEC, THEN CONSTANT .

ORNL-DWG 86-10057R

HYDROGEN RECYCLE FROM CARBON FILMS IS VERY DIFFERENT FROM STAINLESS STEEL

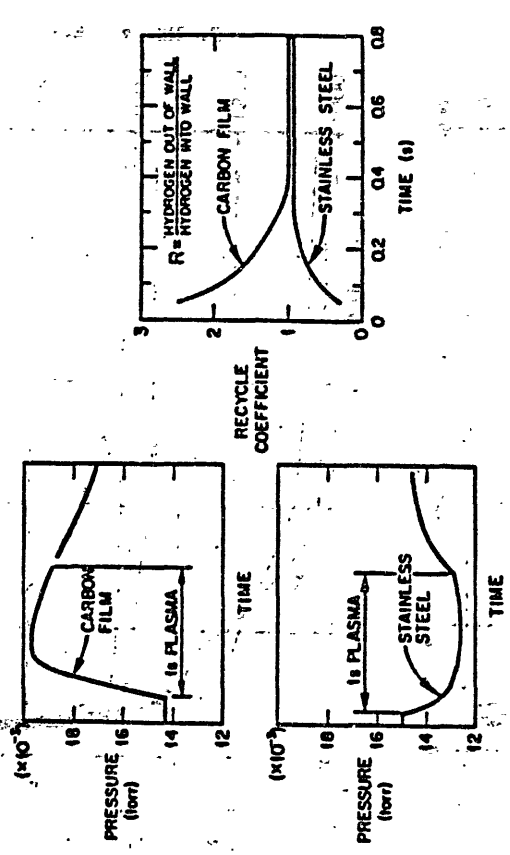

FOR CARBON FILMS:

1. THE INITIAL RECYCLE COEFFICIENT IS USUALLY >>1.
2. ION INDUCED DESORPTION IS THE MOST IMPORTANT RECYCLE MECHANISM FOR TEMPERATURES TO >300°C.
3. RECYCLE IS STRONGLY INFLUENCED BY THE HYDROGEN CONTENT OF THE FILM AND ION ENERGY.

ORNL-DWG 86-18027

SCHEMATIC OF RICS CHAMBER WITH GRAPHITE LINER

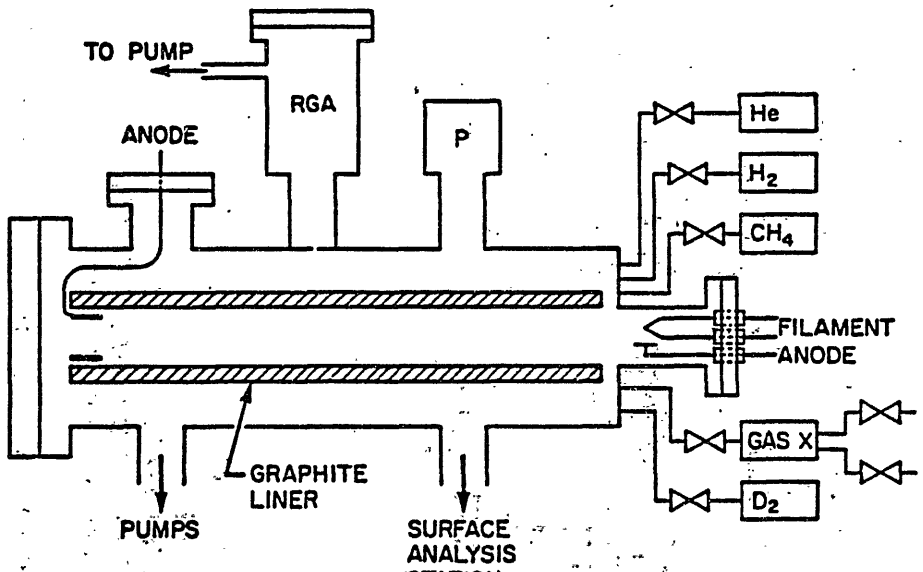

TYPICAL PARAMETERS

ION FLUX: $1-2\times10^{16}$ H/cm^2 s
ION ENERGY: 100–500 eV
TEMP: ROOM TEMP–350°C (≥800°C)
PRESSURE: 15–200 μ

GRAPHITE LINER

ID: 3.8 cm
OD: 6.35 cm
LENGTH: 60 cm

ORNL-DWG 86-10648A

THE RECYCLING-COEFFICIENTS FOR THE 330°C FILM SHOW THE COMBINED EFFECTS OF INCREASING THE TIME INTERVAL BETWEEN PULSES AND PARTIAL REPLENISHMENT OF THE HYDROGEN IN THE FILM BY PRECEEDING PULSES. (this film was degassed for 5h at 330°C before this series began.)

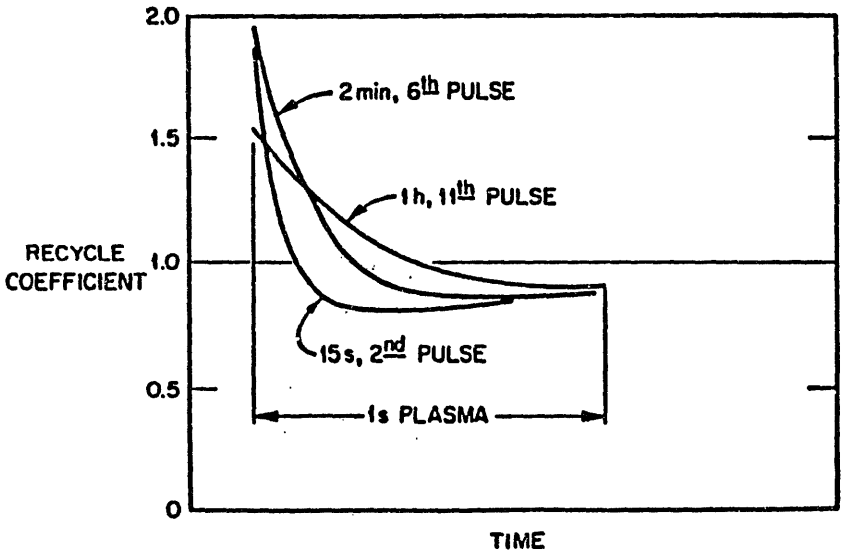

THE RECYCLE COEFFICIENT NORMALLY GOES ASYMTOTICALLY TO ONE DURING A SERIES OF PULSES, BUT IF THE HYDROGEN IS DEPLETED, RECYCLING MAY BE LESS THAN ONE FOR SIGNIFICANT TIMES, UNTIL THE HYDROGEN CONTENT OF THE FILM IS INCREASED SUFFICIENTLY.

Langley/1986

ORNL-DWG 86-2795A FED

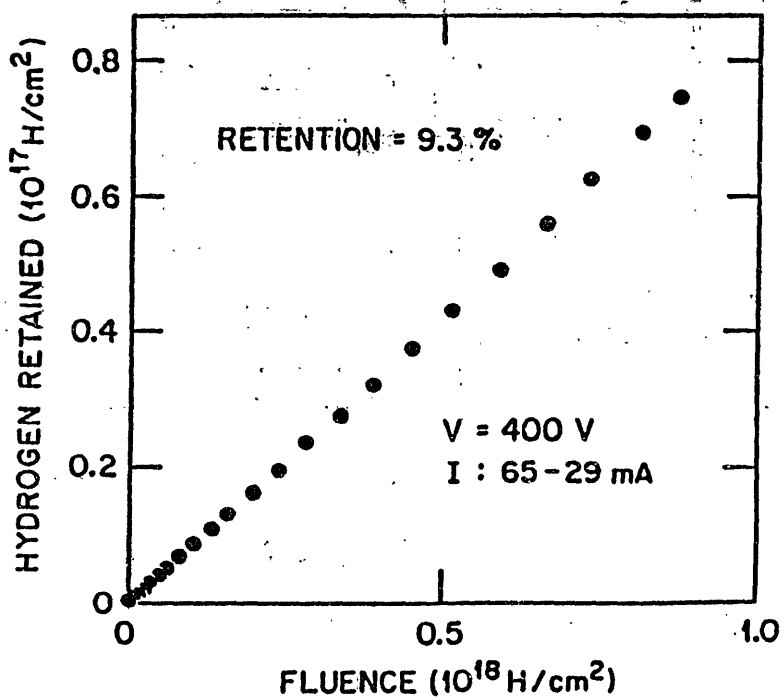

ornl

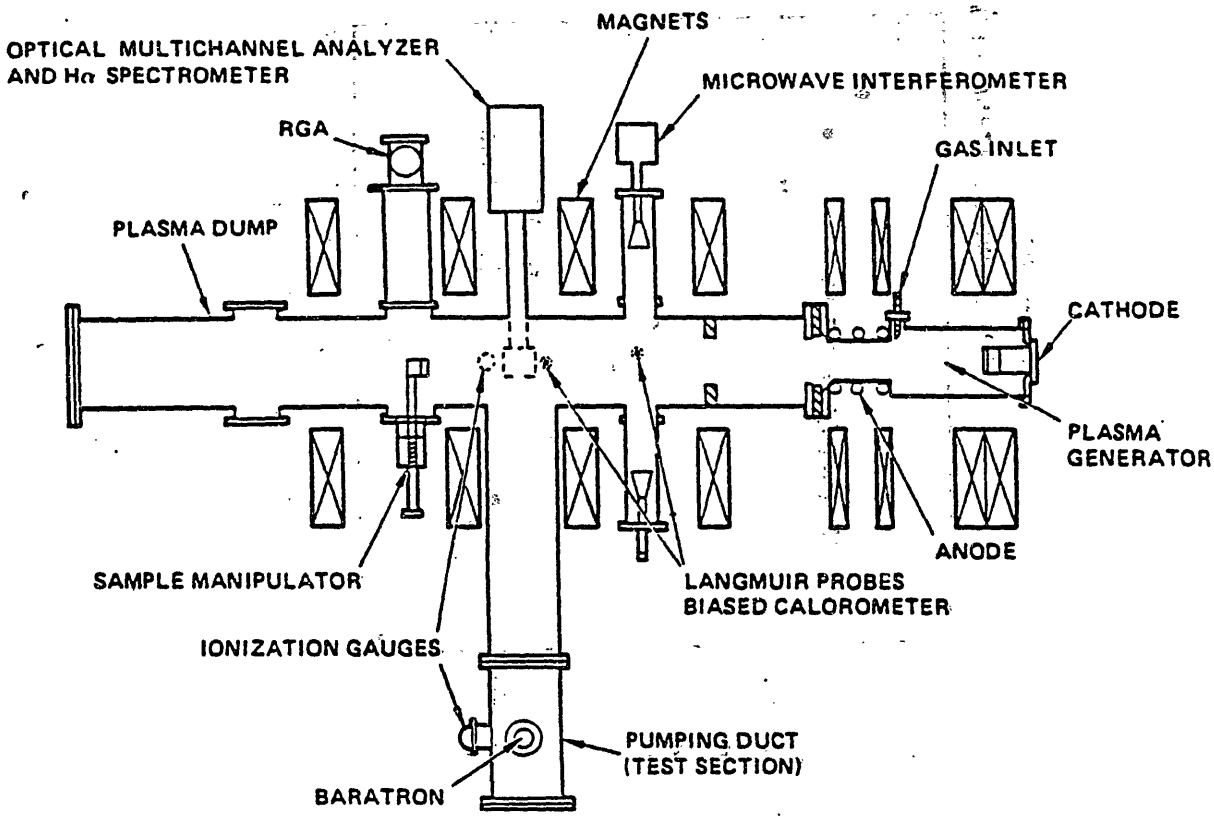
OPTICAL MULTICHANNEL ANALYZER
AND Hα SPECTROMETER
MAGNETS
MICROWAVE INTERFEROMETER
RGA
GAS INLET
PLASMA DUMP
CATHODE
PLASMA
GENERATOR
ANODE
SAMPLE MANIPULATOR
LANGMUIR PROBES
BIASED CALOROMETER
IONIZATION GAUGES
PUMPING DUCT
(TEST SECTION)
BARATRON

UCLA

EROSION AND REDEPOSITION OF GRAPHITE

- CHEMICALLY SPUTTERED HYDROCARBONS ARE REDEPOSITED IN EDGE PLASMAS WITH $n_e > 10^{12}\,cm^{-3}$ AND $T'_e > 10\,eV$
- HYDROCARBON REDEPOSITION REDUCES THE SPUTTERING YIELD AND MODIFIES THE SURFACE STRUCTURE ("SOOT" DEPOSITION)

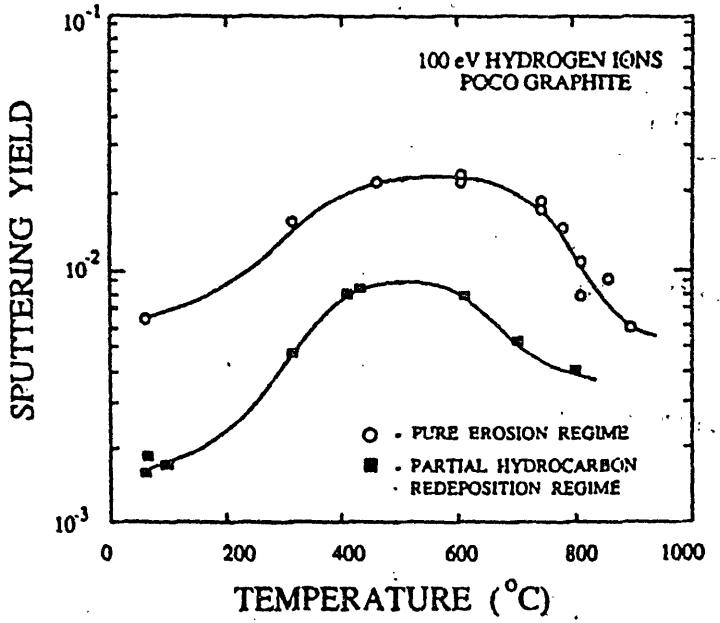

CHEMICAL EROSION OF GRAPHITE AT HIGH PLASMA FLUX

- HYDROGEN AND DEUTERIUM ION BOMBARDMENT AT 2×10^{18} ions/cm^2 sec
- RESULTS
  - CHEMICAL SPUTTERING OCCURS AT HIGH FLUX
  - HYDROCARBON FORMATION AT LOW ENERGY IS OBSERVED

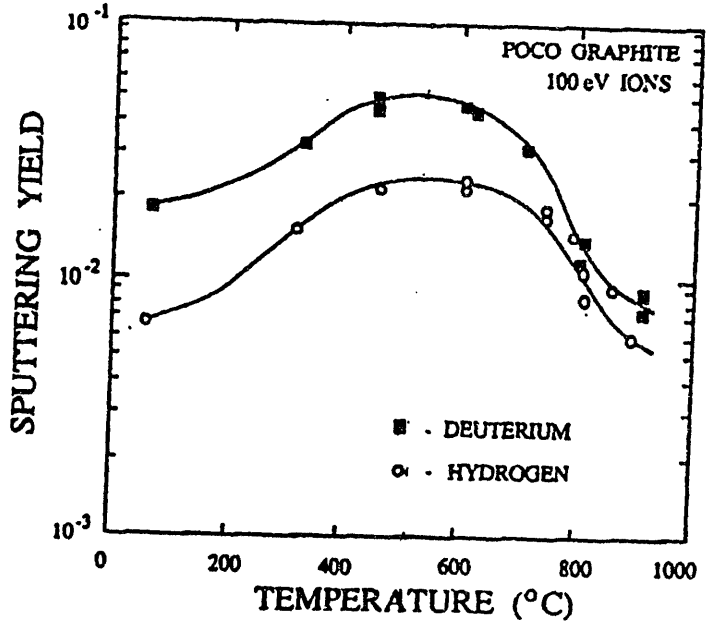

COMPARISON OF GRAPHITES DURING PLASMA BOMBARDMENT

- POCO, ATJ, AND PYROLYTIC GRAPHITES HAVE SIMILAR SPUTTERING YIELDS DURING PLASMA BOMBARDMENT
- 3-D GRAPHITE WEAVES (USED IN ALT-I) PERFORMS AT LEAST AS WELL AS THE STANDARD GRAPHITES TESTED

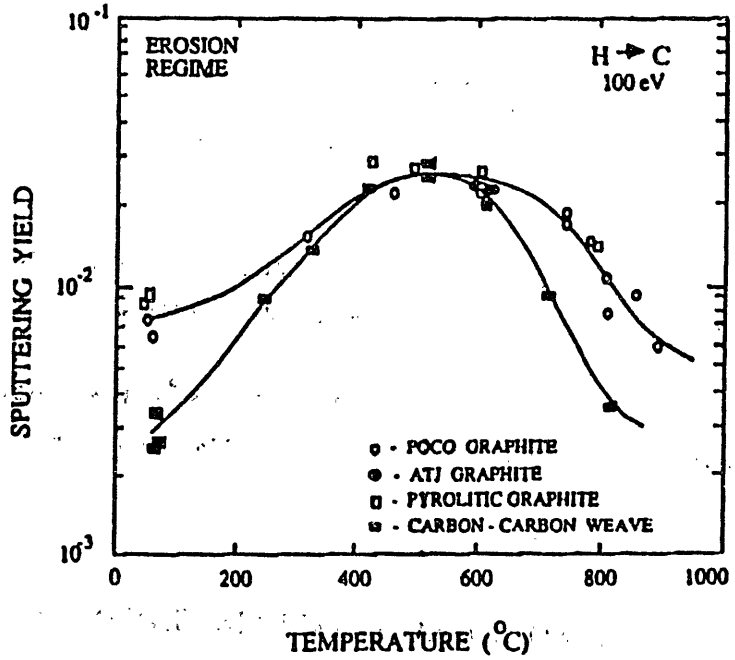

Japanese Efforts on Characterization of Isotropic Graphite Materials for Fusion Reactor

Toshiro Yamashina

Hokkaido University

Abstract

Current activities of Japanese university linkage for characterization of isotropic graphite materials were introduced briefly.

In this research project, 15 graphite materials from 7 Japanese companies have been selected as common testing materials.

Now, characterization of those graphite materials is beeing made by 15 different institutes, in terms of their structure and physical properties from the viewpoint of plasma-wall-interactions.

Special Research Project on Nuclear Fusion

MOE, Japan

Plasma-Wall Interactions Research Group

1986 - 1987

May,	1986	Selection of Candidate Graphite Materials (7 companies)
May,	1986	Group Meeting on PWI Research (Tokyo)
July,	1986	Delivery of 13 Kinds of Graphite to 13 Groups
July,	1986	Domestic Research Meeting on PWI Research (Sapporo) 23 papers presented
Nov.,	1986	Mid-term Meeting on Graphite Materials (Tokyo)
Jan.,	1987	Group Meeting on Graphite Materials (Sapporo) 13 people makers 15 people universities
Mar.,	1987	Final Meeting 1986 on Graphite Materials (Tokyo)
June,	1987	Publication of Report on Graphite Materials

昭和60年12月16－17日
「核融合装置用黒鉛材料の総括的検討と問題点の整理」研究会

1. 共通試料の選択 Selection of Candidate Graphite Materials
黒鉛材料－Isotropic
Anisotropic

2. 表面分析手段の選択 Selection of Characterization Techniques

3. 真空工学的特性評価 Vacuum Engineering
1） 構造と物性
2） 表面形態－マクロ（SEM）
ミクロ（SRF）
3） 気体放出

4. PWI的特性評価 Plasma Wall Interactions
1） エロージョン
2） スパッタリング－Physical
Chemical
3） リサイクリング－水素打ち込み
分布状態
放出過程
4） 重照射
5） トリチウム

5. 熱的・機械的特性評価 Thermal and Mechanical
1） 熱サイクル安定性
2） フラクチュアタフネス

Research Project Characterization of Graphite and Ceramic Materials for Nuclear Fusion

研究計画の概要と方法

核融合炉内材料としての
各種黒鉛とセラミックス
の特性評価

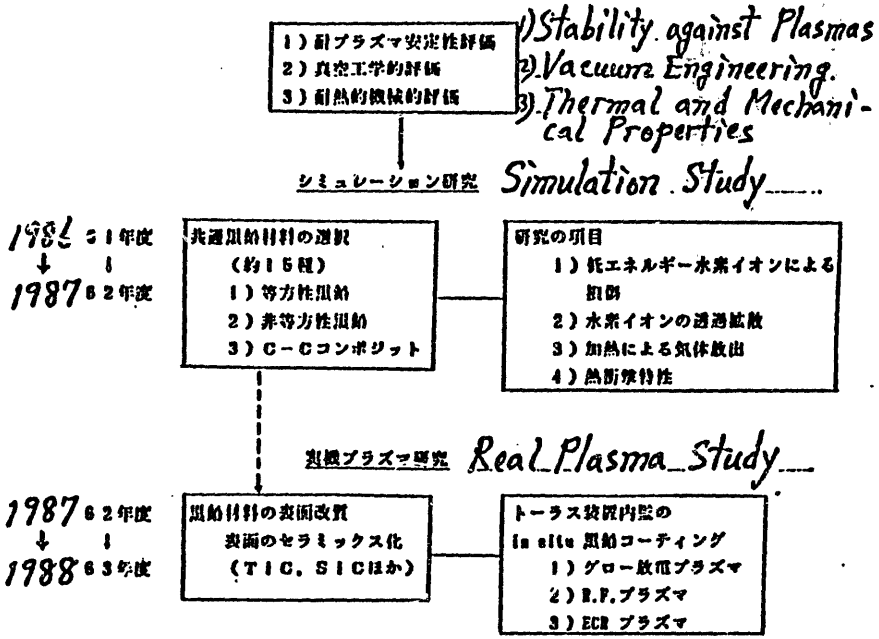

研究の特色

1）各種表面計測手段の活用（科研費による既設設備、の有効利用）
2）実機プラズマの新材料合成への応用
3）大学と官公庁研究機関の協力（実験的研究）
4）民間企業との協力（試料提供、材料開発試験ほか）

昭和６１年度
エネルギー特別研究（核融合）　炉材料及びプラズマ壁相互作用

核融合炉黒鉛材料の特性評価研究グループ（代表者　山科俊郎）

RESEARCH GROUPS OF CHARACTERIZATION
Common Candidate Graphite

研究機関　　研究評価項目

1．北大工　　黒鉛の真空工学的特性評価
Hokkaido Univ.　　VACUUM ENGINEERING

山科俊郎　・全体の総括
日野友明　・ＴＤＳによる脱ガス測定　Thermal Desorption
広畑優子　・ＳＲＦの測定　Surface Roughness Factor
福田伸　・大線量イオン源による照射後，脱ガスとＳＲＦの測定　Hydrogen Ion Irradiation
T. Yamashina

ISOTROPIC GRAPHITE Common Material
共通候補材料（等方性黒鉛）

会社名	VACUUM ENGINEERING 第１種（真空工学的特性）(dense carbon)	THERMAL-MECHANICAL 第２種（熱的機械的特性）(porous carbon)
イビデン IBIDEN	Ｔ－６	ＥＴ－１０
東洋炭素 TOYO TANSO	ＩＳＯ－８００	ＩＧ－１１０
東洋カーボン TOYO CARBON	ＭＴ－Ｋ	ＡＸ－６５０Ｋ
東芝セラミックス TOSHIBA CERAMICS	ＣＰ－１０１ＰＦ	
新日鉄化学 NIPPON STEEL CHEM.	Ｐ－８８０	Ｐ－７８０
東海カーボン TOKAI CARBON	Ｇ－１９５０ＳＳ	Ｇ－３４７Ｓ
日立化成 HITACHI CHEM.	ＨＣＢ－１８（Ｓ）	ＰＤ－６００

6．京大Ｈ研 Kyoto Univ. 野田信明 N. Noda	炭素膜作成と評価 ヘリオトロンＥでカーボニゼーションしたあと膜の評価	IN SITU CARBON COATING Carbonization of Wall Surface of Heliotron E
7．京大Ｈ研 Kyoto Univ. 赤石慎也 N. Akaishi	Ｄ／Ｈの置換 ＤとＨの置換とリテンションの実験的評価	RECYCLING D/H Retention and Replacement D/H in Graphite
8．名大Ｐ研 Nagoya Univ. 川村孝式 K. Kawamura	黒鉛の耐プラズマ安定性の評価 データに関する検討 ＰＷＩのモデリング	THEORETICAL ANALYSIS Analysis of Experimental Data Modeling in PWI
9．理研 RIKEN 坂本雄一 Y. Sakamoto	ＥＣＲプラズマによる炭素膜の作成 ・水素濃度の評価 ・ＲＧとＥＣＲ膜の比較 ・放電パラメータと膜の性質との関係	CARBON COATING BY ECR PLASMA Comparison of Coatings by RG and ECR

2．阪大工 Osaka Univ. 田辺哲朗 I. Tanabe	低エネルギー水素イオンによる黒鉛のエロージョン ・加熱脱ガス測定 ・水素イオンによる表面損耗と表面改質	EROSION / HYDROGEN IONS Thermal Desorption Erosion and Modification
3．富山大 Toyama Univ. 渡辺国昭 K. Watanabe	黒鉛とトリチウムの相互作用 ・Ｈ、Ｄ、Ｔの昇温脱離と同位体効果 ・黒鉛中の水素同位体の捕獲状態 ・Ｔインベントリー	TRITIUM / GRAPHITE INTERACTIONS T-inventory Isotope Effect H, D, T
4．東大工 Univ. Tokyo 山脇道夫 M. Yamawaki	黒鉛中の水素透過と拡散 ・水素注入後、水素透過と再放出試験及び蒸気圧と熱拡散率の評価	PERMEATION, DIFFUSION Hydrogen Permeation in Graphites
5．名大工 Nagoya Univ. 雨宮進 S. Amemiya	黒鉛中の水素の定量測定 ・微量不純物の測定 ・水素同位体の吸蔵と放出	QUANTITATIVE ANALYSIS / H Diffusion of Hydrogen Impurities in Graphite

13. 横浜国大 Yokohama Univ. 宇佐実誠二 S. Usami	水素リサイクリングにおける粒子の表面反射現象 ・低速水素原子との表面反応と付着確率 ・仕事関数測定による電子放出能	HYDROGEN RECYCLING Surface Reaction and Sticking Probability of Atomic H
14. 阪大工 Osaka Univ. 三宅正宣 M. Miyake	被覆炉内材料の熱的疲労特性 ・熱衝撃と熱サイクル試験（電子ビーム）	THERMAL FATIGUE Stability of Graphites against Thermal Shock and Cycle
15. 豊技科大 Toyohashi T. Univ. 逆井基次 M. Sakai	黒鉛材料の亀裂進展低抗性 ・破壊力学パラメータの測定と評価 ・高温度下、真空下での破壊試験	FRACTURE TOUGHNESS Fatigue Examination in Vacuum at High Temperature
10. 電総研 Elec. Tech. Lab. 清水肇 H. Shimizu	低エネルギー水素イオンによる黒鉛のエロージョン ・マイクロ波イオン銃による水素イオン照射 ・レーザによる微量分析	EROSION BY LOW ENERGY H Erosion of Graphites by Large Flux H^+ with Low Energy
11. 金材研 NRIM 岡田雅年 M. Okada	黒鉛の熱サイクルの安定性 ・赤外及び電子線による熱サイクル試験 ・電子線による熱衝撃試験	HEAT CYCLE STABILITY Heat-Cycle Examination by IR and Electron Beams
12. 名大工 Nagoya Univ. 森田健治 K. Morita	低エネルギーイオンと炉材料の相互作用 ・黒鉛中の水素イオンのリテンション ・希ガスイオンのリテンション	INTERACTIONS WITH LOW ENERGY H Retention of Hydrogen Ions in Graphites

Isotropic Graphite Materials

等方性黒鉛材料

構造 Structure	物性 Property	PWI特性 PWI
嵩密度 Density	熱伝導度 Thermal Conductivity	気体放出量 Thermal Gas Desorption
内部表面積 Inner Surface Area	電気伝導度 Electric Conductivity	気体吸脱着 Adsorption & Desorption
結晶粒径 Crystal Size	破壊強度 Fracture Toughness	水素透過性 Hydrogen Permeation
気孔径、気孔長 Pore Size	熱膨張係数 Thermal Expansion	高温強度 High Temp. Strength
気孔率 Pore Density	通気率 Gas Diffusion	熱伝導性 Conductivity
不純物 Impurity		プラズマ安定性 Stability against Plasmas (Sputtering, Erosion....)

黒鉛材料の細孔分布は？

細孔分布の制御は可能か？

What are Pore Size and Ditribution ?

Can We Control Pore Structure of Graphite ?

Carbon Erosion processes for CIT and ETR applications

A.A. Haasz
University of Tronto

Abstract

Graphite has been identified as a primary candidate material for next generation Tokamak (eg, CIT, ETR). Under plasma exposure, graphite erosion occurs through physical sputtering, chemical erosion and radiation-enhanced sublimation. The temperature regimes where these processes dominate the erosion have been identified, and the dependence of erosion yield on graphite temperature and incident plasma particle (H^+, H^0, H_e^+) energies and fluxes have been discussed. The effects of surface and bulk impurities in graphite, as well as oxygen impurity in the plasma, on the erosion rate have been considered.

PHYSICS BACKGROUND OF CARBON

A.A. Haasz
University of Toronto

Scope :

" Laboratory studies aimed at understanding the physical/chemical mechanisms/processes occurring during fusion plasma-materials-interactions, with the objective of making MACHINE-RELEVANT projections of the effects of such processes "

PLASMA PARAMETERS (affecting materials)

Current machines

- energetic ions & charge exchange neutrals
  10's eV – keV's
  fluxes: at limiters : $10^{18} - 10^{19}/cm^2 s$
  at walls : $\sim 10^{16}/cm^2 s$
- Franck-Condon neutrals (few eV energy)
  fluxes: at limiters : $10^{18} - 10^{19}/cm^2 s$
  at walls : $\sim 10^{16}/cm^2 s$
- electrons
- photons
- graphite temperatures :
  up to ~ 1800 K during excursions

Future machines

- in addition to above :
- neutron irradiation
- tritium exposures
- graphite temperatures :
  up to ~ 1800 K without active cooling

EFFECTS ON MATERIALS

Structural effects due to : - fluctuating thermal loads
- neutron irradiation
- etc

Modification of surfaces of plasma-facing materials
- erosion
- redeposition/co-deposition
- H-retention/recycle

Focus of this presentation :

EROSION OF GRAPHITE

viz., our understanding of the erosion processes based on controlled Laboratory experiments

Next presentation (by Dr. Itoh) will deal with some attempts at modelling the erosion processes

1. PHYSICAL SPUTTERING
   - hydrogen (D^+)
   - self-sputtering (C^+)
2. RADIATION-ENHANCED SUBLIMATION (RES?) $T > 1200\,K$
3. CHEMICAL EROSION (due to hydrogen)
   - thermal H° atoms
   - energetic H^+ ions
   - synergistic erosion (thermal H^+ and energetic H^+ or A_r^+)
     - methane formation
     - heavy hydrocarbons
4. CHEMICAL EROSION (due to oxygen)
   - thermal O_2
   - energetic O^+
5. EFFECT OF IMPURITIES ON EROSION

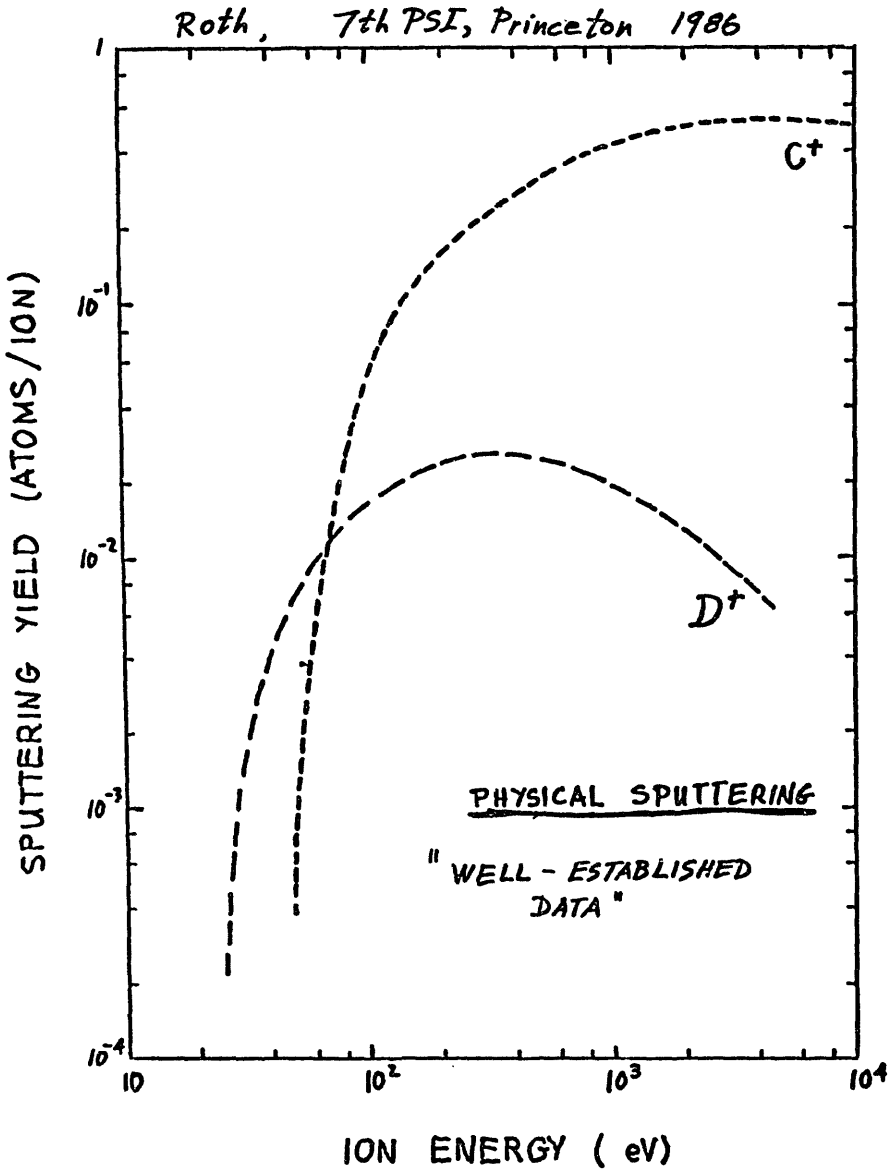

2. RADIATION - ENHANCED SUBLIMATION (RES)

- occurs for $T \gg 1200$ K
- RES is not due to chemical reactions (it also occurs for inert gases, eg. He^+, Ar^+)
- monatomic C is released (for thermal sublimation, C_2 and C_3 clusters dominate)
- the erosion yield (at fixed T) scales with the deposited energy (via nuclear collisions) for various ion energies and ion masses

Roth et al	5th PSI, Gatlinburg (1982)
Philipps et al	5th PSI
Roth et al	FRM, Albuquerque, 1984
Roth et al	6th PSI, Nagoya, 1984

RES MODELS

- energy deposited in surface layer, Roth et al FRM, Alb. 1984
- energy deposited over ion range profile, Roth & Möller Nucl. Inst. Meth in Phys Res. B7/8, (1985) 788
- time-dependence of eroded C flux, Philipps et al. (submitted ?)

models are based on formation of interstitial C atoms, diffusion of C to surface and release of C at surface

CHEMICAL EROSION ($H^0 \rightarrow C$)

STEADY-STATE CH_4 FORMATION

(sub-eV H^0 ON GRAPHITE)

Toronto, AVS 1985

Similar results by Vietzke et al (Jülich)

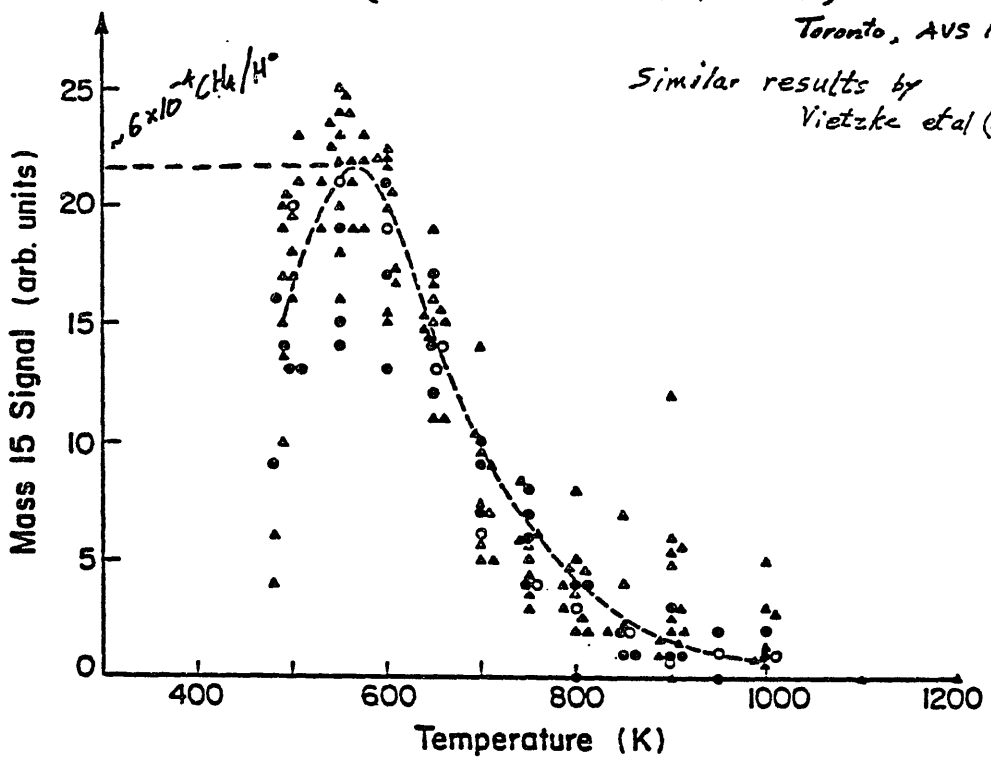

Roth et al, 5th PSI (Gattinburg) 1982

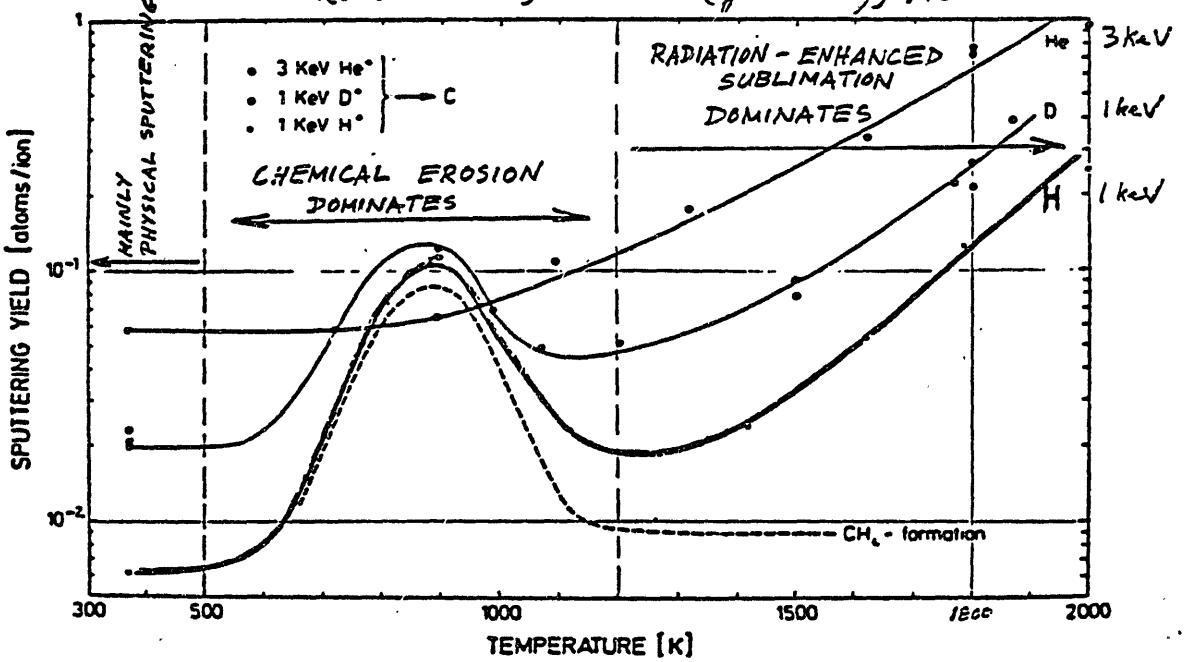

Fig. 1. Temperature dependence of the sputtering yield of PAPYEX carbon paper and pyrolytic graphite for 1 keV D^+ and H^+, & 3 keV He^+ bombardment as measured by weight loss. The yield due to CH_4 formation is indicated for hydrogen.

Also: Results for $Ar^+ \rightarrow C$, Philipps et al, [5.th PSI (Gattinburg)]

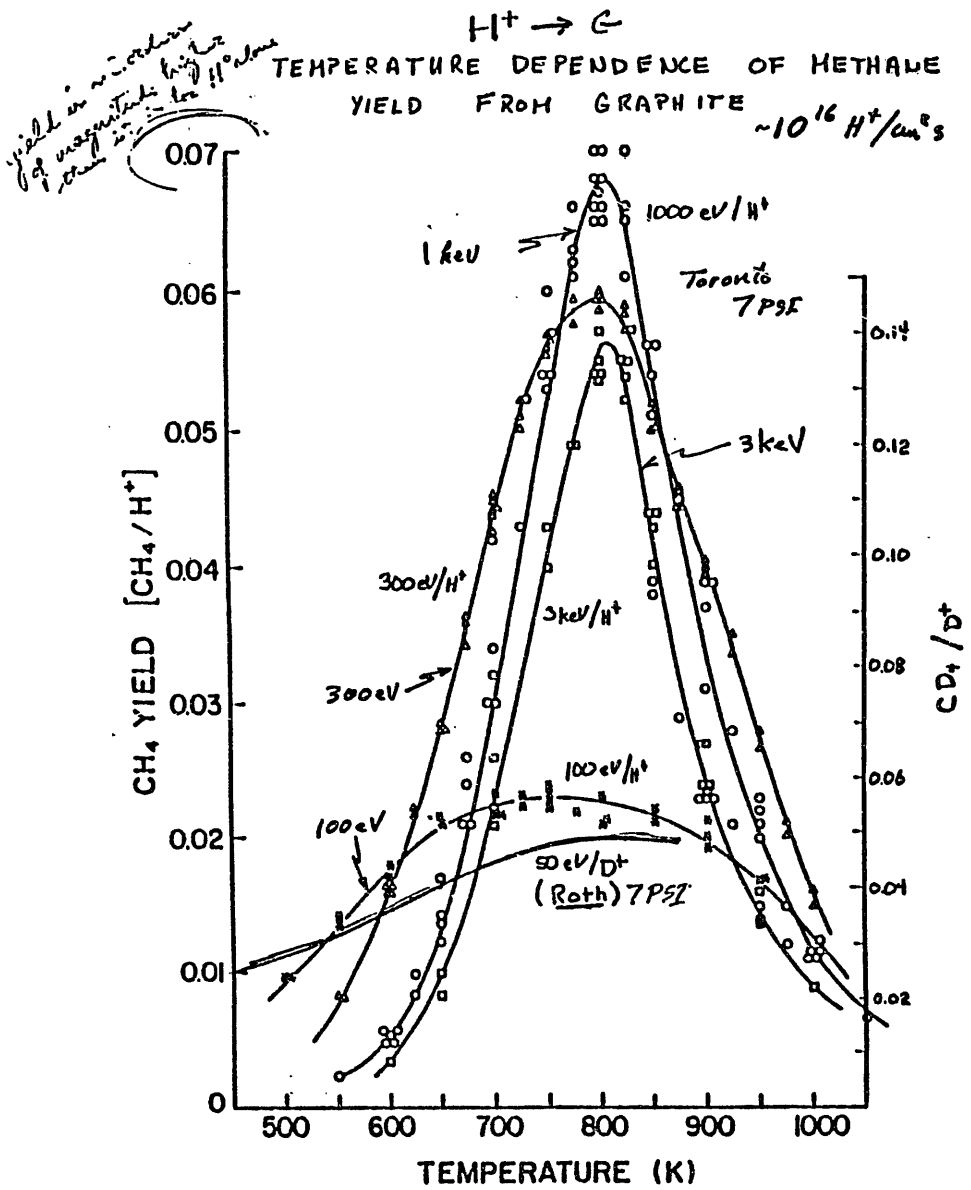

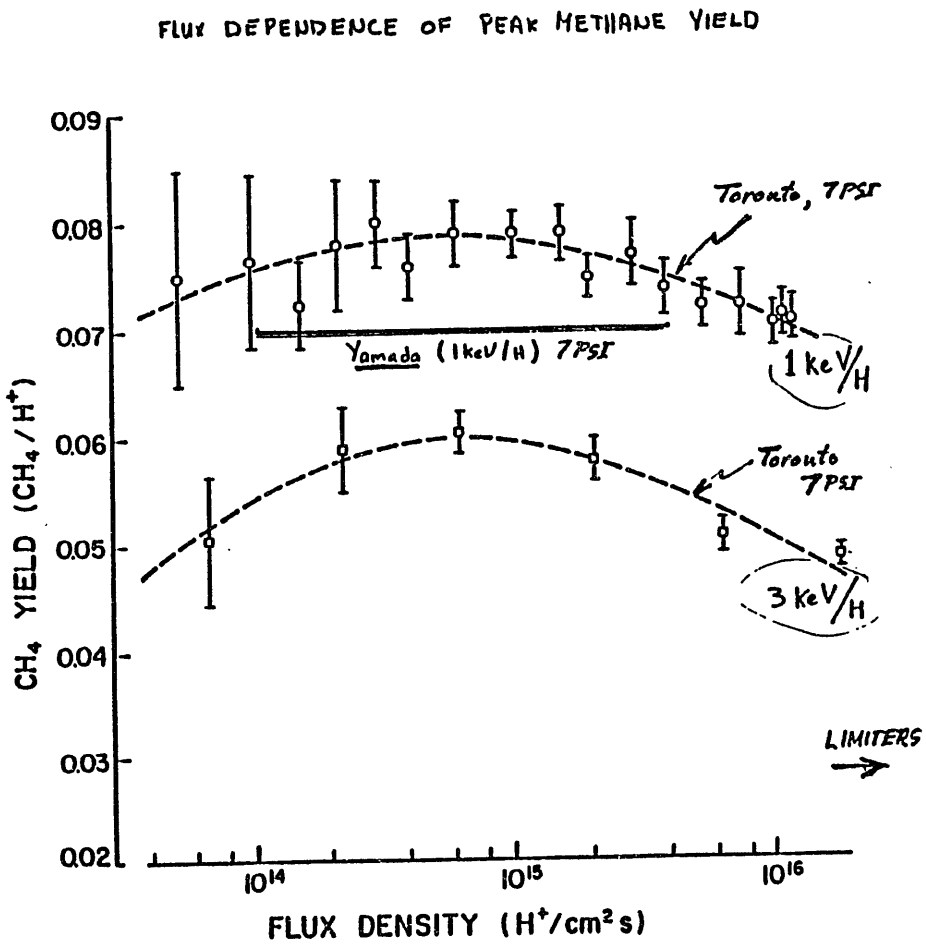

CH_4 YIELD AT T_{max}

CH_4 YIELD vs H^+ ENERGY

H^+ ON P.G.

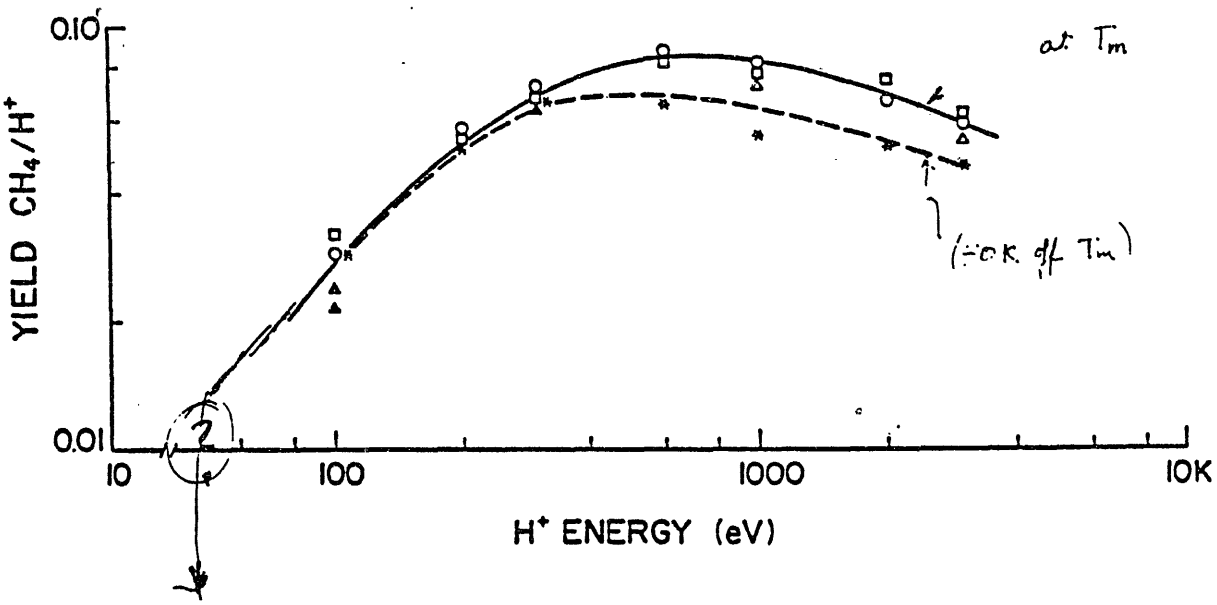

FLUX DEPENDENCE OF METHANE YIELD AT CONSTANT T

750 - 800K

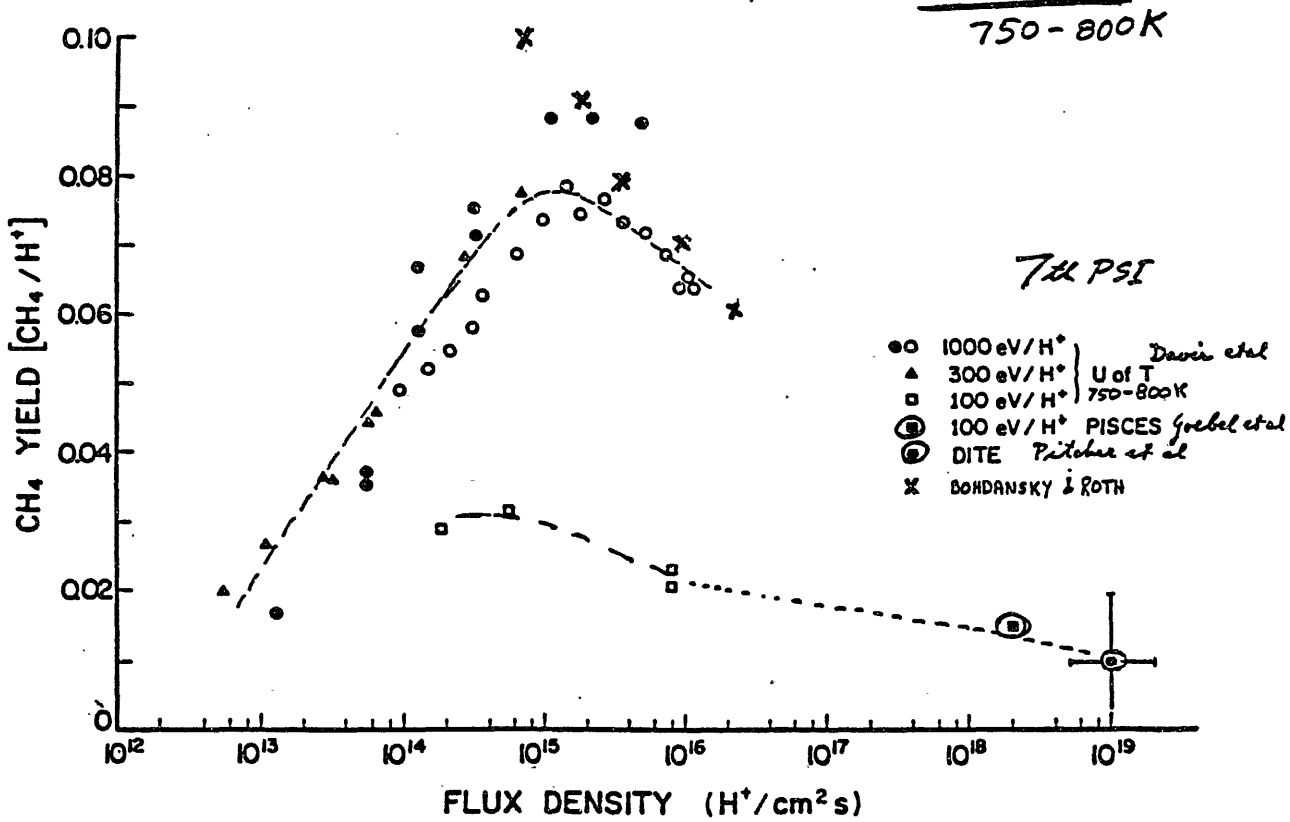

SYNERGISTIC CH_4 FORMATION

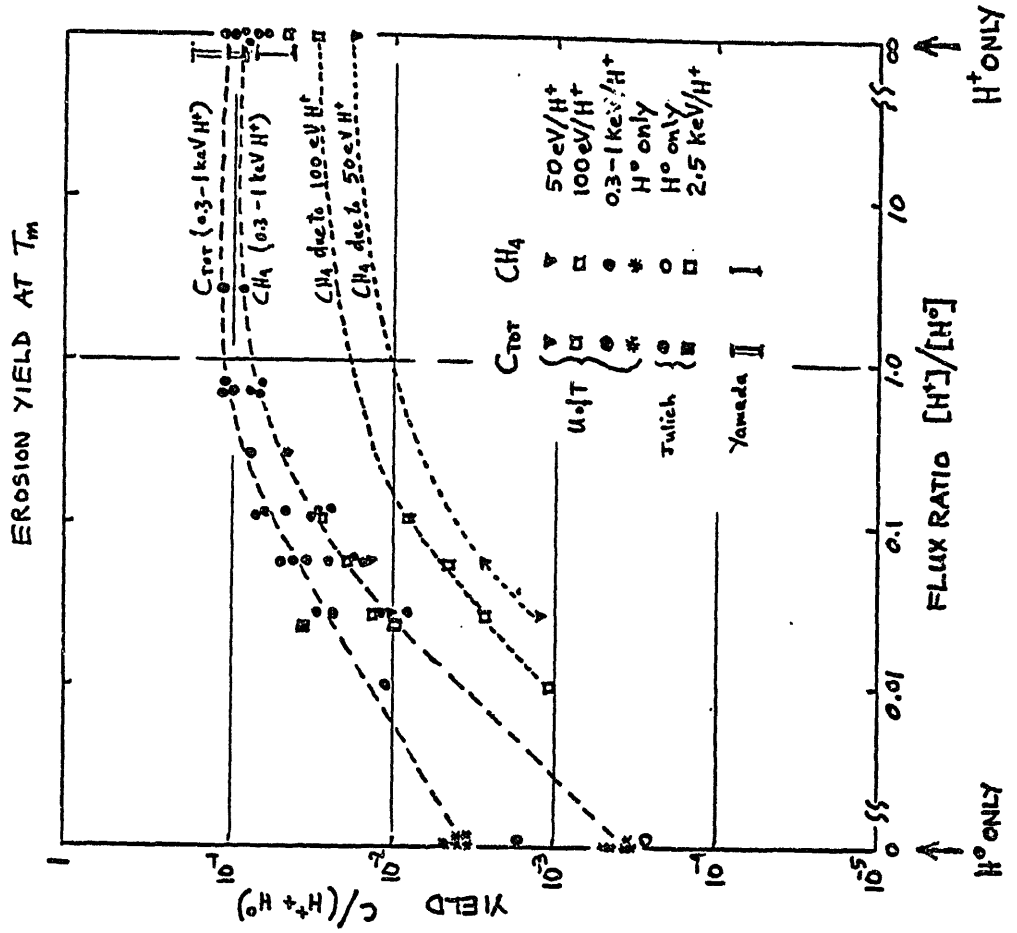

SYNERGISTIC CH_4 FORMATION

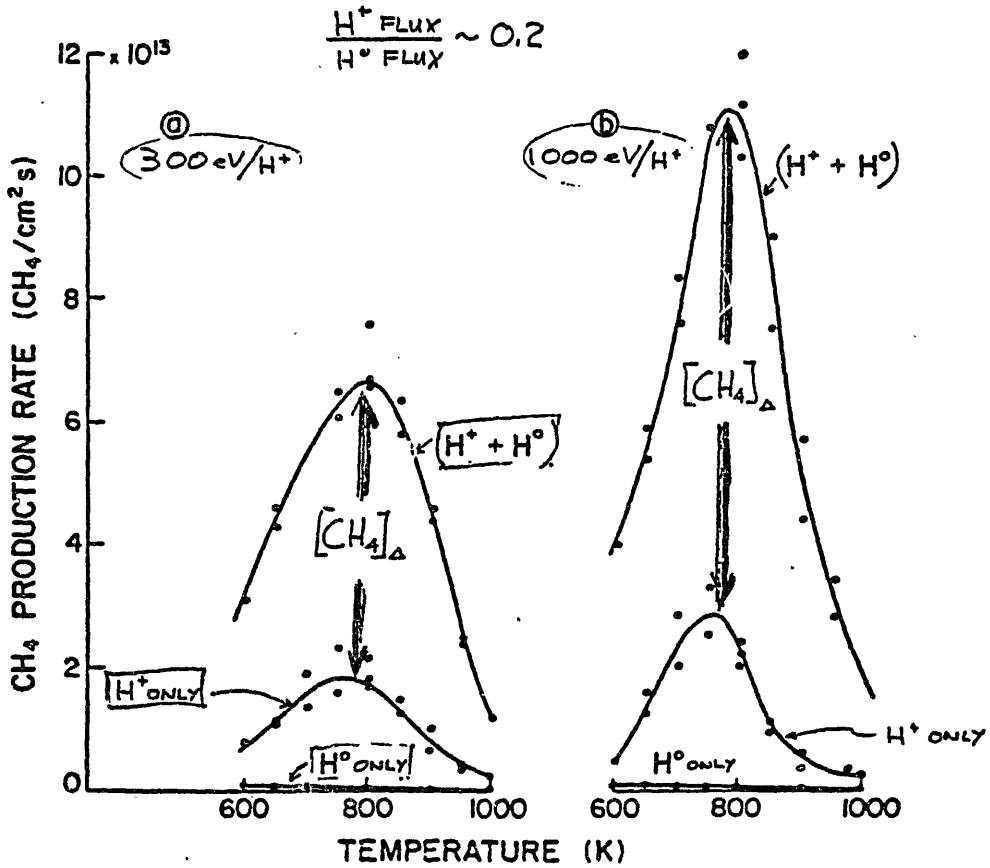

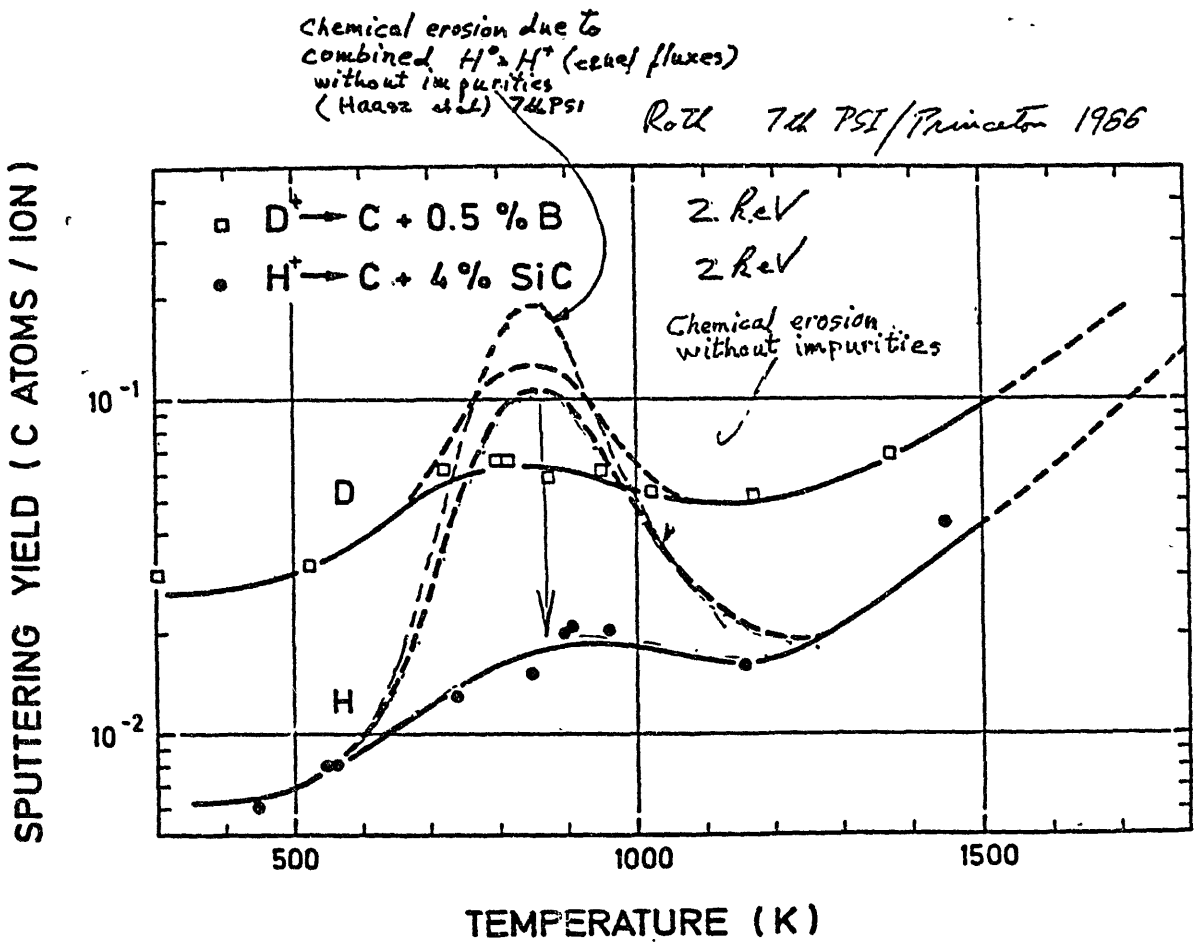

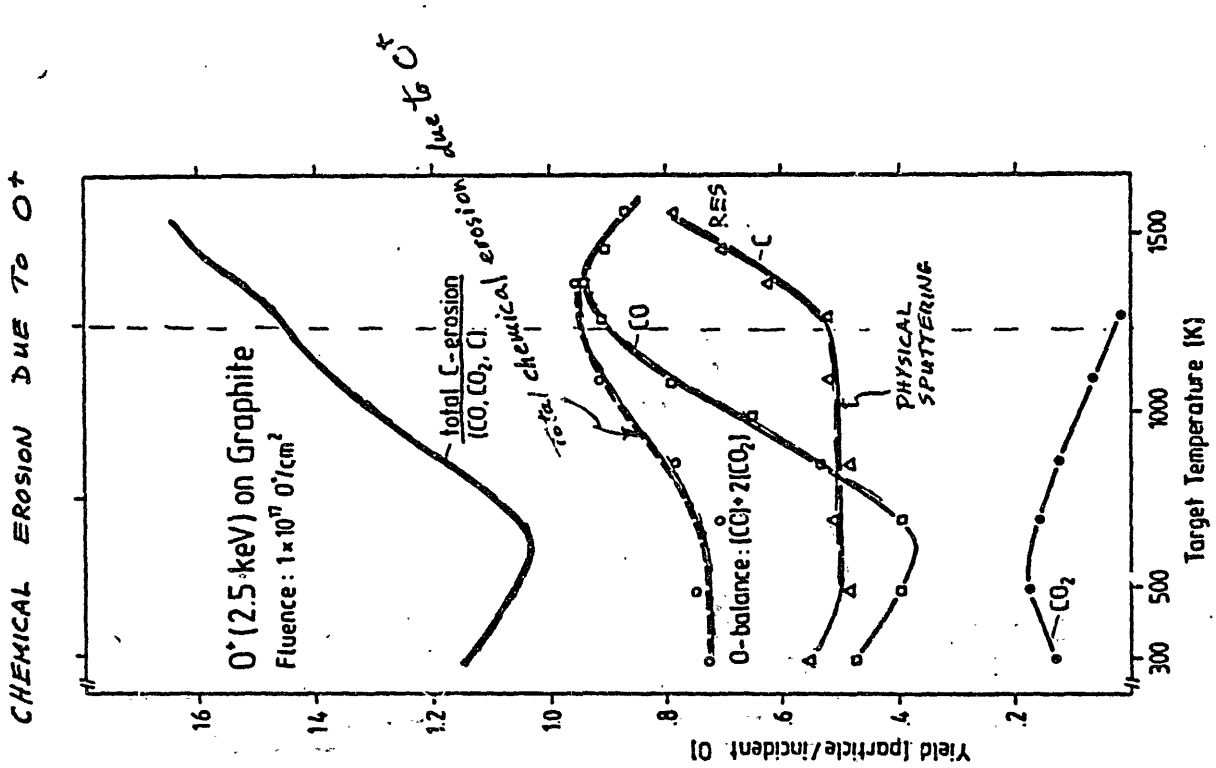

Vietzke et al. 7th PSI/Princeton 1986 (with Tanabe, Osaka U.)

SUMMARY

(i) PHYSICAL SPUTTERING

* extensive data available

(ii) RADIATION-ENHANCED SUBLIMATION

* ion-mass and energy dependence data available
* limited data for effect of impurities
  [Roth et al, 6th PSI, Nagoya 1984]
* need flux dependence data
* need data for < 50 eV (threshold for interstitial C formation)

(iii) CHEMICAL EROSION (due to hydrogen)

* extensive data available for : $< 10^{16}/cm^2 s$
  : > 50 eV energies
* limited data for fluxes $> 10^{16}$ $H^+/cm^2 s$
  [PISCES, Goebel et al, 7th PSI]
* need erosion data for : < 50 eV energies (threshold
  : $> 10^{16}/cm^2 s$ fluxes
* need data for synergistic erosion in presence of surface impurities

(iv) CHEMICAL EROSION (due to oxygen)

* limited data (e.g. Vietzke et al, 7th PSI)
* need data on flux dependence and influence of surface impurities

(v) CHEMICAL EROSION DUE TO COMBINED H^+ & O^+

* need controlled experiments!
  - flux dependence (flux ratio dependence)
  - ion energy dependence
  - graphite temperature
  - effect of impurities

(vi) REDEPOSITED OR CO-DEPOSITED CARBON

* limited data [Goebel et al, 7th PSI]
* does it behave as the co-deposited a-C:H films?
  Some erosion data on a-C:H films exist

  $H^0 \rightarrow$ a-C:H : 'high' level of erosion
  [Vietzke et al, 7th PSI]

  $H^+ \rightarrow$ a-C:H : erosion similar to graphite
  [Yamada, AVS, Baltimore 1986]
  [Davis & Haasz, submitted]

Semi- empirical equations for modelling of chemical erosion of graphite

Noriaki Itoh
Nagoya University

Abstract

A semi-empirical equations for modelling chemical erosion of graphite by energetic hydrogen ions have been developed. The equations are found to explain semi-quantitatively several important features, energy dependence, flux dependence and synergistic effects under simultaneous multi-particle irradiation.

SEMI-EMPIRICAL EQUATIONS FOR MODELING OF CHEMICAL EROSION OF GRAPHITE

Noriaki Itoh* and Yuji Horino**

* Department of Physics,
Faculty of Science, Nagoya University

** Department of Crystalline Materials Science,
Faculty of Engineering, Nagoya University

I. Empirical equations for chemical sputtering

II. Experimental results to be considered in deriving empirical equation

III. New empirical equations

IV. Results of calculation

V. Comparison with experimental results

VI. Concluding remarks

I. Empirical equations for chemical sputtering

[Requirement]

a. Simple
b. Including sufficient number of parameters that have well-defined physical basis

[Advantages of constructing empirical equations to compare experimental data with results of calculation]

a. To clarify the contribution of each elementary physical process on overall phenomena of chemical erosion
b. To single out the deficiency of the model used to construct the empirical equations
c. To approach the final goal, namely to construct the modeling codes for simulation of the behavior of walls, including reflection, erosion, hydrogen retention and re-emission

[Existing empirical equations]

a. Erents et al. (1976)

$$Y \propto \frac{e^{-Q_1/kT}}{\phi\sigma + \tau_0^{-1} e^{-Q_2/kT}}$$

describing temperature dependence of Y and the relation between the incident energy and the temperature T_M where the maximum sputtering yield occurs

b. Yamada (1986)

$$Y \propto (\phi f_d)^L (1 - B) \frac{e^{-Q_1/kT}}{\phi\sigma + \tau_0^{-1} e^{-Q_2/kT}}$$

a modification of the equation by Erents, describing energy and flux dependences of the maximum yield

c. Itoh and Hasebe (1986)

$$Q = \frac{\alpha\beta k_2 n}{\beta(k_1 + \alpha) + \alpha k_2}$$

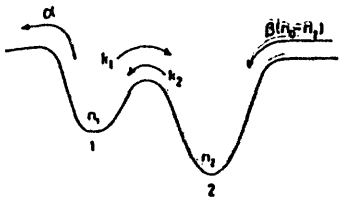

physical two-step model describing synergistic effects

d. Haasz and Davis (1986)

An elaborated equation describing temperature dependence of the yield for thermal hydrogen atoms and for energetic hydrogen ions and the synergistic effects

e. Present model

A modification of the physical two-step model so that it describes several features of chemical sputtering

II. Experimental results to be considered

1. Temperature dependence

a. quantities

Maximum yield Y_M

The temperature T_M where the maximum yield occurs

The half width T_H

b. phenomena

(i) Energy dependence of Y_M and T_M

(ii) Flux dependence of Y_M and T_M

(iii) The hysterisis effects

2. Energy dependence

a. quantities

(i) The energy E_M where the maximum yield occurs

b. phenomena

(i) The fact that E_M ranges near 0.2 keV in some experiments and 2 keV in others

(ii) Elastic stopping power takes a maximum near 0.2 keV

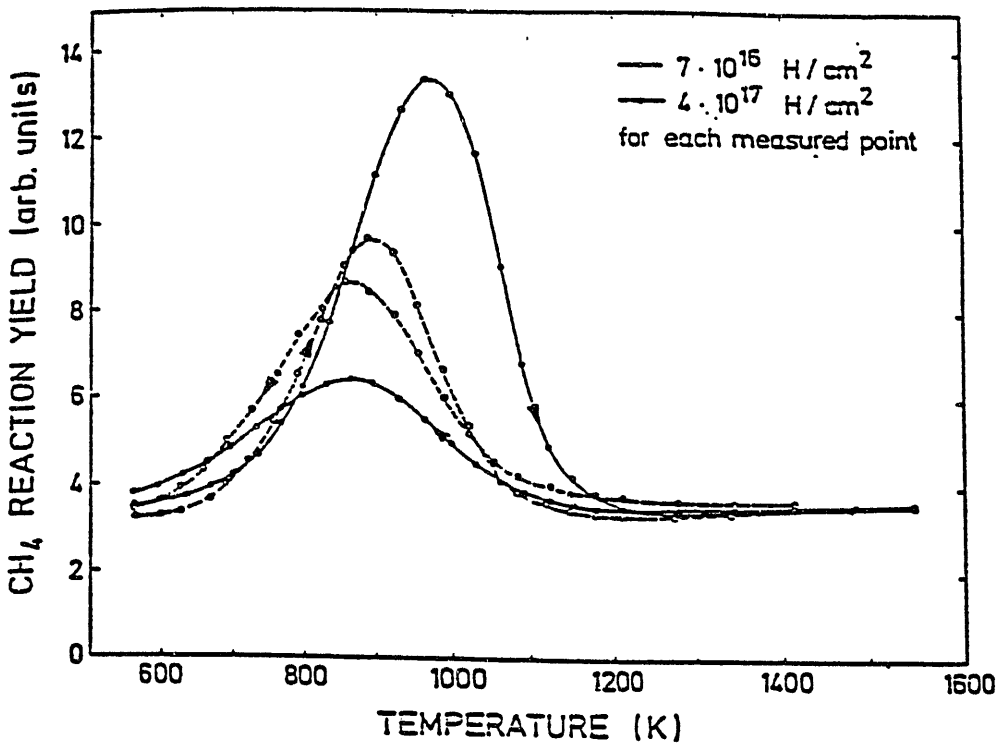
CH_4 REACTION YIELD (arb. units)
TEMPERATURE (K)
$7 \cdot 10^{16}$ H / cm^2
$4 \cdot 10^{17}$ H / cm^2
for each measured point
0
2
4
6
8
10
12
14
600
800
1000
1200
1400
1600

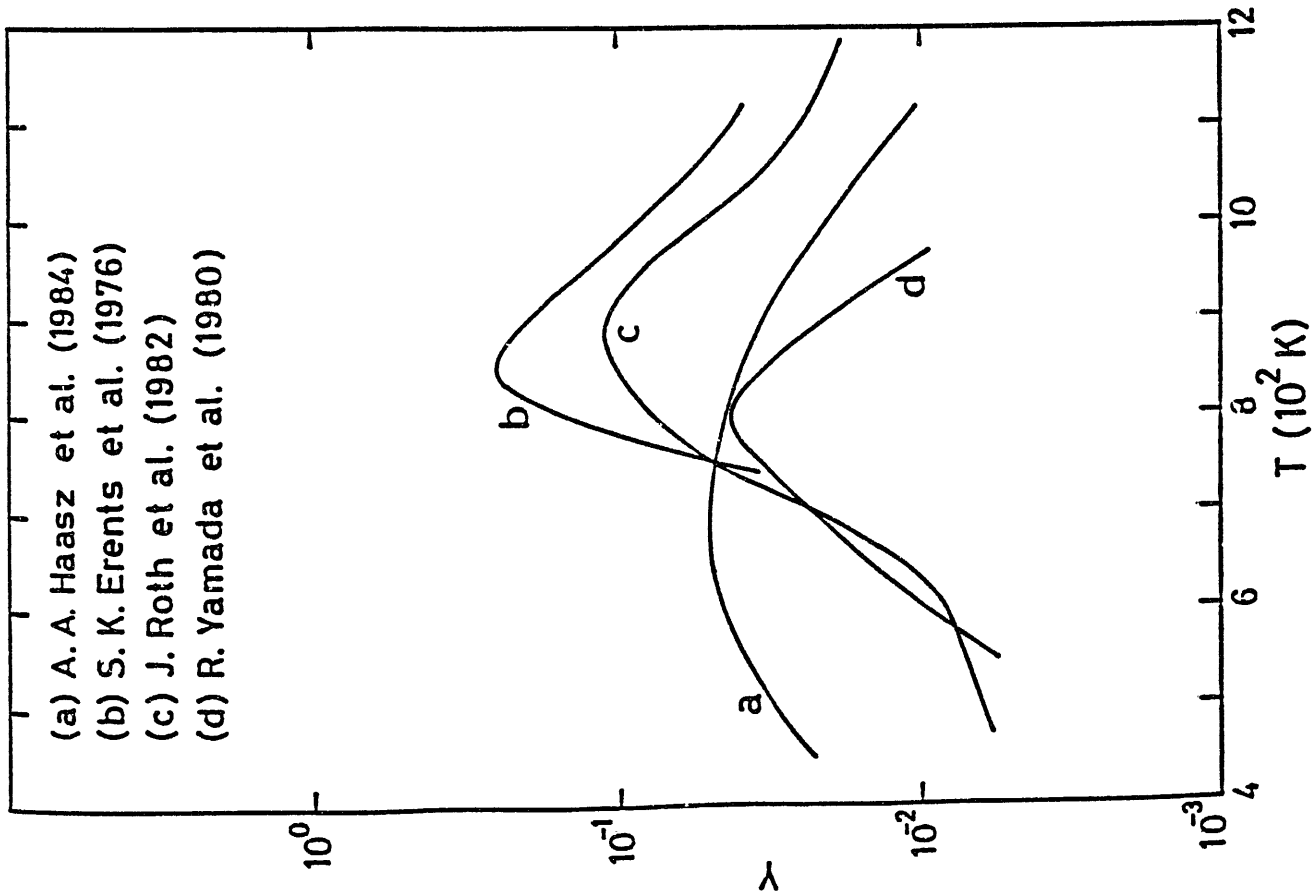
(a) A. A. Haasz et al. (1984)
(b) S. K. Erents et al. (1976)
(c) J. Roth et al. (1982)
(d) R. Yamada et al. (1980)
a
b
c
d
λ
10^0
10^{-1}
10^{-2}
10^{-3}
T (10^2 K)
4
6
8
10
12

III. Empirical equations

$$Q = \frac{\alpha \beta k_2}{\alpha k_2 + (\beta + \gamma)(\alpha + k_1)} n_0$$

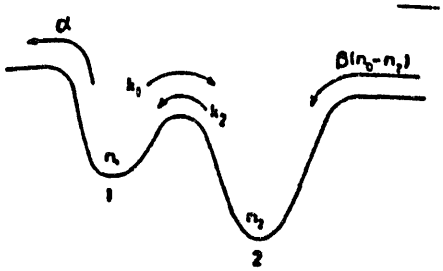

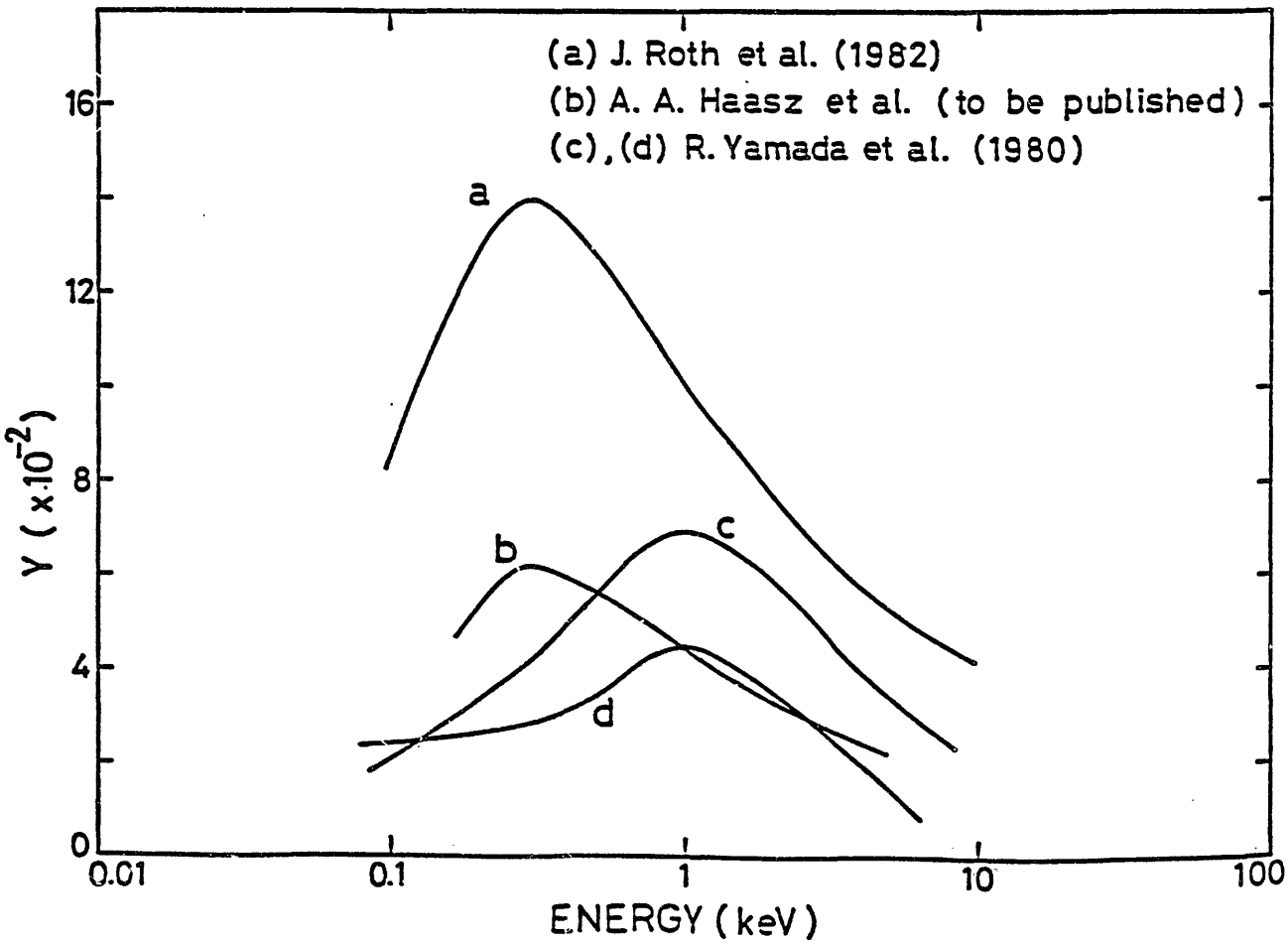

a. $k_1 \gg \alpha, \beta, k_2$

$$k_1 = \nu_1 e^{-E_1/kT}$$

$$Q \approx \frac{\alpha \beta k_2}{(\beta + \gamma) k_1} n_0$$

similar to Erents equation

b. γ back reaction

$$\gamma = c \nu_\gamma e^{-E_\gamma/kT}$$

c is a parameter representing the effective surface concentration of H and is needed to explain the hysterisis effects. Physically, it accounts for the fact that H_2 not H is released from the surface

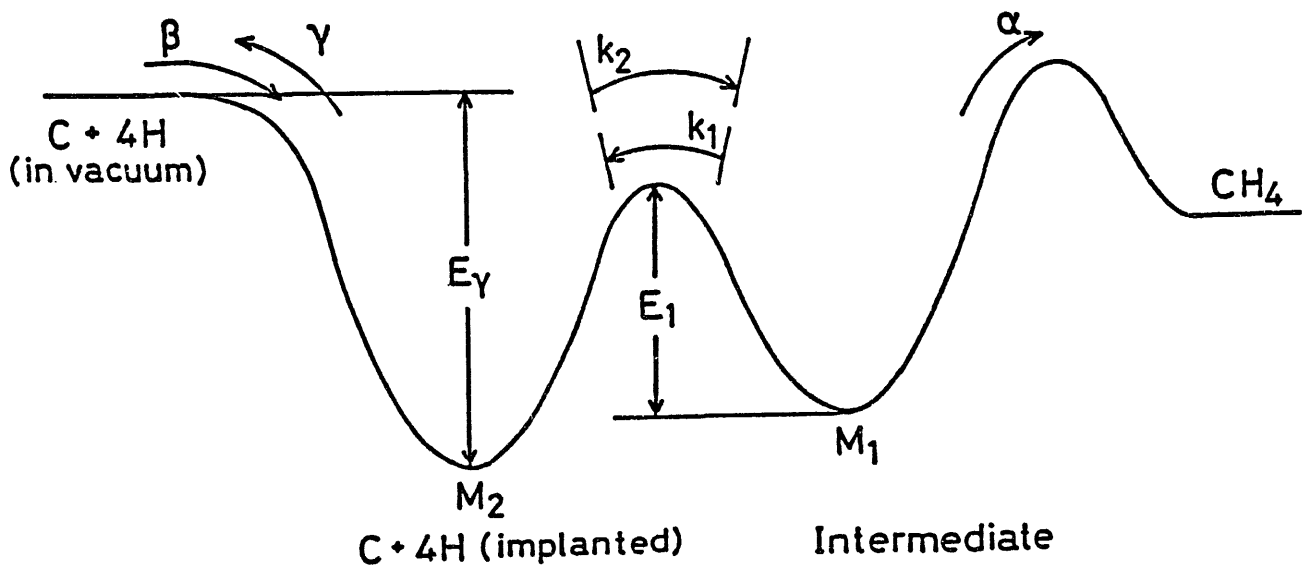

c. β is the rate of supply of H

$$\beta = \frac{\phi}{N_s} f$$

f: fraction of the implanting hydrogen atoms to be effective to chemical erosion

d. $$k_2 = \frac{\phi L}{N_s \epsilon} \frac{dE}{dx}\Big|_{nuclear}$$

ϵ average energy for knockons
L: effective thickness

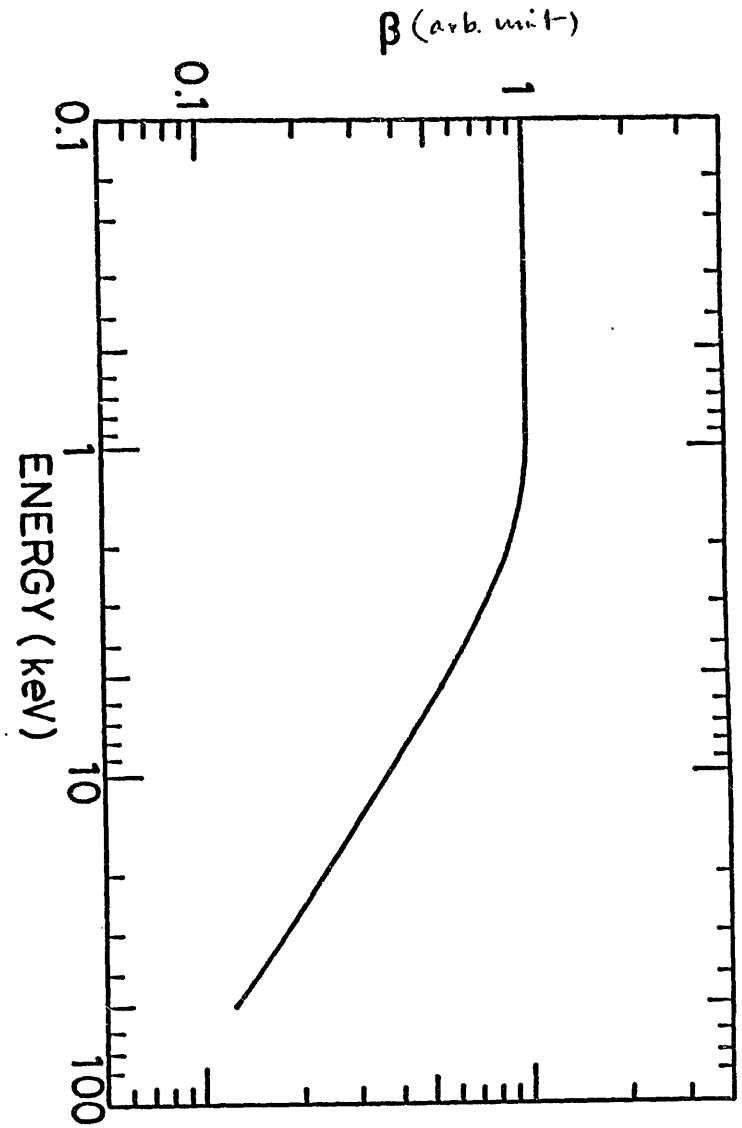

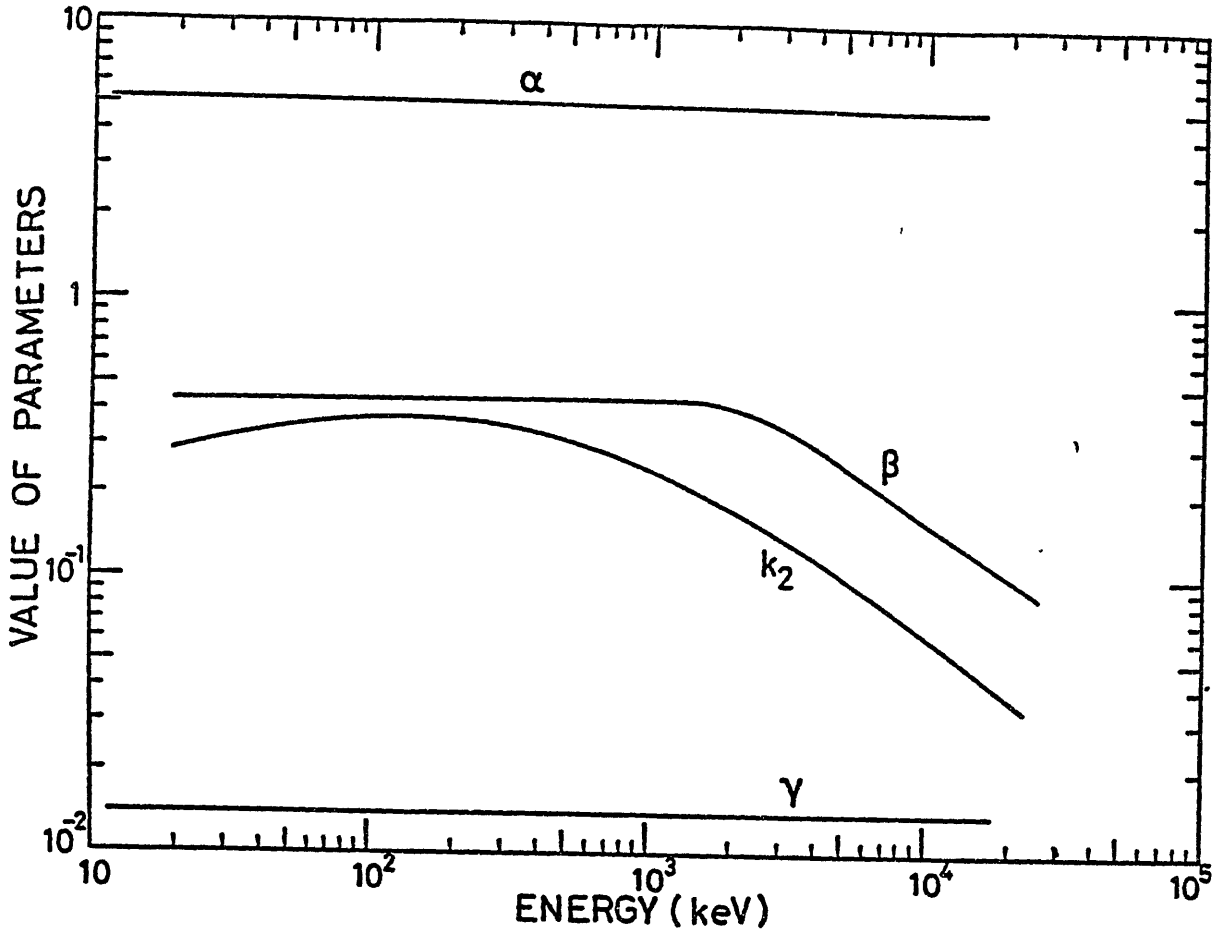

e. $\alpha = \nu_\alpha(c)e^{-E_\alpha/kT}$

ν_α may depend on c, since CH_4 is to be formed for desorption to take place

$$Q = \frac{\nu_\alpha \beta k_2 n_0}{\lambda} \frac{e^{-(E_\alpha - E_1)/kT}}{\beta + c\nu_r e^{E_r/kT}}$$

$$\gamma = \frac{\nu_\alpha(c)\beta_0 k_0 n_0}{\lambda} \frac{e^{-(E_\alpha - E_1)kT}}{\beta_0 + (c/\phi)e^{-E_r/kT}}$$

$(\beta = \beta_0\phi,\ k_2 = k_0\phi)$

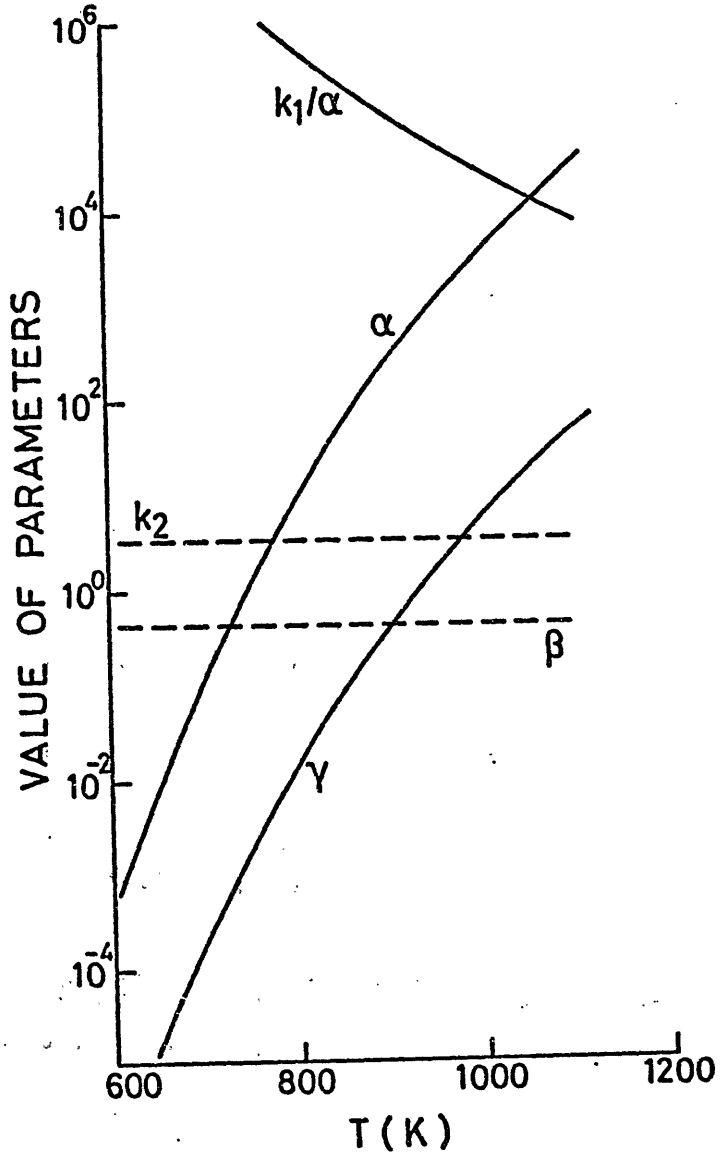

[parameters]

$E_\alpha - E_1 = 1.08$ eV

$E_\gamma = 2.04$ eV

(in accordance with Erents)

pre-exponential factors influence only the absolute values of Y

IV. Results of calculation

c: adjustable parameters

$\nu_\alpha(c)$ = const.

1. Temperature dependence for several c/ϕ (hysterisis)
   E dependence of T_M, Y_M and T_H for several c/ϕ

2. Energy dependence
   The calculated energy dependence takes a maximum near 0.2 keV

3. Synergistic effects
   Temperature dependence
   Dependence on the flux of incident ions

V. Comparison with experimental results
The value of c, the surface concentration is left as an adjustable parameter

1. Temperature dependence
a. Shape of the Y - T curves
(i) dependence on energy
(ii) dependence on flux
(iii) the hysterisis effect

2. Energy dependence
Existence of two types of energy dependence: dependence of T_M on E is weak in both cases
Characteristicis of $\nu_\alpha(c)$ (saturation of ν_α for low energy implantation)

3. Synergistic effects
Y - T curves
Flux dependence

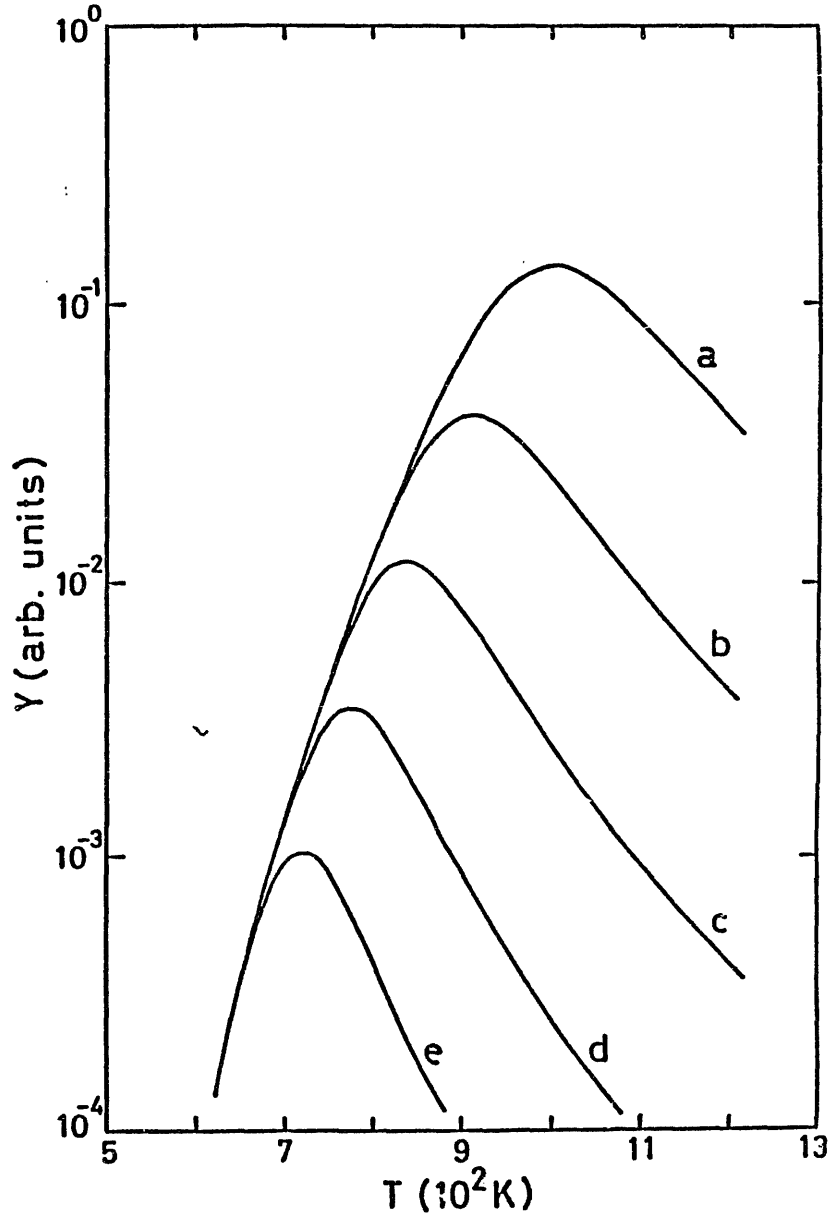

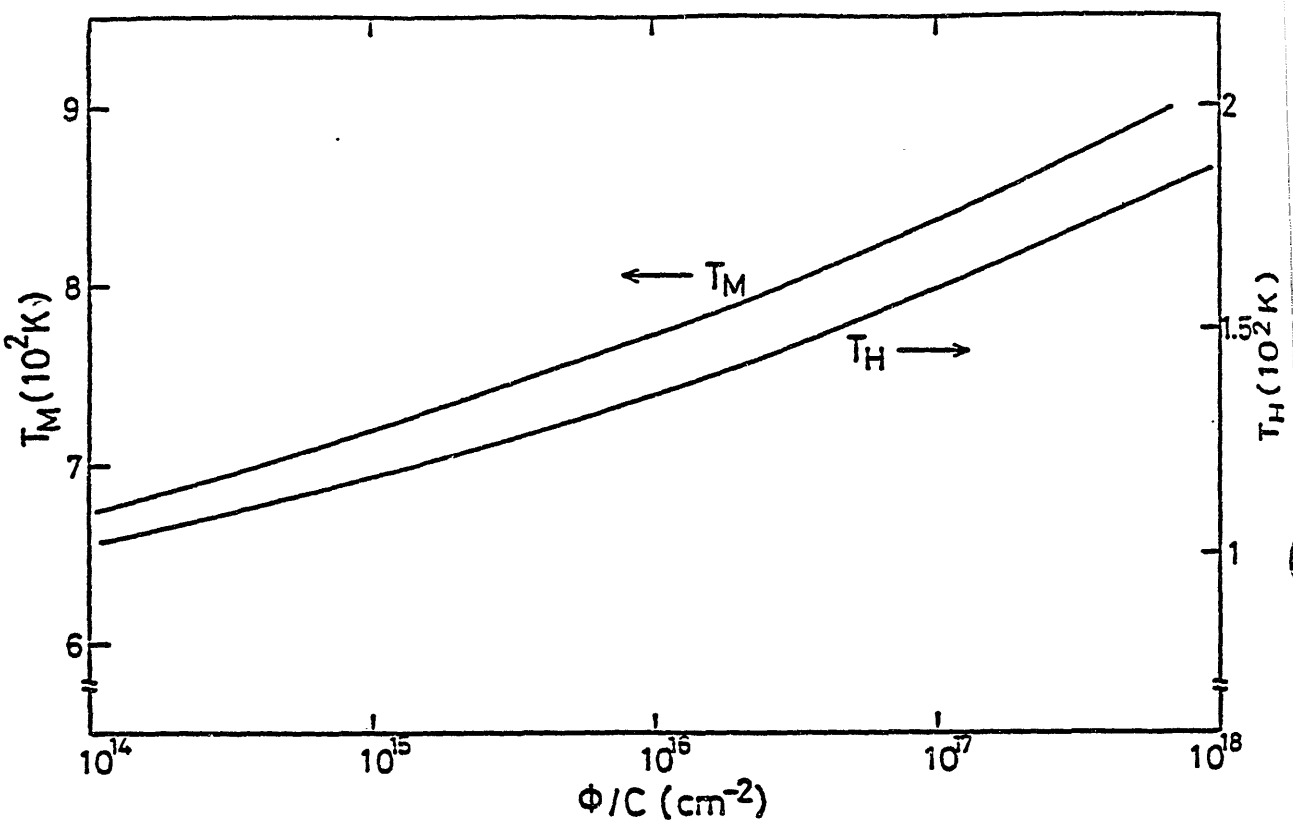
T_M (10^2K)
T_H (10^2K)
T_M
T_H
Φ/C (cm^{-2})

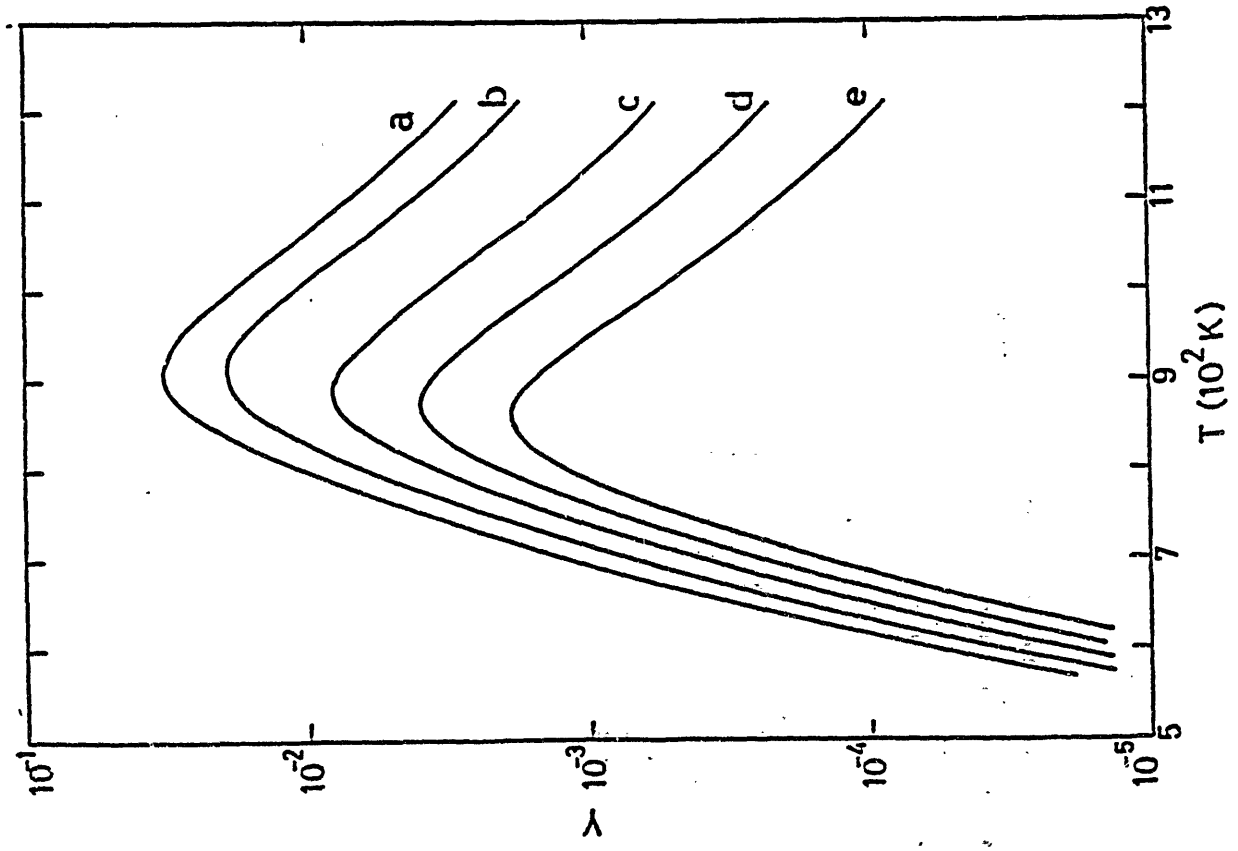
T (10^2K)
a
b
c
d
e
λ

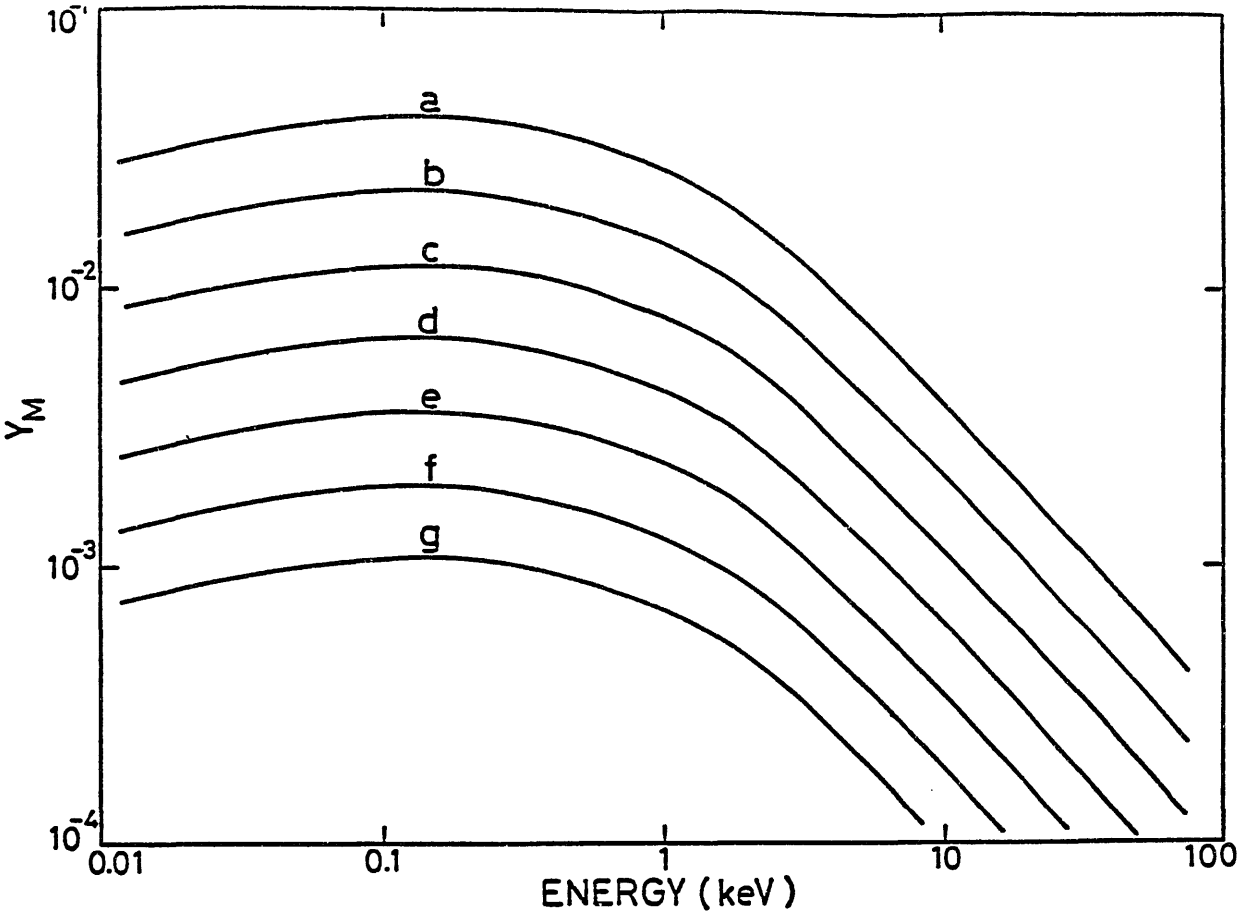
10^{-1}
10^{-2}
10^{-3}
10^{-4}
Y_M
a
b
c
d
e
f
g
0.01
0.1
1
10
100
ENERGY (keV)

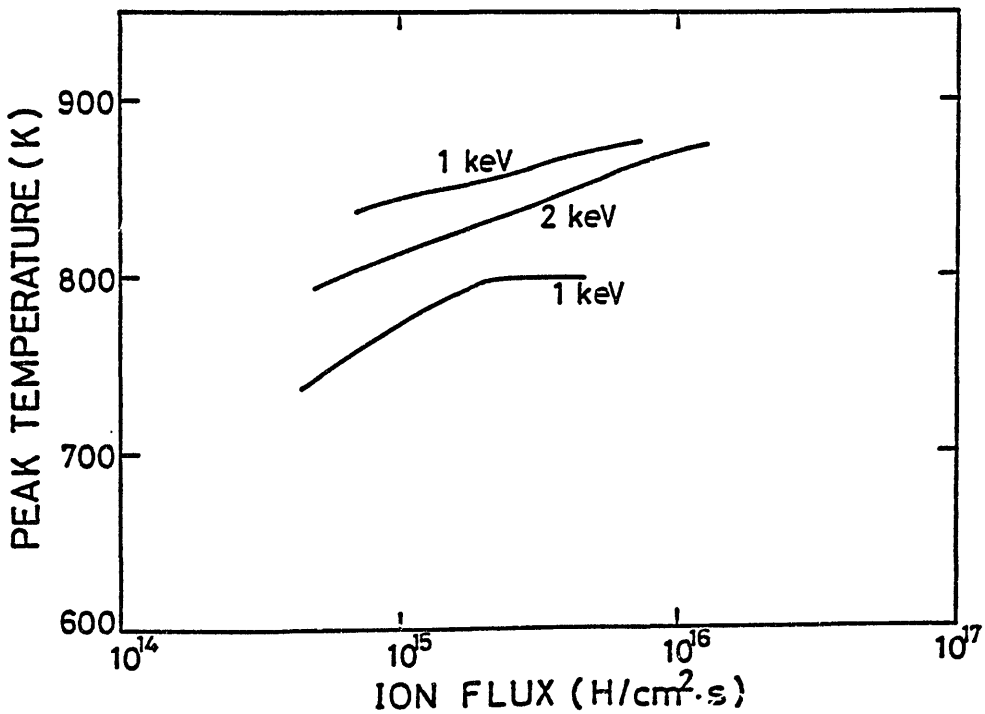
PEAK TEMPERATURE (K)
900
800
700
600
1 keV
2 keV
1 keV
10^{14}
10^{15}
10^{16}
10^{17}
ION FLUX ($H/cm^2 \cdot s$)

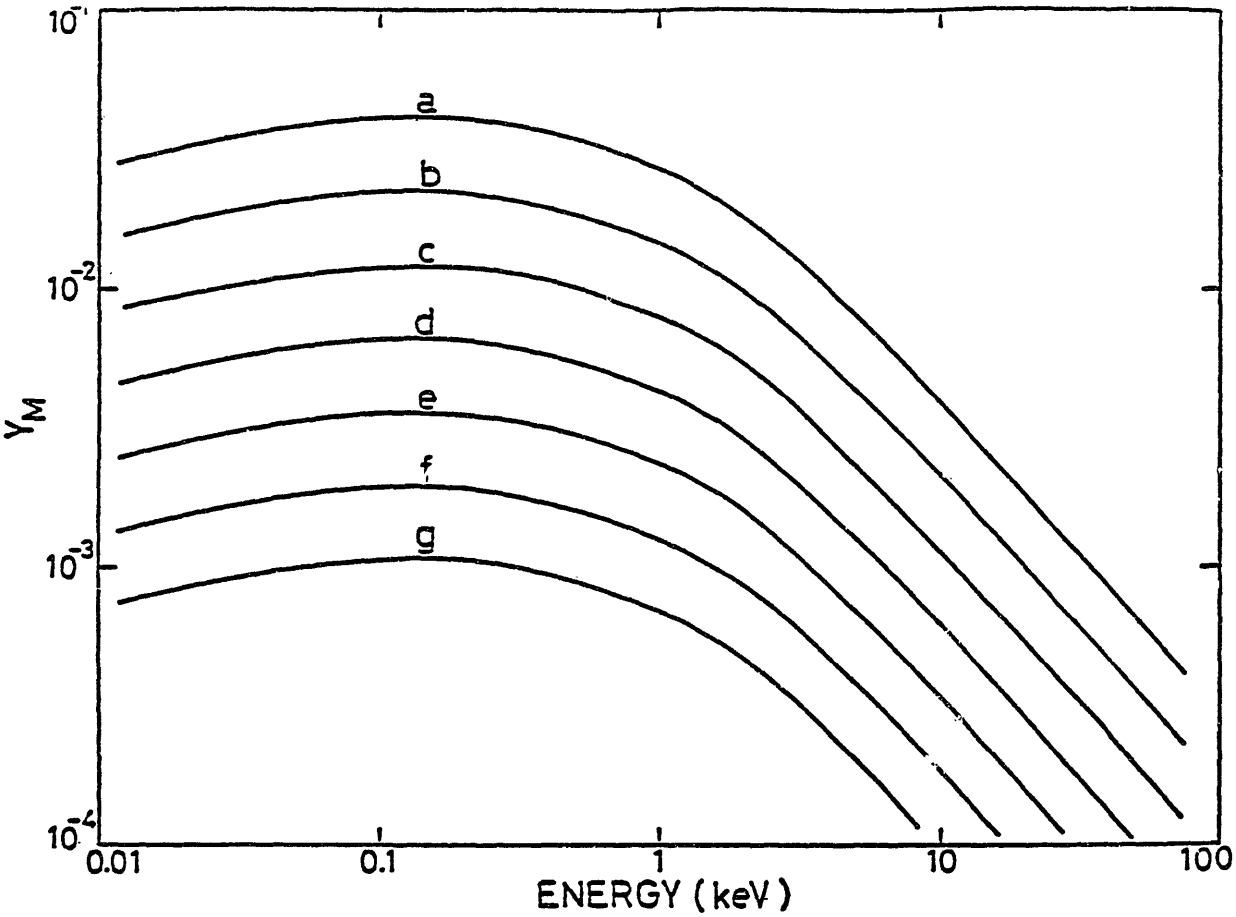
10^{-1}
10^{-2}
10^{-3}
10^{-4}
Y_M
a
b
c
d
e
f
g
0.01
0.1
1
10
100
ENERGY (keV)

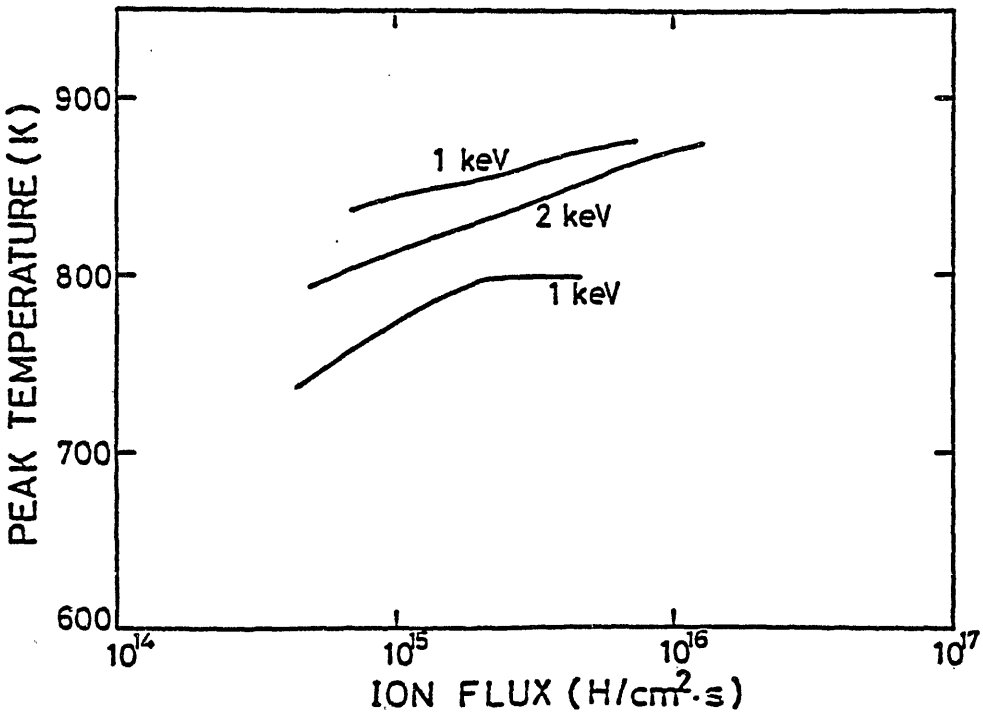
900
800
700
600
PEAK TEMPERATURE (K)
1 keV
2 keV
1 keV
10^{14}
10^{15}
10^{16}
10^{17}
ION FLUX ($H/cm^2 \cdot s$)

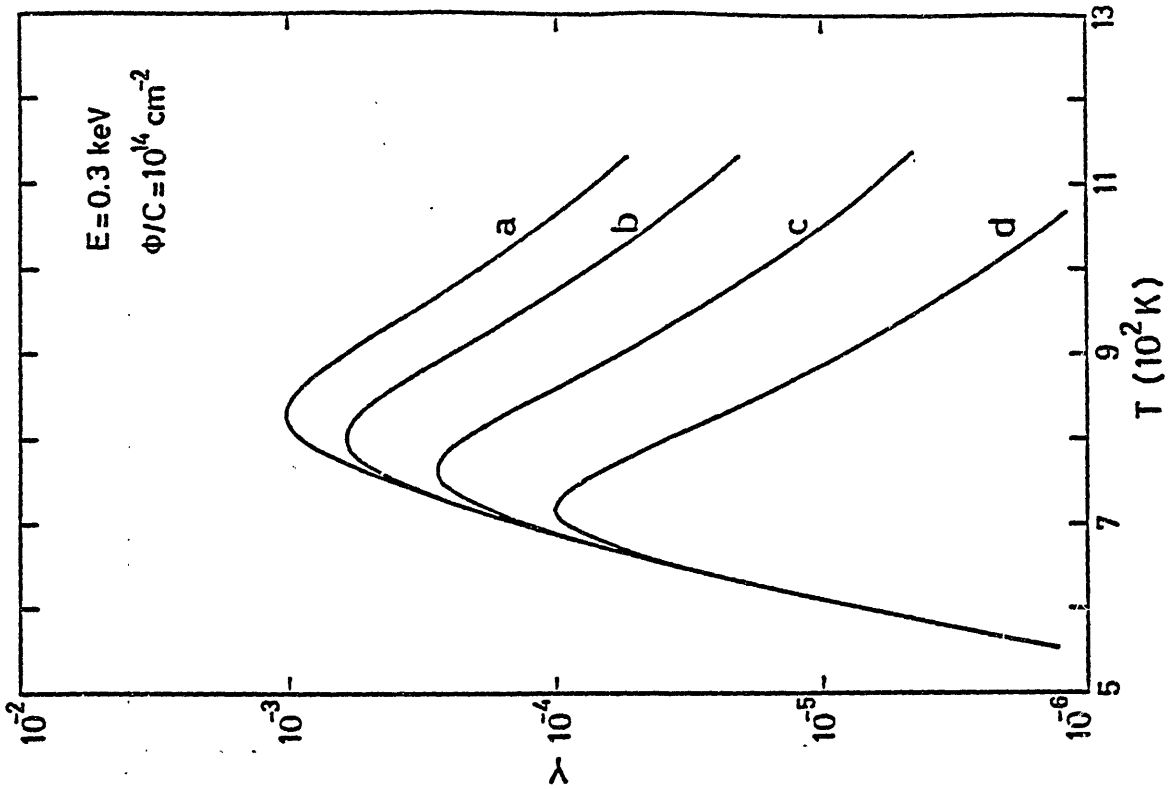
E=0.3 keV
Φ/C=10^14 cm^-2
a
b
c
d
λ
T (10^2 K)

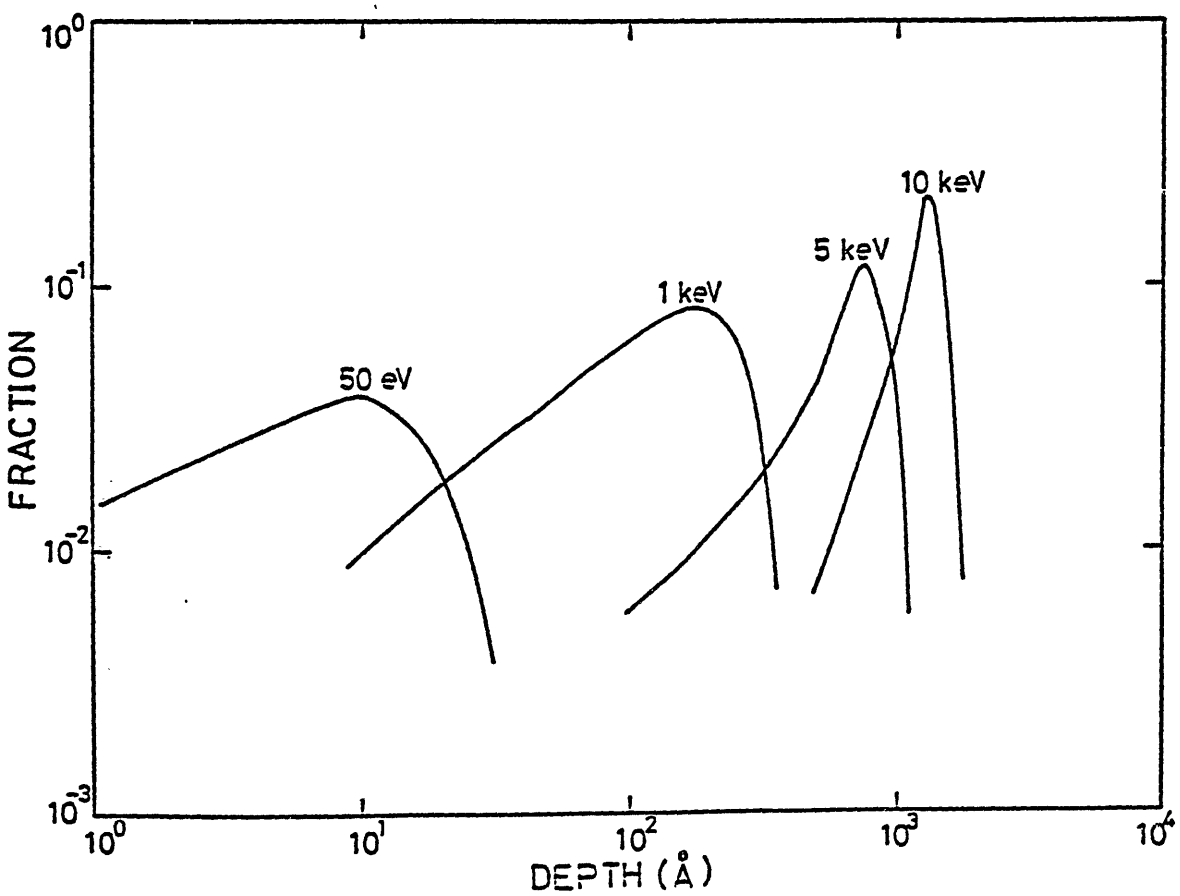
FRACTION
DEPTH (Å)
50 eV
1 keV
5 keV
10 keV

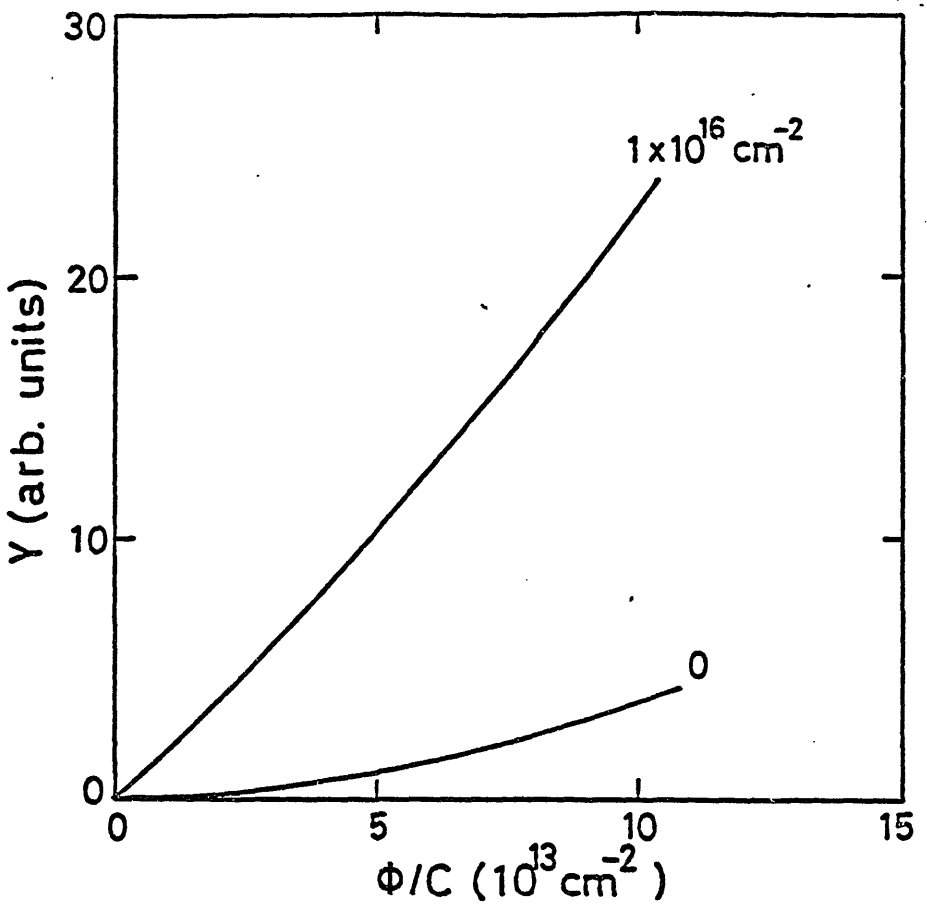
Y (arb. units)
30
20
10
0
1 x 10^16 cm^-2
0
0
5
10
15
Φ/C (10^13 cm^-2)

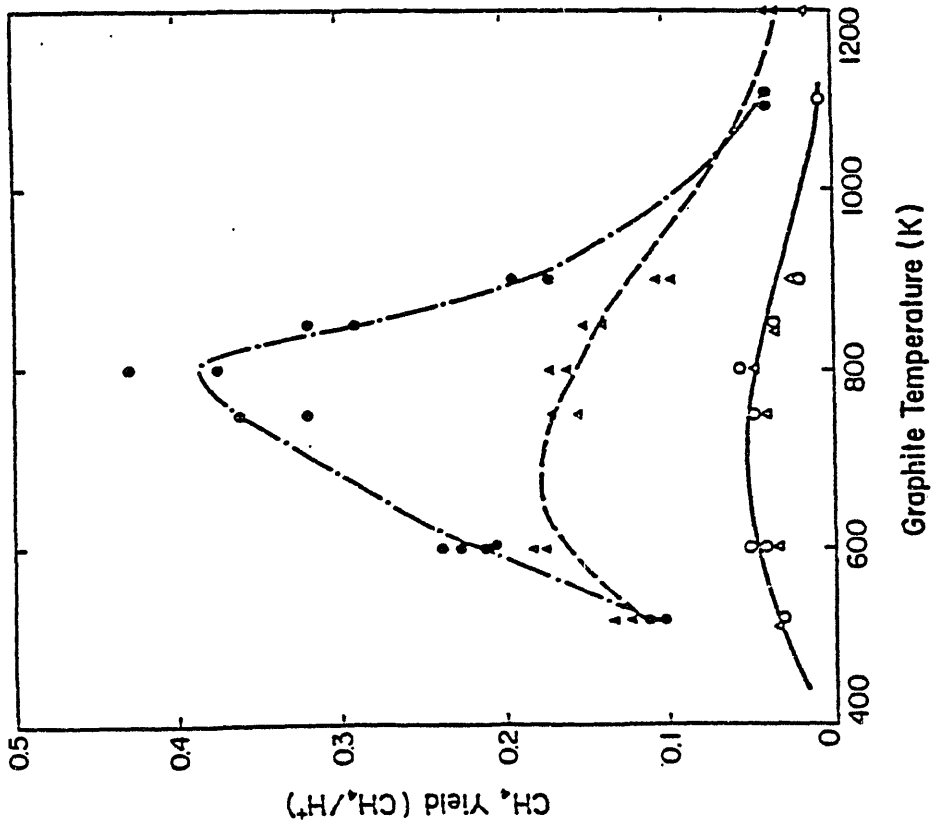
CH4 Yield (CH4/H+)
0.5
0.4
0.3
0.2
0.1
0
400
600
800
1000
1200
Graphite Temperature (K)

IV. Concluding remarks

a. Simple model can describe several important features of chemical sputtering

b. In obtaining experimental data, attention is to be paid on the previous history of treatment, especially on the surface concentration of hydrogen

c. Evaluation of c under various irradiation conditions (temperature, flux, incident energy, sample treatment, ambient hydrogen pressure) is still remained unsolved

d. The chemical sputtering yield may be reduced by increasing hydrogen concentration at the surface

e. It is hoped that the present empirical equation yields a guide for understanding the phenomena and for constructing elaborating modelling codes

Comment on Plasma Facing Material Studies for ETR

Akira Miyahara
Institute of Plasma Physics, Nagoya University
Nagoya 464 Japan

Abstract

ETR faminly has been defined as the next generation machine after present day's devices like JT-60, TFTR, JET and the next step machine like CIT and TORE SUPRA, ASDEX-U, LHS. The requirements to plasma facing materials for ETR are discussed and summarized.

1. Introduction

Recently, the definition of ETR as the next generation fusion machine became more concrete as the result of present day large tokamak researches which gave hopeful issues to discuss the relation between the next step devices such as ignition and long pulse devices and ETR family, namely, NET, TIBER, FER, OTR and INTOR.

Global steps of the nuclear fusion reactor research and development are as shown in fig. 1. The next generation machine is in the third step and we must demonstrate long DT burning, namely, the scientific feasibility in accuarate sense. The fourth step must be dedicated to study energy conversion scheme of higher efficiency in order to fill up the requirement of easier acceptance by public. The last step is commercial feasibility, those are safety, compactness and small impact to environment to obtain good net energy balance including decommissioning.

Minimum requirement for ETR is " to perform long pulse operation with DT burns ". Here, long pulse means longer time than one primary fuel cycle, namely unloading of unburnt fuel, He and impurities exhaust, purification and isotope separation, ice pellet preparation and injections, as shown, in fig. 2.

When we started INTOR design, the primary object of the work was to define the problem related to ETR design clearly. Present day's design efforts both from physics and engineering sides are concentrated to obtain the reality.

2. Requirement from ETR design

In order to obtain the set of well defined problems for ETR plasma facing materials, we have to consider the requirements during fabrication and construction, operation dismantling and decommission as have been done to squeeze condidate materials for BCX. For ETR, remarkable additional conditions are required as mentioned in the following.

(1) To meet requirement of long pulse operation, active cooling is necessary to introduce.

(2) Compatibility with coolant must be considered.

(3) Because of higher neutron fluences up to 5×10^{25}-3×10^{26}n/m^2, activation of PFM including active cooling component must be seriously taken into account.

(4) Radiation damage of PFM by 14MeV neutron is not too serious but still important, becouse the change of physical properties as thermal conductivity will be introduced.

(5) Tritium permeation through cooling pipe wall is important if the coolant temperature is high enough.

Capability of active cooling with PFM if widely investigated with connection to ASDEX-U and TORE SUPRA. Preliminary investigations for PFM of FER are performed in several Japanese industries, but more realistic approch is necessary to fill up requirements. Items described by Dr. W.B. Gauster[1] as in fig. 3, are very important problem to be solved. For ETR family, plasma parameters are given in several papers[2][3][4], however, corresponding requirements to plasma facing materials are not yet clearly given. The aim of

this comment is to stimulate to define the requirements of PFM for ETR and to survey the relation between R and D efforts of the next step devices (CIT, long pulse no burn) and ETR.

Activations of cooling components by 14MeV neutrons are serious problem although people are expecting to avoid the problem by adopting remote maintenance technique. From the stand point of repair and maintenance, activities of the component should be reduced to one thousandth within resonable time for example one month. Also materials with significant activation after 100 years cooling down time must be avoide as discussed by Dr. R. Hancox et al. for structural materials.[5]

Radiation damage of graphite and C-C composite must be investigated from the aspect of the degradiation of physical properties. For example, change of thermal conductivity will introduce change of surface temperature of graphite and enhance the sublimation.

In order to meet such a wide spread requrements to PFM for ETR, we must ask many efforts to be done by plasma physisist, namely to reduce the conditions imposed by plasma side. Perhaps the most important requirement to them is to reduce the number of serious off normal operations such as distruptions and runaway electrons.

3. Conclusion

In conclusion, I will try to identify the ETR's requirements for PFM. Followings are just the preliminary list up of the ploblem area.

(1) Neutron fluences and their effects on each ETR design.

(2) Heat and particle loadings to various components during

normal operations.

(3) Nominate the candidate off normal operations and define the loading conditions.

(4) Estimate the local He loading and its effects.

(5) Evaluate the edge plasma parameters consistent with plasma scenario.

(6) Can divertor concept allow to introduce high z materials? (Impurities, H-mode operation)

(7) Is activation of materials critical issue or not?

(8) Does neutron irradiation introduce serious change of physical properties of graphite?

(9) Realisitic concept of active cooling must be established.

(10) High frequency absorption by wall - material itself and by means of structures comparable to wave length - must be considered especially for synchrotron radiation and ECR heating, power.

Description of TIBER-II/ETR is attached by courtesy of Dr. K.L. Wilson.

References

(1) W.B. Gauster: Private communication

(2) D.R. Harries: The European Community Fusion Materials programme EVR-FV/XII-80/86/65, October 1986

(3) E. Engelmann: Concept and parameters of NET. EVR-FV.XII-80/86/64

(4) K. Tomabechi,et al.: Proc. 9th Int. Conf. on Plasma Physics and Controlled Nuclear Fusion Research, Vol.1, Baltimore, 1982 (IAEA, Vienna, 1983) p.399

(5) R. Hancox, B.Mitchell and G.J. Butterworth: Radiological Implications of Low-Activation Steels as Structural Materials in Fusion Reactors. IAEA-CN-47/H-1-5,1986

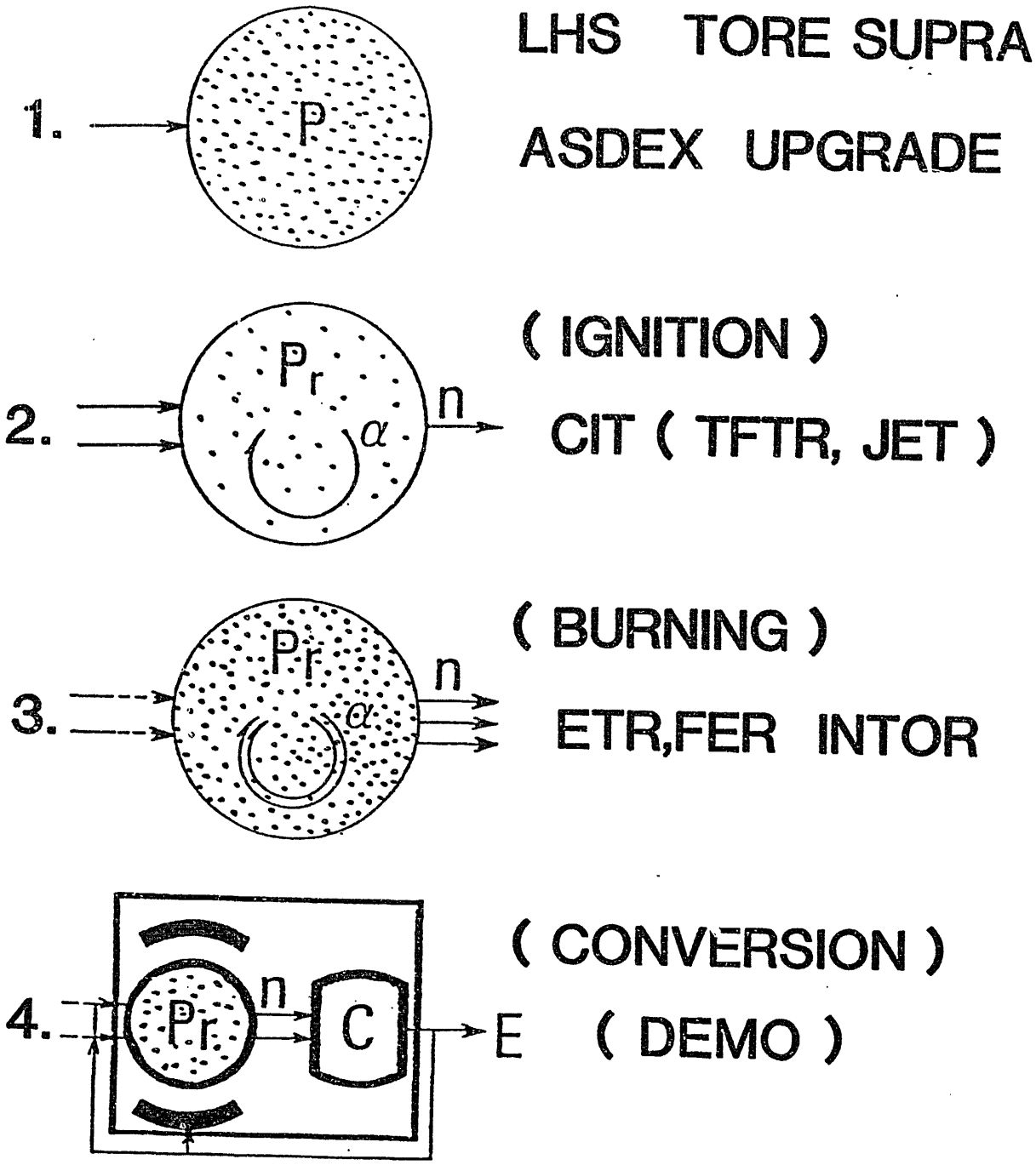

5. ECONOMICS, SAFETY AND ENVIRONMENT

6. COMMERCIAL PLANT

Fig. 1 Each Step of Fusion Reactor Development

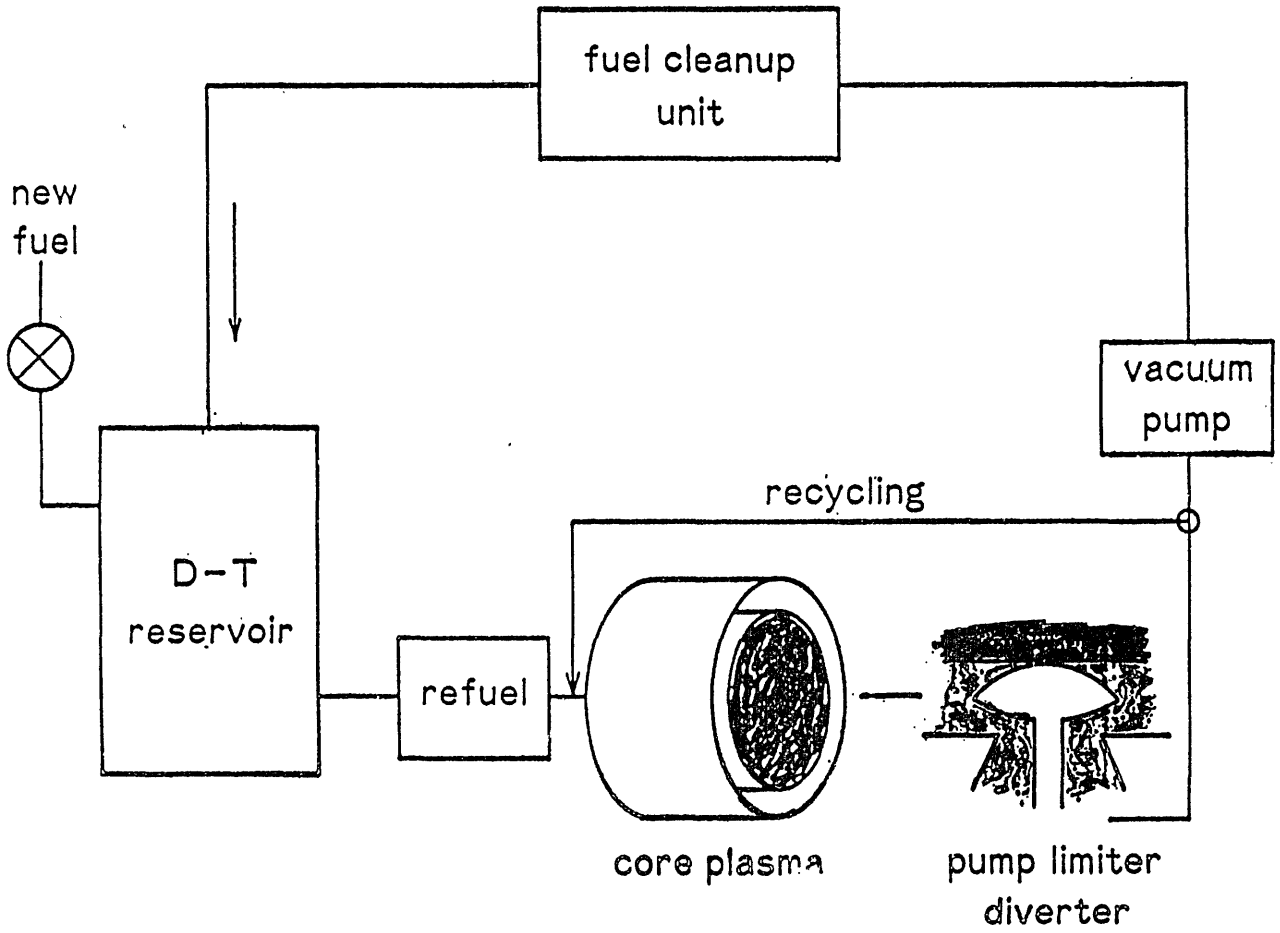

Fig. 2 Scheme of Primary Fuel Cycle

T I B E R II / E T R

C. D. HENNING et al.

REFERENCES:

" TIBER II " UCID-20863 OCT 23, 1986
" TIBER II / ETR " MISC 4399 SEPT/OCT 1986

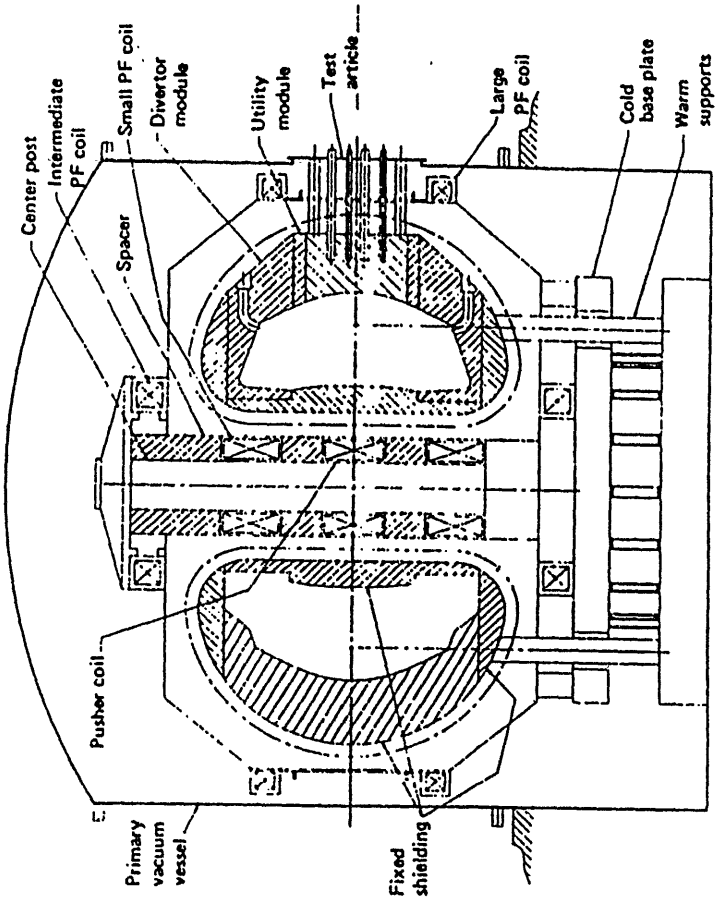

Figure 1-1. TIBER II is the U.S. option for the international ETR.

GOAL OF THE STUDIES PROGRAM

TO DEVELOP THE TECHNICAL & PROGRAMMATIC BASIS
FOR AN INNOVATIVE & LOW COST ETR
TO INFLUENCE A POSSIBLE INTERNATIONAL
CONCEPTUAL DESIGN ACTIVITY.

TIBER-II (USA)

A compact, 3 m radius, steady-state tokamak with ECH/LH current-drive and profile control. Moderate-high end-of-life fluence goal.

FER (Japan)

A 5.2 m pulsed inductive tokamak with conservative design performance. Low wall loading and end-of-life fluence goal.

NET (European Community)

A 5.2 m pulsed inductive tokamak envisaged to be the only step between JET and the DEMO/IFF. Moderate end-of-life fluence goal.

OTR (USSR)

A 6.2 m pulsed inductive tokamak designed to demonstrate electricity and fissile fuel production with complete tritium self-sufficiency in final phase. High end-of-life fluence goal.

	OTR (USSR)	FER (Japan)	TIBER-II (USA)	NET (E.C.)	INTOR IAEA
Fusion power (MW)	520	297	290	600	570
Major radius (m)	6.2	5.2	3.0	5.18	4.9
Auxiliary RF power (MW)	50	50	47	50	40
τ_{burn} (s)	670	2300	Steady-state	670	200
$\hat{\Gamma}$ (MW/m^2)	1.2	0.88	2.0	1.5	1.3
Fluence goal (MW yr/m^2)	5	0.3	3	0.8	0.3-3
Availability goal*	60-70%	Low	$\lesssim$30%	25%	25%
Tritium consumption* (kg/yr)	18	Low	4.5	7.7	6.1

*In final phase.

TIBER II accomodates alternate current drive options, blanket test modules, and materials testing

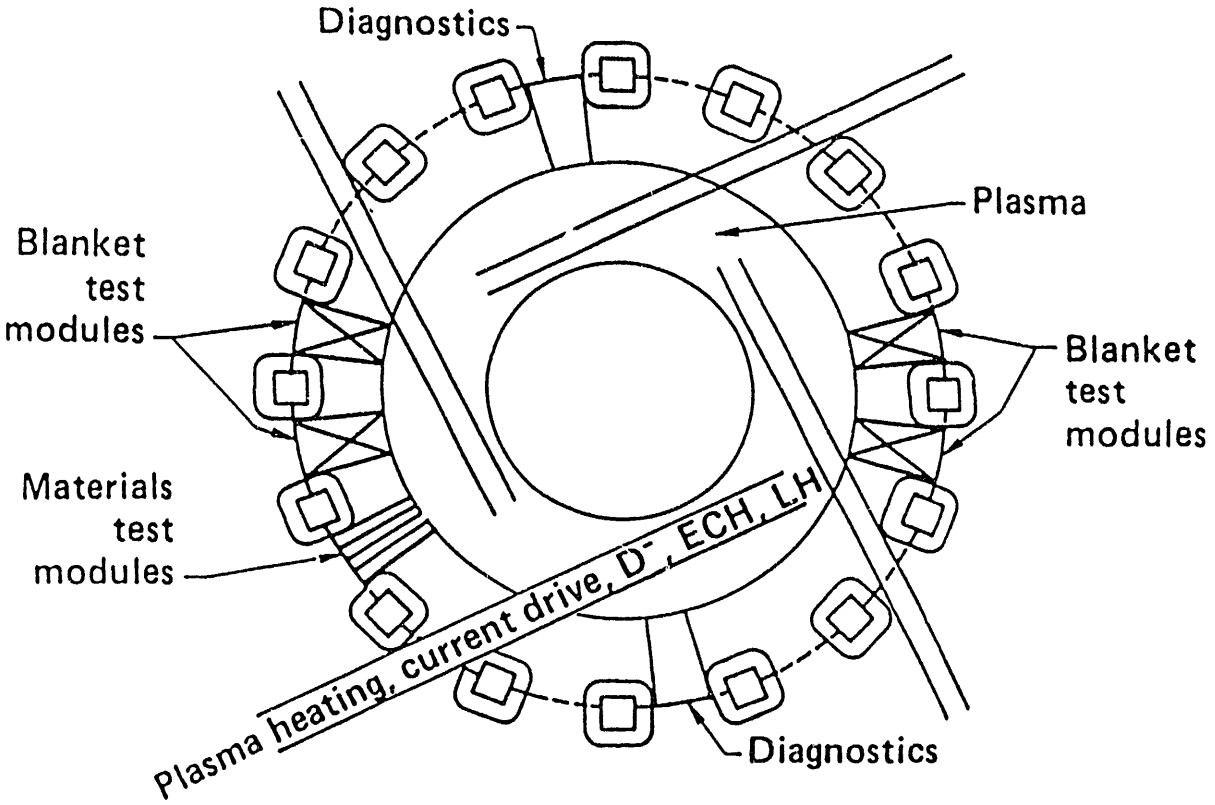

Why steady-state

- A large OH coil leads to a large tokamak.
  - 100 volt-sec corresponds to a 5-m major radius.
  - TIBER (3 m) has about 5 volt seconds of OH.
- Pulsed OH drives lead to:
  - lower current densities in magnets.
  - significant eddy current heat loads.
  - larger structures due to fatigue.
  - thermal fatigue of first-wall and limiter.
- High-fluence nuclear tests require steady-state or very high-duty factor.
- Thermal fatigue of blanket modules may precede damage due to neutrons.
- Equilibrium testing of nuclear components is necessary for realistic results.

Table I. Operating scenarios for TIBER-II.

	I LH ramp-up + L/R decay	II LH ramp-up, OH inductive flat-top + L/R decay	III Current-drive @ 10% avail.	IV Current-drive @ 30% avail.
P_{fusion} (MW)	342	342	290	290
Γ (MW/m^2)	2.3	2.3	2.0	2.0
τ_{burn} (s)	302	724	Steady-state	Steady-state
No. of lifetime cycles	25,000[a]	14,000[a]	<< max. cycles	<< max. cycles
Peak fluence (MW yr/m^2)	0.55	0.73	1.9	5.8
Tritium consumption (kg/yr)	0.46	0.61	1.6	4.8
Availability	~ 4.8%[b]	~ 6.4%[b]	10%	30%

[Machine operating life 10 yr]

[a] 50% of projected cycles to failure.

[b] Required to complete max. no. of cycles in 10 yr lifetime.

Table II. Comparison of current drive methods. (Sept. 1986)

	ECH	NBI	ECH+LH	NBI+LH
P_f(MW)	282	278	320	271
P_{cd}(MW)	30/21	57	23/18	40/15
Q	5.5	4.9	7.9	5.0
Γ(MW/m^2)	1.9	1.9	2.2	1.8
$\langle\Gamma\rangle$(MW/m^2	1.2	1.2	1.4	1.2
I_t(MA)	10	10	6.6/3.4	6.7/3.3
f_{rf}/E_b	185/168 GHz	500 keV	168/5 GHz	500 keV/5 GHz
η_{cd}(A/W)	0.19	0.16	0.29/0.19	0.15/0.22
η_{elec}	0.45	0.45	0.45/0.41	0.45/0.41
$\eta_{elec}Q$	2.5	2.2	3.4	2.2
$\langle T_e\rangle$ (keV)	26	27	24	28
$\langle T_i\rangle$ (keV)	17	38	17	32
$\langle n_e\rangle$ (10^{20}m^{-3})	1.1	0.72	1.2	0.77
F_{trap}	0.71	0.76	0.81/0.85	0.76/0.83
I_{FUEL}(pellet)(A)	245	93	279	133
f_s(%)	--	3.2	--	2.6
Z_{eff}	1.56	2.0	1.56	2.0
$H_{Kay.-Goldston}$	1.3	1.3	1.3	1.3
$\langle\beta\rangle$ %	6	6	6	6

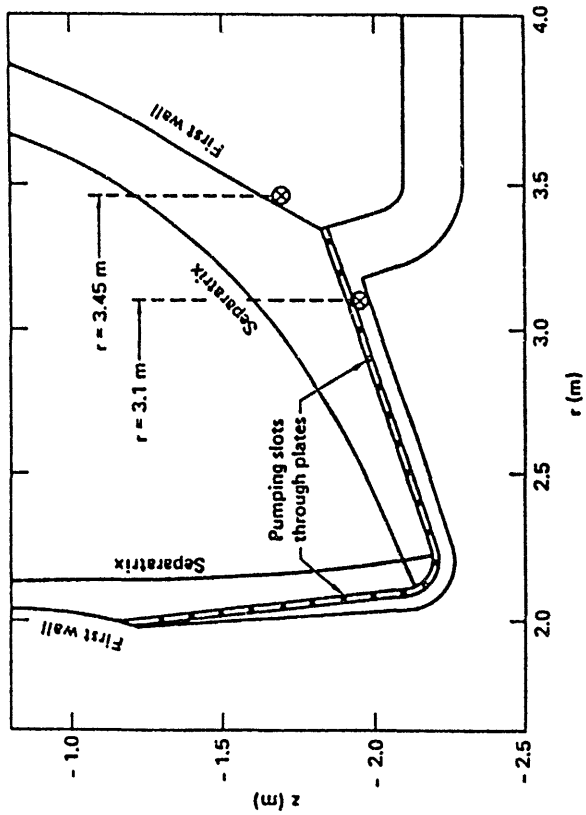

Figure 4-32. TIBER II vacuum-duct dimensions. The ducts are sized to give a pumping speed of 3.5×10^4 L/s for DT molecules at a temperature of 400 K.

Table 4-6. Relative merits of three plasma face materials.

Material	Advantages	Disadvantages
Be	• Low z • Brazable • Can be plasma sprayed • Good thermal conductivity	• Erosion • Low melting point • Susceptible to minor plasma disruptions (narow operating window)
Graphite carbon/carbon	• Low z • Brazable • High thermal shock resistance • Best behavior under plasma-disruption conditions	• RF absorption • Erosion • Expensive (carbon-carbon)
TZM W-5% RE	• Near-zero erosion rate for ETR application • Ductile	• Plasma contamination with high-z material • Susceptible to plasma disruptions

DIVERTOR PLATE DESIGN REQUIREMENTS

- Divertor plates should be remotely replaceable.
- Thermal loads are as follows
  - $q = 6\ MW/m^2$ is defined as the design load for steady-state operation (approximately 2 times higher than the nominal load on divertor plates).
  - Plasma thermal-energy quench time during plasma disruption, $\tau = 0.5$ ms.
- EM loads are as follows
  - Normal operation due to plasma startup and shutdown.
  - Plasma disruption due to current decay in the plasma ($\frac{dI}{dt} = 1$ MA/ms).
- Minimum lifetime requirements and time between replacement, t_r, are as follows
  - Number of full-power plasma disruptions between replacement, $N_p = 150$.
- Assuming an availability factor of 25%, approximately 1.5 years of operation will be allowed between replacement.

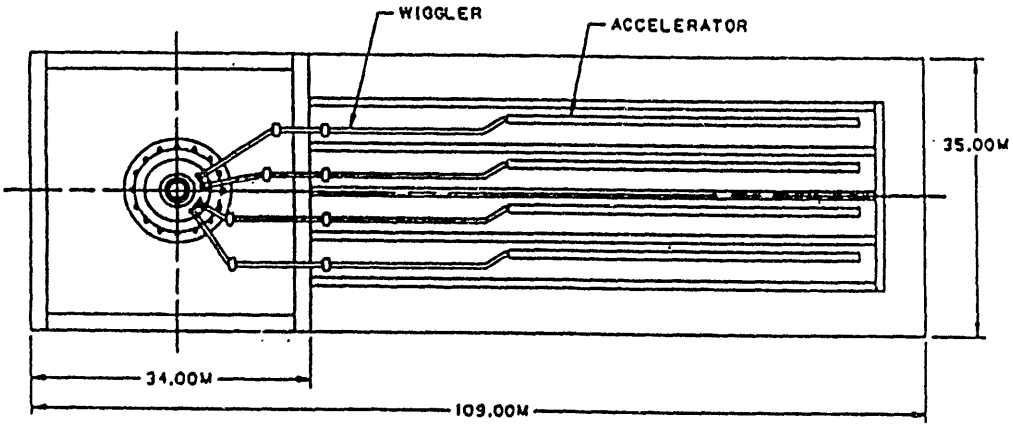

FEL DRIVEN TIBER

Table 4-7. Performance parameters for the coolant channel.

Design heat flux	6 MW/m^2
Be coating thickness	5 mm
Maximum Be temperature	465°C
Be/Cu interface temperature	180°C
Maximum thermal stress in Be	380 MPa
Channel hydraulic diameter	5 mm
Flow velocity	10.4 m/s
Flow rate/channel	0.62 kg/s
Pressure drop in channel	0.18 MPa
Inlet pressure	1.36 MPa
Total flow rate through plates	1500 kg/s

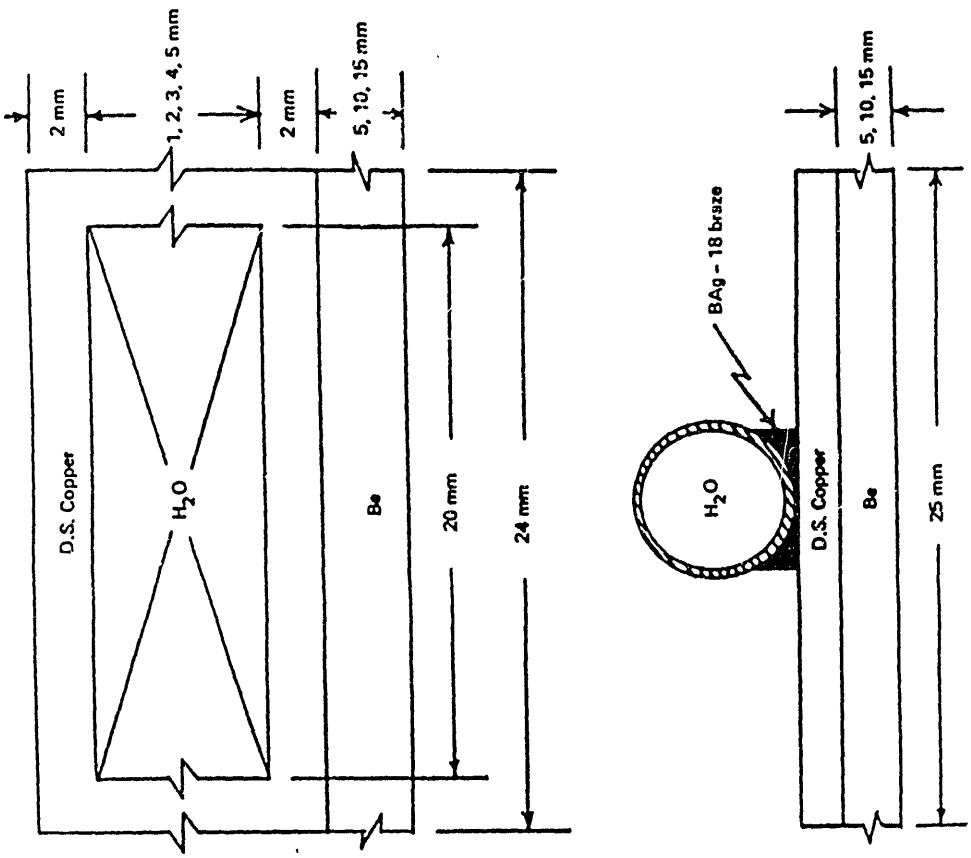

Figure 4-38. Flow channel cross section.

Application of graphite materials to the next generation machine

Masahiro Seki
Japan Atomic Energy Research Institute

Abstract

Performance of graphite tiles to protect the first wall against plasma disruption is discussed.

Two dimensional elastic analysis of the first wall with a bonded graphite tile shows that the stress in the graphite exceeds the Su of IG-11 equivalent graphite to a depth of 0.4mm.

Table I.1-1 Design constraints for the evaluation of first wall/blanket

Lifetime neutron fluence	3 MW·Y/m²
Availability goal	25 %
Neutron wall loading	~1 MW/m²
Divertor performance	Single null
Installation of blankets	Outboard and top regions
Burn time	≧200 sec
Cycle time	≧270 sec
Number of burn cycles	2×10^5 for fully inductive case
	2×10^4 for recharge transformer case
Net tritium breeding	~1.0
Blanket coverage	≧0.6
Maximum external T suplly	1.5 Kg/Y
Blanket/shield thickness	
inboard	0.8 m
outboard	~1.5 m
Surface heat flux during normal operation	0.2 MW/m² for clean plasma option
	0.4 MW/m² for radiation edge option
	0.8 MW/m² for steady state operation mode
Local heat deposition due to	
α-particles	0.2 MW/m²
run-away electrons	TBD
Frequency of major disruptions	5×10^{-3} at Stage I
	1×10^{-3} at Stage II and III
Peak energy flux and deposition time at a major disruption	84 J/cm², 2 ms for fast phase
	76 J/cm², 20 ms for slow phase
Peaking factor	3
Sputtering erosion from first wall	0.2 mm/MW·Y·m⁻² for SS
	2.0 mm/MW·Y·m⁻² for graphite
Structural material	Austenitic Stainless Steel
Additional passive stabilization shell	TBD
First wall protection for disruptions	Armor or guard limiter at least on the Inboard area (if necessary)
Limiters during start-up	Low-Z materials (if necessary)
Permitted T level in FW coolant	10 Ci/l
Electricity generation	none

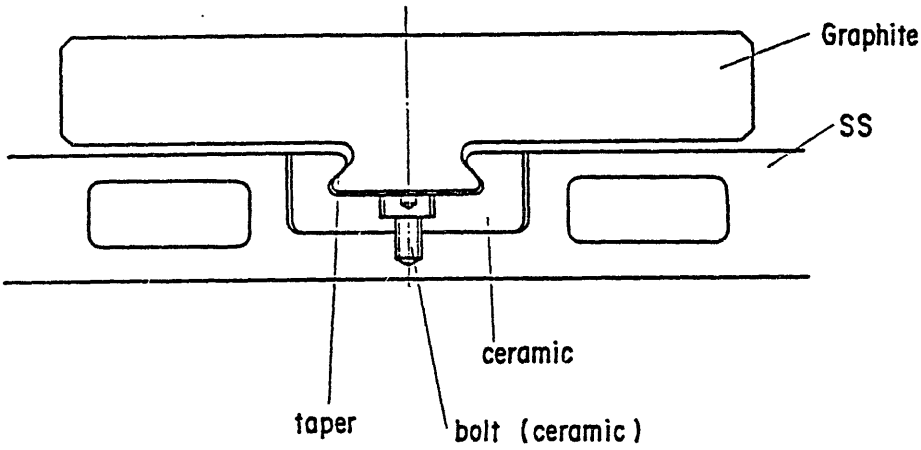

Fig. I.4-2 Mechanically Attached Armor

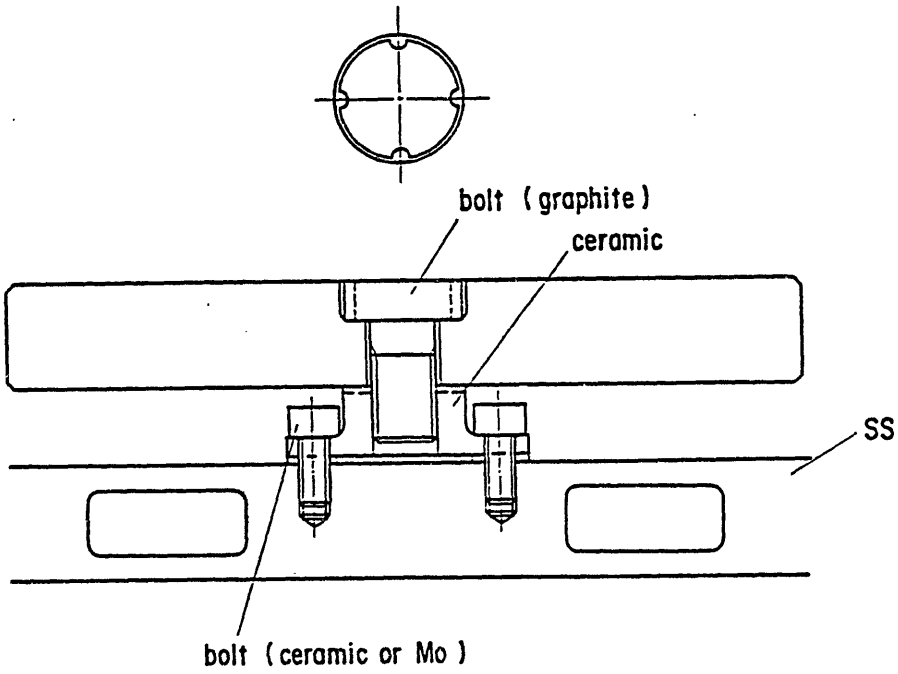

Fig. I.4-1 Mechanically Attached Armor

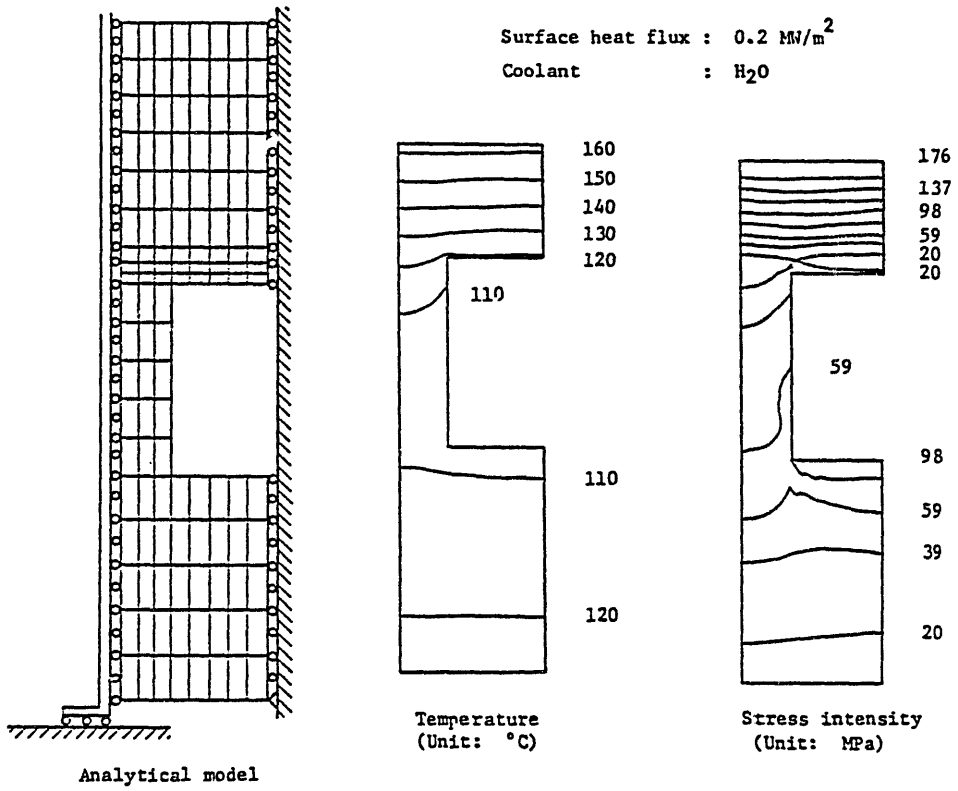

Fig. I.1-2 Analytical Model and Example of Analytical Results

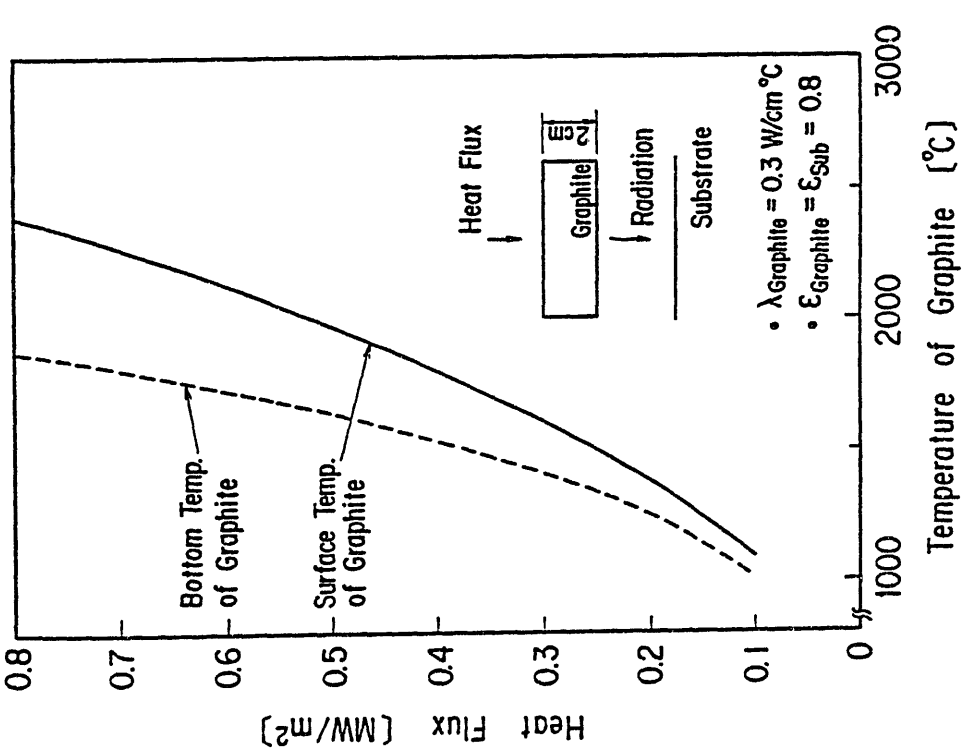

Fig. I.4-3 Temperature of Radiation Cooled Graphite in Steady State

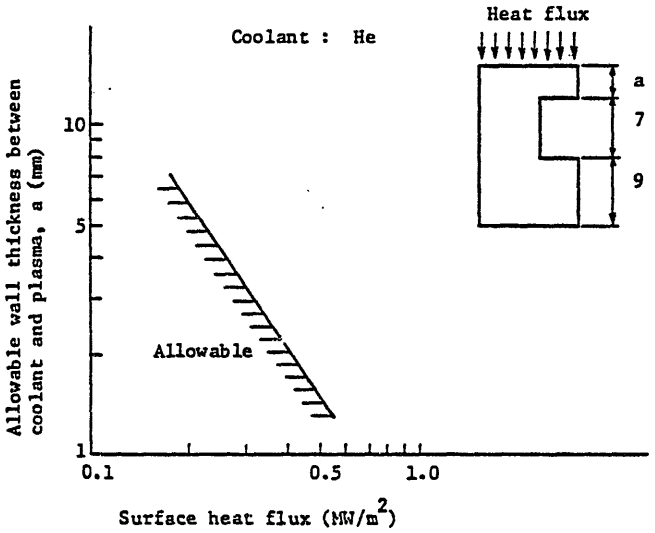

Fig. I.1-4 Relationship between Allowable Wall Thickness, a and Surface Heat Flux

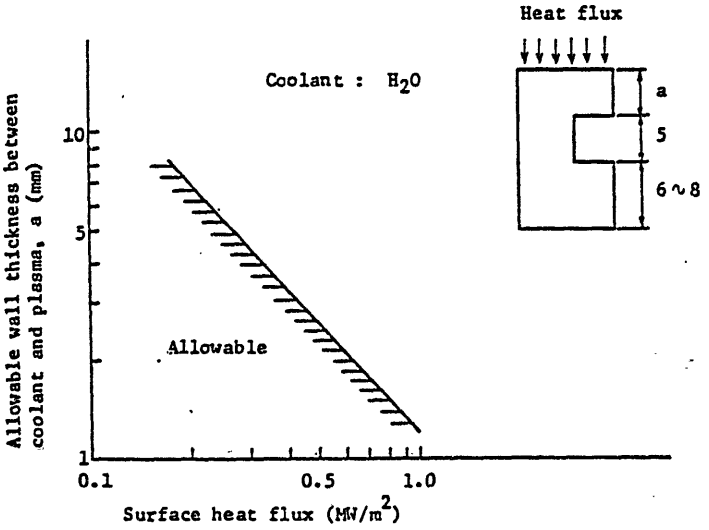

Fig. I.1-3 Relationship between Allowable Wall Thickness, a and Surface Heat Flux

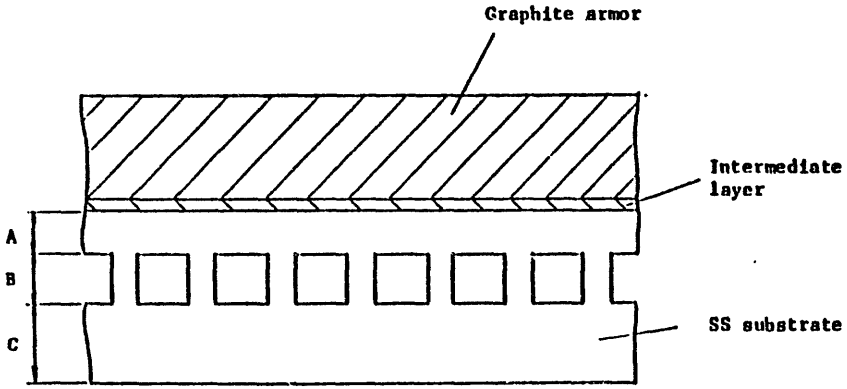

in case of H_2O coolant:

A = 2 mm, B = 5 mm, C = 8 mm

Fig. I.2-1 Graphite Armored FW

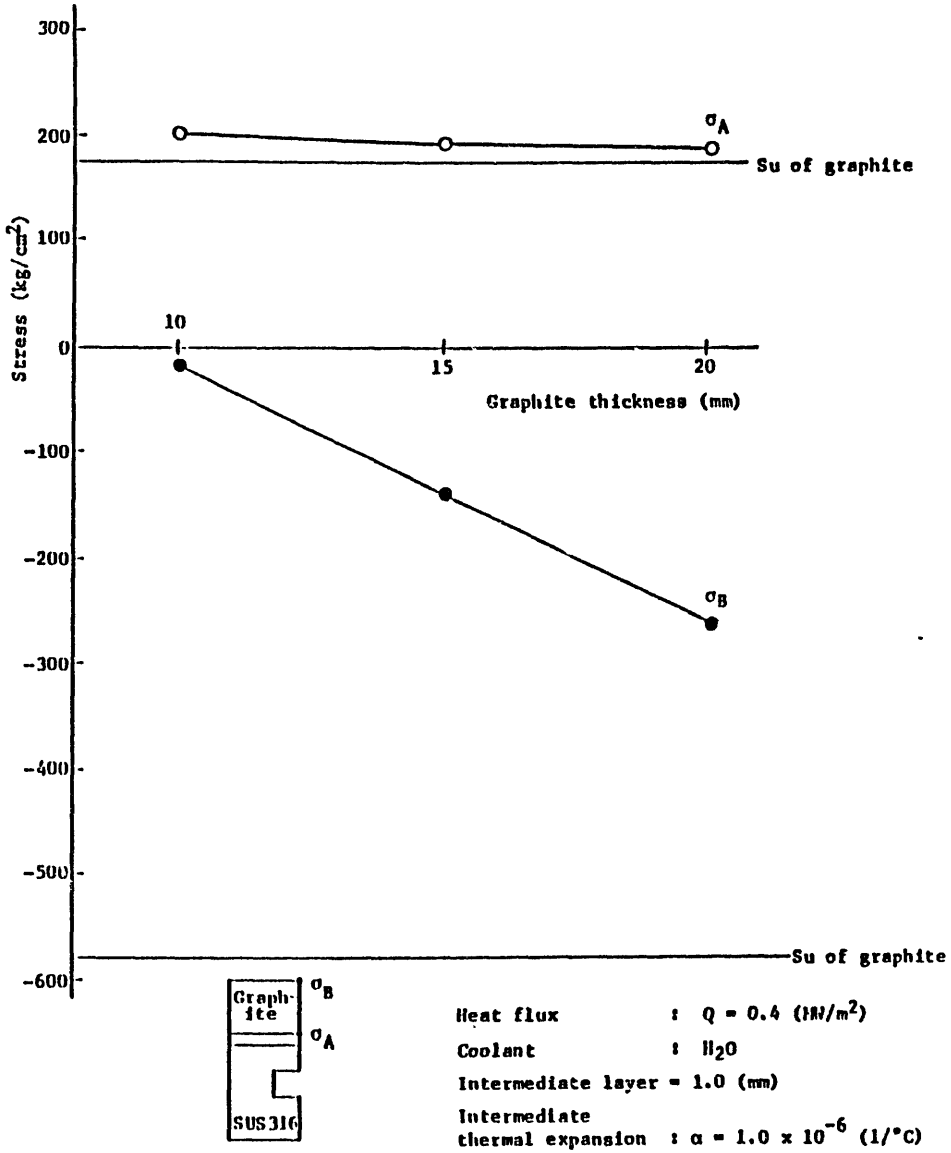

Fig. I.2-2 Effect of Graphite Thickness on Stresses in Graphite

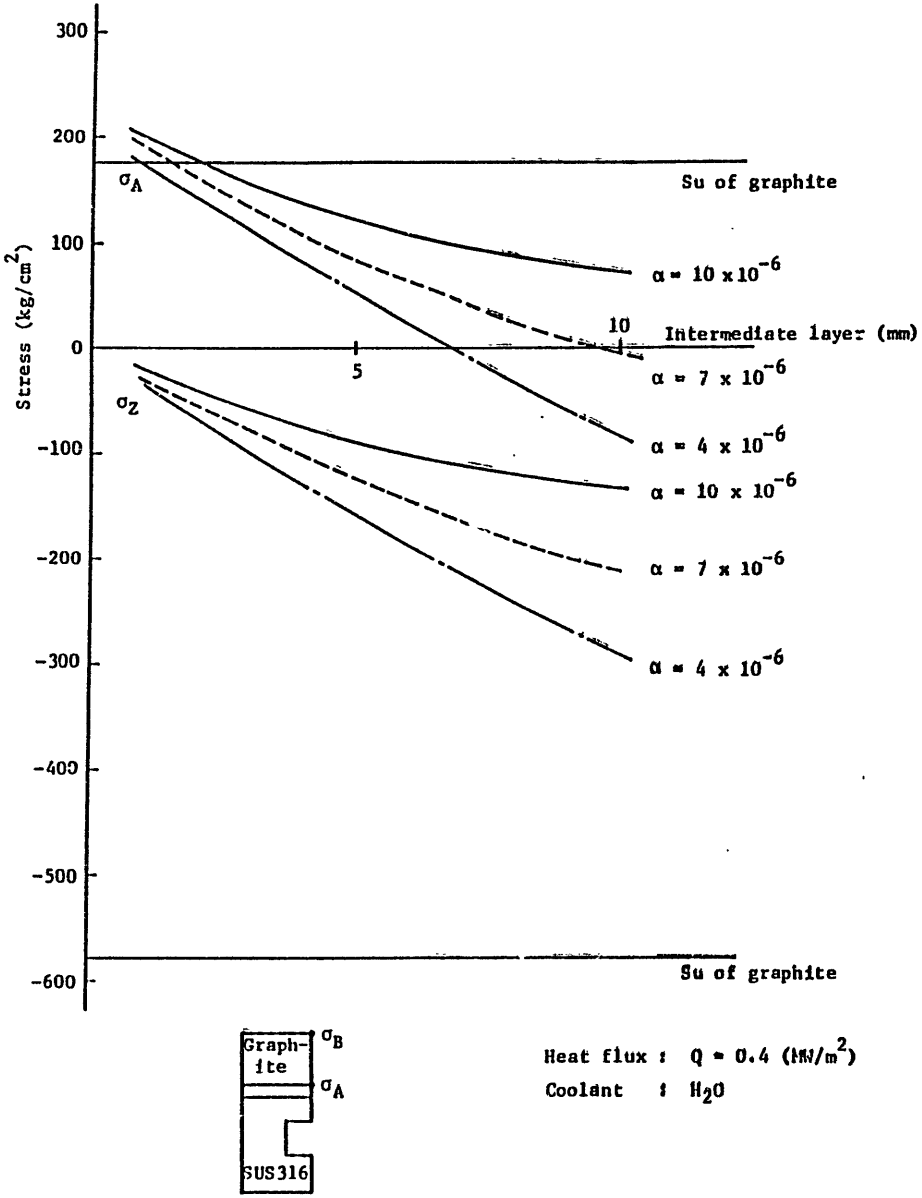

Fig. I.2-3 Effect of Thickness and Thermal Expansion of Intermediate Layer on Stresses in Graphite

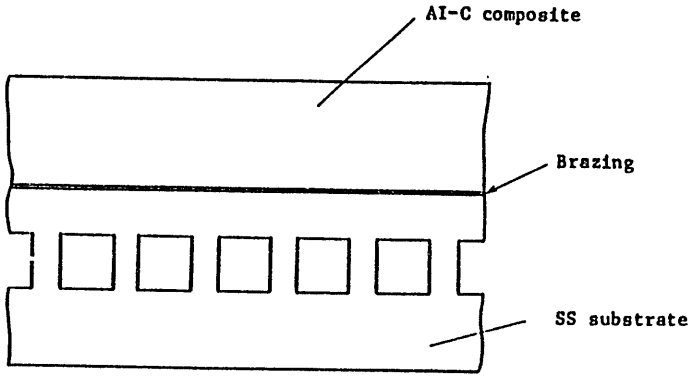

Fig. I.2-4 AI-C Composite Armored FW

Table II.2-2 Results of Disruption Analysis for INTOR First Wall

Material	Stainless Steel	Graphite	Aluminum
Initial Temperature	500 K		
Peak Surface Temperature	2410 K	2740 K	1380 K
Evaporation Loss(disruption)	4.5×10^{-2} μm	5.0×10^{-5} μm	7.4×10^{-4} μm
Evaporation Loss(lifetime)*	9.0 μm	0.01 μm	0.15 μm
Melt Layer Thickness	3.8×10^{-2} mm	–	0.17 mm
Start Time of Melting**	0.83 msec	–	0.48 msec
End Time of Melting**	3.02 msec	–	6.75 msec
Melting Duration	2.19 msec	–	6.27 msec

* : 200 disruptions during reactor lifetime are assumed.

** : time after disruption start.

Table II.2-1 Characterization of Major and Minor Plasma Disruptions

	Major	Minor
Frequency		
Stage I	5×10^{-3}	10^{-2}
Stage II and Stage III	10^{-3}	5×10^{-3}
Time		
fast phase (energy quench)	2 ms	2 ms
slow phase (current quench)	20 ms	-
Energy Deposition		
divertor plate(during fast phase)[1]	100 MJ	25 MJ
first wall (during fast phase)	100 MJ	25 MJ
(during slow phase)	90 MJ	-
peaking factor for first wall	3	
Peak Energy Density		
divertor plate(during fast phase)	290 J/cm^2	70 J/cm^2
first wall (during fast phase)	84 J/cm^2	21 J/cm^2
(during slow phase)	76 J/cm^2	-

1) by a factor 3 wider than the distribution of operating power load.

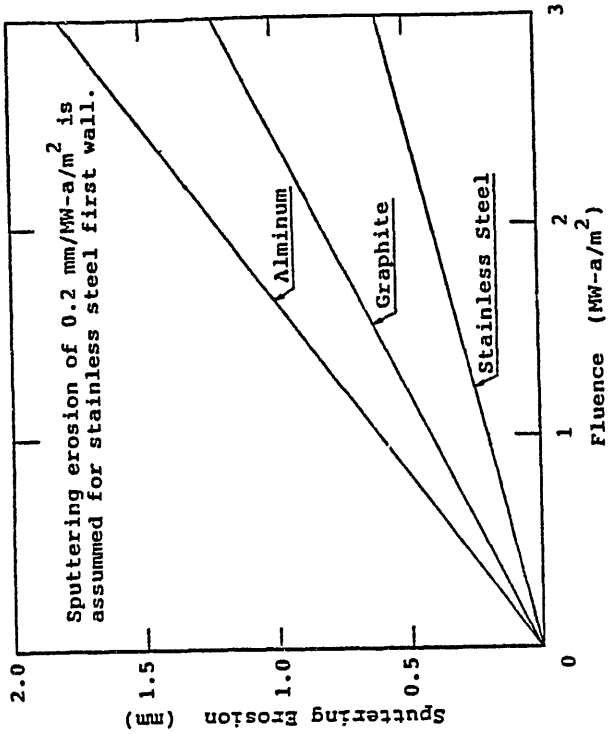

Fig. II.2-1 Physical Sputtering Erosion of First Wall

Table II.2-3 Erosion of INTOR First Wall during Reactor Lifetime (3MW-a/m²)

Material	Stainless Steel	Graphite Armor	Alminum Armor
Erosion due to Physical Sputtering	0.6 mm	1.2 mm	1.8 mm
Erosion due to Chemical Sputtering	-	1.0 mm	-
Erosion due to Evaporation during Disruption	0.0 μm	0.01 μm	0.15 μm
Total	0.6 mm	2.2 mm	1.8 mm

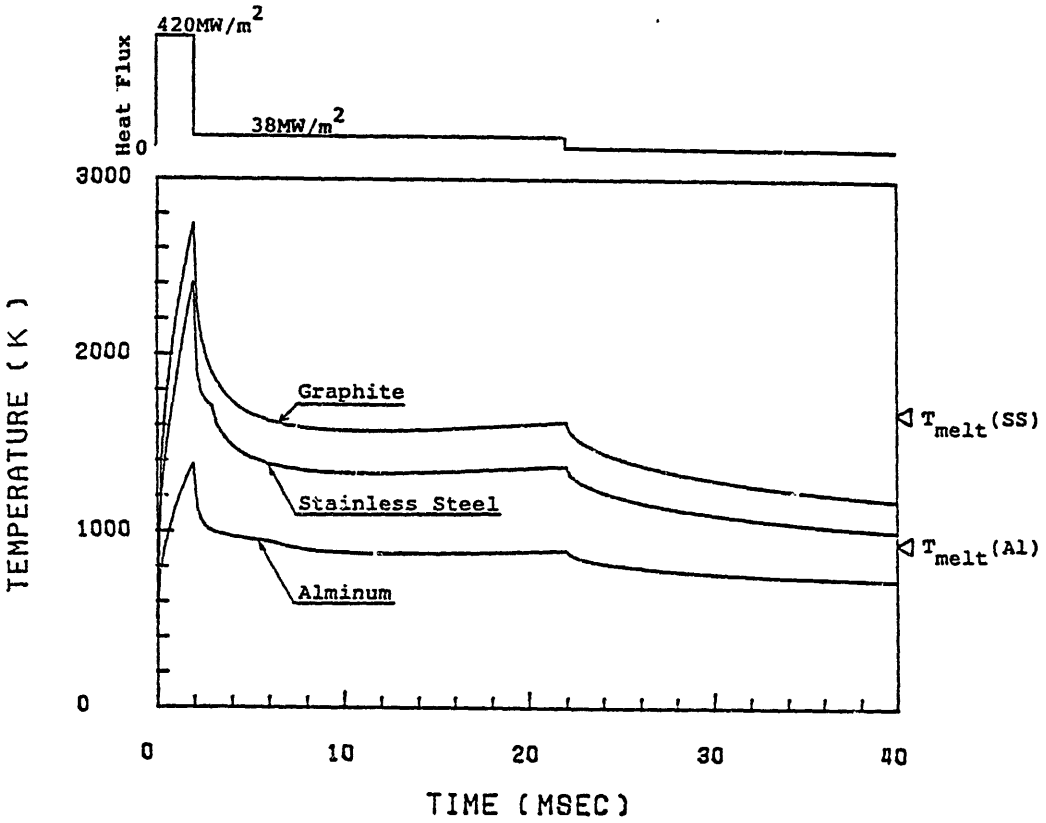

Fig. II.2-4 Temperature Responses at the First Wall Surface during Major Plasma Disruption

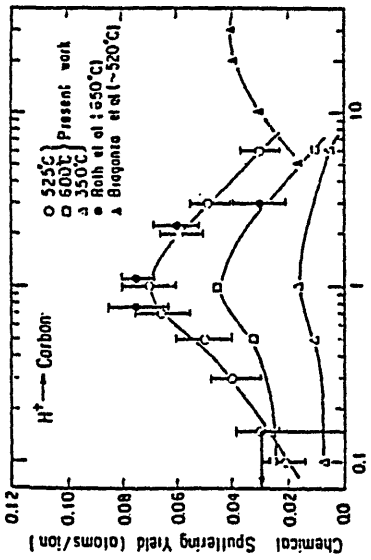

Fig. II.2-2 Energy dependence of the chemical sputtering yield of[1] the basal plane of the PG-A target. The results of Roth et al. are the total erosion yields measured by the weight loss method. Braganza et al. used deuterium ions and the results are determined by CD_4 production rate.

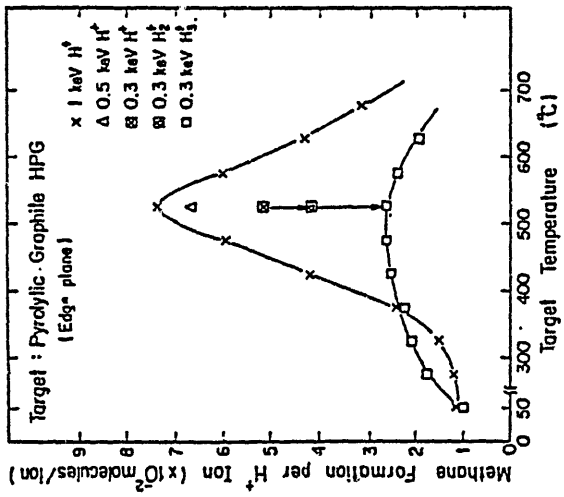

Fig. II.2-3 Methane production rate of the edge plane of HPG.[1]

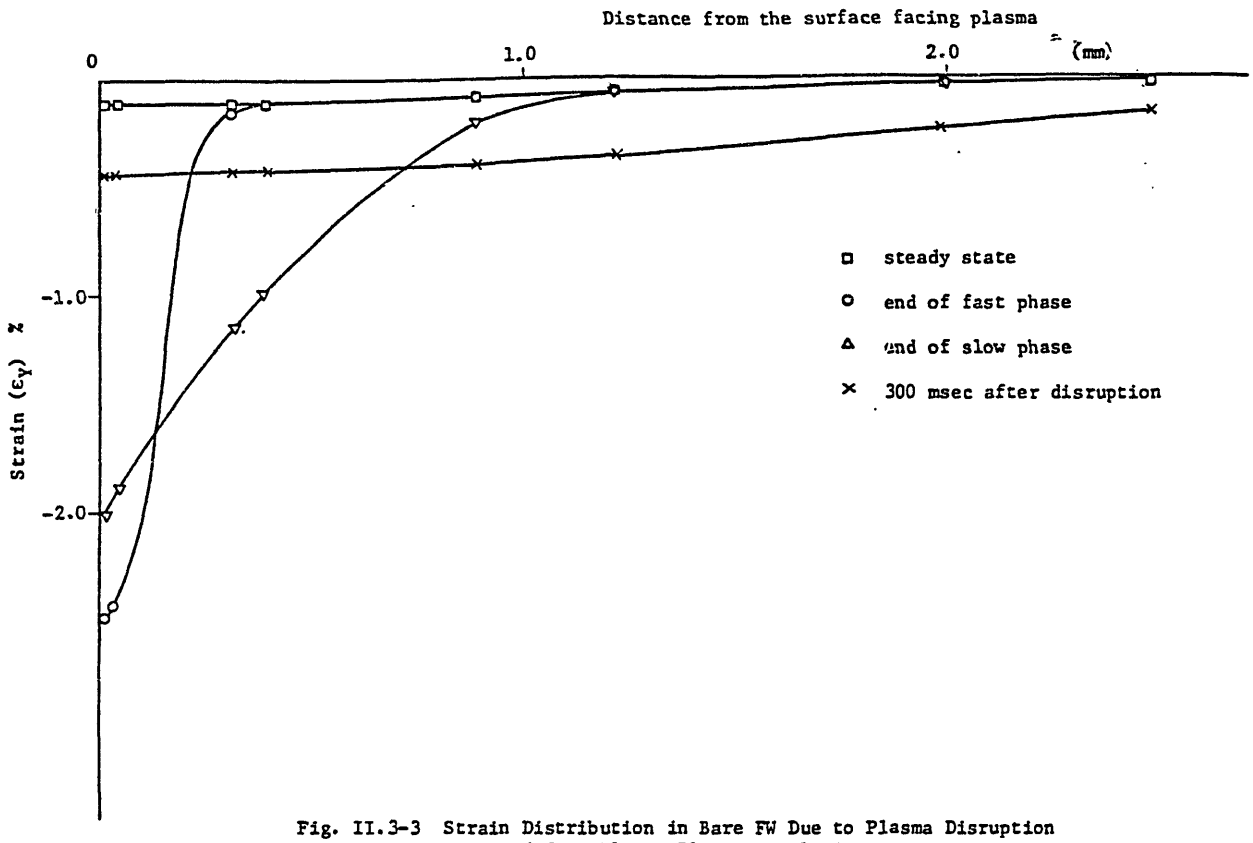

Fig. II.3-3 Strain Distribution in Bare FW Due to Plasma Disruption obtained from Elasto-Plastic Analysis

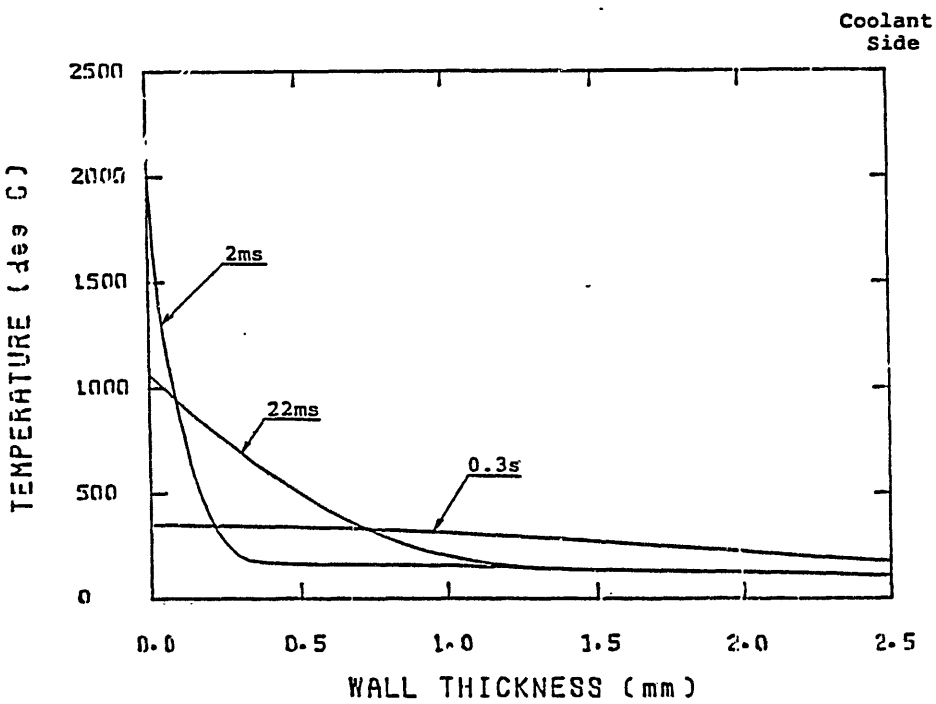

Fig. II.3-2 Temperature Profiles in Stainless Steel First Wall during and after Plasma Disruption

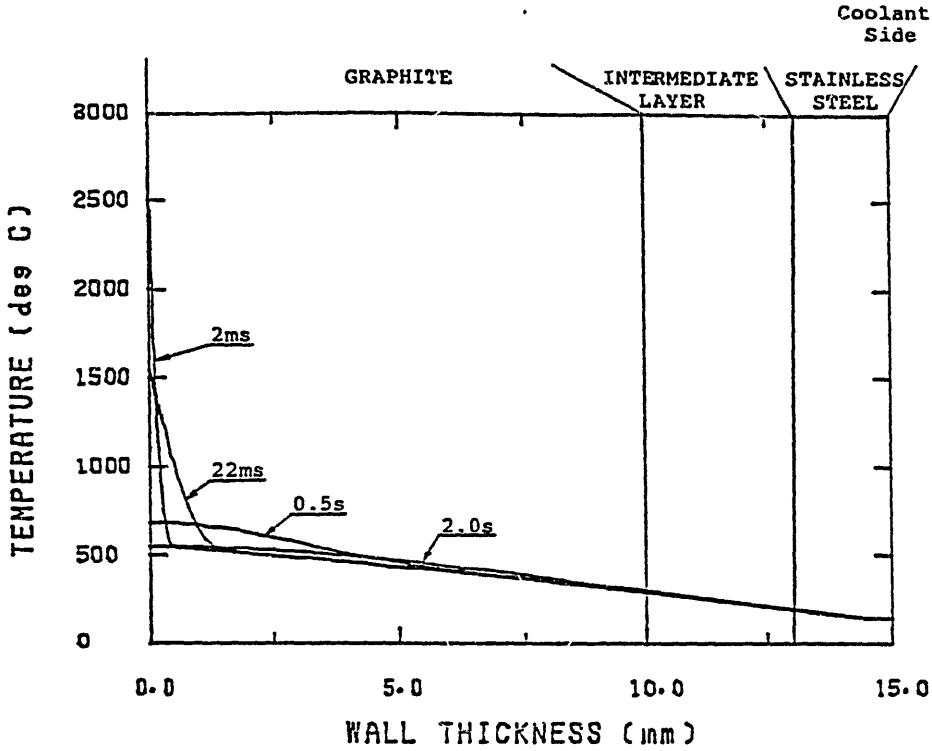

Fig. II.3-6 Temperature Profiles in Graphite Armor during and after Plasma Disruption

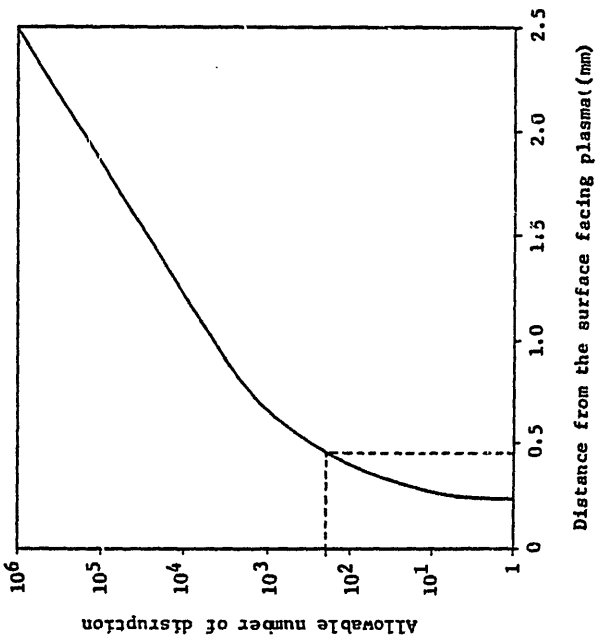

Fig. II.3-4 FW Region where Unaccpetable Fatigue Damage is taken Place by Plasma Disruption

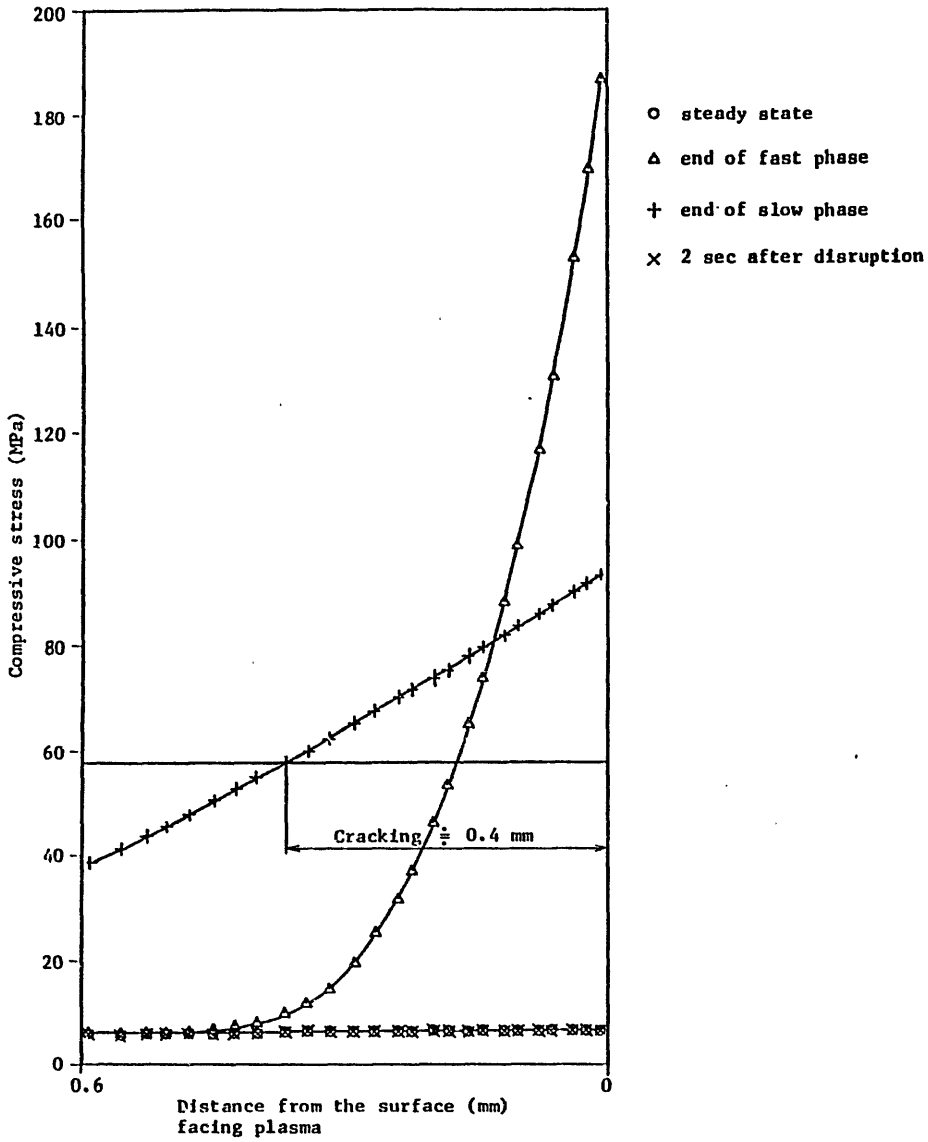

Fig. II.3-7 Stress Distribution in Graphite Due to Plasma Disruption obtained from Elastic Analysis, and Cracking Region

ISSUE OF EACH TOPIC

Some Brief Remarks on Several Critical Aspects of Graphite Data Bases for Fusion Energy Applications

W.P. Eatherly
Oak Ridge National Laboratory
Oak Ridge, Tennessee USA

Abstract

The theory of graphite thermal conductivity is briefly reviewed and the data requirements and manufactures' limitation are summarized. The existence of multiple flaw field in graphite and their role in failure strength and its statistics is traced. The use of fracture mechanics concepts is key and leads to non-destructive(sonic) techniques to predict actural failure strength.

Summary

In the brief time available, I would like to quickly examine a few characteristics of graphite of particular significance to fusion energy devices.

The theory of graphite thermal conductivity is well understood, and is entirely due to lattice waves except near absolute zero temperature. Above room temperature in unirradiated material the phonons(lattice wave packets) scatter of each other(umklapp process) due to the anharmonic nature of the lattice vibrations. With neutron damage, defect(incoherant) scattering quickly dominates. The manufacturer's only control is degree of crystal orientation and material contiguity. Hot-worked pyrolitics exhibit conductivities very near those of single crystals.

Like many ceramics, graphite strengths exhibit the characteristics of multiple flaw fields. Graphite always exhibit a background flaw field introduced through the raw materials and their sizing. A disparate field of larger flaws may be introduced in fabrication. The backgronud flaw field shows Weibull(weakest-link) statistics with the shape facter (Weibull exponent) affected by formingmethod. Hence strength is a function of stress volume and this effect is critical in failure analysis for design.

Principles of fracture mechanics can be used to predict strength from non-destructive test methods. Sonic attenuation senses the background flaw field and, with sonic modulus, yields a strength estimate. Disparate flaws are sensed by sonic reflection and can be the dominant strength-determining feature.

We close by exhibiting a graphite reentry vehicle nose tip ground tested in simulation of steep reentry. Thermal shock occurred under both heat-up and cool down. A disparate flaw occurred at a critical point, was identified sonically prior to test, and later found at the initiating fracture surface. The nose-tip failure was catastrophic.

CONCLUSIONS

1. GRAPHITE IS ESSENTIALLY A LATTICE THERMAL CONDUCTOR
2. THE NUMBER OF PHONONS IS VERY LARGE (I.E., BANDS EXIST AT VERY LOW FREQUENCIES)
3. THEREFORE, GRAPHITE IS AN EXCELLENT THERMAL CONDUCTOR
4. THE ANISOTROPY IN THE LATTICE VIBRATIONAL BEHAVIOR IS SO GREAT, THE IN-PLANE THERMAL EXPANSION CAN BE NEGATIVE

WE.VWG 3 15-NOV-85

INTRODUCTION

GRAPHITE MAY BE CHARACTERIZED AS A

METAL

SEMI-CONDUCTOR

INSULATOR

CERAMIC

PSEUDO-PLASTIC CERAMIC

DEPENDING ON WHAT PROPERTY YOU ARE ATTEMPTING TO DESCRIBE

THIS SIMPLY REPRESENTS THE SAME VERSATILITY OF THE CARBON ATOM AS EXEMPLIFIED IN ORGANIC AND BIOLOGICAL CHEMISTRY

WE.VWG 4 15-NOV-85

MAJOR ROUTES OF GRAPHITE FABRICATION

NUCLEAR AND AEROSPACE GRADES

CONVENTIONAL	NONCONVENTIONAL
CALCINED COKE FILLER (1000–1300°C)	GREEN COKE FILLER (350–600°C)
PITCH BINDER	PITCH BINDER
FORMING (EXTRUSION, MOLDING)	FORMING (MOLDING)
CARBONIZATION (900–1000°C)	
IMPREGNATION	
GRAPHITIZATION (2600–2800°C)	GRAPHITIZATION (2800–3200°C)
COST	
$3.00 – 30.00/LB	$30.00 – $60.00/LB

THE THERMAL CONDUCTIVITY λ OF GRAPHITE IS COMPLETELY DESCRIBED (ABOVE 10°K) BY LATTICE CONDUCTIVITY:

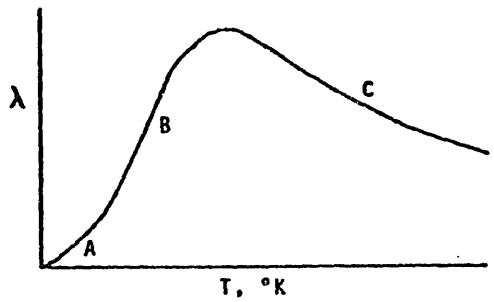

A. REGION OF ELECTRON AND PHONON CONDUCTIVITY LIMITED BY IMPERFECTION SCATTERING.

B. REGION OF PHONON CONDUCTIVITY LIMITED BY IMPERFECTION SCATTERING.

C. REGION OF PHONON CONDUCTIVITY LIMITED BY PHONONS SCATTERING OFF EACH OTHER.

FLAWS IN GRAPHITE APPEAR TO BE DIVISIBLE INTO TWO CLASSES:

1. BACKGROUND FLAWS INHERENT IN THE MATERIAL AND COMPARABLE TO THE GRAIN SIZE. THESE ARE DETECTABLE IN PRINCIPLE BY SONIC ATTENUATION.

2. DISPARATE FLAWS APPARENTLY INTRODUCED IN FABRICATION. THESE ARE DETECTABLE IN PRINCIPLE BY SONIC REFLECTION.

IN "TRANSPARENT" AEROSPACE GRAPHITE THESE FLAWS ARE EASILY IDENTIFIABLE.

FAILURE CRITERIA: FLAWS

- THE STATISTICAL IDENTIFICATION OF THE FLAWS DEPENDS ON IDENTIFICATION OF NEGATIVE OUTLIERS (ATTRIBUTED TO DISPARATE FLAWS) FROM THE DOMINANT DISTRIBUTION (ATTRIBUTED TO BACKGROUND FLAWS) SIMULTANEOUS TO A VARIANCE ANALYSIS.
- THIS DECOMPOSITION HAS BEEN SUCCESSFULLY APPLIED TO THREE SAMPLES: NUCLEAR GRAPHITE H-451, AEROSPACE GRAPHITE M3M, AND FIBROUS CARBON/CARBON INSULATION CBF. THE ANALYSES WERE SUCCESSFUL IN ALL THREE CASES, I.E., INTERNALLY CONSISTENT TO ALL STATISTICAL TESTS APPLIED.
- THE H-451 SAMPLE WAS THE LARGEST: 98 BILLETS OVER THREE LOTS WITH 1166 TENSILE MEASUREMENTS.
- THE RESULTS FOR SPECIMENS OF VOLUME 728 mm^3 WERE:

STRAIN MEASUREMENTS OF N3M GRAPHITE EXHIBIT BIMODALITY

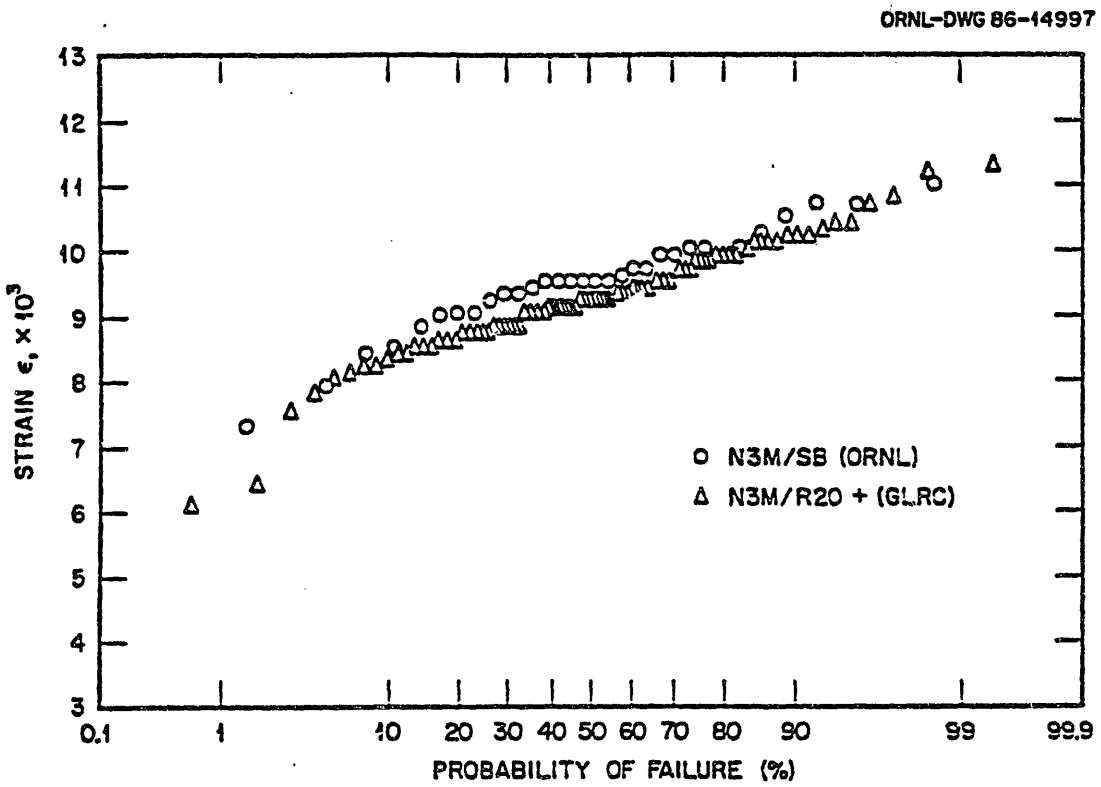

ornl

DATA BASES AVAILABLE AT ORNL

Graphite	Type	Manufactoer	Scope
N3M	Aerospace	Great Lakes	1, 2, 3, 4
H451	Nuclear	Great Lakes	1, 2, 4
AXF, AXM	Specialty	POCO	1, 2, 3, 4,
2020	Specialty	Stackpole	1, 2, 4
ATJ-S	Specialty	Union Carbide	1, 2, 3, 4
TS-1792	Specialty	Union Carbide	1
IG-11	Specialty	Toyo Tanso	1
CBCF	Fibrous Insulation	O R N L	1, 2
Various FRG graphites	Nuclear	Sigri	1, 2, 4

Scope:

1. Non-destructive test survey including statistical variance analysis.
2. Thermomechanicals
3. Thermal shock
4. Neutron damage

H-451 IMPROVEMENT

DISPARATE FLAW SYSTEM

DISPARATE FLAWS COMPLETELY DOMINATE TOLERANCE LIMITS:

	BACKGROUND	DISPARATE
POPULATION	96.2%	3.8%
MEAN	$\bar{x}$	$(\bar{x} - 5.03)$ MPa
STD DEV	1.36 MPa	1.07 MPa
AT 99/95:		
CUT OFF	$(\bar{x} - 4.03)$ MPa	$(\bar{x} + 1.00)$ MPa
CONTRIBUTION	27%	72%

THUS, ABOUT THREE-FOURTHS OF OUR PROBLEM IS REMOVED IF THERE WERE NO DISPARATES

INDIVIDUAL MEASUREMENTS ARE NOT NORMALLY DISTRIBUTED

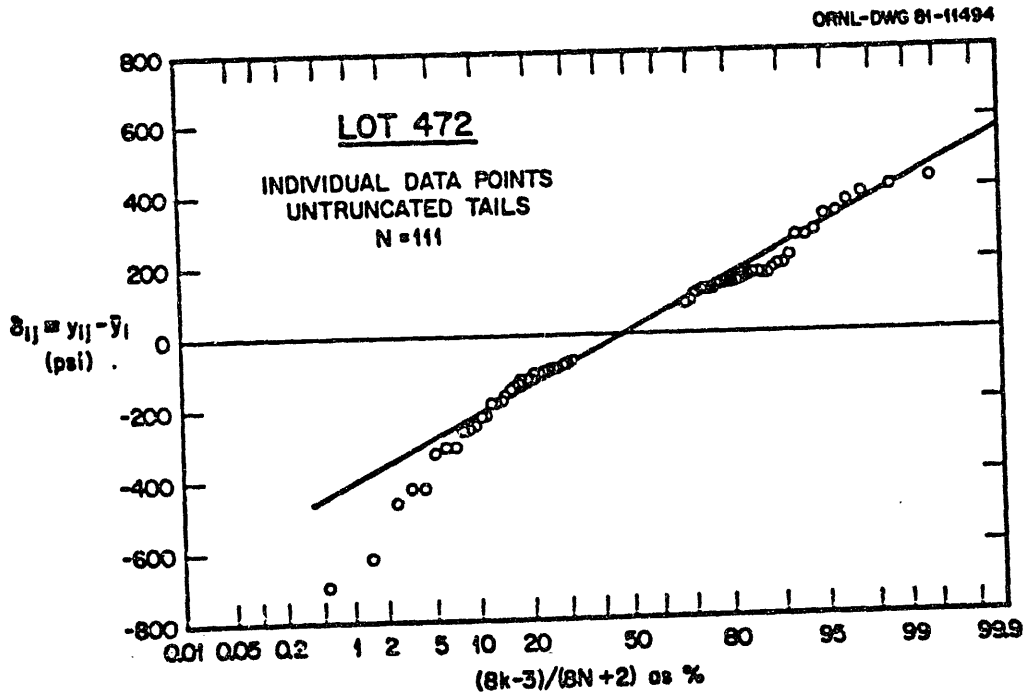

ornl

THE VALUE OF WEIBULL m-PARAMETER VARIES FROM m ≈ 18 FOR FINE-TEXTURE, MOLDED GRAPHITE TO m ≈ 7 FOR EXTRUDED, COARSE-GRAIN GRAPHITE

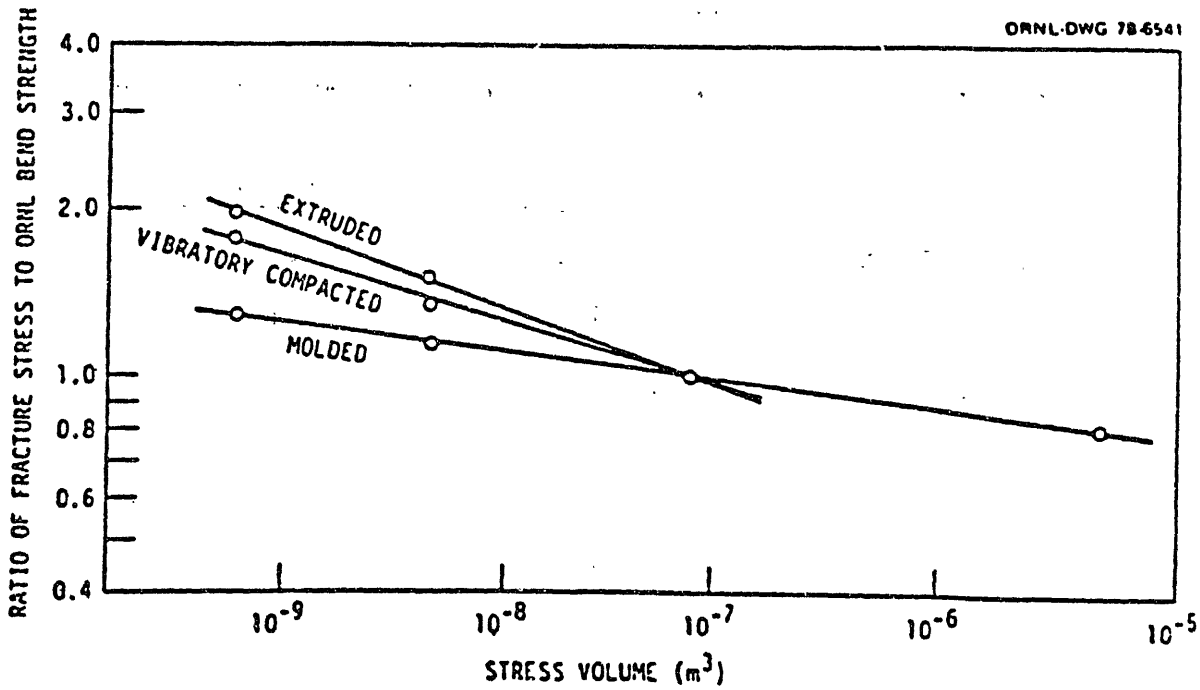

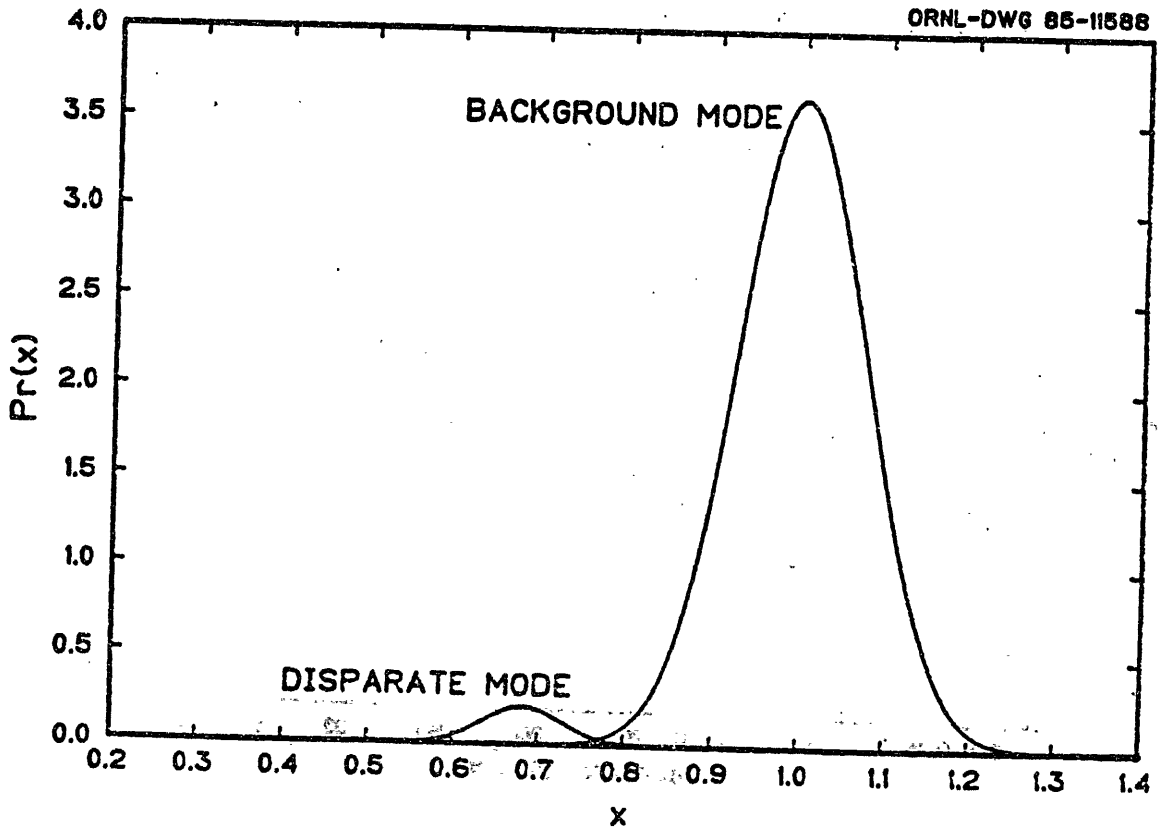

FRACTURE TOUGHNESS DECREASES EXPONENTIALLY WITH POROSITY

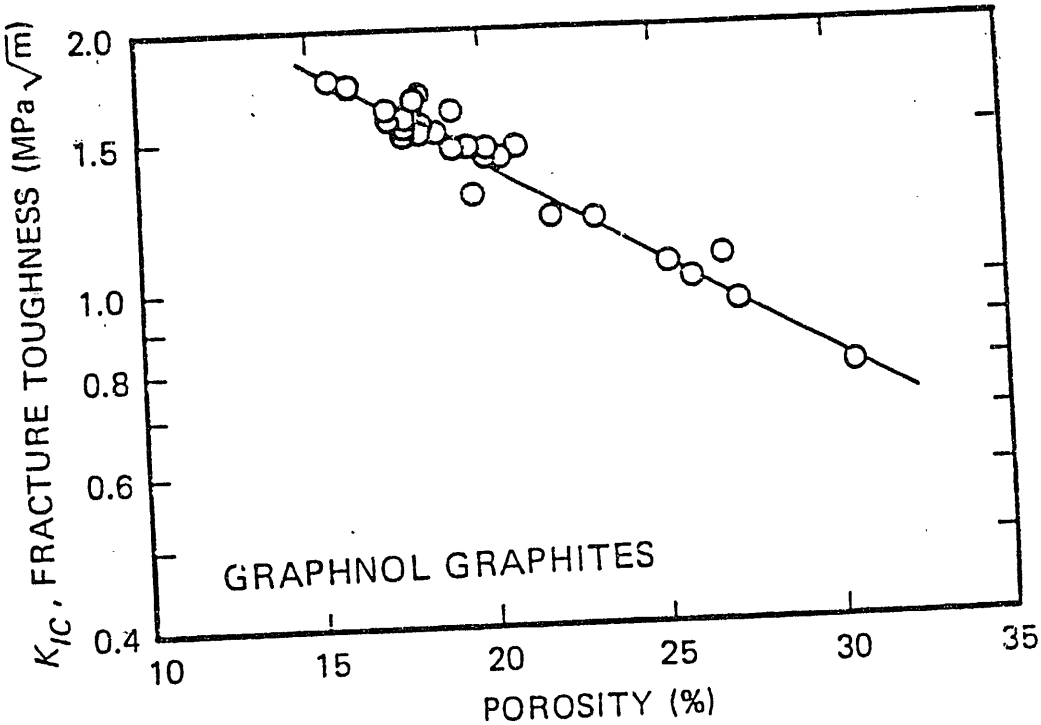

COMPUTER PROGRAMS ALSO USE WEIBULL STATISTICS IN THE CELL ELEMENTS

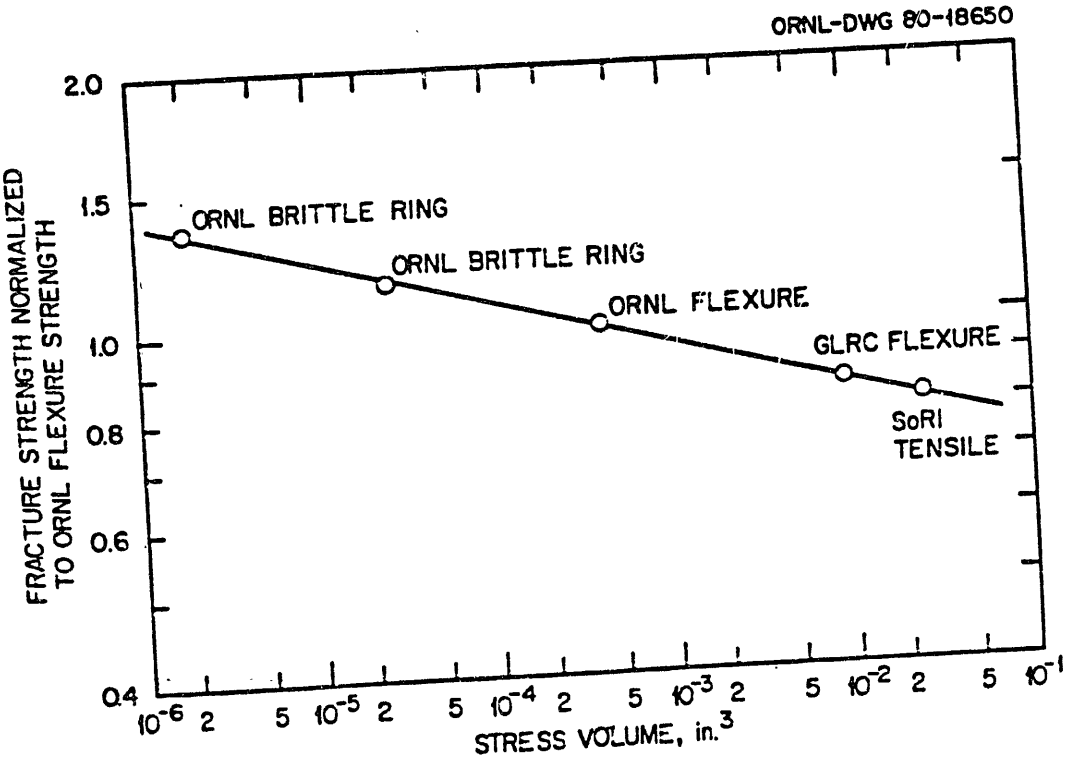

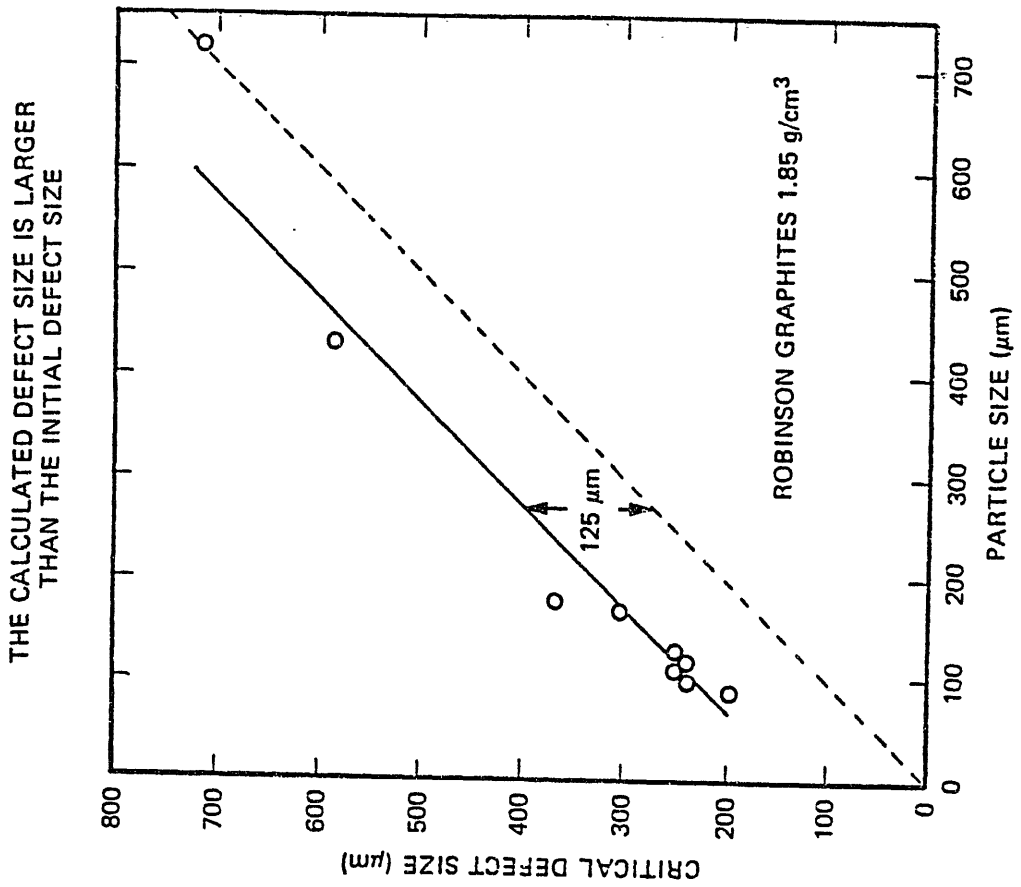

STEAM OXIDATION ALSO REDUCES THE FRACTURE TOUGHNESS EXPONENTIALLY WITH POROSITY

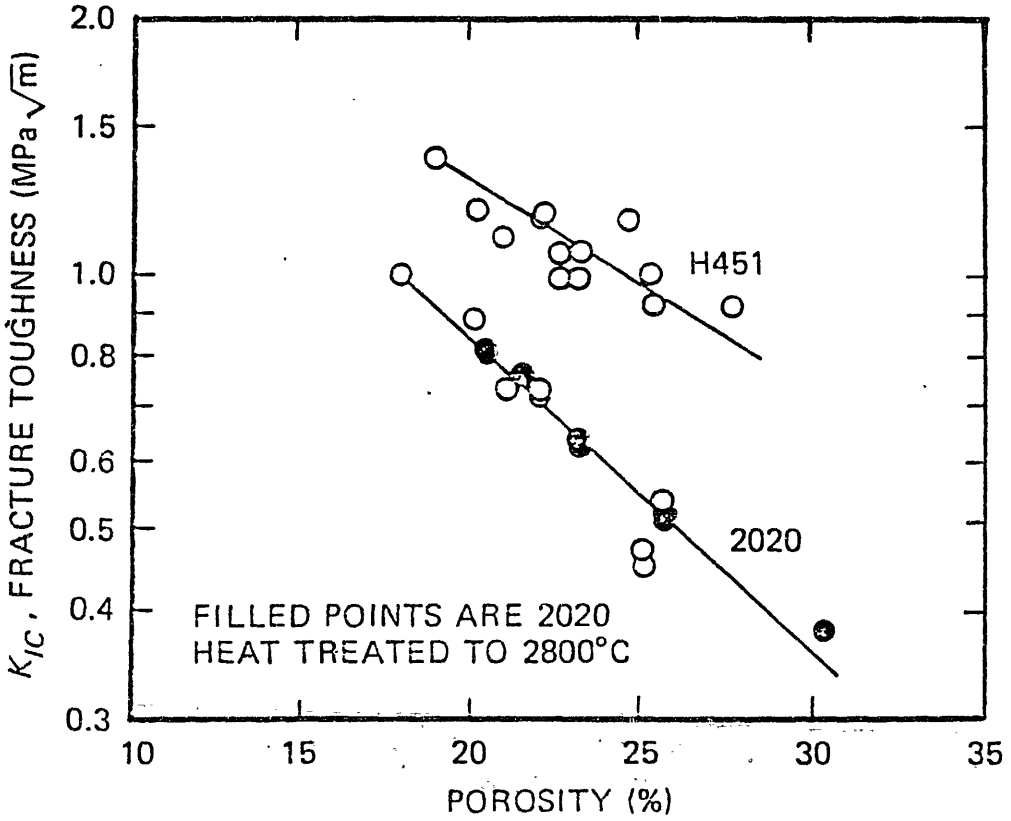

GRAPHITE IS NOT A CLASSICAL BRITTLE MATERIAL

- $a = c + \delta \overline{R}$

  c = INITIAL DEFECT SIZE

  δ = CHANGE IN COMPLIANCE

  $\overline{R}$ = FLAW SIZE GROWTH

- $$\sigma_f = \frac{K_{IC}}{(\pi a)^{1/2}} \; f\left(\frac{a}{W}\right)$$

  $K_{IC} = [E\ G_{IC}]^{1/2}$, FRACTURE TOUGHNESS

THE GRIFFITH-IRWIN EQUATION HAS BEEN DEMONSTRATED TO BE APPLICABLE IN DESCRIBING FRACTURE OF MOST CERAMICS AND GRAPHITES

$$\sigma_f = \left[\frac{G_{IC}\ E}{\pi a (1-\nu^2)}\right]^{1/2} f\left(\frac{a}{W}\right)$$

G_{IC} = STRAIN ENERGY RELEASE RATE

E = YOUNG'S MODULUS

a = CRITICAL DEFECT SIZE

$f\left(\frac{a}{W}\right)$ = GEOMETRIC FACTOR

CONCLUSIONS

FRACTURE MECHANICS

1. ABILITY OF PSEUDO-PLASTIC FRACTURE MECHANICS TO PREDICT FAILURE AT LEAST SEMI-QUANTITATIVELY IS NO LONGER IN DOUBT

2. SURFACE ENERGY PARAMETER G_{IC} IS THE MORE FUNDAMENTAL QUANTITY

3. MUCH WORK REMAINS TO PLACE THEORY ON QUANTITATIVE LEVEL AND FOLD INTO NONDESTRUCTIVE EVALUATION METHODS AND STATISTICS

PARTICLE SIZE DOES NOT AFFECT FRACTURE TOUGHNESS

[ROBINSON FILLER - 1.85 g/cm³ DENSITY]

Particle Size µm	Fracture Toughness, K_{IC}, MPa·m$^{1/2}$	Brittle Ring Fracture Strength, MPa	Critical Defect 2a, µm
725	1.55	46.2	717
430	1.59	52.4	586
180	1.65	68.3	372
170	1.55	71.0	303
125	1.54	79.0	242
110	1.62	81.4	252
100	1.63	84.1	239
90	1.62	86.9	195

SONIC REFLECTION EASILY LOCATES AND DETERMINES PROJECTED AREA OF DISPARATE FLAWS. ARTIFICIALLY INTRODUCED HOLES ARE USED FOR CALIBRATION.

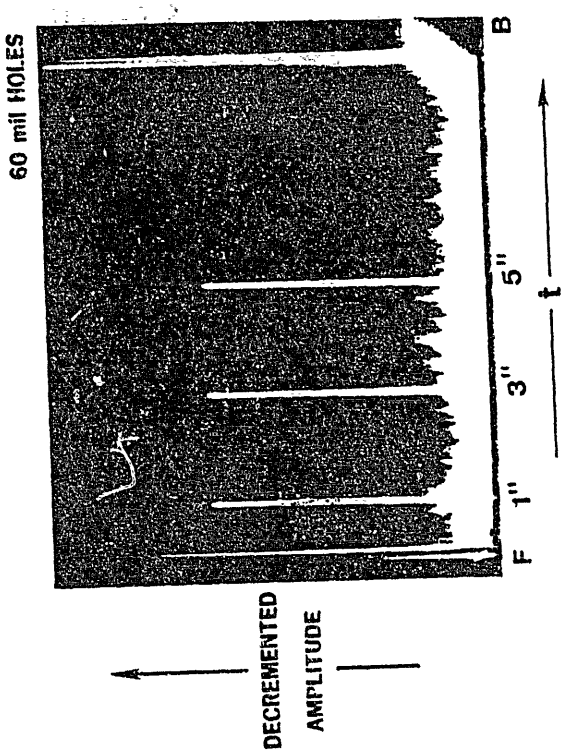

LET US ACCEPT THE HYPOTHESES

G_{1c} IS A TRUE MATERIAL CONSTANT

E IS PROPERLY THE INFINITESIMAL (SONIC) MODULUS

a, THE SONIC ATTENUATION, IS PROPORTIONAL TO DEFECT SIZE (AND NUMBER DENSITY)

THEN

$$\sigma_f \propto \left(\frac{E}{a}\right)^{1/2} = \left(\frac{E}{\alpha}\right)^{1/2}$$

THE VALIDITY OF THIS RELATIONSHIP IS IMPLIED BY BOTH TENSILE AND COMPRESSIVE (SHEAR) FAILURE.

GRAPHNOL/CHARS NOSETIP
N3M NO PRES 11. SEC
CONTOUR OF AXIAL STRAIN

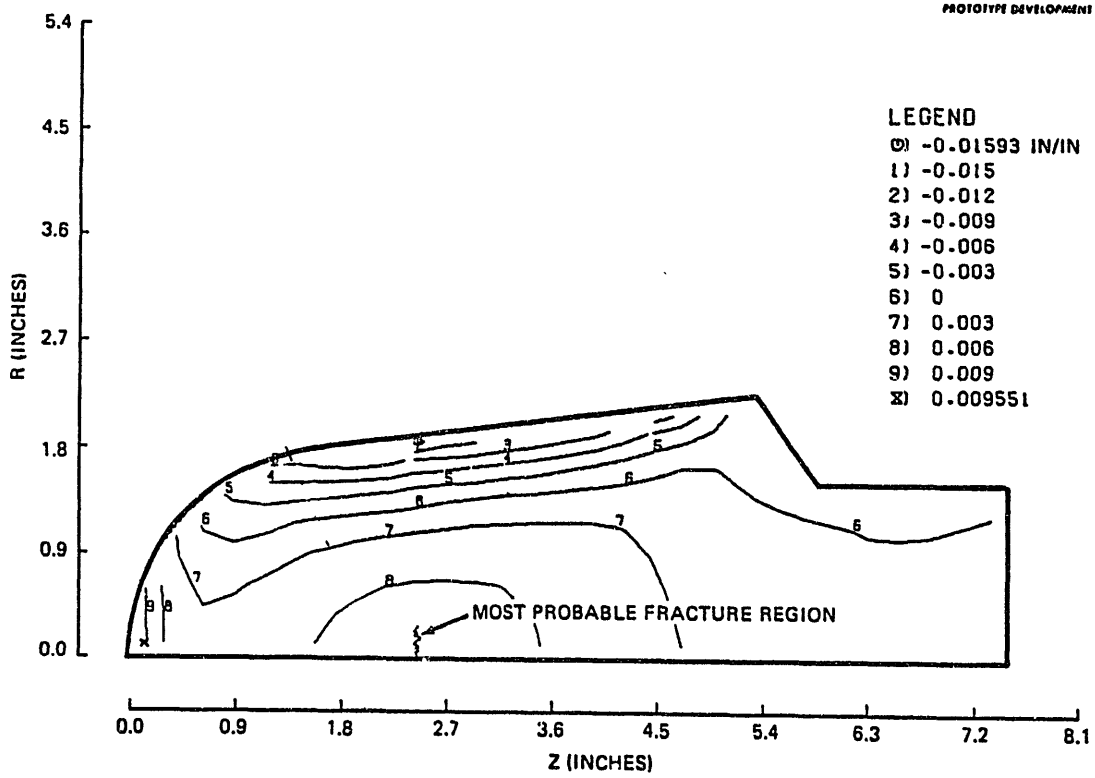

THE EFFECT OF POROSITY ON ATTENUATION:

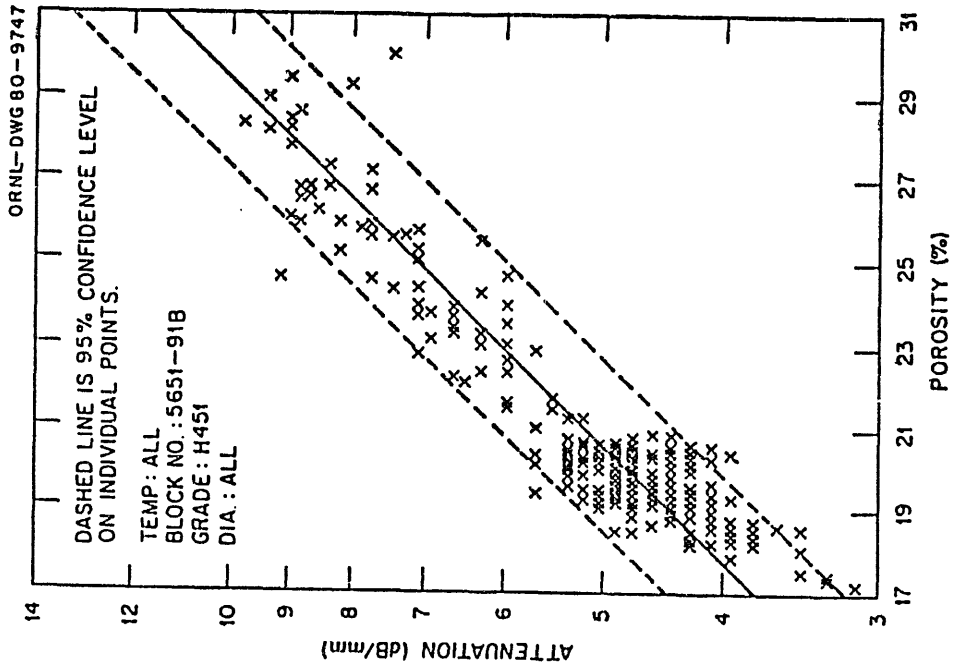

SPECIMENS ARE O-RINGS. DASHED LINE IS 95% CONFIDENCE BAND FOR INDIVIDUAL POINTS.

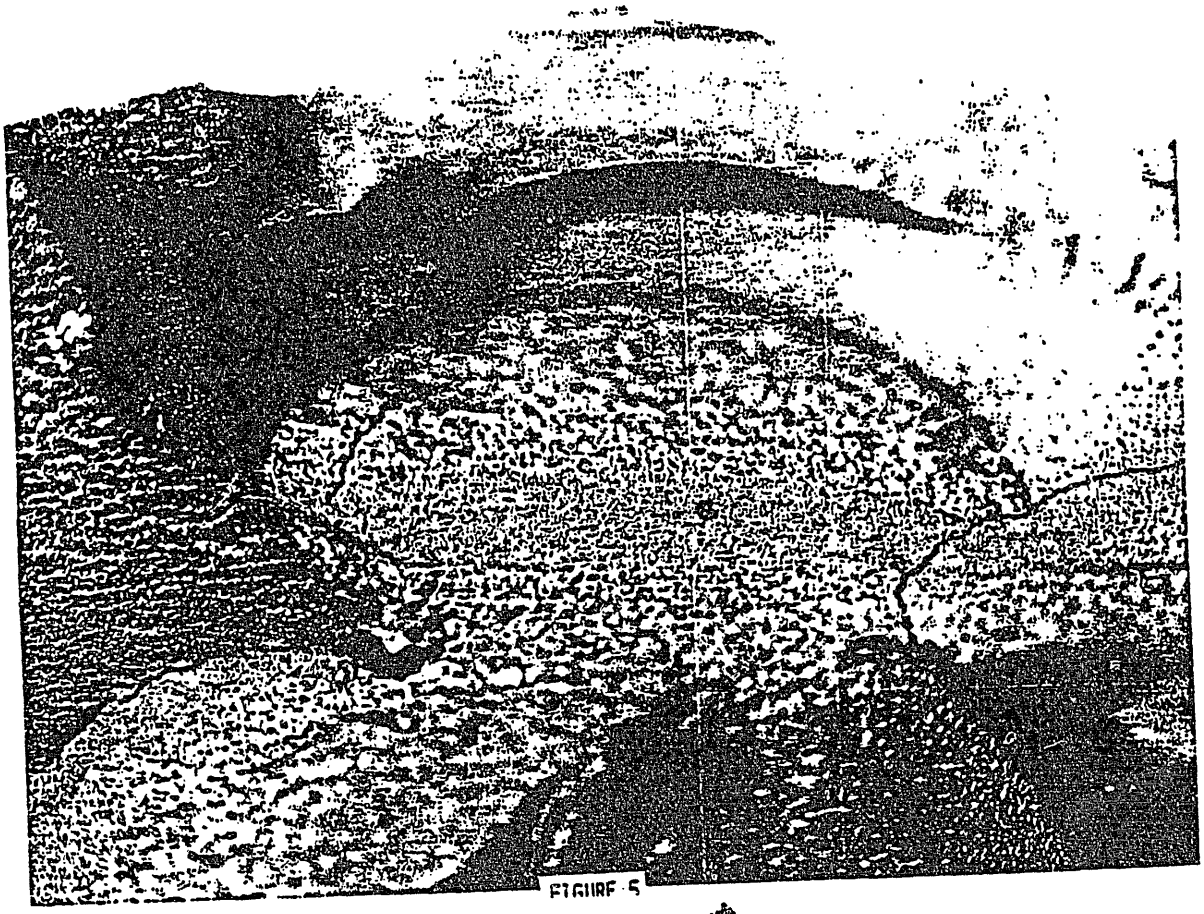

FIGURE 5

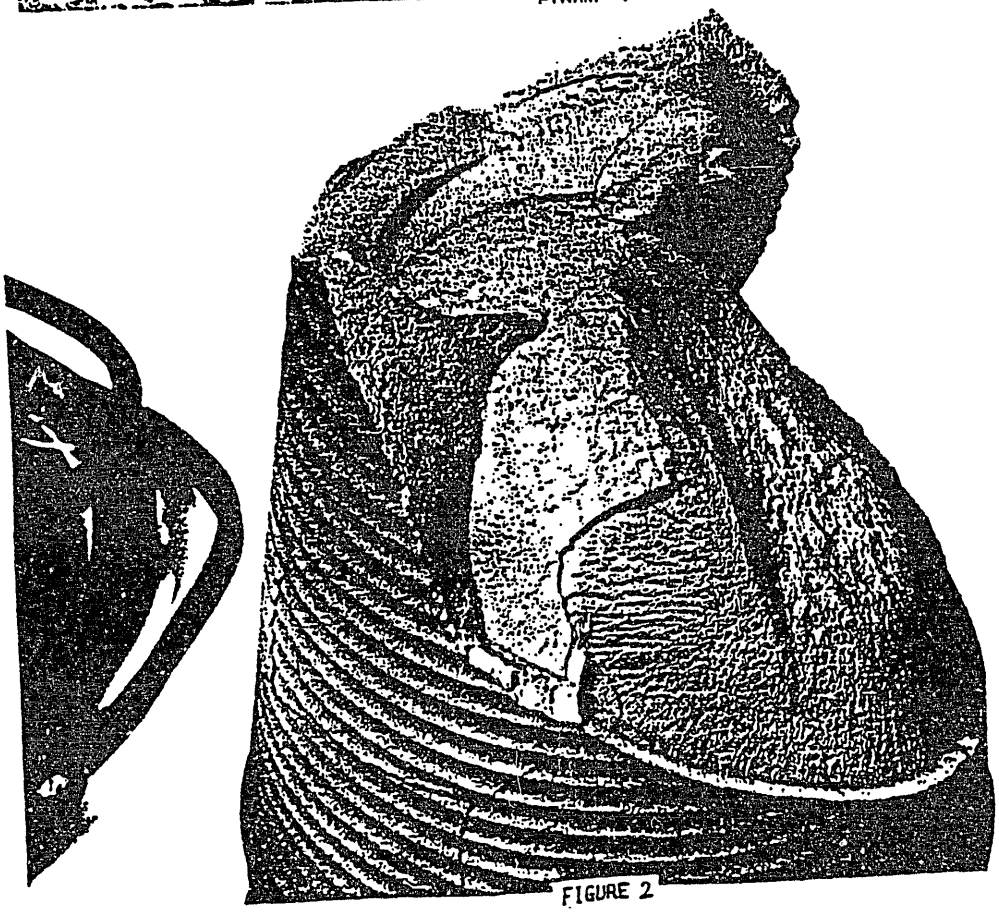

FIGURE 2

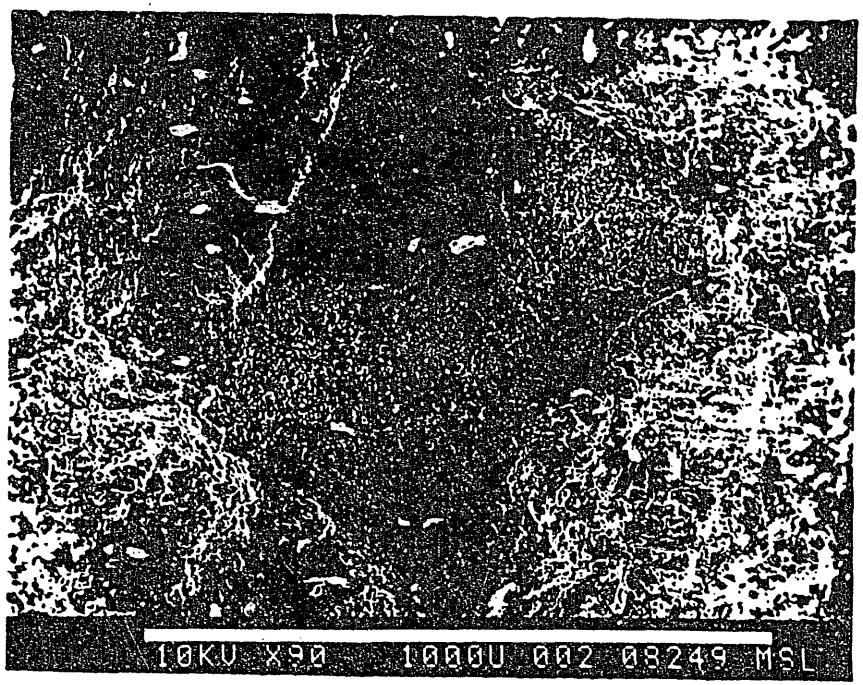

FIGURE 6

Characterization of graphites and C-C-composites

Tatsuo Oku

Japan Atomic Energy Research Institute,

Abstract

Physical and chemical properties are important to foresee the behaviour of graphite tilesunder fusion plasma environment. Data base of this aspect has been overviewed.

Characterization of graphites (and C-C-composites)

- physical properties
  - thermal conductivity
  - electrical resistance
  - young's modulus
  - tensile and flexural strength
  - coefficient of thermal expansion
  - density
- pores
  - porosity
  - size distribution
  - orientation
- quantitative analysis of impurities (2.6)

H. Beske	KFA - ZCH	H. Nickel	KFA - IRW
L. Binkele	KFA - IRW	H. Schiffers	"
W. Delle	"	G. Wolff	KFA - ZCH
G. Haag	"		
H. Heckner	KFA - ZCH		
K. Koizlik	KFA - IRW		
J. Linke	"		

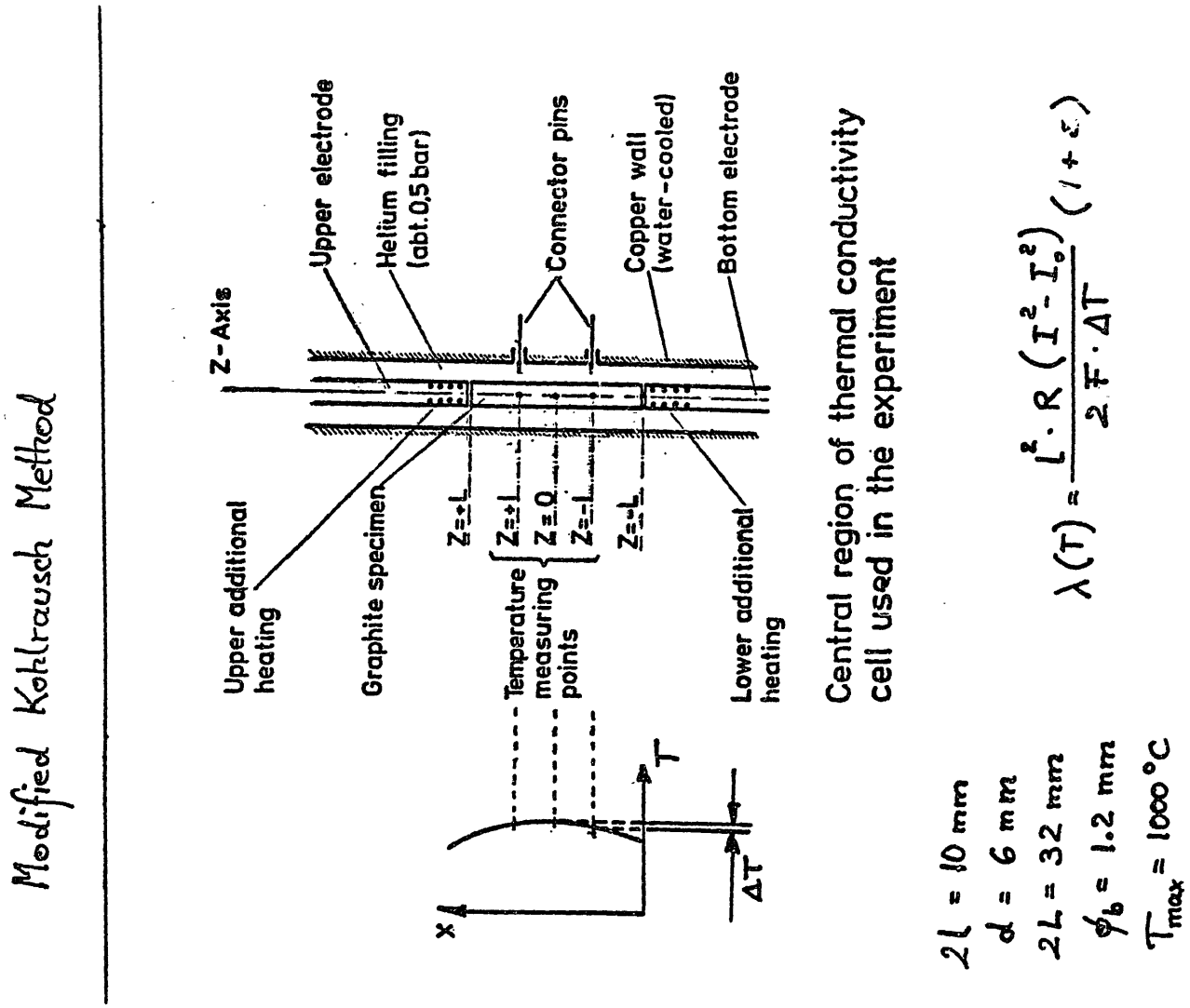

material	manufacturer
EK 98+	Ringsdorff-Werke GmbH, Bonn/D
5890 PT+	Le Carbone-Lorrain, Gennevilliers/F
AXF-5Q+	Poco Graphite, Inc., Decatur, TX/USA
EY-306+	Morganite Spec. Carbons Ltd., London/GB
FP-219+	Schunk Kohlenstoff GmbH, Gießen/D
H-490+	Great Lakes Carbon Corp., Niagaro Falls, NY/USA
ATJ	Union Carbide Corp., Parma, OH/USA
FE-289	Schunk-Kohlenstoff GmbH, Gießen/D
E 5923P*	Dunlop/GB

Tested fine grain graphites and carbon fibre composite material (*). The right hand collumn gives the manufacturers of the materials. The sequence of the graphites was chosen according to the arrival of the materials in IRW. (+ physical data from the IRW-characterization are available).

FP 219
80 orientation

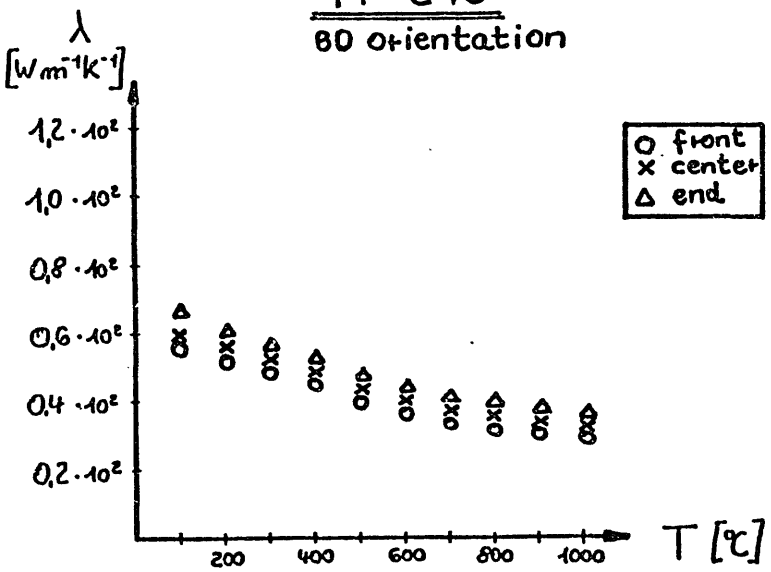

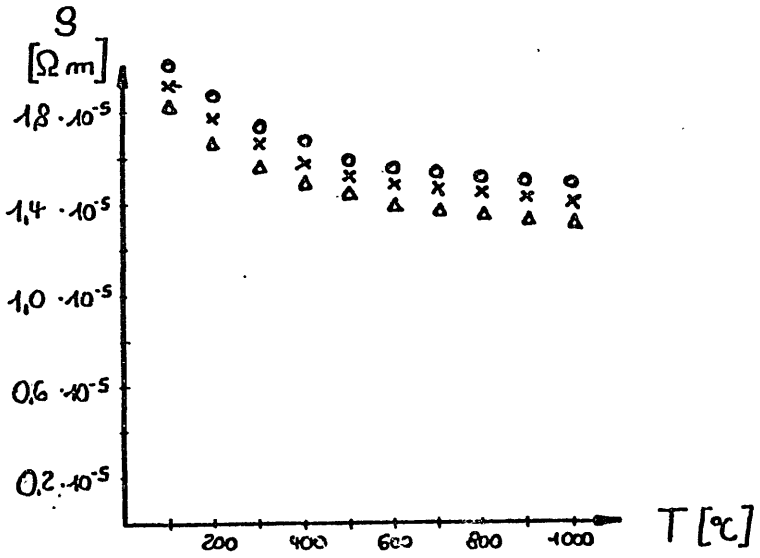

Determination of the dynamic Young's modulus

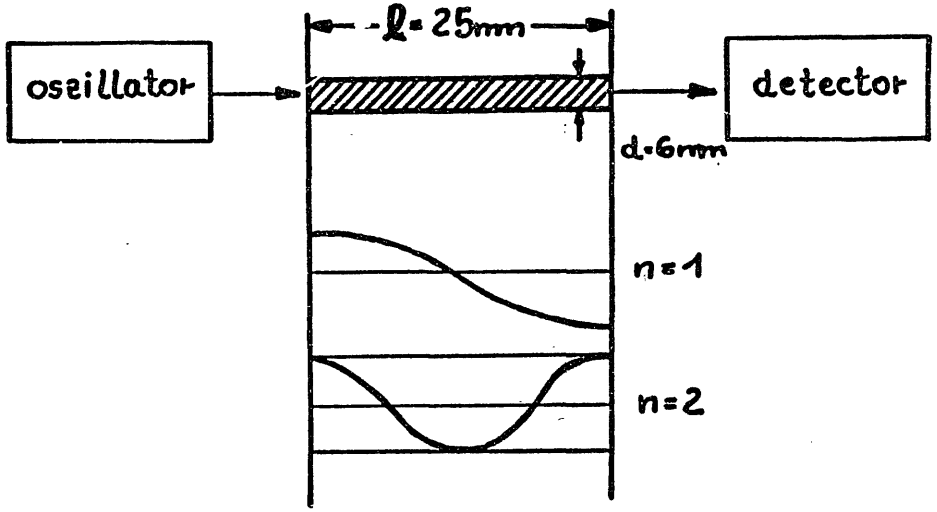

$$C = \sqrt{\frac{E_s}{d}}$$

$$\ell = n \frac{\lambda}{2}$$

$$C = f \cdot \lambda$$

C = propagation speed

d = density

λ = wavelength

f = frequency

$$E_s = \frac{4 \cdot \ell^2 \cdot f^2 \cdot d}{n^2}$$

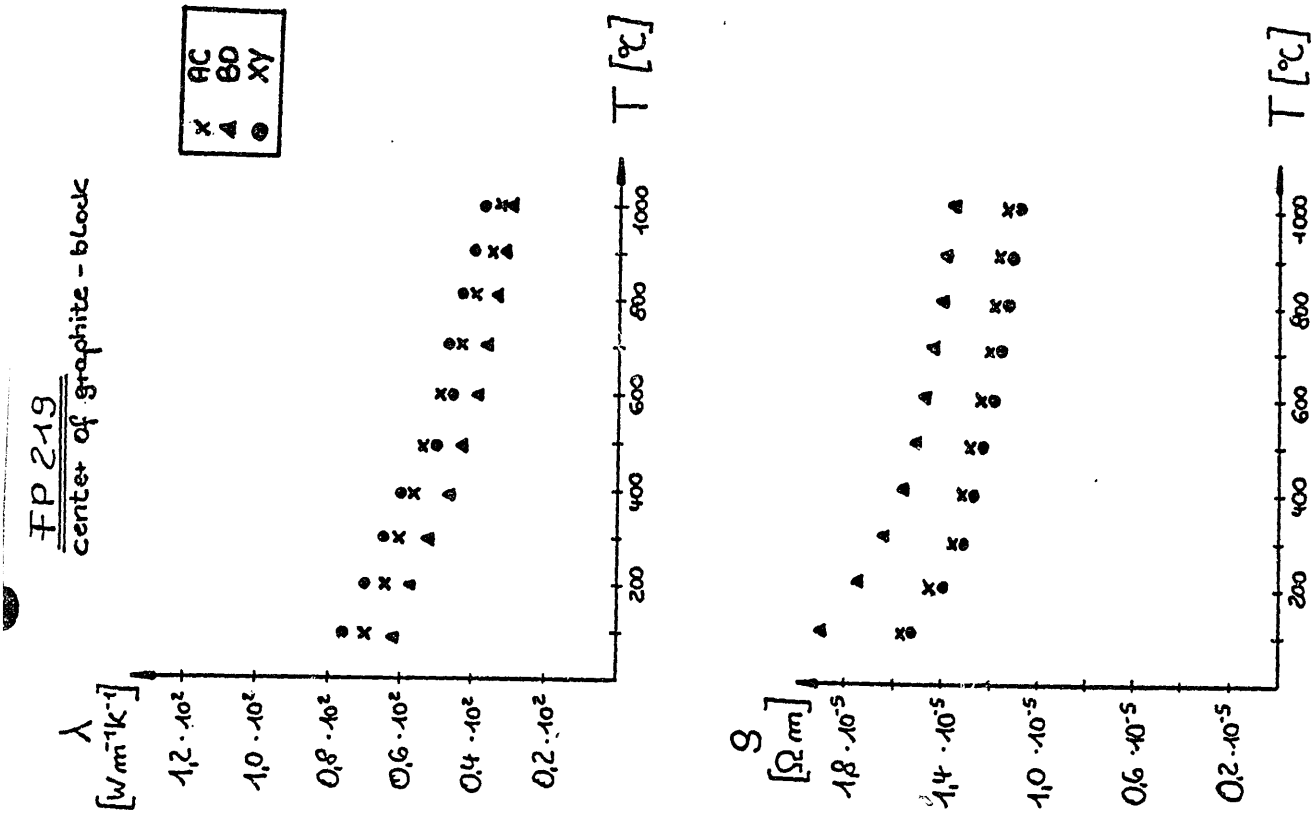

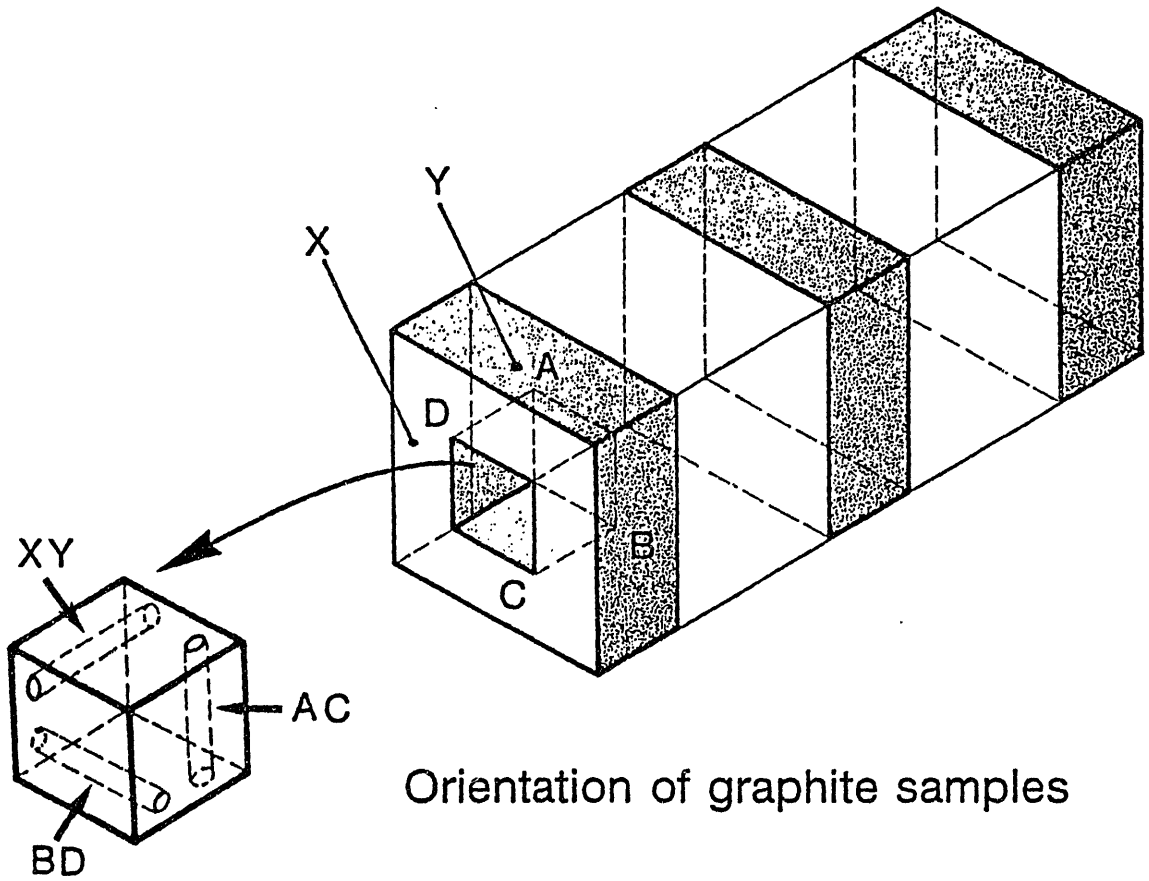

Orientation of graphite samples

HERSTELLER :	POCO	AGL		CARBONE LORRAINE		S+E	RINGSDORFF
QUALITÄT :	AXF-5Q	H-490		5980/PT		FP 219	EK 986
SCHNITTR. :	--	‖	⊥	‖	⊥	--	--
$\overline{R_B}$ (MPa)	87.9	33.6	30.8	53.0	43.0	29.8	47.4
±s (MPa)	10.3	4.1	1.1	3.2	2.5	1.0	1.1
V_p (%)	11.7	12.2	3.6	6.0	5.7	3.4	2.3
$\overline{f_B}$ (mm)	0.407	0.253	0.256	0.314	0.28	0.244	0.284
±s (mm)	0.051	0.03	0.011	0.016	0.014	0.009	0.007
V_p (%)	12.5	12.0	4.4	5.2	5.0	3.6	2.6
Korrel.-koeffiz. R	0.9968	0.9876	0.8582	0.9775	0.948	0.9197	0.8392
PROBEN-ZAHL n	10	10	10	10	10	10	10

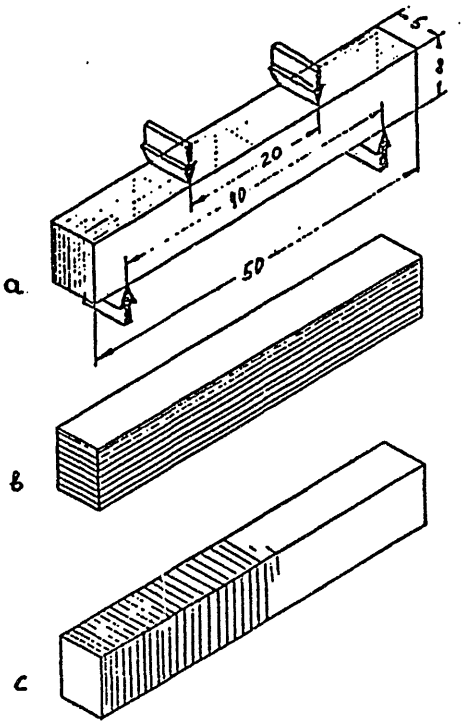

Hersteller:		
Qualität:		
Schnittrichtung:	1a	1b
R_B (MPa) ± S (MPa) V_p (%)	70,1 12,1 17,3	56,4 9,6 17,0
f_B (mm) ±s (mm) Vp (%)	0,259 0,042 16,0	0,293 0,037 12,6
Korrel. Koeffizient R	nicht signifi-kant	0,8715
Probenzahl n	3	7

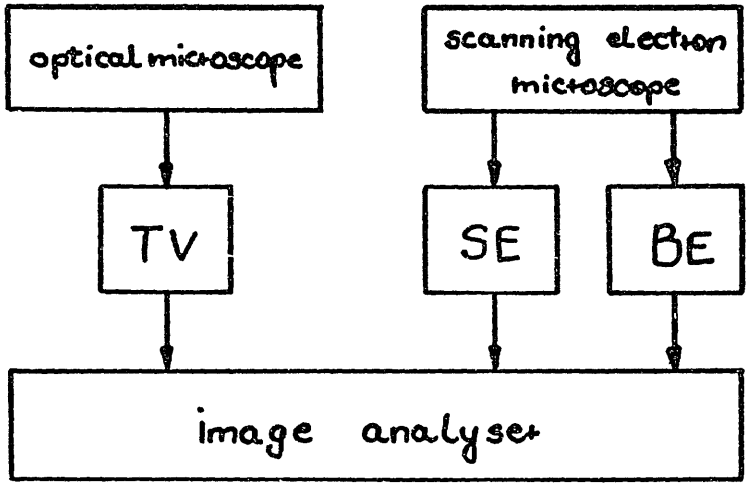

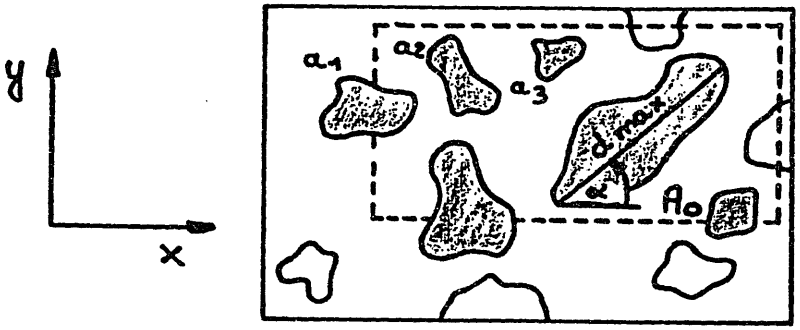

$$\text{porosity} = \frac{\Sigma a_i}{A_0}$$

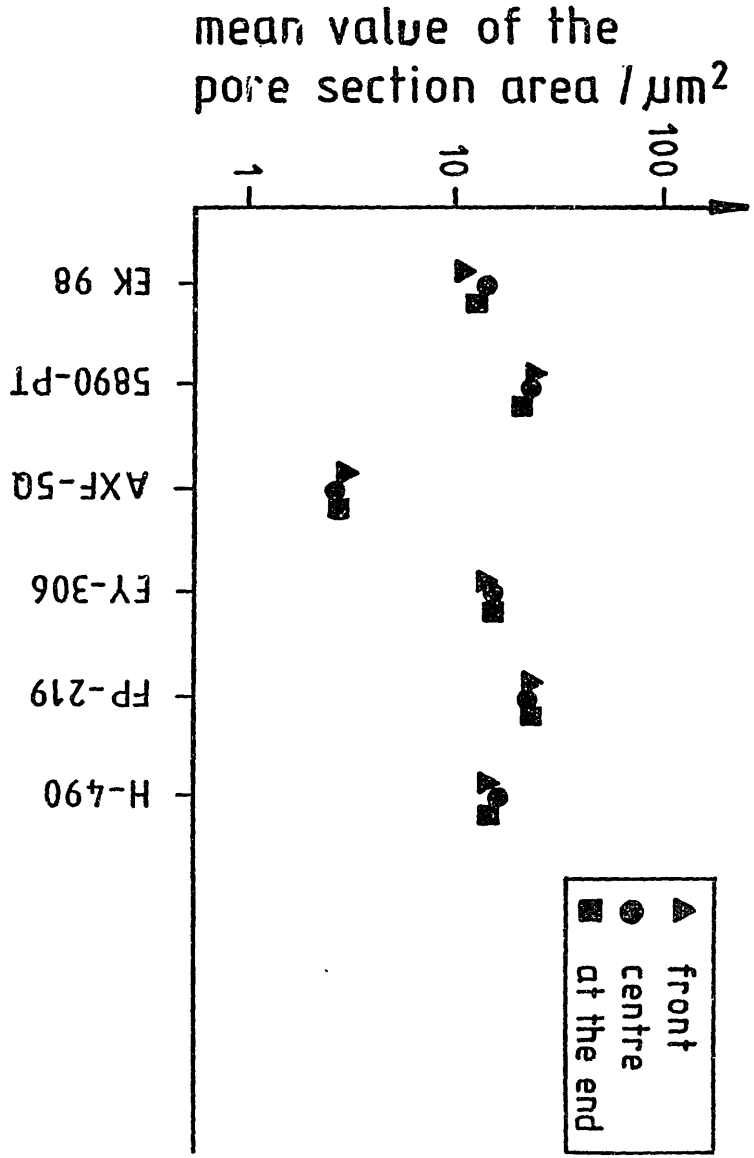

Material Character		Graphite							
		Ek 98	5890-PT	AXF-5Q	EY-306	FP-219	H-490	ATJ	E5923P
Kind of pres.		Isost.	Mould.	Isost.	Isost.	Isost.	Extrus.	Mould.	C-C-Comp.
App. density /gcm^{-3}		1.86	1.79	1.78	1.75	1.76	1.80	1.81	1.91
Open Poros. /V-%		8.2	11.1	18.1	17.6	13.7	13.2	11.5	9.6
Young's Modulus /kNmm^{-2}	XY	11.49	11.83	13.65	10.94	9.84	8.27	14.28	
	AC	11.48	10.79	13.71	11.80	9.68	10.14	12.72	
	BD	11.63	12.20	14.04	11.76	7.88	10.40	9.26	
Therm. Exp. (20-400°C) /10^{-6}K^{-1}	XY	3.35	4.38	8.53	5.90	2.82	4.16	2.28	
	AC	3.45	4.98	8.43	5.62	2.87	3.35	2.41	
	BD	3.33	4.55	8.31	5.47	3.73	3.03	4.08	
Elect. Resistivity /Ωmm^{2}m^{-1}	XY	16.11	16.41	19.16	19.41	17.16	14.06	8.71	3.99
	AC	16.18	17.43	18.77	18.72	17.43	12.03	9.39	17.36
	BD	16.06	15.98	18.31	18.04	20.58	11.69	12.05	

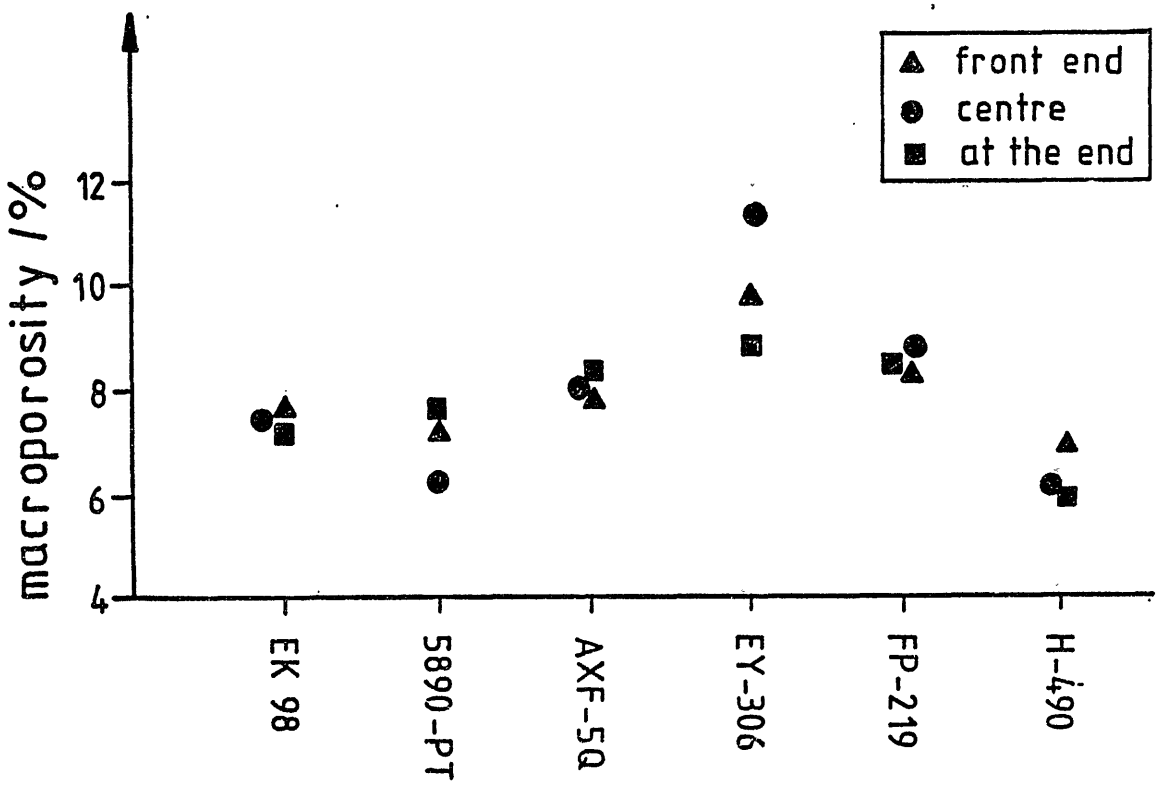

Zusammenfassung für alle untersuchten Graphitproben

Hersteller	Konzentrationsbereich der nachgewiesenen Verunreinigungselemente				
	10-20	20-50	50-100	100-200	> 200 ppm
Poco AFX-5Q	Ba,S	./.	Ca,V,Fe	./.	./.
Carbon Lorraine 5890/Pt	./.	S	./.	./.	V
Schunk und Ebe FP 219	Ca,V Mo	Ti,S	./.	./.	./.
Great-Lakes H-490	Ti	Al,Si, Cr,Ni,S	./.	V	Ca,Fe
Ringsdorff EK 98	S	./.	./.	./.	./.
Morgan	Ca	Al,Fe	./.	./.	./.
ATJ	Si,Ni	./.	S	Fe,Ca	./.
Togo Tanso IG11	./.	Ti,V	./.	./.	./.
Togo Tanso IG110	./.	./.	./.	./.	./.

Tabelle IV Aschegehalte der Graphitproben

	Probe	Asche gefunden ppm	Asche berechnet ppm
AXF 5Q	1.0	150	150
	1.1	161	180
	1.2	405	401
5890 PT	2.0	600	530
	2.1	680	480
	2.2	540	400
FP 219	3.0	100	90
	3.1	150	99
	3.2	100	84
H 490	4.0	1960	1730
	4.1	1510	1480
EK98	5.0	- 50	28
	5.1	50	40
EY 306	6.0	247	209
	6.1	361	326
	6.2	268	235
ATJ	7.0	580	584
	7.1	761	663
	7.2	695	576

Sandia Livermore Conditioning Studies

K.L. wilson

Sandia National Laboratories
Livermore, California USA

Abstract

The Sandia Livermore outgassing database for graphite and carbon-carbon composites is summarized, and testing of a 4-D carbon-carbon composite in TEXTOR is reported.

WALL CONDITIONING IS A CRITICAL ISSUE IN TOKAMAK OPERATION

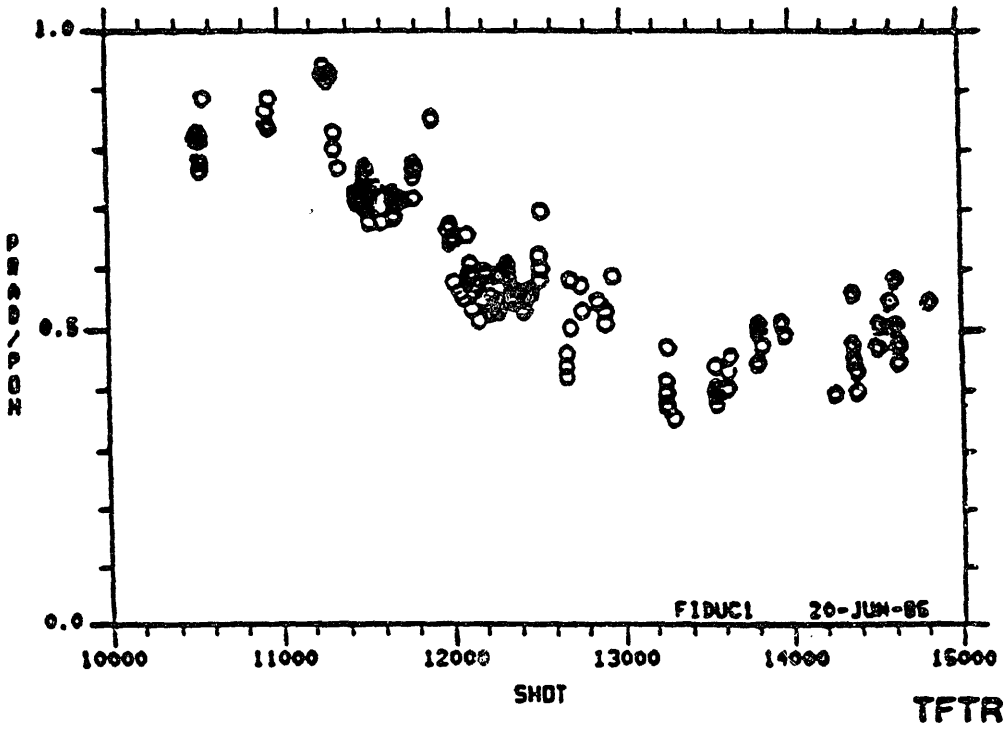

SANDIA LIVERMORE GRAPHITE CONDITIONING STUDIES

-- OUTGASSING

-- CARBON/CARBON COMPOSITE TESTING (TEXTOR)

K. L. WILSON
SANDIA NATIONAL LABS

OUTGASSING OF GRAPHITES AND CARBON/CARBON COMPOSITES

A. E. PONTAU
D. H. MORSE

SANDIA NATIONAL LABORATORIES
LIVERMORE CA 94550

SANDIA OUTGASSING FACILITY

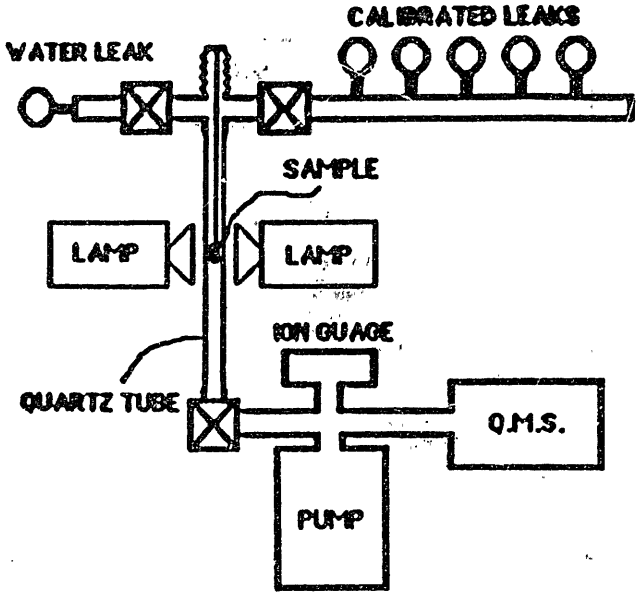

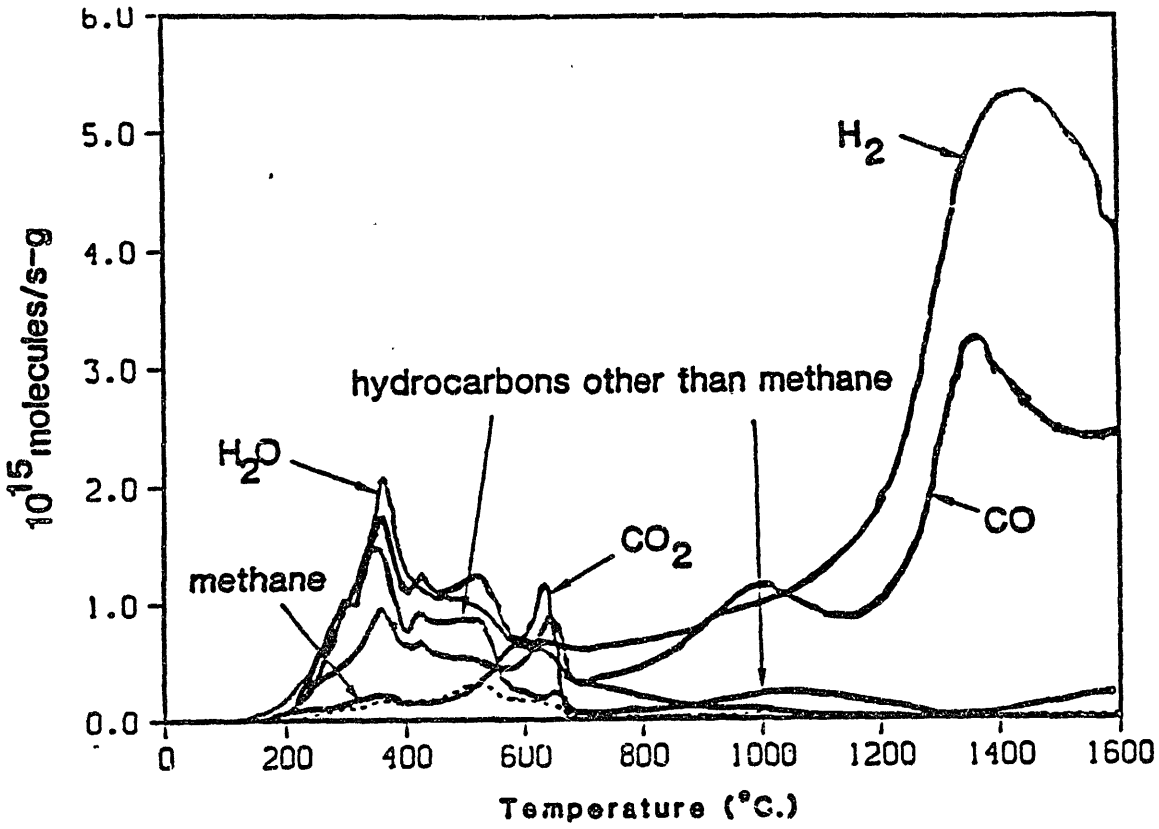

Procedure

a. Bake in vacuum oven 16 hours at 1000°C

b. Expose to air--variable duration

c. Bake in vacuum 1 hour at 125°C

d. Monitor evolving gasses during 1°C/sec ramp.

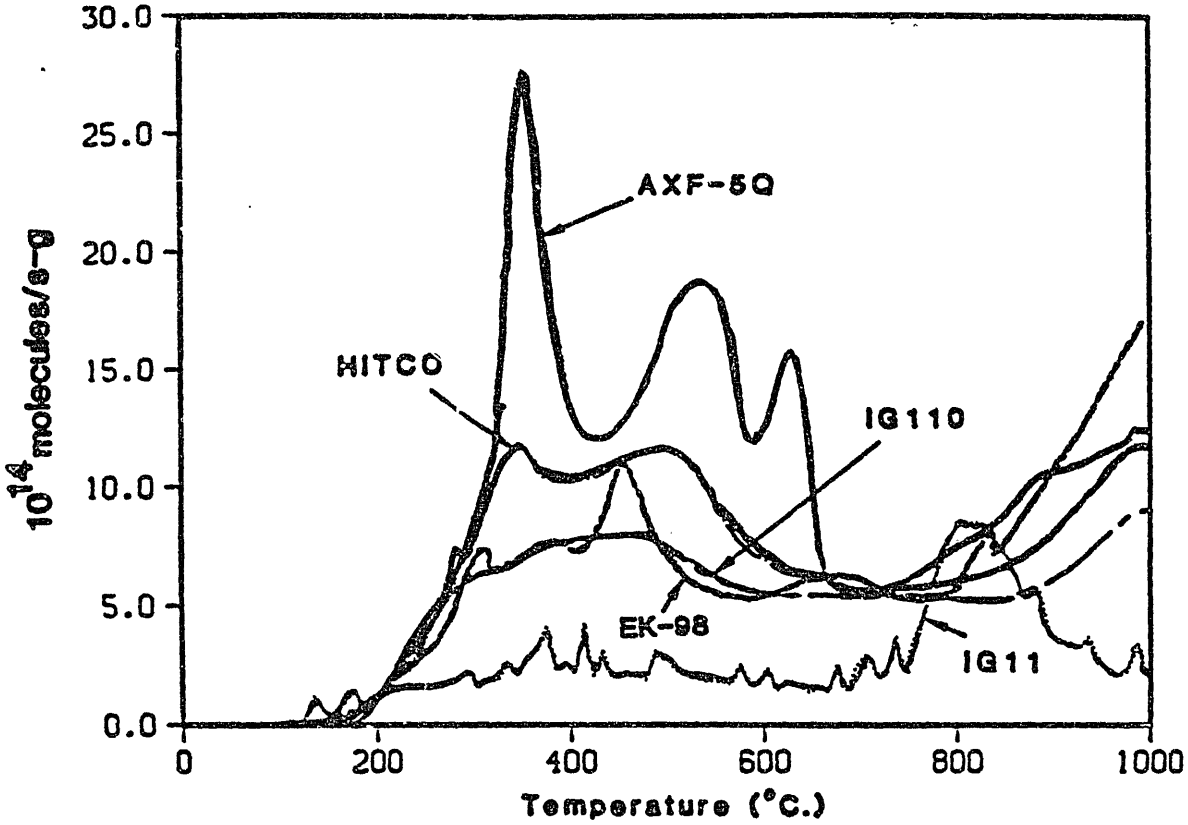
30.0
25.0
20.0
15.0
10.0
5.0
0.0
10^{14} molecules/s-g
AXF-5Q
HITCO
IG110
EK-98
IG11
0
200
400
600
800
1000
Temperature (°C.)

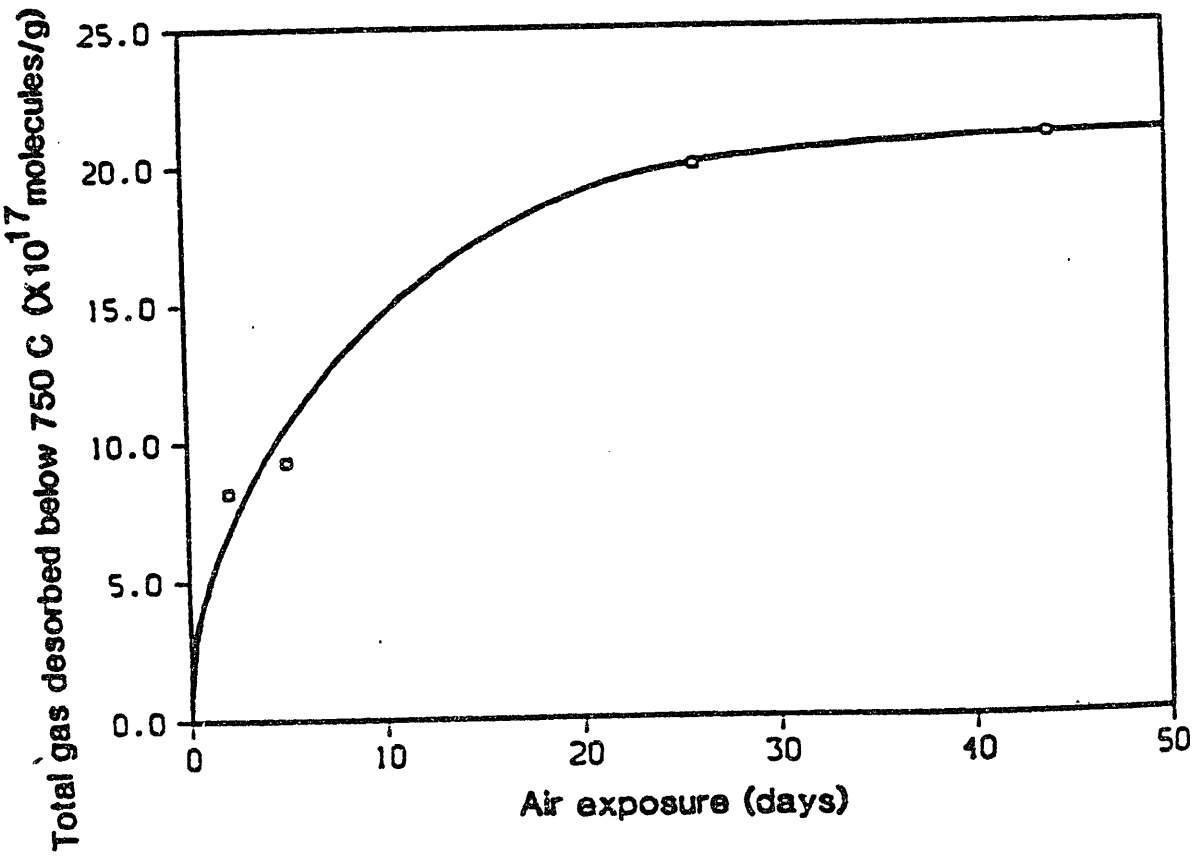
25.0
20.0
15.0
10.0
5.0
0.0
Total gas desorbed below 750 C (X 10^{17} molecules/g)
0
10
20
30
40
50
Air exposure (days)

RELATIVE OUTGASSING BELOW 1000 K FOR CARBON/CARBON COMPOSITES

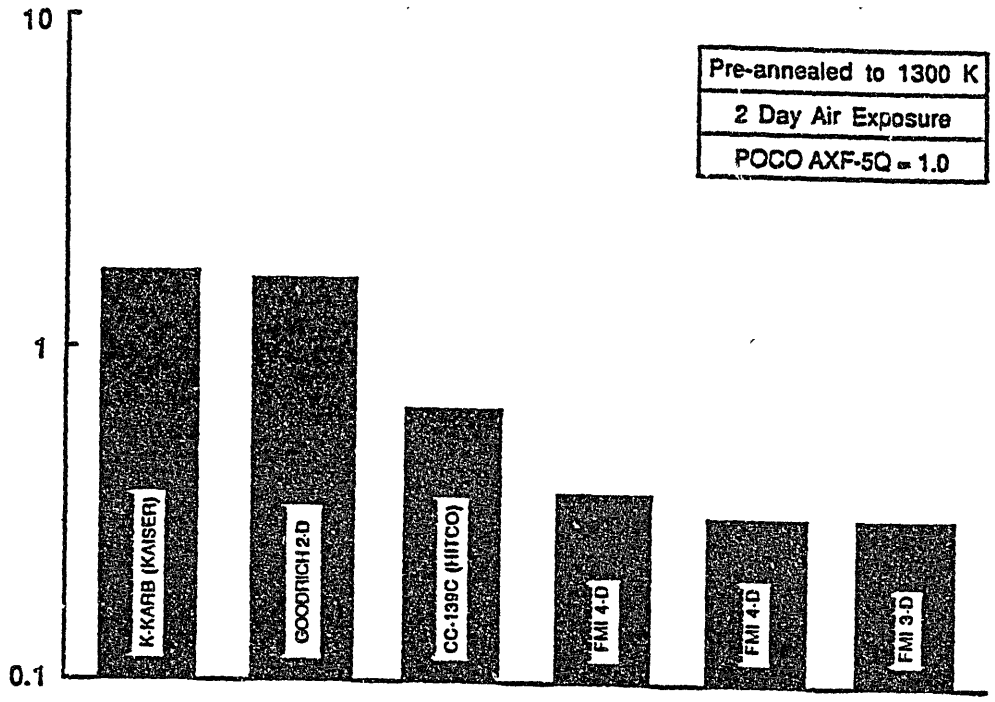

RELATIVE OUTGASSING BELOW 1000 K FOR GRAPHITES

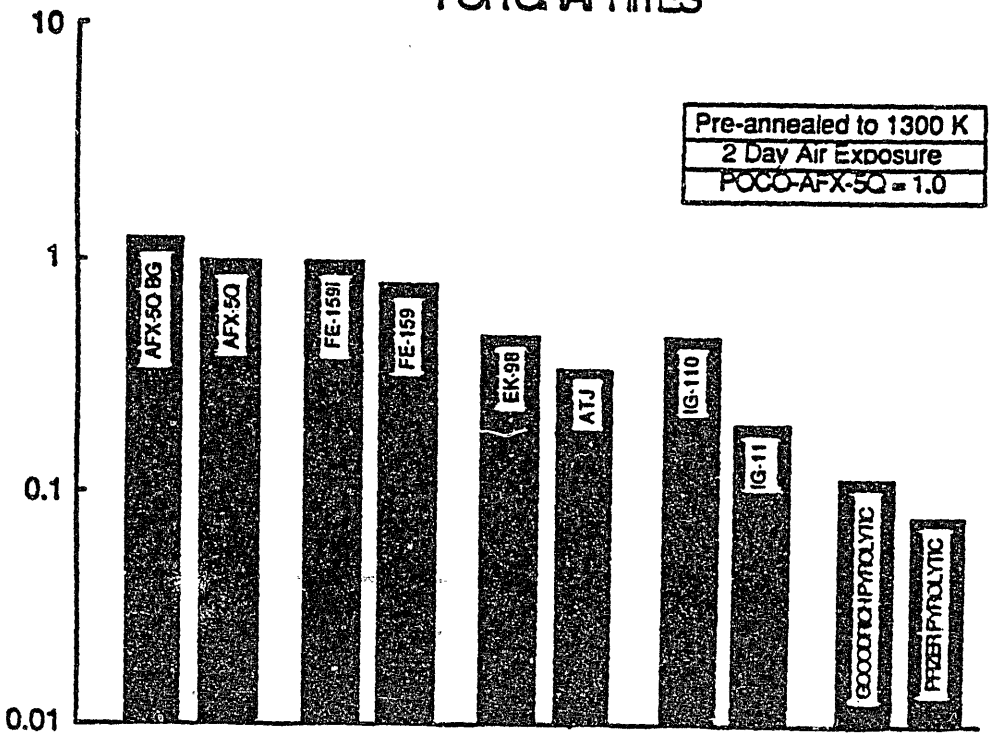

NO CORRELATION BETWEEN BET AND OUTGASSING WAS OBSERVED

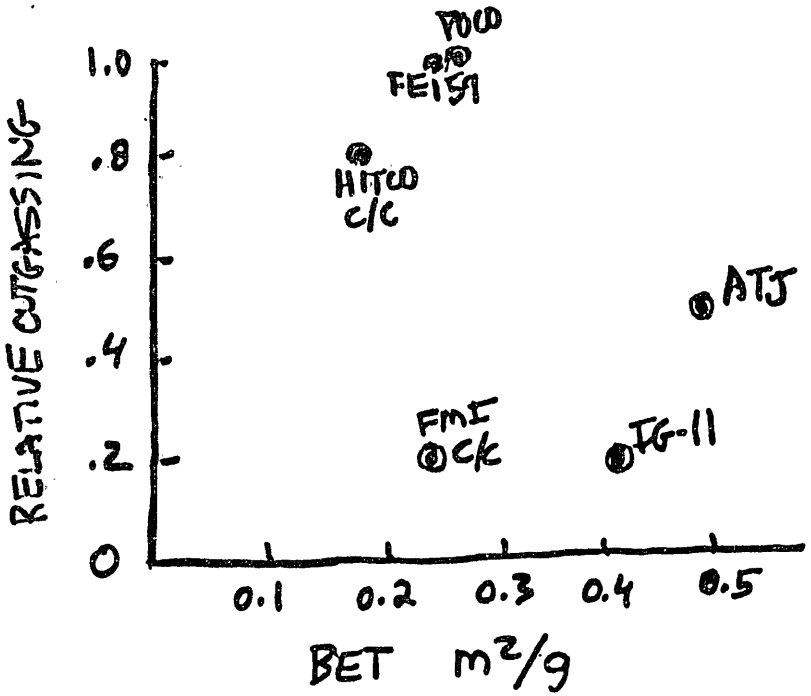

THE BEHAVIOR OF POCO AXF-5Q AND FMI 4-D C/C COMPOSITE DURING PLASMA EXPOSURE

W. L. HSU and A. E. PONTAU
SANDIA

K. H. DIPPEL, J. M. LINKE, U. SAMM
KFA JUELICH

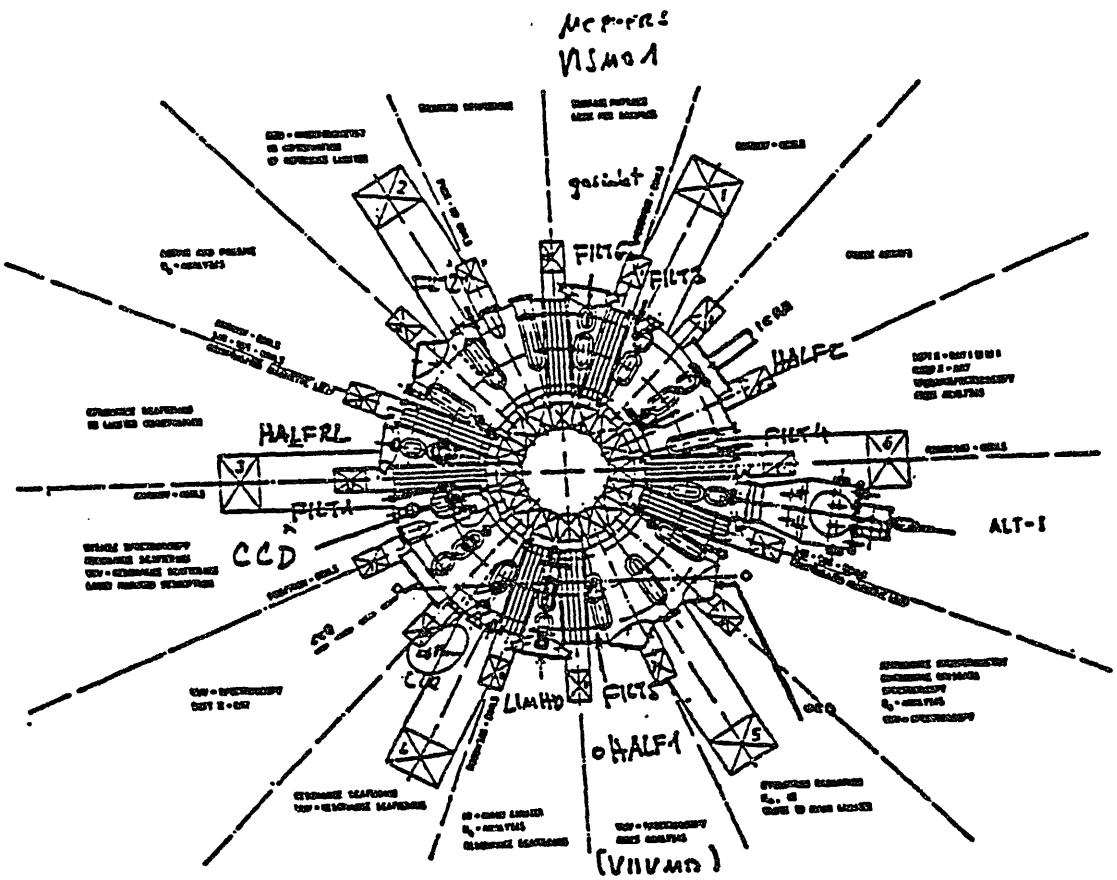

Experimental Arrangement for Laser Metal Fluorescence Measurements at TEXTOR

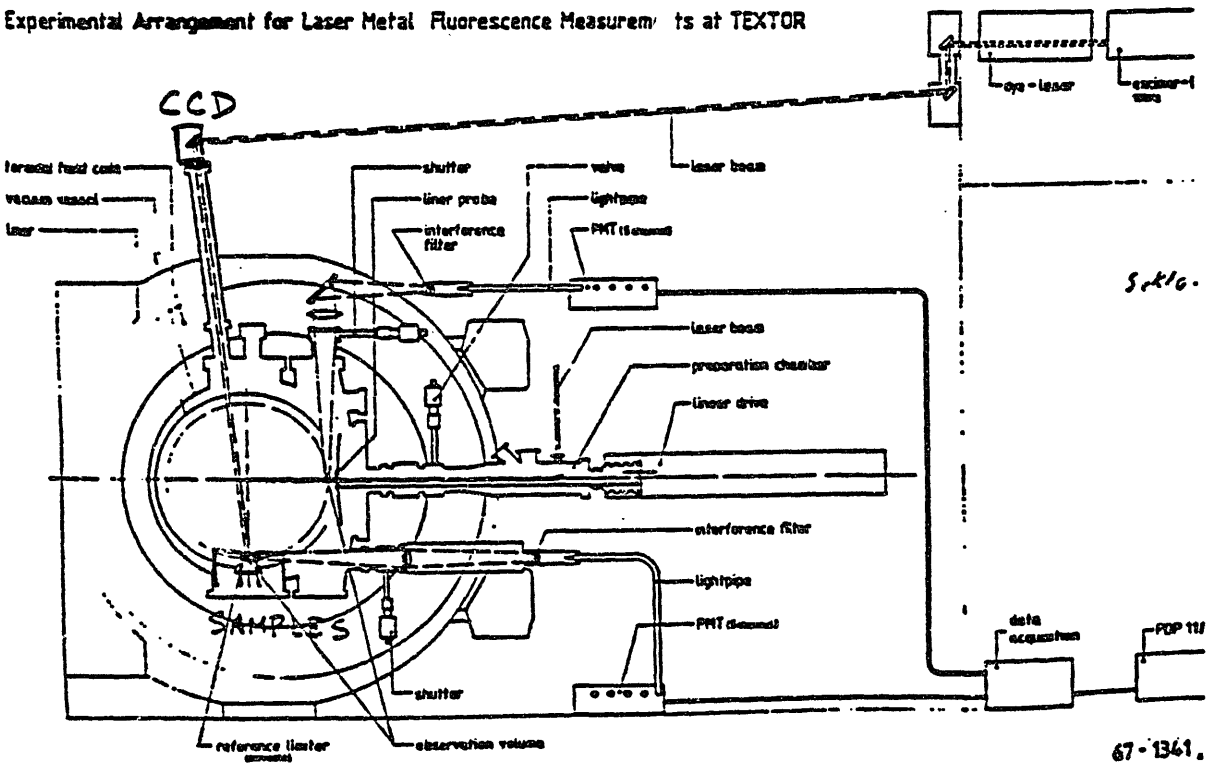

SUMMARY

- SAMPLES WERE HEATED TO > 2500° C IN TEXTOR DISCHARGES
- BOTH POCO AXF-5Q AND THE FMI 4-D C/C COMPOSITE RETAINED STRUCTURAL INTEGRITY
- POCO AXF-5Q HAD 4X OXYGEN OUTFLUX FOR THE FIRST FEW DISCHARGES
- BOTH MATERIALS HAD SIMILAR CARBON OUTLFUX
- THICK REDEPOSITED CARBON LAYERS WERE FORMED IN TWENTY DISCHARGES

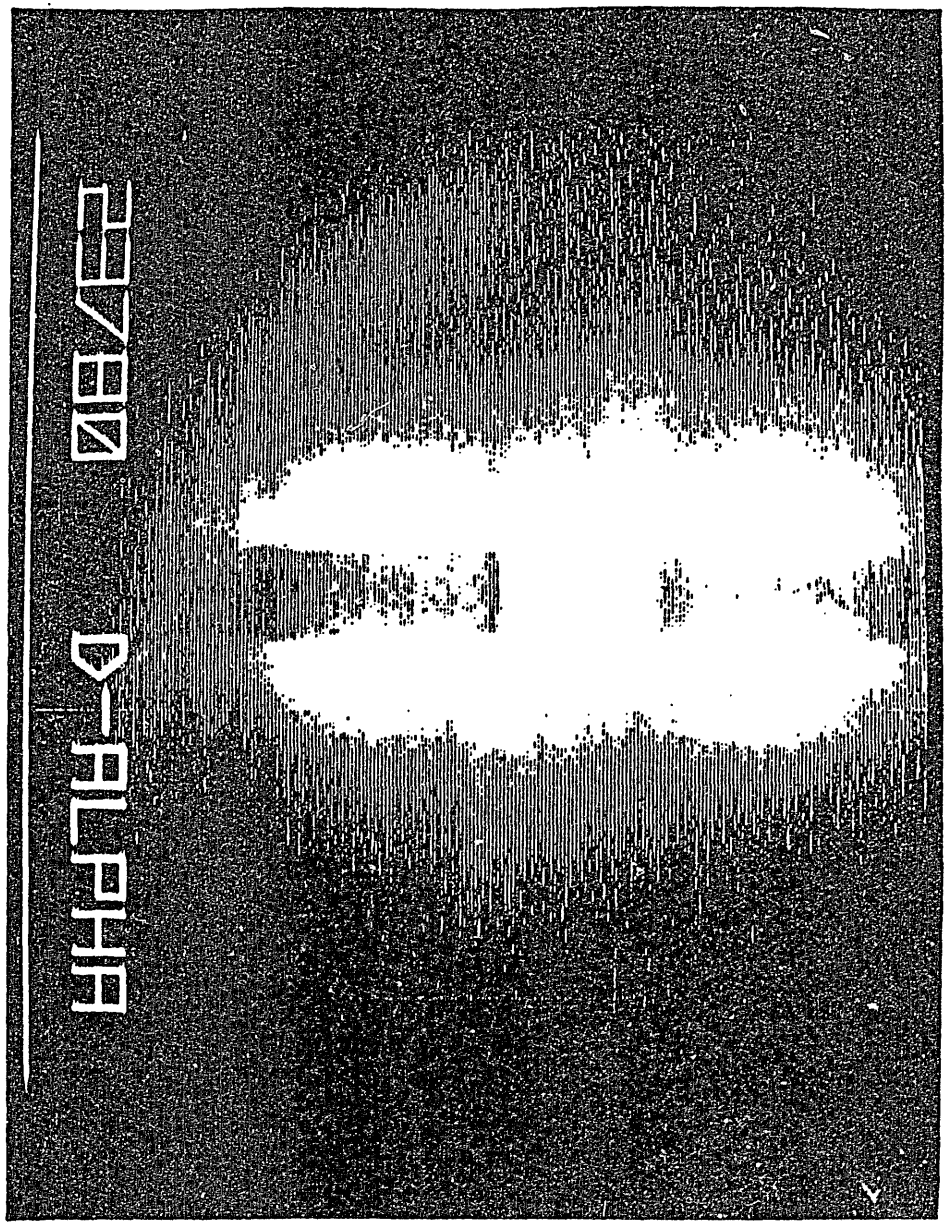

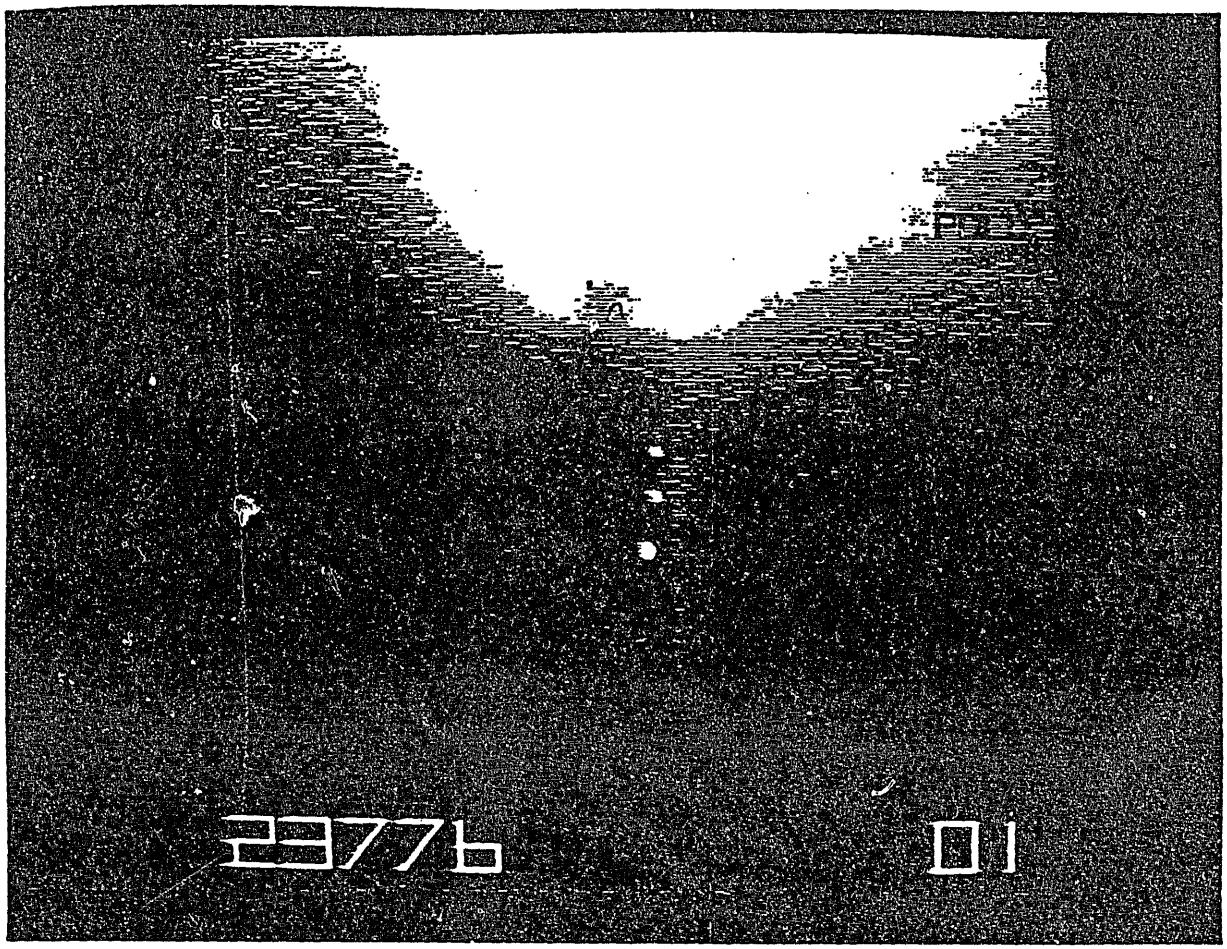
29776
01

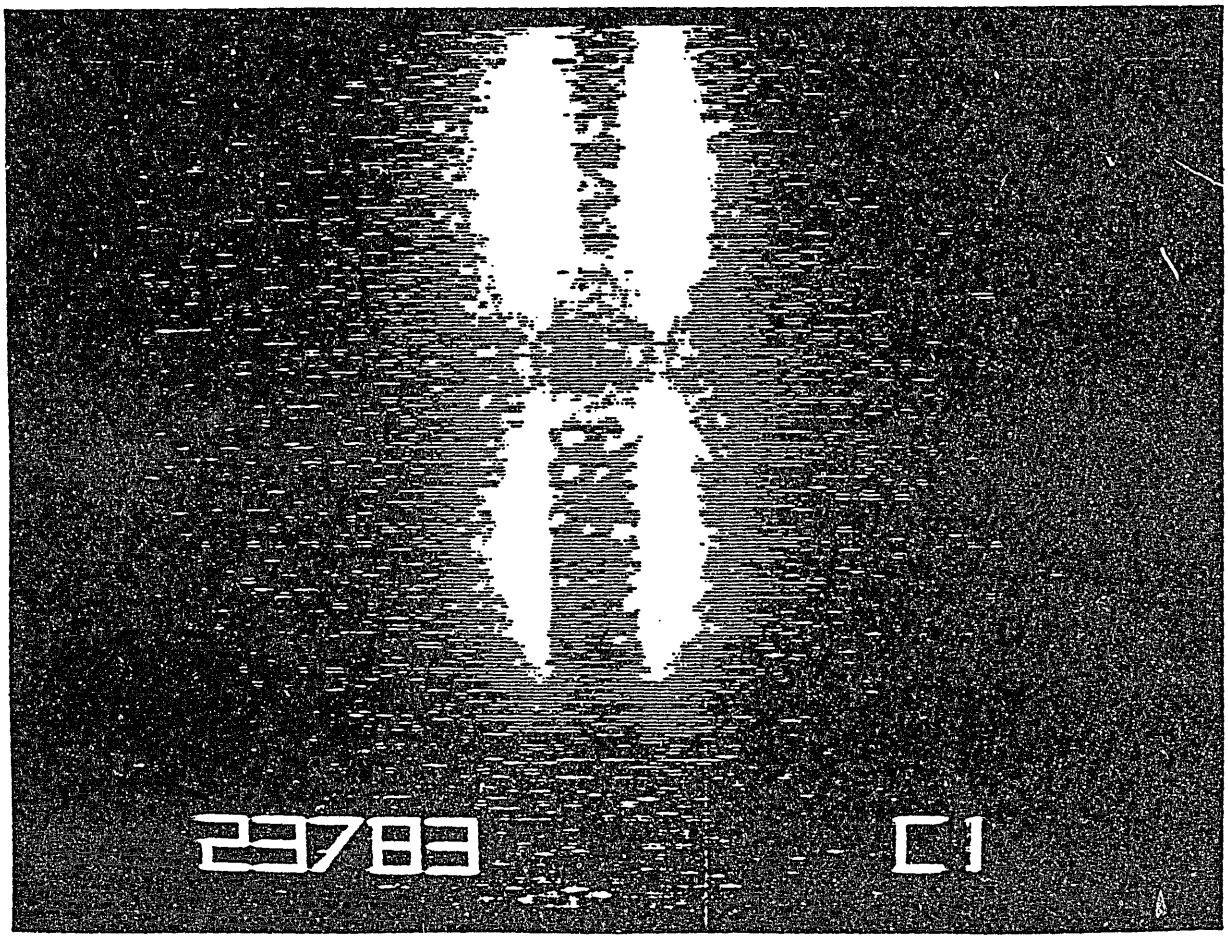
29783
C1

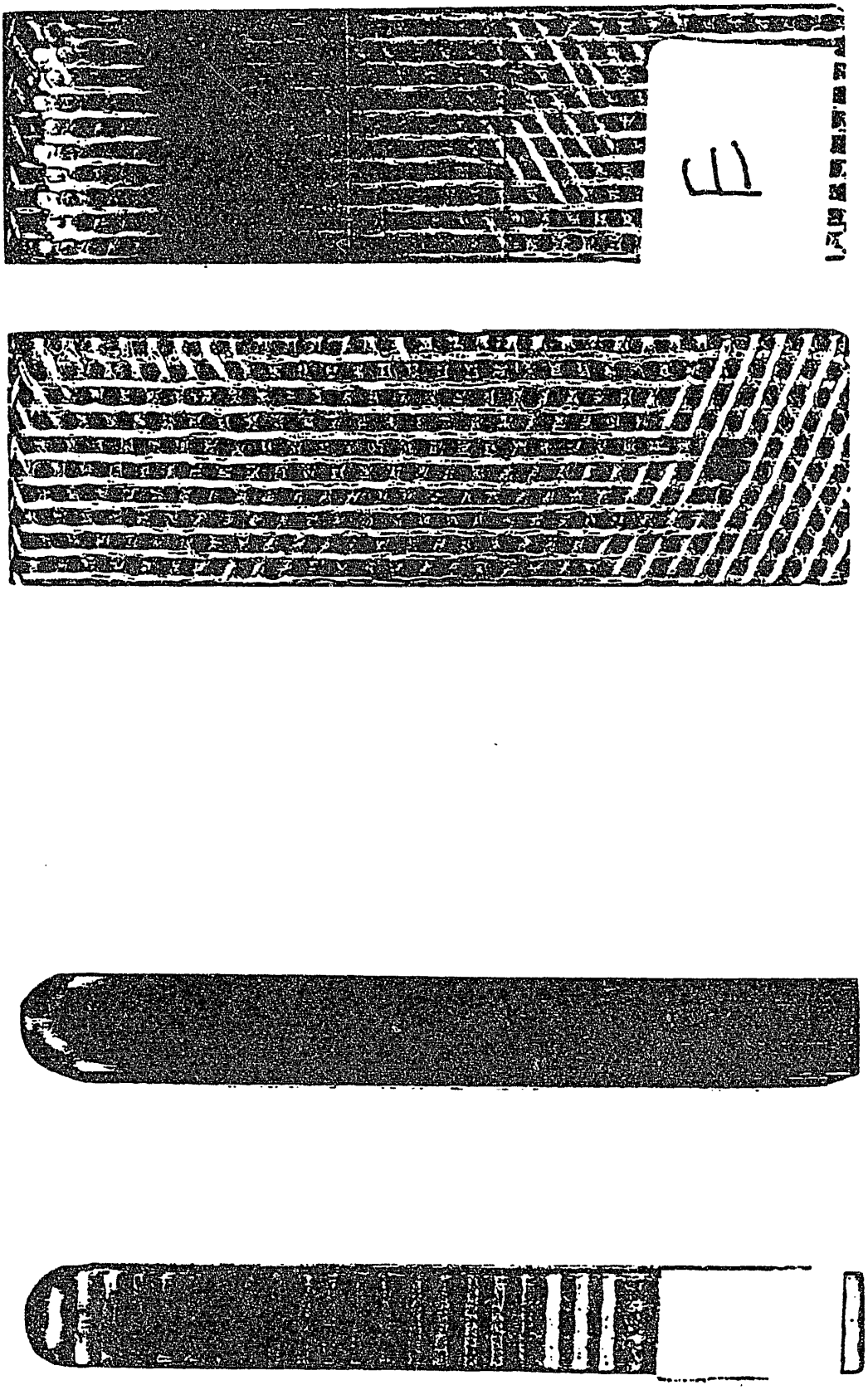

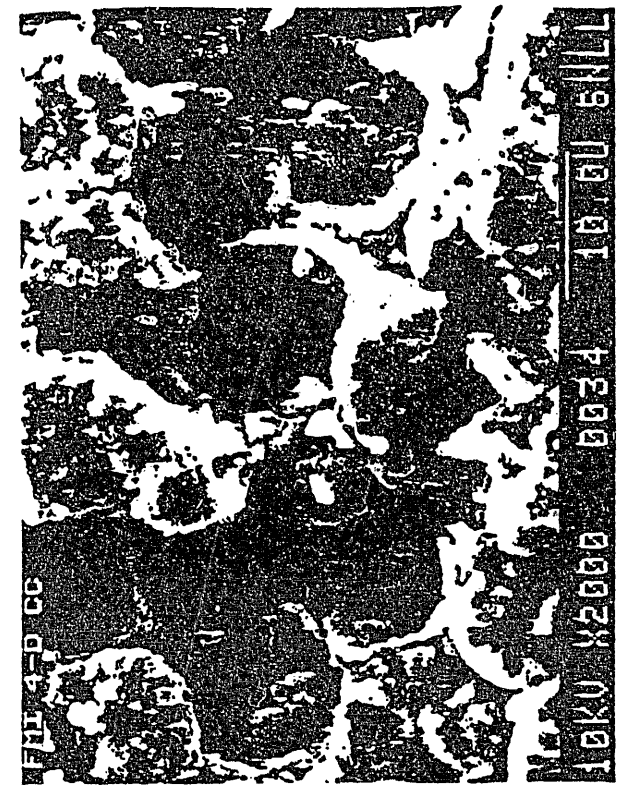
FMI 4-D CC
10KV X2000 0024 10 OU 6MLL

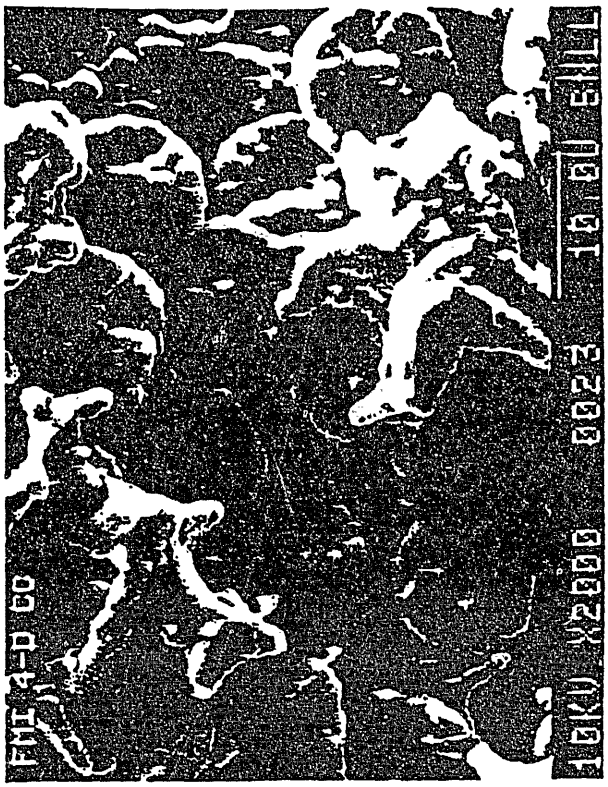
FMI 4-D CC
10KV X2000 0023 10 OU 6MLL

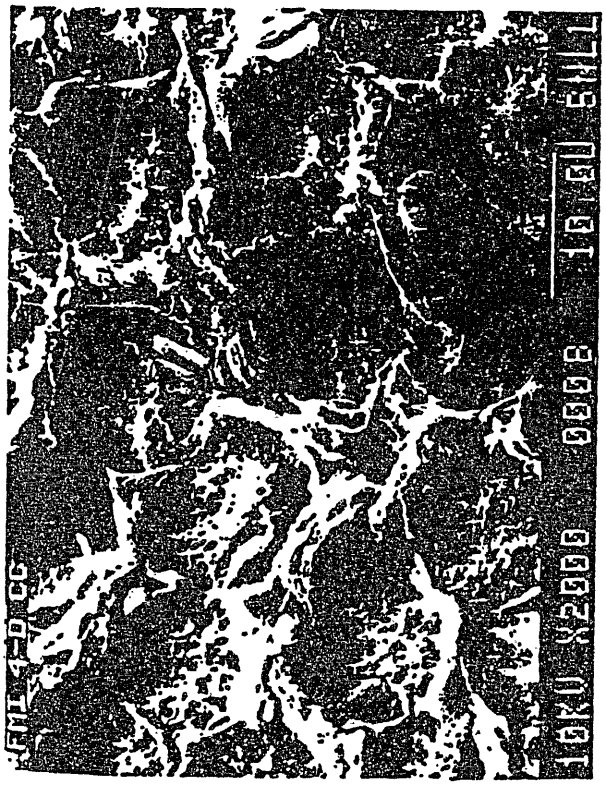
FMI 4-D CC
10KV X2000 0008 10 OU 6MLL

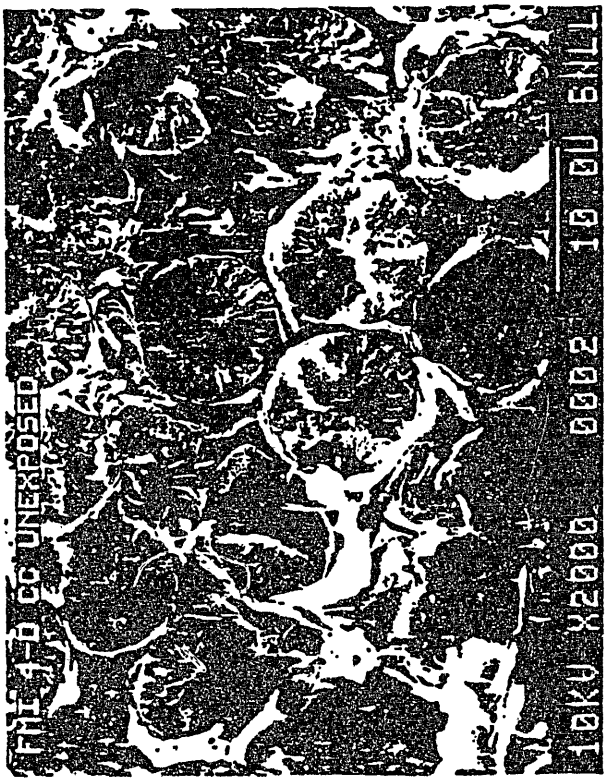
FMI 4-D CC UNEXPOSED
10KV X2000 0002 10 OU 6MLL

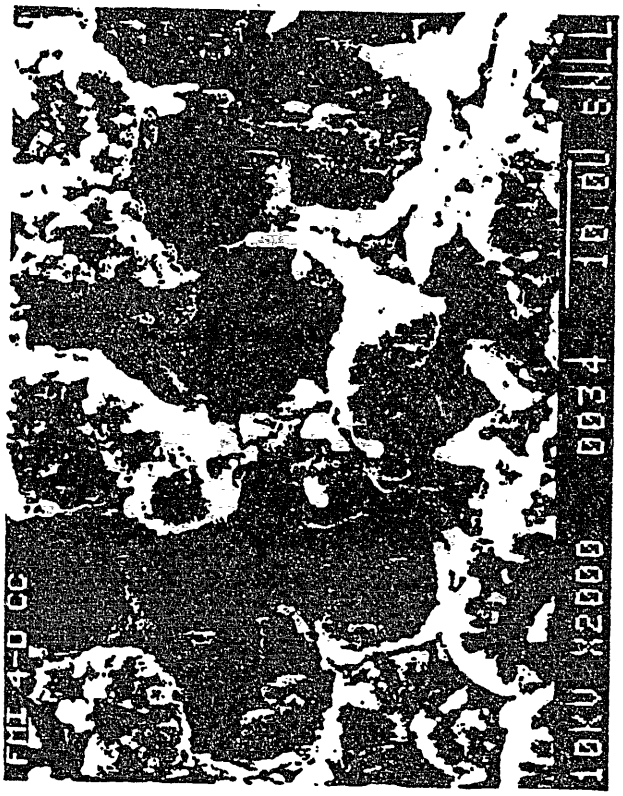
FMI 4-0 CC
10KU X2000 0003 10.0U SNLL

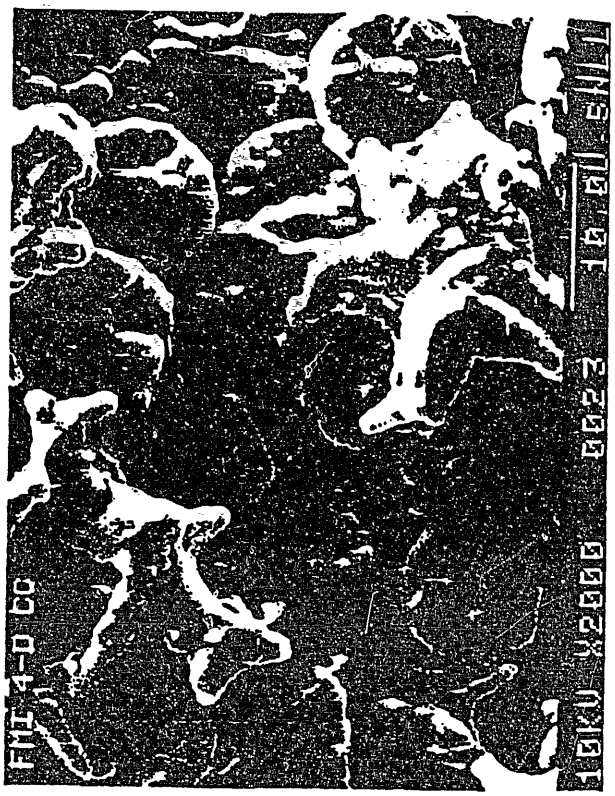
FMI 4-0 CC
10KU X2000 0002 10.0U SNLL

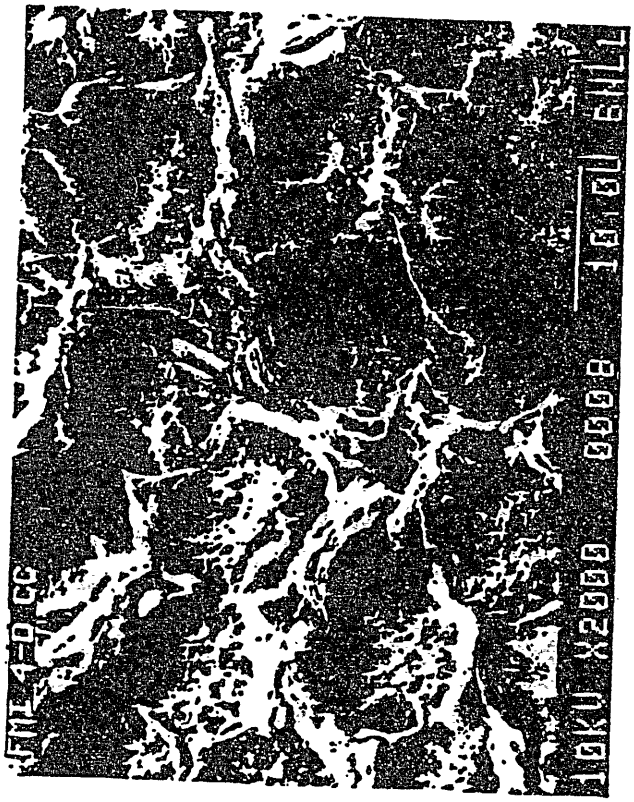
FMI 4-0 CC
10KU X2000 0008 10.0U SNLL

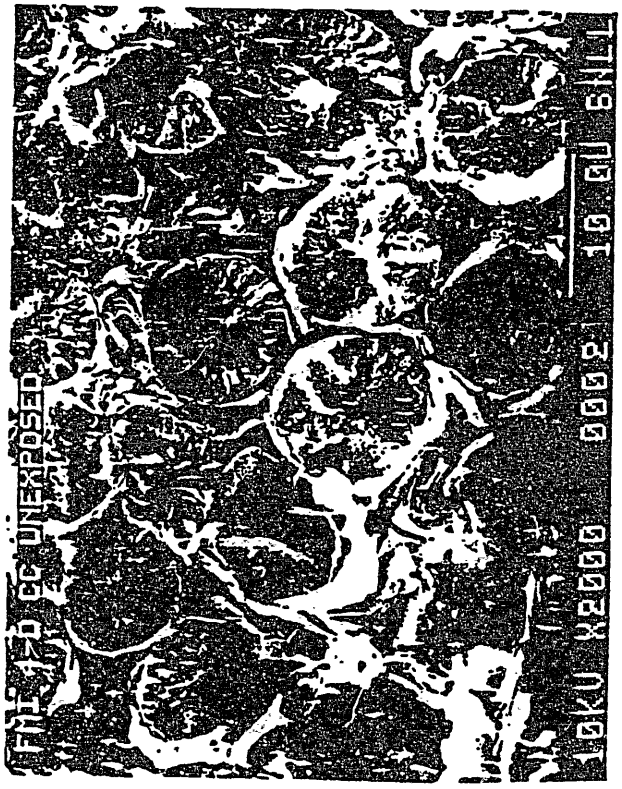
FMI 4-0 CC UNEXPOSED
10KU X2000 0002 10.0U SNLL

Thermal Outgassing of Various Kinds of Graphite

Yusuke Kubota

Institute of Plasma Physics, Nagoya University
Nagoya 464 Japan

Abstract

Thermal outgassing of various kinds of graphites has been measured by using a TDS device and valance for fusion application. The TDS device and a set of results for the effect of kind, pretreatment, and surface area of graphite on the outgassing were reported.

Outgassing of graphites

Y. Kubota IPP-Japan

1) Aims of our investigation

For application of graphite to invessel materials of fusion test devices.

a) Evaluation of the outgassing of graphites

b) Establishment of handling for graphites

TFTR(Poco AXF-5Q), JET( ), TEXTOR(Toyo.T. IG-110U), JT-60(Ibiden ETP-10).

2) Kinds of samples used for the investigation

a) Iso-graphite(13 samples)

b) aniso-graphite(1)

c) C/C composite(3)

3) Standard size of sample used

10mm x 10mm x 50mm (5 cc in volume)

4) Heating parameters

a) Heating ramp rate: 10°C/1min.

b) Maximum temperature: 1400°C

c) Holding time at 1400°C: 30min.

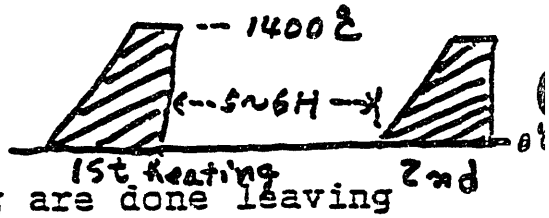

d) 1st heating and 2nd heating are done leaving several hours each other.

5) Measurements carried out

a) TDS measurements for various as-received samples

b) Gas absorption of graphite during storage

c) Effect of pre-treatment on outgassing of graphite

d) Effect of surface area of sample on outgassing

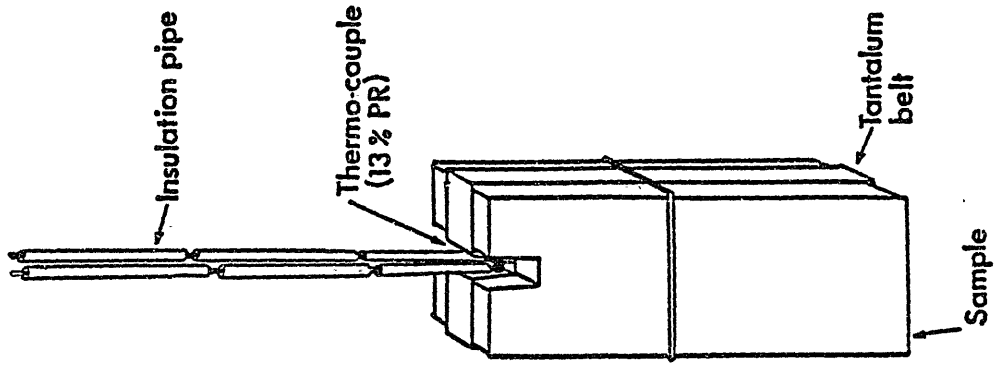

Fig.3 Sample, sample holder, and 13R platinum thermocouple

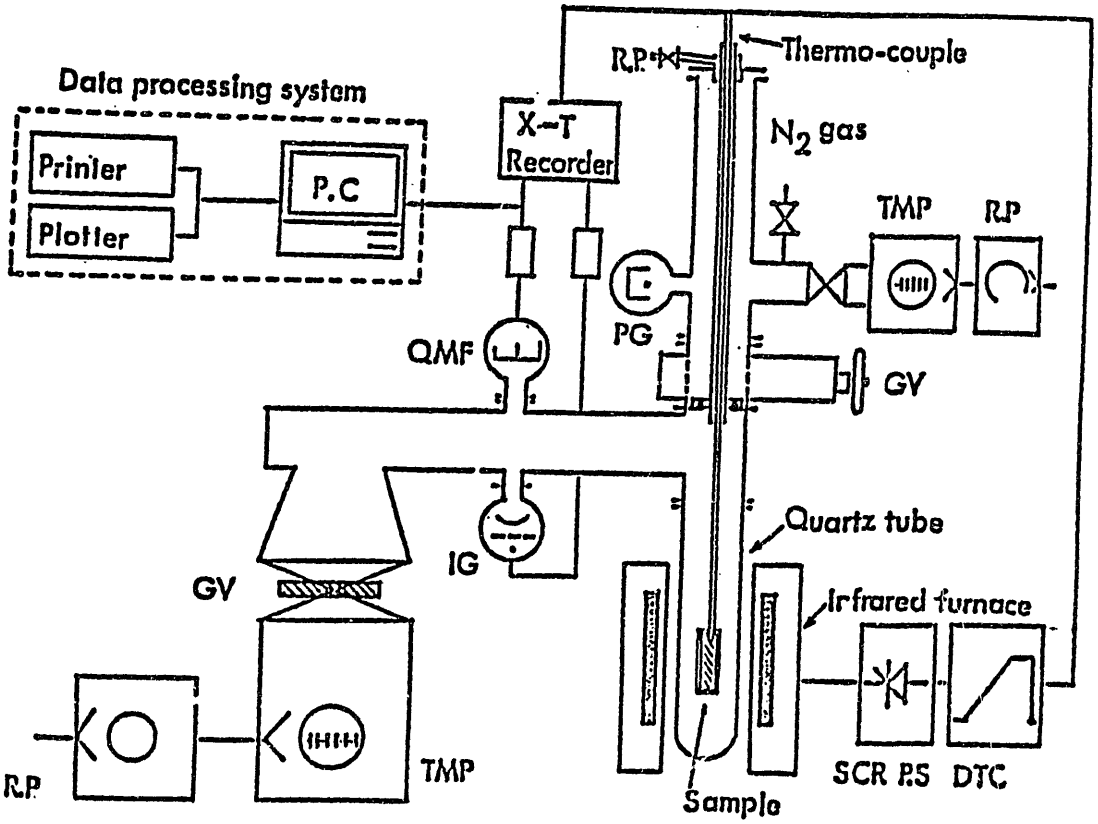

Fig. 1 Block diagram of thermal desorption spectrum appratus.

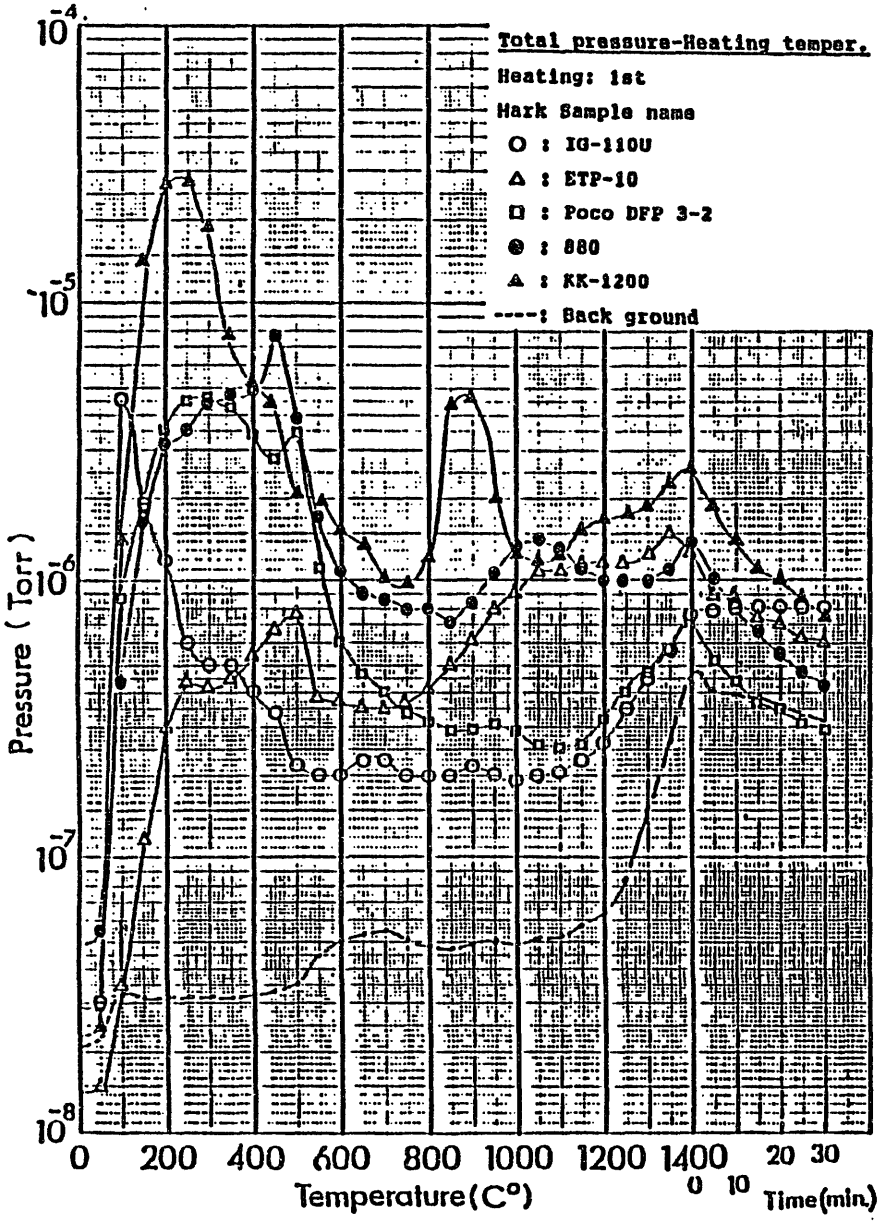

Fig.3. Thermal desorption spectrum of various samples and BG for 1st heating.

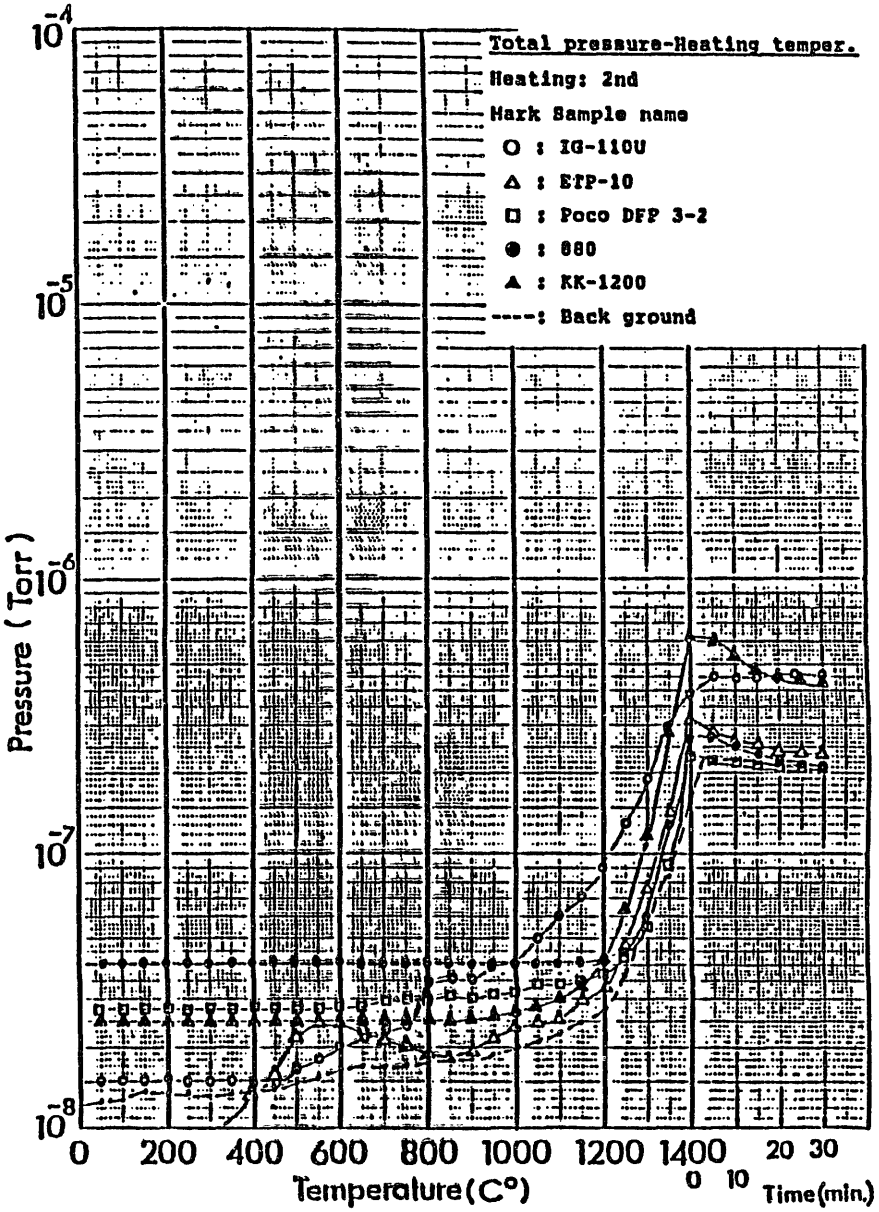

Fig.4. Thermal desorption spectrum of various samples and BG for 2nd heating.

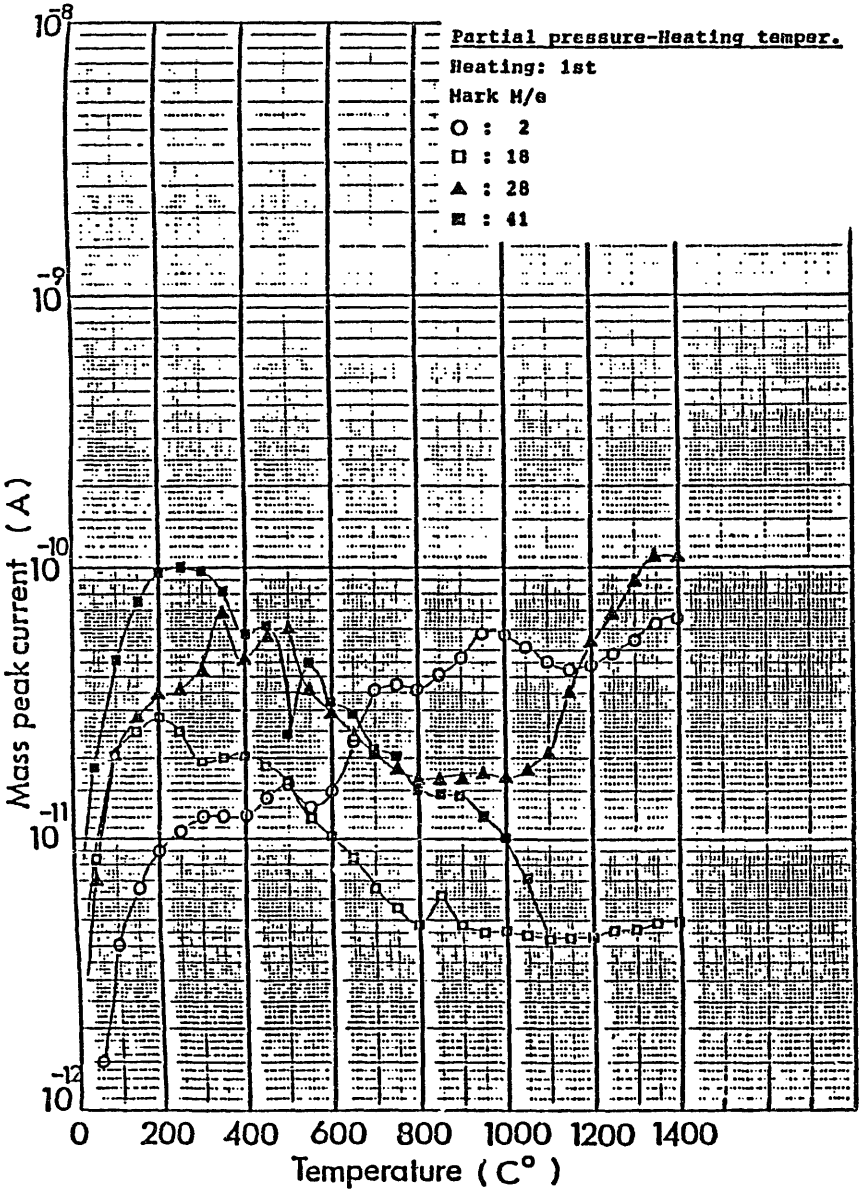

Fig.5. Thermal desorption spectrum for main components of gas desorbed from Poco DFP 3-2 during 1st heating.

Table 1 Thermal outgassing of as-received samples

(without back ground value)

Sample name	Weight (g)	Kind	Desorption(Torr l/g) 1st heating	2nd heating
Shinnitetu 880	8.74	iso-graphite	0.11	0.000
kagaku 980	10.70	〃	0.36	0.000
Toyo Tanso IG-11	8.86	〃	0.25	0.002
IG-110	8.64	〃	0.15	0.000
IG-110U	8.67	〃	0.04	0.006
ISO-63	8.80	〃	0.14	0.002
ISO-630U	9.00	〃	0.01	0.000
ISO-88	9.20	〃	0.15	0.000
Ibiden T-6P	9.25	〃	0.15	0.008
ETP-10	8.49	〃	0.06	0.003
Toyo AX-650K	8.93	〃	0.07	0.003
carbon MT-200	9.21	〃	0.05	0.003
YPD	8.71	aniso-graphite	0.16	0.004
Poco DFP 3-2	9.19	iso-graphite	0.07	0.000
Toray Torayca	8.37	carbon/carbon	0.12	0.001
Hitco C-139	8.20	〃	0.21	0.015
Kaiser KK-1200	4.91	〃	0.56	0.008

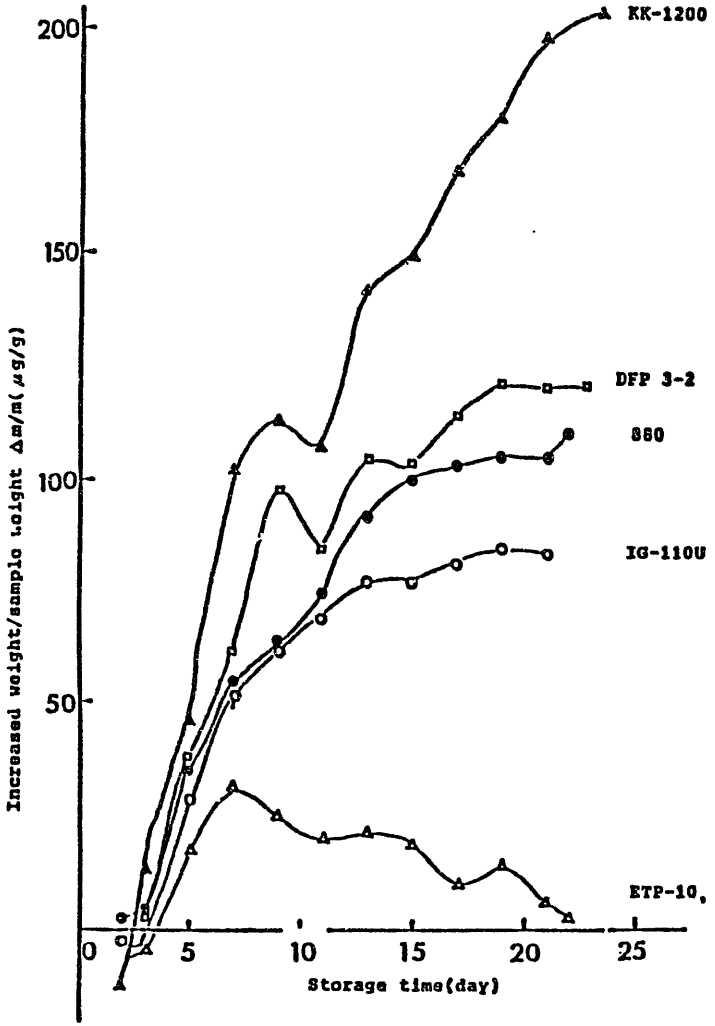

Fig.7. Gas absorption(Δm/m) of various samples degassed against storage time(T).

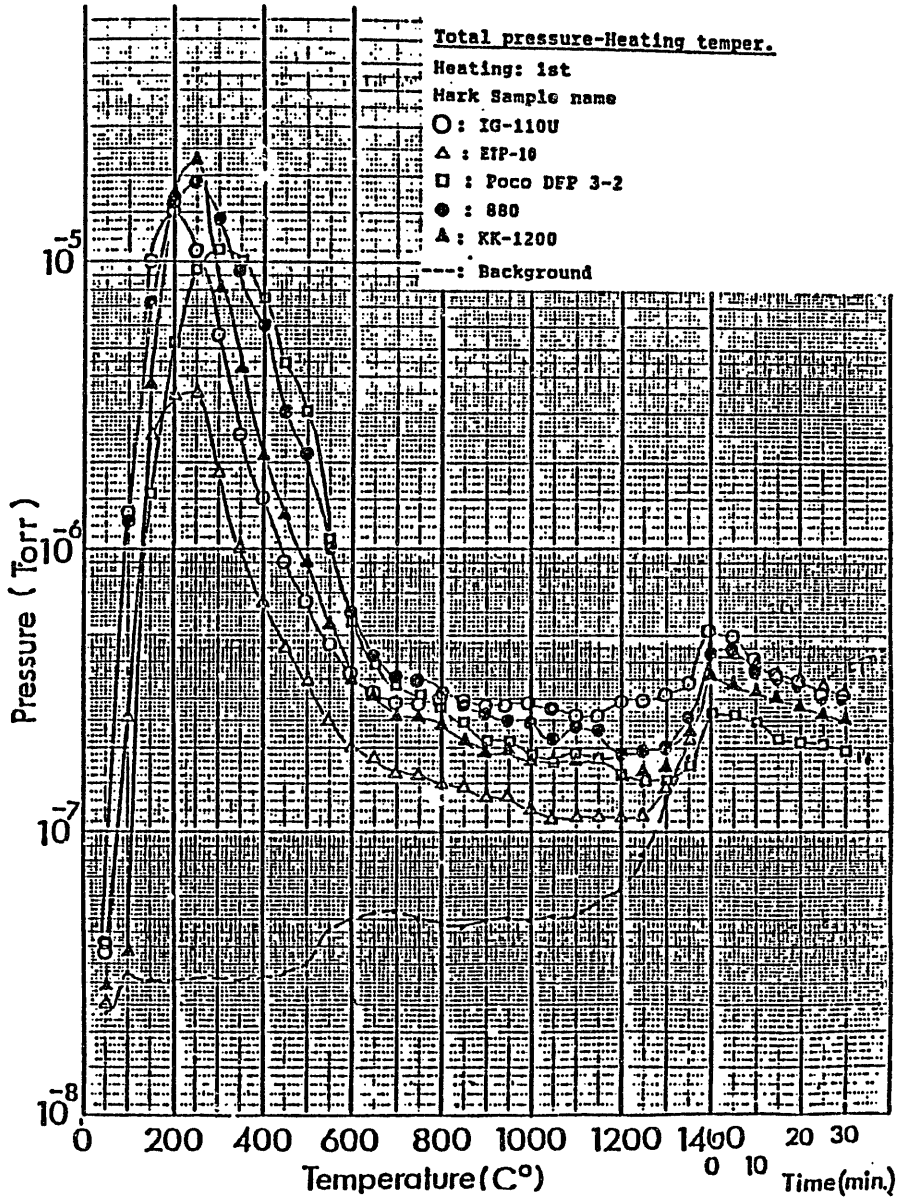

Fig.8. Thermal desorption spectrum of 5 samples stored and BG for 1st heating.

Table 4 Outgassing of as-received and alcohol cleaned samples

Sample name	Desorption(Torr·l/g) for 1st heating	
	As-received	Alcohol cleaned
T-6P	0.187	0.144
ETP-10	o.o71	0.048
IG-11	0.250	0.230

Table 3 Effect of pre-treatments on outgassing of MT-200K sample.

Pre-treatment	Weight (g)	Desorption(Torr·l/g)	
		1st heating	2nd heating
as-received	9.2091	0.067	0.007
cleaned in alcohol	9.1846	0.067	0.005
cleaned in acetone	9.1277	0.080	0.010

Table 2 Gas absorption of 5 samples stored in air for 3 weeks.

Sample name	Sample weight (g)	Increased weight Δm/m(μg/g)	Desorption (Torr·l/g)
IG-110U	8.74095	83	0.124
ETP-10	8.55890	2	0.037
880	9.06428	111	0.189
DFP 3-2	8.70188	120	0.199
KK-1200	4.91471	201	0.267

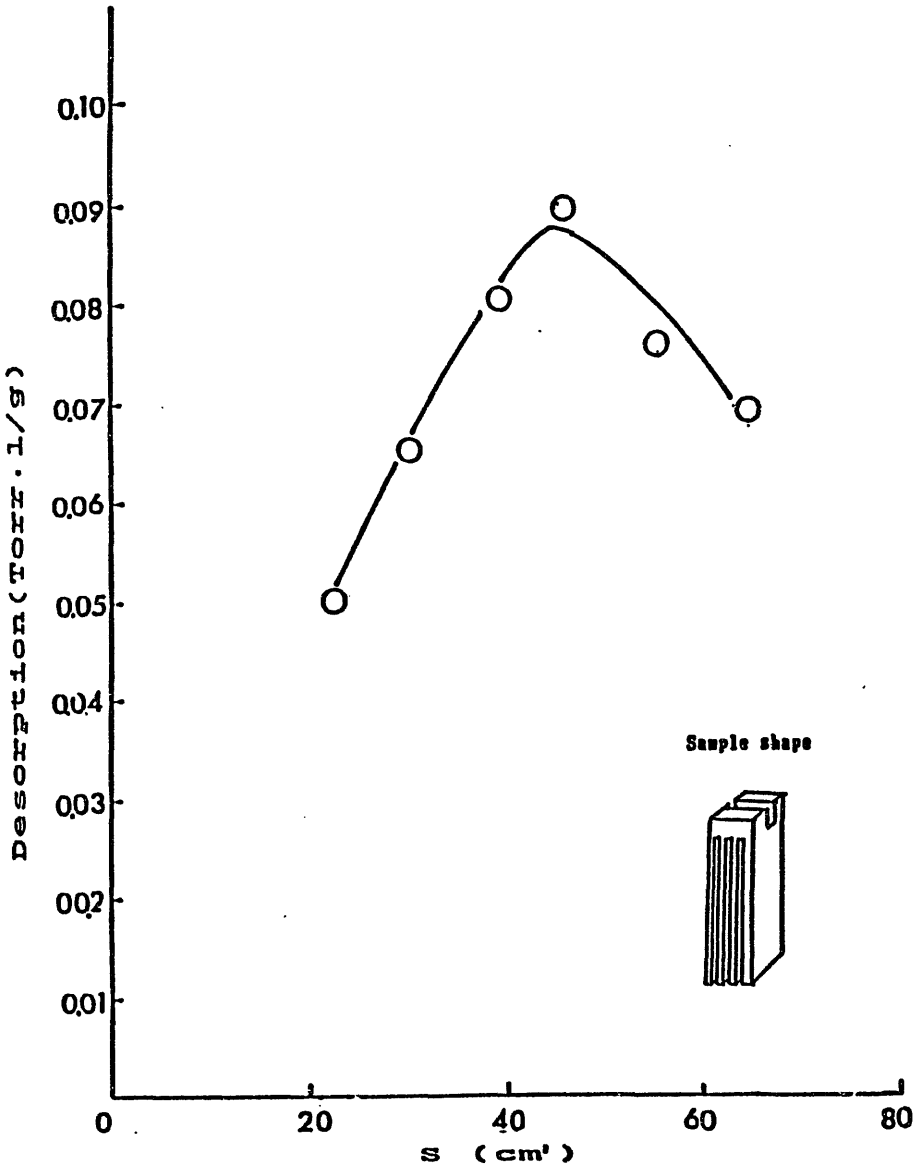

Fig.10. Relationship between the desorption and surface area(cm²) at a constant volumeof 5cc for ETP-10 sample.

1. On Gas Uptake of Coaled and Bare Graphite during exposure

2. Hydrogen and Deuterium Retention in Wall Samples of JET

W. Eckstein

Max-Planck-Institut

Abstract

1. The gas release of carbon probes from diffrent manufacture and the gas-uptake during air exporsure was investigated. Sealing of graphites with pyrocarbon (CVD) does not reduce the short-time gas-uptake in 1 to 2 days, but slows down the farther gas- uptake in one case but not in another one. Also the mass-spectroscopic investigation of desorbed species shows large differences in the composition and in the desorption temperature at equal weight loss.

2. The amount of H and D trapped in vessel walls of carbon-containing tokamaks is of the order of 2×10^{17} to 10^{18}(D+H)/ cm^2 determined from long time samples in JET($\sim10^3$ discharges). The hydrogen is probably trapped by codeposition of H and D with carbon. The total amount of H and D in there layers corresponds to about 100 times the amount of H and D in the plasma.

ON GAS UPTAKE OF COATED AND BARE GRAPHITE DURING EXPOSURE TO AIR

H.VERNICKEL, J.BOHDANSKY,
H.J.KUTSCH, W.OTTENBERGER, J.ROTH,
R.SCHERZER, F.STEINBERGER, E.TRCKA

Samples:

Various graphites from various manufacturers:

- unsealed
- sealed with Pyrocarbon (CVD)
- sealed with SiC (CVD)

note: TiC sealed samples were not included because of the rather high Z of Ti.

Pretreatment: (AS SPECIFIED):

- Cleaning in ultrasonic bath for removal of dust.
- Degassing in vacuum at 1500 to 2000° C.
- Packing in water tight bags (e.g. Hostaphan).

MEASUREMENTS:

- WEIGHT LOSS AND GAIN, MEASURED BY VACUUM MICROBALANCE.
- DEGASSING RATE MEASURED VIA PRESSURE DIFFERENCE ON A CALIBRATED CONDUCTANCE.

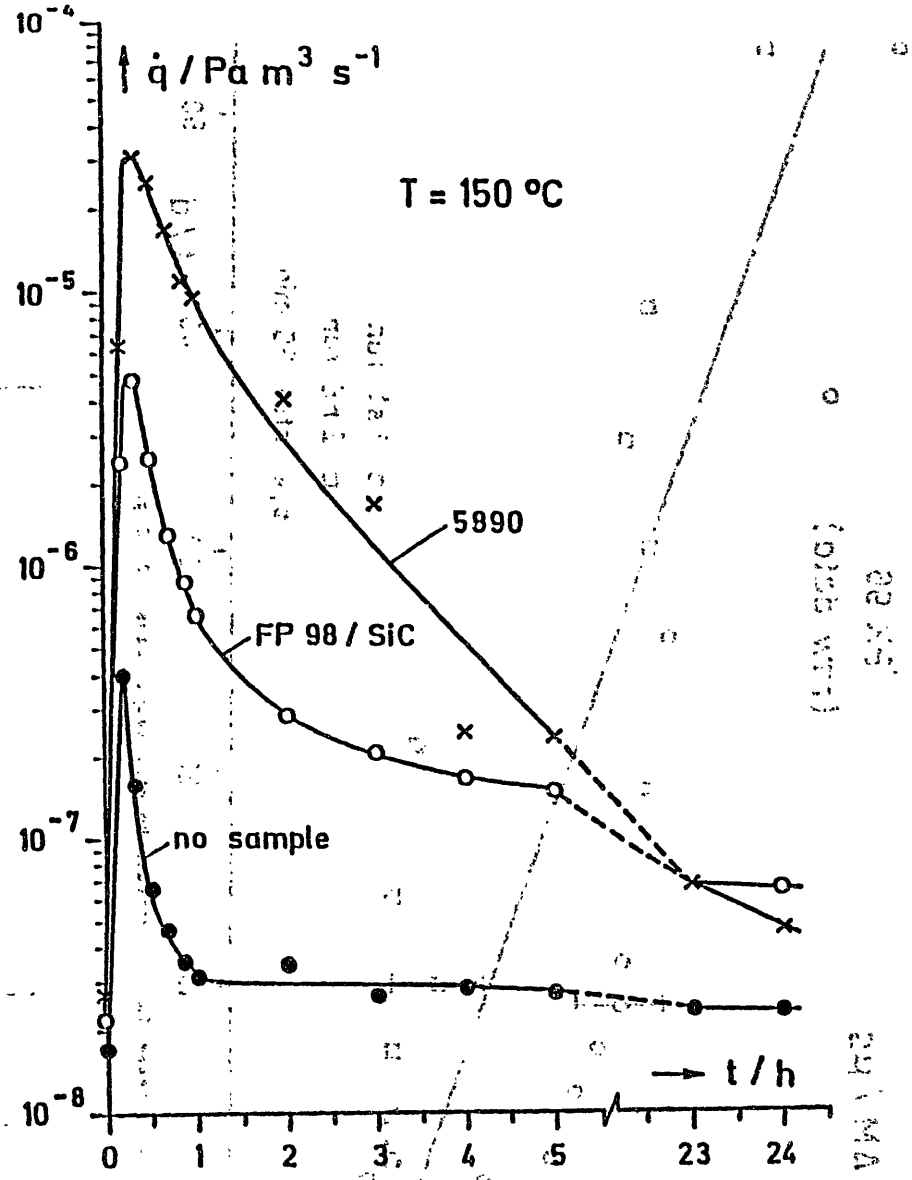

Degassing rate of as-delivered samples at 150° C.
Mass of samples = 2.9 g; t = 0 ... furnace turned on.

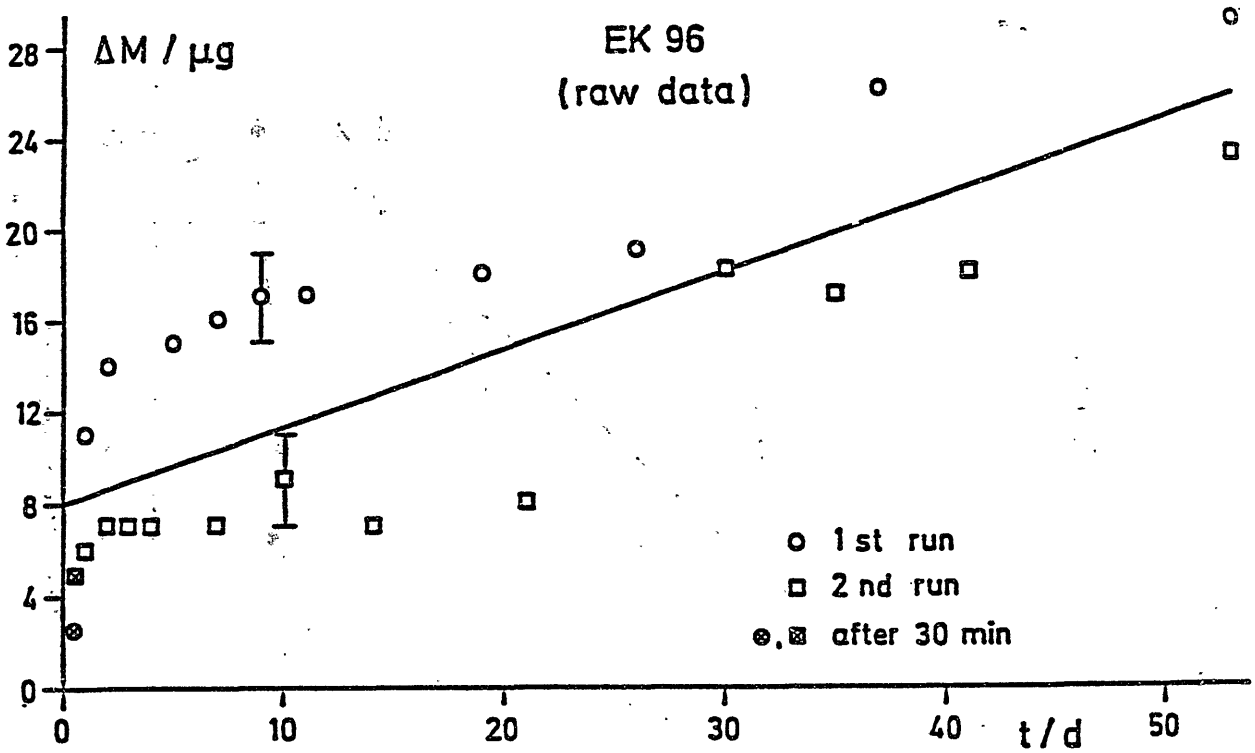

Weight increase during exposure to air; sample mass = 0.43 g.

Table 1: Gas release of the as-delivered samples

Sample	1 24 h at room temp. mtorr · l	2 24 h at 150°C mtorr · l	3 total degassing per g mtorr · l / g	4 weight loss after 750° C µg	5 weight loss per g µg/g
EK96	11	148	55	15	34
5890[1]	37	776	280	88	238
1346[1]	130	680	280	103	260
FP219	11	160	59	8	24
FP98	9	79	30	9	25
EK96/PyC	7	69	26	15	33
5890/PyC[1]	19	291	107	26	65
1346/PyC[1]	11	148	55	17	41
FP219/PyC	(no data)	80	31	7	21
EK96/SiC	13	83	33	27	55
FP98/SiC	50	120	50	18	47
no sample (blank run)	4	17	-	-	-

[1] Samples not properly sealed by the manufacturer.

Notes: 1 mtorr.l = 1 µg if M = 18.

Table 2: Gas uptake during exposure to air

Sample	run	A	B	C	D	D/C	weight of sample g
		µg					
EK96	1	2.5	2.5	29	34	1.17	0.43
	2	5.0	-	23	36	1.57	0.44
5890	1	6.0	6.0	39	52	1.33	0.37
	2	7.5	-	26	35	1.35	0.37
1346	1	6	6	44	50	1.14	0.39
	2	6.5	-	38	45	1.18	0.40
FP219	1	2.5	3	28	40	1.43	0.33
	2	6	-	24	32	1.33	0.34
FP98	1	2.5	3	29	31	1.07	0.36
	2	6.0	-	24	32	1.33	0.36
EK98	1	(3)	-	43	42	0.98	0.50
	2	5.5	-	34	36	1.06	0.41
-	-	-	-	-	-	-	-
EK96/PyC	1	2.5	2.5	8	14	1.75	0.46
5890/PyC	1	11	11	28	20	0.71	0.40
1346/PyC	1	7	8	15	15	1.00	0.41
FP219/PyC	1	2.5	2.5	33	37	1.12	0.34
	2	5.0	-	26	28	1.08	0.34
-	-	-	-	-	-	-	-
EK96/SiC	1	3.5	3.5	21	24	1.14	0.49
FP98/SiC	1	3.5	4	24	32	1.33	0.38

A : Weight gain during 30 min air exposure
B: Weight loss by degassing following A
C: Weight gain during 50 d air exposure
D: Weight loss by degassing following C
Note: D/C = 1.66, if $H_2O \longrightarrow CO + H_2$

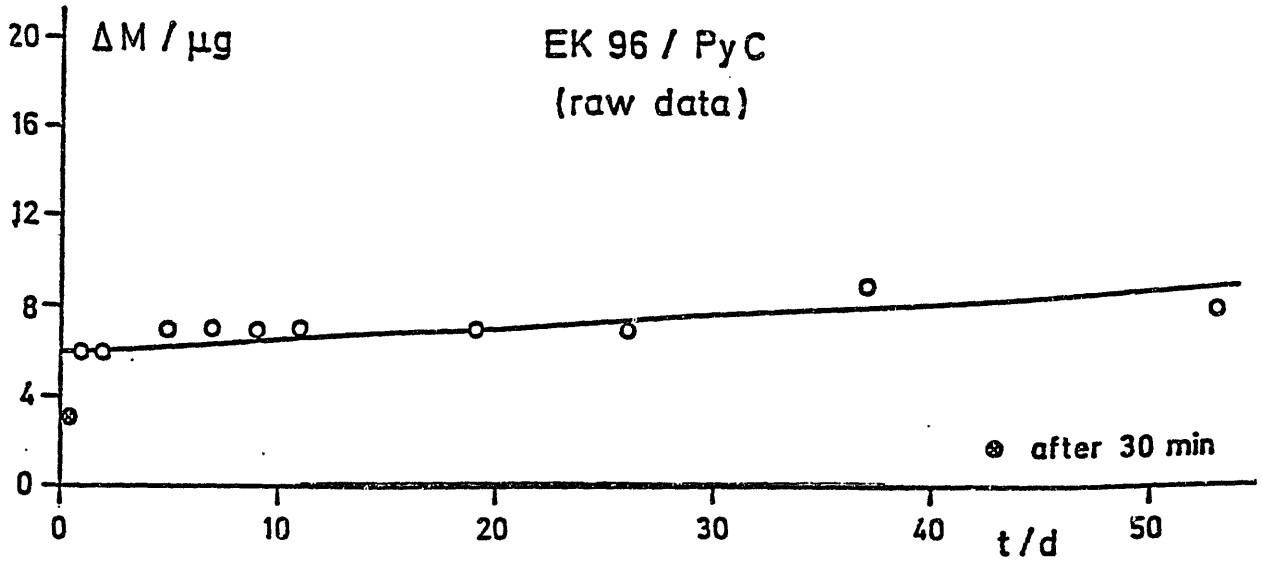

Weight increase during exposure to air: Sample mass = 0.46 g.

Table 3: Gas uptake during exposure to air

Data are presented according to

$$\frac{\Delta M}{M} = a + bt \qquad (2d \leq t \leq 50\ d) \qquad (1)$$

	50 day exposure		long term exposure		
Sample	$a \cdot 10^6$	$b \cdot 10^6/d$	$10^6 \frac{\Delta M}{M}$ (eq.1)	$10^6 \frac{\Delta M}{M}$ (measured)	exposure (d)
EK96	17	0.8	117	79	125
			251	195	292
5890	32	1.1			
1346	35	1.4			
FP219	24	1.0			
FP98	20	1.0			
EK98	18	1.3			
EK96/PyC	18	0.1	31	37	125
5889/PyC	43	0.4	93	85	125
1346/PyC	29	0.2	54	50	125
FP219/PyC	25	1.1	163	105	125
EK96/SiC	20	0.5	83	53	125
FP98/SiC	20	0.9	133	65	125

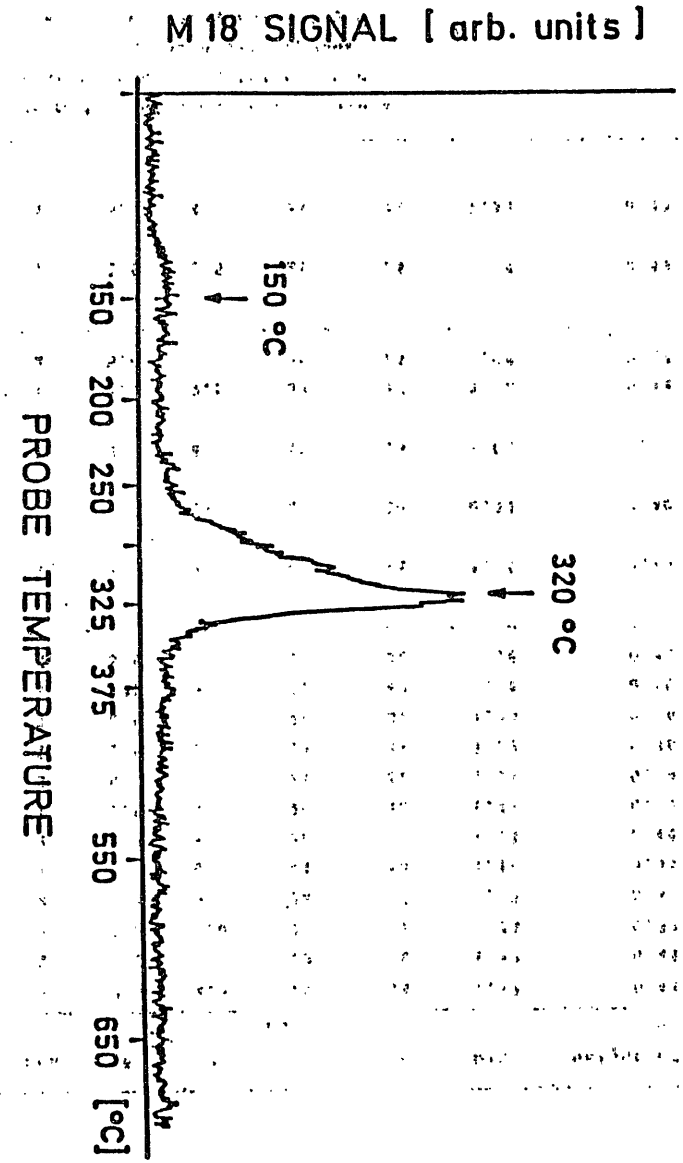

FE 159 c
Graphite liner ASDEX

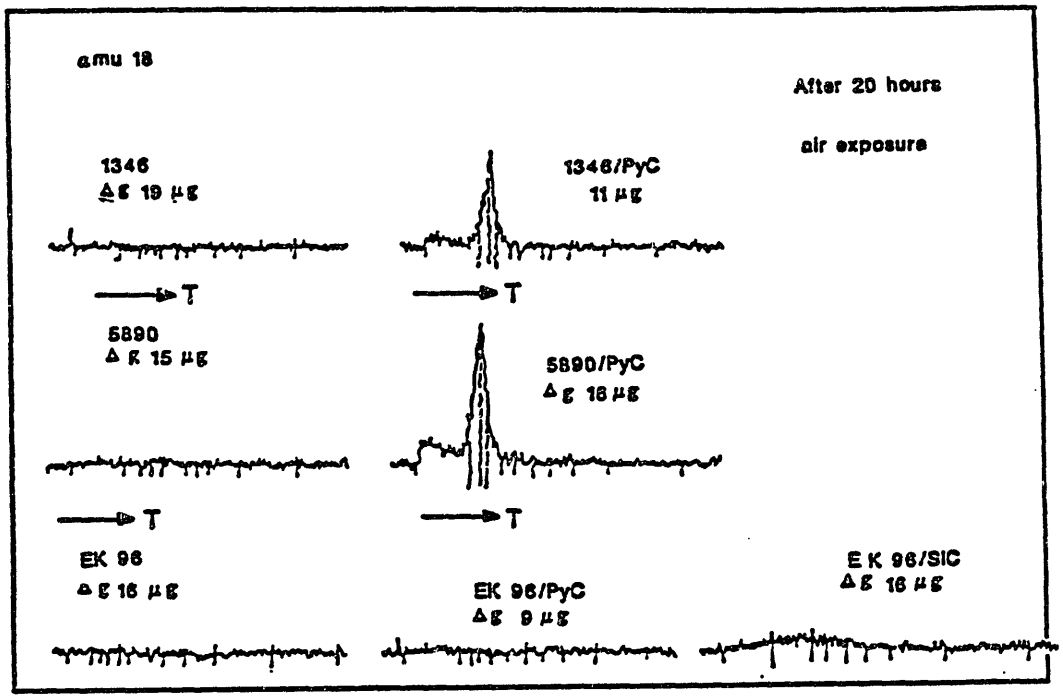
amu 18
After 20 hours
air exposure
1346
Δg 19 μg
1346/PyC
11 μg
T
5890
Δg 15 μg
5890/PyC
Δg 16 μg
T
EK 96
Δg 16 μg
EK 96/PyC
Δg 9 μg
EK 96/SIC
Δg 16 μg

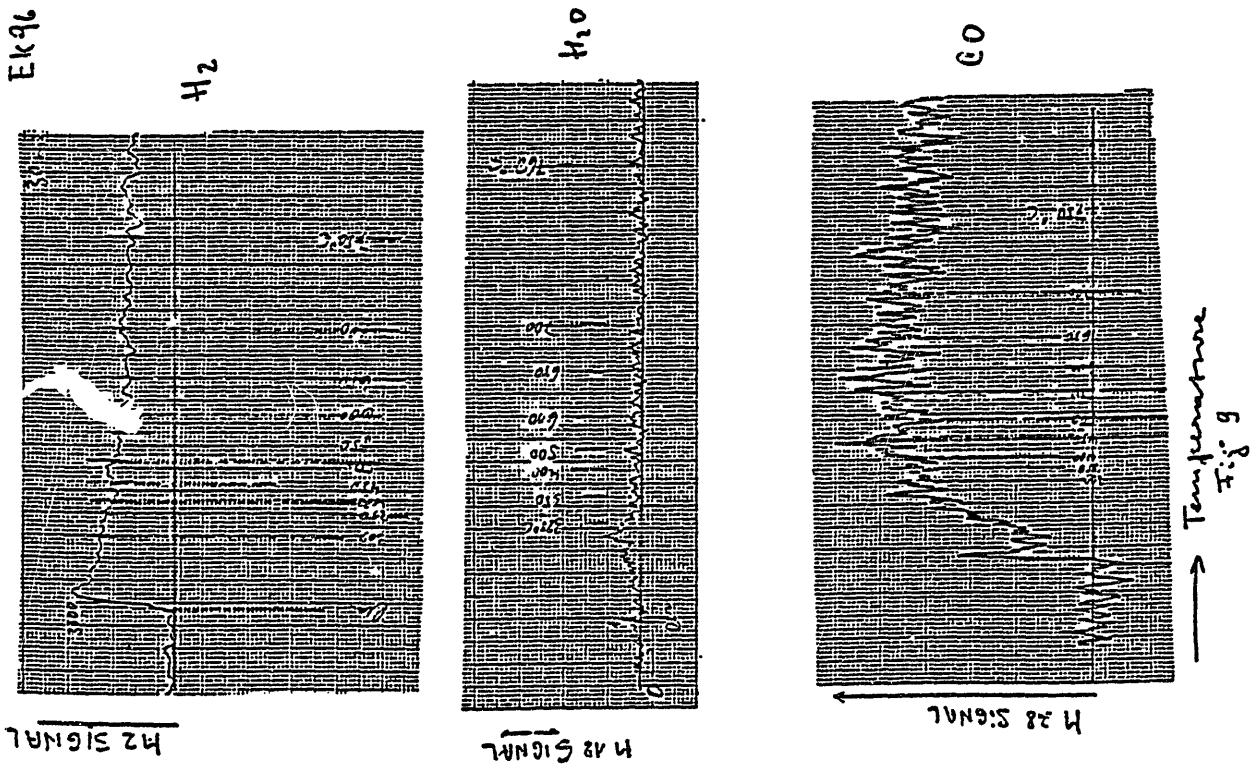
Ek96
H2
H2 SIGNAL
H2O
H2O SIGNAL
CO
CO SIGNAL
Temperature

Fig. 8

Test C: Repeated heating of coated samples in vacuum by a light beam

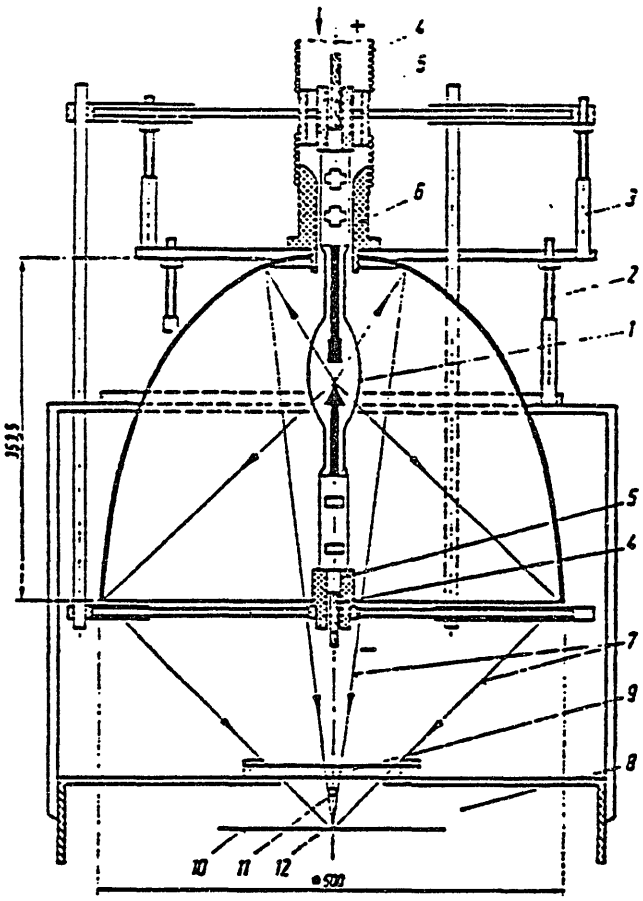

Schnitt durch die Lichtstrahlanlage (1 Lampe, 2 Justierung des Schirms, 3 Justierung der Lampe, 4 Stromzuführungen, 5 Isolierkörper aus Al_2O_3-Keramik, 6 Isolierkörper aus Polyvinylchlorid, 7 Randstrahlen des Strahlungsfeldes, 8 Arbeitskammer, 9 Quarzglasfenster, 10 Arbeitsebene, 11 Hilfsspiegel E1 im Abschattungskegel, 12 Lotprobe P).

Heating to 900° C in 30 sec

Cooling to 300° C in 4 min

250 cycles

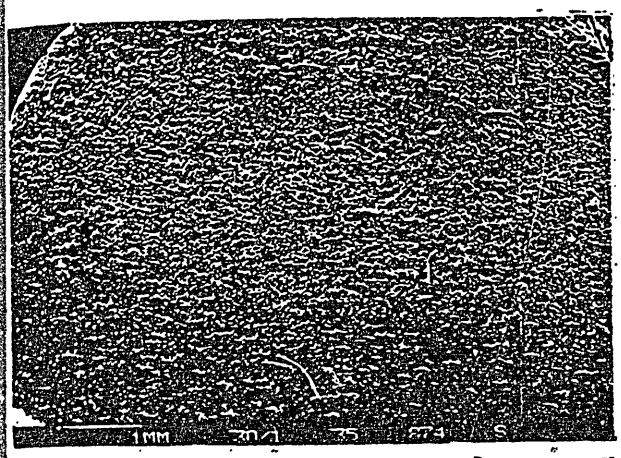
1MM
30/1
35
S

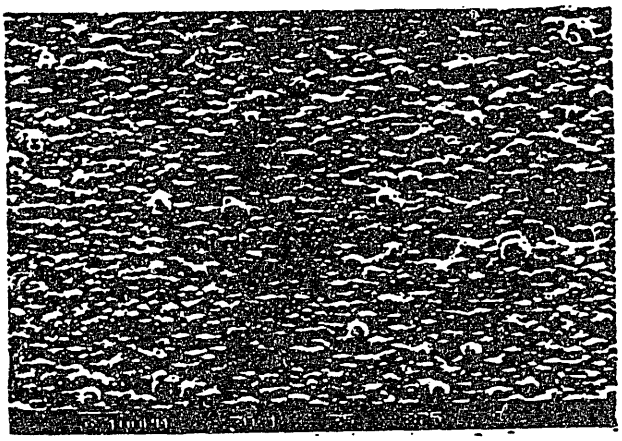

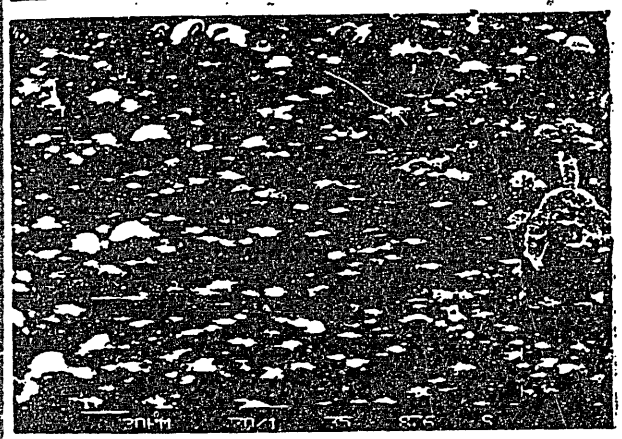
30/1
35
S

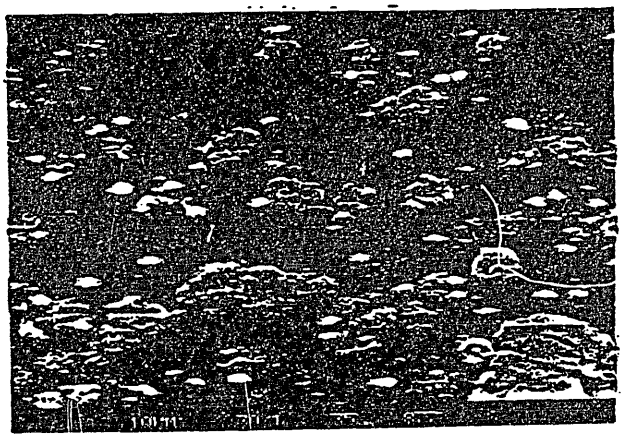

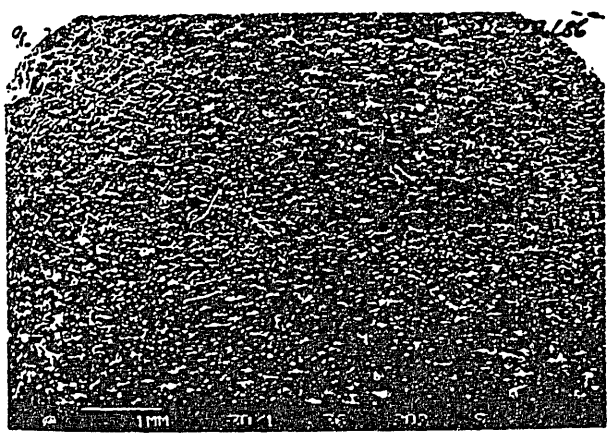
1MM
30/1
S

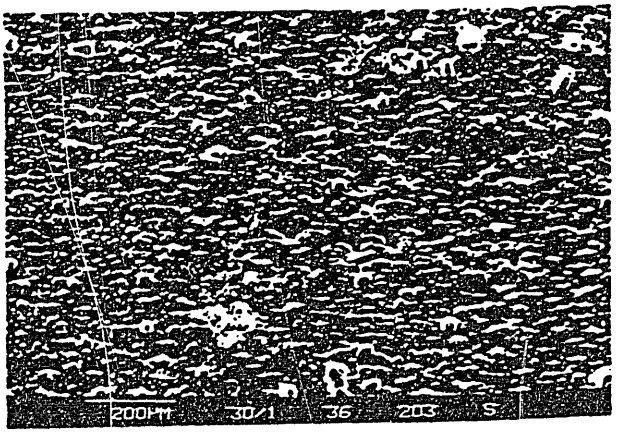
200MM
30/1
36
203
S

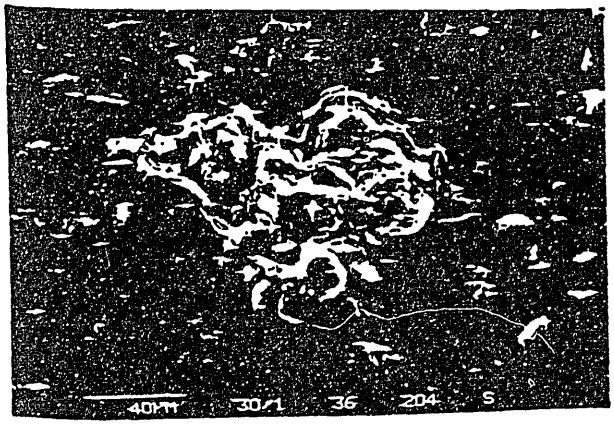
40MM
30/1
36
204
S


20MM
30/1
36
205
S

Hydrogen and Deuterium Retention in Wall Samples of JET

R. Behrisch[+)], P. Børgesen[+)], J. Ehrenberg[+)], M. Wielunski[+)]
A.P. Martinelli[+)], H. Bergsåker[*)], B. Emmoth[*)], J.P. Coad

JET Joint Undertaking, Abingdon, OX 14 3EA, U.K.
+) Max-Planck-Institut für Plasmaphysik, EURATOM Association, D-8046 Garching/München, FRG
*) Research Institute of Physics, S-104 05 Stockholm, Sweden

Aims of the investigations

Determine the amount of D and H in the walls in respect to
- possible release of Hydrogen into the plasma (recycling 1) and
- tritium inventory

Determine the differences in hydrogen trapping in wall samples of different materials with and without carbonisation.

Determine the isotope composition and depth distribution of the hydrogen trapped in the walls.

Analysis

The LTS made of Carbon and Inconel have been analysed in respect to the hydrogen isotopes by

Nuclear reaction $^{3}He(d,p)^{4}He$.
Elastic Recoil Detection using 2.6 MeV ^{4}He ions.

The Carbon layers on Inconel have been measured using H^{+} beams with 1.6 MeV and 1.8 MeV (Rutherford Backscattering with enhanced cross section and resonance cross section). The measurements have been calibrated with standard films

H- AND D- CONTENT IN LONG TERM SAMPLES (ERD MEASUREMENTS) FROM JET (1985) OCTANT III

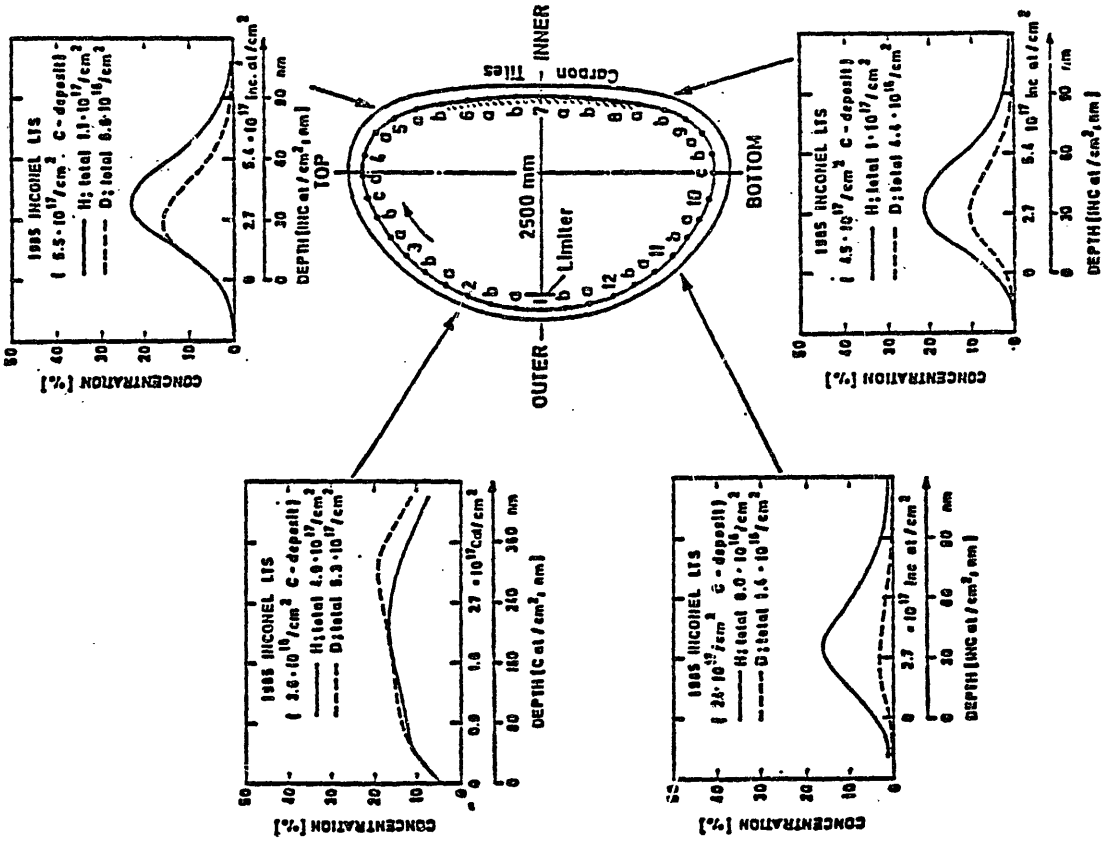

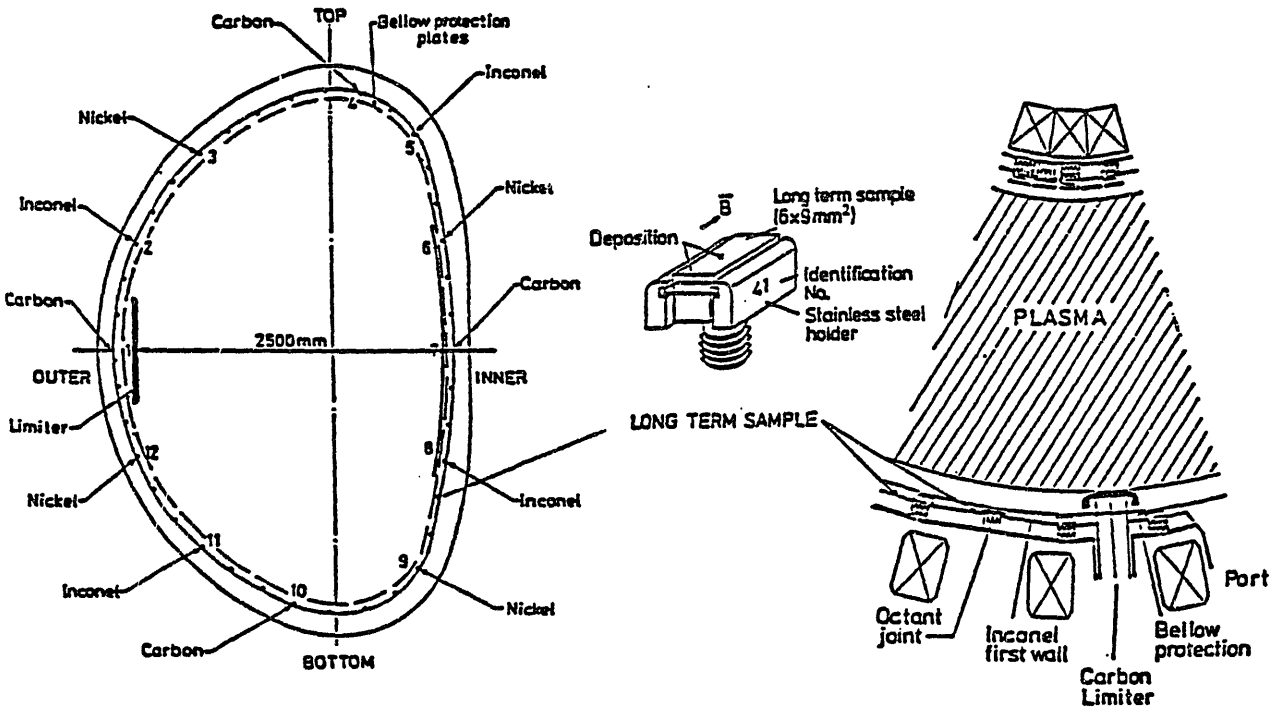

H- AND D-CONTENT IN LONG TERM SAMPLES
(ERD MEASUREMENTS) FROM JET (1984) OCTANT III

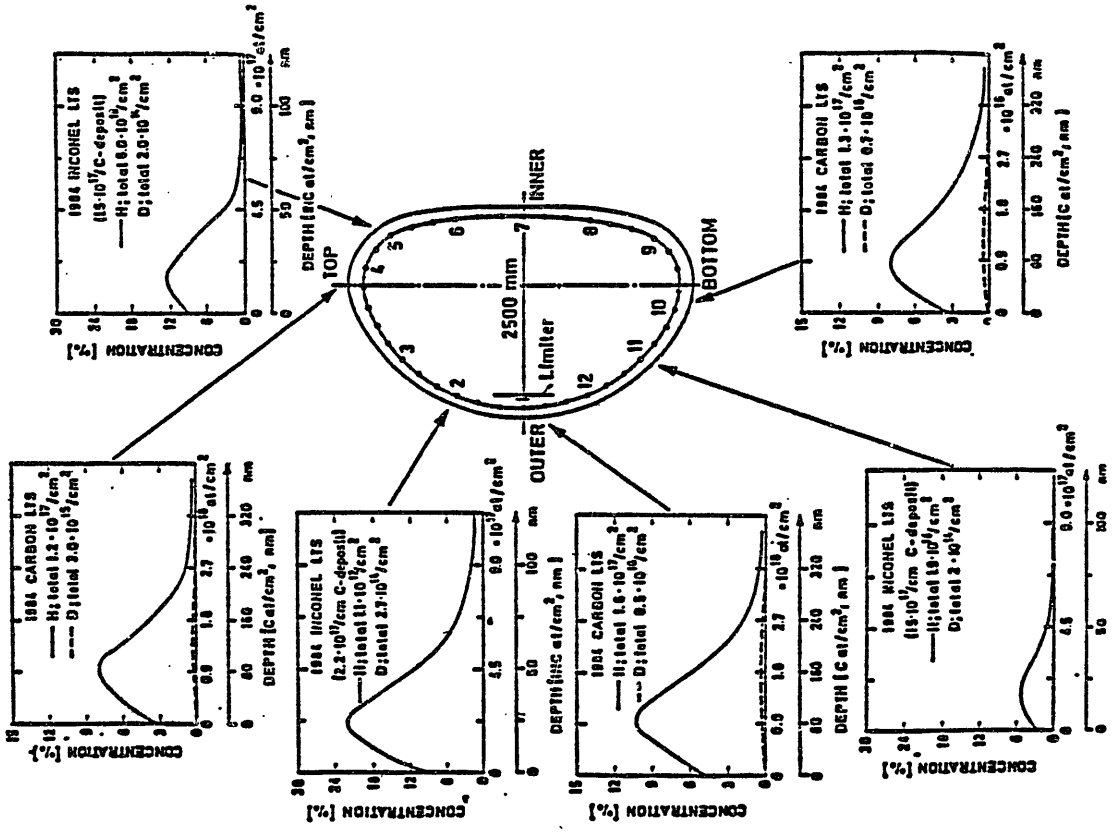

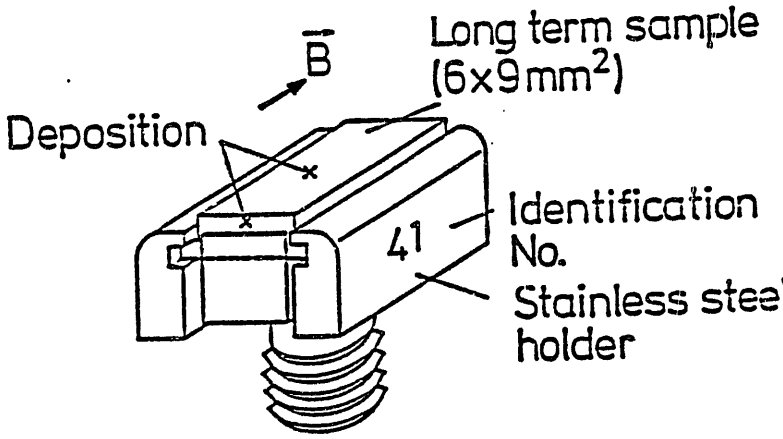

LONG TERM SAMPLE

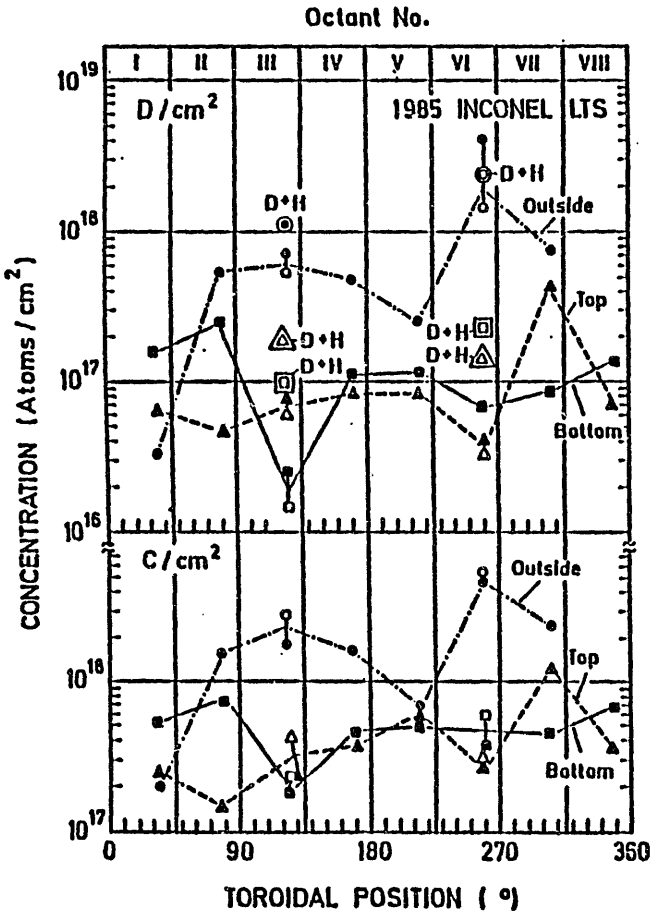
Octant No.
I
II
III
IV
V
VI
VII
VIII
D / cm²
1985 INCONEL LTS
D+H
Outside
Top
Bottom
C / cm²
CONCENTRATION (Atoms / cm²)
TOROIDAL POSITION (°)
0
90
180
270
360

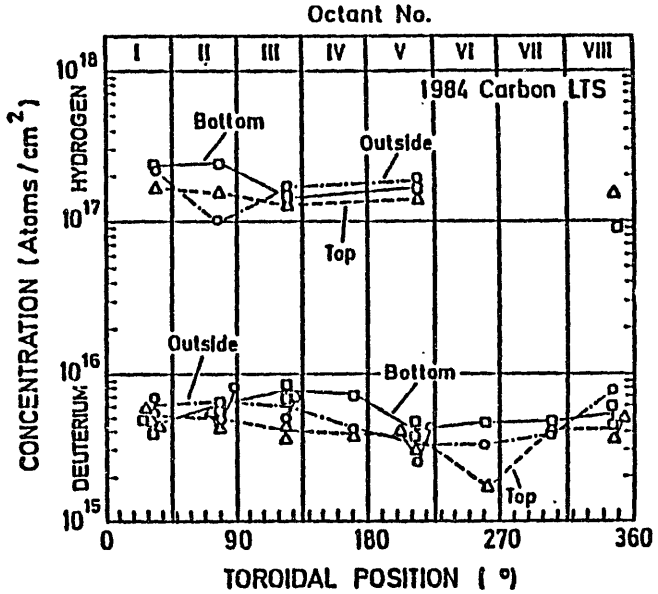
Octant No.
I
II
III
IV
V
VI
VII
VIII
1984 Carbon LTS
HYDROGEN
DEUTERIUM
Bottom
Outside
Top
CONCENTRATION (Atoms / cm²)
TOROIDAL POSITION (°)
0
90
180
270
360

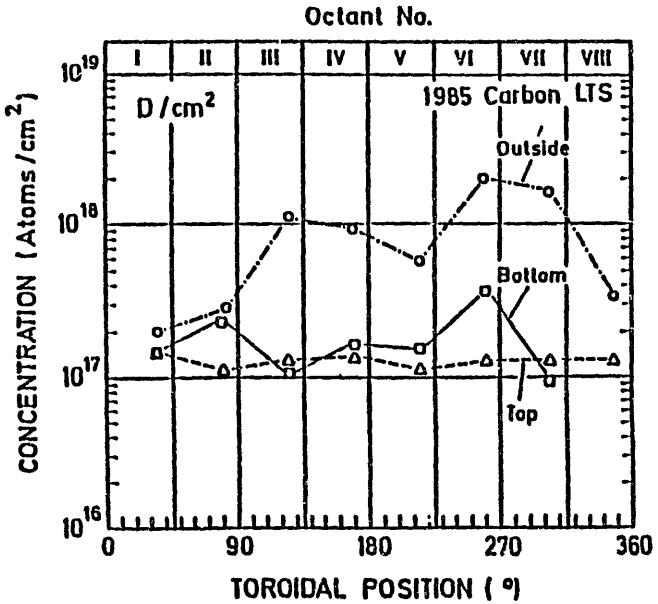
Octant No.
I
II
III
IV
V
VI
VII
VIII
D / cm²
1985 Carbon LTS
Outside
Bottom
Top
CONCENTRATION (Atoms / cm²)
TOROIDAL POSITION (°)
0
90
180
270
360

Conclusions

1) The amount of H, D trapped on the vessel walls in C-containing tokamaks is of the order of $2 \cdot 10^{17}$ to 10^{18} D+H/cm^2.

2) The hydrogen is trapped in a surfacelayer of 200 to 400 um, mostly carbon.

3.) The maximum concentration is about 0.3 to 0.4 D+H/C corresponding to saturation of D, H in carbon

4) The hydrogen is likely trapped by codeposition of H, D with Carbon

5.) This amount of H, D corresponds to about 100 times the amount of H, D in the plasma. It may be reduced at higher wall temperatures.

Absorption and Desorption of D_2 on Graphite

H. Atsumi and M. Miyake
Department of Nuclear Engineering, Faculty of Engineering,
Osaka University, Yamada-Oka, Suita, Osaka 565, Japan

Abstract

Thermal desorption measurements have been performed on the graphite exposed to deuterium gas atmosphere at 200-900 °C under a given pressure within 0.05 - 1 atm for 0.1 - 20h. The typical results of this study are summarized.

Absorption and Desorption of D_2 on Graphite

H.Atsumi and M.Miyake
Department of Nuclear Engineering, Faculty of Engineering,
Osaka University, Yamada-Oka, Suita, Osaka 565, Japan

1. Introduction

For application of graphite to first walls in a fusion reactor, it is important to obtain broad and reliable information on the recycling and inventory of hydrogen on graphite. However, little information is available on the absorption and desorption behavior of hydrogen isotopes on graphite at elevated temperatures. In the present study, thermal desorption measurements have been made on isotropic graphite exposed thermally to deuterium atmosphere under various conditions.

2. Experimental

As shown in Fig.1, these graphite samples (ISOGRAPH-88, Toyo Tanso Ltd., 10×10×1 mm) were degassed at 1100℃ for two hours in a vacuum, and then exposed to deuterium gas atmosphere at 200 - 900℃ under a given pressure within 0.05 - 1 atm for 0.1 - 20 h. Since graphite usually has a large amount of adsorption of hydrogen at graphite grain surfaces or in micro-pores, relatively high temperature and high pressure were chosen in order to produce a much larger amount of deuterium in solution within graphite grains compared with the amount of adsorption. Thermal desorption measurement of deuterium from these graphite samples was made at a constant heating rate of 10 ℃/min in a vacuum below 10^{-5} Pa. Released species from graphite samples (D_2 and CD_4) were determined with a quadrupole mass spectrometer.

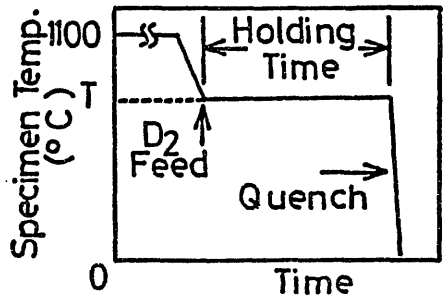

Fig.1 Experimental procedure.

3. Results and Discussion

Deuterium desorption curves on the graphite exposed to D_2 gas show single peaks which exist at about 950 ℃ (Fig.2). And no significant desorption of CD_4 was determined during a series of thermal desorption measurements. The total amount of deuterium released from graphite rises in proportion with the square root of deuterium gas pressure (Fig.3). Therefore, deuterium in the graphite sample would exist as

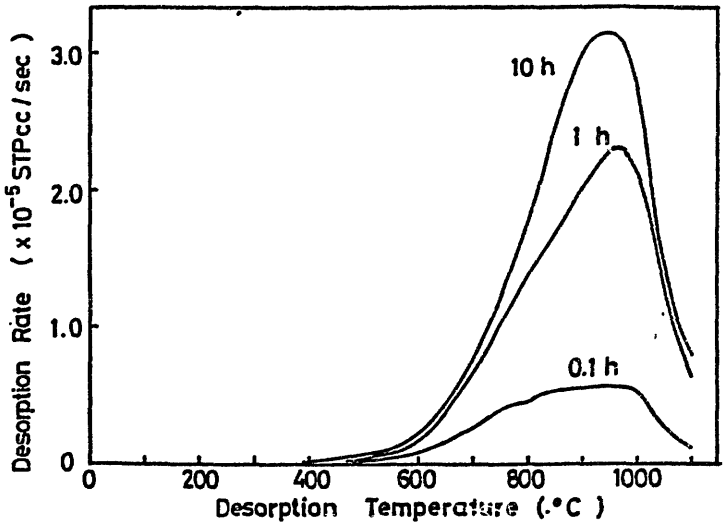

Fig.2 Thermal desorption spectra of D_2 from graphite exposed to deuterium atmosphere for various time (700 ℃, 0.6 atm)

(2) The CD_4 desorption was rather small.

(3) The total amount of released D_2 was proportional to the square root of D_2 gas pressure.

(4) The total amount of released D_2 increased with exposure temperature and decreased above 700 ℃.

(5) Roughly estimated diffusion coefficients of D_2 in graphite were 2×10^{-12} cm^2/sec and 3×10^{-12} cm^2/sec at 800 ℃ and 900 ℃, respectively.

Reference

[1] R.A.Causey, T.S.Elleman, K.Verghese, Carbon 17 (1979) 323.

High heat flux tests on C-materials

Jochen Linke

K F A

Abstract

High heat flux simulation test were performed in electron beam devices (SNLA, KFA) mainly on laboratory scale samples (different grades of graphite,C-C-composites pyrocarbon); besides this actively cooled components also were tested.

Main aspects of these experiments were:

-- erosion behaviour,
-- thermal shock resistance,
-- thermal cycling behaviour,
-- investigation of particle emission.

High heat flux tests on C-materials

e^--beam device KFA-ZAT
- erosion
- cracking behaviour
- surface modifications

(8 fine grain graphites, 1 C-C-composite)

e^--beam device SNLA
- particle emission mechanism
- erosion
- cracking behaviour
- thermal cycling

(11 fine grain graphites, 3 C-C-composites, pyrocarbon, glassy carbon, a:C-H contings)

J. Bohdansky	IPP-Garching	E. Wallura	KFA-IRW
H. Bolt	KFA-IRW	R.D. Watson	SNLA
D. Croessmann	SNLA	J.B. Whitley	"
G. Gutecit	KFA-IRW	J. Winter	KFA-IPP
H. Haven	"		
J. Linke	"		
F. Heuser	"		
E. Sigismund	KFA-ZAT		

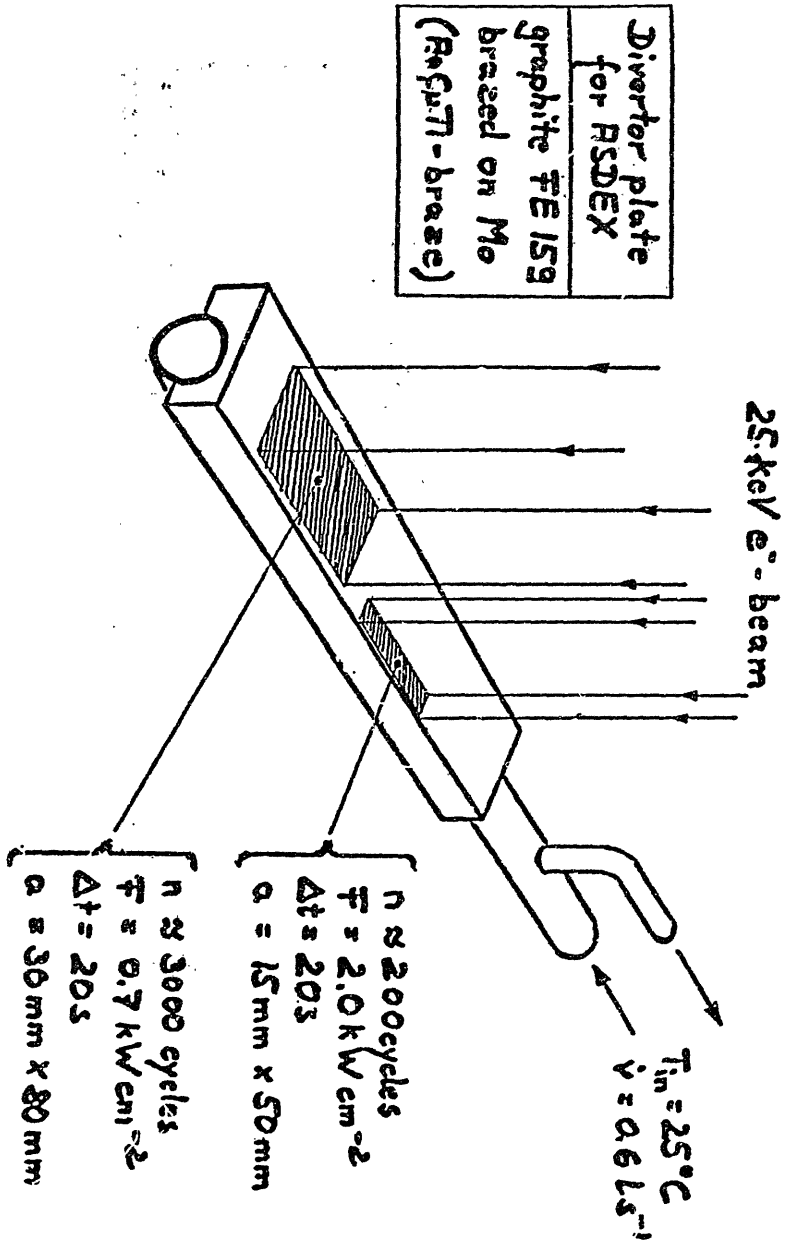

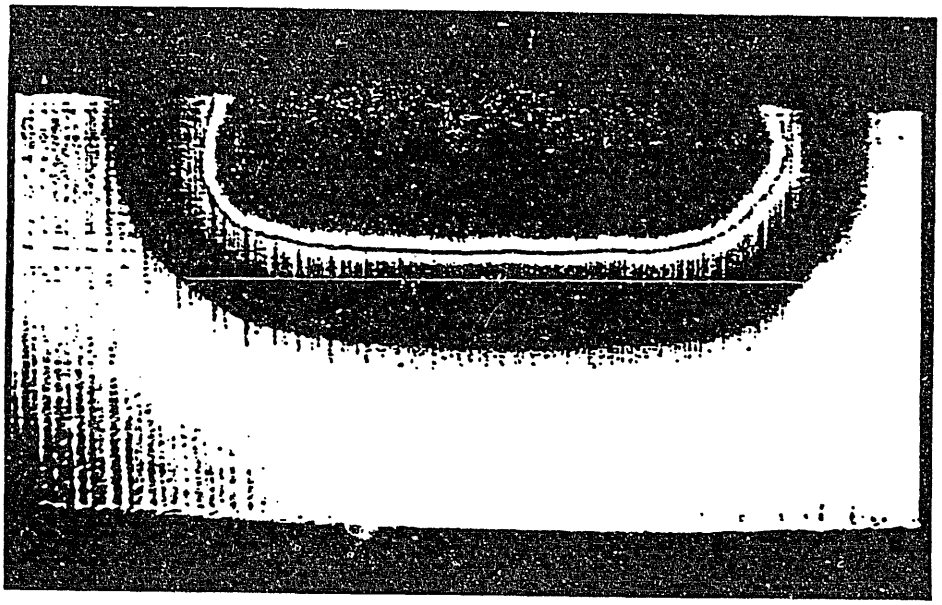

Graphite brazed to a water-cooled Mo-tube after 300 electron beam pulses
($F = 2.0$ kW cm^{-2}, $\Delta t = 20$ s, a = 15 mm × 50 mm)

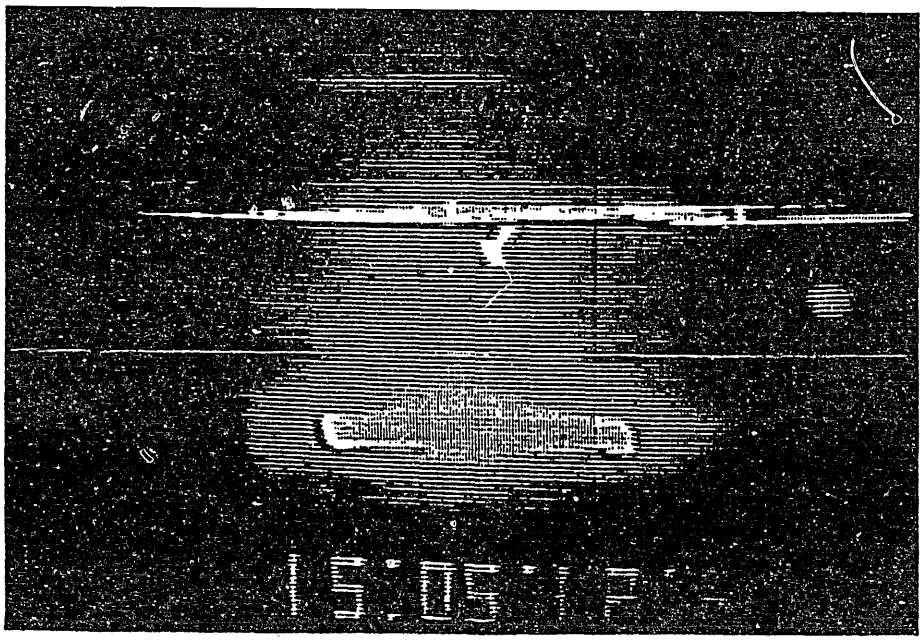

Erosion of the graphite surface by particle emission due to electron beam bombardment ($T_{surf} > 2400°$ C).

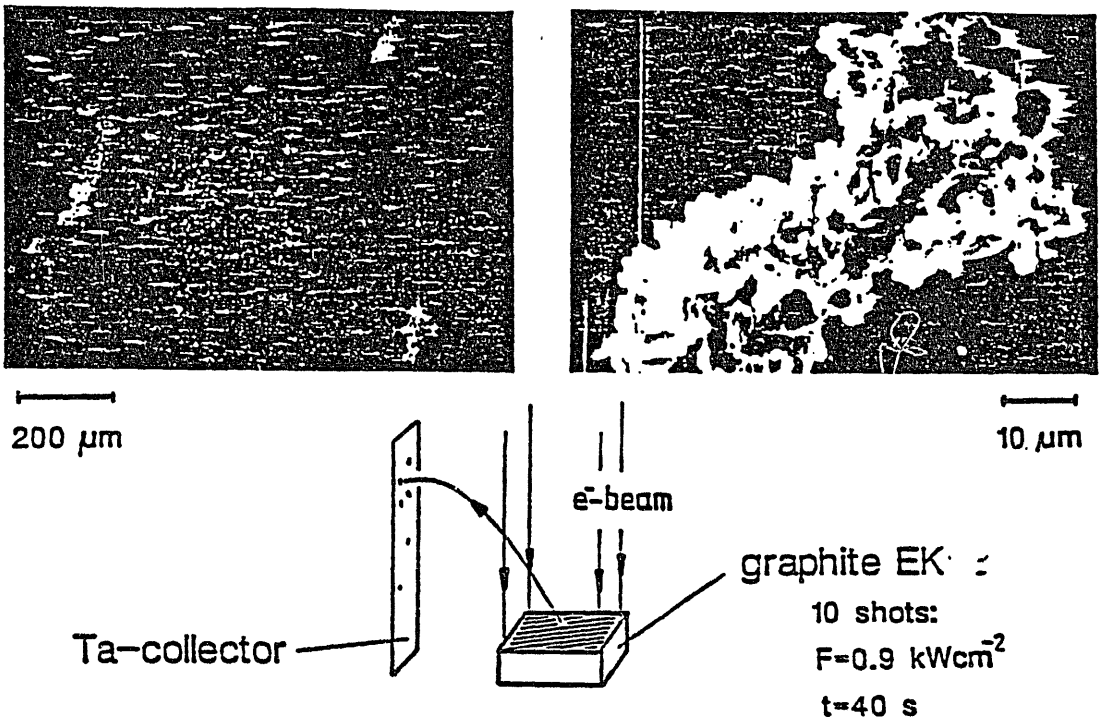

Graphite particles collected on a Ta–foil

material	thermal shock	erosion	thermal cycling
RTJ	x	x	x
* CGW	x	x	
RXF-SG	x	x	x
* RXF-SG-GCI	x	x	x
EK 98	x	x	x
FE 153	x	x	x
* FE 153	x	x	
IG 11	x	x	
# IG 110	x	x	
5890 PT	x	x	
pyrocarbon	x	x	
glassy carbon	x	x	
K-KARB (2D)	x	x	
HITCO (2D)	x	x	
FMI (4D)	x	x	x
sample geometry	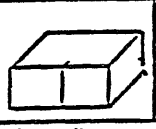	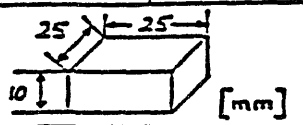	

* densified material # purified material

graphitic material for high heat flux components (tests at SNLA)

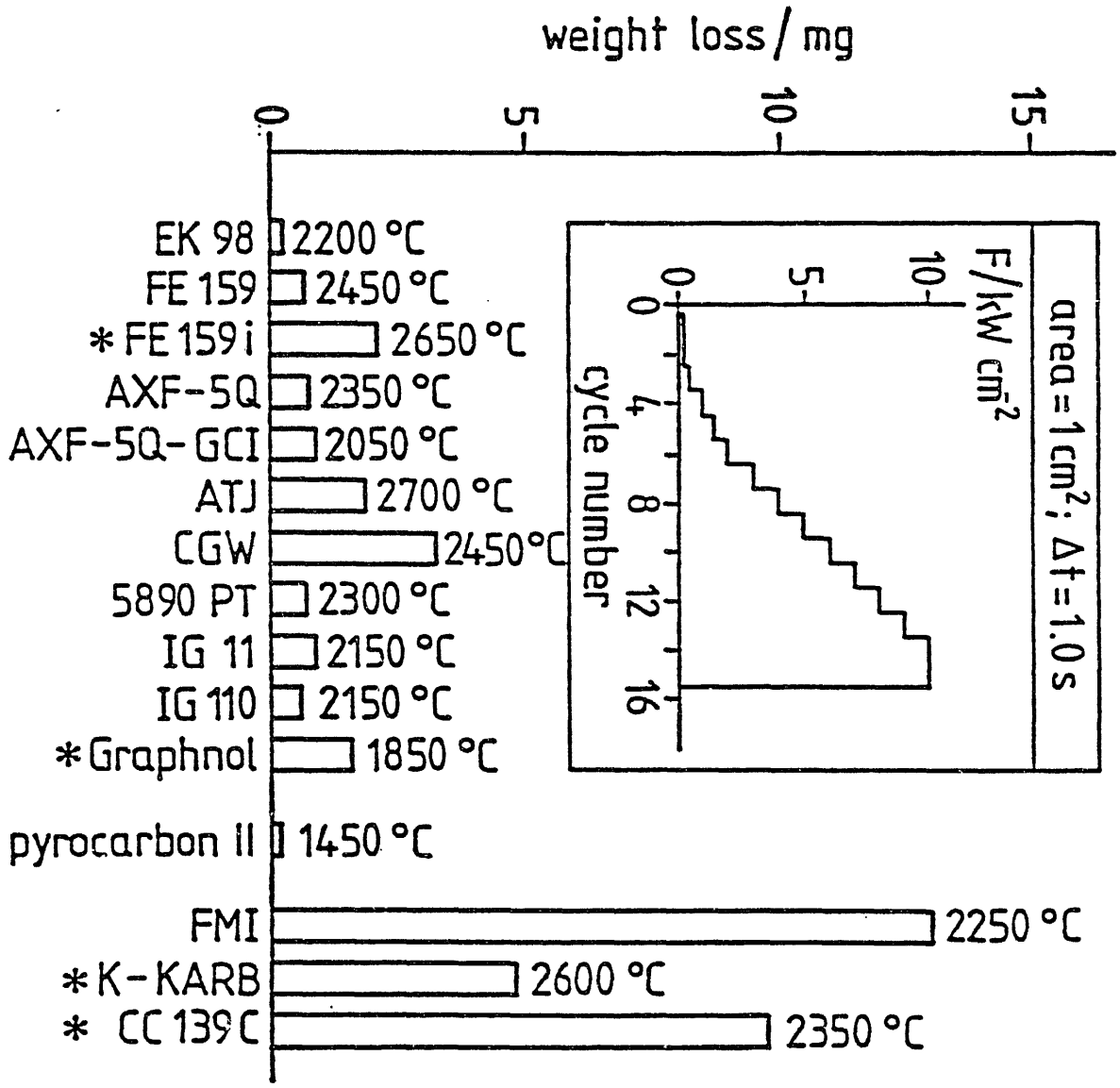

* sample geometry other than 25mm × 25mm × 10mm

Erosion of different graphitic materials due to intense electron beam bombardment

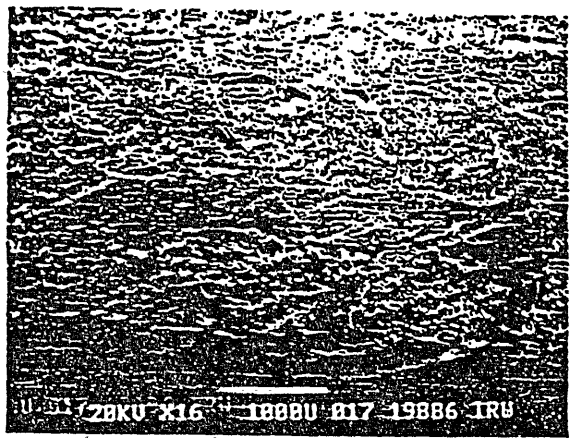

SE

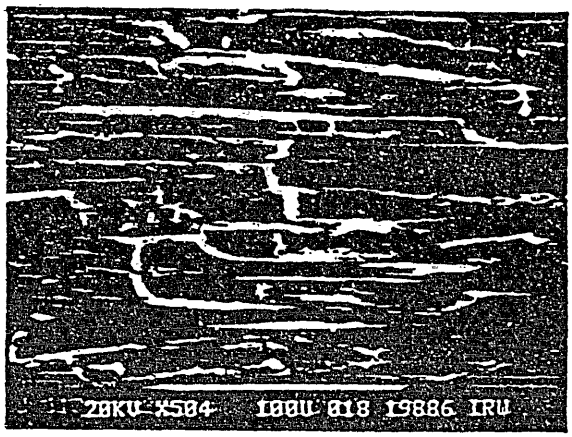

SE

FMI 40 CARBON WEAVE

15 cycle
1s pulse length
0.5 to 10kWcm^{-2}

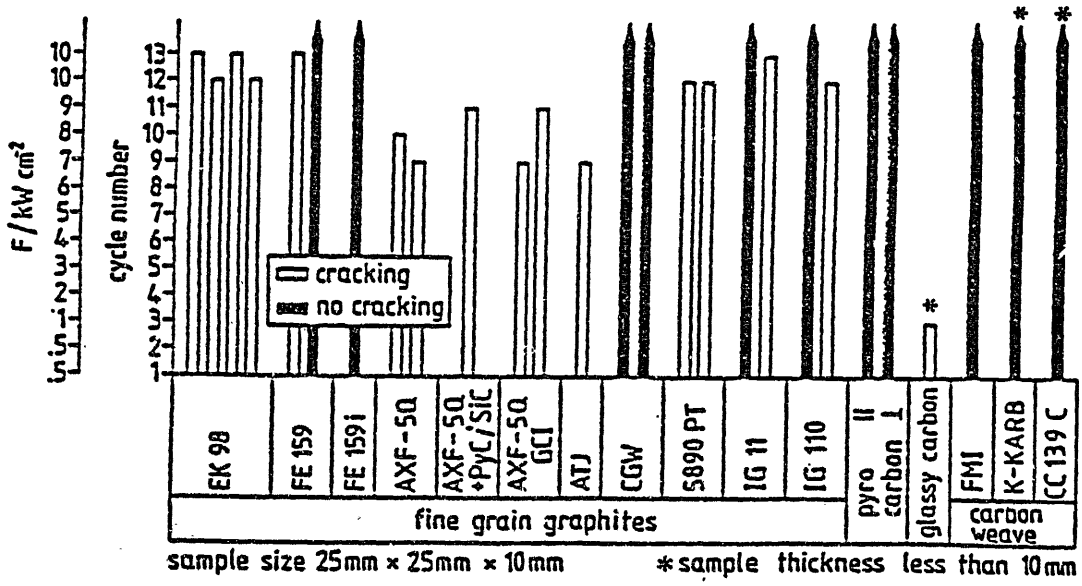

Cracking behaviour of different graphitic materials after successive electron beam shots of 1.5s duration; the power density was raised stepwise from 0.5 to 10kWcm^{-2}.

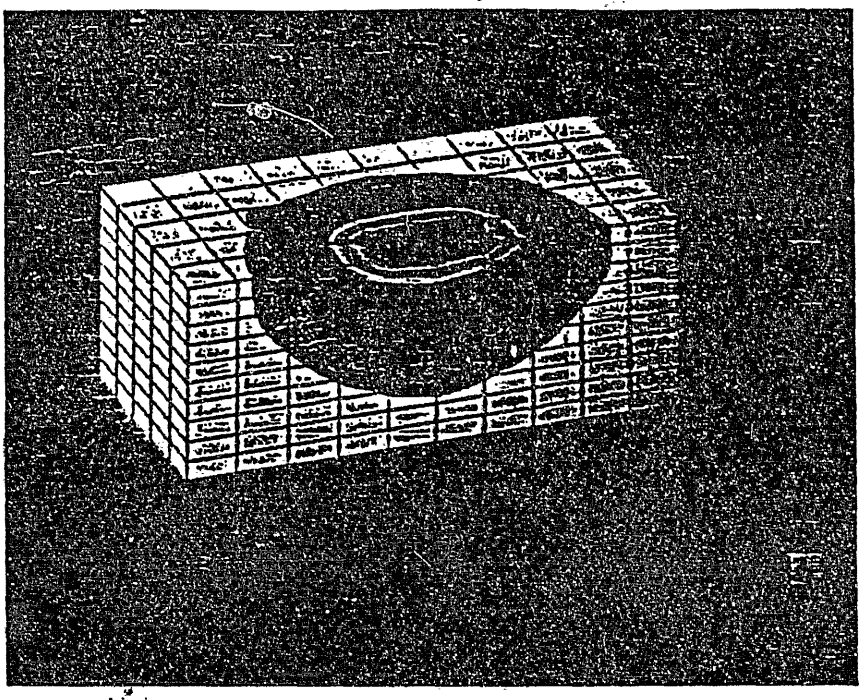

Temperature profiles in a graphite tile after 1.5 s electron bombardment (F = 4 kW cm^{-2}, beam area = 1 cm^2); sample cut up along the midplane.

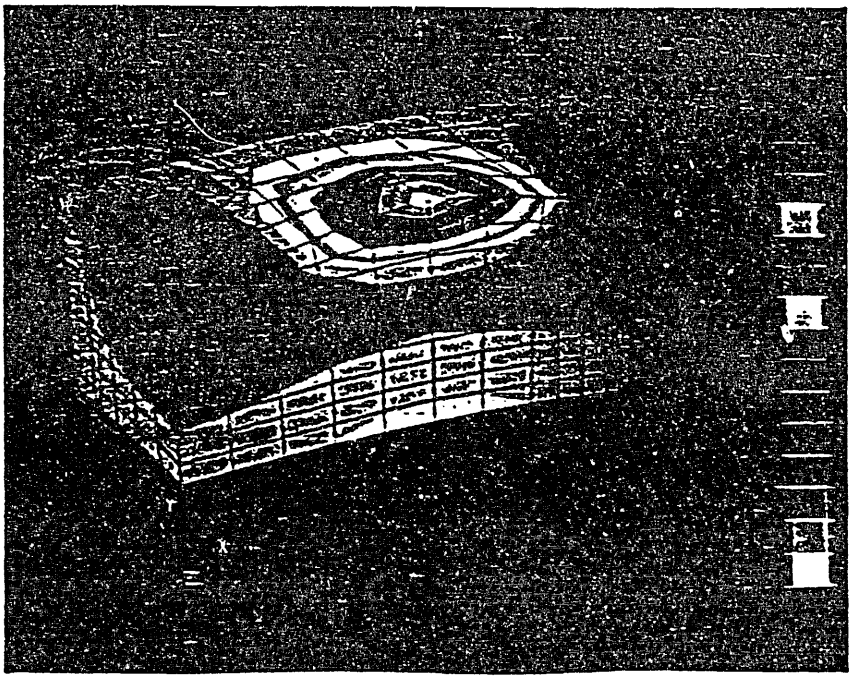

Stresses along the Z-axis in a graphite tile after 1.5 s electror beam exposure (F = 4 kW cm^{-2}, beam area = 1 cm^2). The distortion of the finite element mesh indicates the deformation of the tile due to thermal expansion.

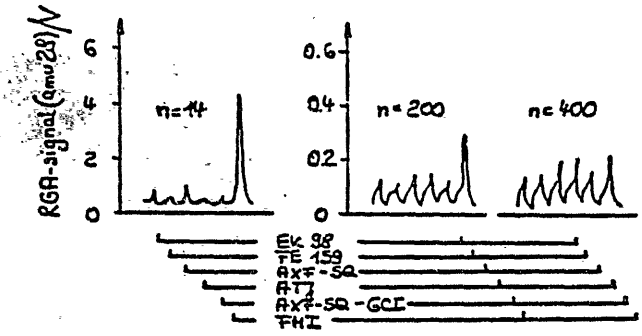

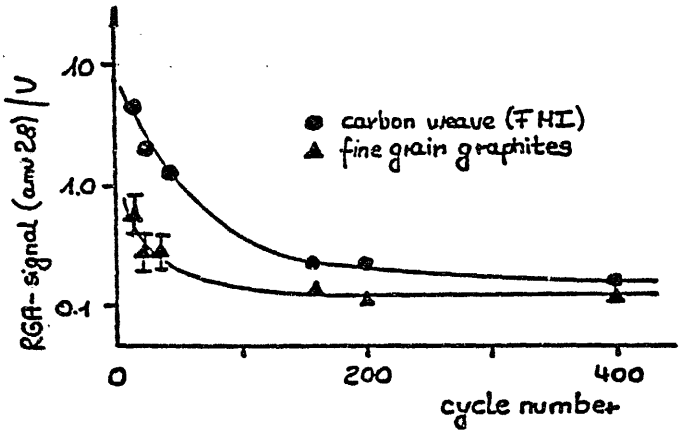

Thermal cycling of fine grain graphites and C-C-composites

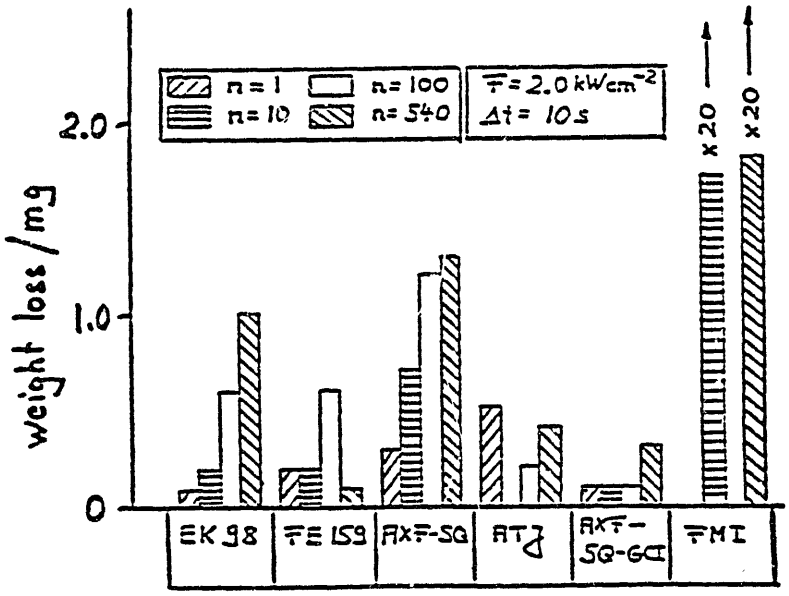

Thermal cycling of different fine grain graphites and C-C-composites

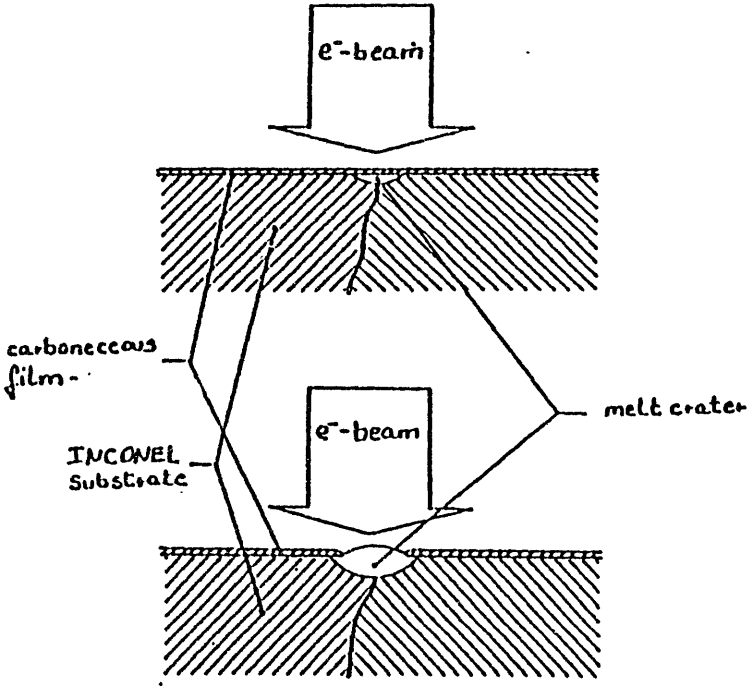

Schematic representation of the C-film dissolution. The melting point of the nickel base alloy is depressed by the enrichment with carbon atoms.

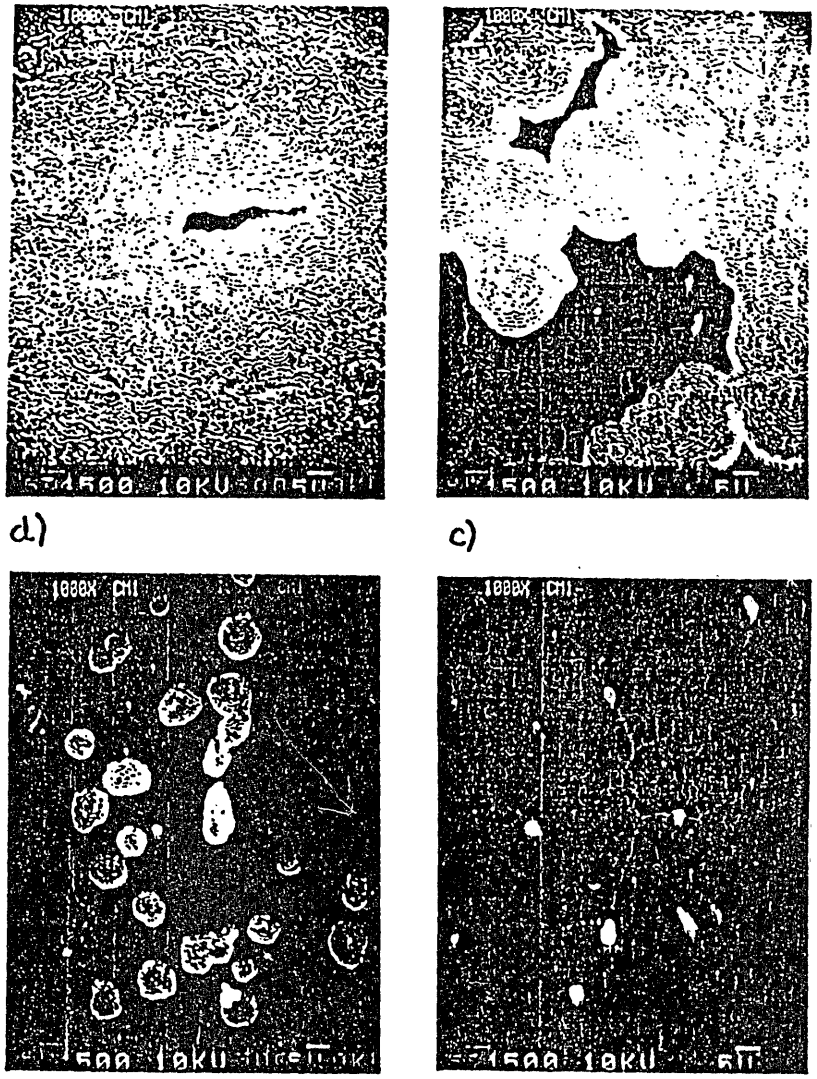

Dissolution of the carboneceous film on INCONEL (increasing heat fluxes from a) to d)) SEM micrographs, 1000x

1. Disruption simulation experiments on graphite by H^+-beam at the 10MW Neutral Beam Injection test stand of the IPP Nagoya

2. Ranaway-electron simulation by electron linear accelerator experiments

H. Bolt

Institute of Plasma Physics, Nagoya
Nagoya 464 Japan

Abstract

1. The behaviour of eleven different graphite grades (US-Japanese and European graphites) under disruption conditions was evaluated. Large size samples (50mm × 50mm surface) were exposed to ion beam pulses of power densities of 90...1000MW/m^2 and pulse length of about 200ms. High strength graphites tended to crack under the heat fluxes whereas isotropic fine grain graphites behaved well.

2. Electron beam of energies of 20 to 30MeV produced by an electron linear accelerator have been used to simulate runaway electron events.

   Bulk graphite showed for superior behaviour to MeV-electron bombardment than stainless steel.

   In activity cooled structures the metal cooling tubes may undergo serious thermal excursions to their failure.

Disruption Simulation Experiments on Graphite by H^+-beam at the 10MW Neutral Beam Injection Test Stand of the IPP Nagoya

H. Bolt[1], C. D. Croessmann[2], A. Miyahara, T. Kuroda, Y. Oka, K. Sakurai

Institute of Plasma Physics, Nagoya University

[1]: on leave from Institute of Reactor Materials, Nuclear Research Center, Juelich, FRG, EURATOM Association
[2]: Sandia National Laboratories Albuquerque, NM, USA

1. Test stand

For the performance of disruption simulation experiments on candidate first wall materials and full size first wall components the 10MW Neutral Beam Injection Test Stand at the IPP Nagoya had been modified. Figure 1 gives a schematic of the rebuilt test stand.

The ion source of the test stand produces H^+-beams of up to 120keV, 75A and 1s pulse duration with a Gauss shaped profile of the beam power density. The elongation factor of the oval shaped beam in vertical direction is roughly 2 and depends on the beam condition applied in experiments. For material tests the deflection coils of the Neutral Beam Test Stand are not in operation thus ions and neutrals are striking the material test pieces at a distance of about 5m from the ion source. A set of test pieces or full size first wall components can be inserted into the vacuum vessel by a lock system without breaking the vacuum of the vessel (about 10^{-7}Torr). A drive mechanism allows the test pieces to be vertically positioned in the H^+-beam. When operated without exposing test pieces to the beam, the beam is dumped into a calorimeter which provides data for the calibration of high heat flux experiments. The repetition rate of the test stand is three to five minutes depending on the power supply mode.

NBI - Test Stand

specifications for disruption simulation experiments on graphites:

H^+-ion beam:	120 keV, 75 A
beam divergence:	0.55^0 (horizontal axis) 1.2^0 (vertical axis)
electrode size:	150mm x 600mm
focal point:	9500mm
heat load on test pieces:	$\leq$ 100 MW/m^2
pulse length:	$\leq$ 1 s
size of components to be tested:	$<$150mm x 400mm

Table 1: test stand specifications for disruption simulation experiments on graphite

2. Experimental procedure

2.1 Pretreatment of samples and test procedure

The graphite samples were machined from larger blocks by dry sawing, milling and drilling of the shape, the slit and the hole for the attachment to the sample holder (Fig. 2). The surface which was to be exposed to the beam was ground. Some samples had polished surfaces.

All samples were cleaned in an ultrasonic bath with ethanol for three times five minutes each time. After each cleaning period the ethanol was exchanged.

The baking for all samples (except YPD, shot no. 23185) was performed at a temperature of 300°C for 20h under a vacuum of 10^{-6}Torr. After the baking the samples were stored under a vacuum of $< 10^{-1}$Torr until the experiment.

For the experiments on graphite a sample holder without cooling system was built. On the 15mm thick copper backing plate of the sample holder four graphite samples with a surface of 50mm x 50mm and 20mm thickness (30mm in the case of EK 98 graphite) were attached in a vertical line. The samples were fixed to the backing plate by bolts to be screwed to metal counterparts which were inserted in a slit machined in the graphite samples (Fig.2).

During the installation to the sample holder the samples were exposed to atmosphere for about 15 minutes. Afterwards they were kept in the back-up vacuum chamber of the lock system for the pump down of the vacuum. Before the experiment the gate valve to the NBI test vessel was opened and the samples inserted for beam exposure. After the experiment the sample holder was withdrawn and the samples removed, or kept for repeated exposure, resp..

2.2 Beam calibration and beam parameters

For the beam calibration the calorimeter of the NBI Test Stand vacuum vessel was used. In this calorimeter 25 shielded thermocouples indicate the temperature rise during the beam impact. The horizontal and vertical spacing of the thermocouples in the plane perpendicular to the beam is 50mm. Since the copper shielding of the thermocouples leads to the measurement of the temperature in the volume of the material, the recorded temperature is proportional to the energy dumped onto this unit. Thus at a preset pulse length the temperature rise indicates the power density of the beam in this location.

After the conditioning of the ion source was finished and the beam conditions for high heat flux experiments - as indicated by the calorimeter values - were satisfied, the test pieces were positioned in the beam line so that during the next pulse the beam could hit the samples with beam conditions similar to the previously calibrated pulse onto the calorimeter with a variation of the beam power of less than 5%.

Figure 3 gives a calibration curve of the beam power density distribution of a pulse as it has beeen applied in the experiments on graphite. The peak power density of the pulses in the experiments varied from 90MW/m^2 to 100MW/m^2. Pulse lengths of 157 to 353 ms were obtained with most pulses at lengths of about 200ms.

2.3 Post experiment treatment of the samples

After an experiment only the graphite sample which has been positioned in the beam center was removed for further examination. The other samples were used as dummy samples to shield the copper backing plate against high heat fluxes.

All samples were examined visually and by SEM as well as the weight loss was measured by means of a microbalance. Aims of the observations were the clarification of the erosion process on graphite materials under high heat flux conditions and the determination of the resistance to thermal shocks under disruption conditions.

2.4 Break down of the ion source and reconditioning

During experiments on graphite the ion source terminated operation after pulse lengths of 157 to 353 ms with most terminations occuring after about 200ms. This termination of the ion source operation is due to arcing between the extraction grids of the ion source which seems to be caused by contamination of the grids. It is still unclear whether the

contamination during the experiments occurs in the form of deposition of hydrocarbons reducing the field resistance against arcing or due to deposition of small carbon particles causing deformation of the electrical field between the grids.

After the experiments and the break down of the ion source caused by grid contamination extensive reconditioning of the ion sorce was needed to remove the contamination from the extraction grids and to reach experimental conditions again.

3. Materials tested and their properties

A list of the graphites subjected to disruption simulation tests and their thermophysical and mechanical properties is given in Table 2. The specific properties of the various grades suggest a distinction into groups of

- high strength, isotropic graphites
  (AXF-5Q, ISO 880, T6-P, MT 200 K)
- isotropic graphites
  (CL 5890 PT, EK 98, ETP-10, IG 110)
- anisotropic graphites
  slight anisotropy: ATJ (not impregnated)
  CGW (impregnated)
  strong anisotropy: YPD

4. Results

For a first orientation a screening test with 14 samples of nine different grades of graphite (AXF-5Q, ISO 880, T6-P, MT 200 K, CL 5890 PT, EK 98, ETP-10, IG 110, and YPD) had been done by means of small samples clamped together and exposed to H^+-beam pulses at the same time. The samples had a surface of 5mm x 10mm and were all placed in the beam center (Fig. 4). They were subjected to three pulses at a power density of 90 to 100 MW/m^2 and pulse lengths of 227ms, 170ms, and 195ms.

On large samples (50mm x 50mm x 20mm) of eleven grades experiments were performed as listed in Table 3.

graphite/ grade	σ_{F_2} (N/mm^2)	σ_{T_2} (N/mm^2)	E (N/mm^2)	α ($10^{-6}/^oC$)	c_p (W/m^oC)
AXF 5Q	90	63	11700	7.7	100
POCO Graphite, Inc.					
ISO 880	95	70	13000	6.5	99
Toyo Tanso					
T6-P	100	50	15000	6.5	57
Ibiden					
MT 200 K	75	45	14000	6	
Toyo Carbon					
CL 5890 PT	60	33	11600	4.6	74
Carbone Loraine					
EK 98	47	30	11500	3.4	69
Ringsdorff Werke					
ETP-10	50	30	11000	3.5	103
Ibiden					
IG 110	40	25	10000	4.6	115
Toyo Tanso					
ATJ	∥:30	∥:30	∥: 8400	∥:2.1	∥:140
Carbon Products Div. of	⊥:25	⊥:22	⊥: 6300	⊥:3.6	⊥: 80
Union Carbide					
CGW					
Carbon Products Div. of					
Union Carbide					
YPD	∥:50			∥:1-2	
Toyo Carbon	⊥:25			⊥:12-13	

Table 2: graphites tested, their mechanical and physical properties (R_T)
σ_F: flexural strength, σ_T: tensile strength, E: Young's modulus, α: linear thermal expansion coefficient, c_p: specific heat

grade	no. of samples tested	no. of pulses per sample	pulse lengths (ms)
AXF 5Q	3	1,1,1	176,233,258
ISO 880	2	1,1	164,214
T6-P	1	1	164
MT 200 K	1	1	183
CL 5890 PT	3	1,1,1	157,176,220
EK 98	3	2,1,1	170,195,227;176,183
ETP-10	2	2,1	176,202;195
IG 110	3	3,1,1	195,202,220;202,214
ATJ	3	1,1,1	170,183,220
CGW	1	1	227
YPD	∥:2; ⊥:1	∥:2,1 ⊥:2	∥ :302,353;309 ⊥ :189,202

Table 3: graphite grades, no. of samples tested, no. of pulses accumulated on each sample and pulse lengths

The pulse lengths obtained in the experiments did not show any dependence on the graphite grade under test with the exception of YPD graphite tested with grain. In these cases the ion source terminated operation at pulse lengths of 353ms, 302ms, and 309ms, thus resulting in a significantly higher heat load on these samples (Chapt. 5.1).

4.1 Small size samples

4.1.1 Cracking

In the screening test on small size samples only on the AXF 5Q and the ISO 880 samples cracking occured.

4.1.2 Erosion

After the experiment the YPD sample (with grain) shows far less signs of erosion compared to the other samples (Fig. 4).

AXF 5Q and ISO 880 show a very homogeneous erosion structure. Other graphites (T6-P, MT 200 K, CL 5890 PT, EK 98, ETP-10, and IG 110) display a more irregular erosion structure with voids occuring at lengths of up to 200µm. The appearence is similar to microcracks but the penetration depth of these voids is very small.It is more likely that just a few binder bridges between grains have failed. The surfaces of T6-P, IG 110, EK 98 and MTK show several voids of about 50µm diameter where obviously particles have been emitted from the surface. It appears as the binder bridges have failed around such particles so that the adherence to the surrounding material was weakened which eases the emission of such a particle.

4.2 Large size samples

SEM micrographs of the sample surfaces after beam exposure (single pulse) in Figures 7 to 17 representing one sample of each grade.

4.2.1 Fracture and cracking

Fracture happened on one YPD sample tested with grain (Fig. 5) after a pulse duration of 308ms. AXF 5Q and ISO 880 show cracks on the surface in net like structure (Fig. 6). On one sample of EK 98 cracks and on another one microcracks occured (Fig. 11). The T6-P and MT 200 K samples show microcracks (Fig. 8,9).

4.2.2 Erosion

The erosion behaviour observed on the large size samples is similar to the one described in section 4.1.2.

The large size samples which were subjected to repeated thermal shocks (i. e. EK 98, ETP-10, IG 110, and YPD) indicate more pronounced the particle erosion process as the samples subjected to single beam exposure. This process means the loosening of the surface structure by the formation of voids along grains which enables the emission of particles from the surface (Chapt. 4.1.2). The rather long voids (about 200µm) which can be found on ETP-10 seem to have been formed already during the production process and thus be preexistent (Fig. 13, left below).

The weight loss per shot on the samples was in the order of 10mg. As the pulse lengths in the experiments varied considerably, the measured weight loss does not allow further conclusions on the differences in the erosion behaviour of the various graphite grades (except YPD). The extended pulse lengths in the tests of YPD graphite (with grain) indicate that this grade shows far less erosion than the other graphites.

4.3 Summary of results

A summary of the results is given in Table 3.

graphite	no. of samples tested	cracking (brackets: no. of samples)	erosion
AXF 5Q	3	netlike crack formation (2)	homogeneous erosion structure
ISO 880	2	netlike crack formation (2)	homogeneous erosion structure
T6-P	1	microcrack (SEM) (1)	loosening of surface structure
MT 200 K	1	microcrack (SEM) (1)	loosening of surface structure
CL 5890	3	---	loosening of surface structure
EK 98	3	crack (1), microcrack (1)	loosening of surface structure
ETP-10	2	---	long voids (∿200µm) (preexistent?)
IG 110	3	---	loosening of surface structure
ATJ (CGW)	3,1	---	
YPD	3	complete fracture (1)	little erosion

Table 3: Summary of the results

5. Discussion

5.1 Fracture and cracking

The disruption simulation experiments show that graphites of high mechanical strength ("High Strength Graphites") tend to crack under the applied heat loads. The only other graphite grades that showed cracking or fracture in the experiments are EK 98 and YPD (with grain).

The result on YPD graphite is to be explained by the anisotropy of properties: The high thermal conductivity in the direction perpendicular to the heated surface leads to lower surface temperatures during the pulse and thus to less erosion compared to the other graphites. Caused

by this the contamination of the ion source grids takes longer time leading to increased pulse lengths which results in an increase of the deposited beam energy on the sample. Additionally to this higher energy deposition YPD graphite has a high linear thermal expansion coefficient and weak mechanical properties in the "against grain" direction. Both together, higher thermal load and disadvantageous mechanical properties in the plane of the heated surface, resulted in the failure of the sample.

The occurance of cracks on the "High Strength Graphite" samples may be caused by their comparatatively high coefficient of linear thermal expansion which leads to increased stresses under thermal loads.

The mechanical and physical properties of EK 98 (Table 1) do not provide any information for an explanation of the inferior behaviour of this grade in the experiments.

5.2 Figure of merit

For engineering purposes it would be helpful to derive a figure of merit for the thermal shock resistance of graphite under disruption conditions which enables to establish a ranking among different graphite grades. The most common figure is the thermal shock resistance parameter R

$$R = \frac{\sigma_F}{E \cdot \alpha} \qquad (1) \quad /1,2/$$

with σ_F : ultimate flexural strength
α : coeff. of linear thermal expansion
E : Young's modulus

To better fit this parameter to the conditions of surface heat loads shorter than the thermal diffusion time t_d

$$t_d = \frac{d^2 \pi \rho c_p}{4k} \qquad (2) \quad /2/$$

with d : thickness of the sample perpendicular to the thermal load incidence
ρ : density
c_p : thermal conductivity
k : specific heat

the thermal conductivity as physical property should be included to form R':

$$R' = \frac{\sigma_F \cdot \sqrt{c_p}}{E \cdot \alpha} \qquad (3)$$

as the surface temperature rise ΔT in one dimensional problems at deposition times shorter the thermal diffusion time is

$$\Delta T = \frac{P}{A} \cdot \sqrt{t} \cdot \frac{2}{\sqrt{\pi \rho c_p k}} \qquad (4) \quad /3/$$

with: P/A : power density
t : time of thermal load

As the thermal ~~conductivity~~ capacity k is very similar among graphites at elevated temperatures /1/ this property can be neglected in the expression for R' (3).

5.3 Correlation of the figure of merit for thermal shock resistivity and the experimental results

The thermal shock resistivity figures of R and R' (chapt. 5.2) for the graphites tested in the experiments are given in Table 4 by using the properties listed in Table 1.

graphite	R	R'
AXF 5Q	1000	10000
ISO 880	1124	11184
T6-P	1026	7746
MT 200 K	893	
CL 5890 PT	1124	9669
EK 98	1202	9984
ETP-10	1299	13183
IG 110	870	9330
ATJ	1700	20115
	1102	9856

Table 4: Figures of merit for thermal shock resistivity R and R'

The experimental results and both of the figures of merit do not show any correlation. This may be due to the strong temperature dependence of the physical and mechanical properties regarded in the figures of merit (σ_f, c_p, E). The data base for these properties at temperatures above 2200°C which seems to be relevant for the case of disruption heat loads and their simulation /4/ is insufficient.

Depending on the raw materials used, the pressing method and the graphitization temperature during the production process the high temperature properties of graphites vary considerably, especially in the temperature region above 2000°C where graphite starts to show increasing ductile behaviour /1/.

Qualitatively the parameters of the thermal shock resistivity figure are dependent on the temperature as follows /1/:

Ultimate strength (tensile, compressive, flexural):
The mechanical properties of graphite improve at elevated temperatures. The maximum values are reached between 2200°C and 2500°C depending on the graphite. At higher temperatures the ultimate strength decreases rapidly due to the increasing plasticity of the material.

Young's modulus:
The value of the Young's modulus at elevated temperatures is highly dependent on the material (degree of graphitization, anisotropy, porosity). In general the Young's modulus increases with temperature until reaching a turn around from which the modulus starts to decrease again. The temperature of this turn around and the gradient of the decrease in the Young's modulus vary over a wide range depending on the material.

Linear thermal expansion coefficient:
With rising temperature the coefficient of linear thermal expansion rises slightly.

Thermal conductivity:
For all graphites the thermal conductivity decreases with increasing temperature quite rapidly to roughly one third from room temperature to 2000°C.

Thus the only parameter left with some reliability for the estimation of the thermal shock properties of various graphites is the linear thermal expansion coefficient as here the temperature dependence is less pronounced. The comparison of the values of the linear thermal expansion coefficient of the graphites tested (Table 2) shows that graphites of high mechanical strength have coefficients larger than 6×10^{-6} whereas the other isotropic and slightly anisotropic graphites have coefficients below 4.6×10^{-6}. As graphites with high mechanical strength at room temperature showed rather unfavourable thermal shock behaviour, the value of the linear thermal expansion coefficient should be taken as a first indicator of the thermal shock properties under disruption conditions.

5.4 Erosion

Previous electron beam experiments on graphites /4,5/ show that under heat fluxes in the disruption regime atomic vaporization, hydrocarbon formation and particle emission contribute to the erosion on graphite surfaces. For vaporization processes analytical approaches exist /3/ which at least can give an approximation of quantities.

The contribution of particle emission processes to the weight loss is not yet quantitatively defined. The erosion of larger particles (about 50µm in diameter) seems to occur as a result of structural changes on the heated surface. Under the deposition of high heat fluxes binder bridges along grains seem to fail and net like void structures on the surface are formed. Thus particles may be emitted from the surface as their adhesion to the substrate is weakened.

All processes together (atomic vaporization, hydrocarbon formation and particle emission) amounted to weight losses in the order of 10mg per pulse.

6. Conclusions

Disruption simulation experiments on 11 different graphites have been undertaken using the 10MW NBI test stand of the IPP-Nagoya.

Power densities of 90 to 100 MW/m^2 were deposited at pulse lengths of 157ms to 353ms on large size samples (surface 50mm x 50mm). Graphites of high mechanical strength (AXF 5Q, ISO 880, T6-P, and MT 200 K) tended to show cracking under these heat fluxes as also EK 98 showed cracking on the heated surface. The other isotropic graphites (CL 5890 PT, ETP-10, and IG 110) did not crack as also the slightly anisotropic grades ATJ and CGW did not show cracking. One sample of the highly anisotropic grade YPD fractured under an energy deposition being about 50% above the value of average pulses.

A correlation of the experimental results to thermal shock resistance parameters could not be found. Only the values of the linear thermal expansion coefficient gave indication of the thermal shock behaviour as all grades with high linear thermal expansion showed unfavourable thermal shock behaviour.

Compared to the other grades YPD showed significantly less erosion due to it's high anisotropy. Besides atomic vaporization and the formation of hydrocarbon compounds the emission of graphite particles seems to contribute to erosion. Measured weight losses were in the order of ten mg per pulse.

References

/1/ W. Delle, K. Koizlik, H. Nickel, Graphitische Werkstoffe fuer den Einsatz in Kernreaktoren, part II, Thiemig, Muenchen (1983)

/2/ R. de Coninck, A. Gijs, M. Snijkers, Rev. int. hautes Temper. Refract., Fr., 16 (1979) 294

/3/ R. Behrisch, J. Nucl. Mater. 93 & 94 (1980) 498

/4/ J. Bohdansky, C. D. Croessmann, J. Linke, 14th SOFT, Avignon (1986)

/5/ C. D. Croessmann, Thesis, Univ. of Wisconsin (1986)

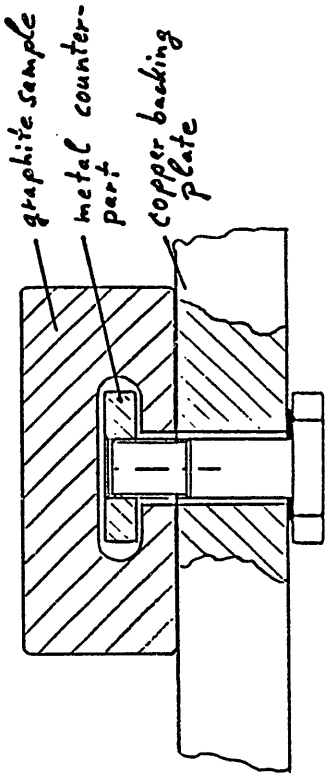

Figure 2: attachment of graphite test pieces to the sample holder (copper backing plate)

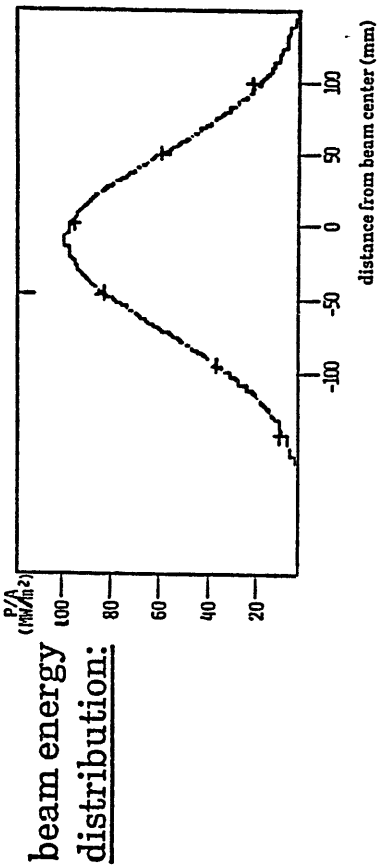

Figure 3: power density distribution profile of the H^+-beam

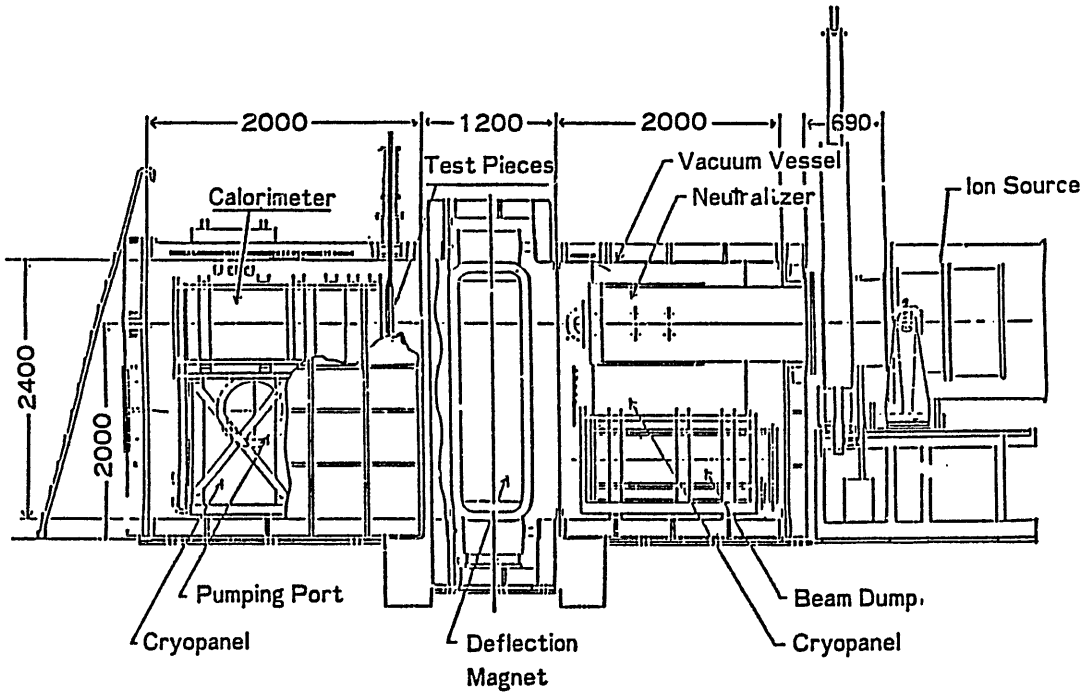

Figure 1: schematic of the test stand

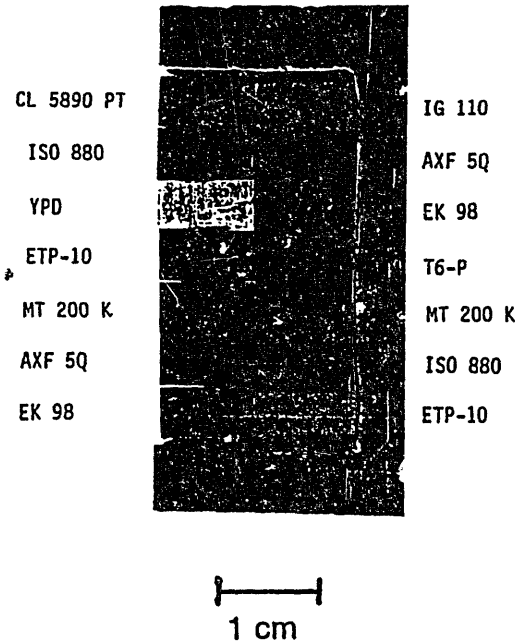

Figure 4: small graphite samples for screening purposes clamped together for beam exposure in the same experiment
experimental parameters: power density 90 to 100 MW/m^2
3 pulses at pulse lengths of 227 ms, 170 ms, 195 ms

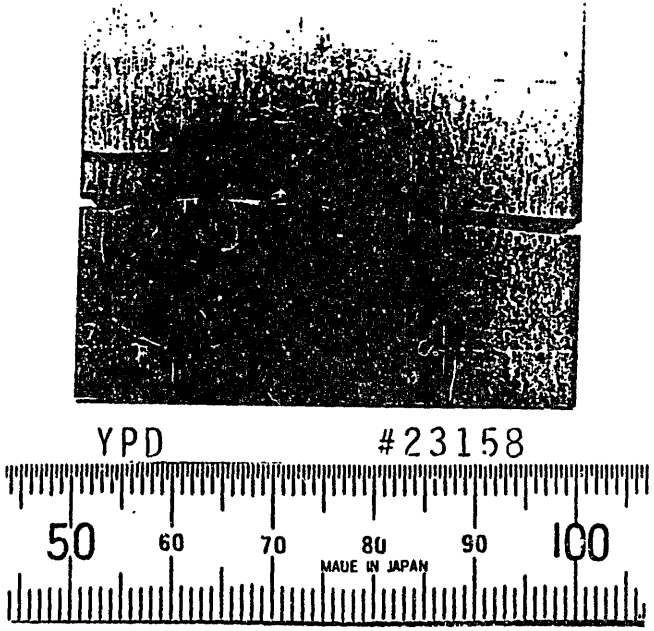

Figure 5: YPD graphite sample after experiment
experimental parameters: power density 90 to 100 MW/m^2
pulse length 308 ms

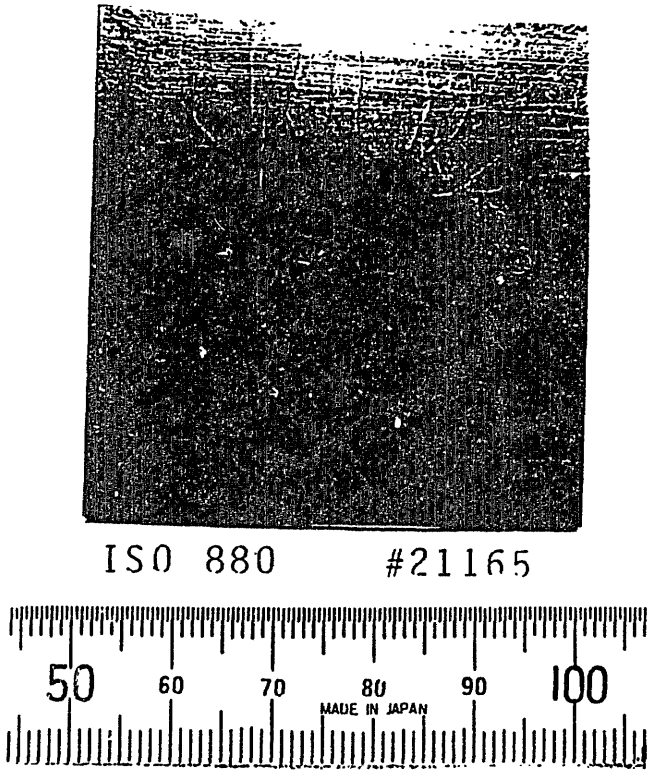

Figure 6: cracks on ISO 880
experimental parameters: power density 90 to 100MW/m^2
pulse length 214 ms

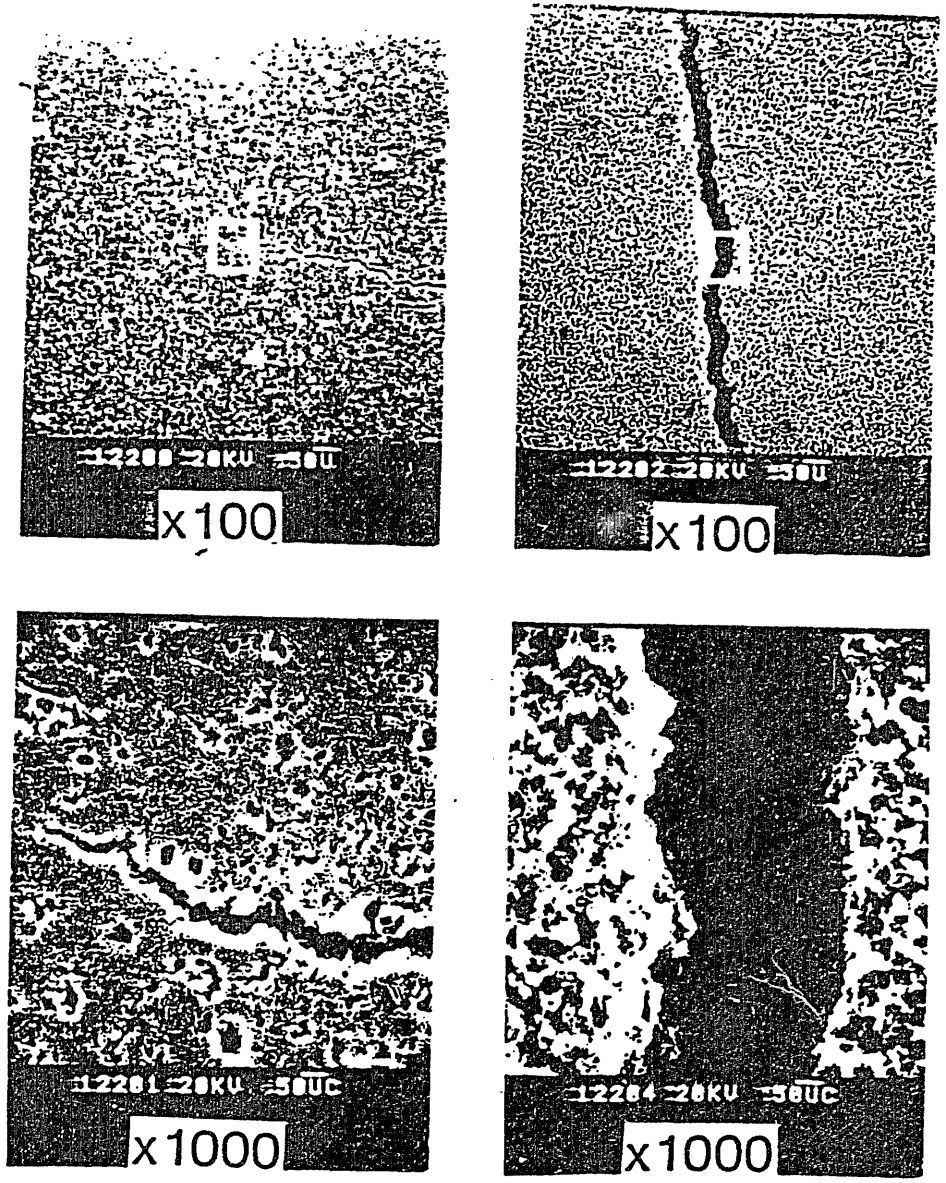

slightly eroded

heavily eroded

Figure 7: experimental parameters: power density 90 to 100MW/m^2
pulse length 233 ms

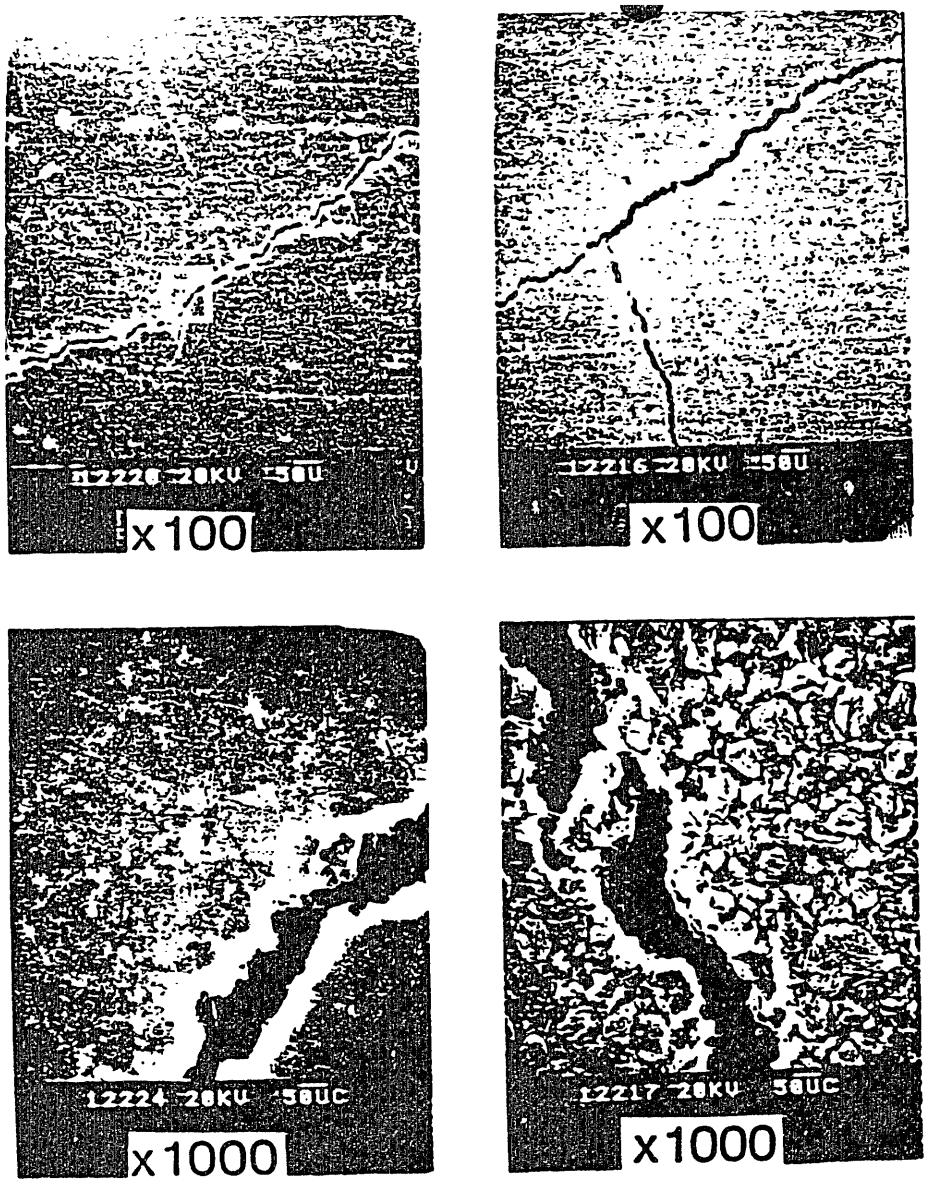

slightly eroded

heavily eroded

Figure 8: experimental parameters: power density 90 to 100MW/m^2
pulse length 214 ms

ISO 880 #21165

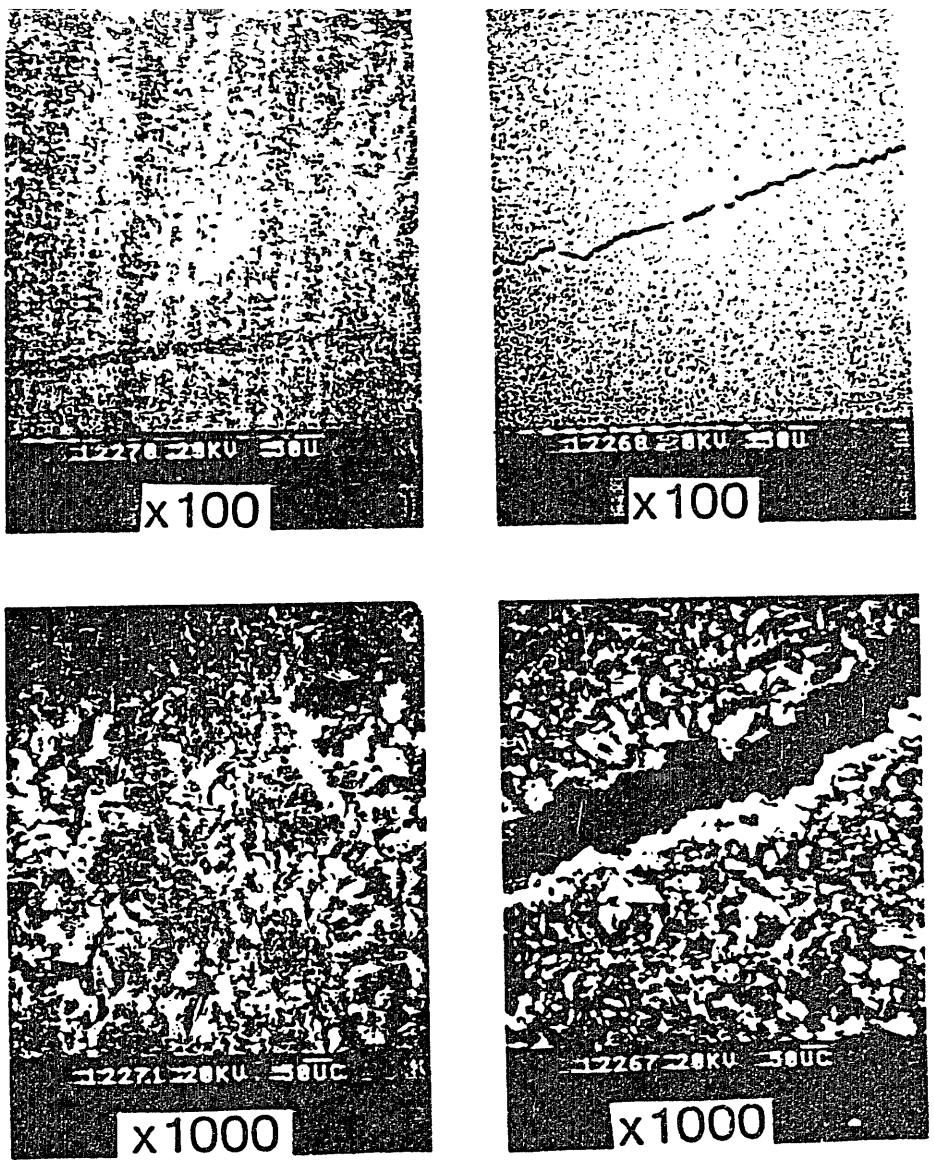

slightly eroded

heavily eroded

Figure 9: experimental parameters: power density 90 to 100MW/m^2
pulse length 164 ms

T6-P #24344

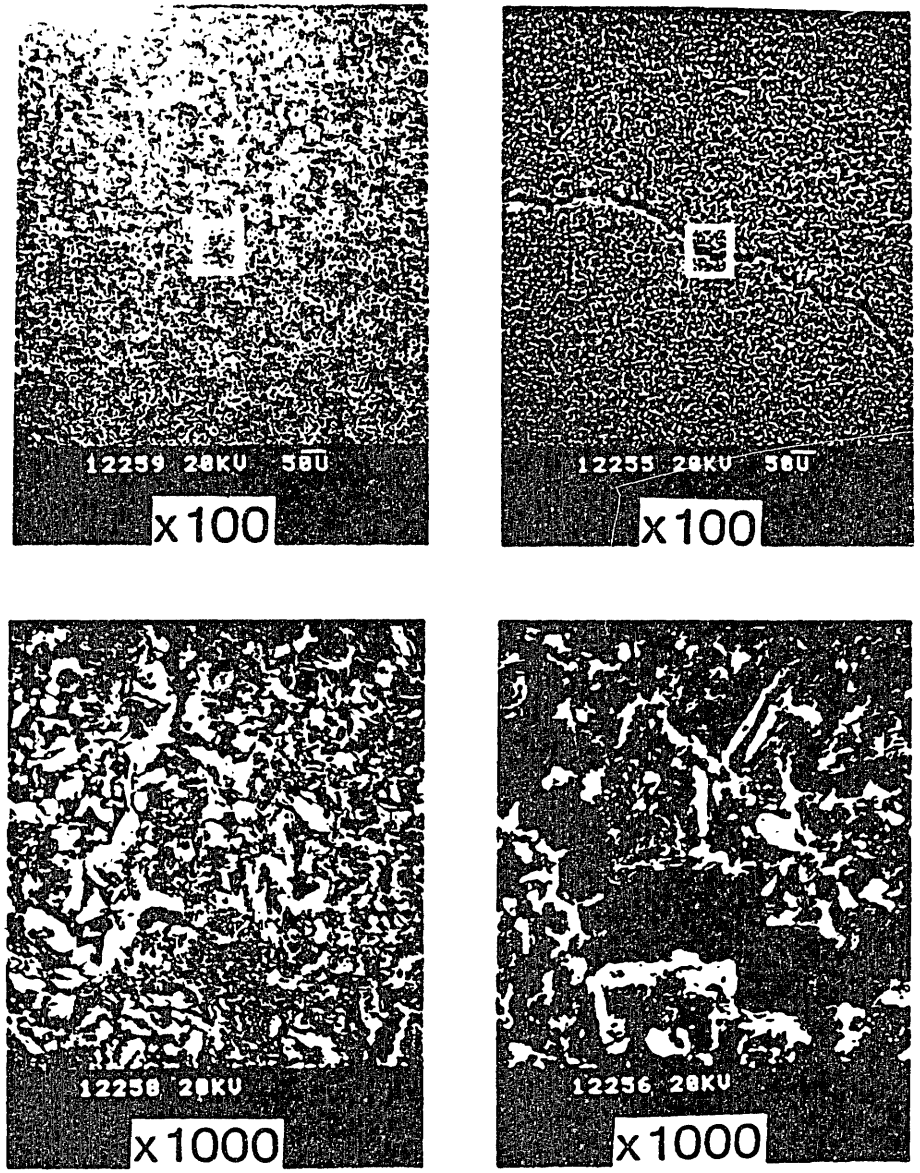

slightly eroded

heavily eroded

Figure 10: Toyo Carbon MT 200 K, (shot no. 23474)
experimental parameters: power density 90 to 100MW/m^2
pulse length 183 ms

MTK #23474

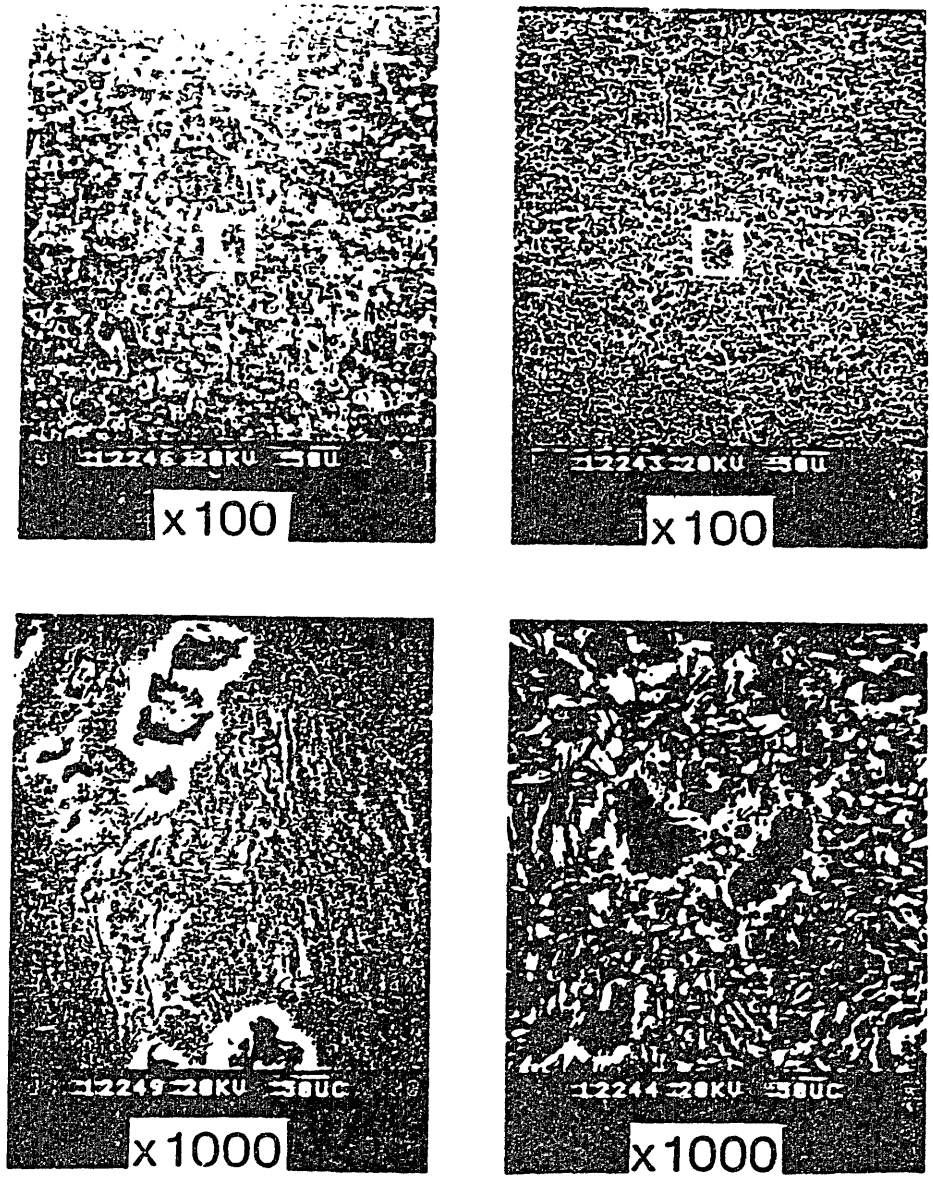

slightly eroded

heavily eroded

Figure 11: experimental parameters: power density 90 to 100MW/m^2
pulse length 220 ms

CL 5890 PT #21120

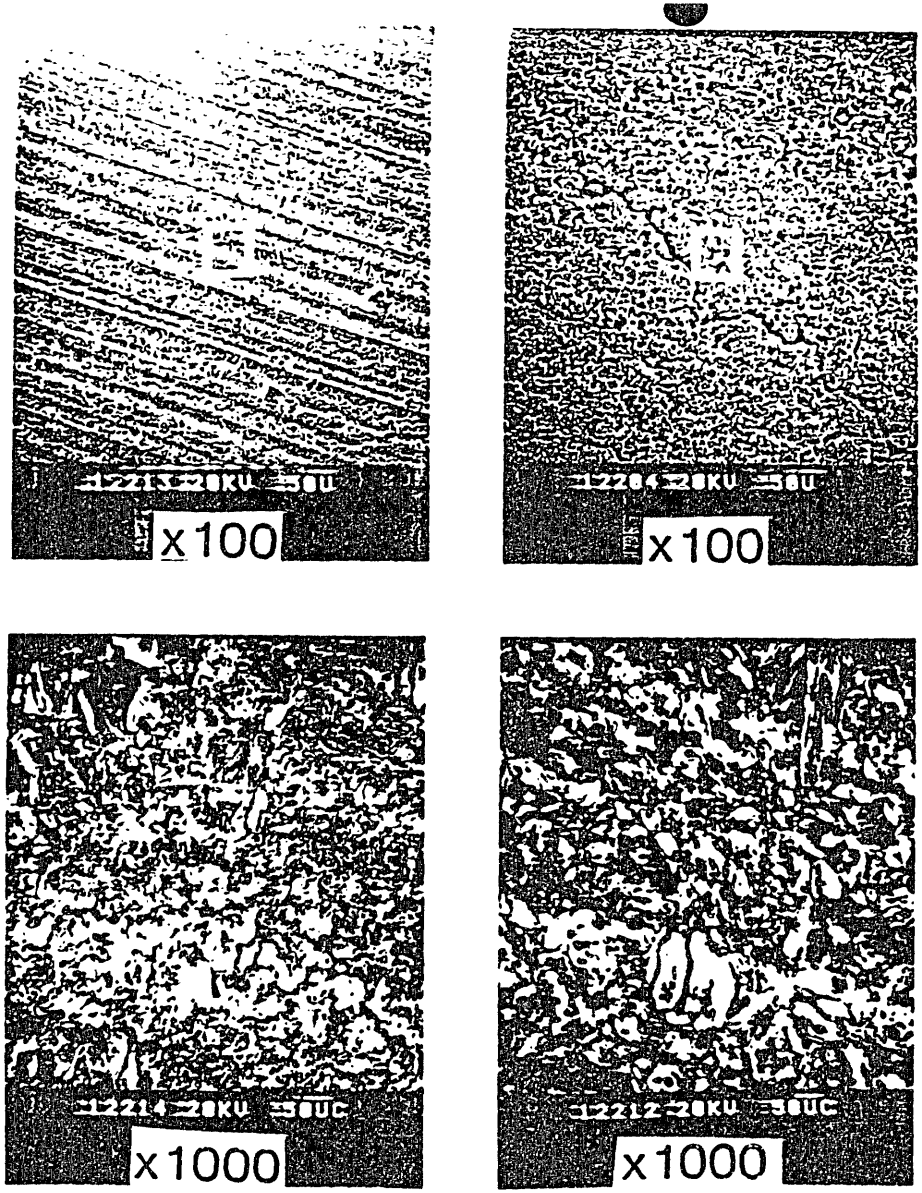

slightly eroded

heavily eroded

Figure 12: experimental parameters: power density 90 to 100MW/m^2
pulse length 176 ms

EK98 #23418

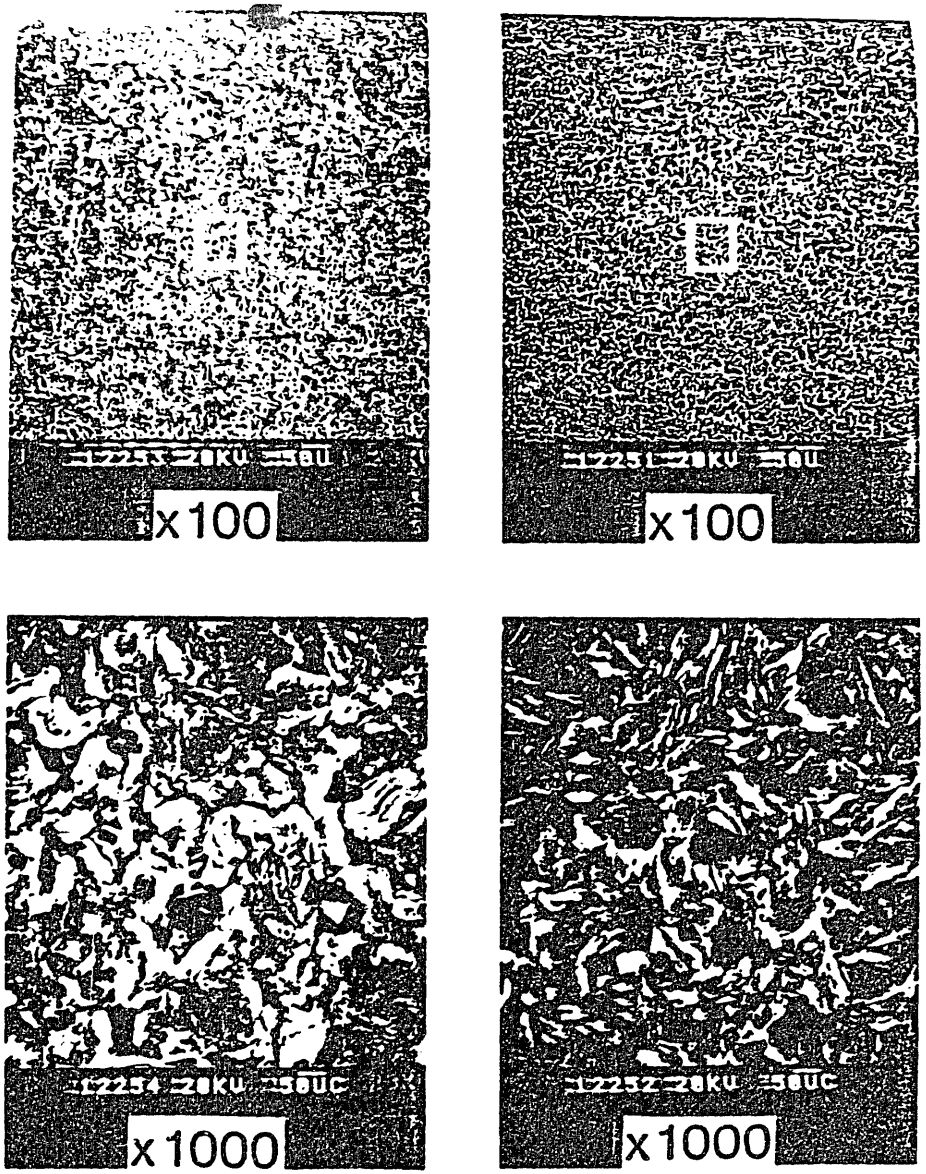

slightly eroded

heavily eroded

Figure 13: experimental parameters: power density 90 to 100MW/m^2
pulse length 195 ms

ETP-10 #23012

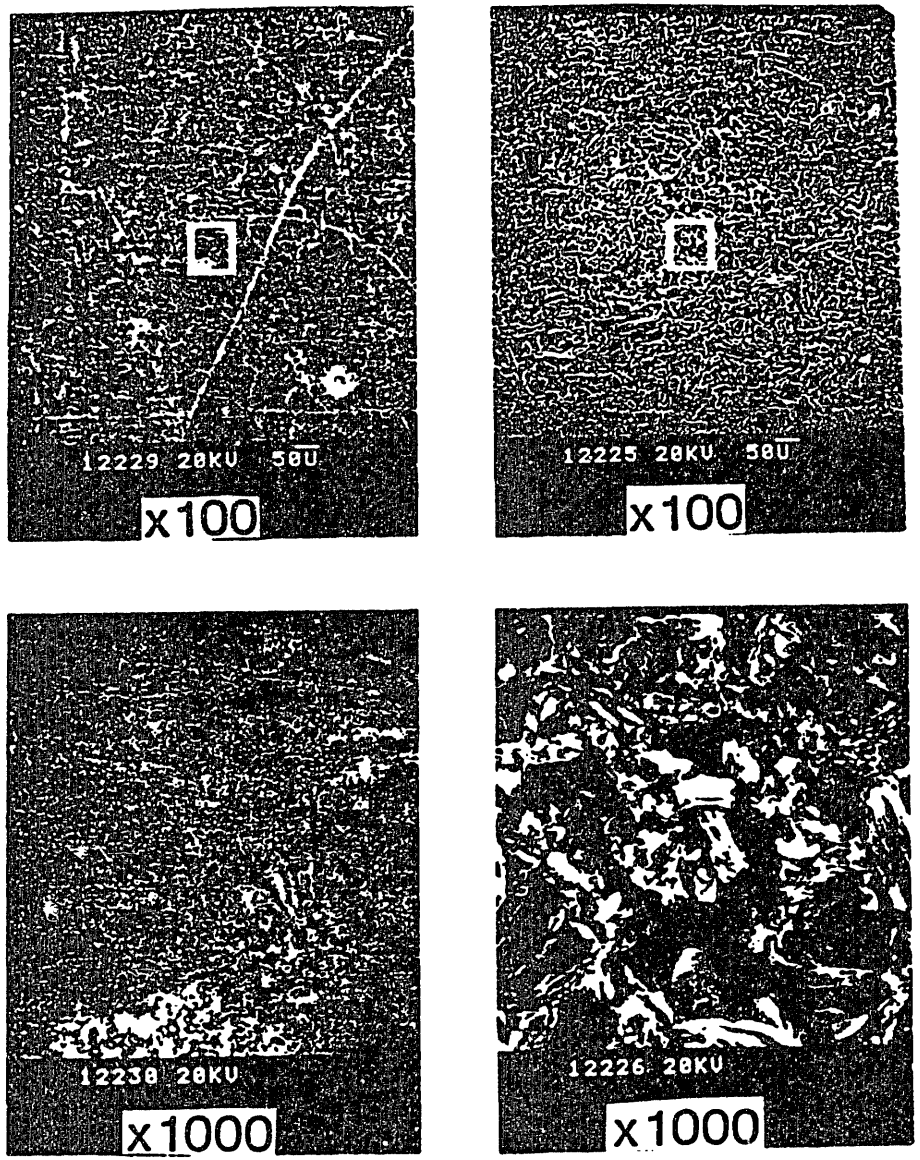

slightly eroded

heavily eroded

Figure 14: Toyo Tanso IG 110, (shot no. 22464)
experimental parameters: power density 90 to 100MW/m^2
pulse length 214 ms

IG110 #22464

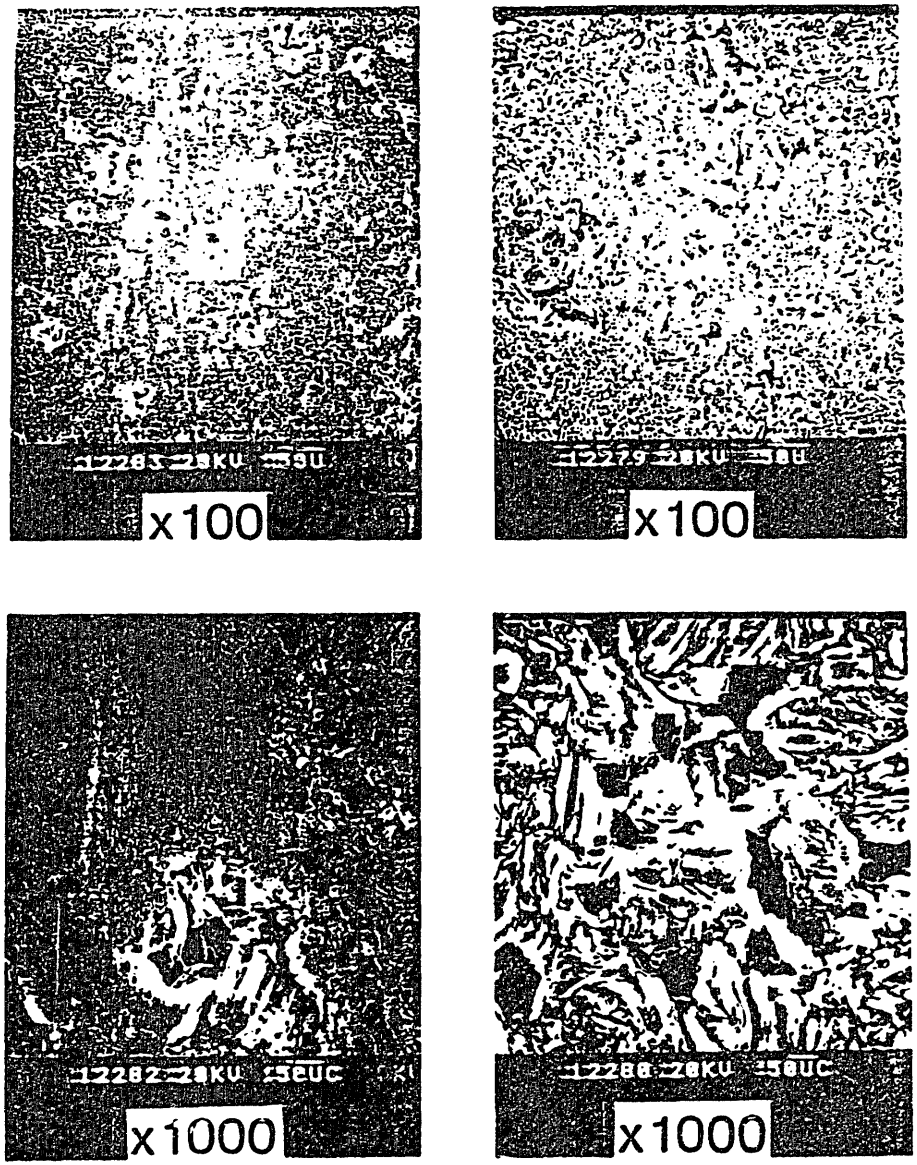

slightly eroded

heavily eroded

Figure 15: experimental parameters: power density 90 to 100MW/m^2
pulse length 220 ms

ATJ #23310

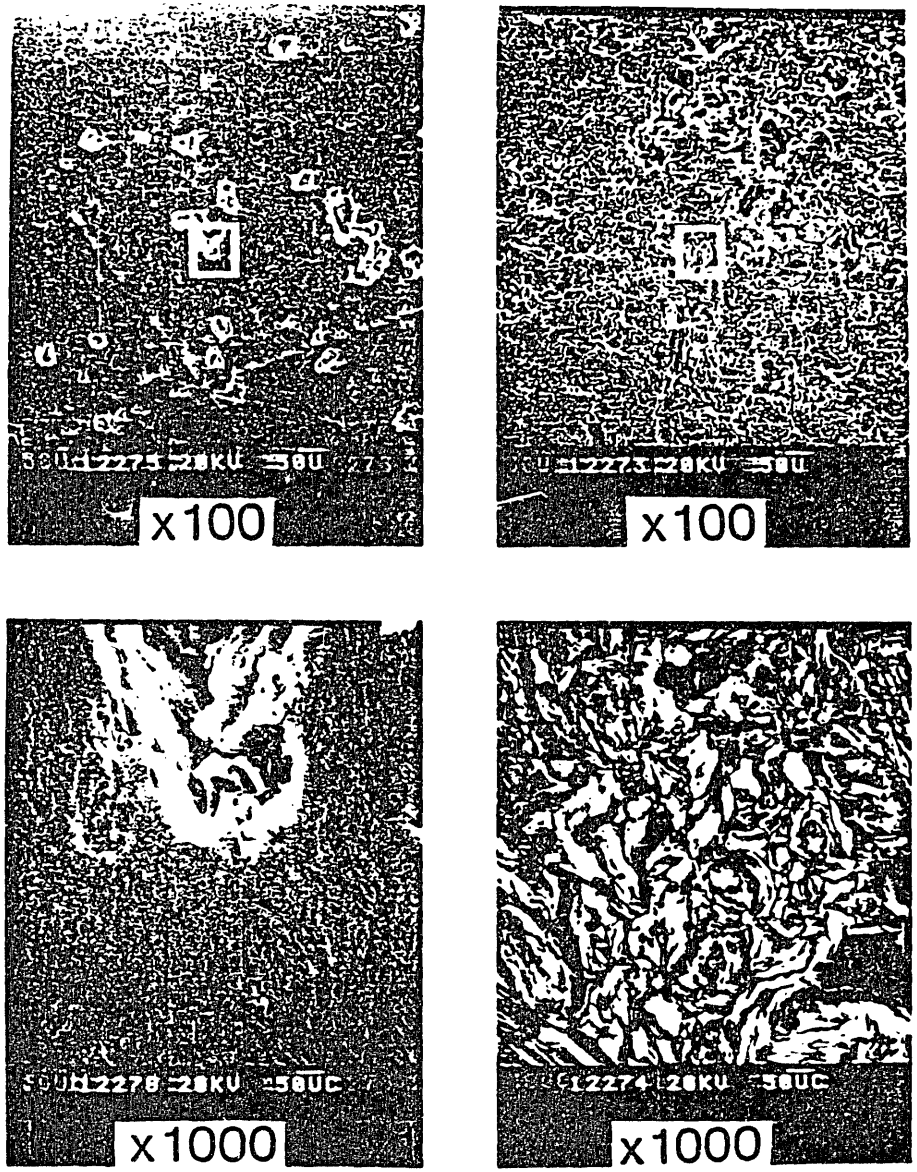

slightly eroded

heavily eroded

Figure 16: experimental parameters: power density 90 to 100MW/m^2
pulse length 227 ms

CGW #22449

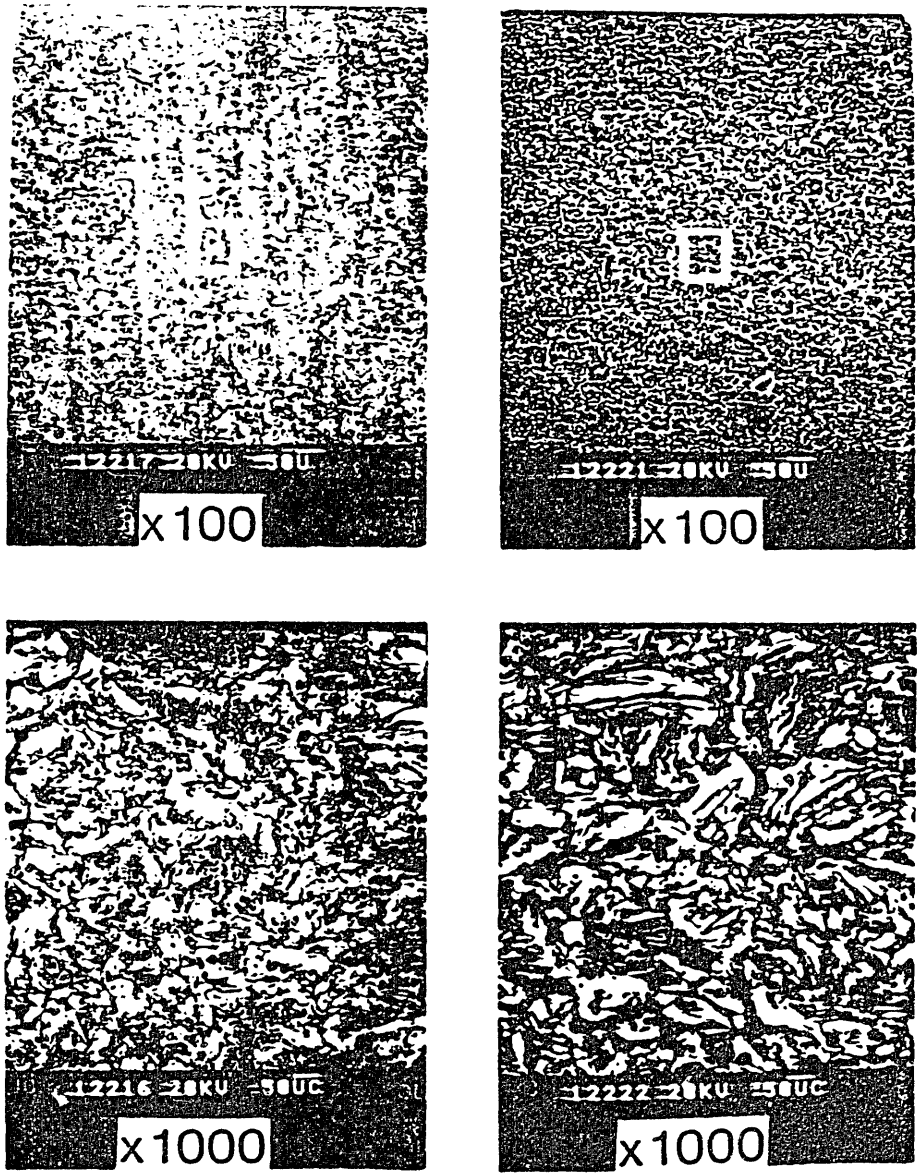

slightly eroded

heavily eroded

Figure 17: experimental parameters: power density 90 to 100MW/m^2
pulse length 309 ms

YPD #23158

Runaway-Electron Simulation by Electron Linear Accelerator Experiments

H. Bolt[1], A. Miyahara[2], M. Miyake[3], T. Yamamoto[4]

1. Inst. for Reactor Materials, Kernforschungsanlage Juelich GmbH, EURATOM-Assoziation, FRG
2. Inst. of Plasma Physics, Nagoya University
3. Dept. of Nuclear Engineering, Osaka University
4. Inst. of Scientific and Industrial Research, Osaka University

I. Introduction

Experimental studies of the interaction between high energy electrons and materials have been initiated. Objective of this study is to determine the development of damages in materials which were subjected to electron beam impact at energies of E=20...30MeV. Specific beam - material interaction effects caused by high energy electrons are volume distribution of the energy, photon production and neutron production. Background of this study is the experimental simulation of runaway-electron events which may occur during upset plasma conditions of tokamak fusion devices.

At low plasma densities, which are likely to be found in the tokamak plasma surface layer and during operational instabilities it is possible for a sheet of electrons to be accelerated to high energies at which their scattering cross section is significantly reduced which again results in further acceleration /1/. In present tokamaks the energy spectrum of highly accelerated (runaway-) electrons ranges from a few MeV in medium sized tokamaks up to about 20MeV in large size devices /1,2/. It is expected that the current driven plasmas of future devices will feature electron sheets of energies up to 100MeV due to the gradually higher RF-energy acceptance of electrons compared to protons and their isotopes.

If these electrons intersect with components of the first wall severe damages like melting, evaporation and cracking result due to electron stopping processes in the first wall materials. Depending on the physical properties of materials runaway-electrons can have large penetration depths into the first wall leading to volume energy deposition but possibly also to severe damages of the cooling tubes of actively cooled first wall modules as well as to attachment structures for plasma facing components.

II. Experimental Facility

Experiments are carried out using the electron linear accelerator of the Institute of Scientific and Industrial Research of Osaka University. Main features of this experimental device are relevant electron energies (E=20...35MeV) and high beam currents during operation. Experimental parameters are given in table 1.

Irradiation Experiments

place	: Radiation Lab., Inst. of Scientific and Industrial Research, Osaka University
apparatus	: Electron Linear Accelerator
beam energies and pulse currents	: E = 20 MeV, I_p = 300 mA
	E = 25 MeV, I_p = 280 mA
	E = 30 MeV, I_p = 240 mA
pulse width	: t_p = 1.5 µs
repetition rate	: f = 120 pps (pulses per sec.)
input power	: P = 1.30 kW
beam diameter	: d = 4 mm
irradiation times	: t_{irr} = 10...60 s

table 1: irradiation facility and runaway-electron simulation parameters

A vacuum chamber has been constructed to prevent beam spread under atmosphere and excessive oxidation of the specimen surfaces. The experimental set-up is shown in Fig. 1. Experiments were carried out under a vacuum of 10^{-1} Torr. The electron beam after being coupled out of the linac tube by a 20µm thick Ti-window is directly led into the target chamber through the same kind of 20µm Ti-window. The target chamber had to be separated from the linac tube guide to prevent contamination of the linac components.

After the decay of induced activity, post experimental examinations were carried out to determine damage caused by high energy electron impact. This included visual examination, metallography, optical light microscopy and SEM observations.

III. Experimental results

III.1 Bulk materials

Graphite, SiC + 2%AlN and stainless steel as reference material have been tested. Their relevant physical properties are listed in Table 2.

The experimental results depending on the experimental conditions are given in Table 3 in the form of damage thresholds.

The irradiation of graphite with 20 to 30MeV at times of up to 60s did not lead to any damages. SiC + 2%AlN showed the same behaviour under irradiation with identical parameters. Stainless steel reacts highly sensitive to shorter irradiation times of 10 to 30s at energies of 20 to 30MeV with grain growth and melts under irradiation with 20MeV for 60s. After solidification of the melt the solidified metal shows interdendritical cracks.

III.2 Experimental results on layer systems

The work focus on layer systems lies in compound systems of plasma facing low Z and low density materials (e.g. graphite) attached to high Z and high density materials (e.g. stainless steel or molybdenum) by brazing or hot isostatic pressing (HIP).

For screening purposes and simplified post-experimental examination initial experiments on layer systems have been carried out with graphite plates of two, five and ten millimeter thickness fixed mechanically with nuts and bolts to 10mm stainless steel and Mo-base plates. Beam incidence was normal to the graphite surface of the specimens.
The parameters and results of the experiments on model layer systems are given in Table 2.

Except for some discoloration at longer irradiation times (t_{irr}= 45s, 60s) the graphite layers did not show damage. A comparison of the results on layer systems with stainless steel substrates and the results on stainless steel bulk specimens does not show significant difference in the damage thresholds for the case of 2mm and 5mm thick graphite layers. Only a shielding of 10mm thick graphite reduces the damage on stainless steel substrates compared to unshielded bulk stainless steel.

The model layer systems of molybdenum covered by graphite suffered serious damage (Fig.2). The molybdenum substrates covered by 2mm resp. 5mm thick graphite were subjected to high temperature excursions. Molybdenum itself shows only (slight) grain growth, similar to the results on bulk molybdenum. The temperature of the substrate nevertheless exceeded the melting temperature of stainless steel thus causing melting of the attachment parts. As in the case of graphite/ stainless steel structures, only a graphite layer of 10mm thickness provides sufficient shielding of the molybdenum substrate to prevent observable damage.

For further determination of high energy electron impact effects on compound systems brazed layer systems have been tested. Figure 3 shows the results of experiments on systems of 5mm and 10mm thick graphite brazed to compound substrates composed of a 2mm Mo layer, a 2.5mm thick Cu layer, and a 2mm thick Mo layer. After irradiation of both samples with E=20MeV, t_{irr}=60s the sample with a 5mm thick graphite layer shows complete melting of the intermediate copper phase. In the location of the brazed zone between the 5mm graphite layer and Mo small droplets are found which may originate from the Cu-Ag-Ti braze used for bonding. The

specimen with a graphite layer thickness of 10mm does not show visible damages. Thus also in the case of brazed layer systems, like in the case of the before mentioned model layer systems, a thickness of 10mm graphite provides significant shielding compared to graphite layers of 5mm thickness.

In situ measurements of the temperature rise of the Cu-phase indicate even earlier failure of the brazed compound structures as after 25s irradiation time temperatures well above 800^0 are reached which result in melting of the braze and thus failure of the bonding.

IV. Discussion

The results obtained on graphite, SiC + 2%AlN and stainless steel are to be explained by the different ranges of high energy electrons in these materials along which they loose their energy in form of radiative and non-radiative collisions. For energies above 1MeV this range S in cm can be approximated as

$$S = 1/\rho \, (5.1 \cdot 10^{-7} E - 0.26) \qquad /3/$$

with density ρ in g/cm^3 and energy E in eV. Thus for an energy of 20 MeV the following ranges can be assumed:

graphite	S = 5.5 cm
SiC + 2%AlN	S = 3.1 cm
stainless steel	S = 1.2 cm

Along this range the energy absorption of materials is not homogeneous but the absorbed power characteristically reaches a maximum at about one third of the range which is then followed by a monotoneous drop to zero over the residual range /3/. Thus the experimental results may be explained by this volume distribution process of beam energy in materials: Obviously on graphite and SiC + 2%AlN no damages were observed because the long range of electrons in this material leads to the distribution of the beam energy in a rather large volume.

layer systems:

With respect to the long range of MeV-electrons in graphite most of the kinetic energy of the electrons is deposited in the metal substrate unless very thick graphite shielding is provided. Thus in the case of 2mm thick and 5mm thick graphite layers only a neglegible fraction of the beam energy is deposited in the graphite layer whereas a layer of 10mm graphite at least absorbs a part of the beam energy which is sufficient to provide some reduction of the thermal load imposed on the substrate material. Like the results on bulk materials stainless steel substrates are more sensitive to high energy electron impact than Mo-substrates. Additionally to this in compound systems special attention has to be paid to the brazed interface. Braze materials with a comparatively low melting point (e.g. Cu-base brazes) may be subjected to melting and structural changes.

V. Conclusions

Compared to stainless steel as reference material graphite and SiC + 2%AlN bulk materials show far higher resistivity against 20...30MeV electron impact.

Results on graphite - metal layer systems indicate the possibility of serious runaway-electron damage to the metal cooling tubes of actively cooled components. For first wall components being potentially exposed to runaway-electron impact

Mo-cooling tubes are preferable to stainless steel (and presumably also copper) cooling tubes due to the higher threshold for thermal damages of Mo. As brazing material a material with high melting point (e.g. Zr-braze) is preferable.

References

/1/ Lomer, W. M., J. Nucl. Mater., 133&134 (1985) 18

/2/ Nishikawa, M., et al., J. Nucl. Mater., 128&129 (1984) 493

/3/ Schiller, S., Heisig, U., Panzer, S., Electron Beam Technology, John Wiley and Sons, New York (1984)

/4/ Brinkschulte,H, private communication, 2nd workshop on graphite materials for fusion applications, KFA Juelich, March 1986

material	graphite	SiC+2%AlN	stainl. steel
supplier/ country	Ringsdorff FRG	Hitachi Japan	Nov nox FRG
trade name	EK 98	Hitaceram	SS 316, 1.4311
specimen geometry (mm)	15x15x30	10x10x25	dia.20x30 dia.20x10
density (g/cm^3)	1.8	3.2	8.0
average atomic no. (Z, Z_{eff})	6	10	25.7
melting point (^oC)		(2425)	1450
thermal conductivity (W/cmK) at RT	0.6	1.0	0.15
spec. heat (J/gK) at RT	0.75	0.75	0.5

Table 2: bulk materials used in electron linear accelerator experiments, specimen size and relevant physical properties

system	energy and irrad. time	observed damages
2mm graphite + 10mm st. steel	30MeV, 10s	twin formation on substrate
5mm graphite + 10mm st. steel	30MeV, 10s	initial twin formation on substrate
10mm graphite+ 10mm st. steel	30MeV, 10s	---
5mm graphite + 10mm st. steel	20MeV, 60s	initial melting of st. steel substrate
10mm graphite+ 10mm st. steel	20MeV, 60s	grain growth on substrate
2mm graphite + 10mm Mo (TZM)	20MeV, 45s	melting of stainless steel attachment bolts, grain growth on substr. (fig. 2)
5mm graphite + 10mm Mo (TZM)	20MeV, 45s	initial melting of attachment bolts, slight grain growth on substrate (fig.2)
10mm graphite+ 10mm Mo (TZM)	20MeV, 45s	--- (fig.2)

table 3: results of linear accelerator experiments on layer systems

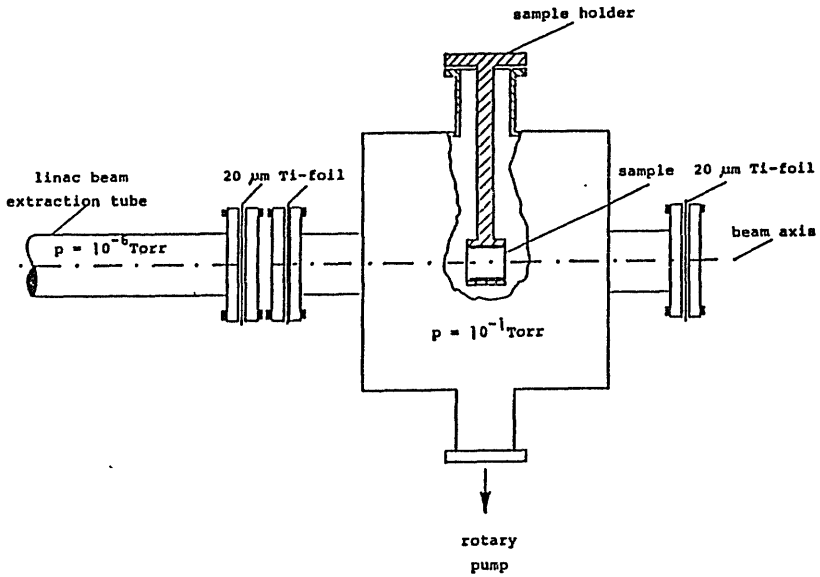

Fig. 1: Set-up for linear accelerator experiments. The electron beam is coupled into the target chamber via 20µm thick Ti-foils. Beam incidence onto the specimen surface is perpendicular.

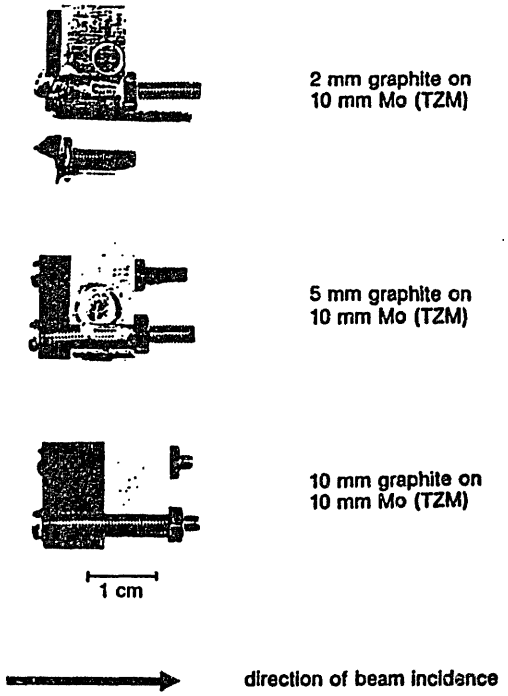

Fig. 2: Model layer systems after electron irradiation with E=20MeV, t_{irr}=45s. Graphite layers (left) have been attached to Mo-substrates (right) by stainless steel nuts and bolts. Thermal excursions of the substrates inthe case of thin graphite layers caused melting of the attachment parts.

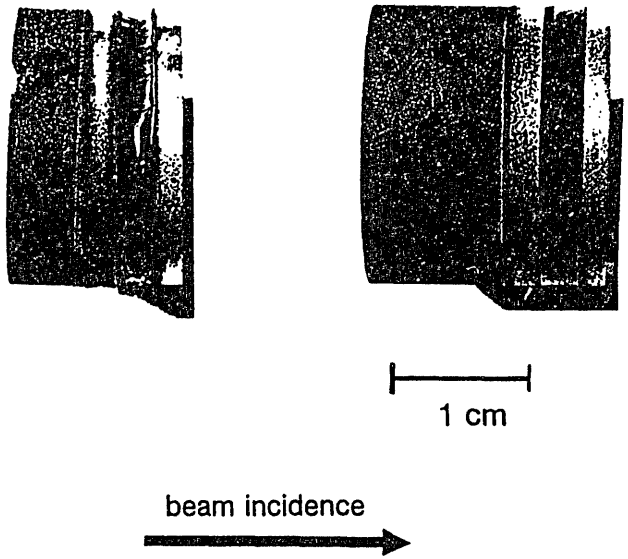

Fig. 3: Brazed layer systems of graphite brazed to Mo-Co-Mo substrate after electron irradiation with E=20MeV, t_{irr}=60s. The specimen with a graphite layer of 5mm thickness (left) underwent melting of the Cu-phase and degradation of the braze zone between graphite and Mo. The specimen with a 10mm thick graphite layer (right) shows no damages.

THERMAL SHOCK AND FRACTURE TOUGHNESS CONSIDERATIONS FOR GRAPHITE IN TOKAMAK REACTORS

Presented by R.T. McGrath
Division 6248

PI-- J.J. Stephens
Division 1832

Sandia National Laboratories
Albuquerque, New Mexico 87185

OUTLINE

- Survey of thermal shock parameter for existing graphites
  - Both major directions
- Fracture Toughness Testing of Graphites
  - Previous data base - 3 point bend or compact tension specimens (pre-cracking is required)
  - Present study - use short bar specimen (no pre-cracking needed)
- Problem: Graphites which rank highest in thermal shock parameter do not rank highest in fracture toughness
- Possible new directions

"Thermal Shock and Fracture Toughness Considerations for Graphite in Tokamak Fusion Reactors"

for

"Materials Data Needs for the Next Step and Steady State Devices", Nagoya, Japan.

Suggested order of View Graphs

1. Title
2. Outline
3. Thermal Shock Parameter
4. Room Temperature Properties of Graphites
5. Thermal Shock Parameter, WG
6. Thermal Shock Parameter, AG
7. Fracture Toughness Testing
8. Elevated Temperature Fracture Toughness Testing of Graphite
9. Previous Data on Fracture Toughness Testing of Graphite
10. Short Bar/Rod Fracture Toughness Test Simplifies Testing of Brittle Materials
11. Six different orientations can be easily tested
12. Short Bar Test Permits Large Numbers of Samples
13. Relative Ranking of Available Graphites
14. Possible New Experimental Directions

2. Focus of talk: to show that the exact mechanical selection criteria for selection of a particular graphite is not clear. [We at Sandia have selected AXF5Q Poco because of high thermal expansion (brazing consideration), isotropic properties - but it ranks low in thermal shock parameter.] Work in progress here has focused on measuring static (as opposed to impact) fracture toughness of graphites of interest for Tokamaks. Preliminary results show that ranking of graphites according to best thermal shock parameter does not correlate with ranking according to fracture toughness.

3. Over the years, engineers have attempted to rank various material groups' resistance to thermal shock and fracture by the [illegible]

It should be noted that some workers use a slightly different thermal shock parameter, M:

$M = M'(1-\nu) = S_{UTS}\, k\, (1-\nu)/(\alpha E)$ where ν is Poisson's Ratio

There is no question that a specific thermal shock test for a specific application is preferred to the use of M', but "you have got to start somewhere"

4. Room Temperature data which was used to obtain M' at room temperature. A majority of the data was taken from graphs from a previous Fusion workshop: Materials Handbook For Fusion Energy Systems (MHFES) (copy of plots and summary page enclosed). The PT5890 graphite is the exception here. We would like to ask the Japanese if temperature dependent k, E, S_{UTS}, and α data are available for Toyo Tanso grades ISO-880U and ISO-630U.

5. Thermal Shock Parameter, With Grain Orientation:

1. Graphnol looks best, at least at room temperature.
2. Surprisingly, ATJ-S is found to be better than ATJ at RT
3. AXF-5Q are very similar in M' as F(Temp) - later we will see that AXF-5Q is clearly better from a fracture toughness standpoint.

6. Thermal Shock Parameter, Across Grain Orientation:
1. Pretty much same ranking as WG, except: ATJ is much poorer near room temperature.

7. Fracture Toughness Testing: Determination of plane strain fracture toughness gives designers an aid in control of flaw sizes and experimental loads in order to avoid catastrophic fracture. This view graph summarizes ASTM standard methods for measuring fracture toughness assuming linear elastic fracture mechanics applies:
1. pre-crack specimen (easy to do for metal, hard to do for graphite)
2. measuring crack opening displacement and load, load to fracture. Obtain K_c from peak load, and from appropriate equation given particular sample geometry.
3. determine if plane strain conditions are applying, in order to see if test is valid K_{Ic} experiment.

8. Fracture toughness testing at elevated temperatures is a very non-trivial adventure - only one study completed.

9. Summary of previous fracture toughness data on graphites - (there may be some ORNL data that is fairly recent that I don't have my hands on) AFXQ1 is apparently an earlier version of isotropic graphite made by Union Oil (Poco Graphite). Guess/Hoover work was performed at SNLA.

10. *CURRENT WORK* : use of short bar specimen (short rod is shown in figure) to measure fracture toughness of graphites.
1. Sample is relatively easy to prepare
2. No need to precrack
3. Planar cracks are virtually always achieved. This is often difficult for some other types of frature toughness specimen designs when testing brittle materials.

11. Isotropy of fracture toughness can be tested - by looking at all of the possible crack orientations in a slab of graphite. Results of our tests show isotropy in fracture toughness for both Poco AXF5Q and PT5890. Bar to bar variation (leading to bimodal stats.) is evident in PT5890 and not in AXF5Q.

12. Histograms of results: total population for each graphite = 24=2bars x 6 orientations x 2 specimens(duplicate runs). As above, the two bars of PT5890 were not uniform, and larger populations would probably show bimodal stats.

13. Relative ranking of the available graphites: arranged in order of best from worst in terms of thermal shock parameter. Note also that a very different ranking would be found if one were to rank according to fracture toughness.

14. Possible new directions: • are there standardized tests for thermal shock that Tokamak people can agree to? This would be more desireable than calculated M'. • it would be useful to do fracture toughness testing of graphites that have been exposed to actual Tokamak conditions. (Would want to have unexposed material as a control. Conversely, we have additional pieces if people were interested in exposing our samples in say, sandwich limiters!)

THERMAL SHOCK PARAMETER

- A phenomenological parameter which is used to rank varying aerospace materials' tendency for fracture due to rapid thermal transients.

- We will use the following definition:

$$M' = S_{UTS}\, k / (\alpha E) \qquad \text{(Watts/Meter)}$$

S_{UTS} = Tensile Strength (MPa)
k = Thermal Conductivity (Watts/meter/°C)
α = Thermal Expansion Coefficient (/°C)
E = Young's Modulus (measured in tension, first loading) (MPa)

- All four quantities vary as a function of temperature, thus M' also shows strong temperature dependence.

- Effect of anisotropy: WG gives higher M', hence posesses better thermal shock resistance than AG

ROOM TEMPERATURE PROPERTIES OF GRAPHITES

TYPE & PRODUCER	DENSITY (gm/cc)	THERMAL CONDUCTIVITY (watt/m/°C)	YOUNG'S MODULUS (10^4 MPa)	TENSILE STRENGTH (MPA)	THERMAL EXPANSION (10^{-6}/°C)	THERMAL SHOCK PARAM. (10^4 watts/m)	FRACTURE TOUGHNESS (MPa(m)$^{1/2}$)
AXF-5Q "POCO" UNION OIL	1.88	100.	1.10	64.6	7.4	7.9	1.67
ATJ UNION CARBIDE	1.76	125.(WG) 100.(AG)	0.84(WG) 0.85(AG)	29.9(WG) 27.2(AG)	2.3(WG) 3.4(AG)	17.7(WG) 9.4(AG)	
ATJ-S UNION CARBIDE	1.83	130.(WG) 103.(AG)	1.14(WG) 0.85(AG)	36.5(WG) 30.0(AG)	3.2(WG) 4.2(AG)	13.0(WG) 8.8(AG)	0.93(WG) 0.89(AG)
GRAPHNOL N3M GREAT LAKES CARBON	1.85	185.(WG)	0.80(WG) 0.74(AG)	42.2(WG) 38.5(AG)	5.3(WG) 5.8(AG)	18.6(WG) 16.8(AG)	1.44(AG)
PT5890 CARBON-LORRAINE	1.81	88.1(WG) 72.4(AG)	1.17(WG) 0.99(AG)	42.8(WG) 41.5(AG)	3.8(WG) 3.75(AG)	8.5(WG) 8.1(AG)	1.23

J.J. Stephens, SNLA Div. 1832

THERMAL SHOCK PARAMETER, ACROSS GRAIN

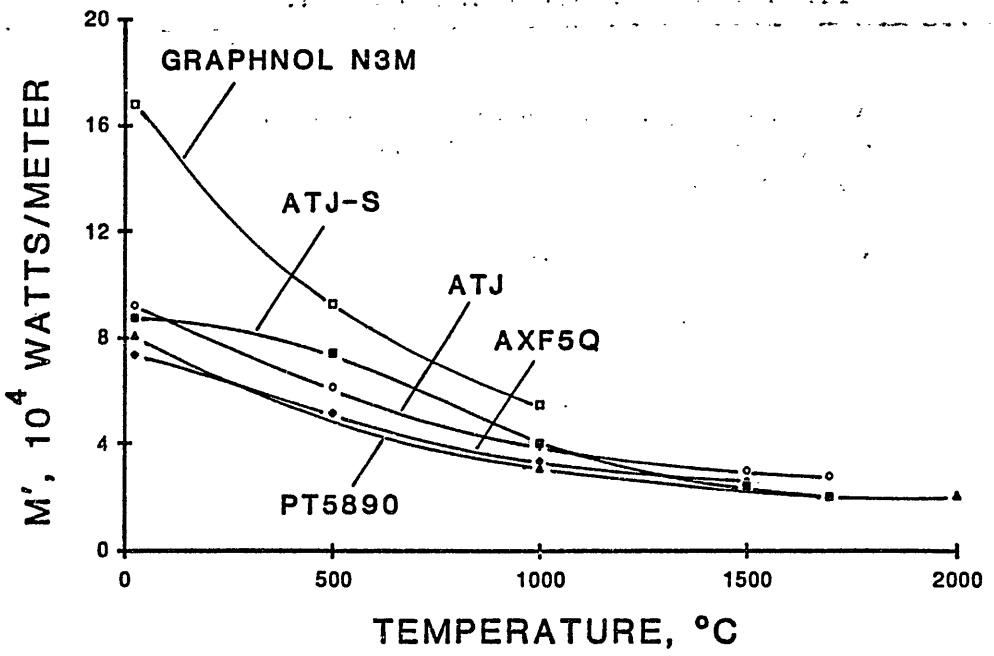

J.J. Stephens, SNLA Div. 1832

THERMAL SHOCK PARAMETER, WITH GRAIN

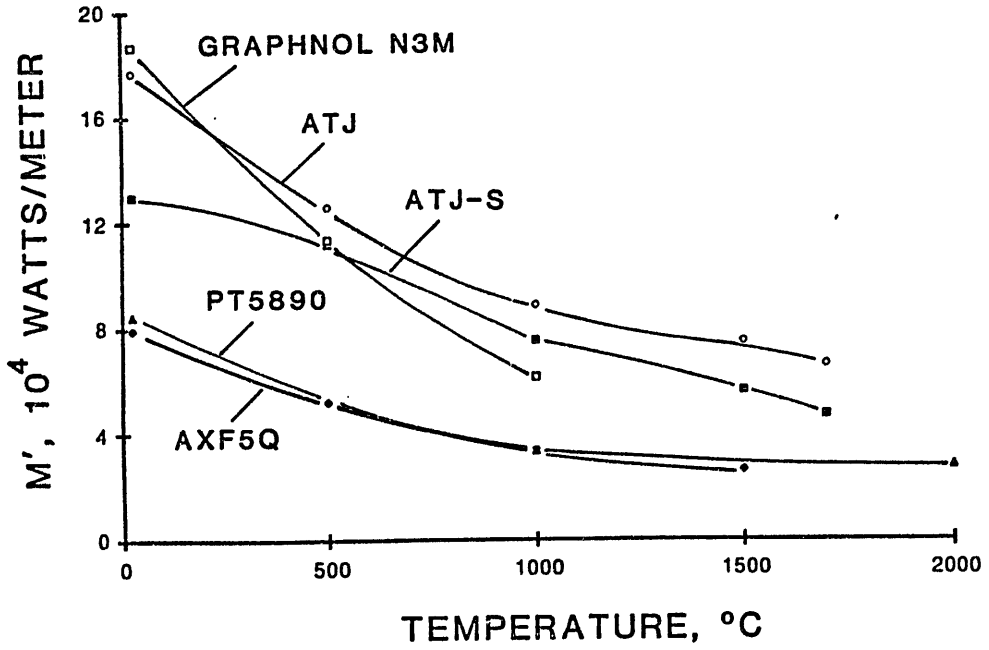

J.J. Stephens, SNLA Div. 1832

ELEVATED TEMPERATURE FRACTURE TOUGHNESS TESTING OF GRAPHITE

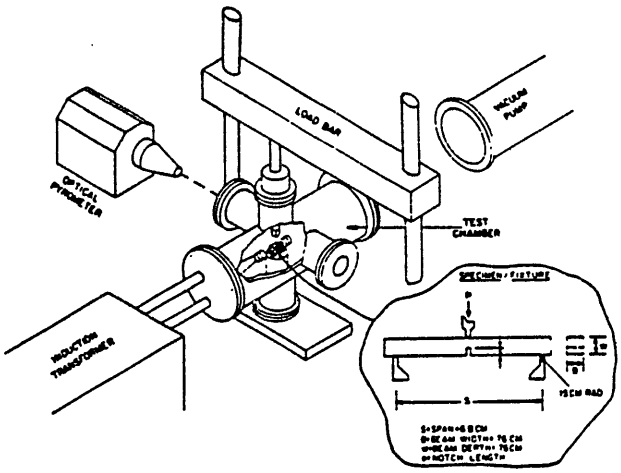

FIG. 1—*Schematic illustrations of test apparatus and specimen/fixture design for determining fracture toughness of graphitic materials at elevated temperatures.*

REF: L.R. Hettche and T.R. Tucker, ASTM STP 601, 1976.

FRACTURE TOUGHNESS TESTING

- **Fracture toughness provides a measure of the load a structure can withstand without catastrophic failure due to fracture**
  - **The plane strain fracture toughness, K_{Ic}, is related to the critical energy release rate, G_{Ic}, for crack extension:**

$$(K_{Ic})^2 = G_{Ic}\,(1-\nu^2)\,E$$

where ν is poisson's ratio and E is the elastic modulus.

- **ASTM E399 is the standard for fracture mechanics testing, using either compact tension or bend test specimens. These tests require a precracked specimen.**

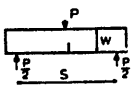

Thickness B

$$K_I = \frac{PS}{BW^{3/2}}\left[2.9\left(\frac{a}{W}\right)^{1/2} - 4.6\left(\frac{a}{W}\right)^{3/2} + 21.8\left(\frac{a}{W}\right)^{5/2} - 37.6\left(\frac{a}{W}\right)^{7/2} + 38.7\left(\frac{a}{W}\right)^{9/2}\right]$$

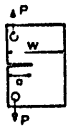

Thickness B

$$K_I = \frac{P}{BW^{1/2}}\left[29.6\left(\frac{a}{W}\right)^{1/2} - 185.5\left(\frac{a}{W}\right)^{3/2} + 655.7\left(\frac{a}{W}\right)^{5/2} - 1017\left(\frac{a}{W}\right)^{7/2} + 638.9\left(\frac{a}{W}\right)^{9/2}\right]$$

PREVIOUS DATA ON FRACTURE TOUGHNESS OF GRAPHITE

Material	Method	Temp (°C)	Fracture Toughness ($MPa(m)^{1/2}$)
Graphnol N3M	Compact Tension	25.	1.44
Ref: B. Johnson, Southern Research Institute, Personal Communication, Sept. 30, 1985.			
ATJ-S(AG)	3 Point Bend	25.	0.83
Ref: T.R. Guess, W.R. Hoover, J. Composite Materials, vol 7, p. 2 (1973).			
ATJ-S(AG)	3 Point Bend	25.	0.89
		1000.	1.06
		1500.	1.07
ATJ-S(WG)		25.	0.93
		1000.	1.15
		1500.	1.18
Ref: L.R. Hetchie, T.R. Tucker, ASTM STP 601, 1976.			
AFXQ1	4 Point Bend	25.	1.25
Ref: R. Stevens, Carbon 1971, vol. 9, 573, (1971).			

- Other data in the literature are for nuclear grades of graphite, most of which are no longer available. (eg: AGOT, SGBF, pile grade "A", Airco-Speer RC4, PGX grades)

SHORT BAR/ROD FRACTURE TOUGHNESS TEST SIMPLIFIES TESTING OF BRITTLE MATERIALS

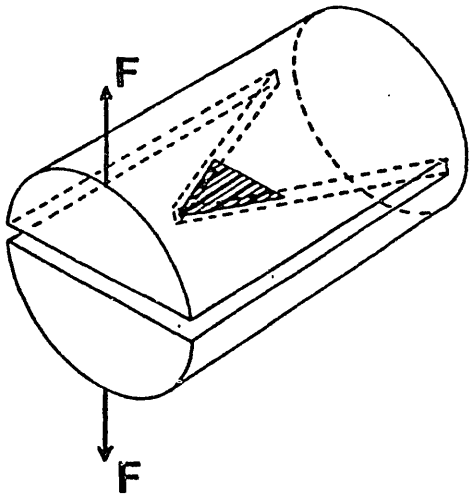

Short rod specimen. The shaded area denotes the crack. F denotes the opening load applied at the mouth of the specimen.

- Thin slots are machined longitudinally in the specimen - leaves a "V" shaped ligament in crack plane
- As load is applied to the specimen, a crack is initated at the "V" and requires increasing load to produce crack growth
  - The increasing load required for crack growth produces a stable, planar crack
- Thus, fracture toughness (termed K_{IcSR}) can be measured easily and without precracking the specimen

POSSIBLE NEW EXPERIMENTAL DIRECTIONS

- Development of standardized thermal shock testing appropriate for Tokamak environment?
- Fracture toughness testing after exposure to actual service conditions?

RELATIVE RANKING OF AVAILABLE GRAPHITES

TYPE	THERMAL SHOCK PARAMETER (10^4 WATTS/m)	FRACTURE TOUGHNESS (MPa(m)$^{1/2}$)
Grahpnol N3M	18.6 (WG) 16.8 (AG)	1.44 (AG)
ATJ-S	13.0 (WG) 8.8 (AG)	0.93 (WG) 0.89 (AG)
PT5890	8.5 (WG) 8.1 (AG)	1.23*
AXF5Q Poco	7.9	1.67*

* average of 6 different orientations x 2 blocks (duplicate specimen for each condition).

High Flux Plasma Bombardment of Graphite

Yoshihiko Hirooka

U C L A

Abstract

Resent experimental results of high flux ($\sim 10^{18}$ ions/sec/cm^2) hydrogen plasma bombardment experiments in PISCES, Particulary on graphite, are reviewed. Under a typical redeposition conditions, the erosion yield is reduced by a factor of 2 $\sim$ 3. Various graphite materials including ATJ, POCO, Pyro-graphite and 3D C-C weave are compared with respect to the erosion yield. The C-C weave is found to be the best material so far.

Also the first experimental result of controlled graphite pumping experiments is presented. High fluence helium plasma (10^{21-22} ions/cm^2) activates the graphite surface for pumping neutrals. The activated graphite surface showed retarded hydrogen reemission characteristic which might be one of the key factor for TFTR's supershot.

TABLE OF CONTENTS

PISCES PLASMA AND TOKAMAK EDGE-PLASMA CHARACTERISTICS

	PISCES	TYPICAL TOKAMAKS
DENSITY($1/cm^3$)	10^{11} - 10^{13}	$2X10^{12}$ - $5X10^{13}$
ION FLUX($1/cm^2$ sec)	10^{17} - 10^{19}	10^{17} - 10^{19}
ELECTRON TEMP.(EV)	3 - 30	10 - 100
SHEATH POTENTIAL(-V)	10 - 500 (Negative bias)	5 - 250
PRE-SHEATH(-V)	5 - 50 (-1.5 kT_e/e)	5 - 50 (-0.5 kT_e/e)
HEAT FLUX(W/cm^2)	5 - 500	200 - 500 (Limiter)
OPERATION	CONTINUOUS (UPTO HOURS)	PULSE (UPTO 10 SEC)

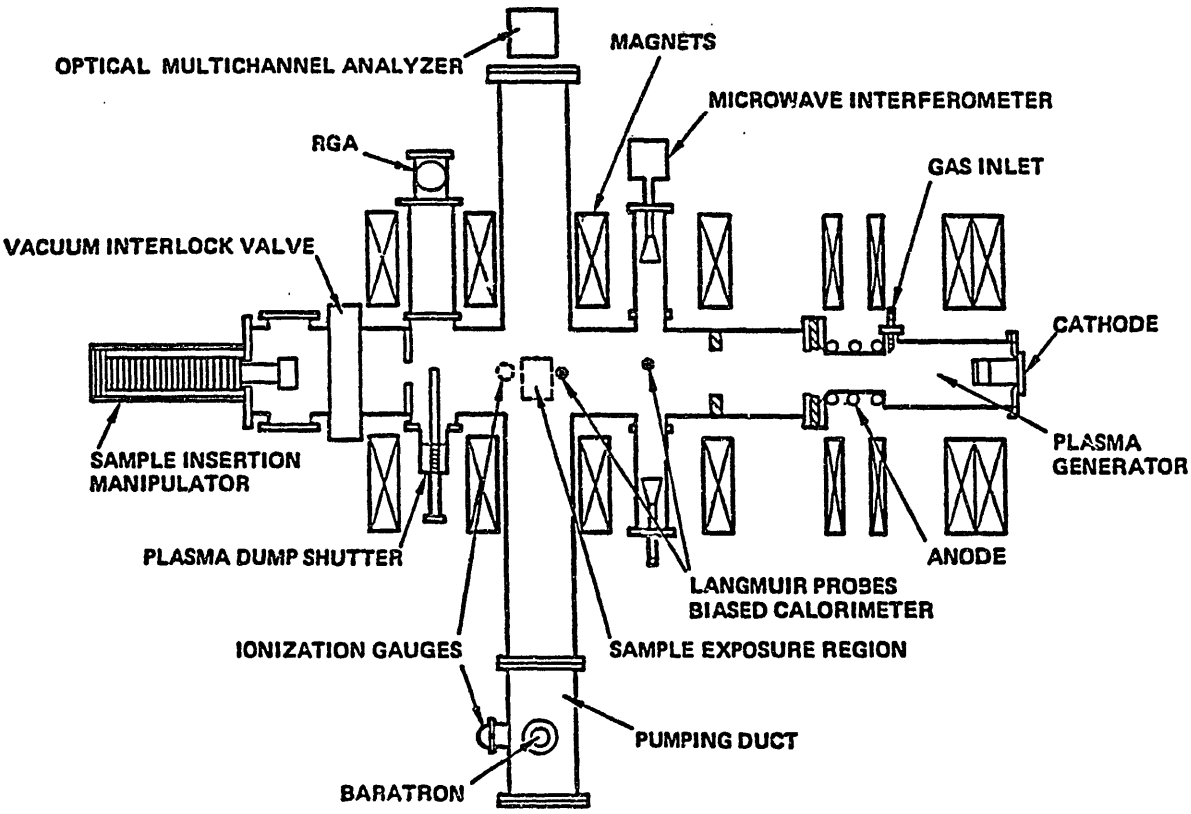

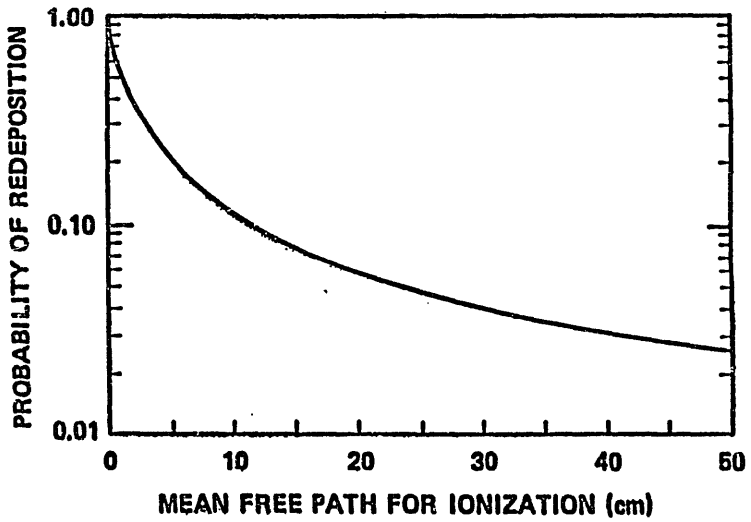

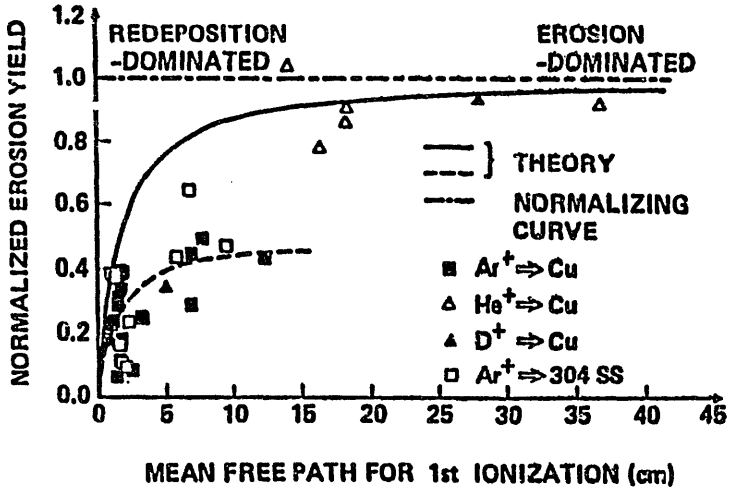

ELECTRON TEMPERATURE EFFECT ON MFP

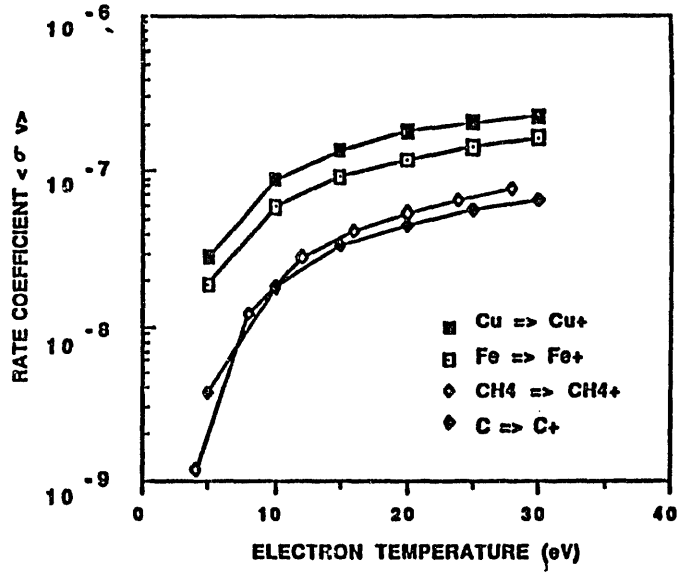

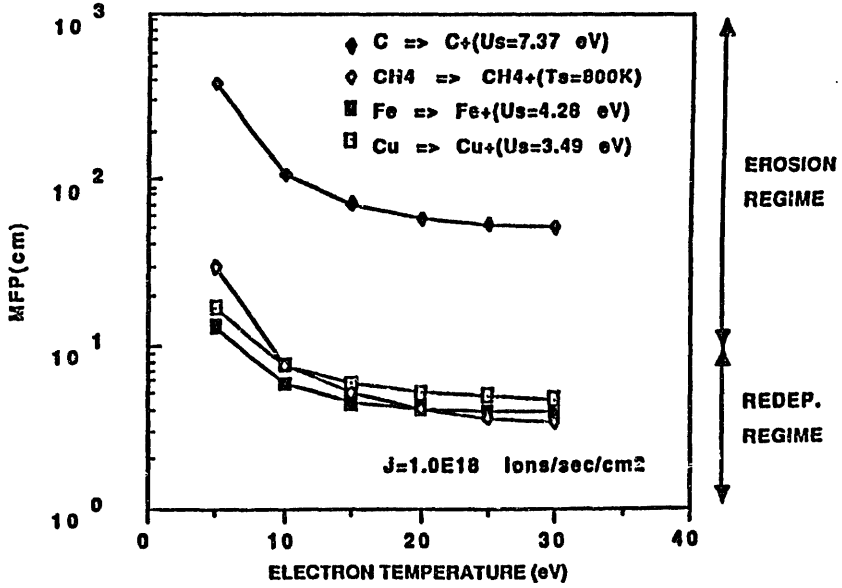

EROSION AND REDEPOSITION CONDITIONS

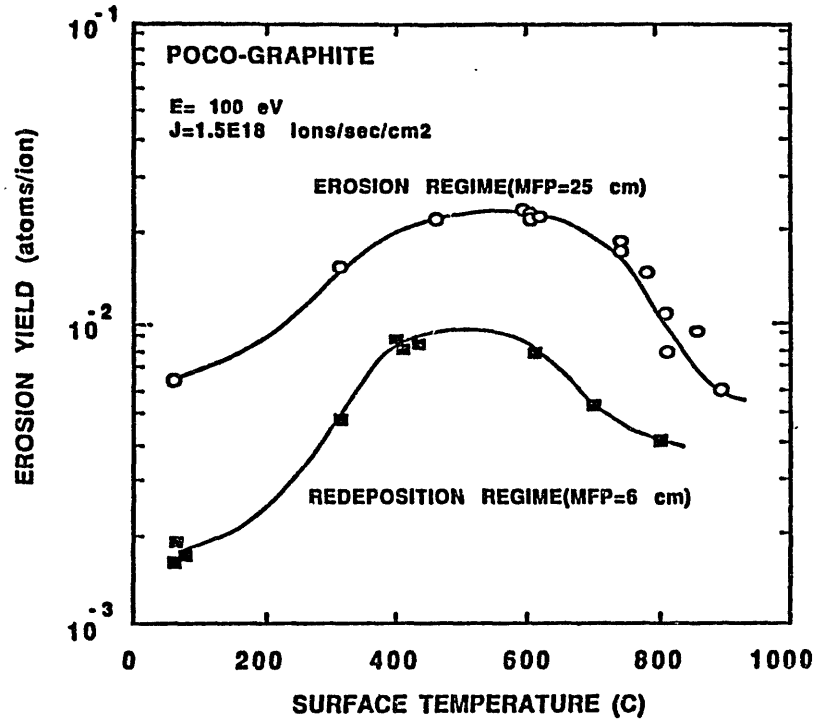

SURFACE TEMPERATURE EFFECT ON MFP FOR METHANE

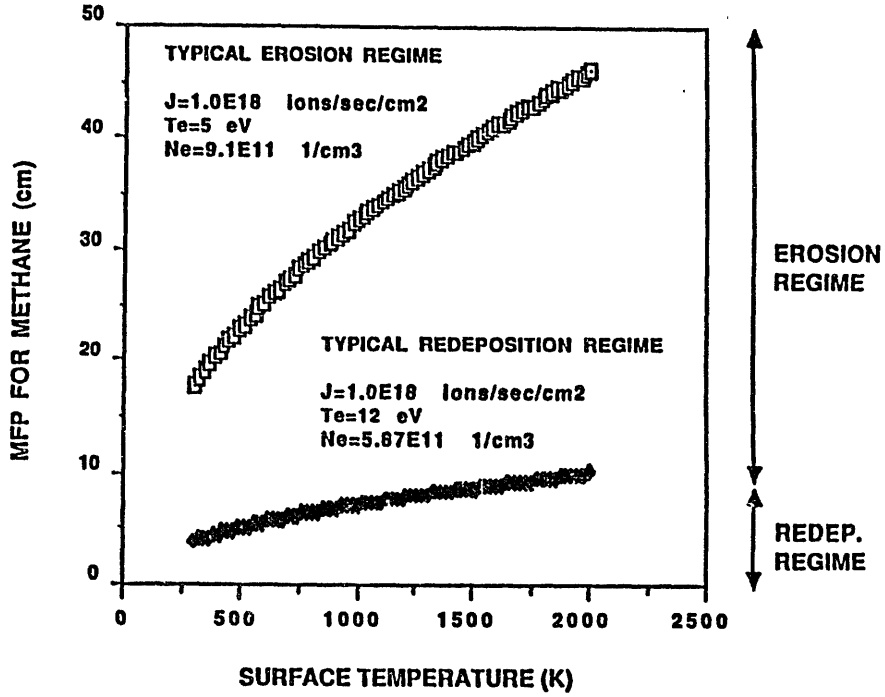

COMPARISON OF VARIOUS GRAPHITE MATERIALS

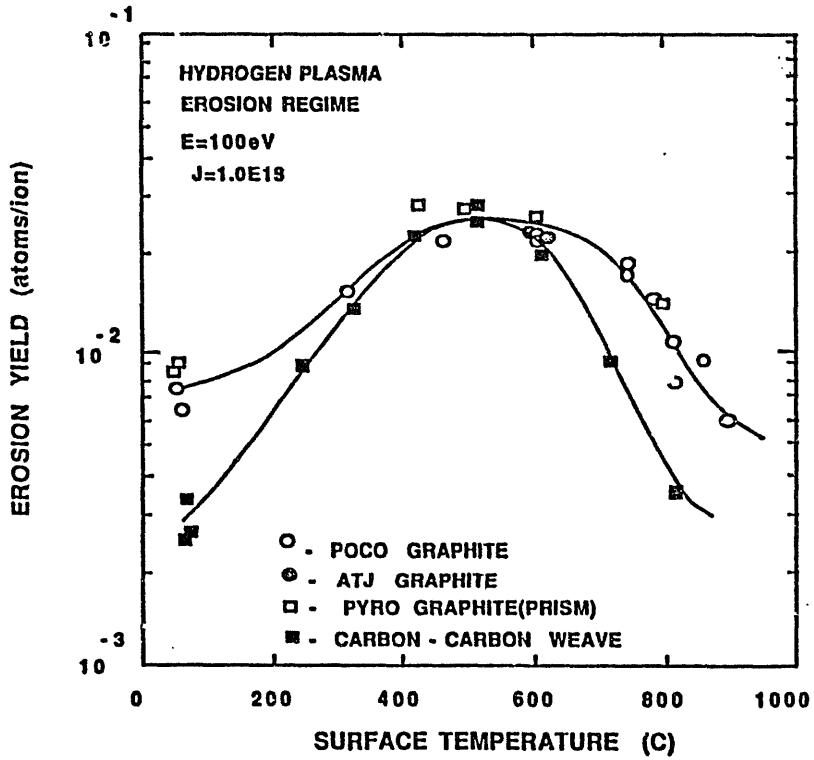

A SCHEMATIC ILLUSTRATION OF GRAPHITE PUMPING EXPERIMENTS

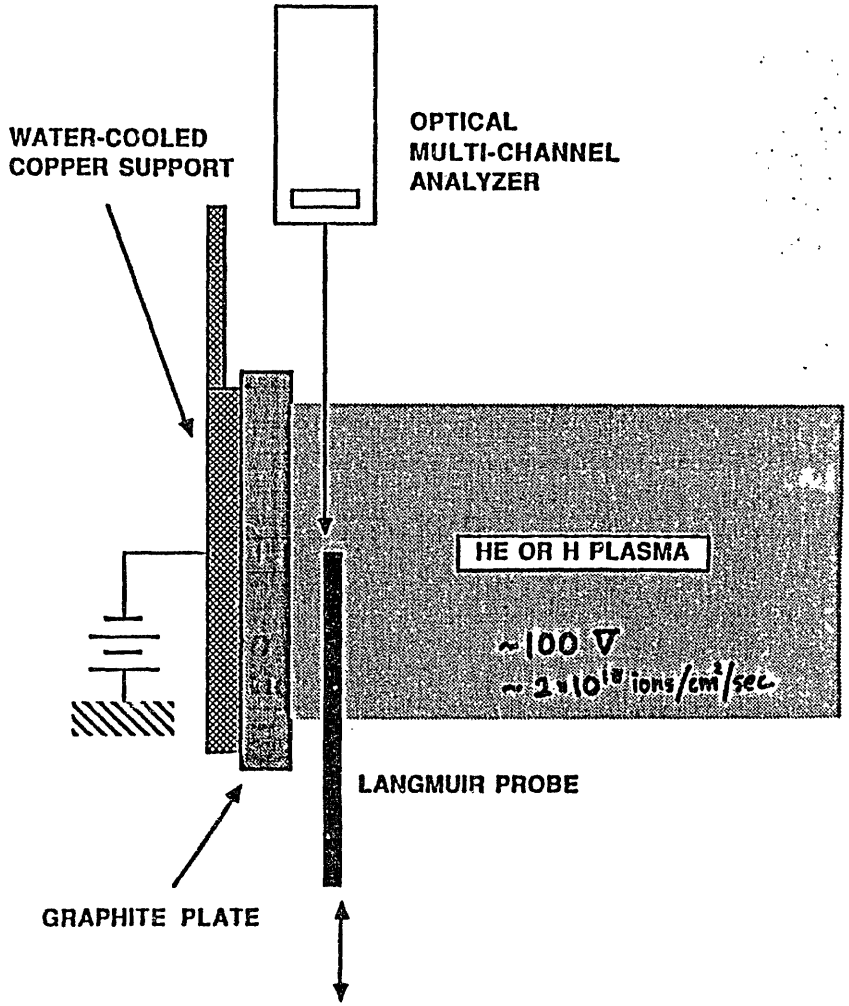

PUMPING BY PLASMA-ACTIVATED GRAPHITE

(ATJ TYPE NUCLEAR GRADE GRAPHITE)

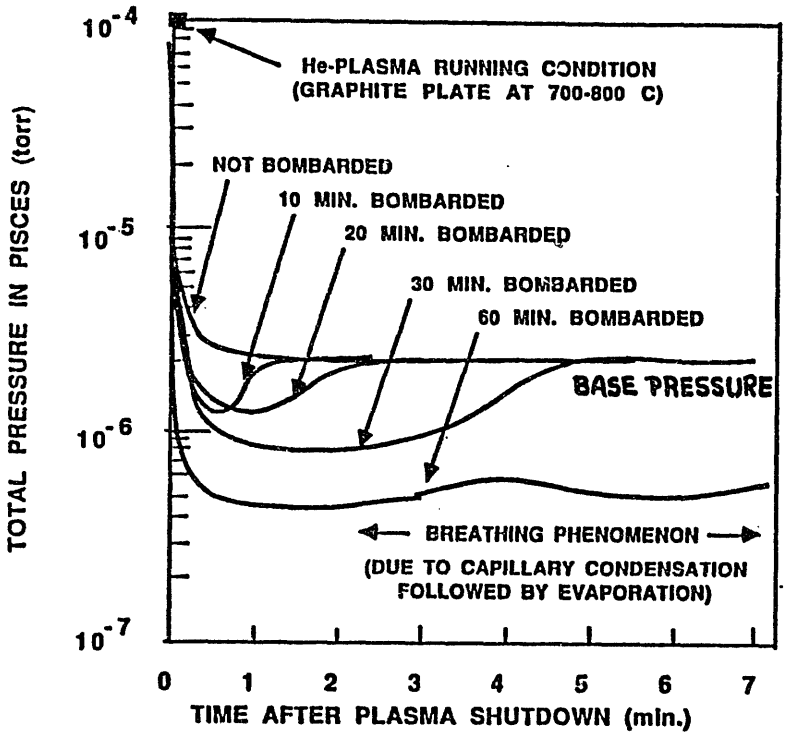

MAX. PUMPING SPEED (AT 10E-6 torr) = 200 litter/sec/cm2
(TYPICAL TI-GETTERED SURFACE, 30 litter/sec/cm2)

ACTIVATED PUMPING CONTINUES FOR 1-1.5 HOURS
PUMPING CAPACITY = 1.0E18 molecules/cm2

KEY ASPECTS ON PLASMA ACTIVATION OF GRAPHITE SURFACE

1. THERMAL OUTGASSING EFFECT UNDER HIGH FLUX (30 W/cm2) PLASMA BOMBARDMENT (ACTIVATION TEMPERATURE = 700-800C).

2. SURFACE MODIFICATION BY PHYSICAL SPUTTERING TO INDUCE OPENING SURFACE PORES (ETCHING RATE=1-10 MONOLAYERS/SEC BY 100 eV He-PLASMA, WITH A FLUX OF 2E18 ions/sec/cm2).

   RADIATION DAMAGED
3. ACTIVE ADSOTPTION SITES PROTECTED BY INNERT HELIUM UNTIL EXPOSED TO HYDROGEN ETC.

PORES CLOSED WITH DUSTS
ADSORBED WITH GASES

OPEN PORES AND (INCREASED)
FRESH SURFACE FOR ADSORPTION
(RADIATION DAMAGE SITES)

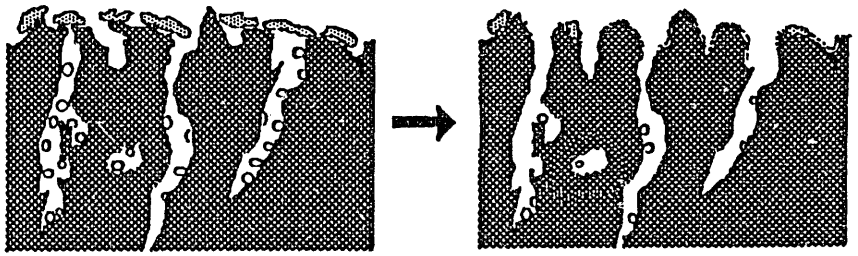

BEFORE ACTIVATION

AFTER ACTIVATION

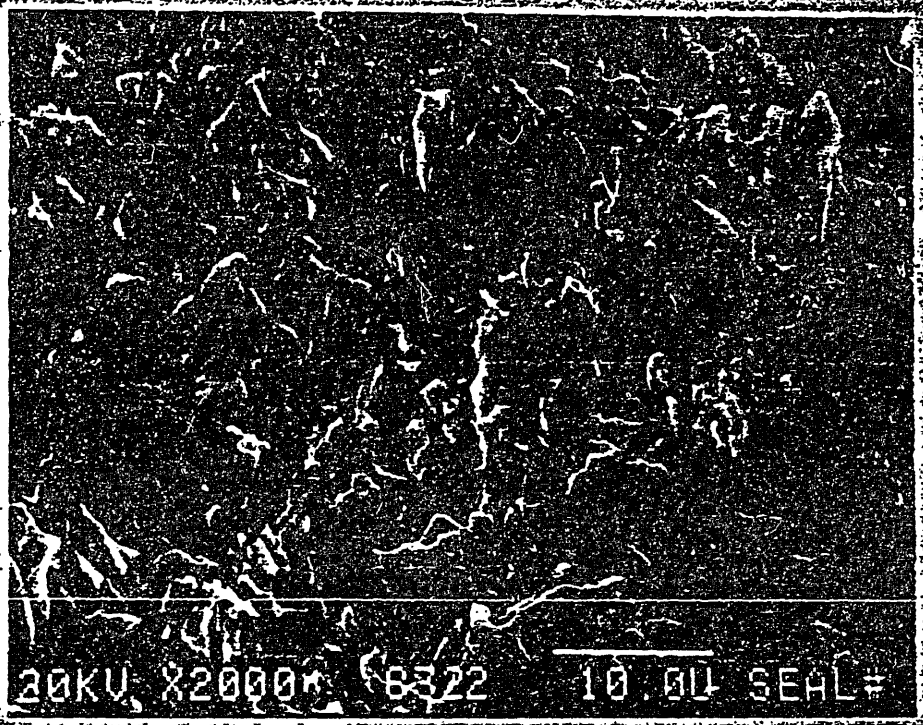

Low fluence (10^{20} ions/cm^2)

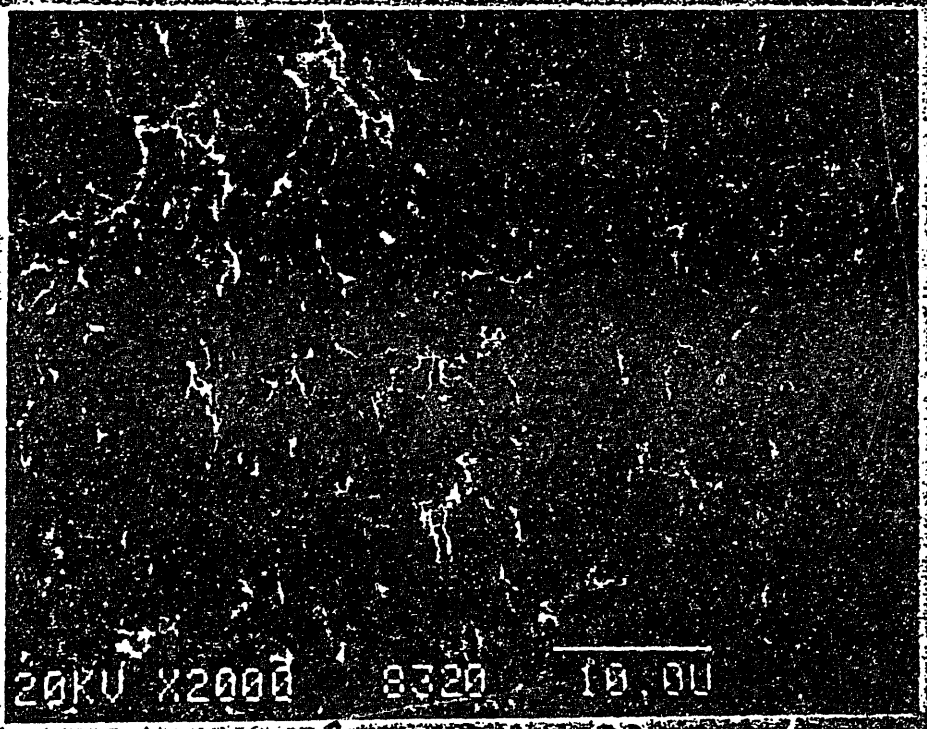

High fluence (10^{22} ions/cm^2)

HYDROGEN RECLYCLING OVER PUMPING AND SATURATED GRAPHITE

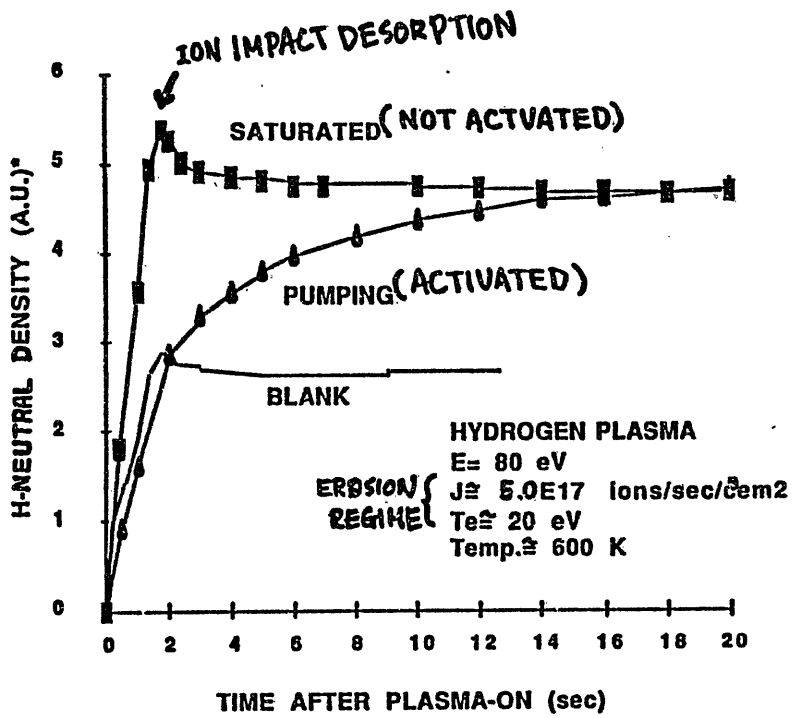

*H-ALPHA INTENSITY $\propto N_e \underset{\uparrow}{N_o} \langle \sigma v \rangle$

H-NEUTRAL

IMPLANTATION AND DAMAGE PROFILES (COMPUTED WITH TRIM PROGRAM)

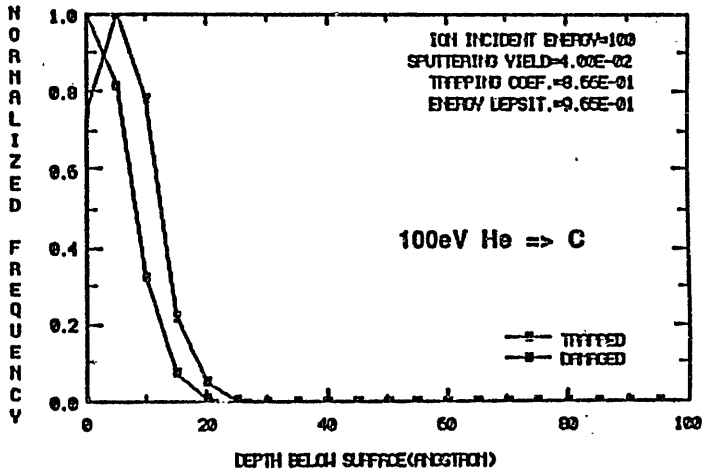

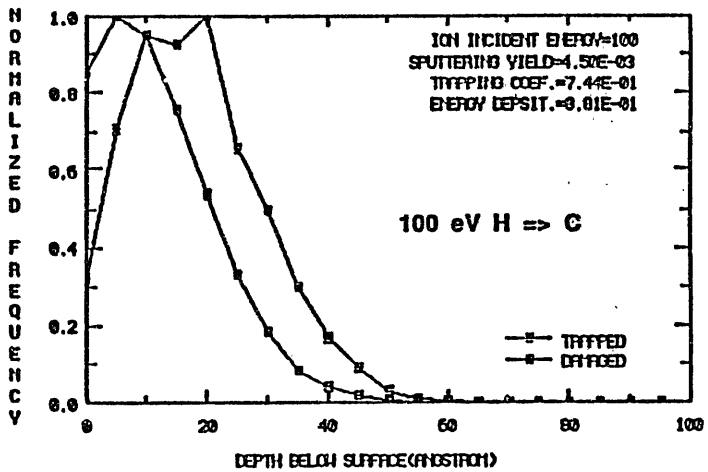

POSSIBLE MECHANISMS FOR RETARDED REEMISSION FROM ACTIVATED GRAPHITE

1. SURFACE CHEMISTRY

1-1. SURFACE RECOMBINATION MIGHT BE HINDERED AT ACTIVATED ADSORPTION SITES (IF RECOMBINATION DOMINATED).

AND/OR

2. SURFACE PHYSICS

2-1. NEAR-SURFACE DAMAGE PROFILE BY HELIUM BOMBARDMENT MIGHT RETARD HYDROGEN MIGRATION UP TO THE SURFACE (IF DIFFUSION DOMINATED).

AND/OR

2-2. HYDROGEN IS RE-IMPLANTED INTO THE DEPLETED REGION GENERATED BY HELIUM BOMBARDMENT (IF ION-IMPACT DESORPTION DOMINATED).

↑

Mike Ulrickson at TFTR

SUMMARY

1. GRAPHITE EROSION EXPERIMENTS

1-1. REDEPOSITION of HYDROCARBON results in a REDUCTION of the erosion yield by a factor of 2-3.

1-2. GRAPHITE WEAVE showed equal or BETTER erosion performance than ATJ or POCO.

2. GRAPHITE PUMPING EXPERIMENTS

2-1 High fluence INNERT GAS plasma bombardment can activate the graphite surface for PUMPING.

2-2. GRAPHITE PUMPING results in RETARDED REEMISSION of subsequentely implanted hydrogen.

Assessment of graphite for limiter/divertor and first wall tiles in CIT and ETR-type machines

A.A. Haasz
University of Tronto

Abstract

The expected range of operating graphite temperature and plasma parameters for CIT and ETR-type machines were identified. The available database for graphite erosion was evaluated with respect to first wall and limiter/divertor requirements. Physical sputtering, chemical erosion, radiation/enhanced sublimation and synergistic erosion were discussed. The effects of surface impurities, bulk impurities, plasma impurities, redeposition/codeposition and use of carbon/carbon composites were also addressed.

$H^+ \rightarrow$ a- C:H

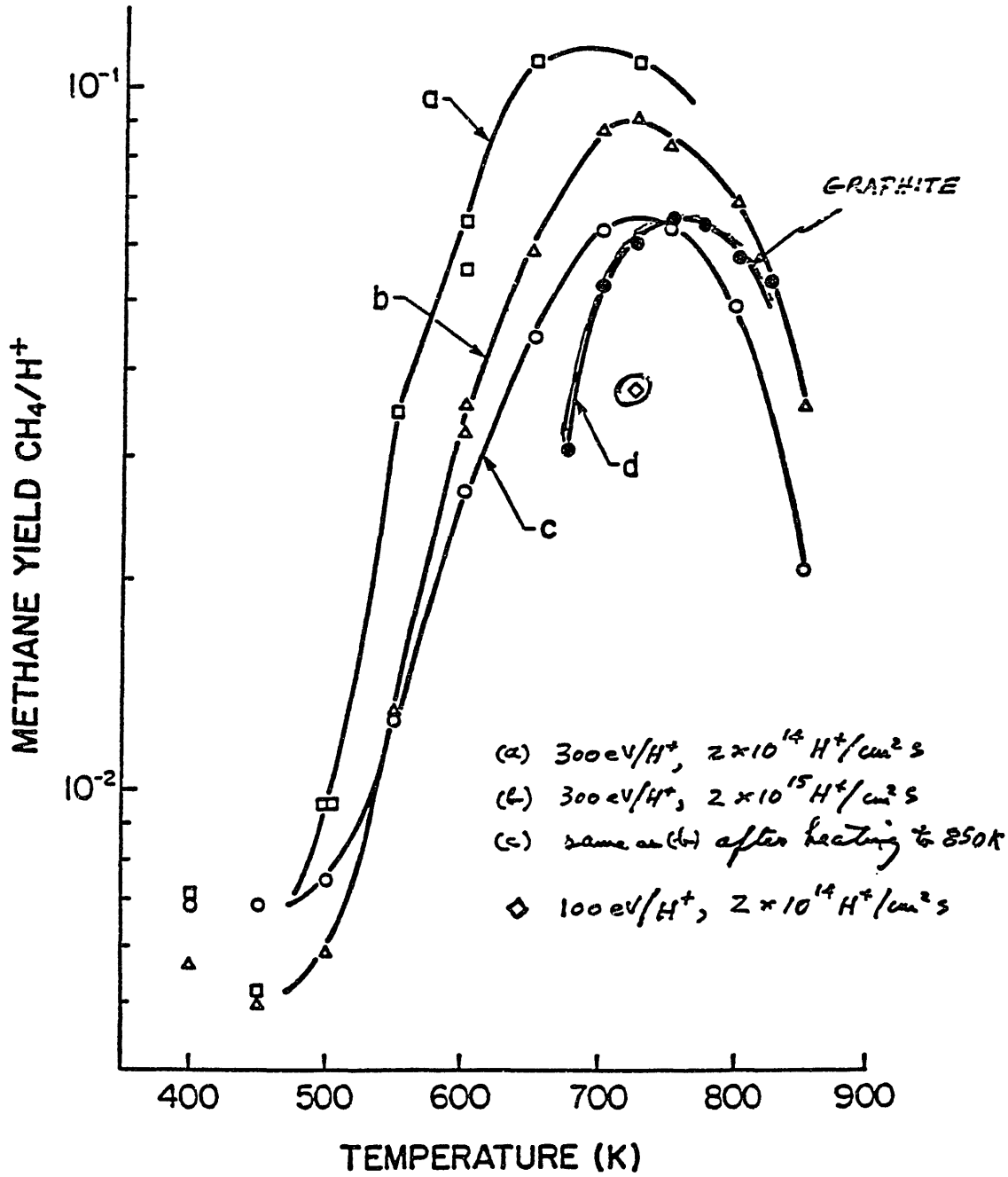

Fig 1 Davis & Heavy

Ion-Induced Sputtering and Interfacial Reaction of Metals or Metal Carbides Deposited on Graphite at Temperatures

Kenji Morita

Department of Crystalline Materials Science
Faculty of Engineering, Nagoya University
Nagoya 464 Japan

Abstract

It has been shown, concerning of suppression of chemical sputtering, that sputtering of metal atoms from metal layer (Ni) or metal carbide layer (TiC, Cr_7C_3) deposited on graphite is substantially suppressed, below certain critical ion flux, by coverage of the surface with segregated carbon atoms, which are continuously supplied via diffusion from graphite substrate.

Motivation of This Work

- It has been experimentally shown that deposition of metal or metal carbide layer on graphite reduces the reaction probability of CH_4 formation responsible for chemical sputtering
- It has been observed that metal atoms, sputtered off from the first wall, are redepodited on to the graphite limiters

Aim of This Work

- To investigate the yields of sputtering of metals deposited on graphite at high temperatures as a function of ion flux and how metals deposited on graphite are modified at high temperatures

Main Results

* Sputtering of Metals deposited on graphite at high temperatures is substantially suppressed, below certain critical ion flux, by coverage of the surface with segregated carbon atoms, which are continuously supplied via diffusion from graphite substrate.
* When thickness of metal layer is smaller than range of bombarding ion, suppression of sputtering is enhanced and carbon composition of metal carbide formed is increased.

Japan-US Workshop on Plasma Materials Interaction/ High Heat Flux
Data Needs for the Next Step Ignition and Steady State Devices
January 26-30,1987 IPP Nagoya University

Ion-Induced Sputtering and Interfacial Reaction of Metals or Metal-Carbides Deposited on Graphite at High Temperatures

K. Morita

Department of Crystalline Materials Science
Faculty of Engineering, Nagoya University

Collaborators:

Y. Horino
Y. Hasebe
K. Kondoh
Nagoya Univ.

S. Sukenobu
Y. Gomay
Toshiba Corp.

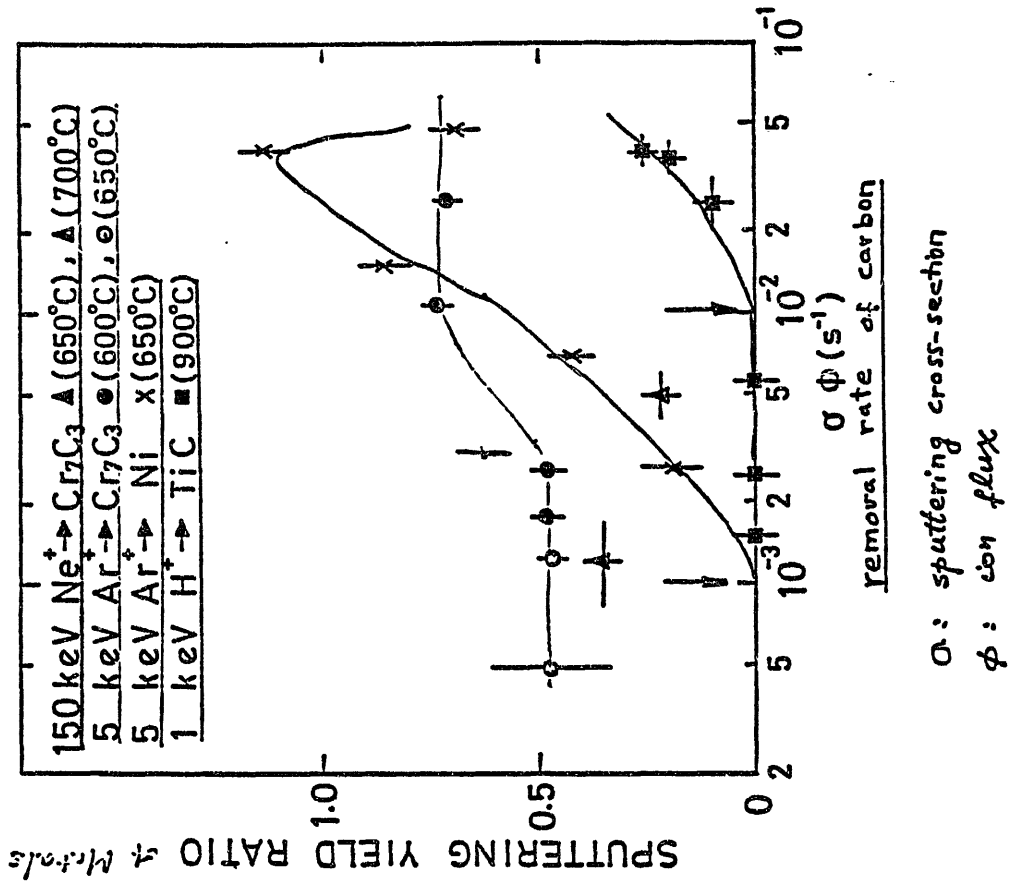

Materials Deposited on Graphite and Irradiation Conditions

		prepartion methode	thickness	ion	temperature	carbon enrichment
1)	TiC	CVD	3000 Å	1 keV H^+	900°C	strong
2)	Ni	PVD	5000 Å	5 keV Ar^+	650°C	strong
3)	Cr_7C_3	PVD and Annealing	3000 Å	5 keV Ar^+	650°C, 700°C	weak
4)	Cr_7C_3		1000 Å	150 keV Ne^+	650°C, 700°C	

When these specimens are heated at appropriate temperatures, it has been observed that the material surface is enriched by segregated carbon atoms

In the cases of 1), 2) and 3)

Projected range of ions $\ll$ thickness of deposited layer

In the case of 4)

Projected range of ions $\gtrsim$ thickness of deposited layer

In the latter case, maximal energy density deposited by elastic collisions of bombarding ions is situated at the interface between the Cr_7C_3 layer and graphite.

** Effects of interfacial reaction has been observed

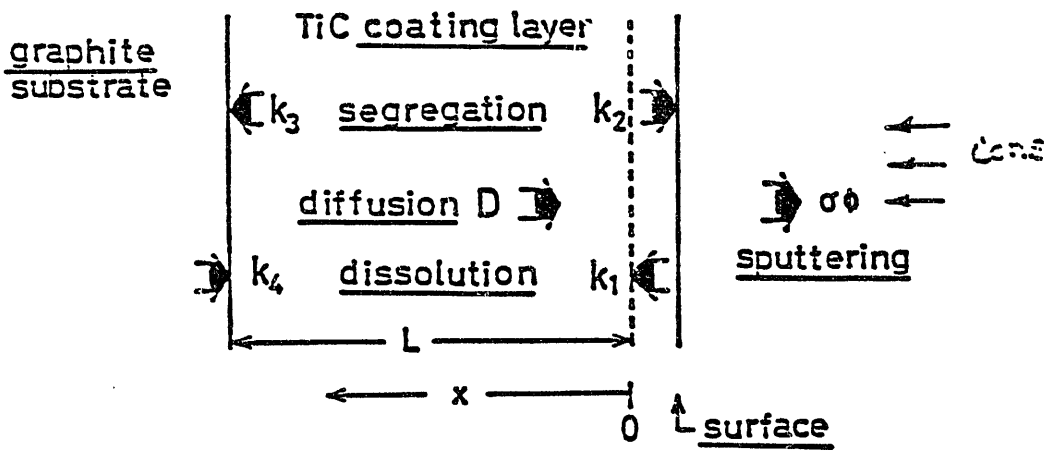

Steady State Surface Concentration of Carbon $C_s(\phi)$

$$C_s(\phi) = \frac{C_s^{\circ}}{1 + (\sigma\phi/k_1)(1 + Q_1 + Q_2)}$$

$$Q_1 = \frac{k_2}{k_3}, \quad Q_2 = \frac{k_2}{(D/La)}, \quad C_s^{\circ} \approx 1$$

σ : sputtering cross-section ϕ : ion flux

k_1 : dissolution rate at the surface

k_2 : segregation rate at the surface

k_3 : segregation rate at the interface

k_4 : dissolution rate at the interface

Under the present experimental conditions

$$Q_1 \sim 1 \qquad Q_2 \ll 1$$

The critical ion flux for suppression of metal sputtering

$$\phi_c \sim 0.1 \frac{k}{2\sigma} \qquad \text{for 90\% reduction}$$

Under ion irradiation, the rate constant is enhanced by defect formation. Thus we consider supply of carbon atoms to the surface is limited by the rate constant of k_4 at the interface

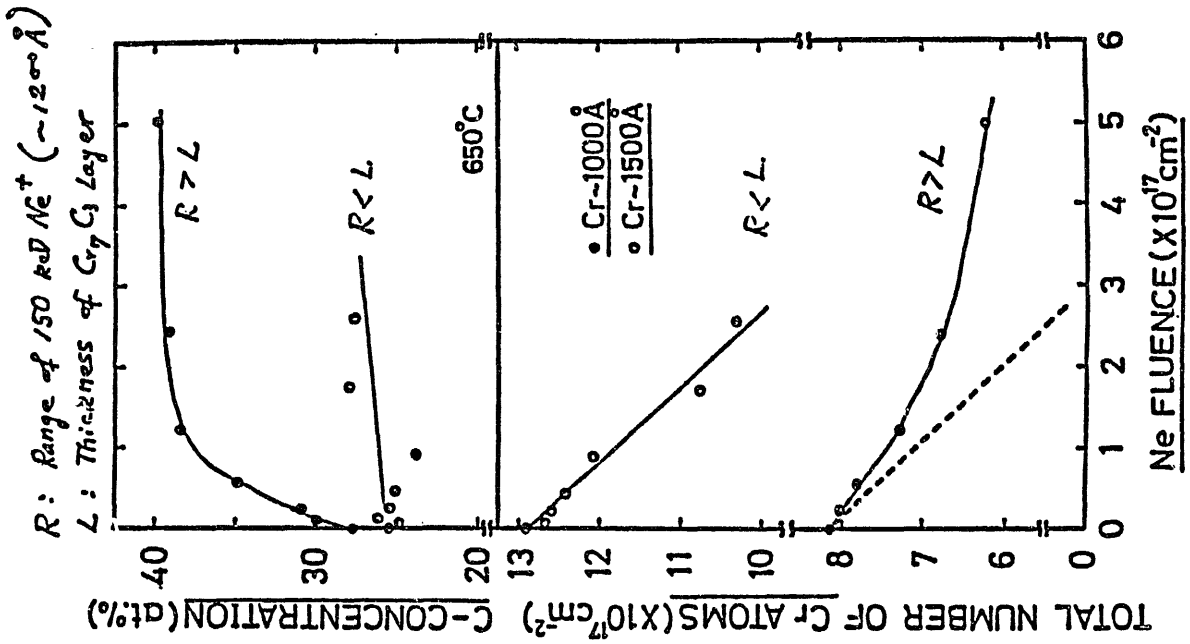

Conclusions

- It has been experimentally observed that sputtering(or resputtering) of metals deposited on graphite at high temperatures is substantially reduced by coverage with segregated carbon atoms below certain critical ion flux.
- The critical ion flux is dependent on sputtering cross section(or yield) of carbon and temperature, namely the rate constants of both dissolution of carbon from graphite and segregation of carbon onto the bombarded surface

When the edge temperature of plasma is lowered, it is expected that sputtering of metals is suppressed at ion fluxes higher than a critical ion flux of $1\times10^{15}/cm^2.s$ on bombardment of 1 keV H^+ on TiC in the present experiment.

Chemical Erosion of graphite and Diamond materials due to low energy hydrogen bombardment

Reiji Yamada
Japan Atomic Energy Research Institute

Abstract

Chemical erosion of graphite due to hydrogen ion bombardment in the regime of low energy(≤several keV) and low flux ($\leq 10^{16}/cm^2$ sec) bombadment measured by JAERI was compared with the data of Toronto group and Garching group. The difference between three groups is rather small and consistent.

Diamond compacts and film produced by CVD method at 900°C for the subrate temperature shows low chemical erosion compared with graphite.

Dose Dependence of CH_4 Production

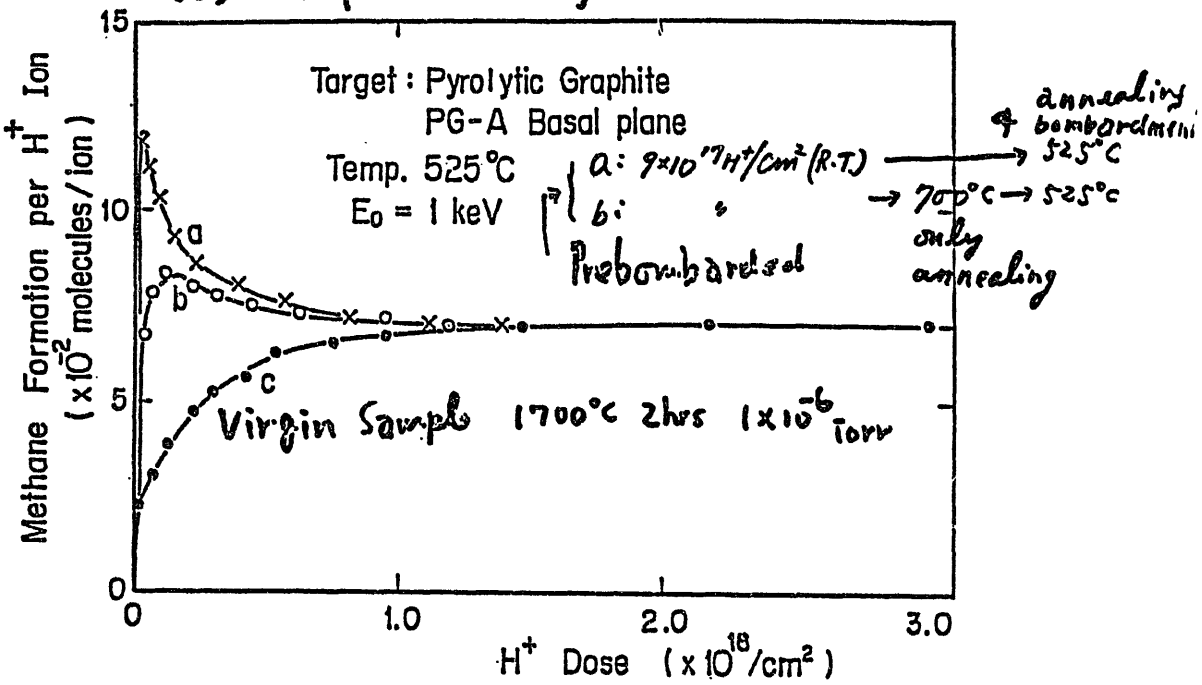

R. Yamada et al
J. Nucl. Mater. 95 (1980) 278

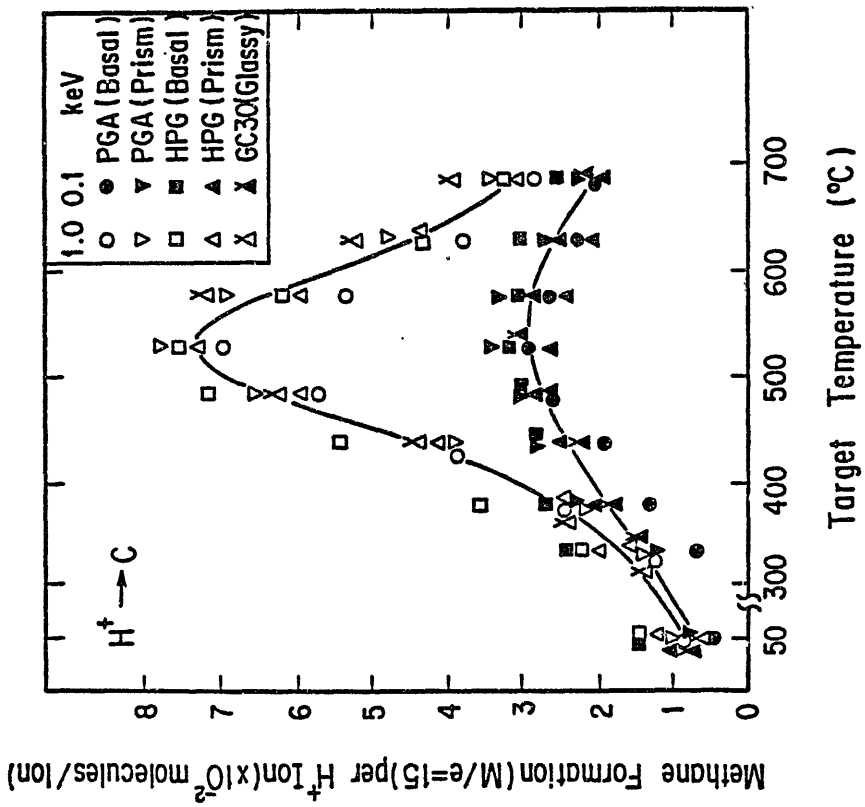

R. Yamada et al
J. Nucl. Mater. 95 (1980) 278

V. Philipps et al. J. Nucl. Mater. 122+123 (1984), 1990
$A_r^+ + H^0 \rightarrow C$. P.G. Poco. Papyex. Isotropic.

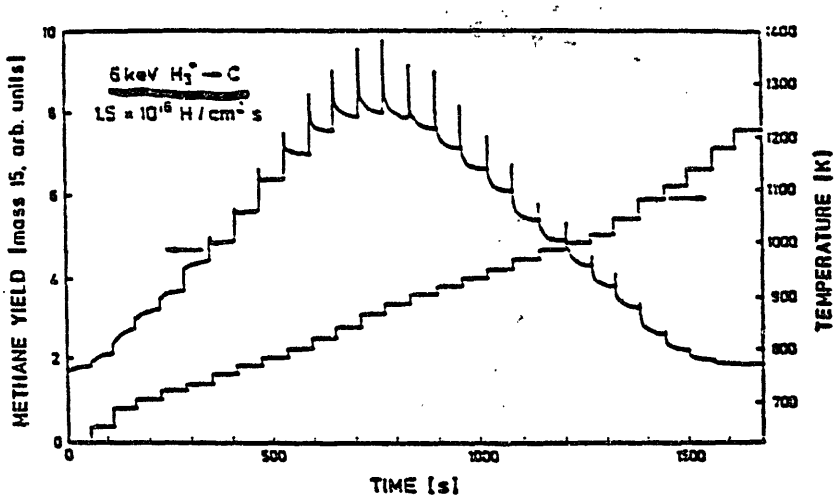

Fig. 2. The time dependence of the methane yield during continuous bombardment of PAPYEX carbon paper with hydrogen ions for stepwise increasing temperature.

J. Roth et al. J. Nucl. Mater. 111 & 112 (1982) 775

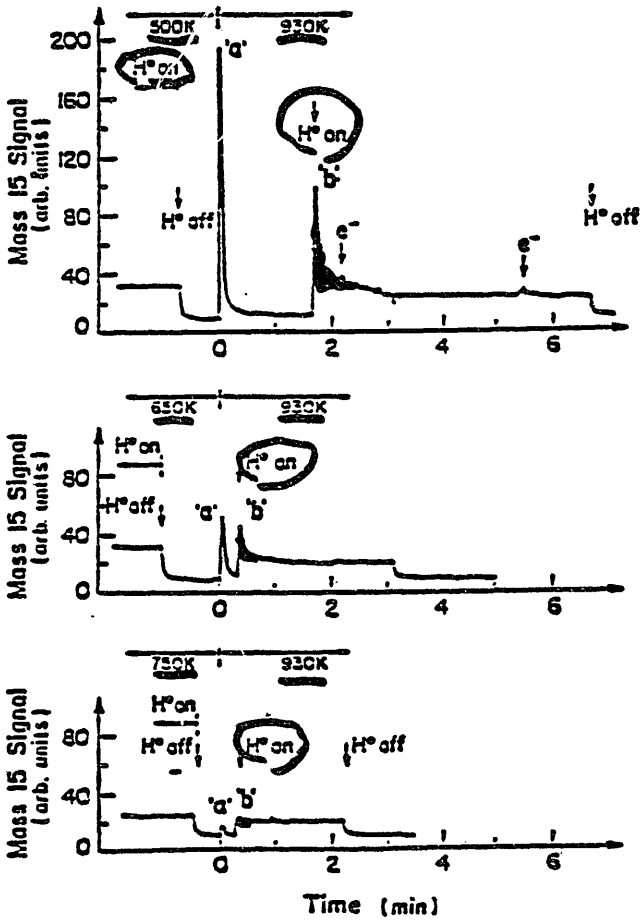

A. A. Haasz et al. J. Vac. Sci. Technol. A 4 (1986) 1179

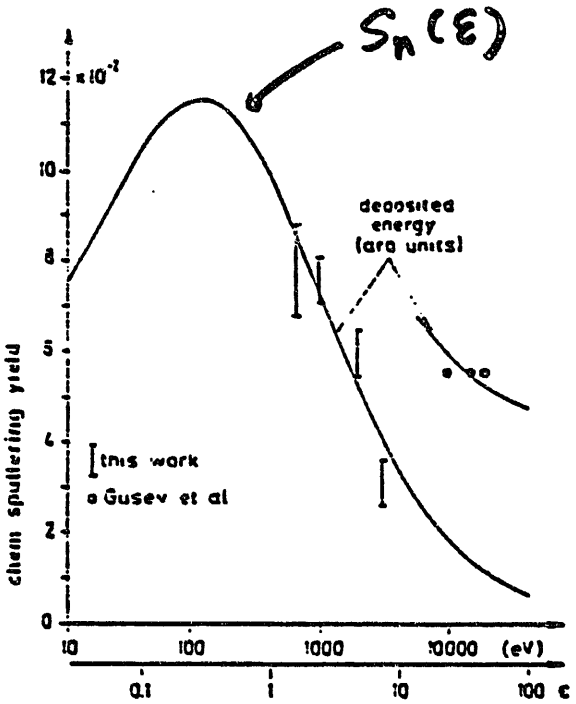

Fig. 5. Energy dependence of the erosion due to chemical sputtering for the bombardment of graphite with hydrogen ions at 650° C. For comparison the calculated energy deposited in the surface layer has been introduced.

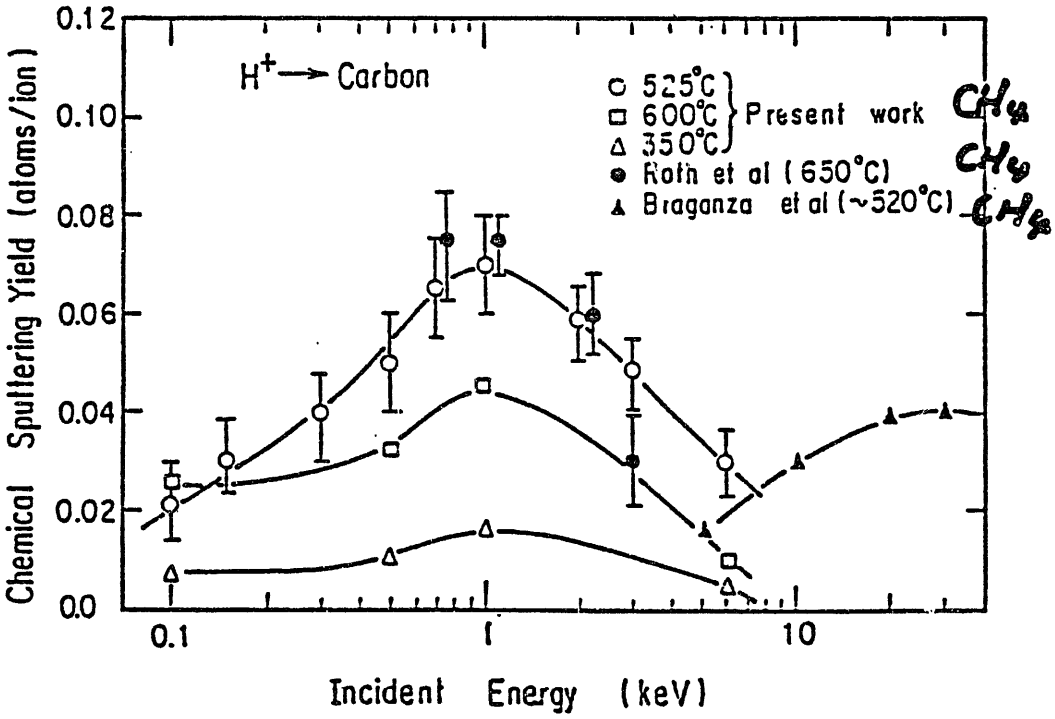

R. Yamada et al. J. Nucl. Mater. 95 (1980) 278
R. Yamada & K. Sone J. Nucl. Mater. 116 (1983) 20

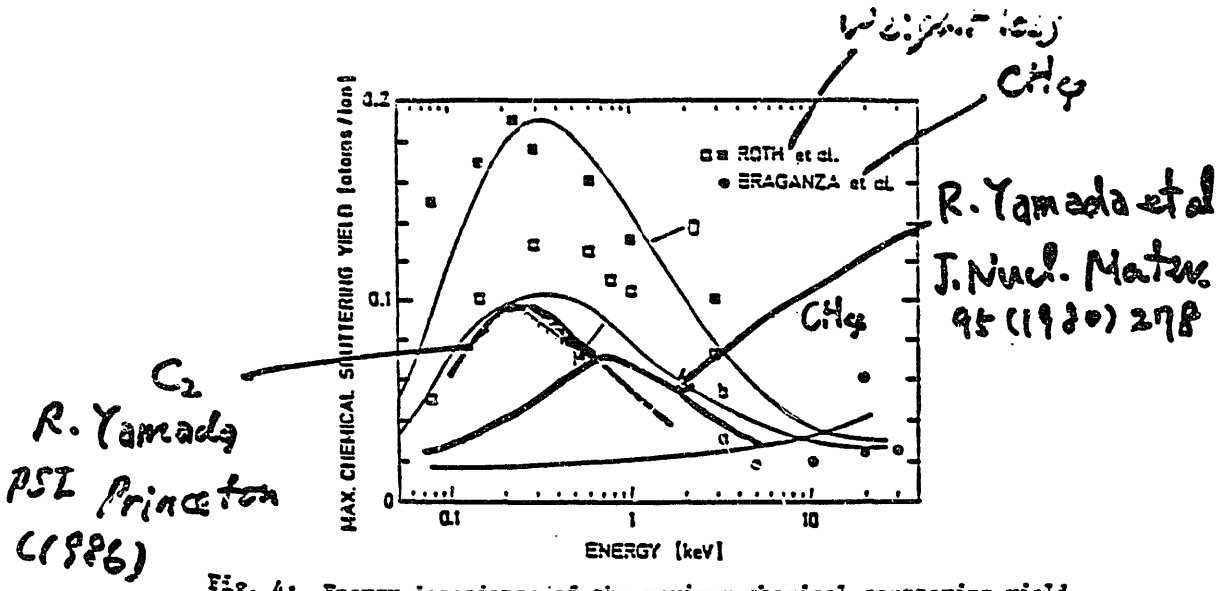

Fig. 4: Energy dependence of the maximum chemical sputtering yield for a constant hydrogen ion flux of 10^{15} H/cm² sec. Open points are for hydrogen, full points for deuterium ions. Curve a is calculated from eq. (4), curves b from eq. (6).

J. Roth. NATO ASI series Vol B 131 P. 389 (1986)

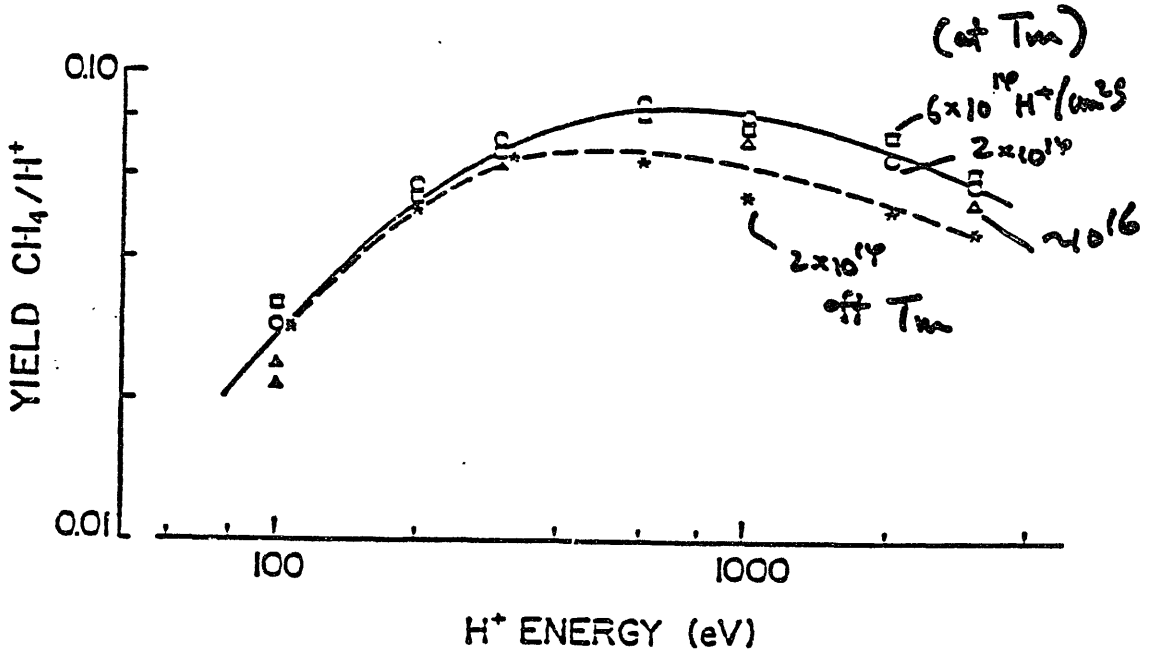

J.W. Davis, A.A. Haasz et al
PSI Princeton (1986)

From J. Roth NATO ASI series Vol 131 (1986) 397

For energetic ion bombardment more global balance equations were used to explain the observed temperature dependence /8, 9/. In steady-state the reemitted hydrogen flux is equal to the incident ion flux Γ_H. The surface concentration c_{sH} can be calculated depending on the residence time of the hydrogen and is assumed to be proportional to the reaction yield. This yields

$$\Gamma_H \left(1 - \frac{c_{sH}}{c_{so}}\right) = \frac{\Gamma_H}{\tau_o} e^{-Q_2/kT}$$

where the residence time is equal to $\tau_o e^{Q_2/kT}$ and c_{so} is the surface saturation concentration.

$\propto \frac{1}{\sigma}$

Then

$$Y \propto \frac{e^{-Q_1/kT}}{\Gamma_H/c_{so} + \frac{1}{\tau_o} e^{-Q_2/kT}} \qquad (2)$$

S.K. Erents et al J. Nucl. Mater. 63 (1976) 399

This predicts a maximum at a temperature

$$T_m = \frac{Q_2}{k} \left(\ln \frac{(Q_2 - Q_1)\, c_{so}}{\Gamma_H\, Q_1\, \tau_o}\right)^{-1} \qquad (3)$$

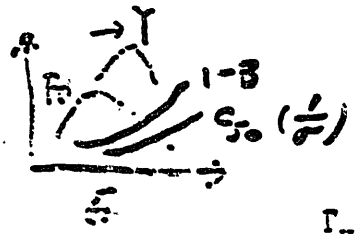

$$Y = A \left(\frac{\Gamma_H F_D}{\nu_o e^{-Q_3/kT}}\right)^{\ell} \frac{(1-B)\, e^{-Q_1/kT}}{\frac{\Gamma_H}{c_{so}} + \frac{1}{\tau_o} e^{-Q_2/kT}}$$

R. Yamada & K. Sone J. Nucl. Mater. 116 (1983) 200

Here B is the energy dependent reflection coefficient of hydrogen at the carbon surface, $F_D(E)$ the deposited energy in the surface layer. $\Gamma_H \cdot F_D$ is the production rate and $\nu = \nu_o e^{-Q_3/kT}$ is a jump frequency proportional to the annealing rate of radiation-incuded vacancies and interstitials. By taking $F_D(E)$ from physical sputtering calculations they could reasonably fit the measured dependence of the methane production rate on the ion energy with the exponent ℓ between 0.5 and 1 and $A(\nu)^{-\ell}$ as a fitting factor. The activation energies Q_1, Q_2 and Q_3 could be extracted from the temperature dependence of the methane yield.

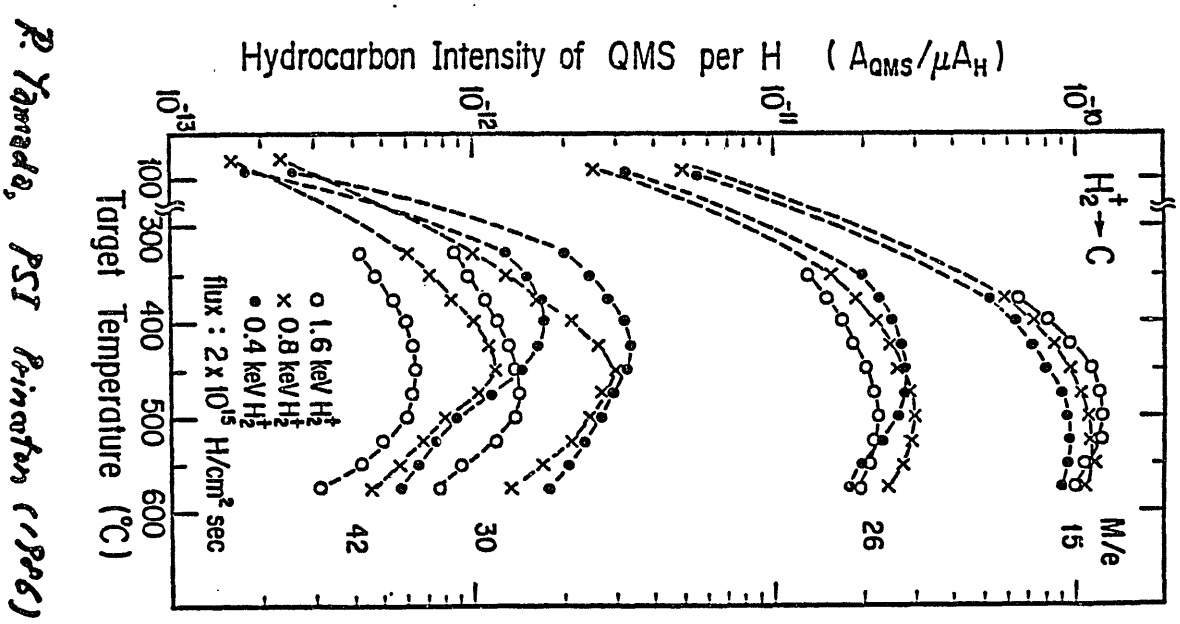

R. Yamada, PSI Princeton (1986)

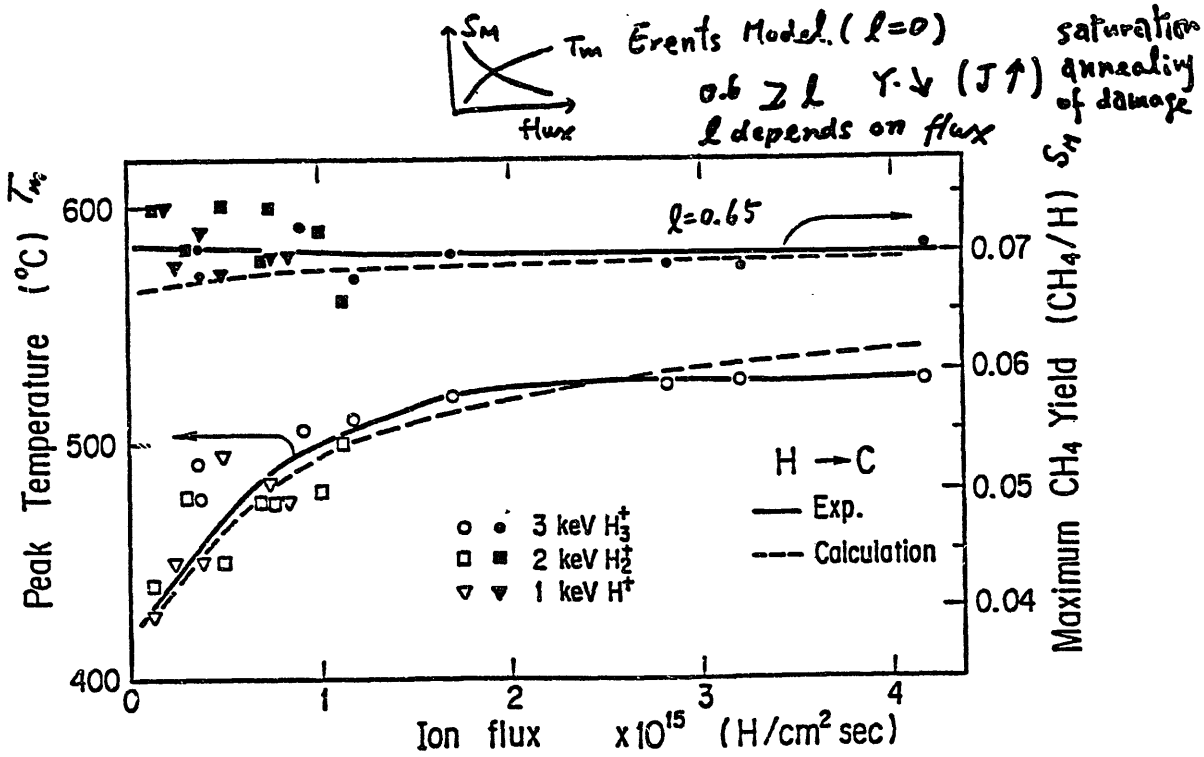

R. Yamada, PWI Princeton (1986)

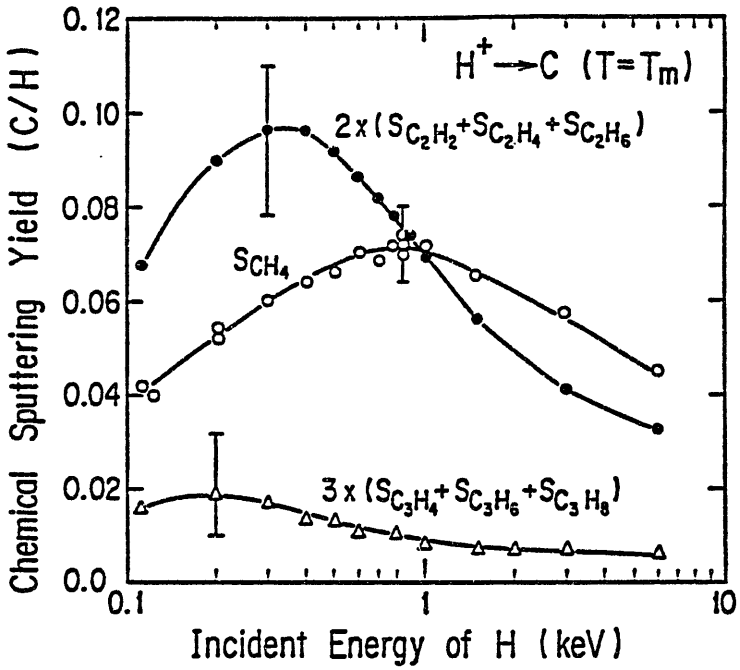

R. Yamada, PSI Princeton (1986)

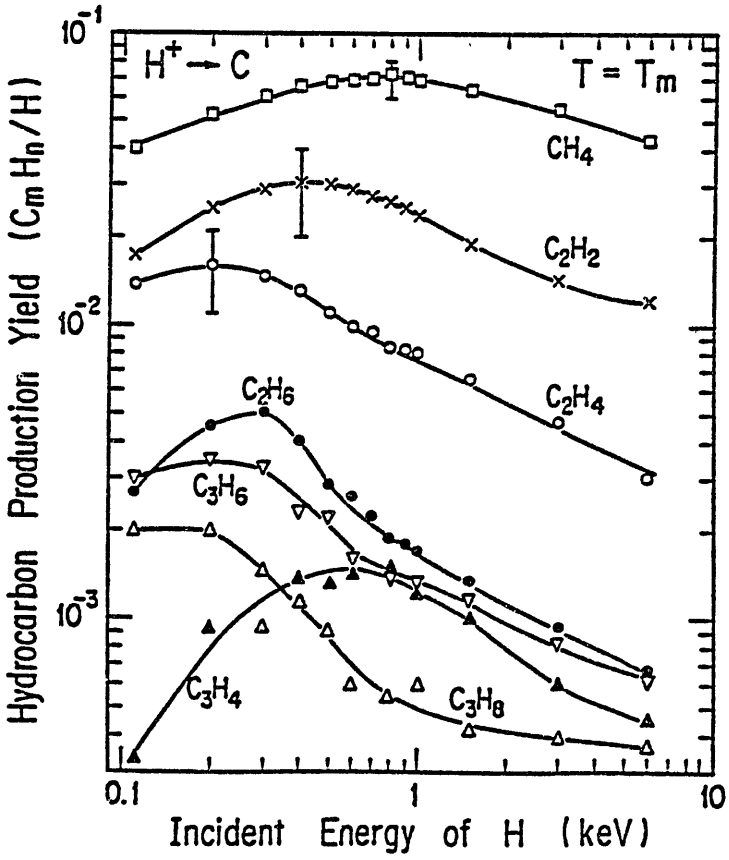

R. Yamada PSI Princeton (1986)

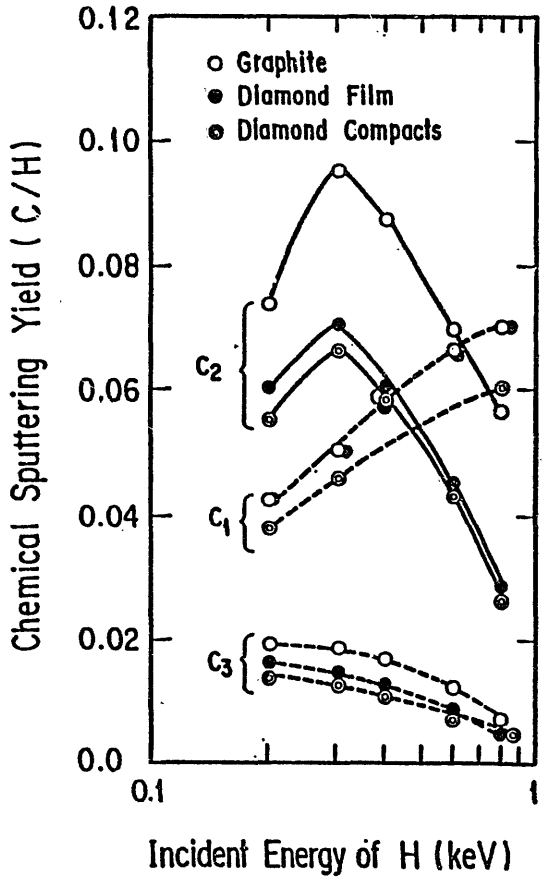

R. Yamada, J. Vac. Sci. Technol. A (1987)

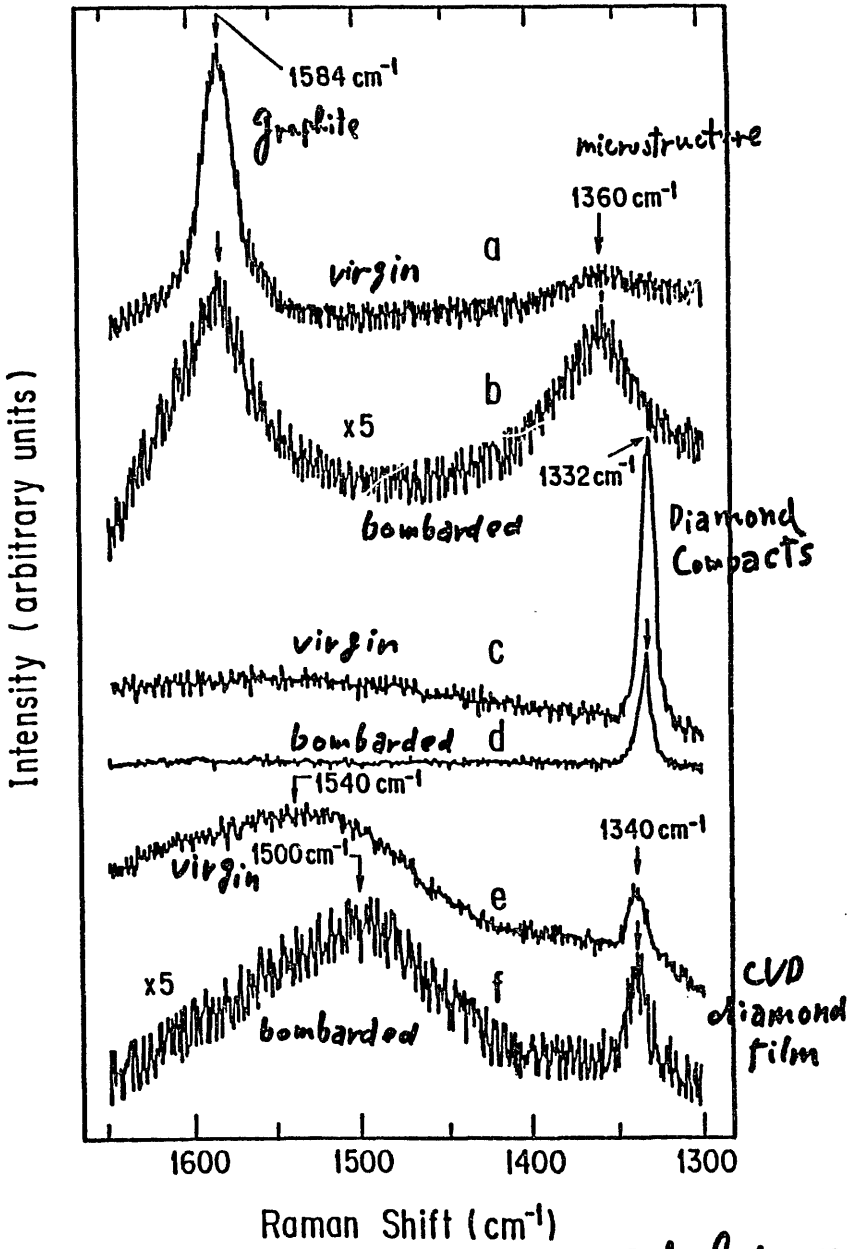

R. Yamada, J. Vac. Sci Technol A (1987)

Comment on erosion of graphite

Volker Philipps

K F A

Abstract

Radiation enhanced sublimation; The interstitial model to explain the radiation enhanced sublimation has been further proofed. If predicts a threshold down to small energies similar as for the production of Frenhel pairs. A flux dependence is predicted, so that the yield ciell decrease propartional to $(P)^{314}$ (P: Frenhel pair production rate).

Chemical erosion of hydrocarbon films; Which the chemical erosion of pure graphite differs significantly when using either thermal atomic hydrogen or energetic ions (yield increases from 5×10^{-4} to $\sim5\times10^{-2}$ C/H), a-C:H films are highly reactive against atoms alone.

The erosion yield of a-C:H films when bombarded with thermal atoms is in the maximum 800k of the order $0/10^{-1}$ and so similar as that of energetic ions on these films which is quite similar to the yield of pure graphite.

If has been further found that hydrogen saturated graphite layers shows also a high reactivity against atoms alone.

Radiation enhanced sublimation

Model

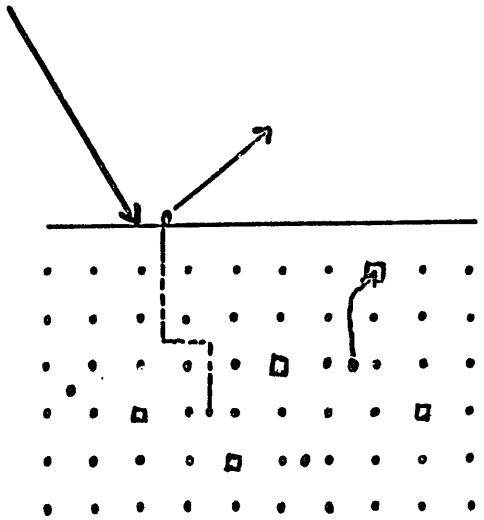

— Production of Frenkel pairs

— Thermal diffusion of vacancy and interstitials

— Recombination of vacancy and interstitial

interstitial arrives at the surface and desorbs

↓

ion induced sublimation

Test of the model

— weak bonding of interstitials to the surface

→ simulation experiment ✓

(To be published in surface science)

— time dependence of the emitted C-atom flux

predicted time evolution of the interstitial flux to the surface (qualitatively)

— start phase:

interstitial concentration ≈ vacancy concentration

⟹ large interstitial flux to the surface

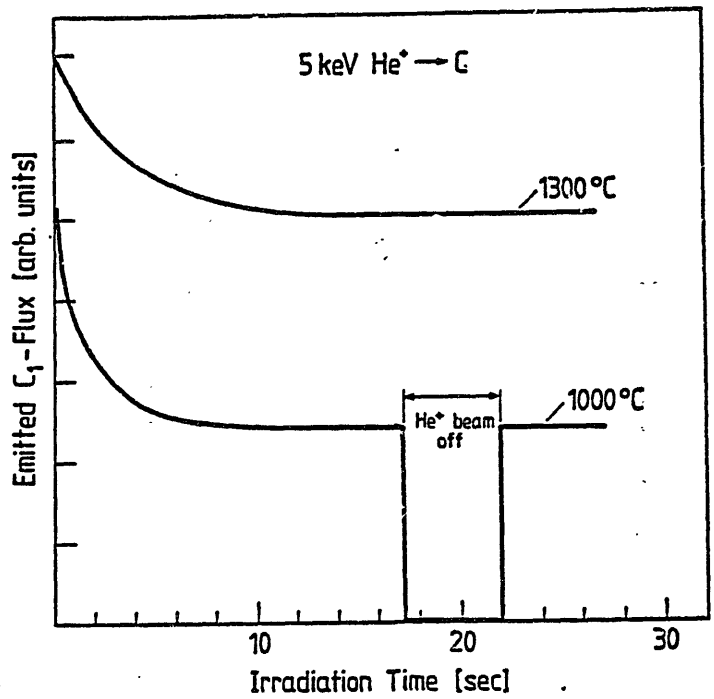
5 keV He⁺ → C
1300 °C
1000 °C
He⁺ beam off
Emitted C₁-Flux [arb. units]
10
20
30
Irradiation Time [sec]

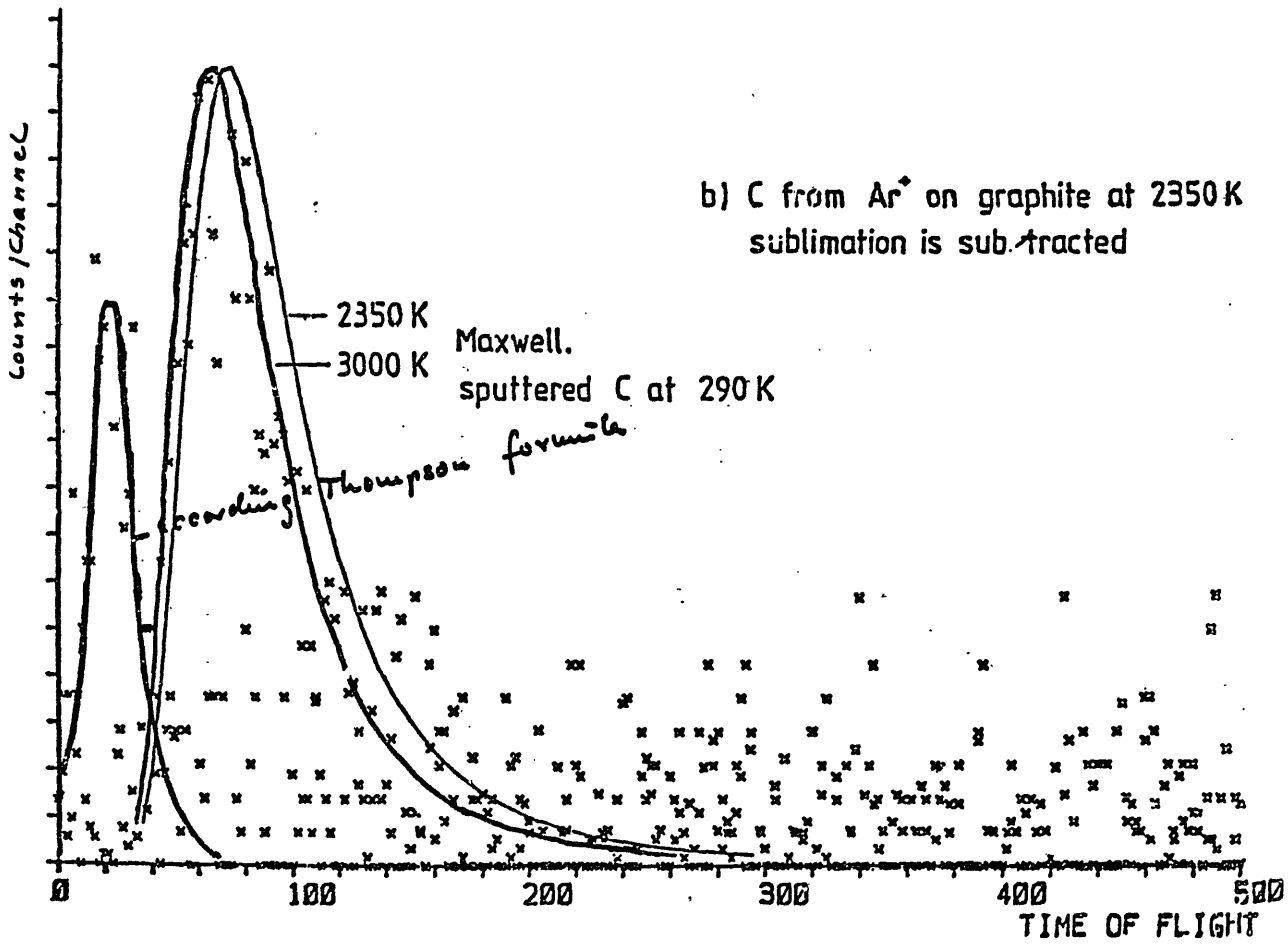
b) C from Ar⁺ on graphite at 2350 K
sublimation is sub-tracted
2350 K
3000 K
Maxwell.
sputtered C at 290 K
according Thompson formula
Counts/Channel
0
100
200
300
400
500
TIME OF FLIGHT

⇒ Analytical Model

Predictions of the interstitial model

- Yield $\sim (D_v)^{1/4} \sim e^{-0.9\,eV/kT}$

  ↑ vacancy Diffusion $D_v \sim e^{-3.5\,eV/kT}$

- Yield $\sim (P)^{3/4} \sim (\text{Flux})^{3/4}$

  ↑ Frenkel pair Production rate

- Threshold for small energies equal to the threshold for Frenkel-pair production

Chemical Erosion

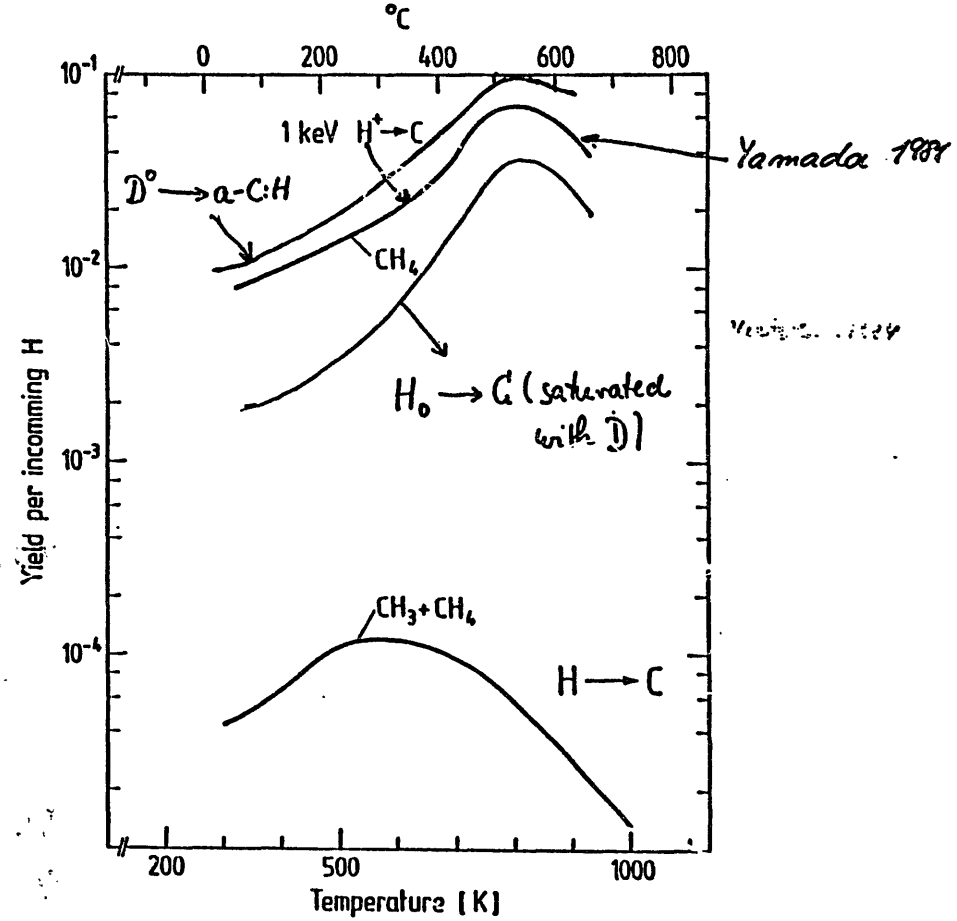

spectral distribution of hydrocarbons

	CH_x	C_2H_x	C_3H_x	$x \geq 4$	total C-erosion
$H^0 \rightarrow$ a-C:H	1	0.8	0.5	~0.2	~5×CH_x
$H^+_{2.5keV} \rightarrow$ a-C:H	1	0.3	<0.1	<0.07	2·CH_x
pure graphit					
$H^+_{2.5keV}$ C (Yamada)	1	0.4	0.13		~2×CH_x

⇒ thermal atomic hydrogen exposure

⇒ erosion is dominated by C_2, C_3- hydrocarbons

⇒ Edge behaviour ?

Thermal Desorption Process and Surface Roughness of POCO Graphite Irradiated by Hydrogen Ion Beam

Tomoaki Hino
Hokkaido University

Abstract

POCO Graphite samples were irradiated by H_3^+ ion beam (9keV), and the thermal desorptions of H_2 and CH_4 were studied by thermal desorption spectroscopy. The peak temperature, which gives a maximum of H_2 desorption, increased at lower irradiation number but decreased at higher irradiation number. For CH_4, the peak temperature was roughly constant for the irradiation number. The surface roughness factor of the graphite decreased as the irradiation number.

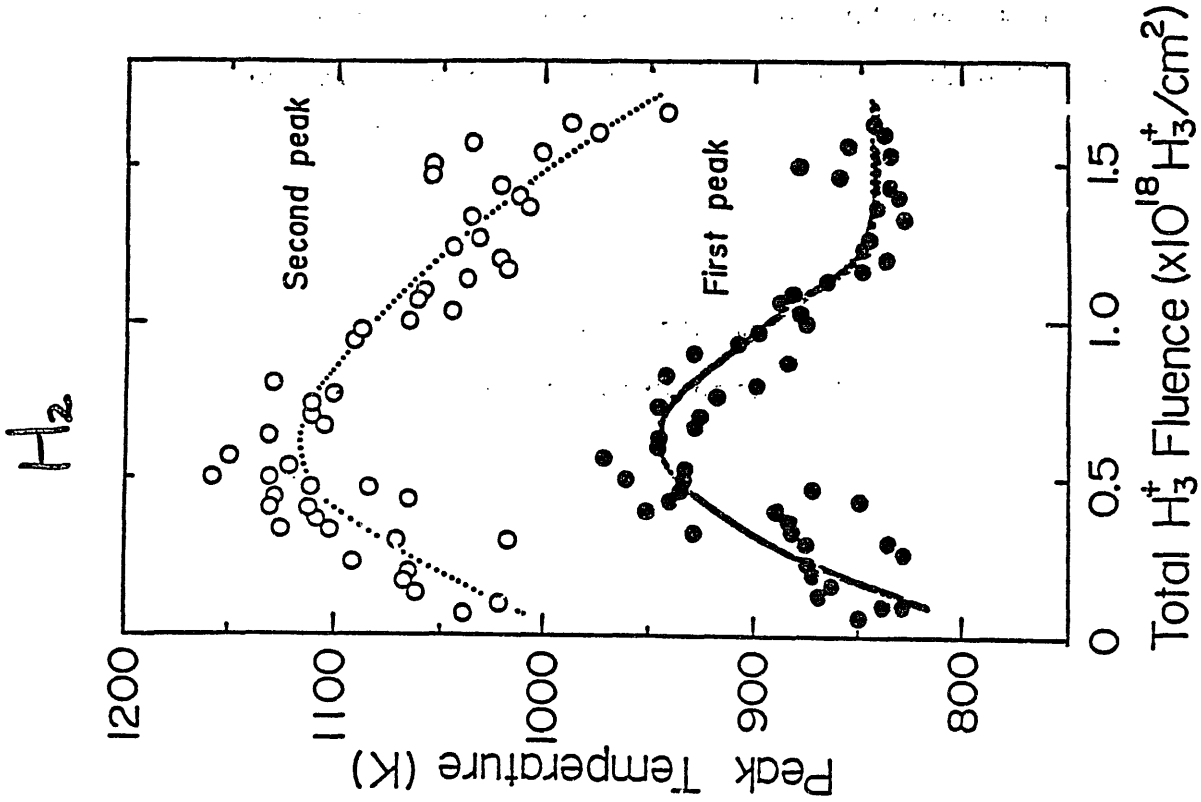
H_2
Second peak
First peak
Peak Temperature (K)
1200
1100
1000
900
800
0
0.5
1.0
1.5
Total H_3^+ Fluence ($\times 10^{18}$ H_3^+/cm^2)

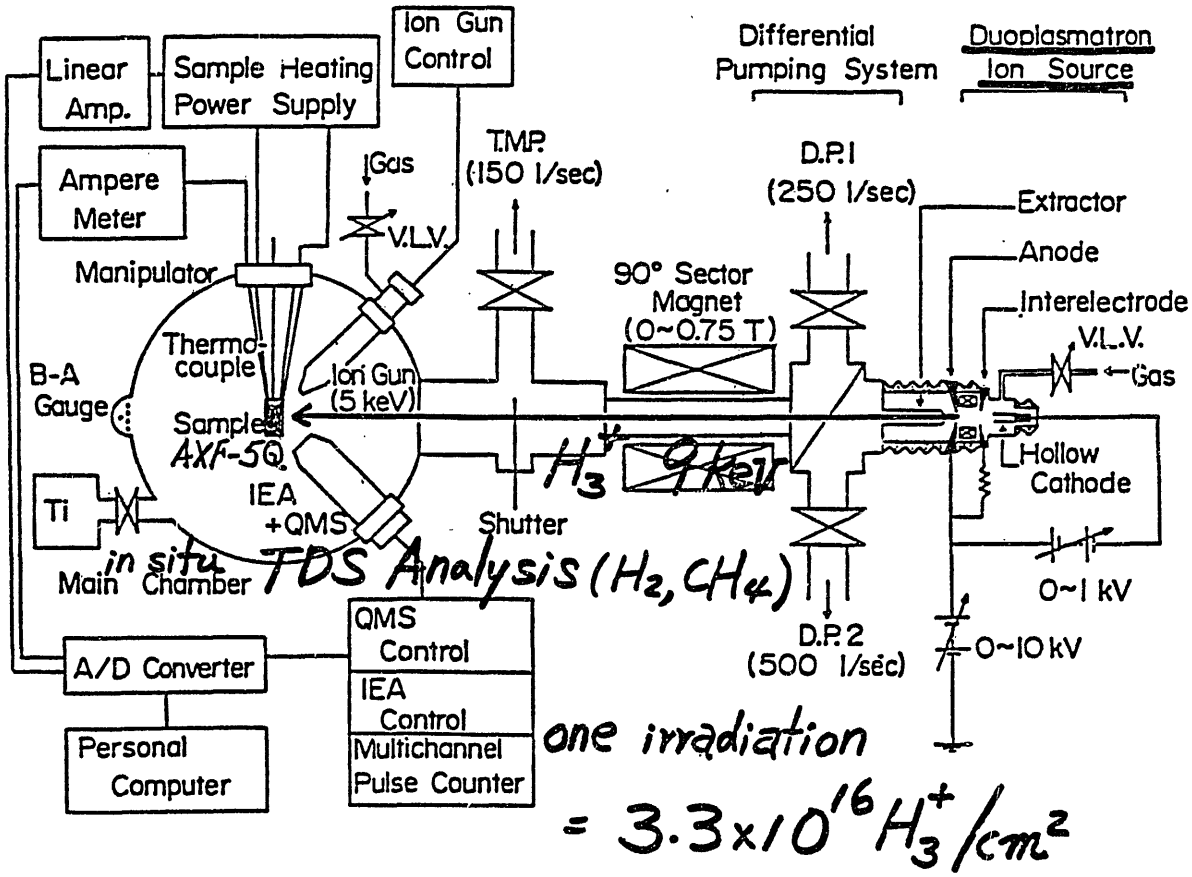
Linear Amp.
Sample Heating Power Supply
Ion Gun Control
Differential Pumping System
Duoplasmatron Ion Source
Ampere Meter
Gas
V.L.V.
T.M.P. (150 l/sec)
D.P.1 (250 l/sec)
Extractor
Anode
Interelectrode
V.L.V.
Gas
Manipulator
90° Sector Magnet (0~0.75 T)
Thermo-couple
Ion Gun (5 keV)
B-A Gauge
Sample
AXF-5Q
H_3^+
9keV
Hollow Cathode
Ti
IEA +QMS
Shutter
in situ TDS Analysis (H_2, CH_4)
Main Chamber
0~1 kV
D.P.2 (500 l/sec)
0~10 kV
A/D Converter
QMS Control
IEA Control
Multichannel Pulse Counter
Personal Computer
one irradiation
$= 3.3\times10^{16} H_3^+/cm^2$

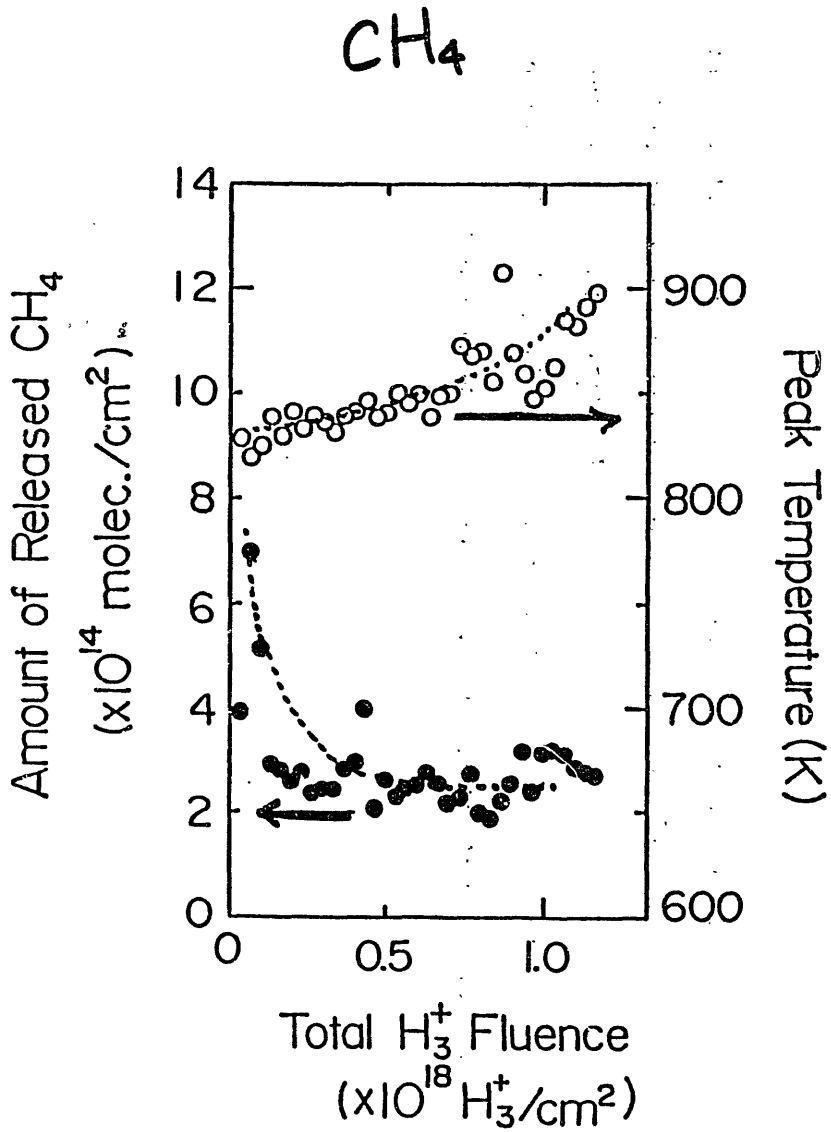
CH4
Amount of Released CH4
(x10^14 molec./cm^2)
Peak Temperature (K)
Total H3+ Fluence
(x10^18 H3+/cm^2)
0
2
4
6
8
10
12
14
600
700
800
900
0.5
1.0

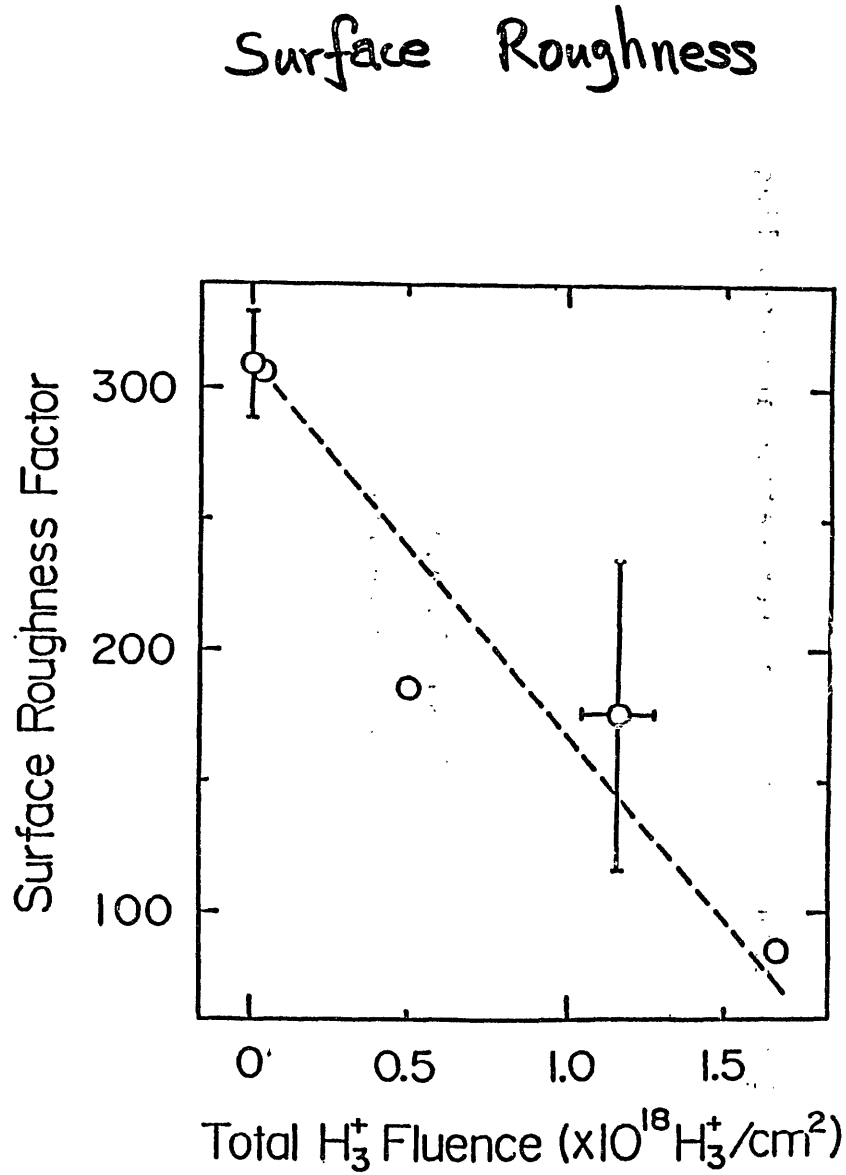
Surface Roughness
Surface Roughness Factor
100
200
300
0
0.5
1.0
1.5
Total H3+ Fluence (x10^18 H3+/cm^2)

Estimation of Retention, Permeation and Recycling

Tetsuo Tanabe

Osaka University

Abstract

For estimation of hydrogen recycling properties, the importance of effect of gaseous hydrogen background is emphasized based on the recent data showing the rather high silubility of hydrogen in graphite. The importance of time transient behavior is also mentioned.

Estimation Retention, Permeation and Recycling

T. Tanabe(Osaka Univ.)

Importance of time transient behavior

Importance of background hydrogen gas

Effect of impurity

Main problem seems to be originated from
high retnetion in the first wall

Large tritium inventory

High probavility of DT and DD reaction

Large Permeation

Large fractuation of hydrogen recycling

Hydrogen embrittlement

Recommendation

High (but no so high) temerature operation

Main problem seems to be originated from
high retention in the first wall

Large tritium inventory

High probavility of DT and DD reaction

Large permeation

Large fractuation of hydrogen recycling

Hydrogen Embrittlement

Recommendation

High(but not so high) temperature operation

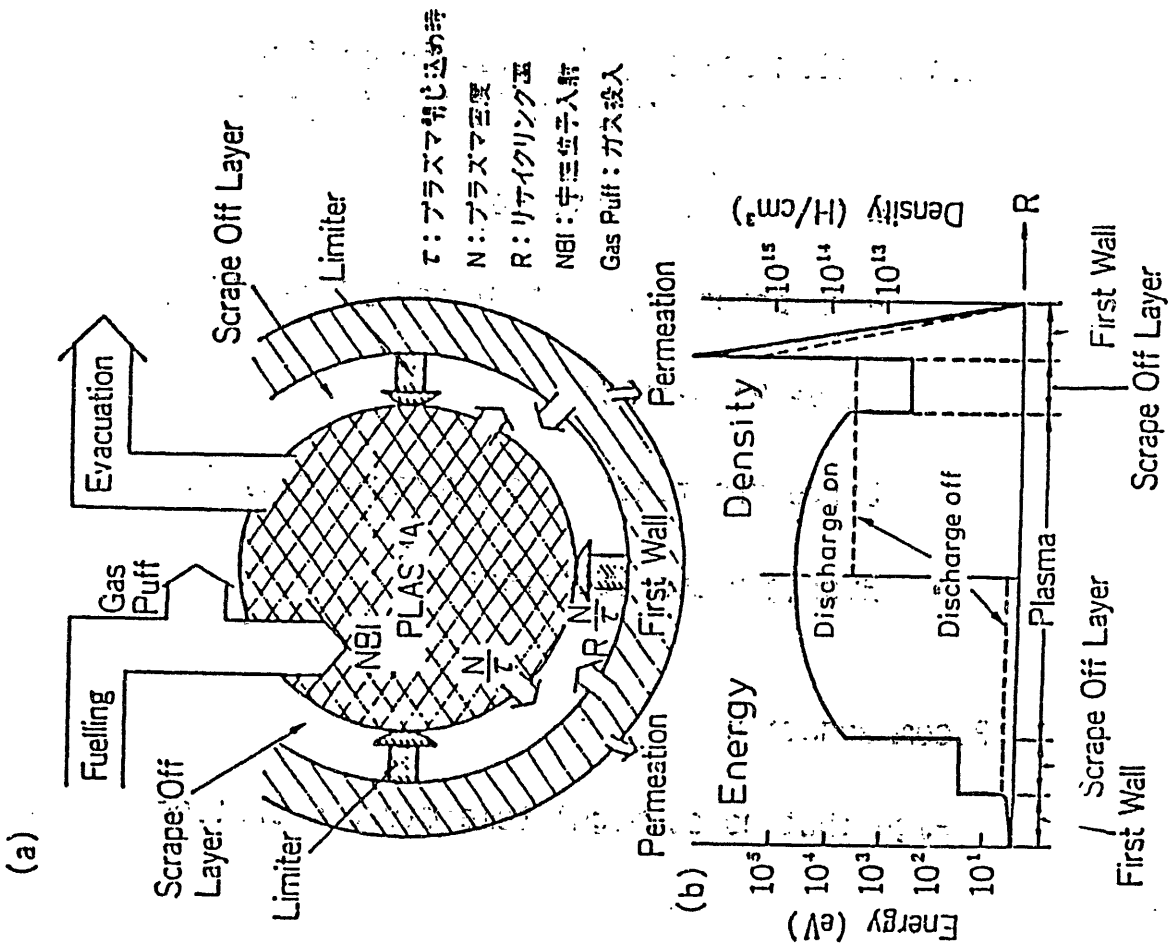

$$J_2 \geq \alpha \cdot \phi = \frac{r}{d}\phi \quad \text{(DD regime)}$$

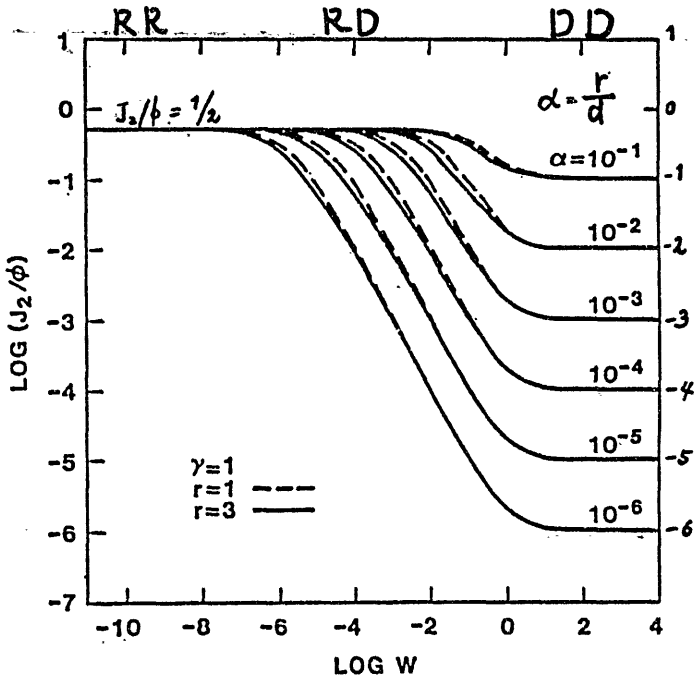

$W \propto k_r^{1/2}/D$

FIGURE 3 Log-log plot of v^r, for $r=1$ and 3, versus the transport parameter for several values of α and for $\gamma=1$. Each of these curves represents exact solutions to Eq. (30) and the dashed curve is for $r=1$.

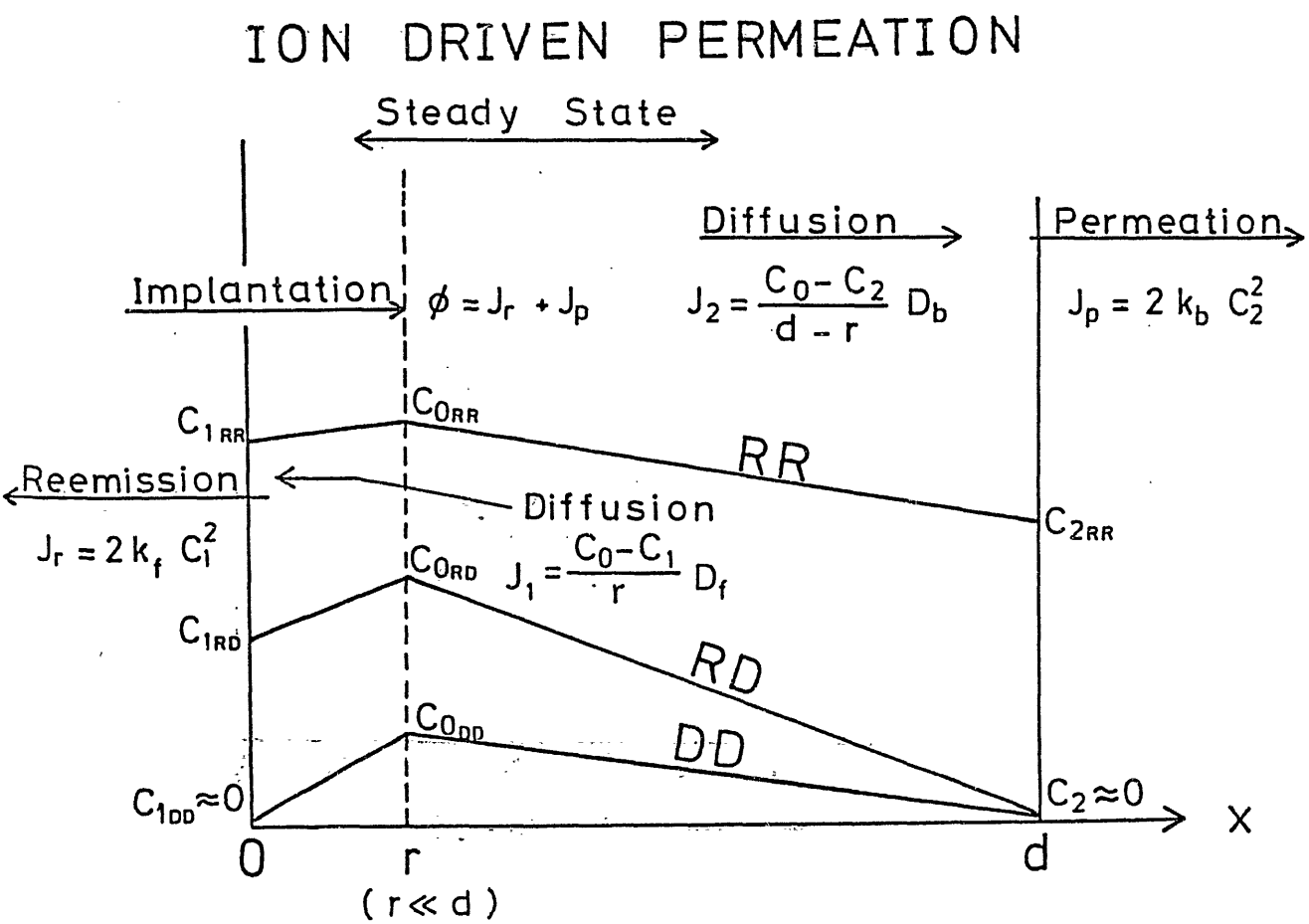

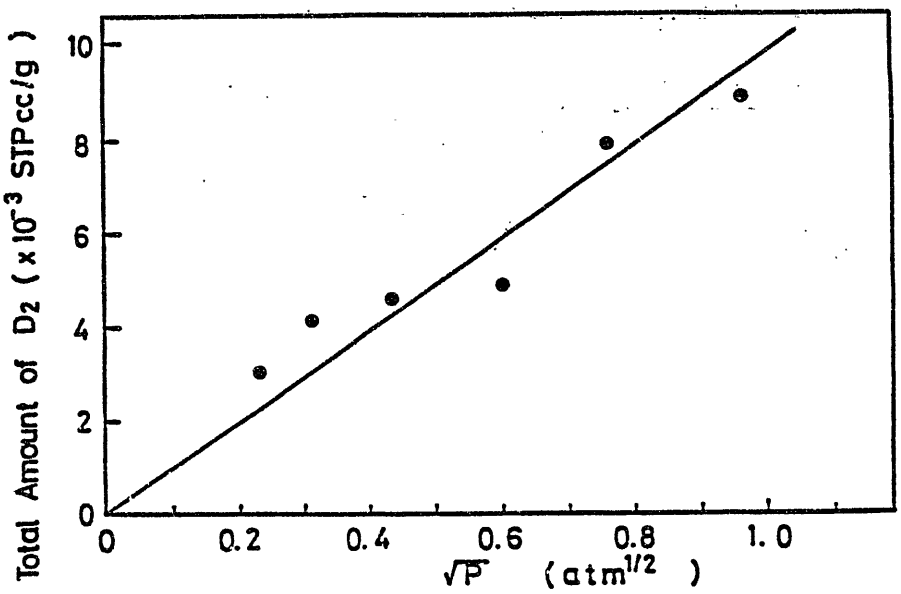

Fig. 8 D_2 Gas Pressure Dependence of Total Amount of D_2 Released from Graphite.

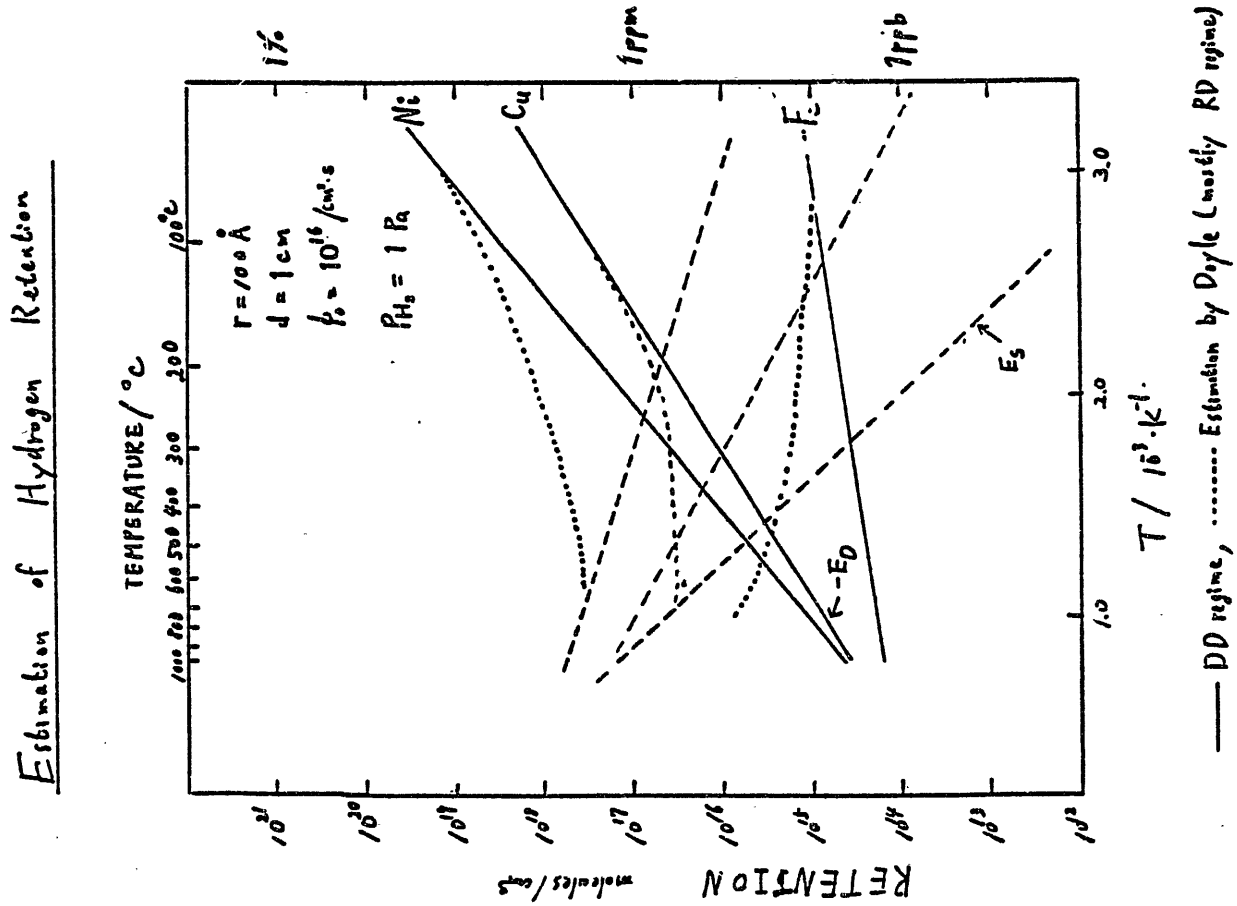

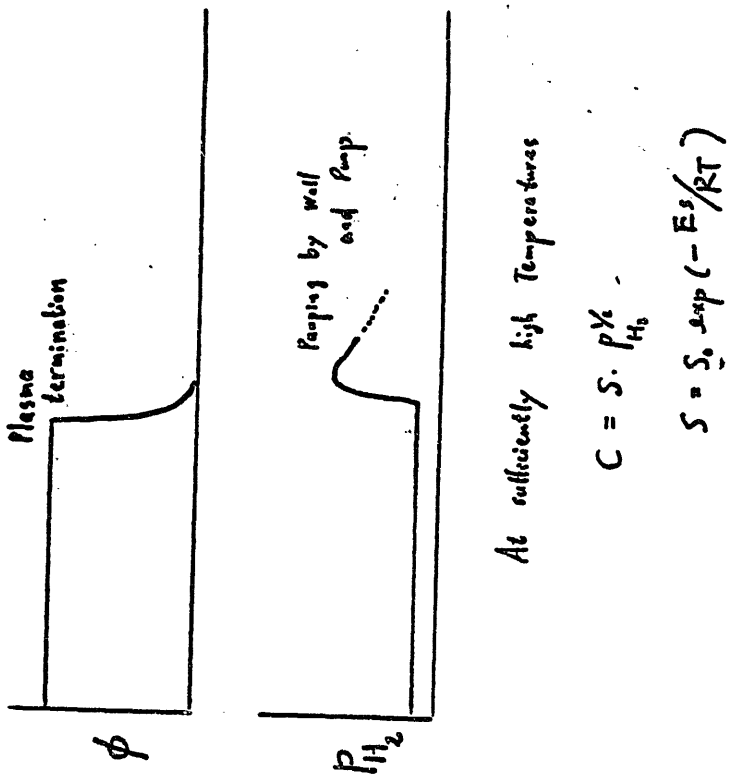

At sufficiently high Temperatures

$C = S \cdot p_{H_2}^{1/2}$

$S = S_0 \exp(-E_s/RT)$

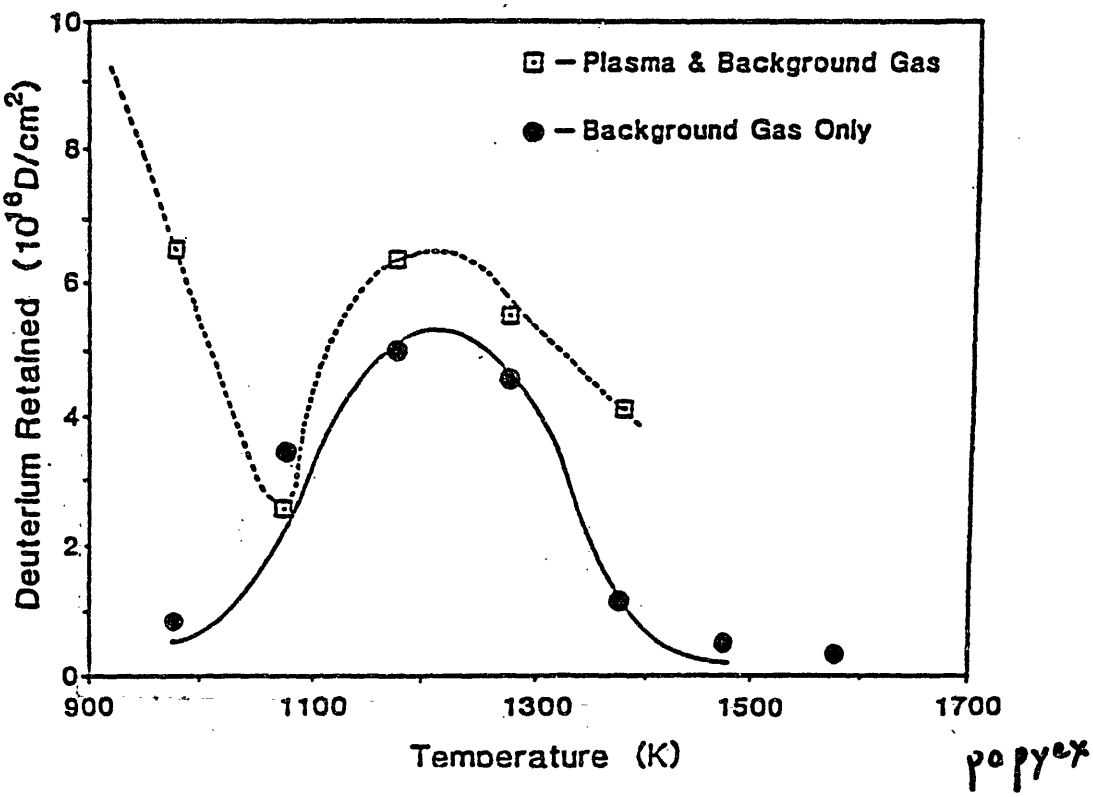

papyex

Causey

Estimation of Hydrogen Permeation

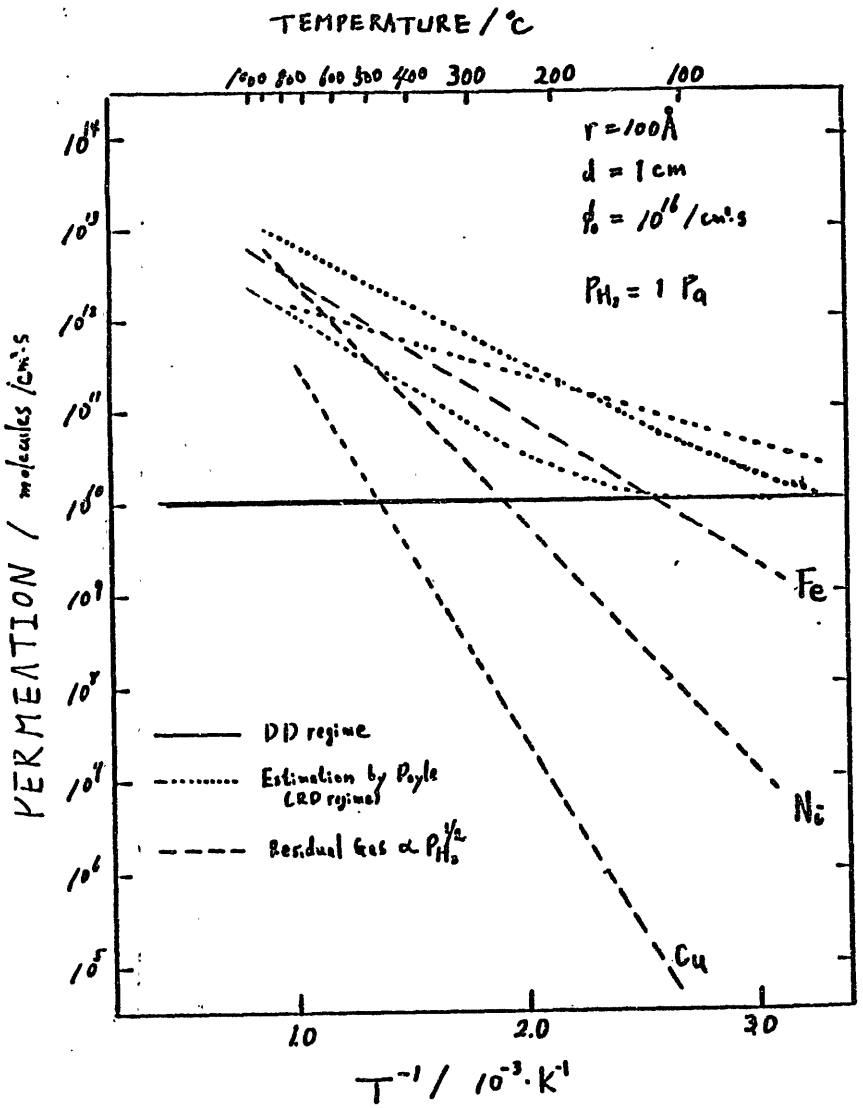

Transition State

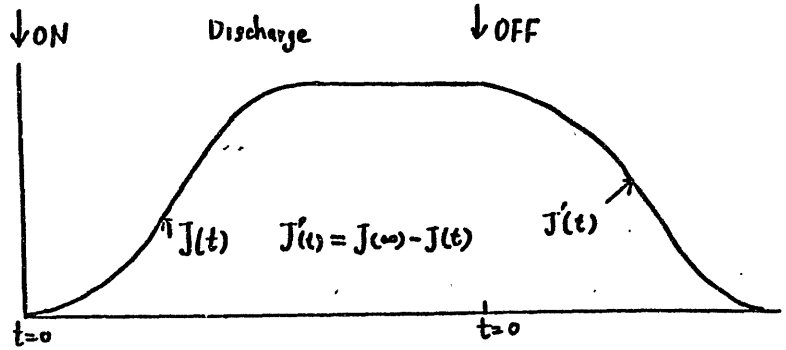

No change in
- Diffusion (D)
- Recombination (k_r, σ)
- Reversible Trapping (T)

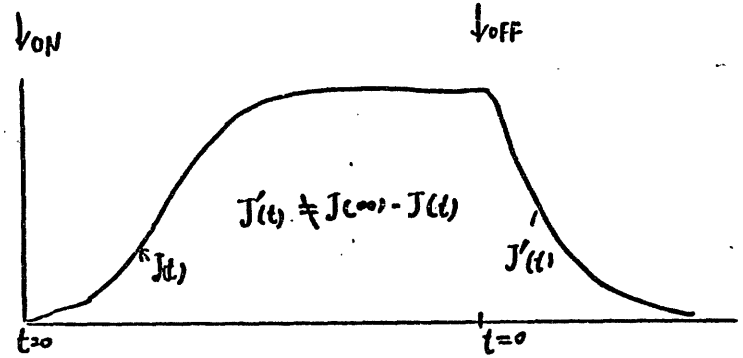

Irreversible change in
- D
- k_r, σ
- T

Trap production during discharge

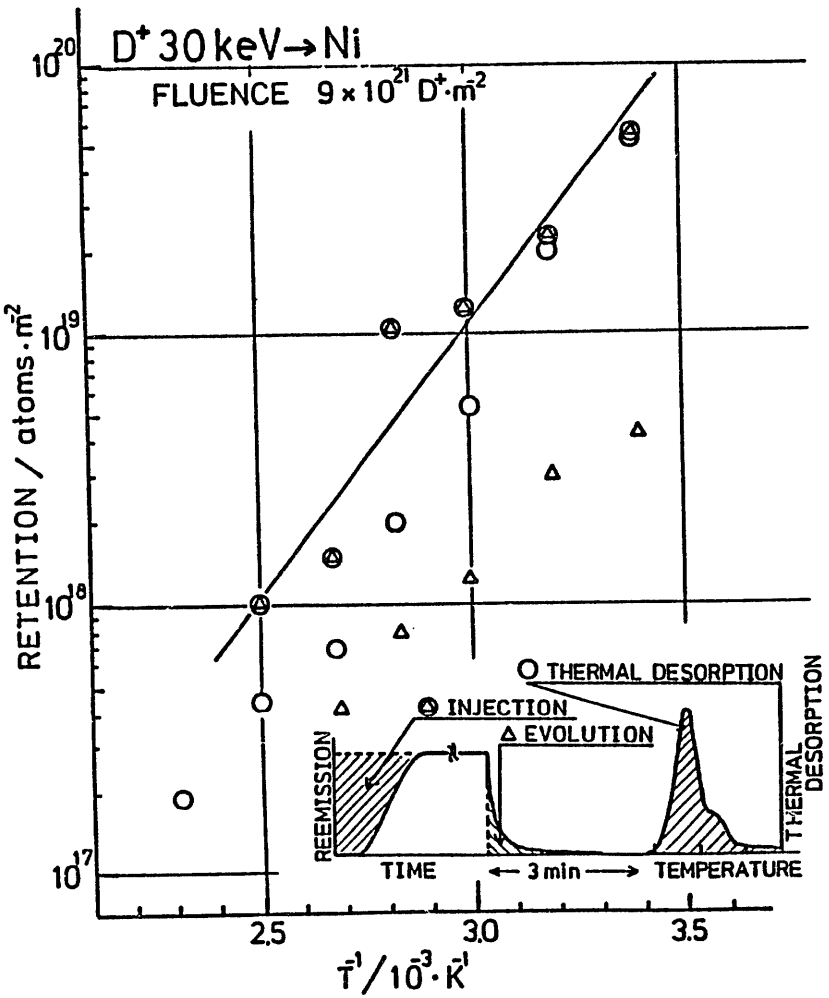
D+ 30 keV → Ni
FLUENCE 9 × 10^21 D+·m^-2
RETENTION / atoms·m^-2
10^20
10^19
10^18
10^17
2.5
3.0
3.5
T^-1 / 10^-3·K^-1
THERMAL DESORPTION
INJECTION
EVOLUTION
REEMISSION
THERMAL DESORPTION
TIME
3 min
TEMPERATURE

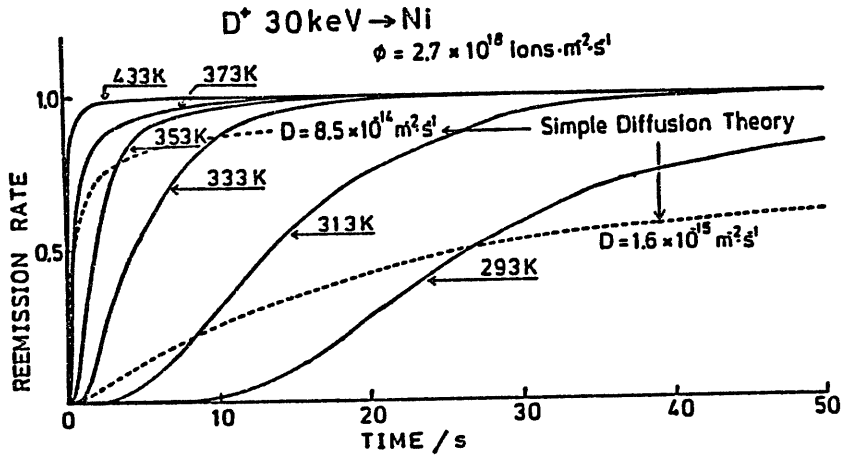
D+ 30 keV → Ni
φ = 2.7 × 10^18 ions·m^-2·s^-1
433K
373K
353K
333K
313K
293K
D = 8.5 × 10^-14 m^2·s^-1
Simple Diffusion Theory
D = 1.6 × 10^-15 m^2·s^-1
REEMISSION RATE
1.0
0.5
0
10
20
30
40
50
TIME / s

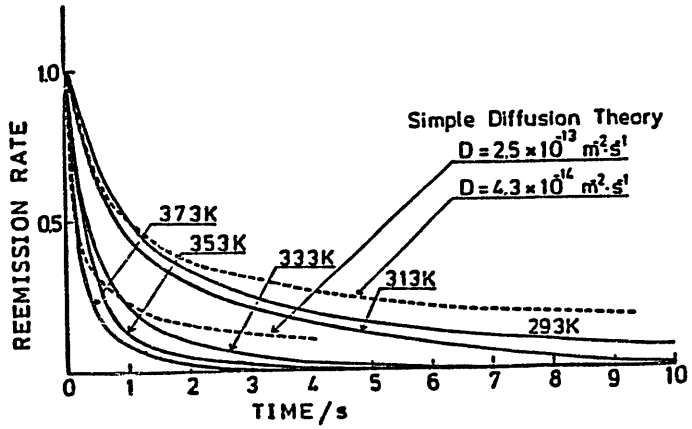
Simple Diffusion Theory
D = 2.5 × 10^-13 m^2·s^-1
D = 4.3 × 10^-14 m^2·s^-1
373K
353K
333K
313K
293K
REEMISSION RATE
1.0
0.5
0
1
2
3
4
5
6
7
8
9
10
TIME / s

Change of Reemission and Retention with TIME and Flux

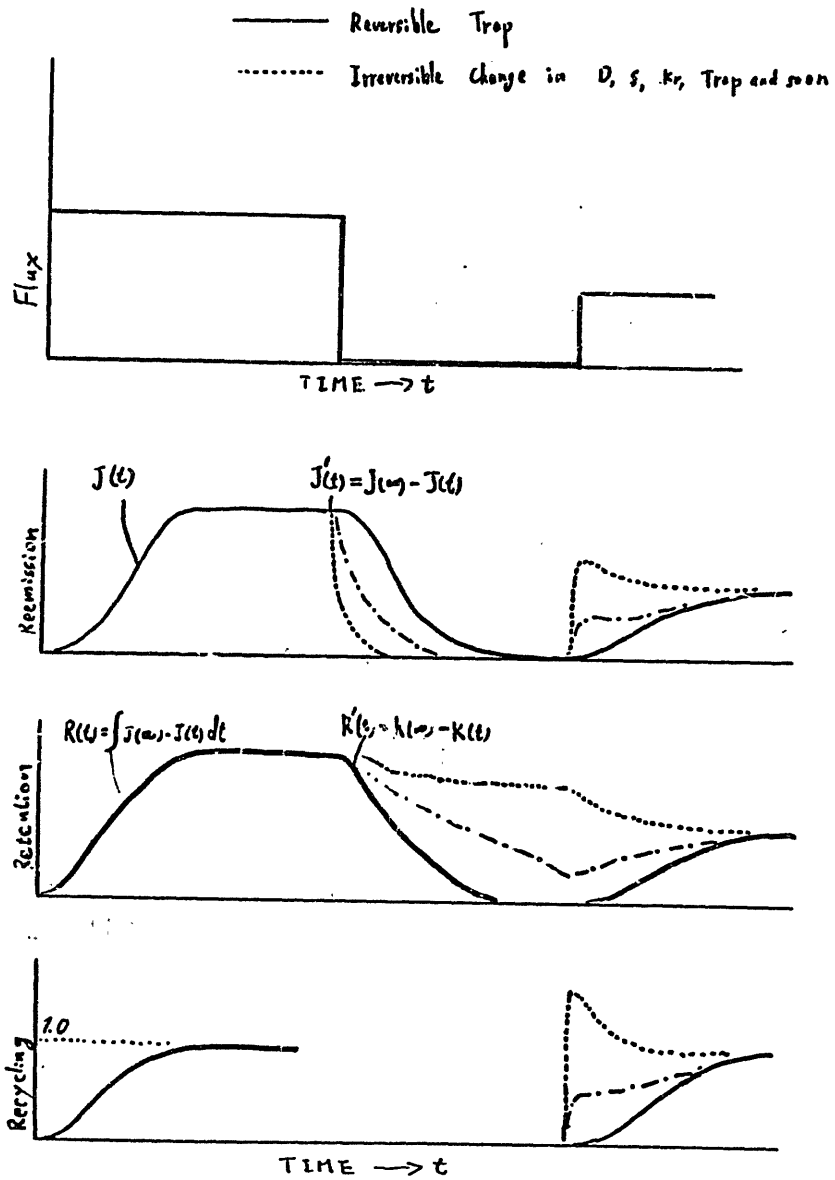

Change of Reemission and Retention with TIME and TEMPERATUR

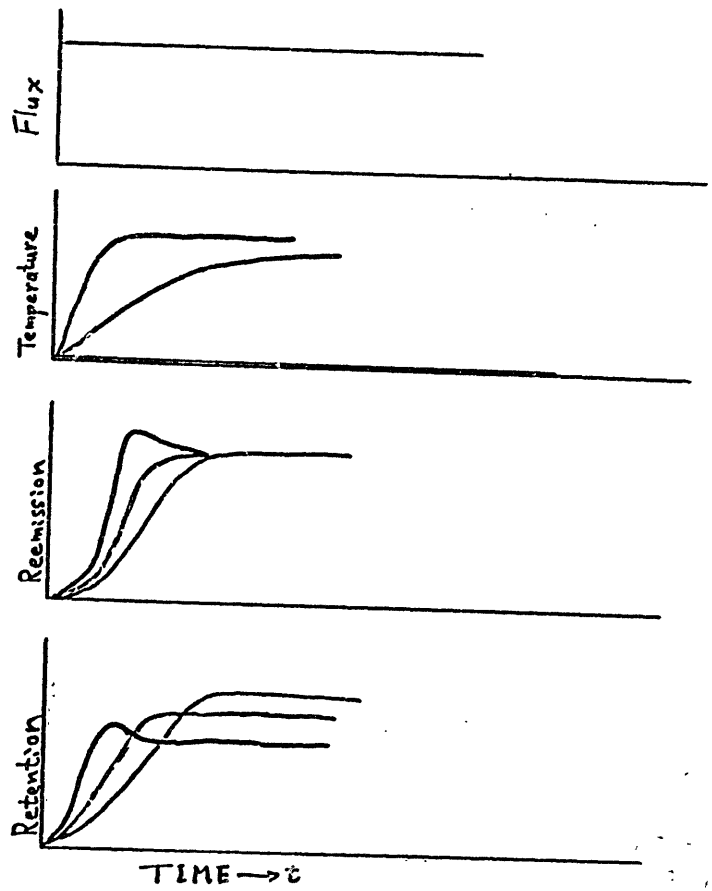

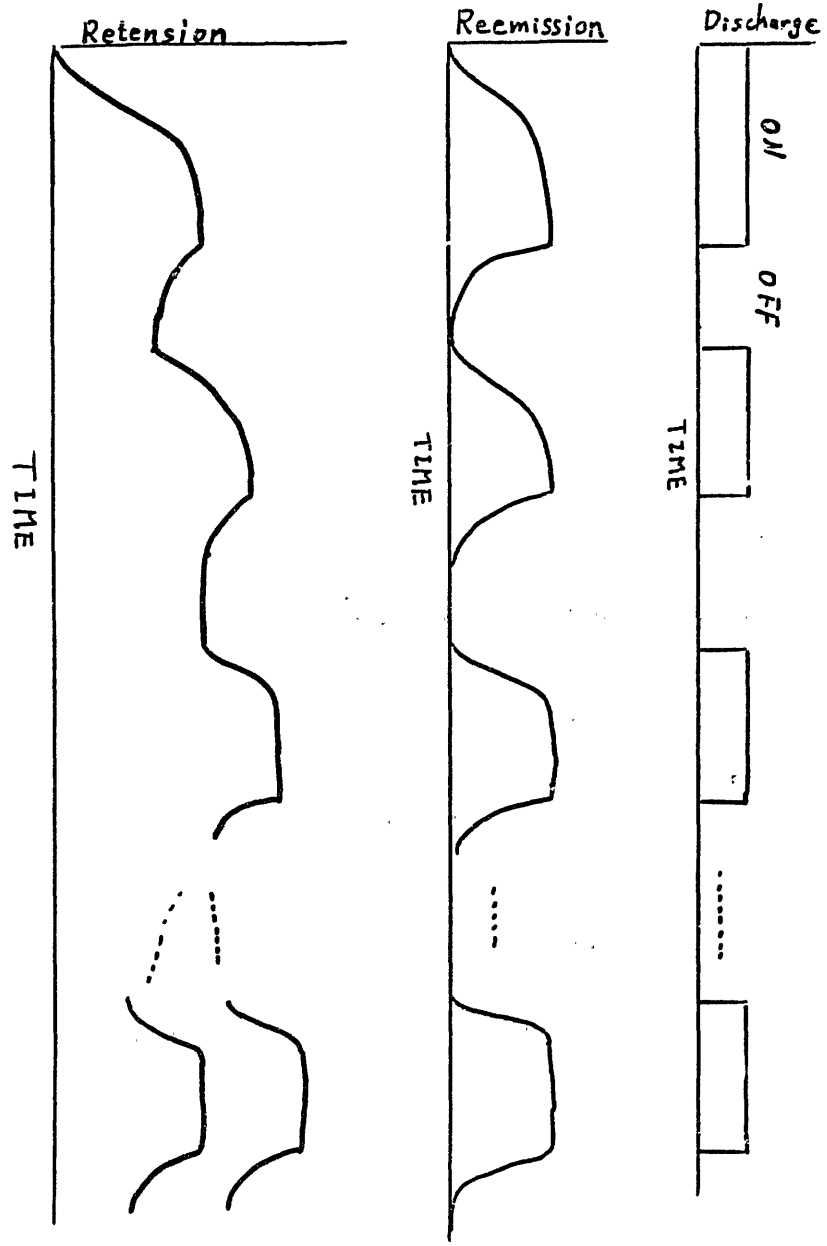

Change of Reemission and Retention with Sample history

Estimation of Retention, Permeation and Recycling

T. Tanabe(Osaka Univ.)

Material parameters	Data Needs
Solubility	for low H_2 pressure
Diffusivity	
Permeability	
Recombination	
Trapping	above RT

Plasma Parameters

Plasma density

Confinement time, Pulse length, Duty ratio

Particle loading (Energy and FLUx)

Heat loading (Radiation, Particle)

Scenario for time and temperature variation

Speciality of Graphite

- large trapping energy
- Significant Solubility of H_2 at high temperature

  $C \approx S \cdot p^{1/2}$
- Chemical reaction during the desorption

Estimation of Retention, Permeation and Recycling

T. Tanabe(Osaka Univ.)

Material parameters

- Solubility
- Diffusivity
- Permeability
- Recombination
- Trapping

Plasma Parameters

- Plasma density
- Confinement time, Pulse length, Duty ratio
- Particle loading (Energy and FLUx)
- Heat loading (Radiation, Particle)

Scenario for time and temperature variation

Tritium Inventory

K.L. Wilson

Sandia National Laboratories
Livermore California, USA

Abstract

Tritium inventory estimates for TFTR and CIT are summarrized. Modeling is too imprecise to provide accurate calculations. Instead, tritium inventory is estimated using an empirical approach.

HYDROGEN-GRAPHITE RECYCLING

I. HYDROGEN RETENTION IN GRAPHITE

-- MECHANISMS

-- SUPERSHOT CONDITIONING IN TFTR

II. THE CO-DEPOSITION MECHANISM

-- WALL PUMPING IN JET

-- LABORATORY SIMULATION

III. TRITIUM INVENTORY IN GRAPHITE DEVICES

-- THEORETICAL APPROACH

-- EMPIRICAL APPROACH

presented by:

K. L. Wilson
Sandia National Laboratories
Livermore CA 94550

THERE ARE AT LEAST FOUR MECHANISMS FOR HYDROGEN RETENTION DURING PLASMA-GRAPHITE INTERACTION

- SATURATED LAYER
- POROSITY
- TRANSGRANULAR DIFFUSION AND TRAPPING
- CO-DEPOSITION

CONTRIBUTORS

SANDIA
M. BASKES
D. BRICE
R. CAUSEY
B. DOYLE
W. HSU
A. PONTAU
K. WILSON

ORNL
R. CLAUSING
R. LANGLEY

PPPL
F. DYLLA
D. HEIFETZ
P. LA MARCHE
M. ULRICKSON

LABORATORY STUDIES HAVE IDENTIFIED THREE SOURCES OF HYDROGEN RETENTION IN GRAPHITE

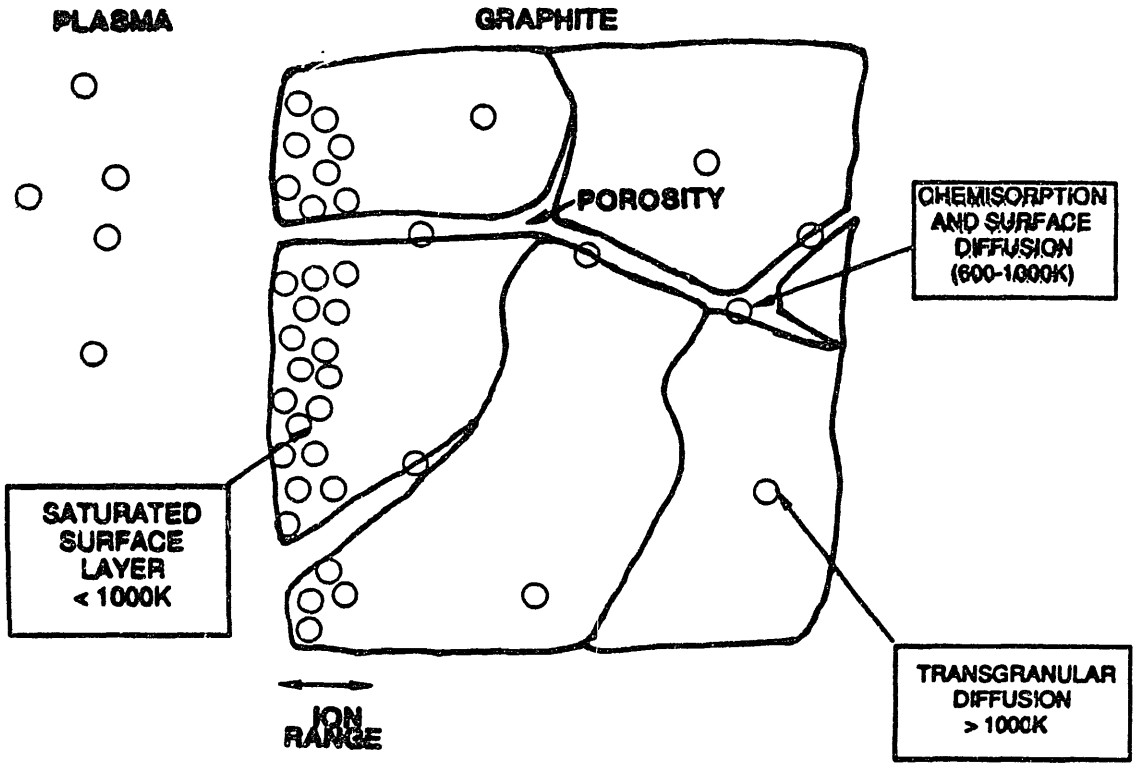

H. HYDROGEN RETENTION IN GRAPHITE

THE LOCAL MIXING MODEL CAN PREDICT ISOTOPE EXCHANGE IN THE SATURATED LAYER

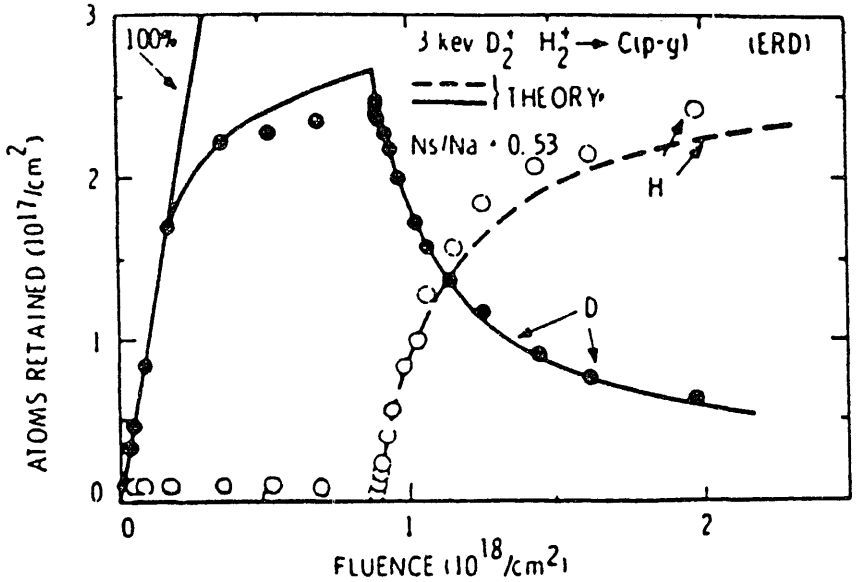

RELEASE OF H DEPENDS ON LOCAL $H/_{H+D}$ RATIO

DOYLE et al. (1980)

TRITIUM RETENTION IN GRAPHITE IS TEMPERATURE DEPENDENT

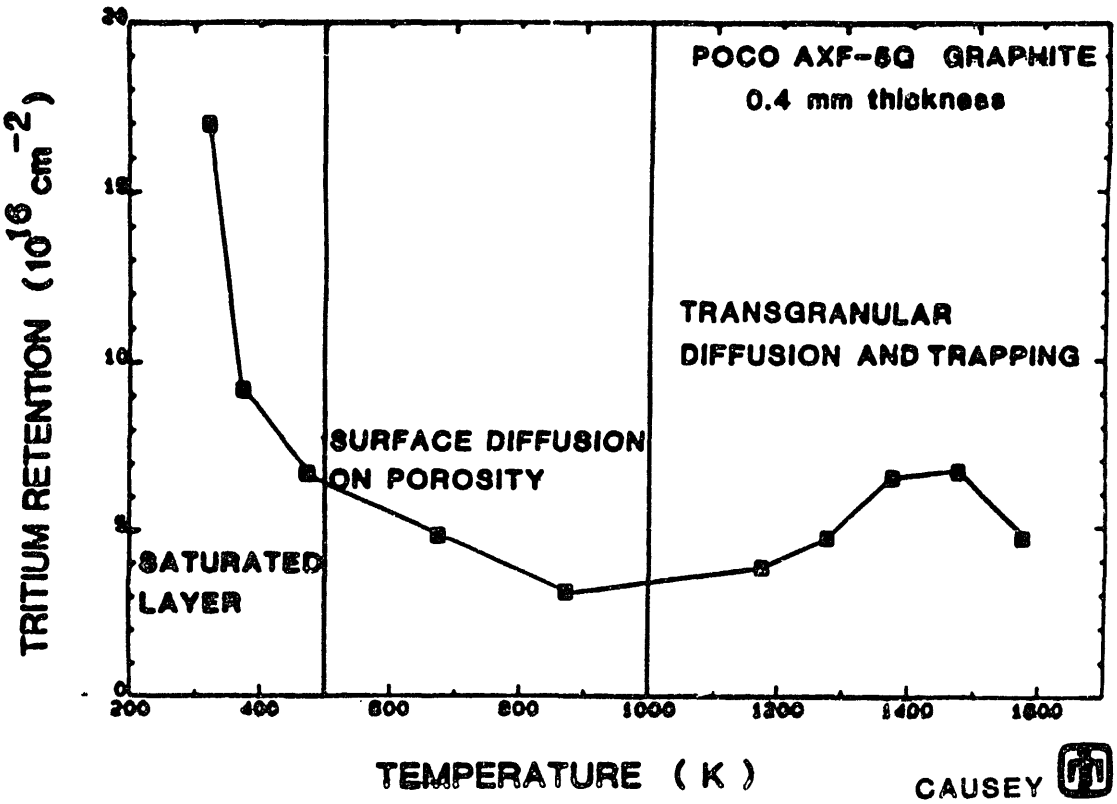

CAUSEY

TRANSGRANULAR DIFFUSION AND TRAPPING IS OBSERVED IN POCO AXF-5Q GRAPHITE ABOVE 1000K

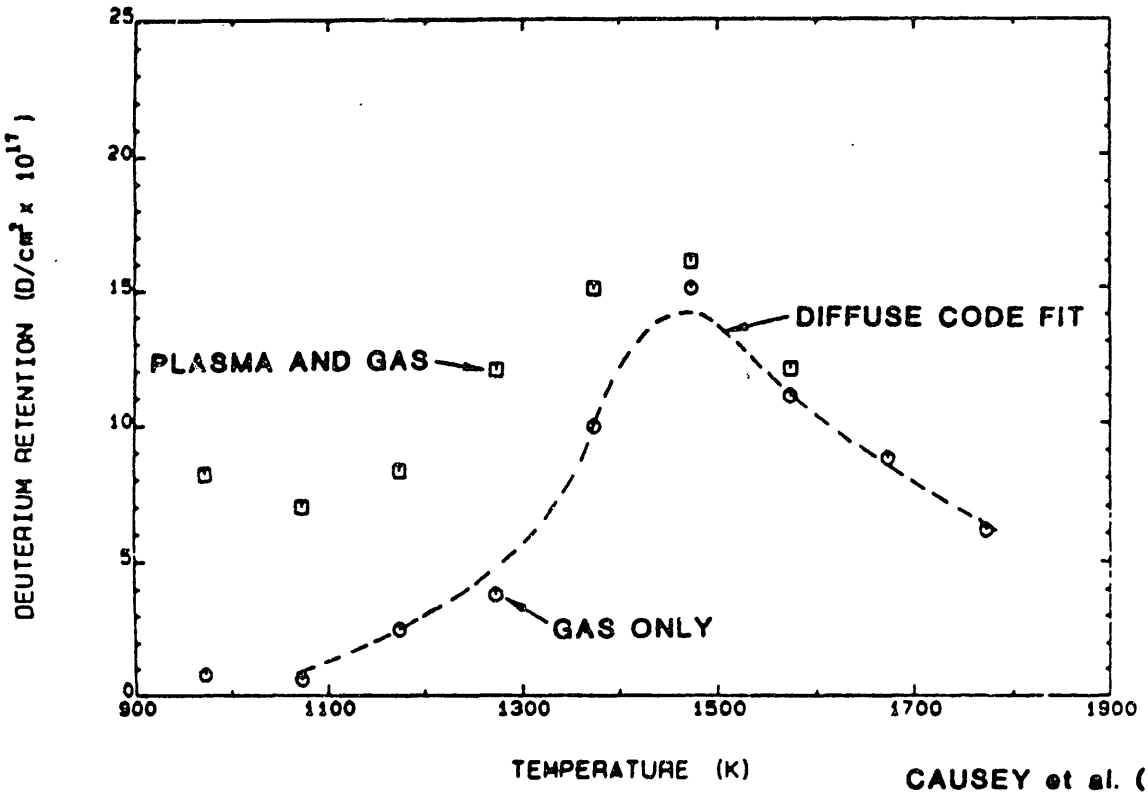

CAUSEY et al. (1986)

SURFACE DIFFUSION OF TRITIUM INTO POCO AXF-5Q GRAPHITE FOR 1.5 HOURS

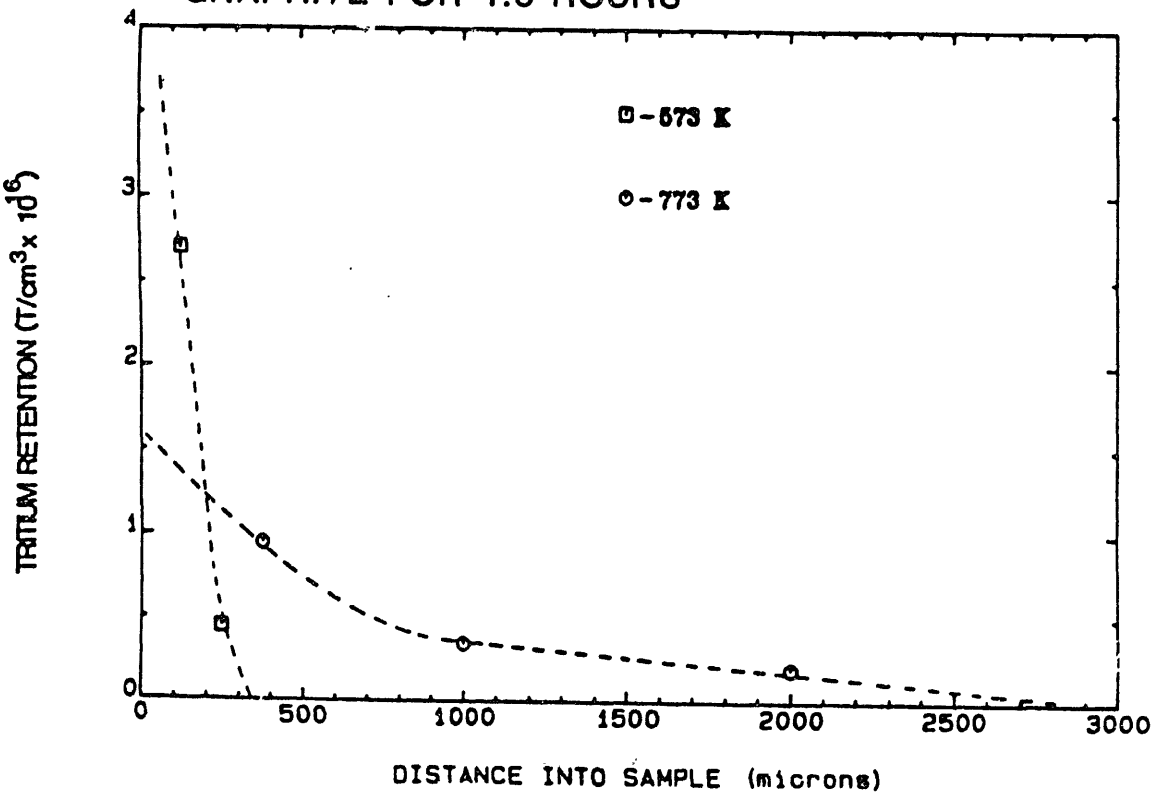

CAUSEY

TFTR SUPERSHOTS 23260

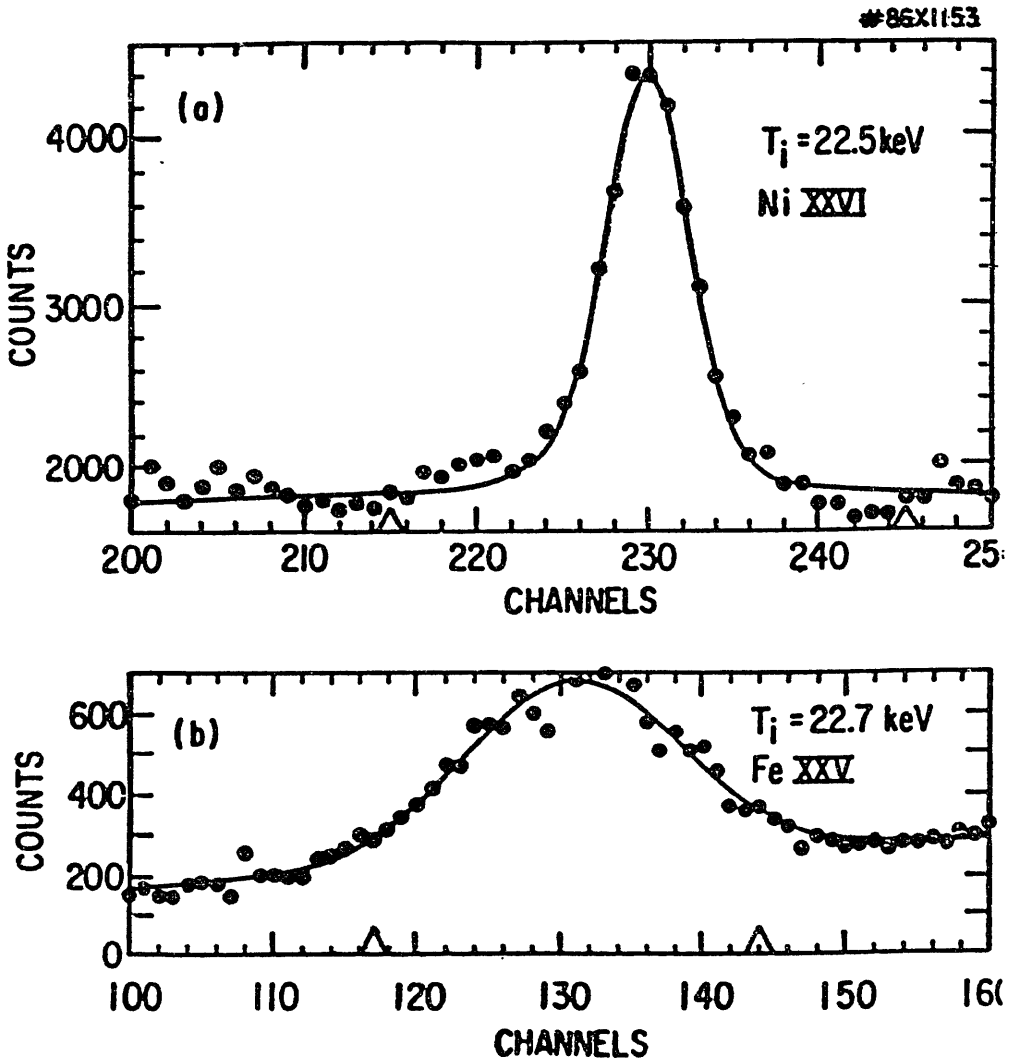

SUPERSHOT CONDITIONING IN TFTR

- Supershots require approx. 10 conditioning discharges of low density deuterium or helium.
- The conditioning discharges have $Z_{eff} \sim 6$ (i.e., carbon).
- After conditioning, the global recycling coefficient is ≤ 0.5 (versus approx. 1.0 before conditioning) for a limited number of shots.
- A gas input of 100 t-l/s will reload the graphite and degrade the low recycling conditions.
- Depletion of the saturated layer (approx. 10nm thickness) by the conditioning shots can account for the observed transient pumping.

Adapted from Dylla, et al.

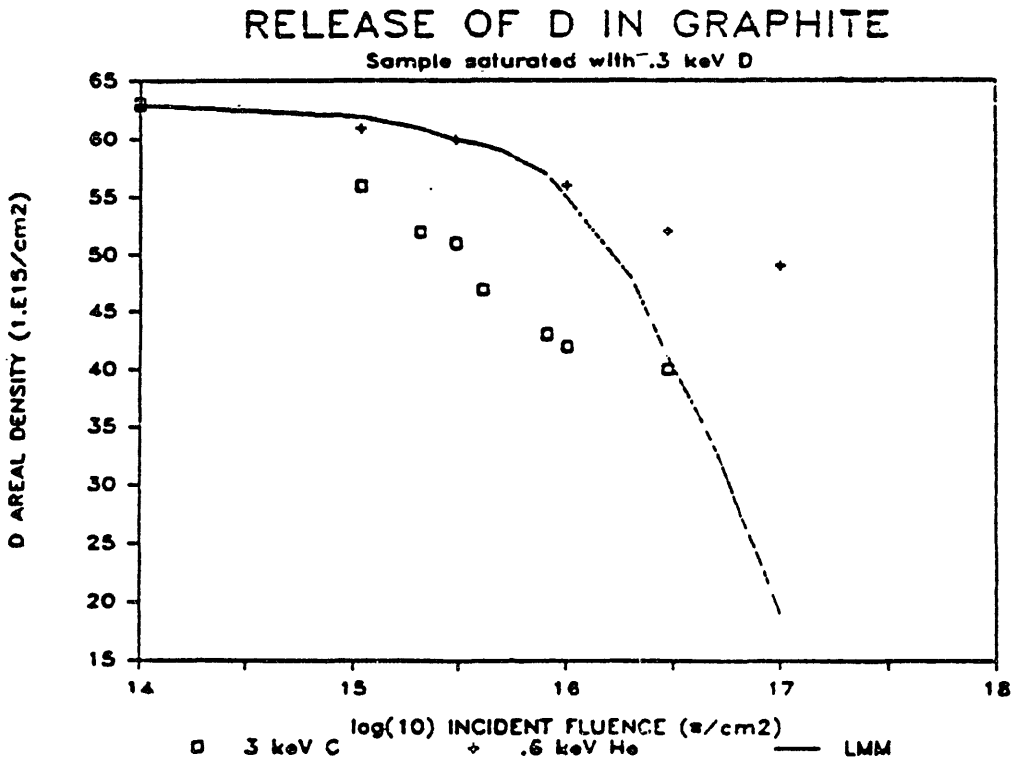
RELEASE OF D IN GRAPHITE
Sample saturated with .3 keV D
D AREAL DENSITY (1.E15/cm2)
65
60
55
50
45
40
35
30
25
20
15
14
15
16
17
18
log(10) INCIDENT FLUENCE (#/cm2)
3 keV C
.6 keV He
LMM

DOYLE

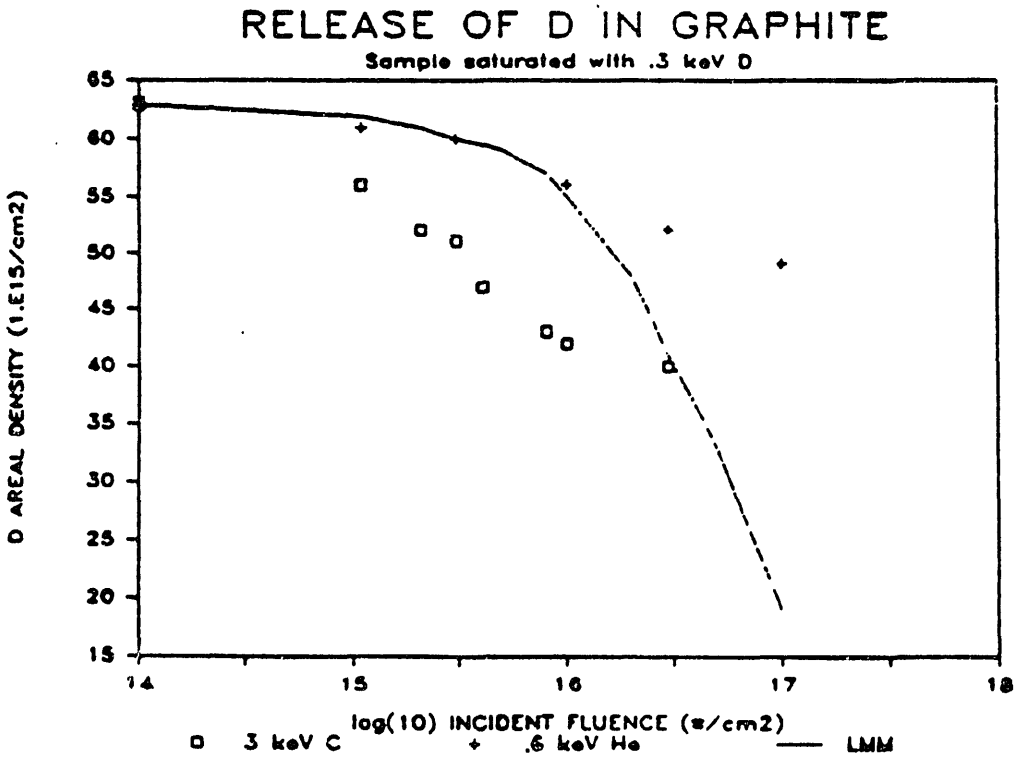
RELEASE OF D IN GRAPHITE
Sample saturated with .3 keV D
D AREAL DENSITY (1.E15/cm2)
65
60
55
50
45
40
35
30
25
20
15
14
15
16
17
18
log(10) INCIDENT FLUENCE (#/cm2)
3 keV C
.6 keV He
LMM

DOYLE

ORNL-DWG 86-18025

RESULTS:

* Beneficial removal of surface D caused by ion-induced release.
  - -Sputtering and burial negligible
  - -C more efficient at releasing D than is He.

* Release cross-section monotonically increases with energy into atomic collisions.

* D retrapped in self-inflicted or releasing-ion damage.

* He ions produce H traps in graphite which are much stronger than H-produced traps.

HYDROGEN RECYCLING CAN BE DECREASED BY USING HELIUM PLASMAS TO DEPLETE THE HYDROGEN CONTENT OF GRAPHITE

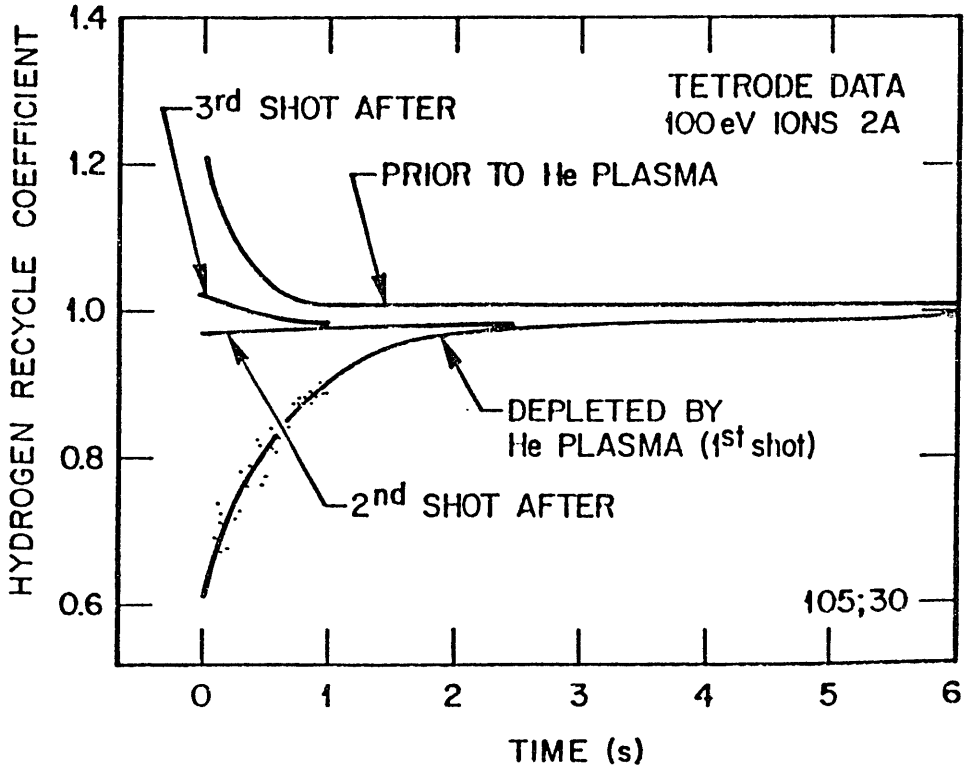

CLAUSING

ornl

Hydrogen Pumping With POCO-AXF5Q Graphite Electrodes

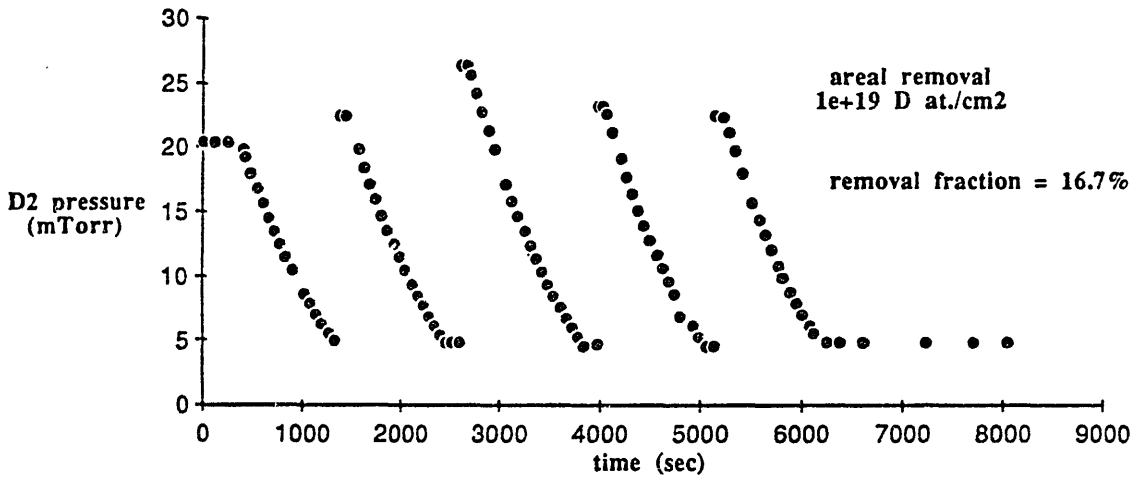

Hydrogen Removal Cannot be Explained by Retention in Graphite

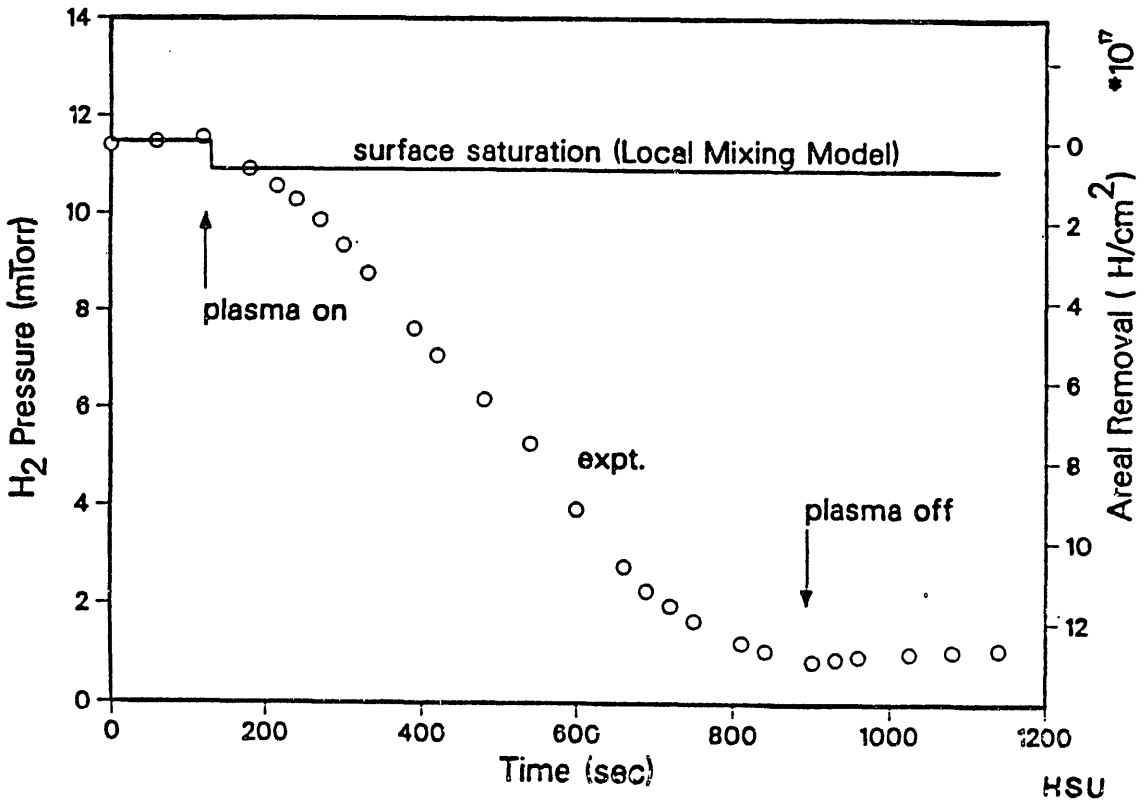

"No deterioration or saturation of the pumping rate has been observed... from shot to shot."

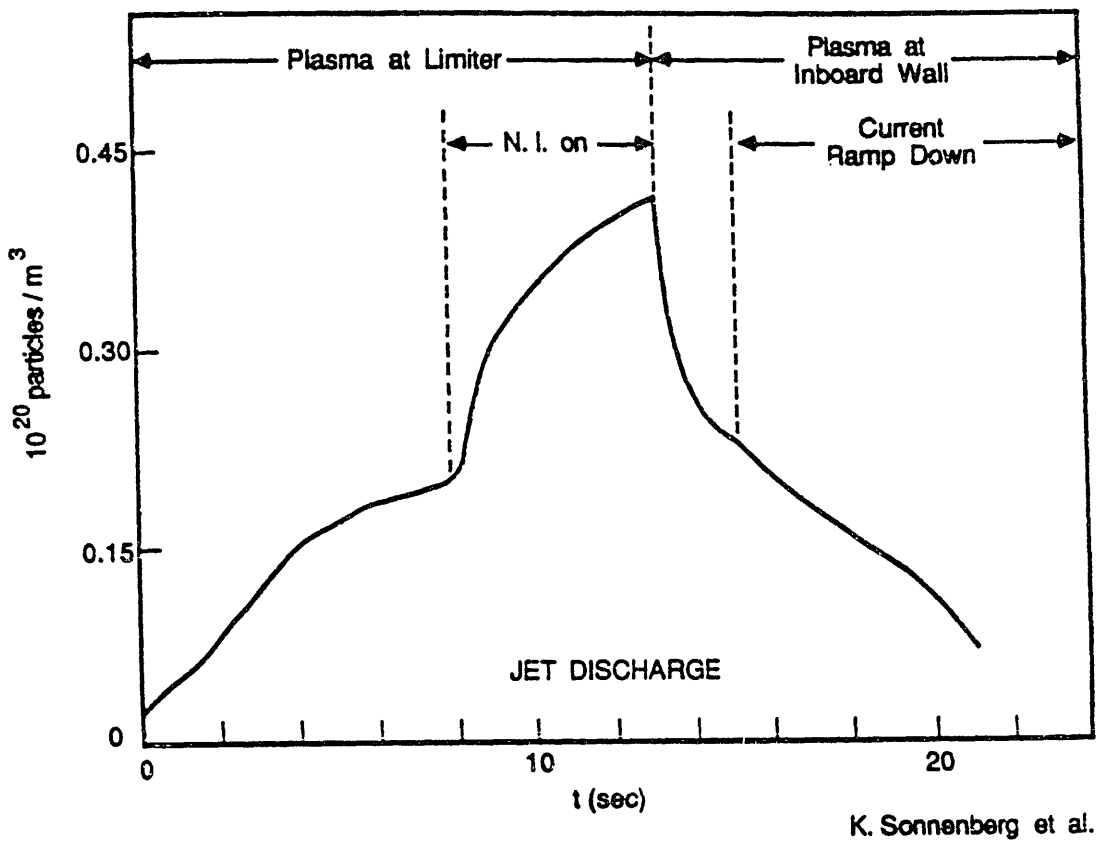

K. Sonnenberg et al.

II. CO-DEPOSITION

CO-DEPOSITION IS THE DOMINANT HYDROGEN REMOVAL MECHANISM

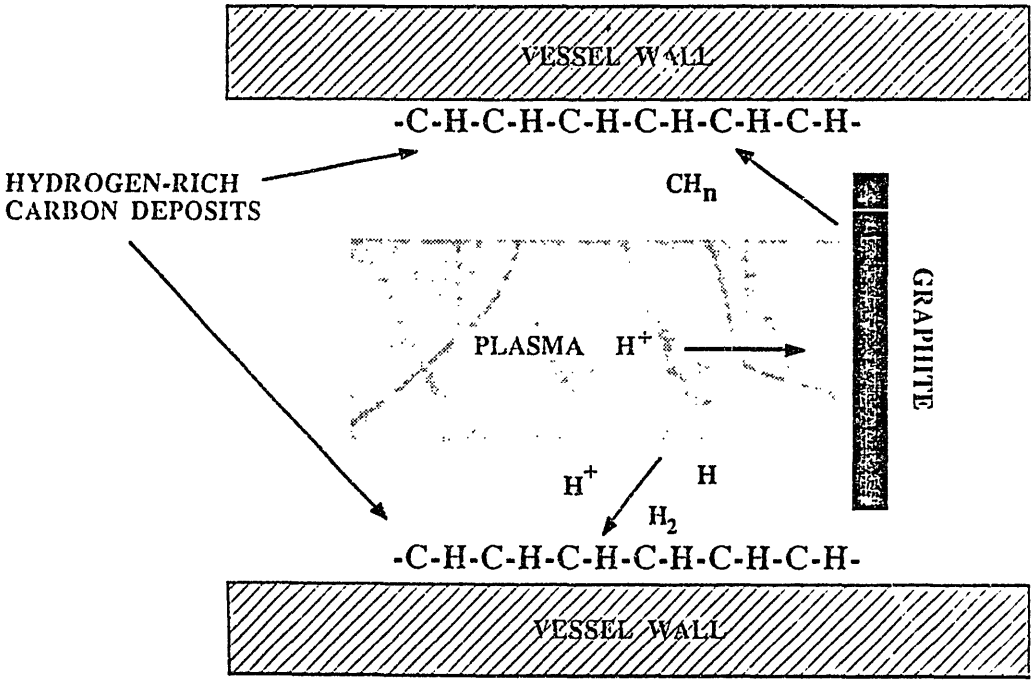

Large Hydrogen Pumping Is Observed Using Dense Carbon Materials (Pyrolytic Carbon)

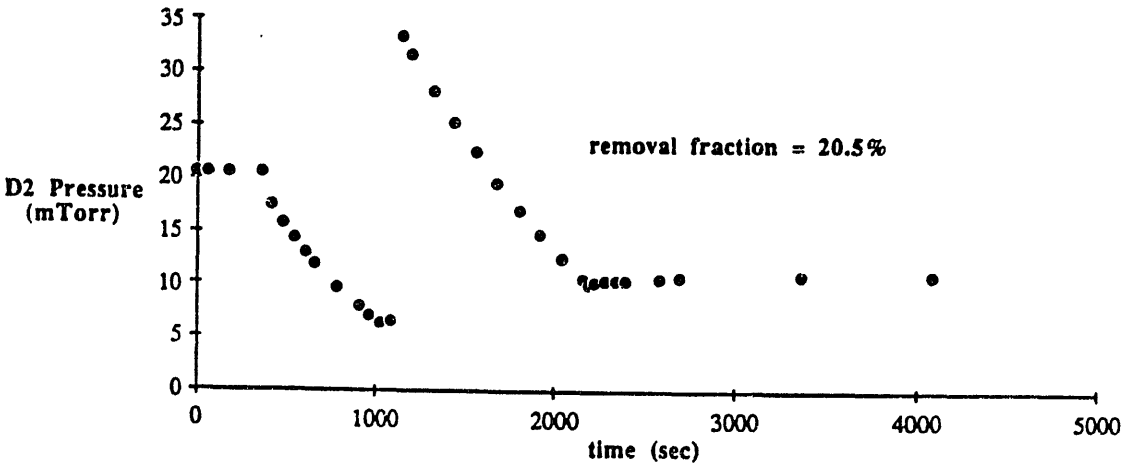

HSU

Hydrogen Removal With SS Electrodes is Consistent With Theory Based on DIFFUSE

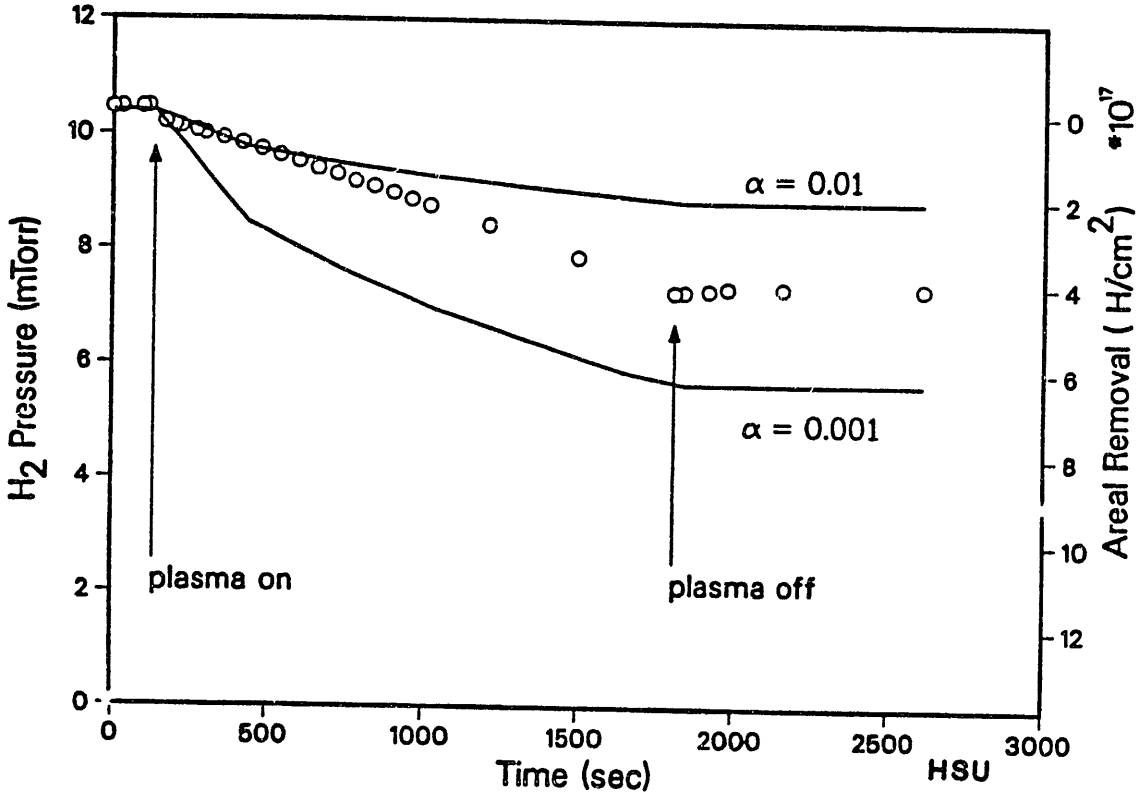

PENNING DISCHARGE

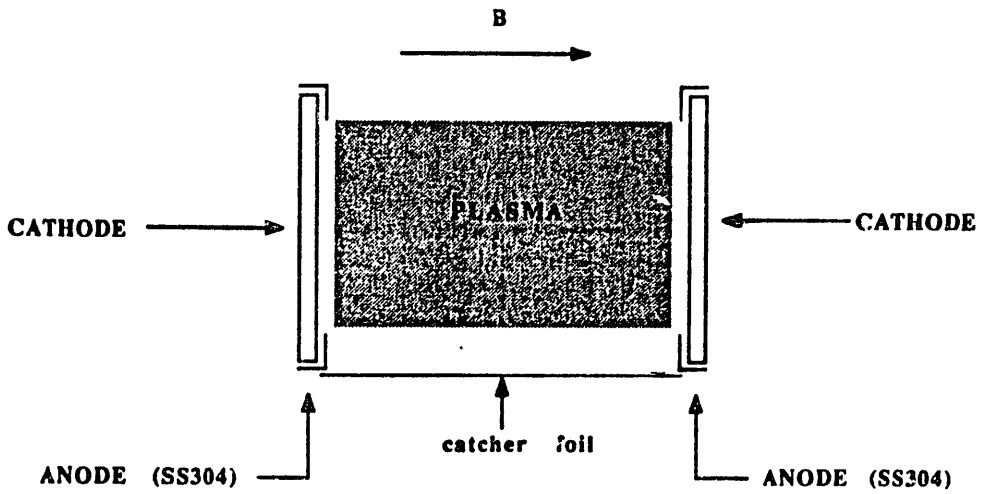

HSU

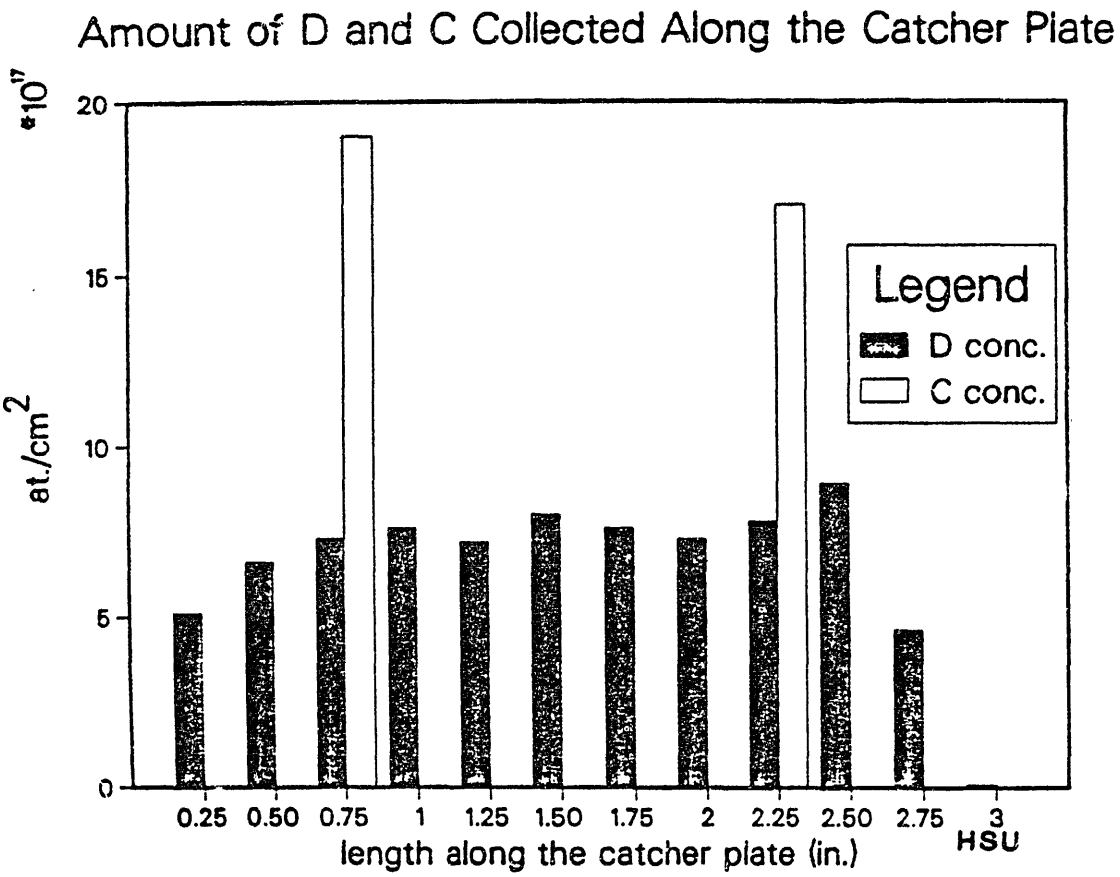

Catcher Strip 8/18/86

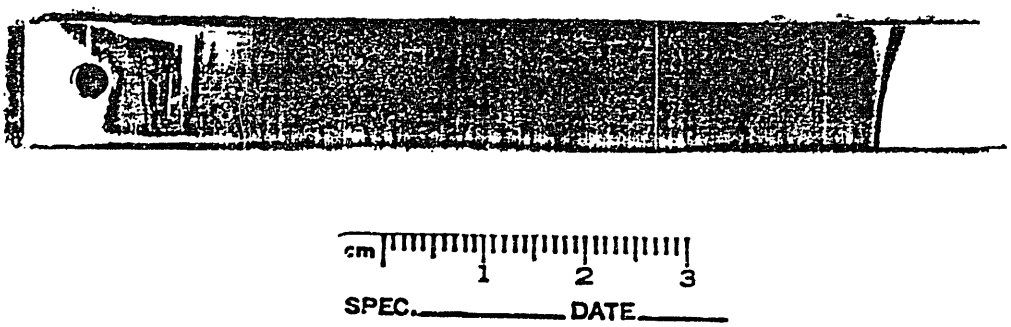

ORNL-DWG 86-18023

HYDROGEN "RETENTION" DOES NOT SATURATE AND SEEMS TO DEPEND ON THE EXPERIMENTAL ARRANGEMENT

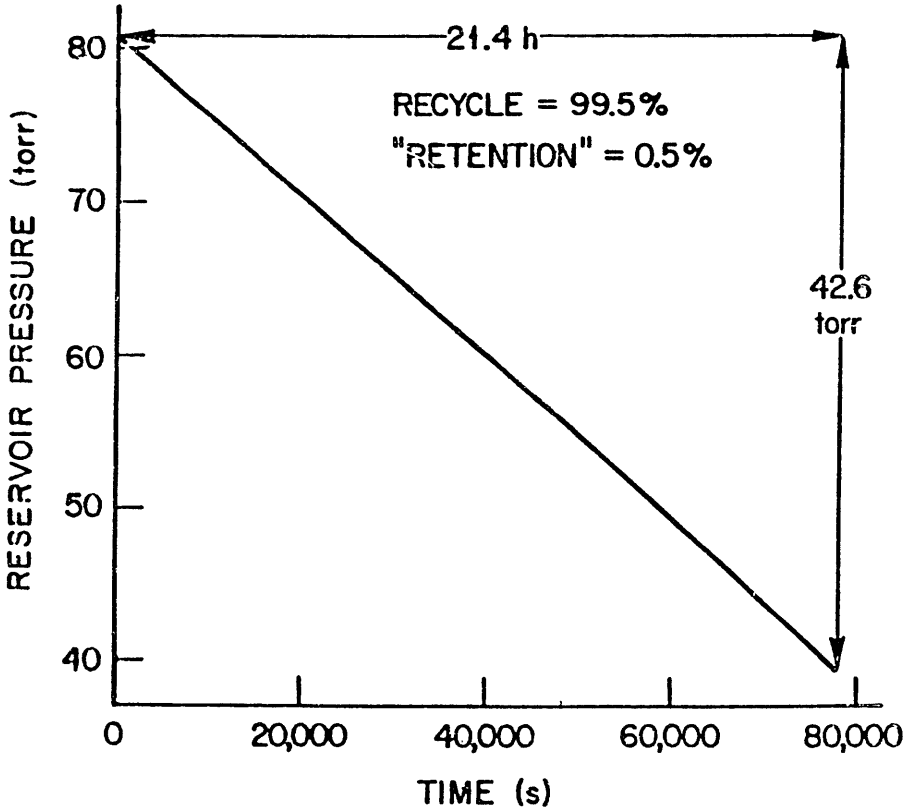

5A GLOW DISCHARGE (no pumping)
145°C ±5, 600cm^2 GRAPHITE
FLUENCE ~ 1×10^{21}/cm^2, "RETAINED" 5×10^{18}/cm^2

CLAUSING ornl

Langley/1986

ORNL-DWG 86-2792 FED

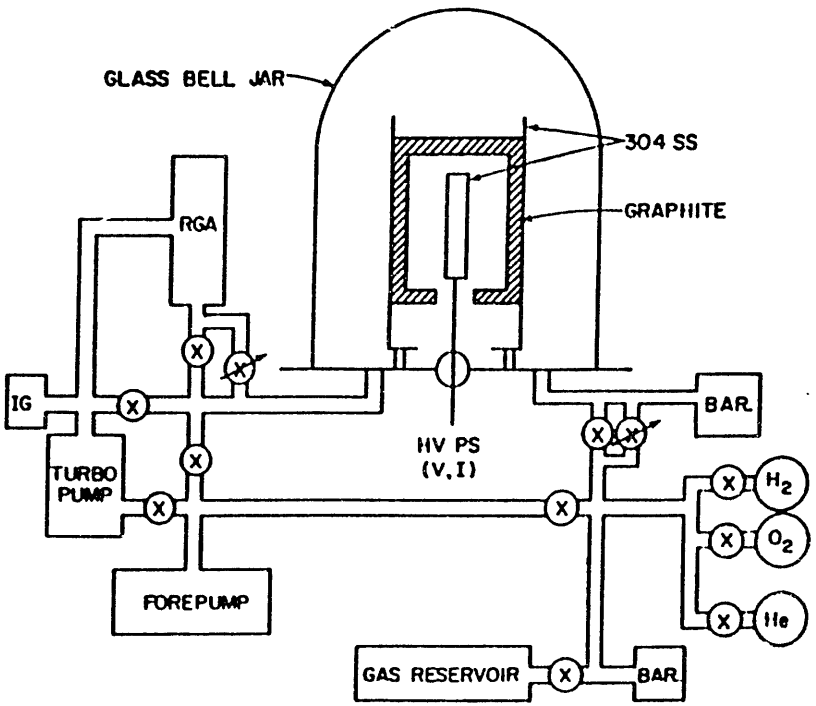

DEUTERIUM IS RETAINED IN THE REDEPOSITED 'TOKAMAKIUM' LAYER

WAMPLER et al. (1986)

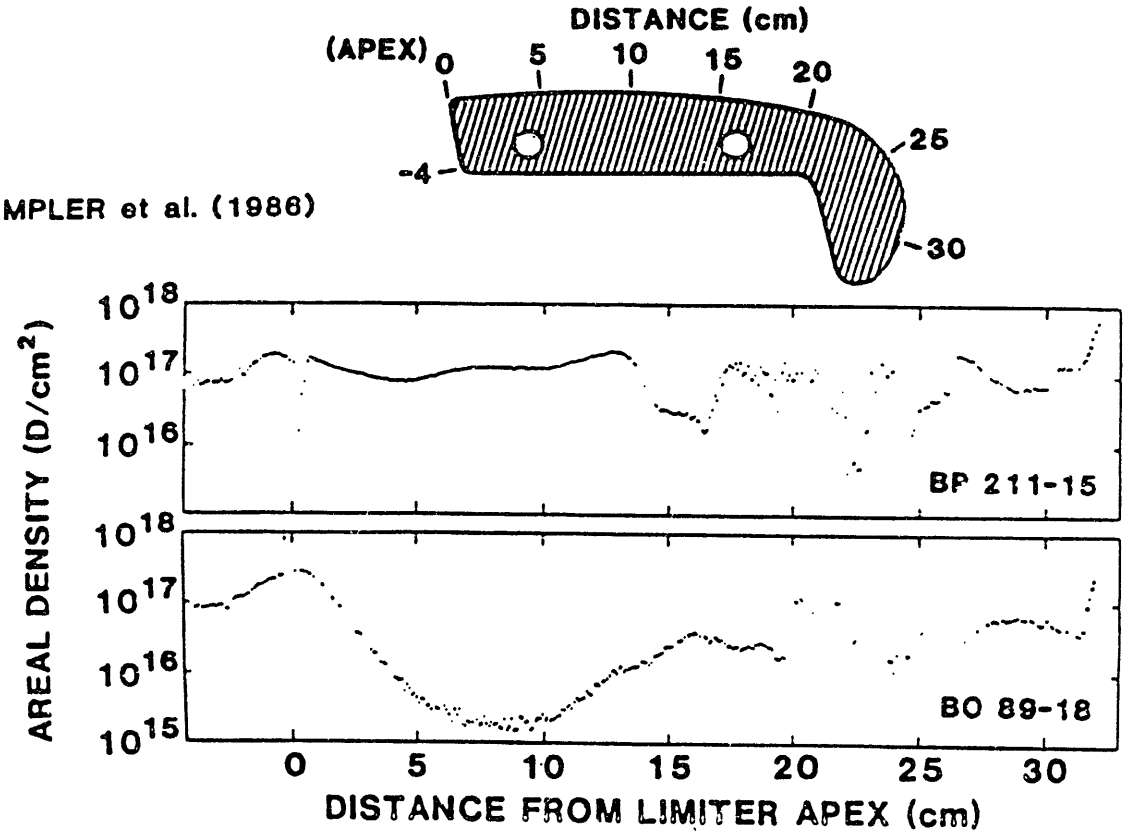

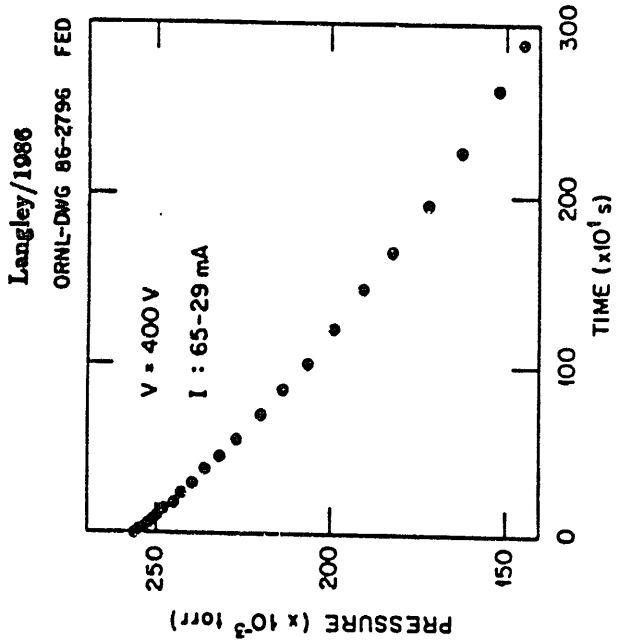

QUANTITATIVELY SIMILAR RESULTS HAVE BEEN REPORTED FOR JET

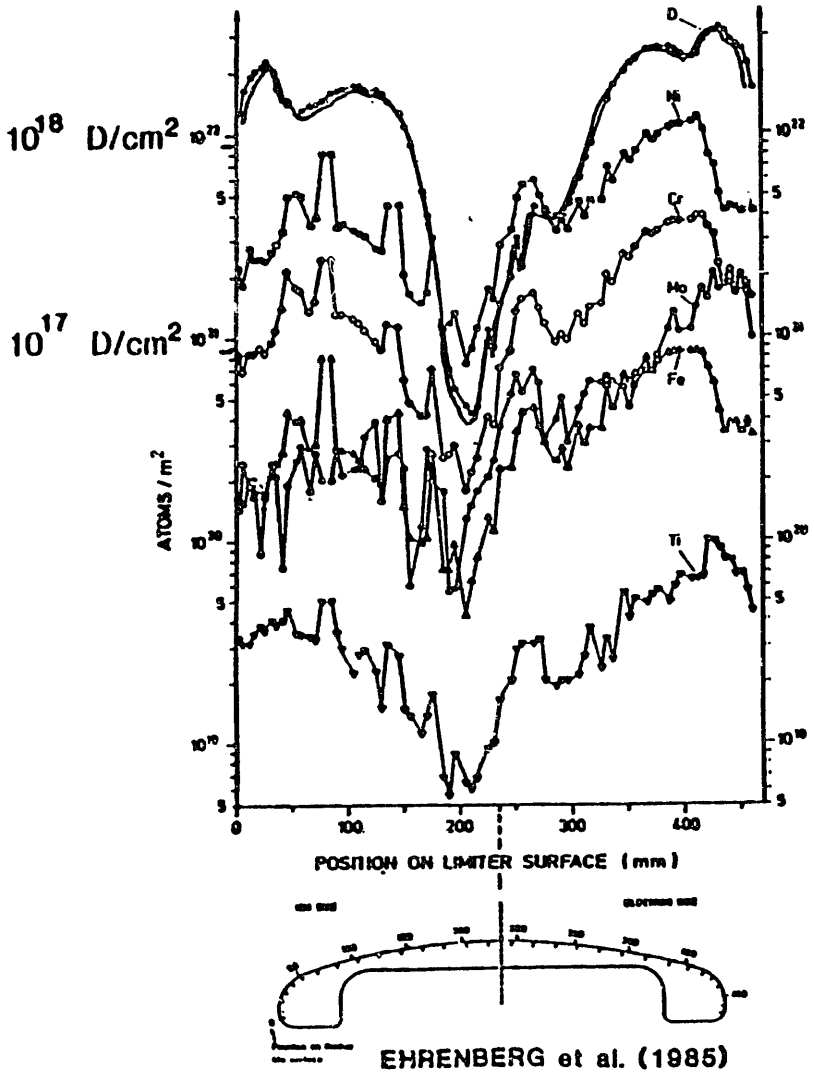

EHRENBERG et al. (1985)

TFTR HAS OVER 2000 kg OF GRAPHITE

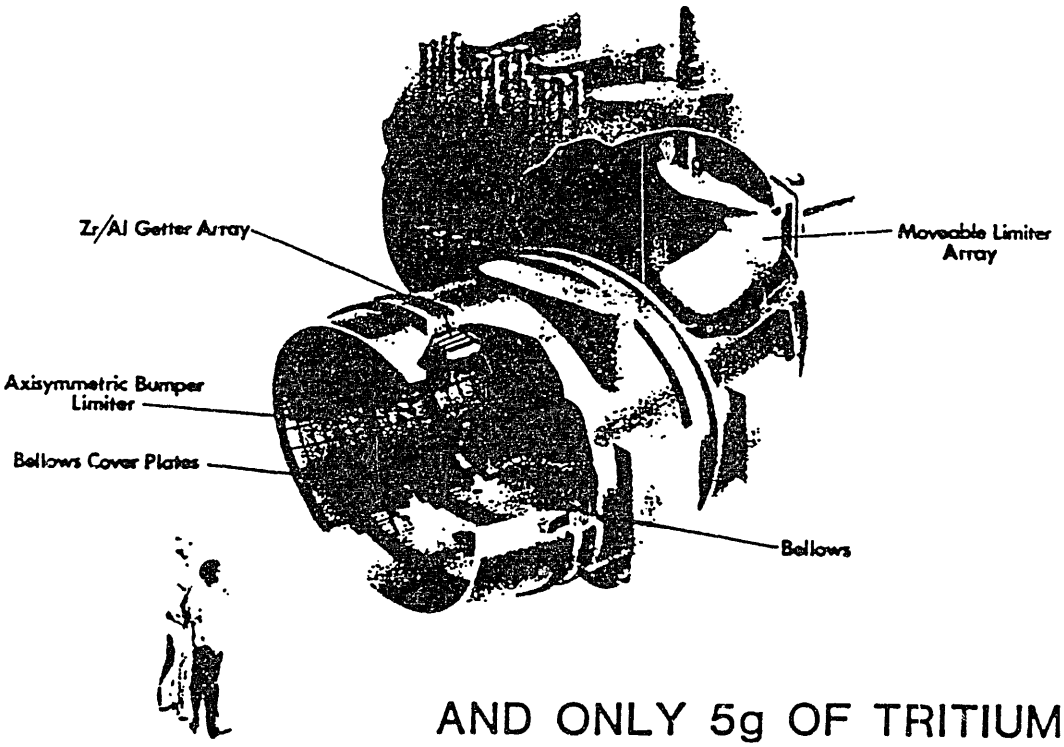

AND ONLY 5g OF TRITIUM

III. TRITIUM INVENTORY

GEOMETRY USED IN TFTR RECYCLE CALCULATIONS WITH DEGAS

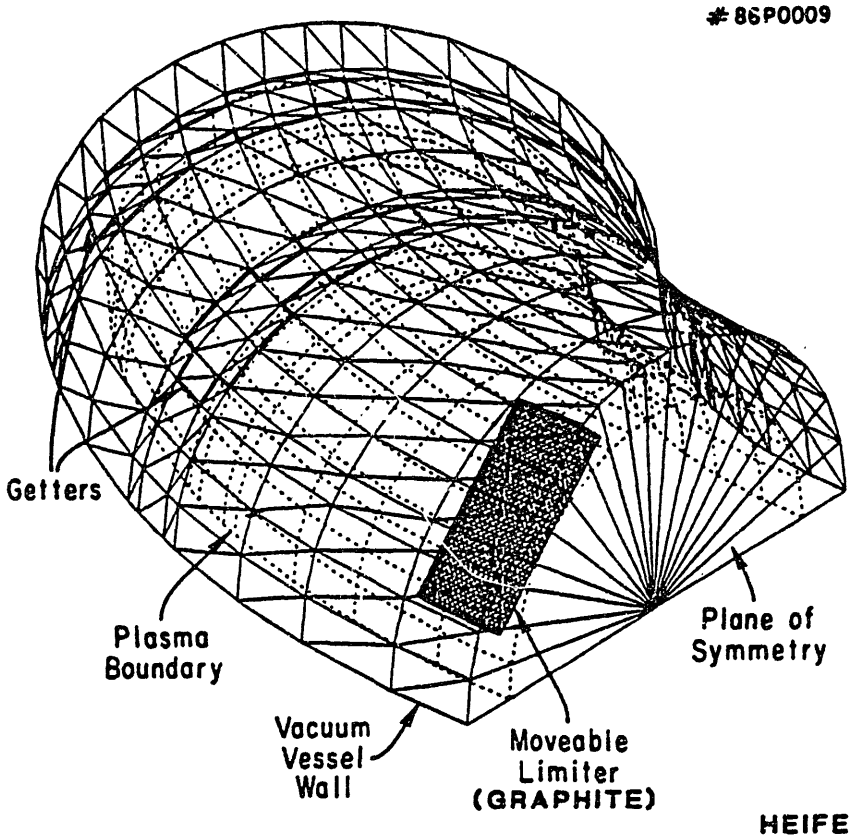

HEIFETZ, PPPL

TFTR RECYCLING CODE

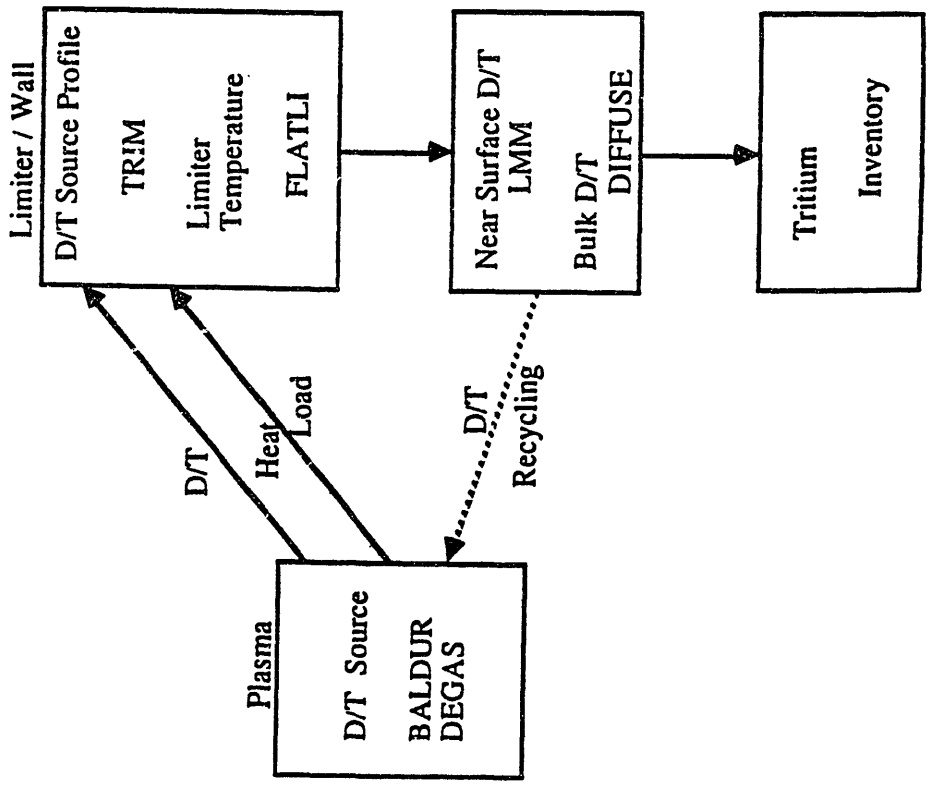

PUMP & DUMP SHOULD NOT BE SEEN IN TFTR BECAUSE OF THE LARGE VARIATION IN POWER FLUX AND TEMPERATURE

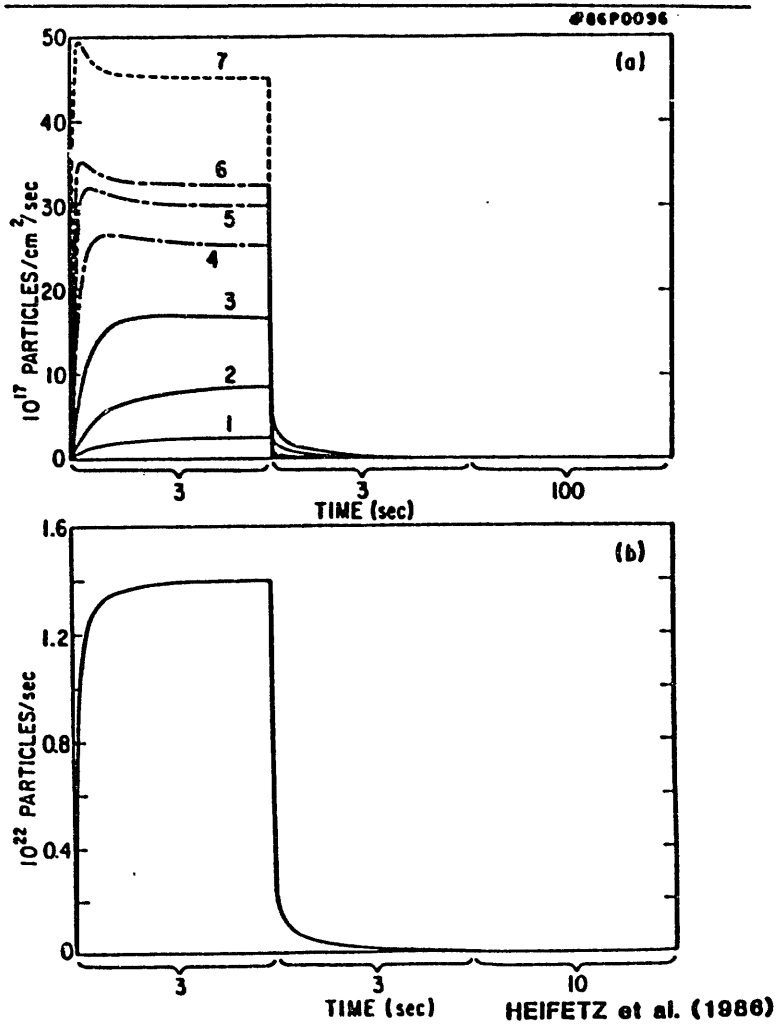

HEIFETZ et al. (1986)

DEGAS CALCULATIONS FOR RECYCLING IN TFTR

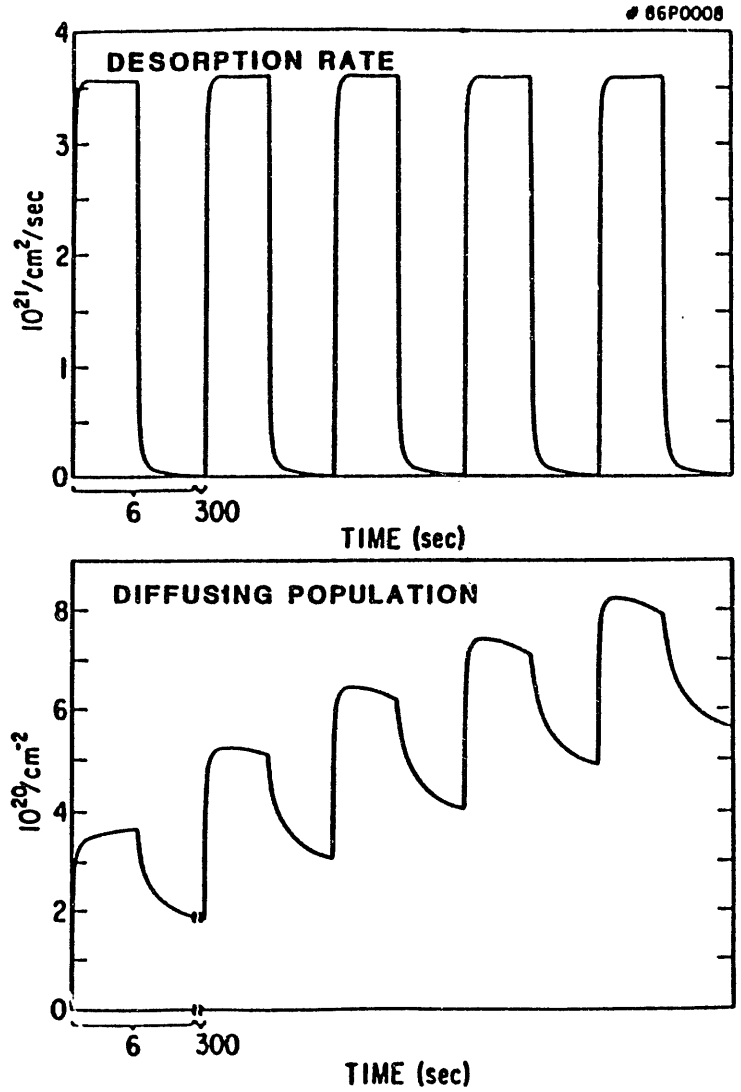

HEIFETZ, PPPL

Tritium Inventory in TFTR (grams)--1986 in vacuum (torus and neutral beams)

Torus geometric surface area coverage: 10^{17} T/cm^2

Neutral beam injector surface areas: 2×10^{14} T/cm^2

Graphite bulk loading: 5 ppm

Metal bulk loading: 0 ppm except T beam dumps

	Surface:	Bulk
Bumper Limiter	0.1	1.7
NB Protection Armor	0.05	0.9
Wall	0.55	—
Getters	—	—
Antenna Limiter	0.02	0.07
Neutral beam	0.03	0.5
TOTAL	3.9 grams	

PONTAU

KEY EXPERIMENTAL OBSERVATIONS

TFTR TILES:

AVERAGE SURFACE LOADING: 10^{17} cm^{-2}

MAXIMUM SURFACE LOADING: 10^{18} cm^{-2}

BULK LOADING: 5 ppm

LABORATORY:

BULK LOADING MAXIMUM: 20 ppm

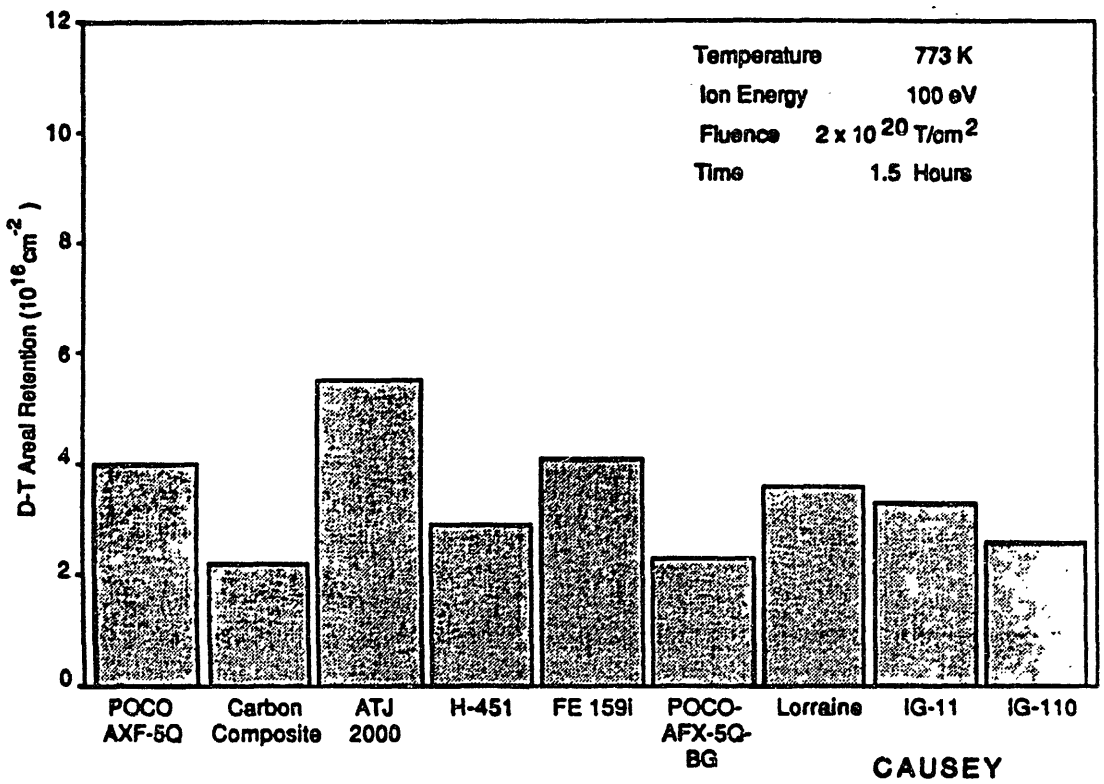
Temperature 773 K
Ion Energy 100 eV
Fluence 2 x 10^20 T/cm^2
Time 1.5 Hours
D-T Areal Retention (10^16 cm^-2)
0
2
4
6
8
10
12
POCO AXF-5Q
Carbon Composite
ATJ 2000
H-451
FE 159i
POCO-AFX-5Q-BG
Lorraine
IG-11
IG-110
CAUSEY

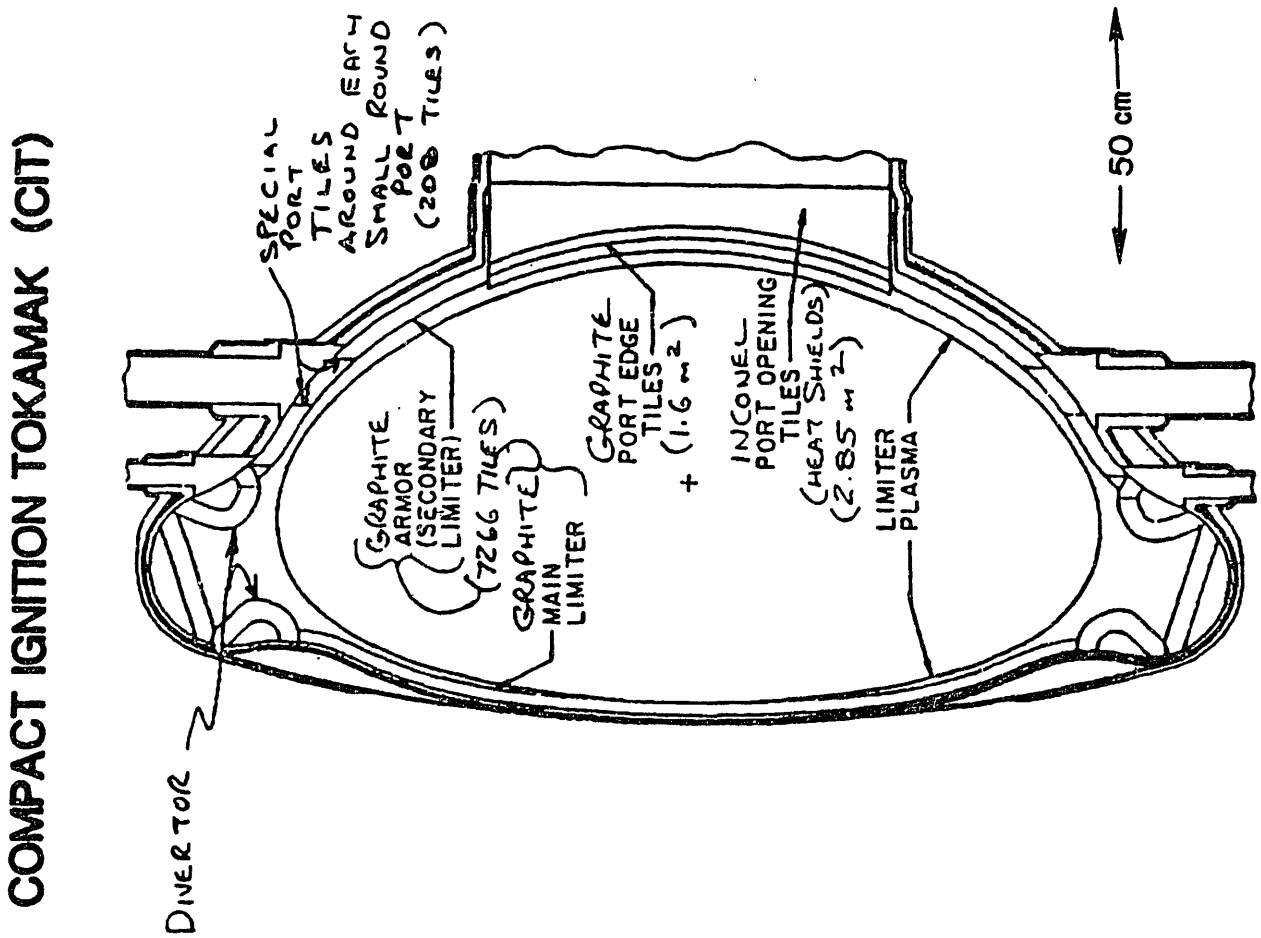
COMPACT IGNITION TOKAMAK (CIT)
SPECIAL PORT TILES AROUND EACH SMALL ROUND PORT (208 TILES)
GRAPHITE ARMOR (SECONDARY LIMITER)
(7266 TILES)
GRAPHITE MAIN LIMITER
GRAPHITE PORT EDGE TILES (1.6 m²)
+
INCONEL PORT OPENING TILES (HEAT SHIELDS) (2.85 m²)
LIMITER PLASMA
DIVERTOR
50 cm

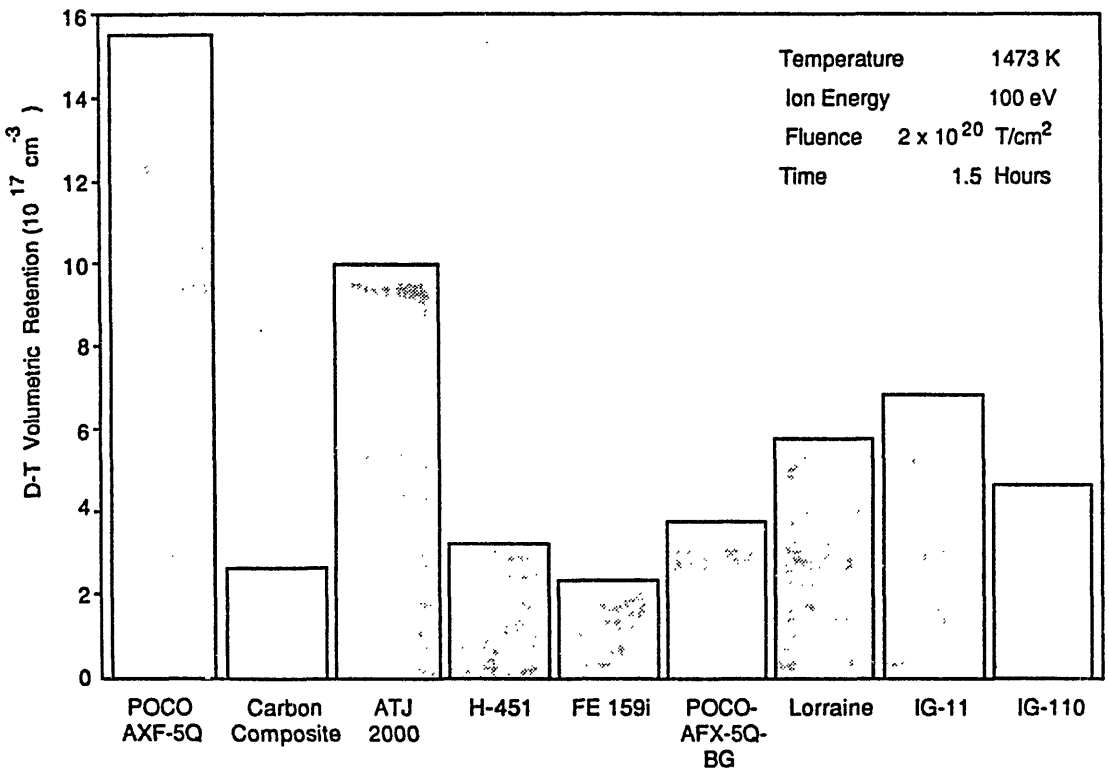
D-T Volumetric Retention (10^{17} cm^{-3})
16
14
12
10
8
6
4
2
0
Temperature 1473 K
Ion Energy 100 eV
Fluence 2×10^{20} T/cm^2
Time 1.5 Hours
POCO AXF-5Q
Carbon Composite
ATJ 2000
H-451
FE 159i
POCO-AFX-5Q-BG
Lorraine
IG-11
IG-110

Trapping-Release Behaviours of Hydrogen Isotopes in/from Graphite

--- Modification by the Presence Fe Impurity ---

Kenji Ichimura

Toyama University

Abstract

In trapping-release of hydrogen isotopes in/from graphite trapping states and thermal release mechanisms were determined, and recombination factor and Inventory were evaluated.

Graphite characteristics was modified by Ion bombardments (D_2^+ and H_e^+) and by presence Fe impurity. The surface recombination factor of the iron-coated graphite was smallerthan that of pure graphite below 600°C.

INTERACTIONS BETWEEN TRITIUM AND GRAPHITE

K. Ichimura, K. Ashida, M. Matsuyama, and K. Watanabe
Tritium Research Center, Toyama University

1. Trapping-Release Behaviours of Hydrogen Isotopes in/from Graphite

1-1. Trapping States : XPS - SIMS (- TDS)

1-2. Thermal Release : Mass Analyzed Thermal Desorption Spectroscopy (MATDS)

1-3. Recombination Factor

1-4. Inventory and/or Retention

2. Modifications of Graphite Characteristics by Irradiation and/or Impurity

2-1. By Ion Bombardment (Hydrogen Isotopes and Helium) : XPS-SIMS-Raman

2-2. By Presence of Fe Impurity : XPS (- SIMS) - MATDS

TRAPPING-RELEASE BEHAVIORS OF HYDROGEN ISOTOPES IN/FROM GRAPHITE

—— MODIFICATION BY THE PRESENCE Fe IMPURITY ——

K. Ichimura, K. Ashida, M. Matsuyama, and K. Watanabe
Tritium Research Center, Toyama University

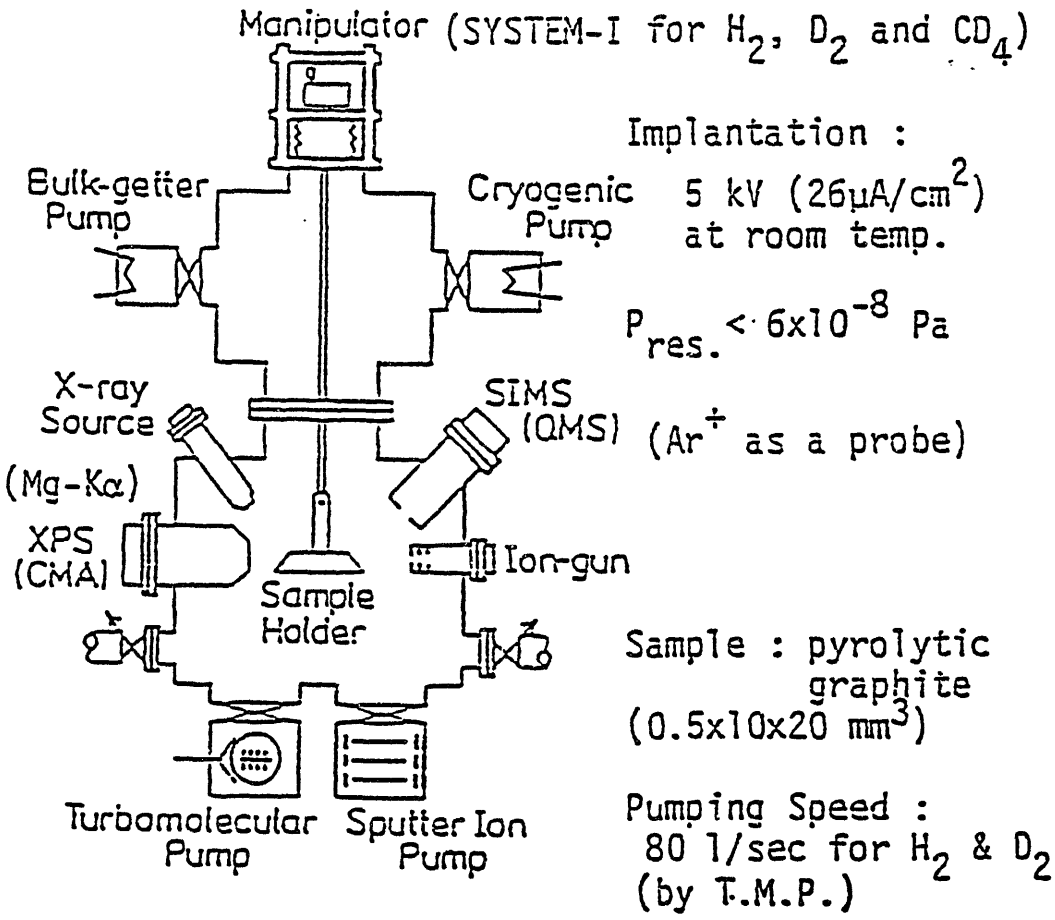
Manipulator (SYSTEM-I for H_2, D_2 and CD_4)
Implantation :
5 kV (26μA/cm^2)
at room temp.
Bulk-getter Pump
Cryogenic Pump
$P_{res.} < 6 \times 10^{-8}$ Pa
X-ray Source
(Mg-Kα)
SIMS (QMS)
(Ar^+ as a probe)
XPS (CMA)
Ion-gun
Sample Holder
Sample : pyrolytic graphite
(0.5x10x20 mm^3)
Turbomolecular Pump
Sputter Ion Pump
Pumping Speed :
80 l/sec for H_2 & D_2
(by T.M.P.)

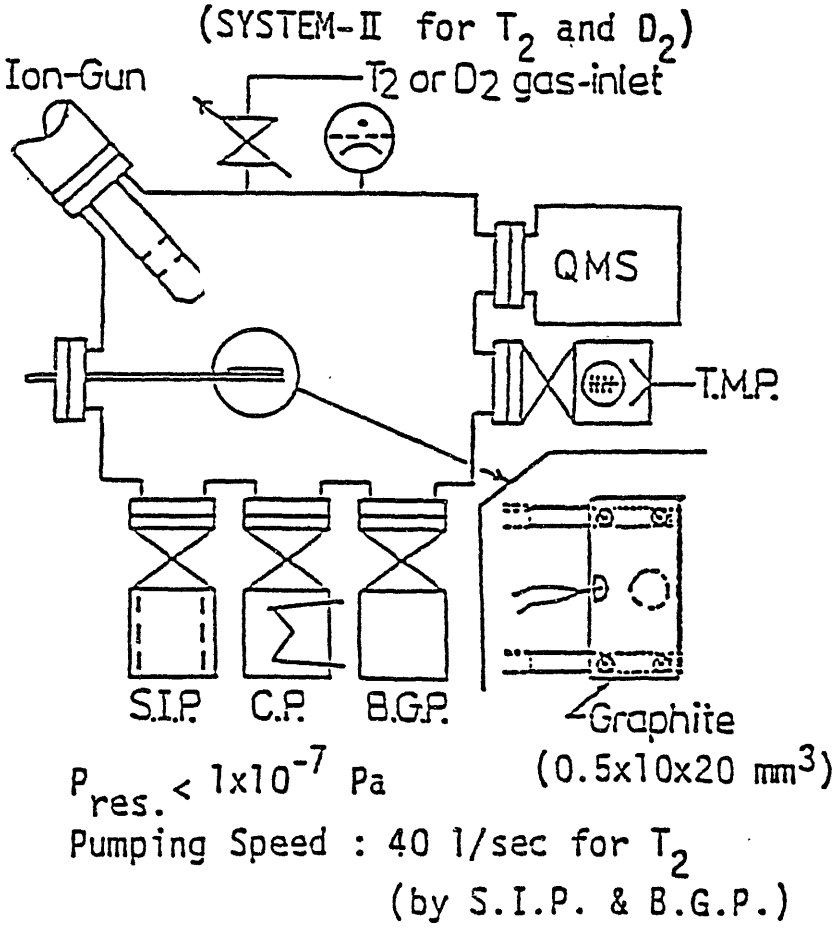
(SYSTEM-II for T_2 and D_2)
Ion-Gun
T_2 or D_2 gas-inlet
QMS
T.M.P.
S.I.P.
C.P.
B.G.P.
Graphite
(0.5x10x20 mm^3)
$P_{res.} < 1 \times 10^{-7}$ Pa
Pumping Speed : 40 l/sec for T_2
(by S.I.P. & B.G.P.)

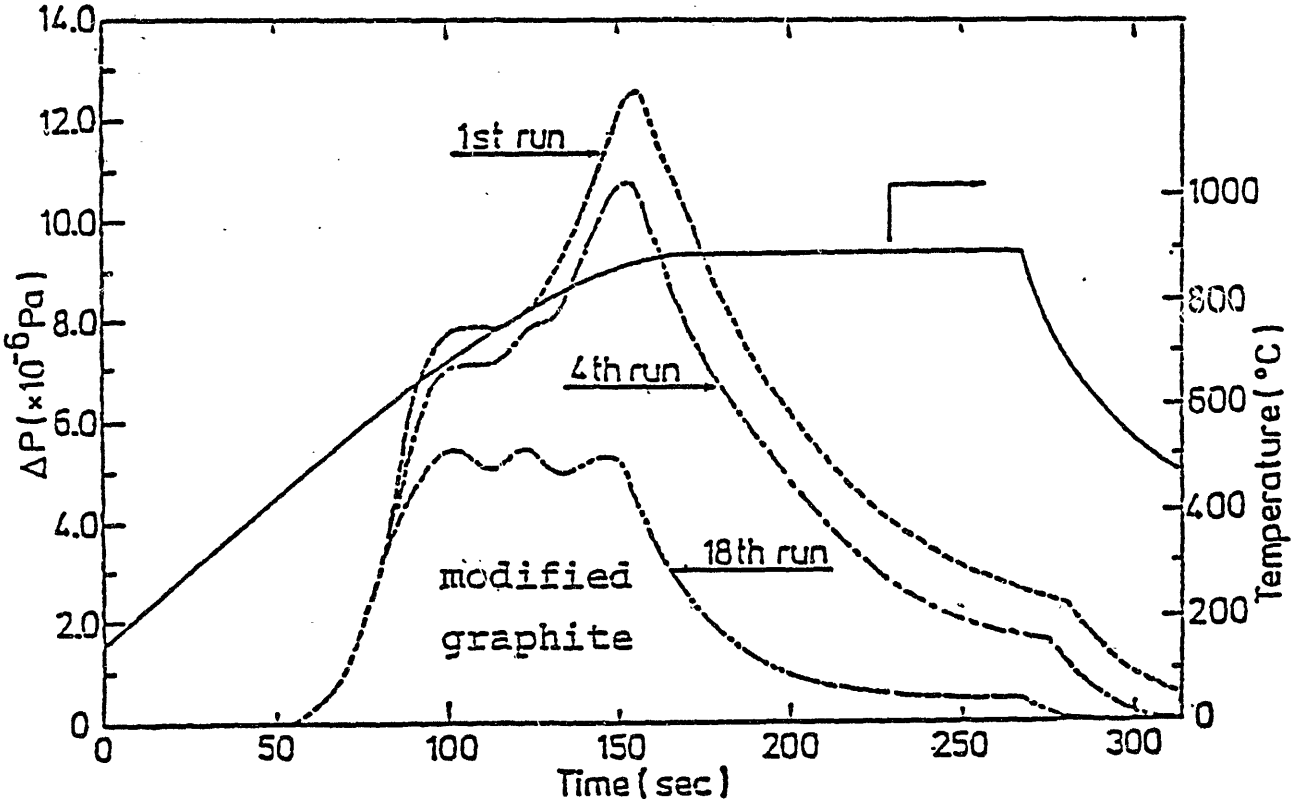

Change in the desorption spectra of D_2
with repeating implantation-desorption cycle

Deuterium ion fluence : 6×10^{17} ions/cm^2
(with 5 keV, 26 μA/cm^2)

Temperature ramp : 5 °C/sec

after 18th run, the spectral shape and the amount of desorption became reproducible.

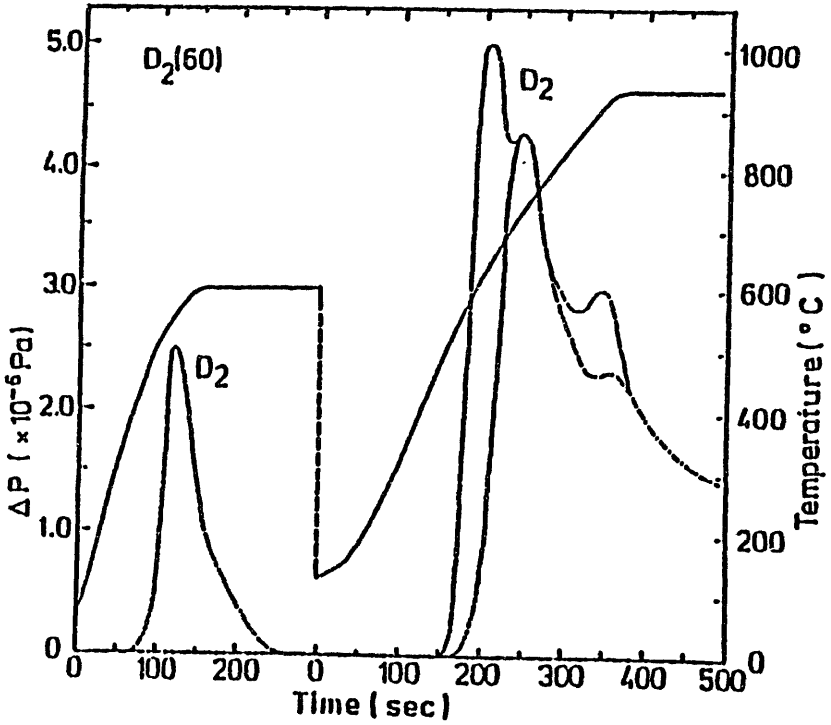

Two-step desorption spectra of D_2 after the deuterium-ion implantation (8×10^{16} ions)

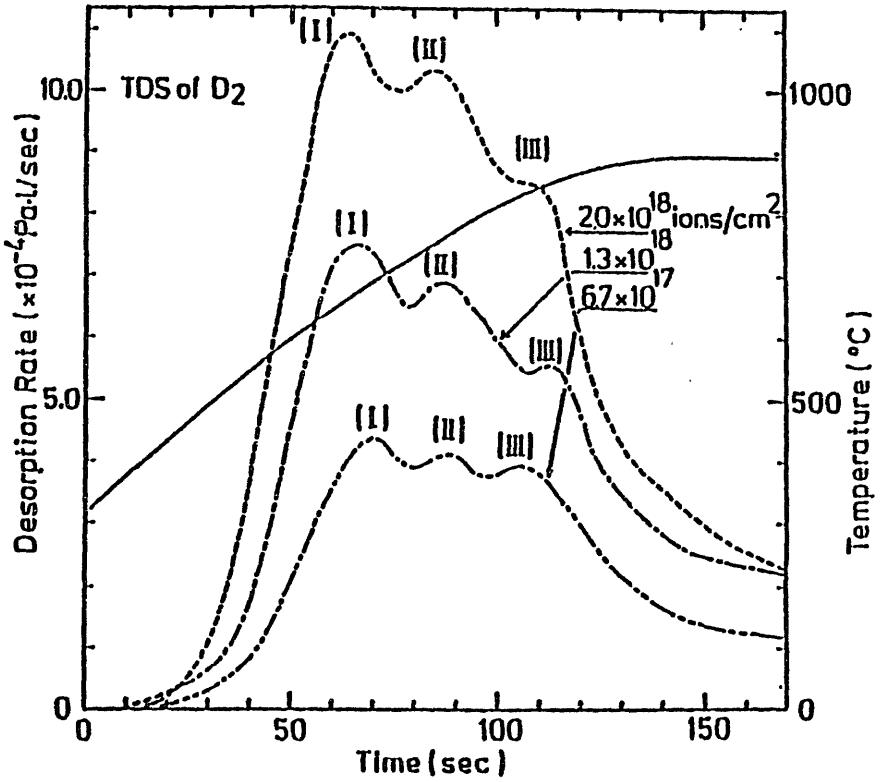

Thermal desorption spectra of D_2

Temperature ramp : 5 °C/sec

Peask [I] shifted to the lower temperature side with the increase of the amount of implantation

Table 1. Summary of the rate constants for PG-A and PAPYEX

	PG - A	PAPYEX
$k_d(H_2)_I$	$(1.5\times10^{-6})\exp(-43.0\times10^3/RT)$	$(2.5\times10^{-7})\exp(-46.0\times10^3/RT)$
$k_d(D_2)_I$	$(4.0\times10^{-7})\exp(-44.0\times10^3/RT)$	
$k_d(T_2)_I$	$(9.3\times10^{-6})\exp(-45.0\times10^3/RT)$	
$k_d(H_2)_{II}$	$(7.5\times10^{-4})\exp(-59.0\times10^3/RT)$	$(1.0\times10^{-4})\exp(-61.0\times10^3/RT)$
$k_d(D_2)_{II}$	$(2.4\times10^{-4})\exp(-59.0\times10^3/RT)$	
$k_d(T_2)_{II}$	$(1.3\times10^{-3})\exp(-59.0\times10^3/RT)$	

unit: [1/sec·molec]

Table 2. Summary of recombination factors for PG-A.

	PEAK I	PEAK II
$k_r(H_2)$	$(13.0\times10^{-19})\exp(-44.0\times10^3/RT)$	$(9.06\times10^{-16})\exp(-59.0\times10^3/RT)$
$k_r(D_2)$	$(7.18\times10^{-19})\exp(-44.0\times10^3/RT)$	$(5.74\times10^{-16})\exp(-59.0\times10^3/RT)$
$k_r(T_2)$	$(5.26\times10^{-19})\exp(-44.0\times10^3/RT)$	$(15.8\times10^{-16})\exp(-59.0\times10^3/RT)$

unit: [cm^4/sec·molec]

EVALUATION OF RECOMBINATION FACTOR

Surface Reaction : $2\,S-H \xrightarrow{A} 2\,S + H_2\,(gas)$

$$-(1/2)d[C_s]/dt = -d[H_2]/dt = N(t) = k_s C_s^2$$

Bulk-Surface Equilibrium : $B - H + S \rightleftharpoons B + S - H$

$$C_b \quad (N_s - C_s) \quad (N_b - C_b) \quad C_s$$

$$C_s = KN_sC_b/(N_b-C_b-KC_b)$$

Total Numbers of Ad/absorbate : $n_T = C_sS + C_bV$

$$C_s = KN_s(n_T-C_sA)/[VN_b-(1-K)(n_T-C_sA)]$$

$N(t)$: desorption rate [molec/sec·cm^2]
N_s : surface site density [sites/cm^2]
N_b : bulk site density [sites/cm^3]
C_s : surface concentration [atoms/cm^2]
C_b : bulk concentration [atoms/cm^3]
K : equilibrium constant
S : surface area [cm^2]
V : volume [cm^3]

Surface Recombination Factor : $k_r = k_d^{obs}(V^2/A)$

A : implantation area

in the recycling of tritium in the graphite first wall.

The surface recombination factor, k_s, can not be evaluated from the observed rate constants, because the equilibrium constant, K, is unknown. We define here the pseudo surface recombination factor, k_sK^2. From Eq. (17), this is described as

$$k_sK^2 = (N_b/N_s)^2(V^2/A)k_{ob}$$
$$= (N_b/N_s)^2(V^2/A)\nu_d \exp(-E_d/RT) \quad (24)$$

In this equation, the volume (V) and area (A) have been evaluated as the above. The trapping site densities, N_s and N_b, are calculated as follows. The atomic densities of carbon in graphite are $2.2\times10^{15}/cm^2$ on the surface and $1.1\times10^{23}/cm^3$ in the bulk. The saturation concentration of hydrogen atoms in graphite has been determined as $[H]/[C] \cong 0.5$[13,16,17]. Thus, the trapping site densities are $N_s = 1.1\times10^{15}/cm^2$ and $N_b = 6.6\times10^{22}/cm^3$. By use of these values, the pseudo surface recombination factors are evaluated as

$$k_sK^2(H_2) = (4.68\times10^{-3})\exp(-44.0\times10^3/RT)[cm^2/sec\cdot molec] \quad (25)$$
$$k_sK^2(D_2) = (2.58\times10^{-3})\exp(-44.0\times10^3/RT) \quad (26)$$
$$k_sK^2(T_2) = (1.89\times10^{-3})\exp(-44.0\times10^3/RT) \quad (27)$$

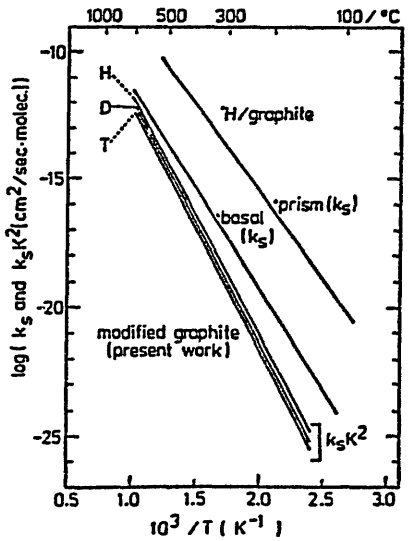

Fig. 4. Comparison of the pseudo surface recombination factor, k_sK^2, evaluated from the present data with the surface recombination factor, k_s, for graphite.
* The data for k_s are taken from ref. [18]

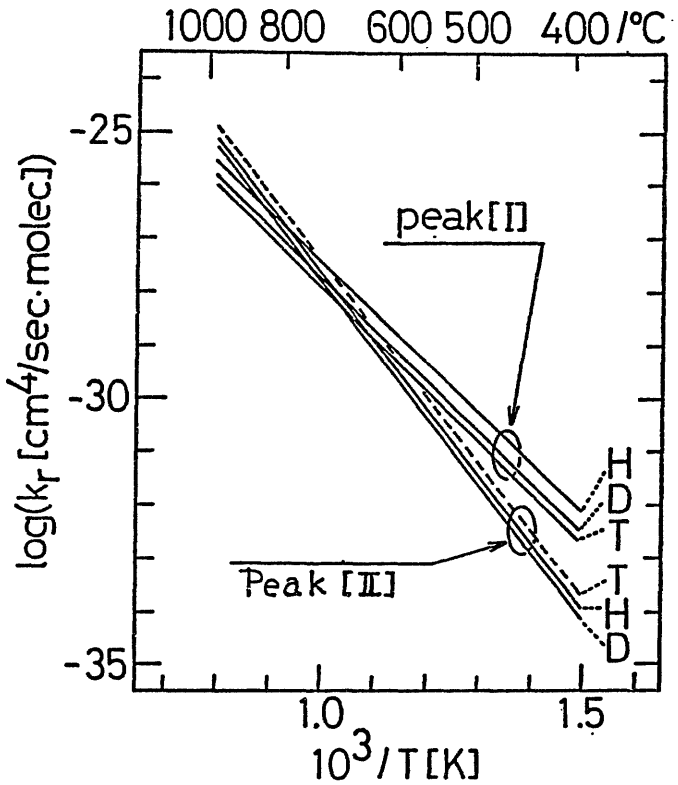

and Eqs. (4), (5), (6) and (20), the recombination factors averaged over the sub-surface layer of the modified graphite for three hydrogen isotopes are determined as

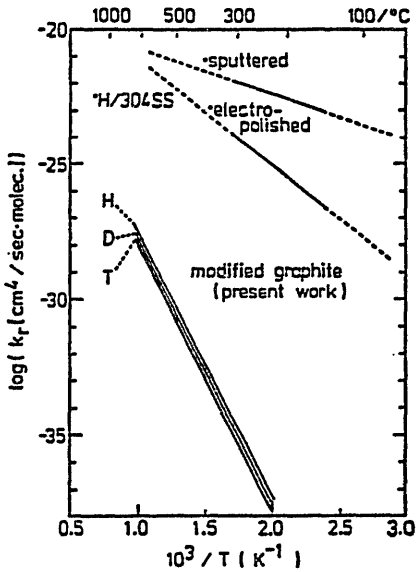

Fig. 3. Comparison of recombination factor, k_r, for graphite with that for stainless steel.
*The data for stainless steel are taken from ref. [14]

$$k_r(H_2) = (13.0\times10^{-19})\exp(-44.0\times10^3/RT)[cm^4/sec\cdot molec] \quad (21)$$

$$k_r(D_2) = (7.18\times10^{-19})\exp(-44.0\times10^3/RT) \quad (22)$$

$$k_r(T_2) = (5.26\times10^{-19})\exp(-44.0\times10^3/RT) \quad (23)$$

The recombination factors evaluated above are plotted in Fig. 3, where those for stainless steel are quoted from Langley[13] for the sake of comparison. It is seen in the figure that the recombination factors for the graphite are about five order of magnitude smaller than those for the stainless steel even at 1000℃.

The surface recombination rate of tritium estimated from the above factor is only 1×10^{14} molec/sec·cm² at 500℃ even at saturation concentration (c. a. 7×10^{22} atoms /cm³) in graphite. The desorption rates of hydrogen isotopes forming the peak II and III should be far smaller than the above value. This indicates that the thermal release plays only a minor role for tritium recycling in the graphite first wall, especially at low temperature region : other mechanisms such as ion induced desorption will predominate

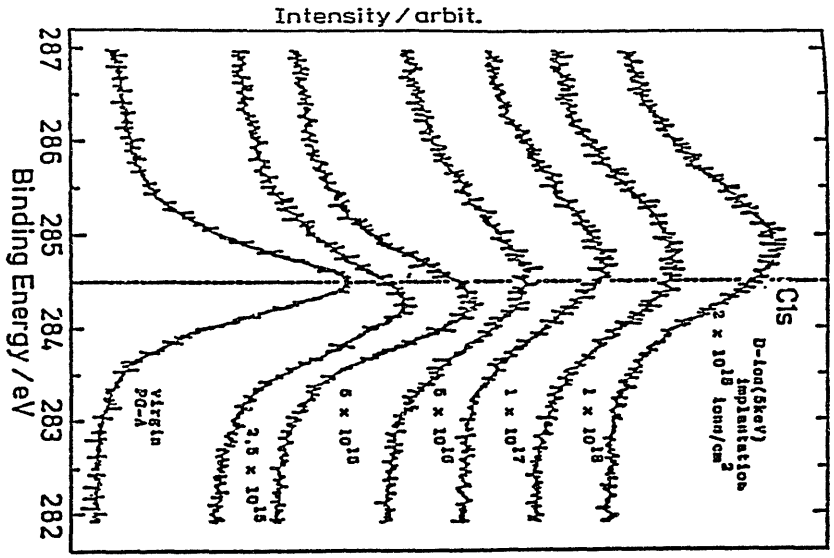

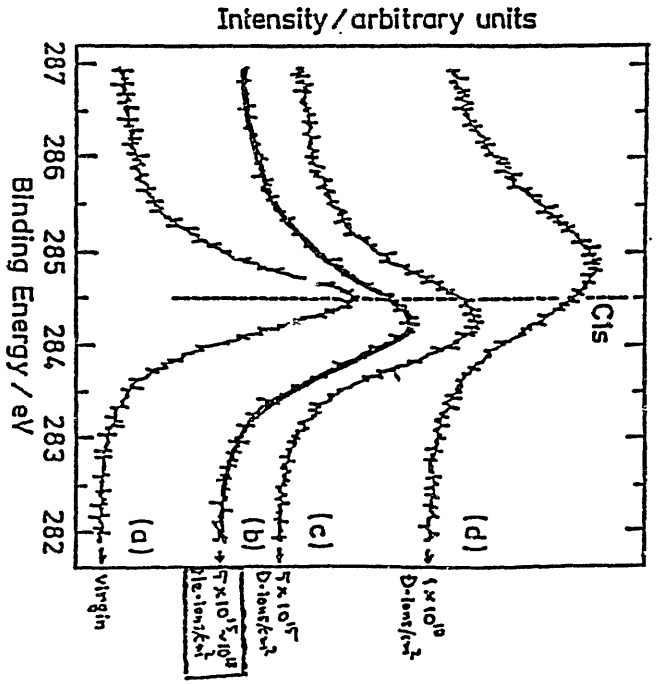

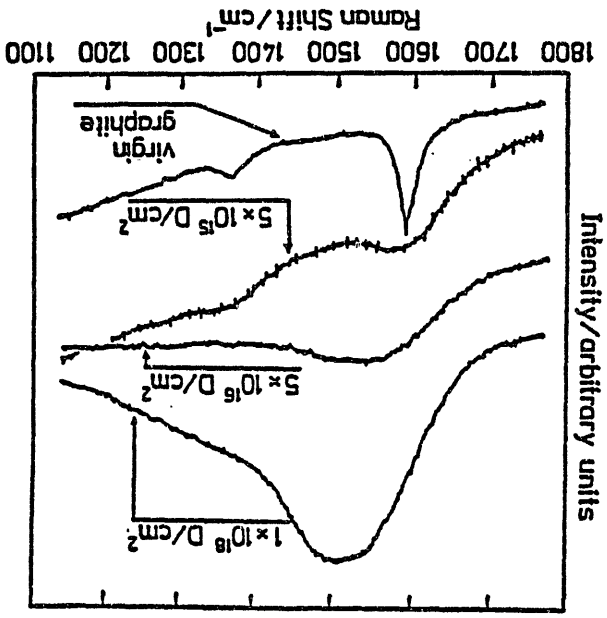
Intensity/arbitrary units
Raman Shift/cm⁻¹
1×10¹⁸ D/cm²
5×10¹⁶ D/cm²
5×10¹⁵ D/cm²
virgin graphite
1800 1700 1600 1500 1400 1300 1200 1100

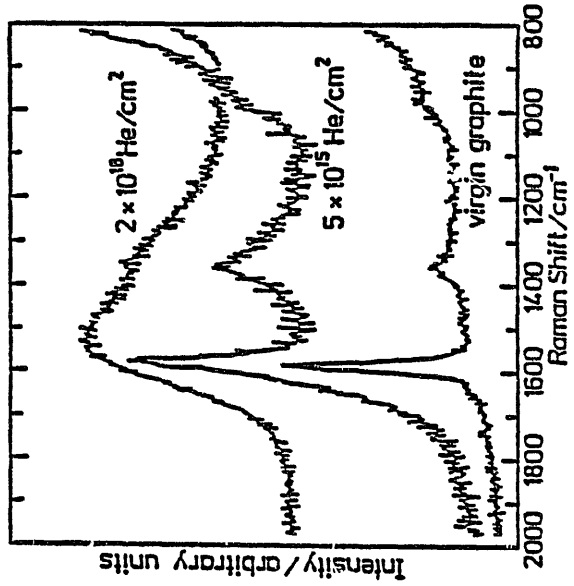
Intensity/arbitrary units
Raman Shift/cm⁻¹
2×10¹⁸He/cm²
5×10¹⁵He/cm²
virgin graphite
2000 1800 1600 1400 1200 1000 800

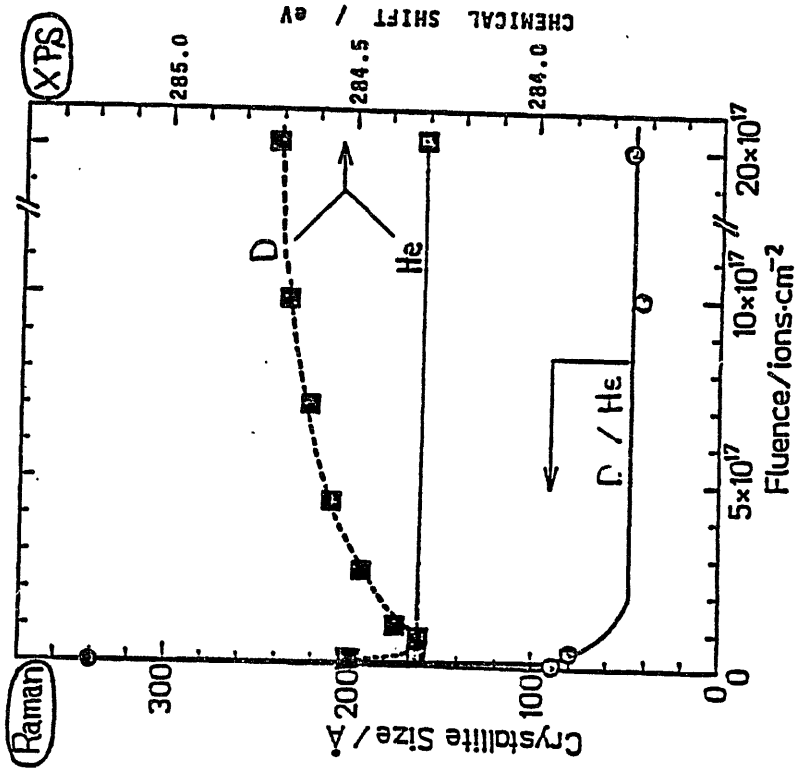
Raman
XPS
Crystallite Size / Å
CHEMICAL SHIFT / eV
Fluence/ions·cm⁻²
D
He
D / He
0
100
200
300
284.0
284.5
285.0
5×10¹⁷
10×10¹⁷
20×10¹⁷

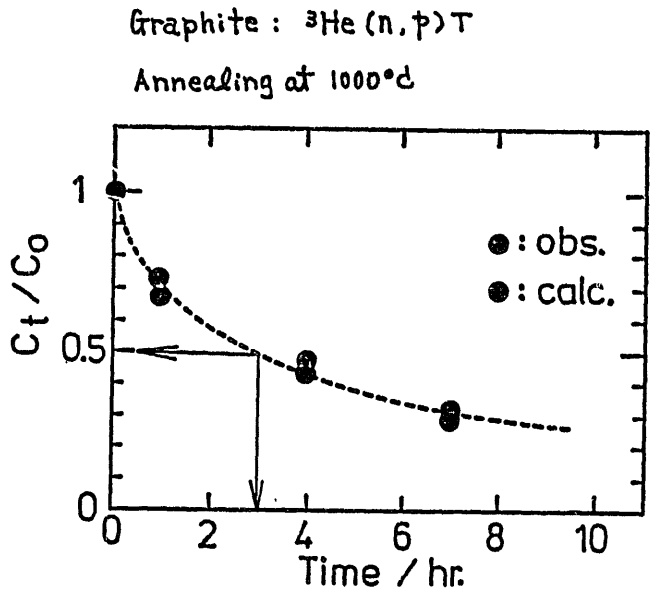

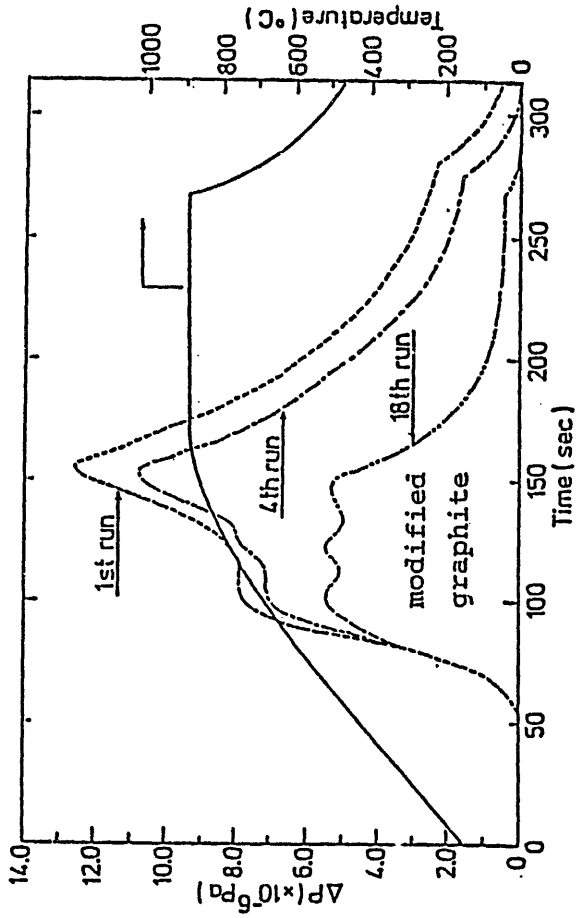

Change in the desorption spectra of D_2 with repeating implantation-desorption cycle

Deuterium ion fluence : 6×10^{17} ions/cm^2 (with 5 keV, 26 μA/cm^2)

Temperature ramp : 5 °C/sec

after 18th run, the spectral shape and the amount of desorption became reproducible.

SUMMARIES OF INTERACTIONS BETWEEN TRITIUM AND GRAPHITE

K. Ichimura, K. Ashida, M. Matsuyama, and K. Watanabe
Tritium Research Center, Toyama University

1. Trapping-Release Behaviours of Hydrogen Isotopes in/from Graphite

1-1. Trapping States : XPS - SIMS (- TDS)

(1) Graphite Normal Lattice (Chem. Shift in XPS, CD^- in SIMS)

(2) Damaged Site by Irradn. (Peak Broadn. in XPS, C_2D^- in SIMS)

"At least, two trapping sites have been identified."

1-2. Thermal Release : Mass Analyzed Thermal Desorption Spectroscopy (MATDS)

(1) Desorption from/by Normal Lattice and Damaged Site/2nd Order

(2) Desorption from the Bulk by Diffusion

"Three desorption mechanisms have been identified and determined."

1-3. Recombination Factor

(1) $k_r(D_2)_I = (7.18\times10^{-19})\exp(-44.0\times10^3/RT)$

(2) $k_r(D_2)_{II} = (5.74\times10^{-16})\exp(-59.0\times10^3/RT)$

"Recombination factors for peaks I and II have been evaluated."

2. Modifications of Graphite Characteristics by Irradiation and/or Impurity

2-1. By Ion Bombardment (Hydrogen Isotopes and Helium) : XPS-SIMS-Raman

(1) Disruption of C-C Bonds and Decrease in Crystalline Size; Electronic Defect/Increase in Electronic Charge

(2) Asymmetry of C-C Bond Angle

2-2. By Presence of Fe Impurity : XPS (-SIMS) - MATDS

(1) Iron doped in graphite becomes carbide by vacuum heating above 800°C.

(2) Electronic density of graphite increases due to presence Fe of ca. 3 at% on the surface.

(3) TDS spectra of Fe/graphite is remarkably altered; the peak [I] disappears.

(4) The rate determining step of the desorption is the association process of hydrogen isotope atoms on the surface.

INTERACTIONS BETWEEN TRITIUM AND GRAPHITE

K. Ichimura, K. Ashida, M. Matsuyama, and K. Watanabe
Tritium Research Center, Toyama University

1. Trapping-Release Behaviours of Hydrogen Isotopes in/from Graphite

1-1. Trapping States : XPS - SIMS (- TDS)

1-2. Thermal Release : Mass Analyzed Thermal Desorption Spectroscopy (MATDS)

1-3. Recombination Factor

1-4. Inventory and/or Retention

2. Modifications of Graphite Characteristics by Irradiation and/or Impurity

2-1. By Ion Bombardment (Hydrogen Isotopes and Helium) : XPS-SIMS-Raman

2-2. By Presence of Fe Impurity : XPS (- SIMS) - MATDS

TRAPPING-RELEASE BEHAVIORS OF HYDROGEN ISOTOPES IN/FROM GRAPHITE

—— MODIFICATION BY THE PRESENCE Fe IMPURITY ——

K. Ichimura, K. Ashida, M. Matsuyama, and K. Watanabe
Tritium Research Center, Toyama University

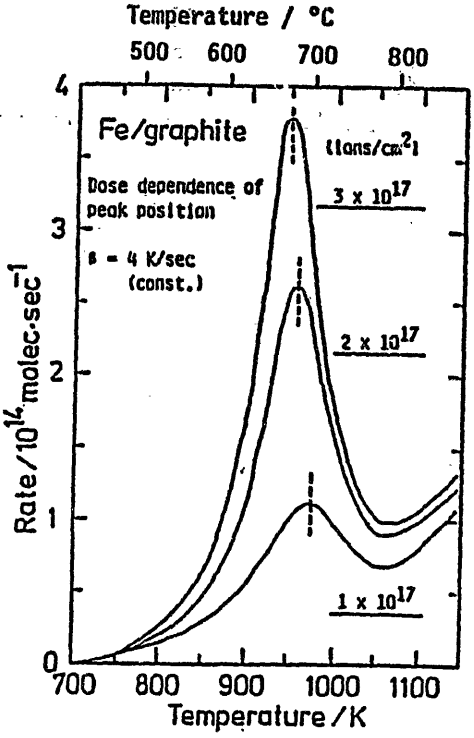
Temperature / °C
500
600
700
800
Fe/graphite
Dose dependence of peak position
β = 4 K/sec (const.)
[Ions/cm²]
3 x 10¹⁷
2 x 10¹⁷
1 x 10¹⁷
Rate/10¹⁴ molec·sec⁻¹
0
1
2
3
4
700
800
900
1000
1100
Temperature/K

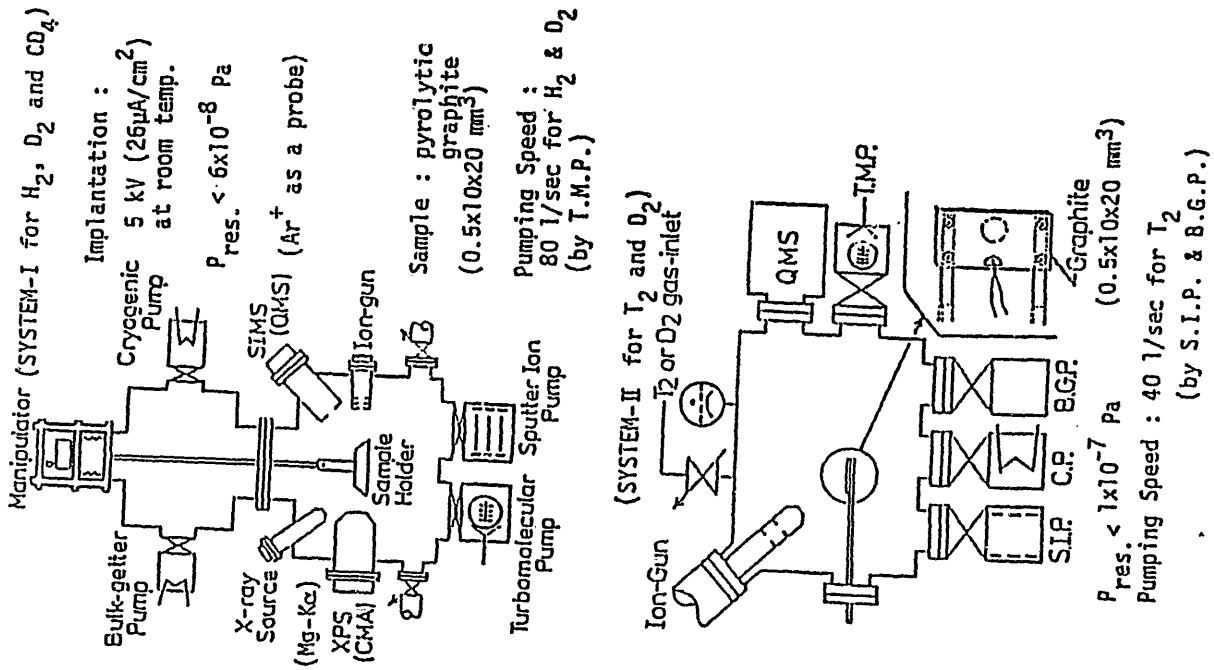
Manipulator (SYSTEM-I for H2, D2 and CD4)
Implantation : 5 kV (26μA/cm²) at room temp.
Cryogenic Pump
P res. < 6x10⁻⁸ Pa
SIMS (QMS) (Ar⁺ as a probe)
Ion-gun
Sample : pyrolytic graphite (0.5x10x20 mm³)
Pumping Speed : 80 l/sec for H2 & D2 (by T.M.P.)
Bulk-getter Pump
X-ray Source (Mg-Kα)
XPS (CMA)
Sample Holder
Sputter Ion Pump
Turbomolecular Pump
(SYSTEM-II for T2 and D2)
T2 or D2 gas-inlet
Ion-Gun
QMS
T.M.P.
Graphite (0.5x10x20 mm³)
B.G.P.
C.P.
S.I.P.
P res. < 1x10⁻⁷ Pa
Pumping Speed : 40 l/sec for T2 (by S.I.P. & B.G.P.)

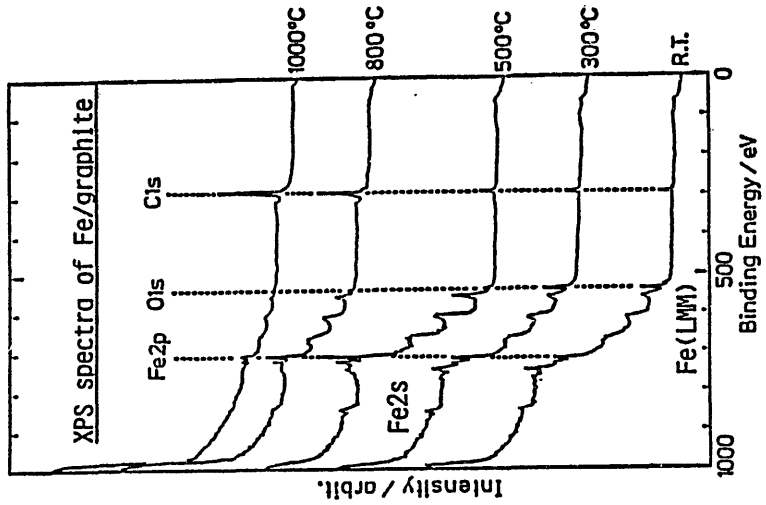
XPS spectra of Fe/graphite
Fe2p
O1s
C1s
Fe2s
Fe(LMM)
1000°C
800°C
500°C
300°C
R.T.
Intensity / arbit.
Binding Energy / eV
0
500
1000

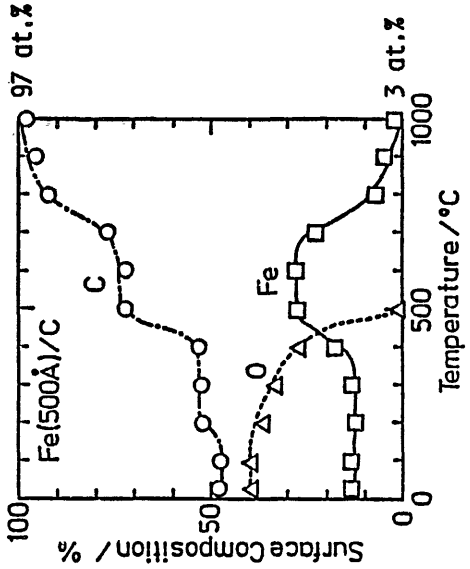
Fe(500Å)/C
C
O
Fe
97 at.%
3 at.%
Surface Composition / %
100
50
0
Temperature / °C
0
500
1000

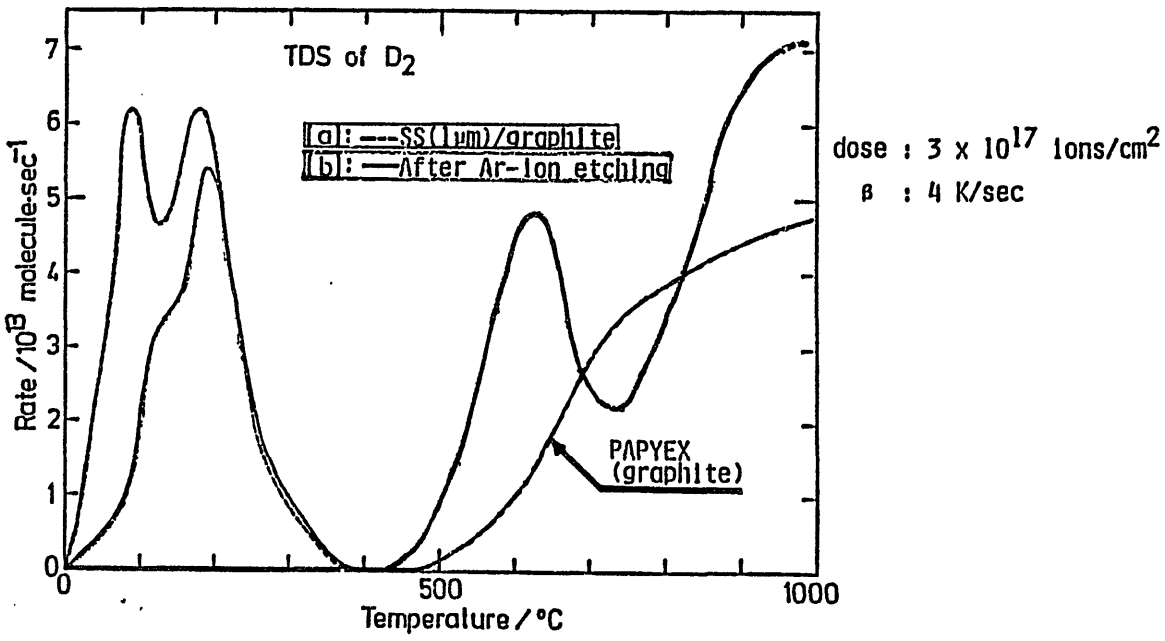
TDS of D_2
[a]: ---SS(1μm)/graphite
[b]: —After Ar-ion etching
PAPYEX (graphite)
dose : 3 x 10^{17} ions/cm^2
β : 4 K/sec
Rate / 10^{13} molecule·sec^{-1}
Temperature / °C
0
1
2
3
4
5
6
7
500
1000

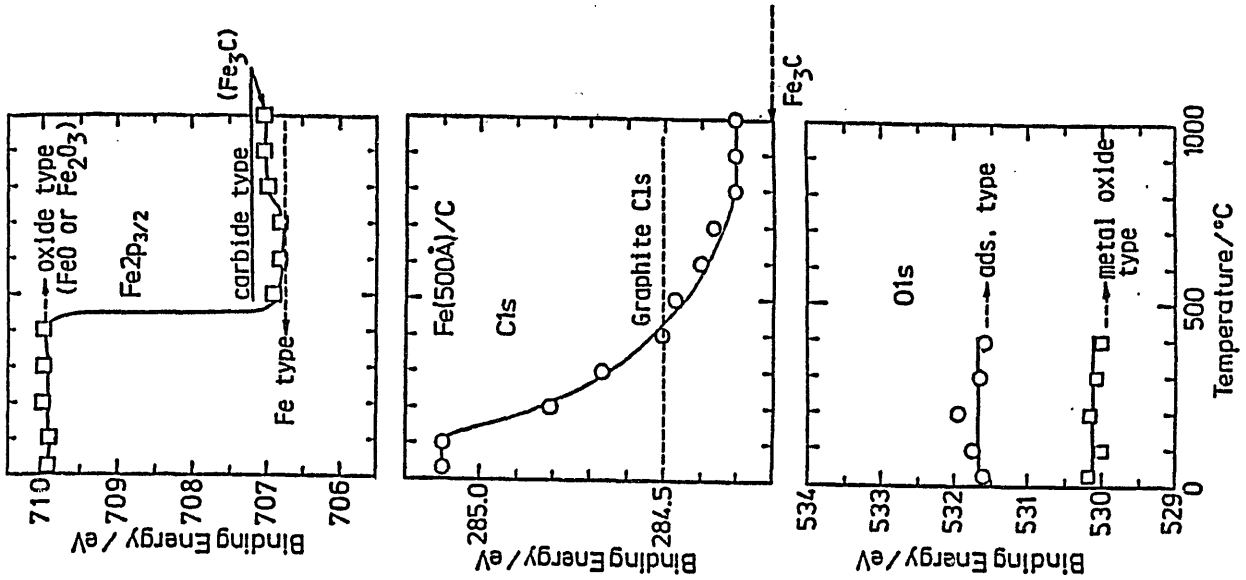
oxide type
(FeO or Fe_2O_3)
$Fe2p_{3/2}$
carbide type
(Fe_3C)
Fe type
Binding Energy / eV
710
709
708
707
706
Fe(500Å)/C
C1s
Graphite C1s
Fe_3C
285.0
284.5
O1s
ads. type
metal oxide type
534
533
532
531
530
529
0
500
1000
Temperature/°C

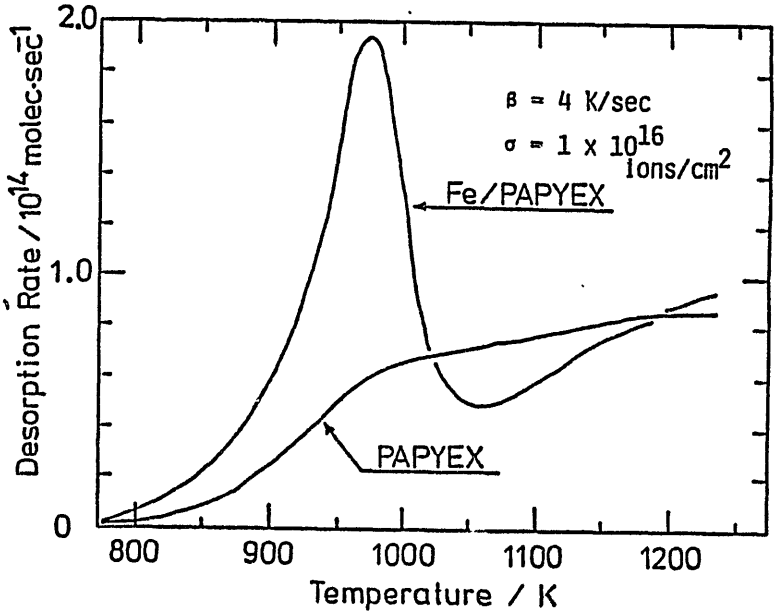
Desorption Rate / 10^{14} molec·sec^{-1}
2.0
1.0
0
β = 4 K/sec
σ = 1 x 10^{16} ions/cm^2
Fe/PAPYEX
PAPYEX
800
900
1000
1100
1200
Temperature / K

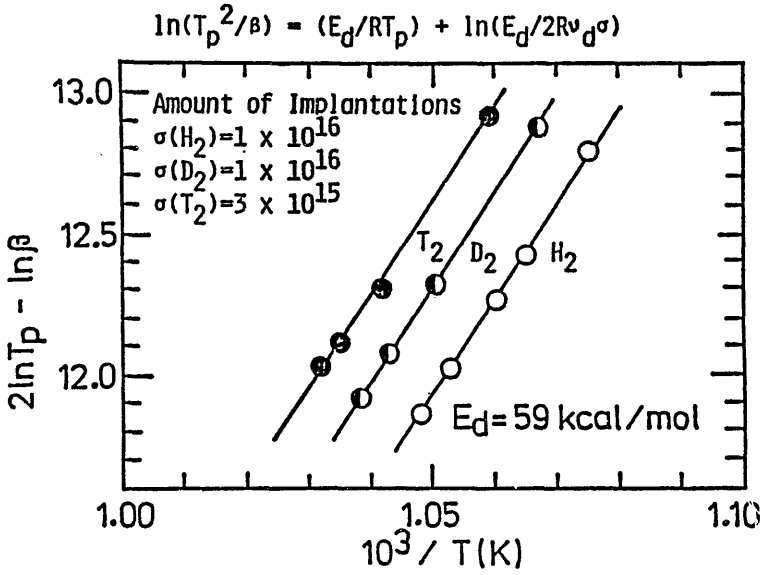
ln(Tp2/β) = (Ed/RTp) + ln(Ed/2Rνdσ)
Amount of Implantations
σ(H2)=1 x 10^16
σ(D2)=1 x 10^16
σ(T2)=3 x 10^15
T2
D2
H2
Ed=59 kcal/mol
2lnTp - lnβ
13.0
12.5
12.0
1.00
1.05
1.10
10^3 / T(K)

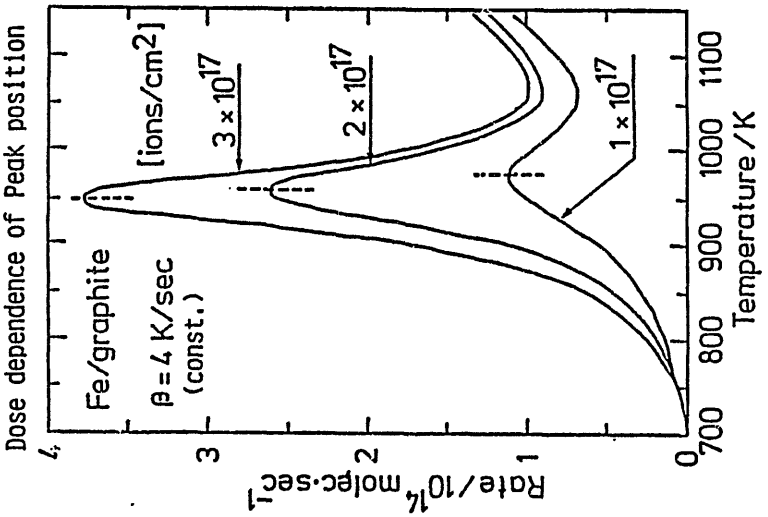
Dose dependence of Peak position
Fe/graphite
β=4 K/sec
(const.)
[ions/cm2]
3 x 10^17
2 x 10^17
1 x 10^17
Rate/10^14 molec·sec^-1
0
1
2
3
4
700
800
900
1000
1100
Temperature/K

Table 3. Summary of rate constants and recombination factors.

	k_d	k_r
H_2	$(7\times10^{-4})\exp(-59.0\times10^{3}/RT)$	$(1.51\times10^{-15})\exp(-59.0\times10^{3}/RT)$
D_2	$(4\times10^{-4})\exp(-59.0\times10^{3}/RT)$	$(9.56\times10^{-16})\exp(-59.0\times10^{3}/RT)$
T_2	$(1\times10^{-3})\exp(-59.0\times10^{3}/RT)$	$(2.63\times10^{-15})\exp(-59.0\times10^{3}/RT)$

unit: [1/sec·molec] [cm^4/sec·molec]

Table 1. Summary of the rate constants for PG-A and PAPYEX

	PG-A	PAPYEX
$k_d(H_2)_I$	$(1.5\times10^{-6})\exp(-43.0\times10^{3}/RT)$	$(2.5\times10^{-7})\exp(-46.0\times10^{3}/RT)$
$k_d(D_2)_I$	$(4.0\times10^{-7})\exp(-44.0\times10^{3}/RT)$	
$k_d(T_2)_I$	$(9.3\times10^{-6})\exp(-45.0\times10^{3}/RT)$	
$k_d(H_2)_{II}$	$(7.5\times10^{-4})\exp(-59.0\times10^{3}/RT)$	$(1.0\times10^{-4})\exp(-61.0\times10^{3}/RT)$
$k_d(D_2)_{II}$	$(2.4\times10^{-4})\exp(-59.0\times10^{3}/RT)$	
$k_d(T_2)_{II}$	$(1.3\times10^{-3})\exp(-59.0\times10^{3}/RT)$	

unit: [1/sec·molec]

Table 2. Summary of recombination factors for PG-A.

	PEAK I	PEAK II
$k_r(H_2)$	$(13.0\times10^{-19})\exp(-44.0\times10^{3}/RT)$	$(9.06\times10^{-16})\exp(-59.0\times10^{3}/RT)$
$k_r(D_2)$	$(7.18\times10^{-19})\exp(-44.0\times10^{3}/RT)$	$(5.74\times10^{-16})\exp(-59.0\times10^{3}/RT)$
$k_r(T_2)$	$(5.26\times10^{-19})\exp(-44.0\times10^{3}/RT)$	$(15.8\times10^{-16})\exp(-59.0\times10^{3}/RT)$

unit: [cm^4/sec·molec]

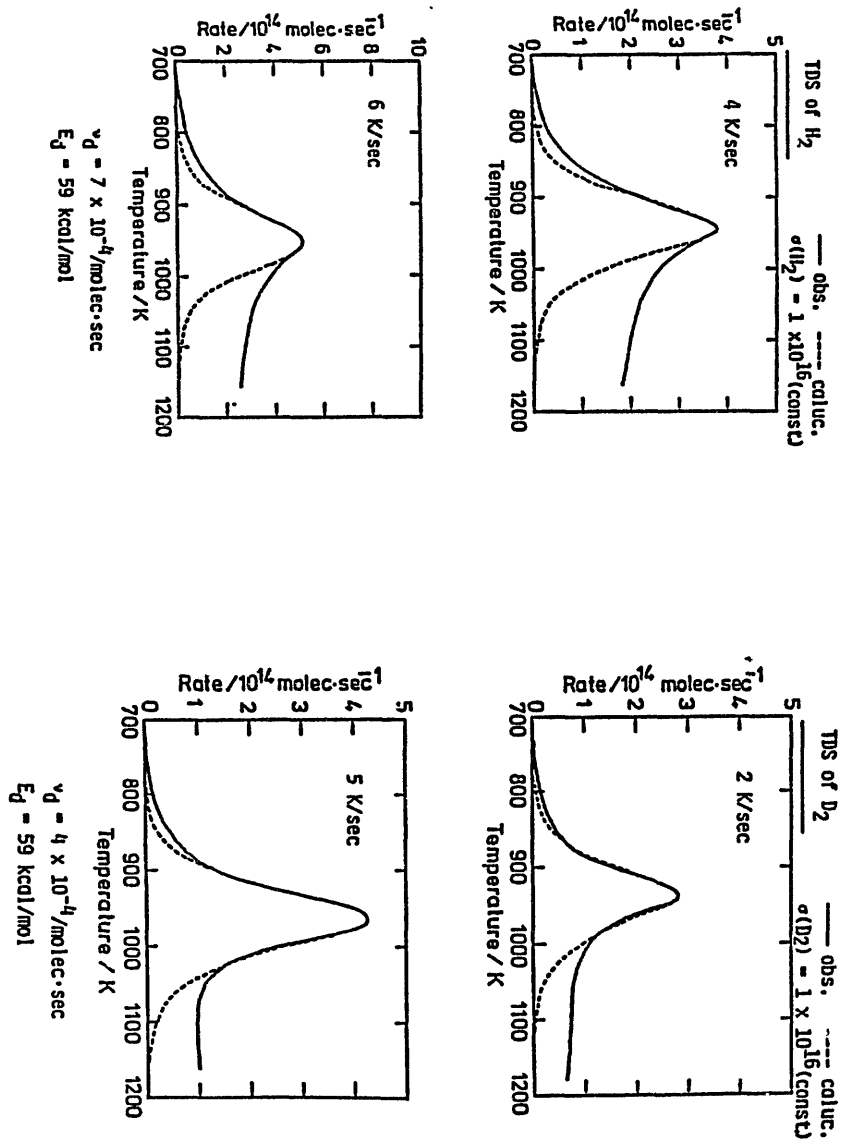

Table 3. Summary of rate constants and recombination factors.

	k_d	k_r
H_2	$(7\times10^{-4})\exp(-59.0\times10^{3}/RT)$	$(1.51\times10^{-15})\exp(-59.0\times10^{3}/RT)$
D_2	$(4\times10^{-4})\exp(-59.0\times10^{3}/RT)$	$(9.56\times10^{-16})\exp(-59.0\times10^{3}/RT)$
T_2	$(1\times10^{-3})\exp(-59.0\times10^{3}/RT)$	$(2.63\times10^{-15})\exp(-59.0\times10^{3}/RT)$

unit: [1/sec·molec] [cm^4/sec·molec]

Table 1. Summary of the rate constants for PG-A and PAPYEX

	PG-A	PAPYEX
$k_d(H_2)_I$	$(1.5\times10^{-6})\exp(-43.0\times10^{3}/RT)$	$(2.5\times10^{-7})\exp(-46.0\times10^{3}/RT)$
$k_d(D_2)_I$	$(4.0\times10^{-7})\exp(-44.0\times10^{3}/RT)$	
$k_d(T_2)_I$	$(9.3\times10^{-6})\exp(-45.0\times10^{3}/RT)$	
$k_d(H_2)_{II}$	$(7.5\times10^{-4})\exp(-59.0\times10^{3}/RT)$	$(1.0\times10^{-4})\exp(-61.0\times10^{3}/RT)$
$k_d(D_2)_{II}$	$(2.4\times10^{-4})\exp(-59.0\times10^{3}/RT)$	
$k_d(T_2)_{II}$	$(1.3\times10^{-3})\exp(-59.0\times10^{3}/RT)$	

unit: [1/sec·molec]

Table 2. Summary of recombination factors for PG-A.

	PEAK I	PEAK II
$k_r(H_2)$	$(13.0\times10^{-19})\exp(-44.0\times10^{3}/RT)$	$(9.06\times10^{-16})\exp(-59.0\times10^{3}/RT)$
$k_r(D_2)$	$(7.18\times10^{-19})\exp(-44.0\times10^{3}/RT)$	$(5.74\times10^{-16})\exp(-59.0\times10^{3}/RT)$
$k_r(T_2)$	$(5.26\times10^{-19})\exp(-44.0\times10^{3}/RT)$	$(15.3\times10^{-16})\exp(-59.0\times10^{3}/RT)$

unit: [cm^4/sec·molec]

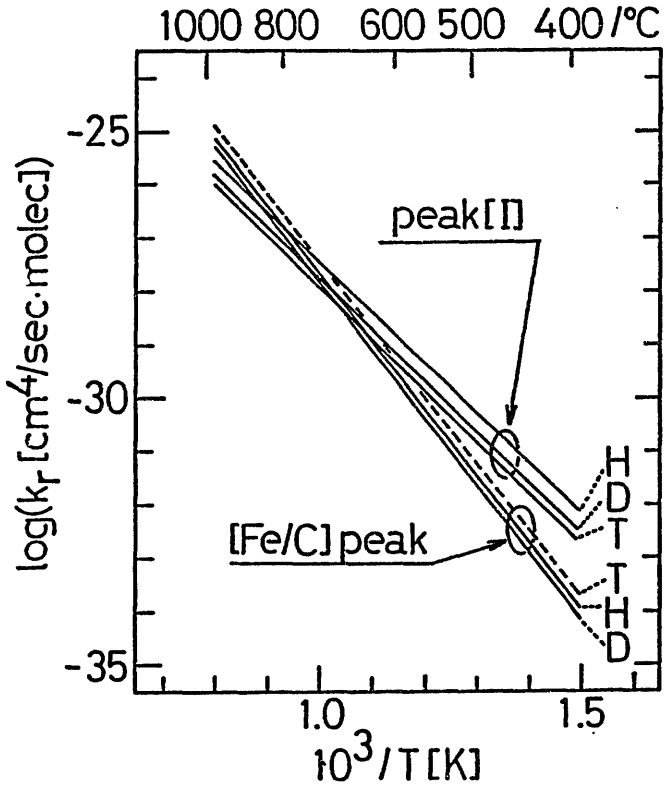

SUMMARIES OF INTERACTIONS BETWEEN TRITIUM AND GRAPHITE

K. Ichimura, K. Ashida, M. Matsuyama, and K. Watanabe
Tritium Research Center, Toyama University

1. Trapping-Release Behaviours of Hydrogen Isotopes in/from Graphite

1-1. Trapping States : XPS - SIMS (- TDS)

(1) Graphite Normal Lattice (Chem. Shift in XPS, CD^- in SIMS)

(2) Damaged Site by Irradn. (Peak Broadn. in XPS, C_2D^- in SIMS)

"At least, two trapping sites have been identified."

1-2. Thermal Release : Mass Analyzed Thermal Desorption Spectroscopy (MATDS)

(1) Desorption from/by Normal Lattice and Damaged Site/2nd Order

(2) Desorption from the Bulk by Diffusion

"Three desorption mechanisms have been identified and determined."

1-3. Recombination Factor

(1) $k_r(D_2)_I = (7.18\times10^{-19})\exp(-44.0\times10^3/RT)$

(2) $k_r(D_2)_{II} = (5.74\times10^{-16})\exp(-59.0\times10^3/RT)$

"Recombination factors for peaks I and II have been evaluated."

2. Modifications of Graphite Characteristics by Irradiation and/or Impurity

2-1. By Ion Bombardment (Hydrogen Isotopes and Helium) : XPS-SIMS-Raman

(1) Disruption of C-C Bonds and Decrease in Crystalline Size; Electronic Defect/Increase in Electronic Charge

(2) Asymmetry of C-C Bond Angle

2-2. By Presence of Fe Impurity : XPS (-SIMS) - MATDS

(1) Iron doped in graphite becomes carbide by vacuum heating above 800°C.

(2) Electronic density of graphite increases due to presence Fe of ca. 3 at% on the surface.

(3) TDS spectra of Fe/graphite is remarkably altered; the peak [I] disappears.

(4) The rate determining step of the desorption is the association process of hydrogen isotope atoms on the surface.

Hydrogen Permeation through Graphite

Michio Yamawaki
University of Tokyo

Abstract

Graphite is porous material so that gaseous diffusion through pores and atomic diffusion on pores are intrinsically important in evaluating the hydrogen retention and permeation rate of graphite. Linear pressure dependence of permeability was found in the down to $\sim 10^{-2}$ Pa region suggesting the viscous flow limiting kinetics. Extremely large temperature dependence of permeability was observed, but could not be adequately explained by the existing models.

Extensive studies are needed to understand this aspect of hydrogen behavior in graphite.

HYDROGEN PERMEATION THROUGH GRAPHITE

M. YAMAWAKI
Univ. of Tokyo

H CONCENTRATION IN A WALL

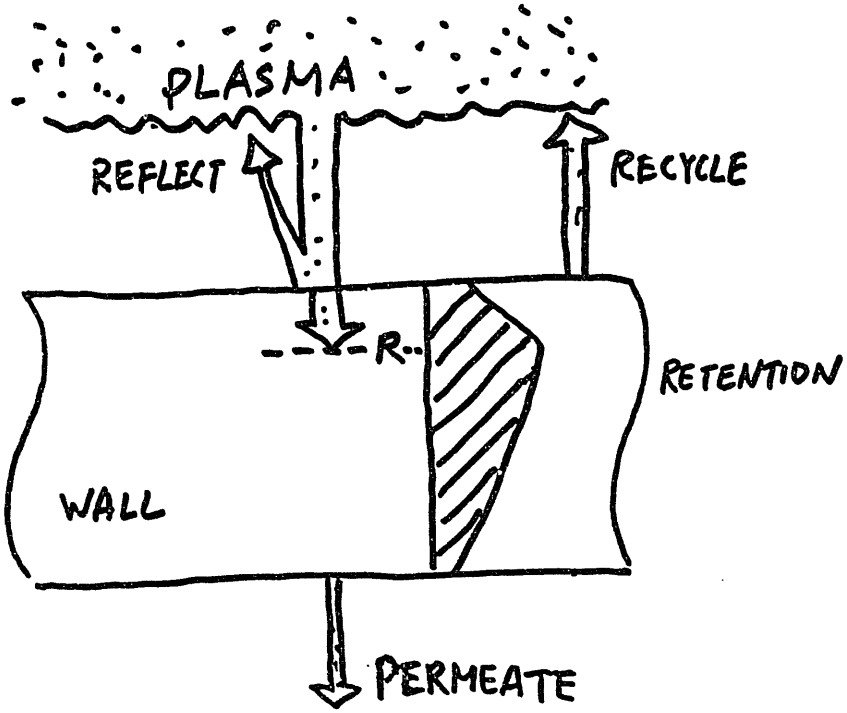

- PORE SIZE DISTRIBUTION
- SHAPE OF PORES
- TORTUOSITY FACTOR

PREVIOUS PERMEATION DATA:

(A) Common Graphite:

$K = 1 \sim 10\ cm^2/s$

(B) TREATED GRAPHITE:

$K = 10^{-1} \sim 10^{-6}\ cm^2/s$

(C) IMPERVIOUS GRAPHITE:

$K \leq 10^{-11}\ cm^2/s$

. PERMEATION
. DIFFUSION

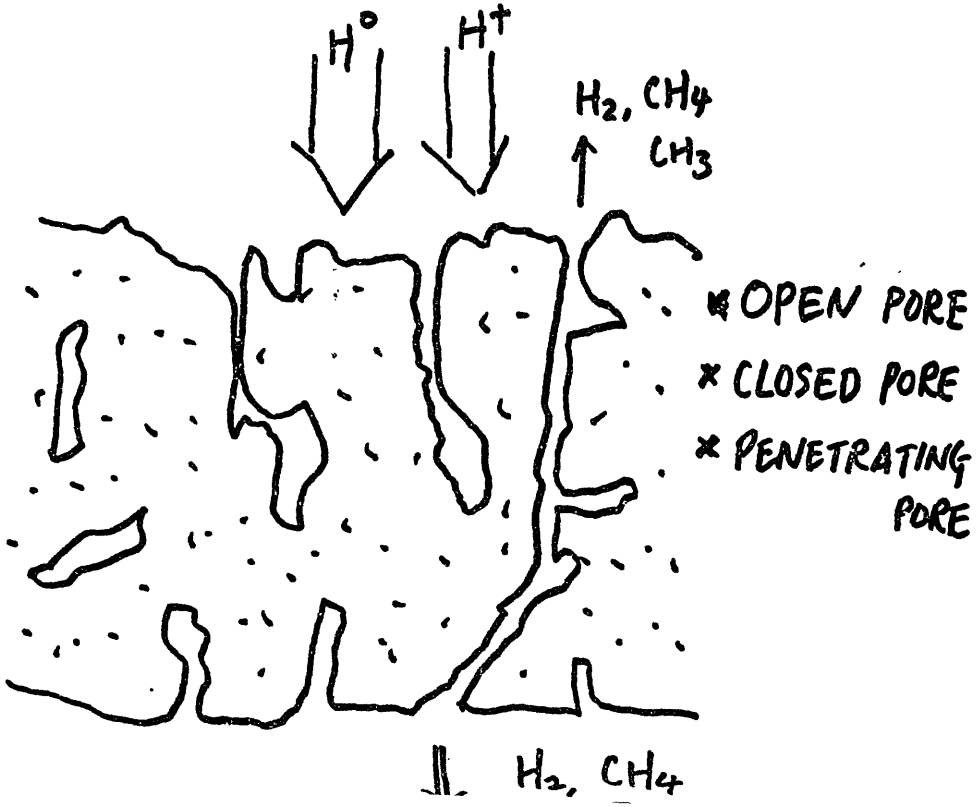

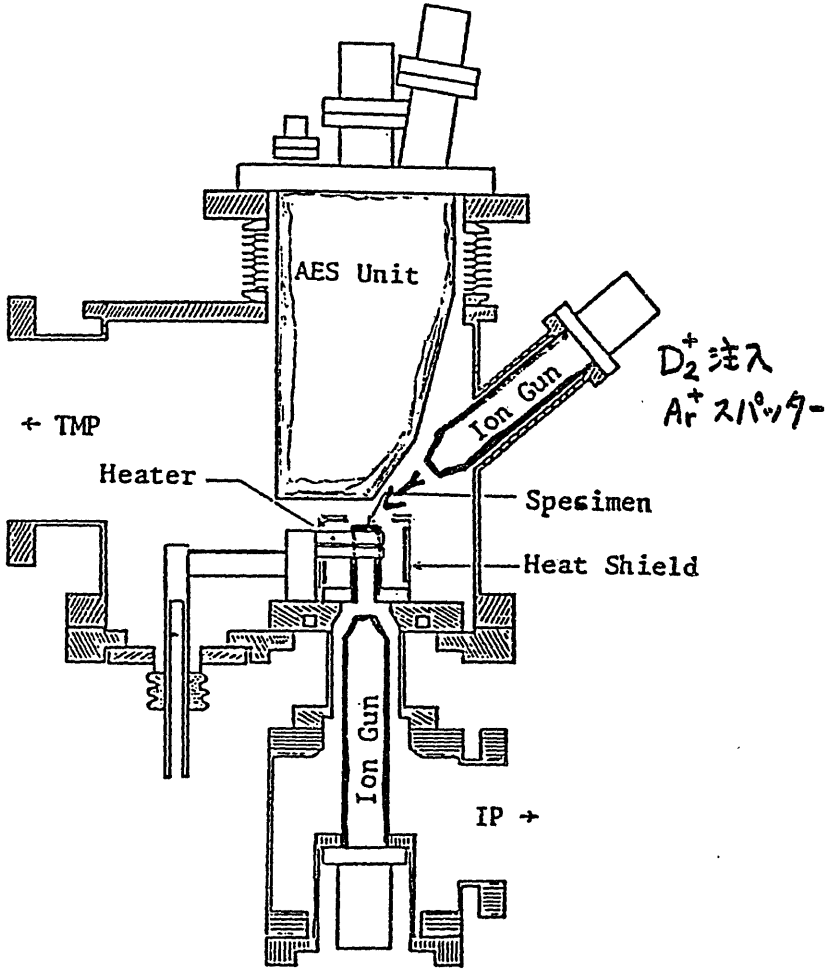

図 1. 装置断面図

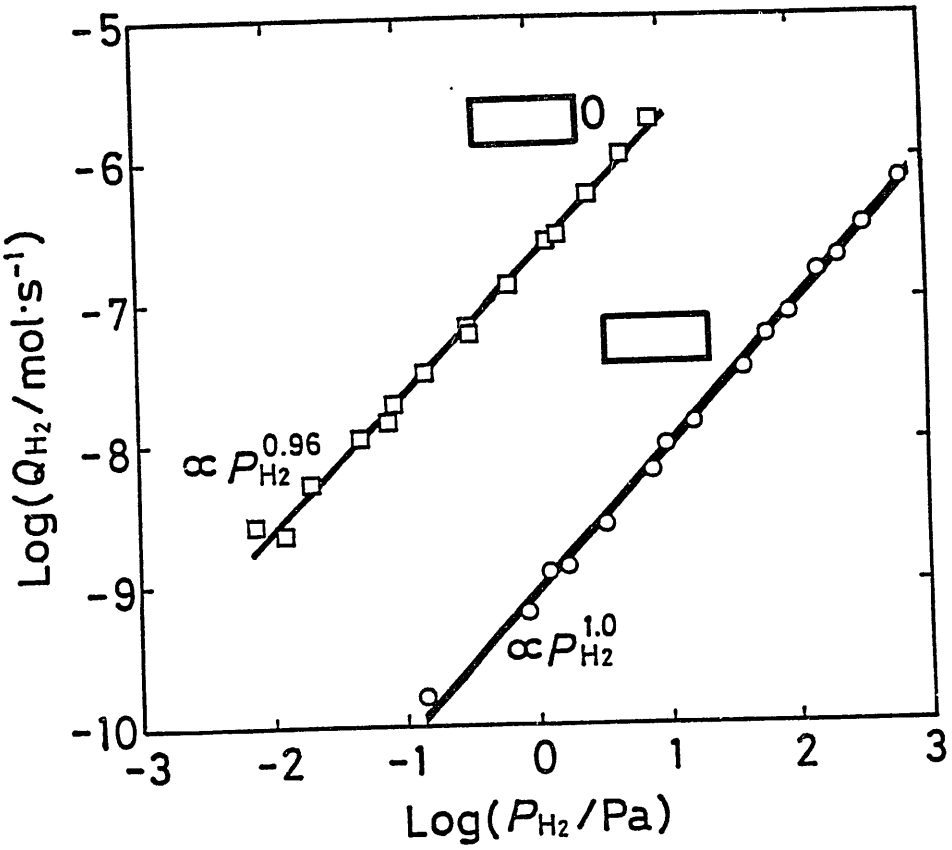
-5
-6
-7
-8
-9
-10
-3
-2
-1
0
1
2
3
Log(Q_{H_2}/mol·s^{-1})
Log(P_{H_2}/Pa)
$\propto P_{H_2}^{0.96}$
$\propto P_{H_2}^{1.0}$

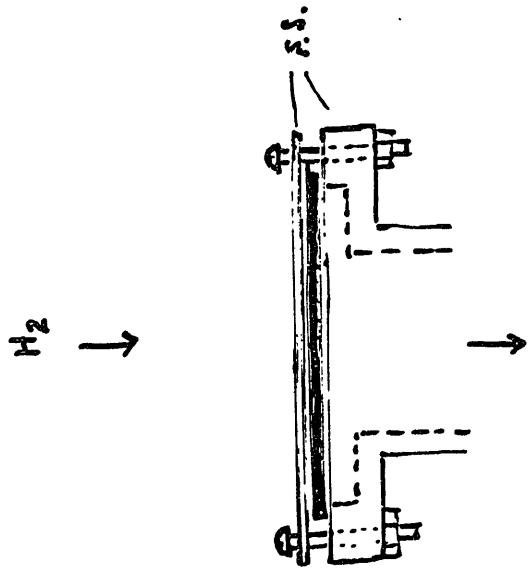
H_2

Darcy の法則

$$u = -B_0 \frac{\partial p}{\partial l} \qquad \dot{u}\ (\mathrm{cc/cm^2 \cdot sec})$$

$$u_0 = \frac{B_0}{L\,p_0} \cdot \frac{p_1 + p_2}{2} \cdot (p_1 - p_2) = \frac{B_0}{L} \cdot \frac{p_m}{p_0} \cdot \Delta p$$

Viscous Flow:

粘性流

$$q_m = A u_m = \frac{B_0}{L} \cdot A \cdot \Delta p$$

$$B_0 = q_m \cdot \frac{L}{A \cdot \Delta p}$$

Slip Flow:

分子流 (slip flow)

$$q_m' \cdot p_m = K_0 \cdot \frac{A}{L} \cdot \Delta p$$

$$q_m + q_m' = (\overset{V}{p_m B_0} + \overset{S}{K_0}) \frac{A}{p_m} \cdot \frac{\Delta p}{L}$$

$$= K \cdot \frac{A}{p_m} \cdot \frac{\Delta p}{L}$$

$$K = \frac{(p_m q_m) L}{A \cdot \Delta p}$$

$$K = \overset{S}{K_0} + \overset{V}{B_0 p_m}$$

Carman's eq.:

$$K = \underbrace{\frac{B^\circ}{\eta} \cdot p_m}_{V} + \underbrace{\frac{4}{3} K^\circ \sqrt{\frac{8RT}{\pi M}}}_{S}$$

Kinetic Theory of Gaseous Molecules

Poiseulli's Law

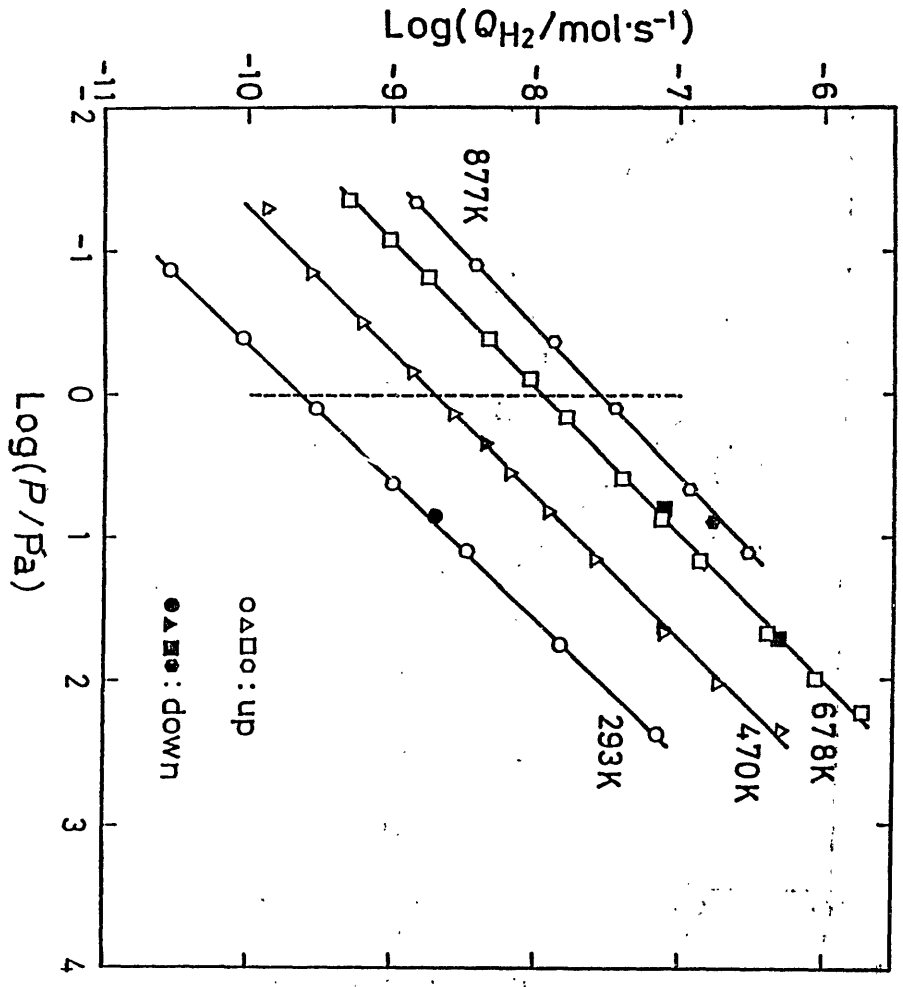

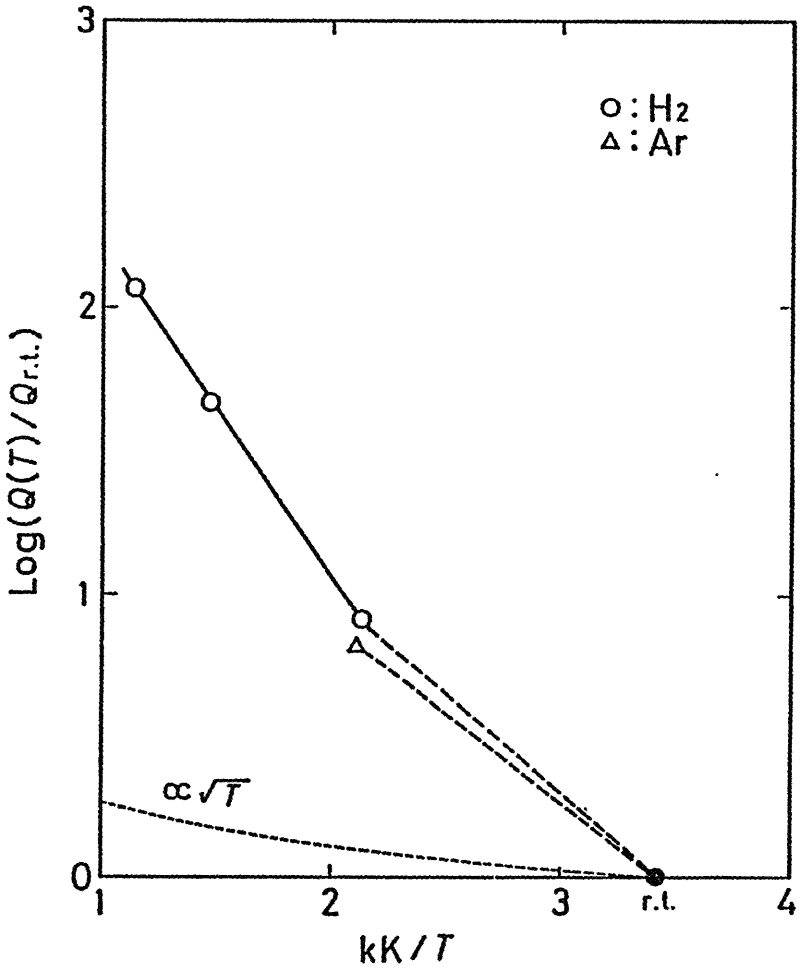

ITEMS OF PROBLEMS

— Permeation of H_2 —

(1) Temperature Dependence

— No Adequate Model

(2) Effect of Implantation

(3) Effect of (Surface) Impurities

(4) Change of Rate-limiting Steps: Viscous to Molecular Flow

Comments on recycling and hydrogen inventory

Volker Philipps

K F A

Abstract

Recycling behaviour in tokamaks with metals walls can be understood based on materials parameters of diffusion constants, recombination rates, solubilities etc of hydrogen in metals. The expected recycling in fusion devices with carbon walls is believed to be determined by the saturation of graphite due to hydrogen impact. This world result in R=1 after a transient pumping with R<1 and further change in the recycling would be only caused by temperature excurtions of the walls. In contrast, present observations in tokamaks(JET, TFTR, TEXTOR) can not be explained by this simple picture. The final clarification of the observed phenomena is still open. The answer of this behaviour will also drastically influence the expected tritium investory in fusion machines.

Recycling with carbon (carbonised) walls

(density control problem
→ Mlichson, Dietz, Wilson, Hirooka ...)

Expected behaviour from laboratory carbon data:

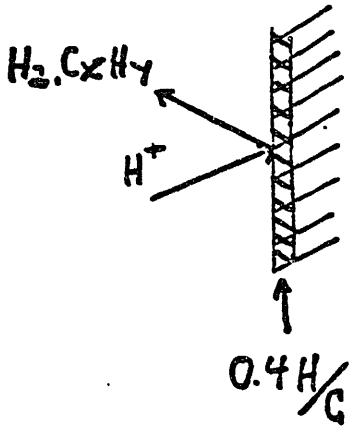

⇒ for a transient time:
strong wall pumping $R \ll 1$

⇒ in the steady state : $R = 1$
(no pumping)

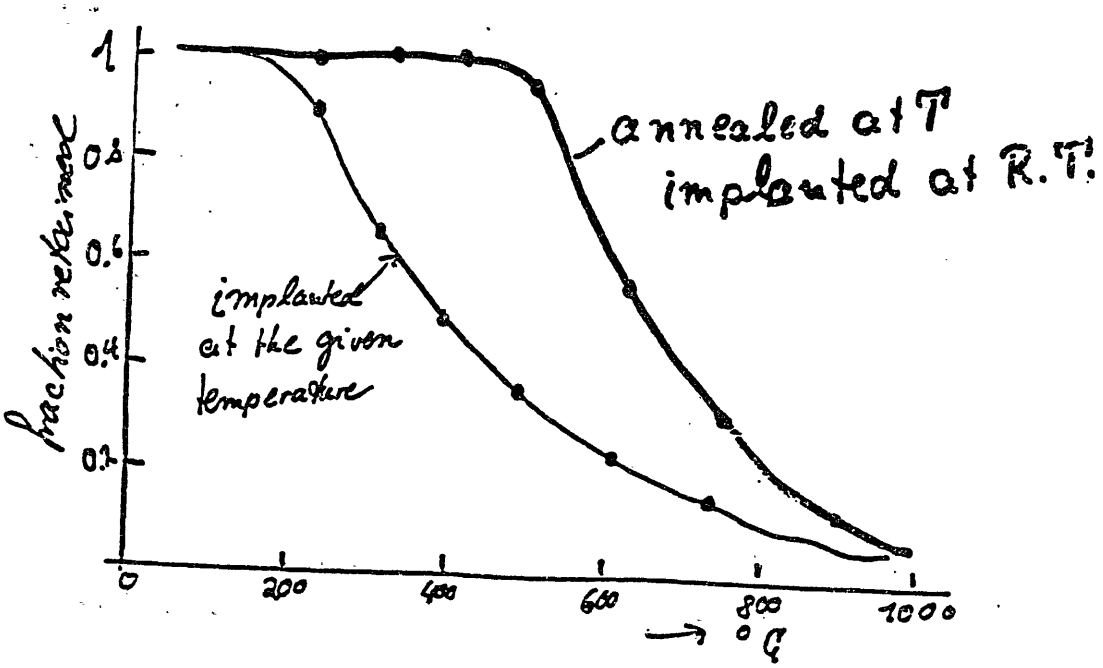

$R \doteq 1$ occurs only due to temperature excursion of the walls

<u>in contrast:</u>

<u>Observations in Tokamaks (JET, TFTR, TEXTOR) on recycling and wall pumping can not be explained by this simple trapping model</u>

<u>Main observations</u>

Reproducible wall pumping occurs due to plasma shifts (used as density control method)

Possible models to explain the wall pumping

- „Diffusion" model (long range Diffusion of hydrogen in graphit)
- „Hydrocarbon" model

} Hydrogen remains in the machine ⇒ <u>Tritium</u>

- „Transient" model

(under bombardment of H^+, the steady state hydrogen concentration depends from the fluxes (and energies) → (do not agree with lab..)

Some Considerations on Selection Criteria for Graphites as Fusion Materials

T. Oku

Japan Atomic Energy Research Institute

Abstract

Some considerations are made on the selection criteria for graphite materials when they are used for the fusion reactor components. The selection criteria are examined considering that the graphite might fracture due to internal stresses.

The internal stresses consist of a thermal stress based on temperature gradient in the components and irradiation-induced stress associated with dimensional changes due to neutron irradiation. It is stressed that the irradiation-induced stress is particularly important.

There may be impossible for the graphite to fracture if a stress generated is smaller than the fracture stress and a stress intensity factor or a J-integral value which controls initiation and extension of cracks is smaller than the respective fracture toughness value. From such viewpoints the selection criteria for graphite materials are examined and the present status of the data base on properties which are considered to be significant is reviewed. As a result, the data group which should be intensively obtained are defined.

1. Introduction

2. Service Conditions of Graphite as a Fusion Reactor Material

3. Definition of Important Phenomena

4. Definition of Selection Criteria for Graphite Materials

5. The properties Related to the Selection Criteria and Their Correlations

6. Present Status of Data Base

7. Examples of Calculation for the Irradiation-Induced Stresses

8. Concluding Remarks

* The selection criteria are defined taking note of that the crack in graphite may extend due to internal stress.

* The internal stresses consist of thermal stress based on the temperature gradient in the components and irradiation-induced stress generated from temperature dependence of dimensional changes.

* There exists a possibility of fracture which comes from initiation and extension of cracks due to internal stresses. In this case the properties we have to obtain are stress intensity factor and J integral value. and fracture toughness values.

* The first question is what properties are related to thermal stress, irradiation-induced stress, stress intensity factor and J-integral value. The second one is that under what conditions data on the properties are needed.

* The content of the selection criteria should be that stresses and stress intensity factors generated in the components are sufficiently smaller than the fracture stress and the fracture toughness values.

* In this paper it is shown that the irradiation-induced stress is particularly important and some examples of data base on properties related to it are examined and reviewed.

* The IEA Workshop report(May 1983) says that the most severe conditions in fusion reactor environment correspond to 7 dpa/MW/m^2/year and 1300 ppmHe/MW/m^2/year. And also it says that the life of the existing graphite is, from the dimensional changes data,

  30 dpa at 450 C

  20 dpa at 600 C

  ~10 dpa at 900-1400 C.

  Under the conditions above stated no sufficient data are available at present time and an intensive data acquisition is needed.

2. Service Conditions of Graphite as a Fusion Reactor Material

* According to the report of G. Hopkins and E. Opperman in the last Workshop the graphite receives the following neutron fluences.

1 MW year/m^2 = 1.4×10^{25}n/m^2(14 MeV-n)

= 7×10^{25}n/m^2(all energies)

TCFX(BCX)	TEST REACTOR(INTOR)
(0.2MW y/m^2)	(2MW y/m^2
1×10^{25}n/m^2	1×10^{26}n/m^2
(~1.4dpa)	(~14dpa)

3. Definition of Important Phenomena

From the viewpoint of the design and service life the following phenomena are considered to be important.

* fracture due to thermal stress and thermal cycle
* fracture due to irradiation-induced stress
* initiation and extension of cracks and fracture due to thermal stress and irradiation-induced stress.

4. Definition of Selection Criteria for Graphite Materials

The selection criteria should be derived from the condition that the service life for graphites becomes maximum. A graphite material to be selected must meet the following three conditions:

1) A margin of the strength to the stresses generated in operation is maximum.

2) A margin of the strength to irradiation-induced stresses in shut down is maximum.

3) A margin of the fracture toughness to the stress intensity factor or J-integral values is maximum.

5. The Properties Related to the Selection Criteria and Their Correlations

The stresses produced in the graphite components are generally dependent upon the geometry of the components. Therefore, the stresses produced cannot be obtained in a generic form unless the shape and size are determined. In order to know an intrinsic relation of the stresses generated with different kind of properties, let us consider for simplicity the stresses in a cylinder of inner and outer radii r_1 and r_2 respectively.

We assume that heat does not flow to z-direction but to r-direction only. Then, we have temperature difference in the r-direction only.

temperature of inner surface; T_1

temperature of outer surface; T_2

Young's modulus; E

Poisson's ratio; ν

thermal expansion coefficient; α

The thermal stresses $\sigma_\theta(r_1)$ and $\sigma_\theta(r_2)$ are expressed as follows

$$\sigma_\theta(r_1)=\sigma_z(r_1)=\sigma_{th}(r_1)$$
$$= \alpha E(T_1-T_2)/(1-\nu)[1/2\ln(r_2/r_1)-r_2^2/(r_2^2-r_1^2)] \quad (1)$$
$$\sigma_\theta(r_2)=\sigma_z(r_2)=\sigma_{th}(r_2$$
$$= \alpha E(T_1-T_2)/(1-\nu)[1/2\ln(r_2/r_1)-r_1^2/(r_2^2-r_1^2)] \quad (2)$$

When the heat source exists in the inner side of the cylinder, the following holds.

$$\sigma_{th}(r_1)<0<\sigma_{th}(r_2)$$

In the case of inner surface, that is $\sigma > 0$,

$$\sigma = \sigma_{th} + \tfrac{1}{2}(\varepsilon_{i2} - \varepsilon_{i1})E - K\sigma\Phi E \qquad (3)$$

In the case of outer surface, that is $\sigma < 0$,

$$\sigma = \sigma_{th} - \tfrac{1}{2}(\varepsilon_{i2} - \varepsilon_{i1})E + K\sigma\Phi E \qquad (4)$$

Therefore

$$\sigma_i = [2\sigma_{th}(r_1) + (\varepsilon_{i2} - \varepsilon_{i1})E]/2(1+KE\Phi) \qquad (5)$$

$$\sigma_0 = [2\sigma_{th}(r_2) - (\varepsilon_{i2} - \varepsilon_{i1})E]/2(1-KE\Phi) \qquad (6)$$

Accordingly, the maximum tensile stress in these stresses is $\sigma_{th}(r_2)$ Eq. (2) or σ_i when $\sigma_{th}(r_1) = 0$ in Eq. (5), that is, the stress in shut down of the reactor, say σ_i', becomes:

$$\sigma_i' = (\varepsilon_{i2} - \varepsilon_{i1})E/2(1+KE\Phi) \qquad (7)$$

On the other hand, the temperature difference between inner and outer surfaces of the cylinder can be expressed by the following equation.

$$T_1 - T_2 = q \ln(r_2/r_1)/2\pi\lambda \qquad (8)$$

where q is the heat generation rate per length and λ thermal conductivity. Then thermal stress at $r = r_2$ is expressed by

$$\sigma_{th}(r_2) = [q\beta'(r_1, r_2)/2\pi][\alpha E/\lambda(1-\nu)] \qquad (9)$$

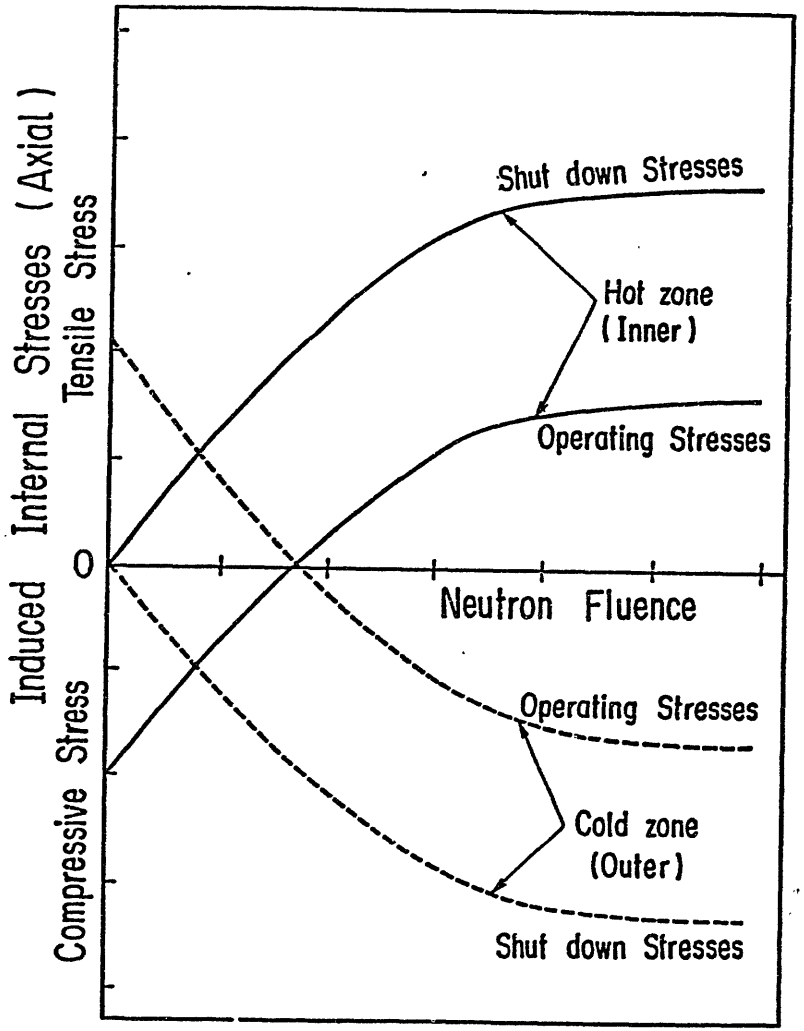

Ratios of the stresses to the mean tensile strength σ_t are expressed

$$\sigma_i'/\sigma_t = \tfrac{1}{2}(\varepsilon_{i2}-\varepsilon_{i1})E/(1+KE\Phi)\sigma_t \qquad (10)$$

and

$$\sigma_{th}(r_2)/\sigma_t = [q\beta'(r_1,r_2)]\{\alpha E/\lambda(1-\nu)\sigma_t\} \qquad (11)$$

The smaller the above ratios become, the smaller the fracture probability will be.

On the other hand, the stress intensity factor K_I at the crack tip (length a) is expressed by

$$K_I = C\cdot\sigma\sqrt{\pi a} \qquad (12)$$

where C is a constant which depends on the shape of the component.

J-integral values can be expressed by the following equation in a small scale range of yielding.

$$J_I = (1-\nu^2)K_I^2/E \qquad (13)$$

If these values are sufficiently smaller than the fracture toughness values K_{IC} and J_{IC}, there is extremely small possibility of initiation and extension of cracks. It should be noted that the extension of crack depends upon not only stress, Young's modulus and Poisson's ratio but also crack length a. Therefore, it is required for predicting the extension of cracks to know the maximum crack size before using the material.

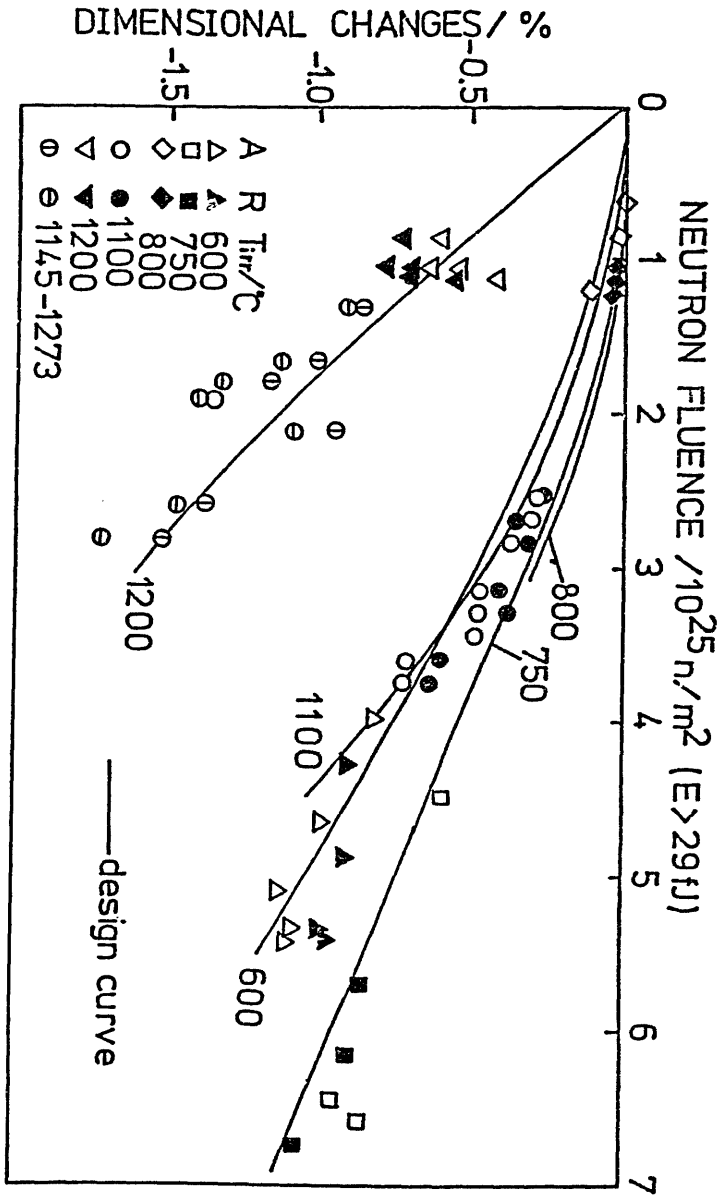

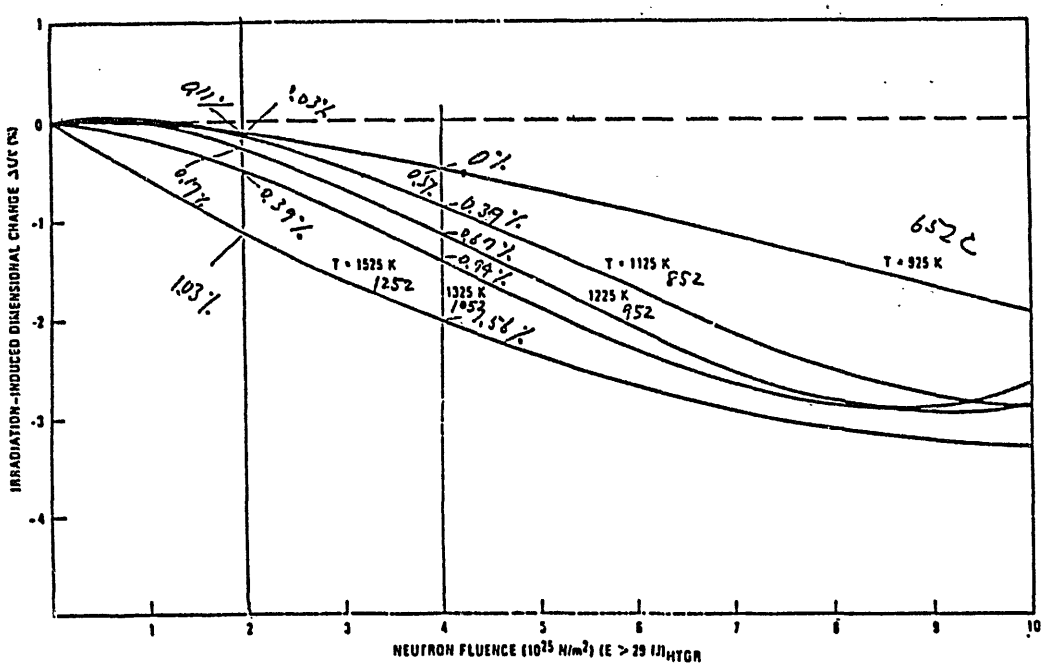

Fig. 5-3 (a). Irradiation-induced dimensional change in H-451 graphite, axial orientation - design curves

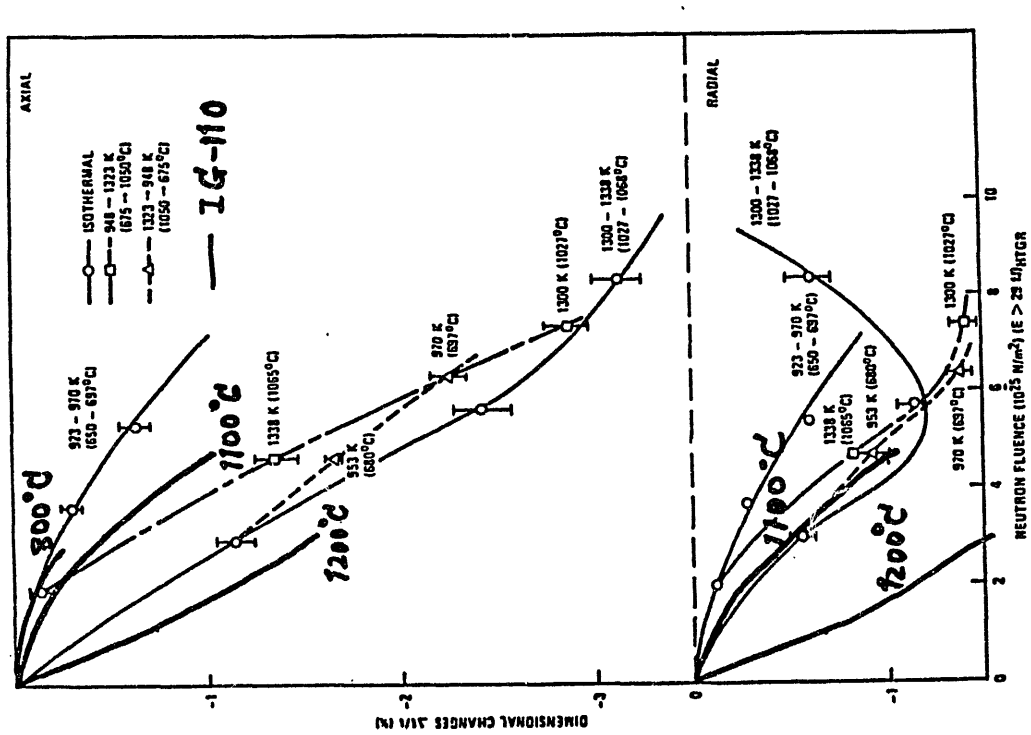

Fig. 5-7. Dimensional changes in H-451 graphite irradiated with changes in temperature

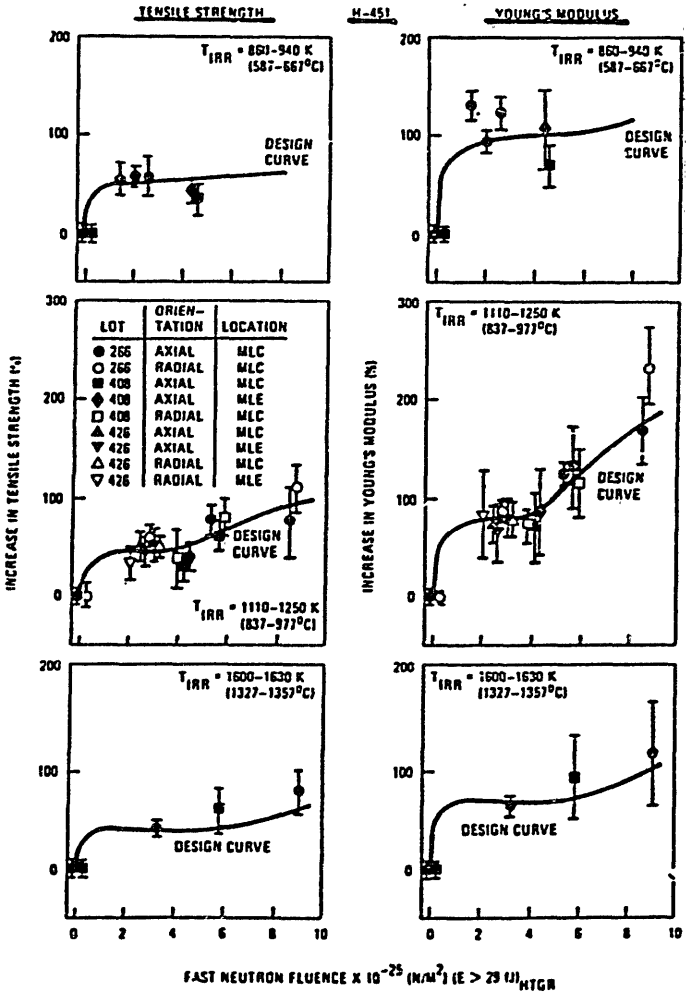

Fig. 7-1. Changes in tensile strength and Young's modulus of H-451 graphite as a function of fast neutron fluences. Error bars denote ± one standard deviation

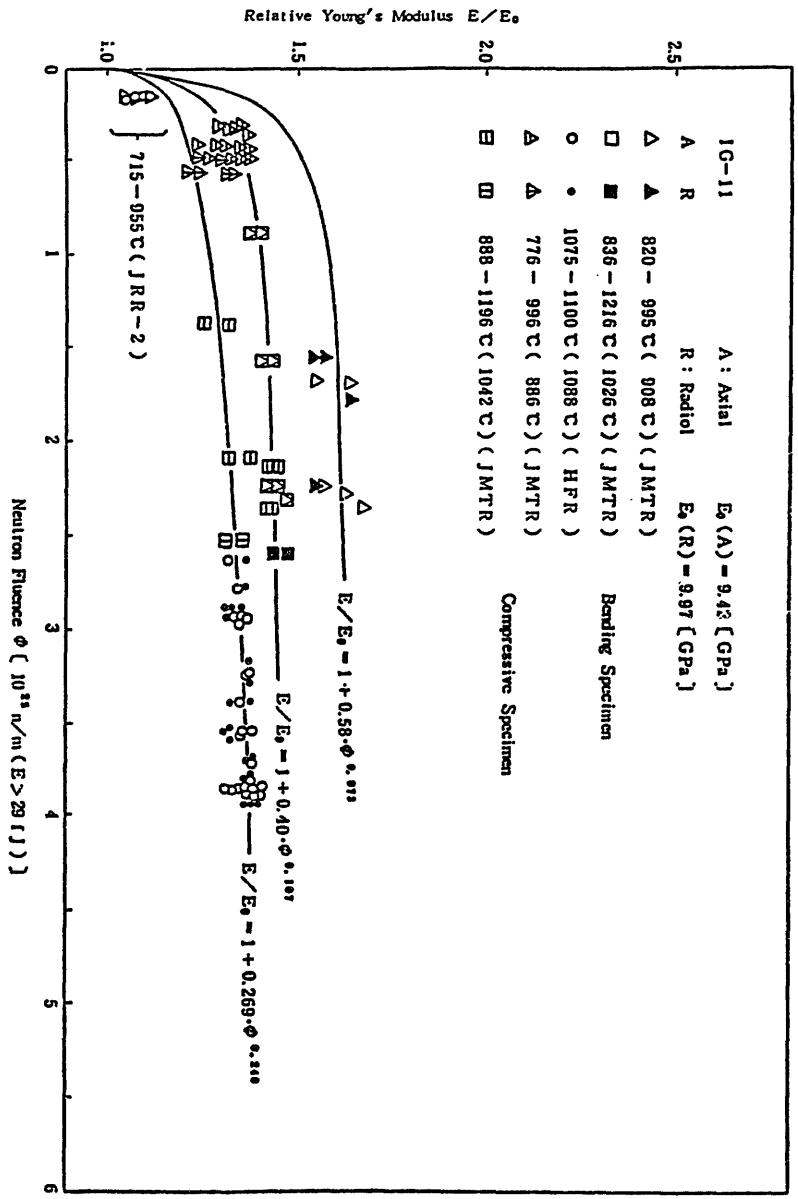

$$\sigma/\sigma_0 = (E/E_0)^{0.64}$$

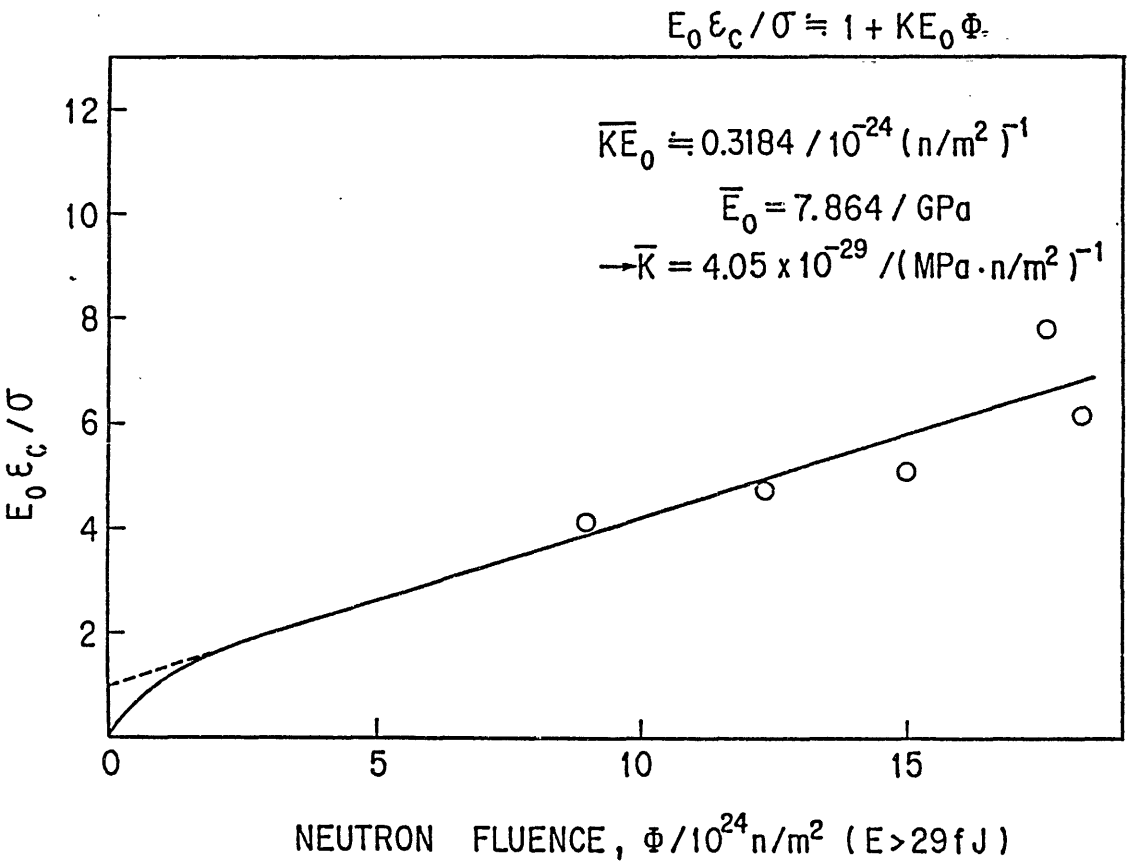

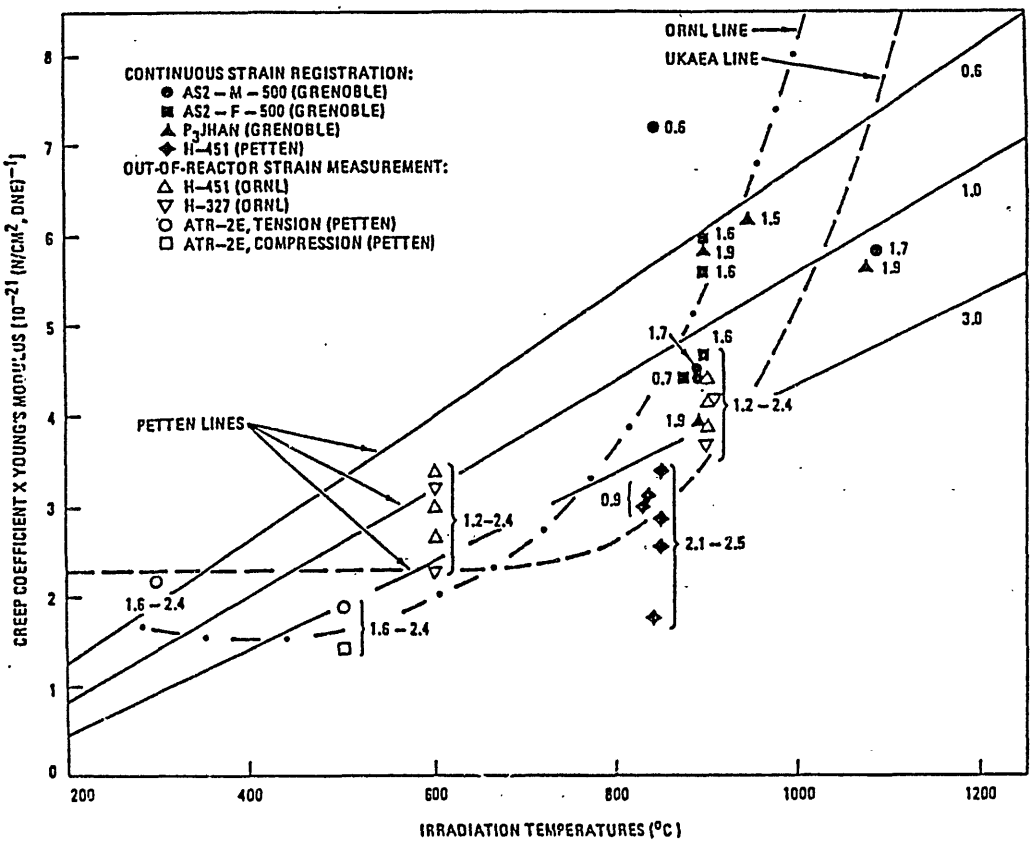

Fig. 17. Composite plot of creep coefficient multiplied by initial Young's modulus as a function of temperatures

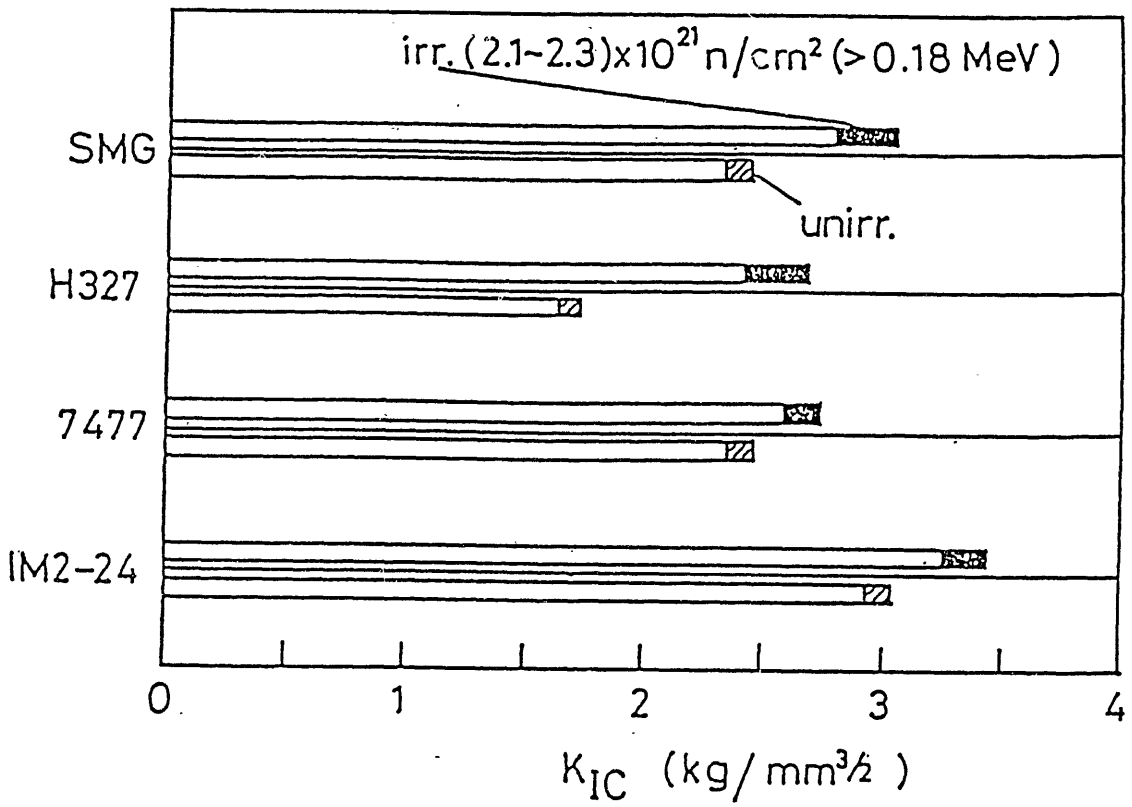

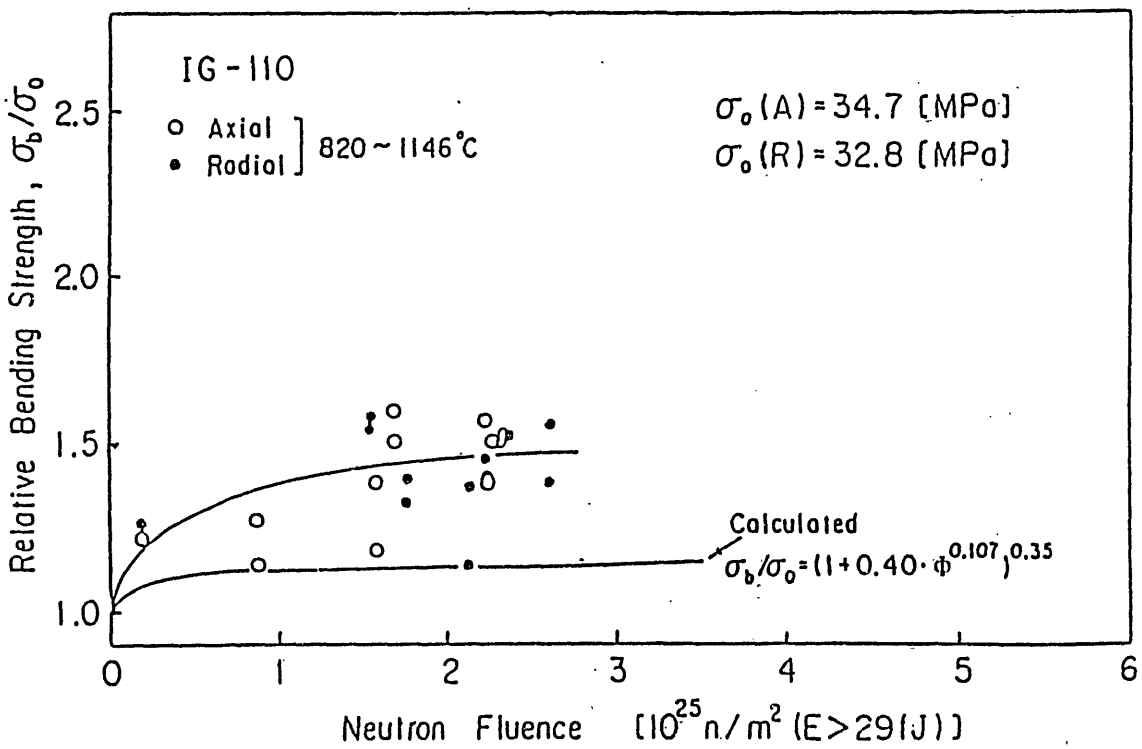

Fig. Relative change in the bending strength of IG-110 graphite as a function of neutron fluence

7. Examples of Calculation for the Irradiation-Induced Stresses

We attempt to obtain the values of Eqs.(7) and (10) by using the design data on IG-110 and H-451 graphites. Let us consider the case of T_1=1050 C, T_2=950, 850 C and 2×10^{25} and 4×10^{25}n/m^2 for neutron fluence. Table 1 shows dimensional changes, $\varepsilon_{12}-\varepsilon_{11}$, the Young's modulus of unirradiated materials , E_0 and KE_0. If we use these values, σ_i' are obtained as shown in Table 2. σ_t and σ_i'/σ_t are also listed in the same table.

Table 1 Dimensional changes, Young's modulus and creep coefficient.

Grade	Φ	$\varepsilon_{12}-\varepsilon_{11}$/%		E_0	KE_0
	10^{25}n/m^2	T_2/C		GPa	(n/m^2)$^{-1}$
		950	850		
	0	-	-	10.5	-
IG-110	2	0.209	0.343	15.5	2.5×10^{-25}*
	4	0.343	0.579	17.0	2.5×10^{-25}*
	0	-	-	10.4	-
H-451	2	0.22	0.36	18.0	2.5×10^{-25}**
	4	0.27	0.55	18.0	2.5×10^{-25}**

* design value

** the mean value of 1.39×10^{-25}~3.63×10^{-25}

7) The stress intensity factor and J-integral value requires an information on the initial crack size in addition to the parameters needed for stress calculation.

8) Since irradiation effects data on the fracture toughness values are not enough for evaluating the crack extension, the intensive data acquisition is required in the future.

Intro: It may be understood that one of the purpose of the present workshop is to make clear the feasibility of graphite for the next fusion facilities.
The question we have is what we should do or what we can do to examine the feasibility.
The next problem is howlong is the graphite is usable for the fusion facilities. It is not easy for us to choose a graphite from different kinds.
As a result, a selection criteria for graphite materials is needed.

Fig. 7: This is a schematic viewgraph which shows thermal stresses and irradiation-induced stresses. Very clearly, the stress in question is generated in a hotzone(inner surface) in shutdown of the facility.

Before data base:
First, one of the important phenomena is the dimensional change. Secondly, E, K and σ_f are needed.

Table 2: This table indicates that there is no significant difference in the results of IG-110 and H-451 graphites. Here, it should be noted that the important property is the difference in the dimensional changes due to the difference in irradiation temperature. This is considerd to be quite large contribution to σ_i. There is an another information that the K may be slightly smaller for much higher neutron fluences.

Presentations on Graphite Technology

W.P. Eatherly

Oak Ridge National Laboratory
Oak Ridge, Tennessee USA

Abstract

The properties Kic, E, and ultimate tensile strength have been measured on three graphite irradiated to neutron fluences beyond dimensional turn-around.
Kic is relatively uneffected, while the effective flaw size monotonically decreases.
Gic as caluculated from Kic monotonically decreases consistent with the model of original flaw heating accompanied by generation of many new small flaws.

THE SHORT ROD TEST IS ALSO A QUICK AND EASY TEST TO RUN

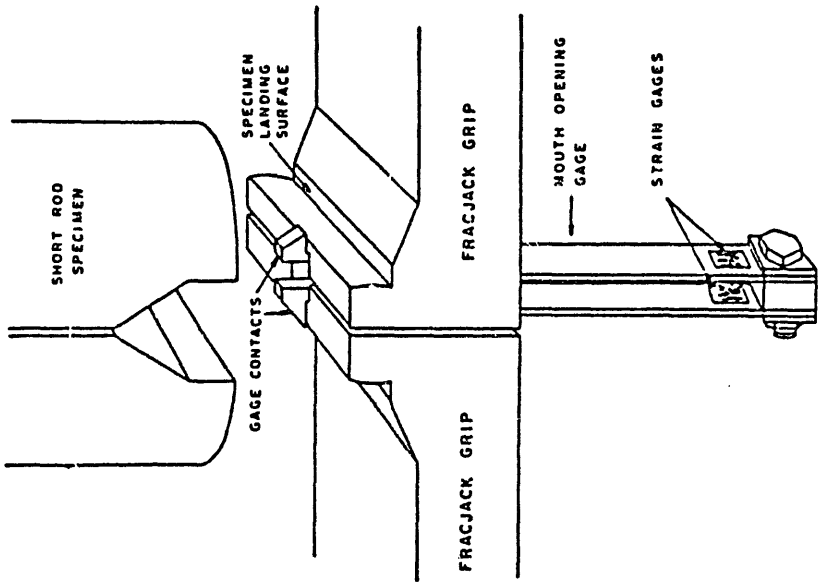

THE SHORT ROD SPECIMEN IS COMPATABLE WITH OXIDATION AND IRRADIATION TESTING

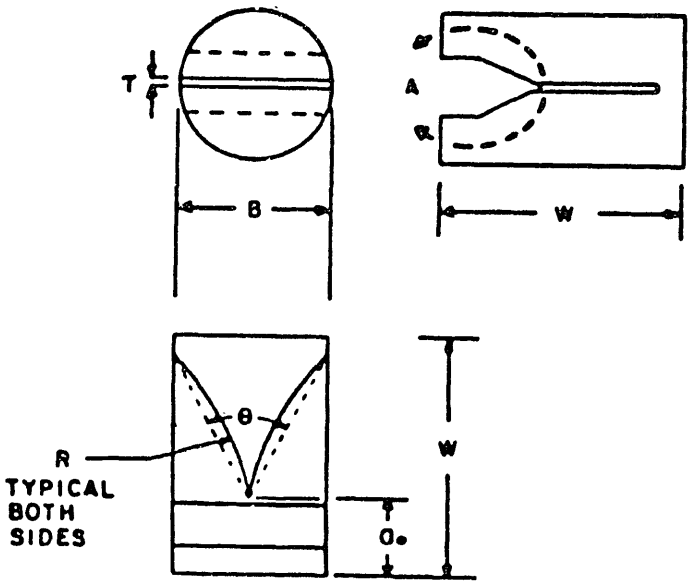

SHORT ROD

THE GRIFFITH-IRWIN EQUATION HAS BEEN DEMONSTRATED TO BE APPLICABLE IN DESCRIBING FRACTURE OF MOST CERAMICS AND GRAPHITES

$$\sigma_f = \left[\frac{G_{Ic}\, E}{\pi\, c}\right]^{1/2} = \frac{K_{Ic}}{[\pi\, c]^{1/2}}$$

G_{Ic} = STRAIN ENERGY RELEASE RATE

E = YOUNG'S MODULUS

c = HALF WIDTH OF DEFECT

K_{Ic} = CRITICAL STRESS INTENSITY FACTOR

THE DIFFERENCE BETWEEN WITH–GRAIN AND AGAINST–GRAIN STRENGTH IS A RESULT OF DEFECT ANISOTROPY

	RATIO
FRACTURE STRENGTH	1.57
SQUARE ROOT OF ATTENUATION	1.56

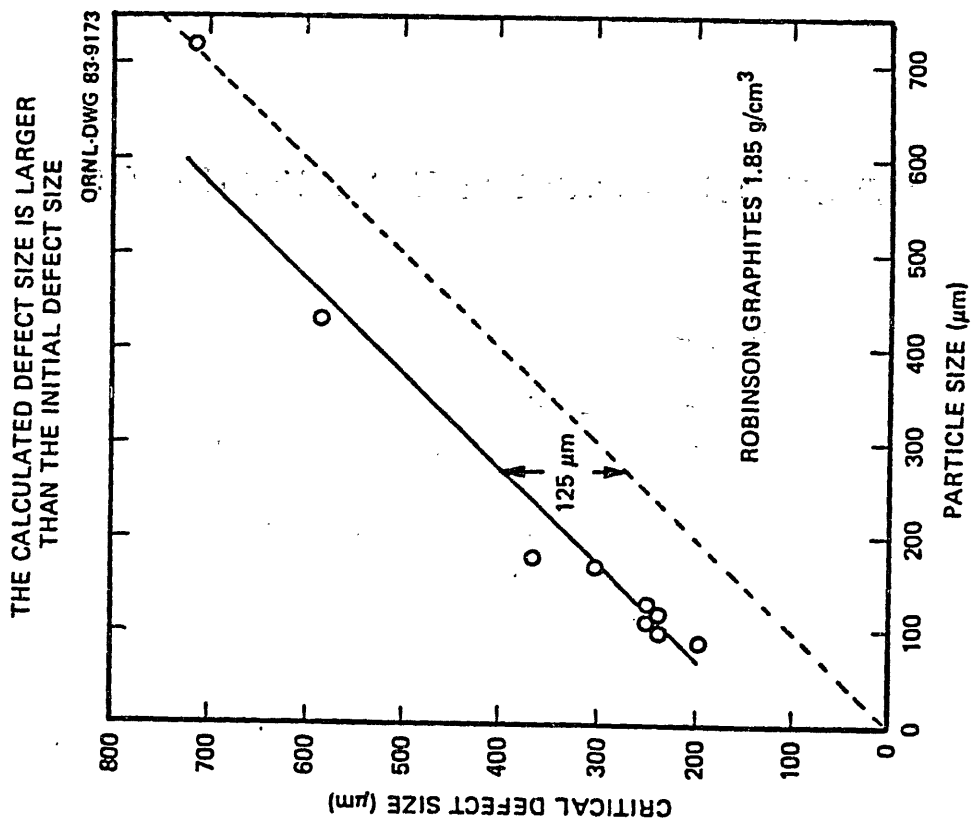

SUMMARIZING THE EFFECT OF ANISOTROPY

- K_{IC} DOES NOT VARY
- PARTICLE ANISOTROPY YIELDS DEFECT ANISOTROPY
  - AGAINST GRAIN STRENGTH REDUCED BY LARGER DEFECT SIZE
- G_{IC} MEASURED IS TOTAL WORK OF FRACTURE

STRENGTH IS INCREASED BY IRRADIATION

- ASSUMPTIONS
  - G_{IC} CONSTANT
  - CRITICAL DEFECT SIZE CONSTANT
- STRENGTH CAN THEN BE PREDICTED BY MODULUS CHANGE

CRACK GROWTH REDUCES THE SENSITIVITY TO DISPARATE FLAWS.

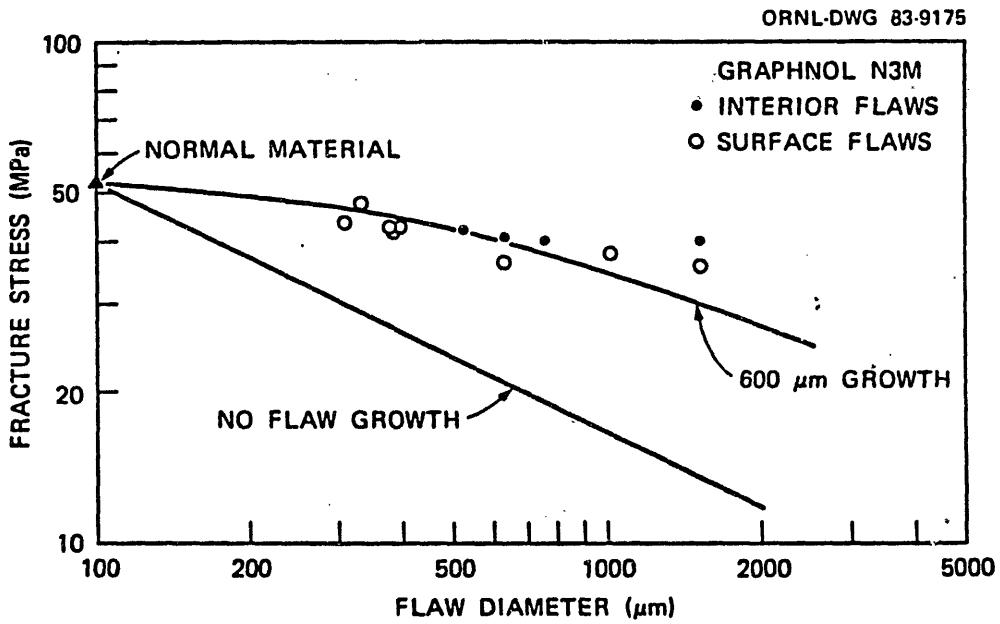

THE ASR1RS FRACTURE TOUGHNESS SPECIMENS WERE IRRADIATED PAST MAXIMUM DENSIFICATION AT 900C

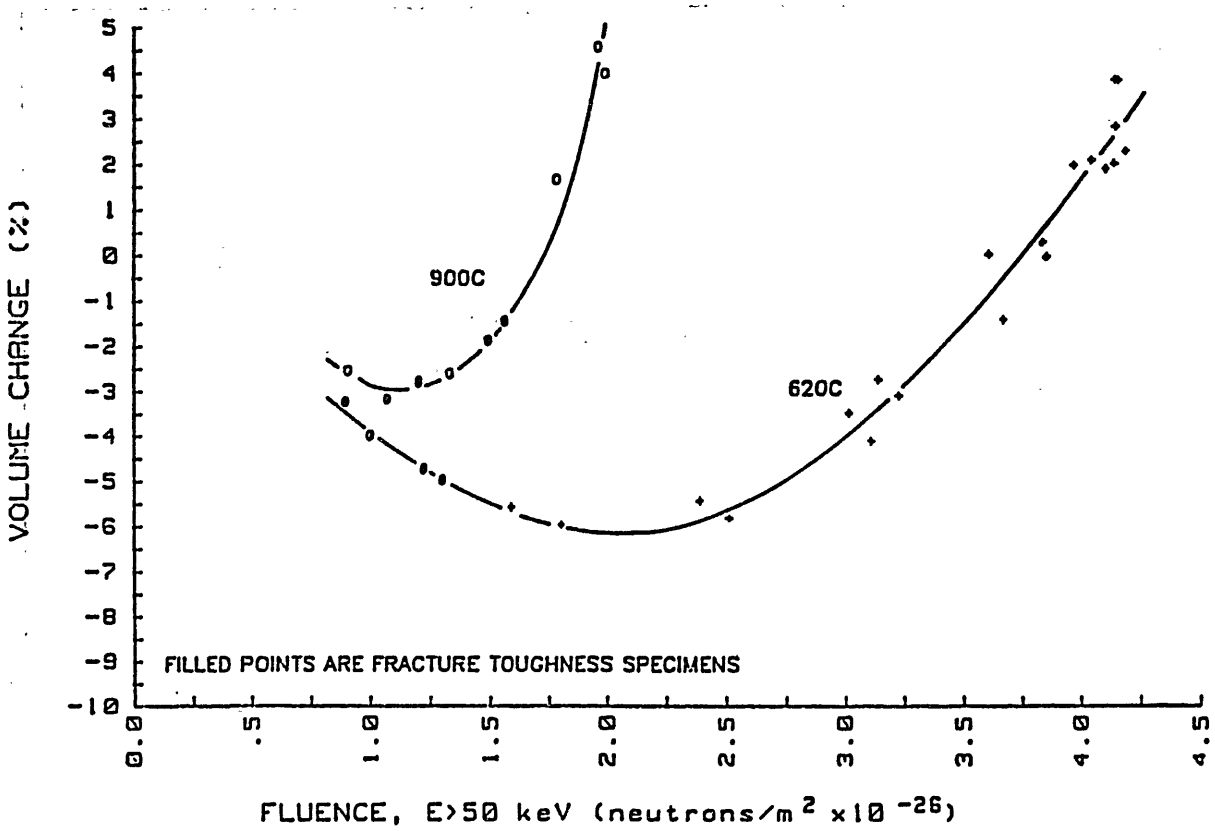

ALL OF THE GERMAN AND US GRAPHITES ARE FAIRLY ISOTROPIC

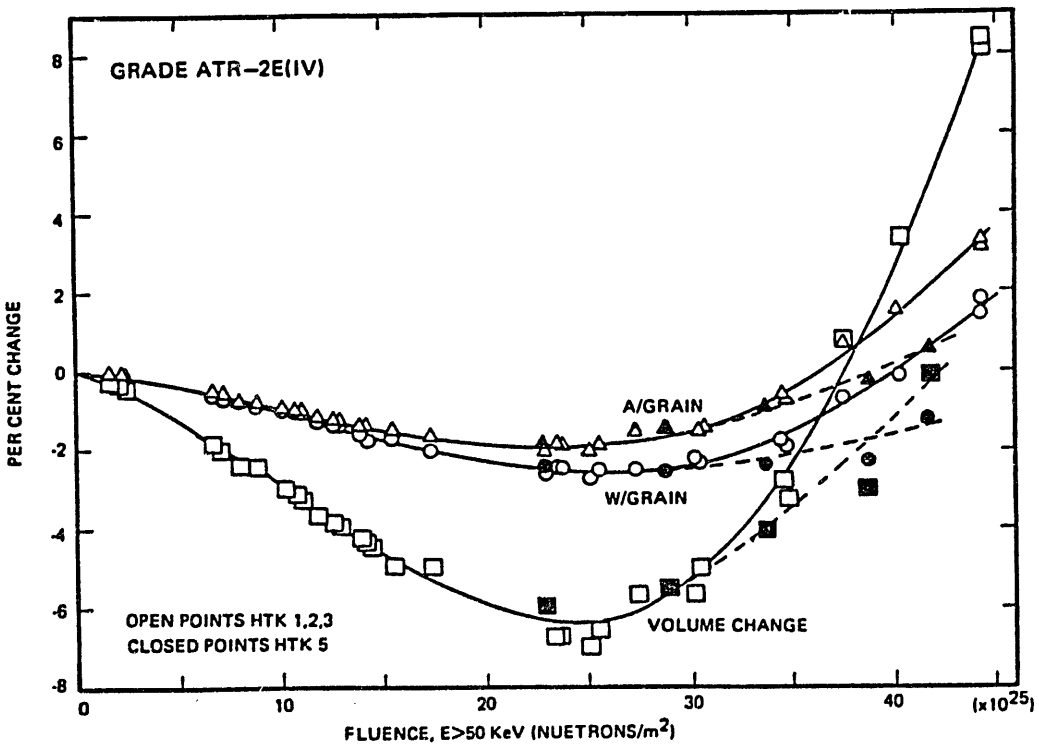

FRACTURE TOUGHNESS DOES NOT VARY MUCH WITH FLUENCE

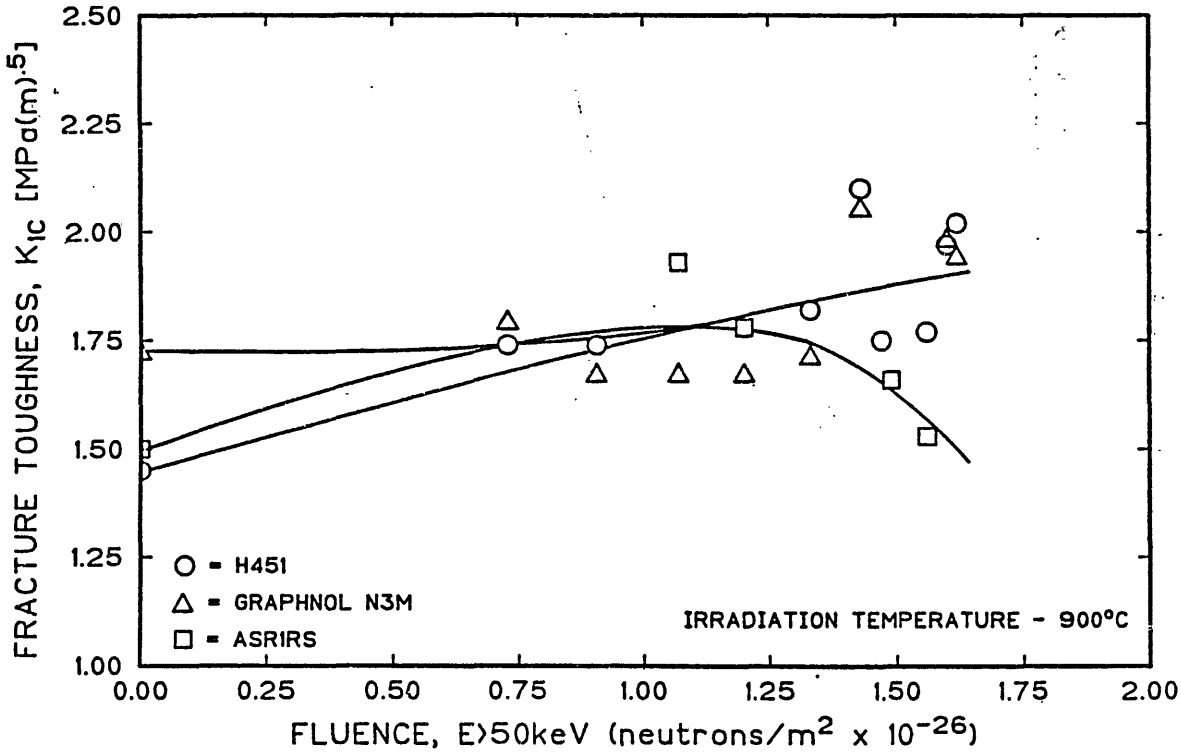

THE MODULUS IS SIGNIFICANTLY INCREASDED BY IRRADIATION

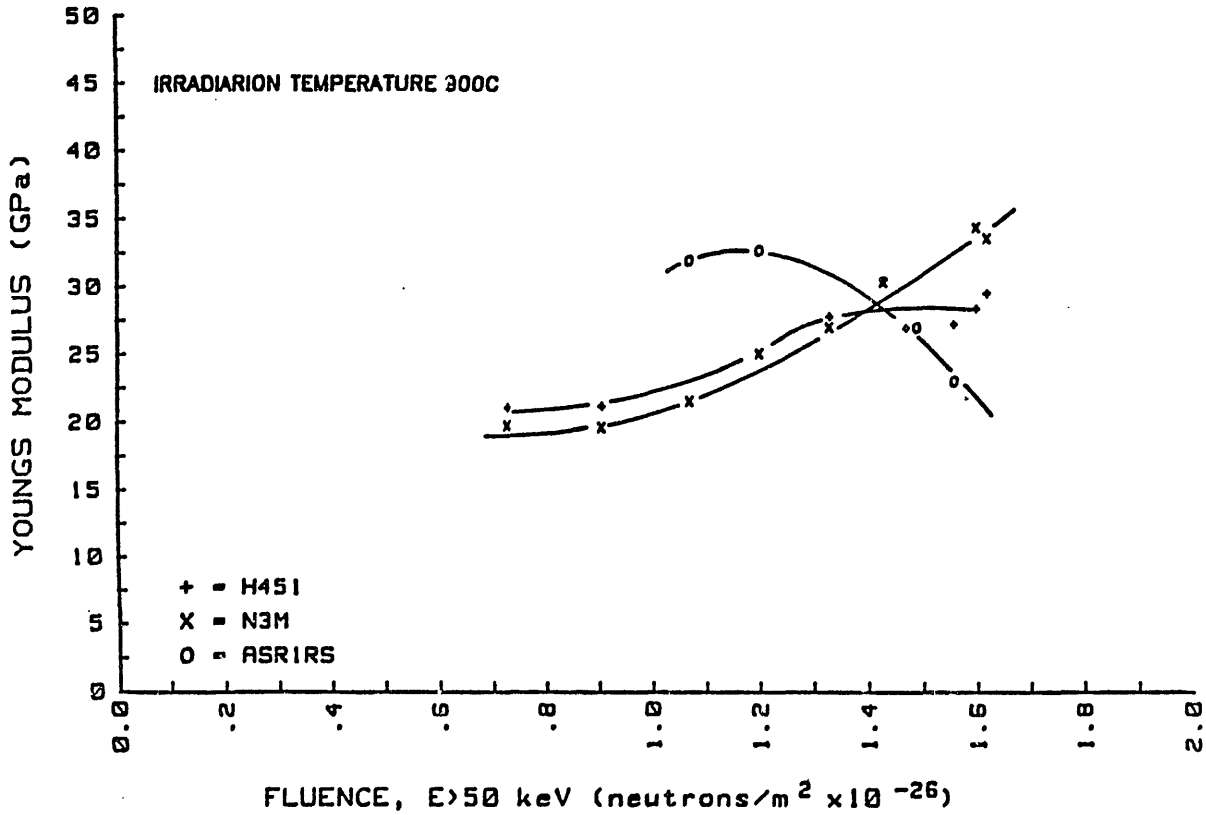

THE CRITICAL DEFECT SIZE IN ALL GRADES DECREASES WITH FLUENCE

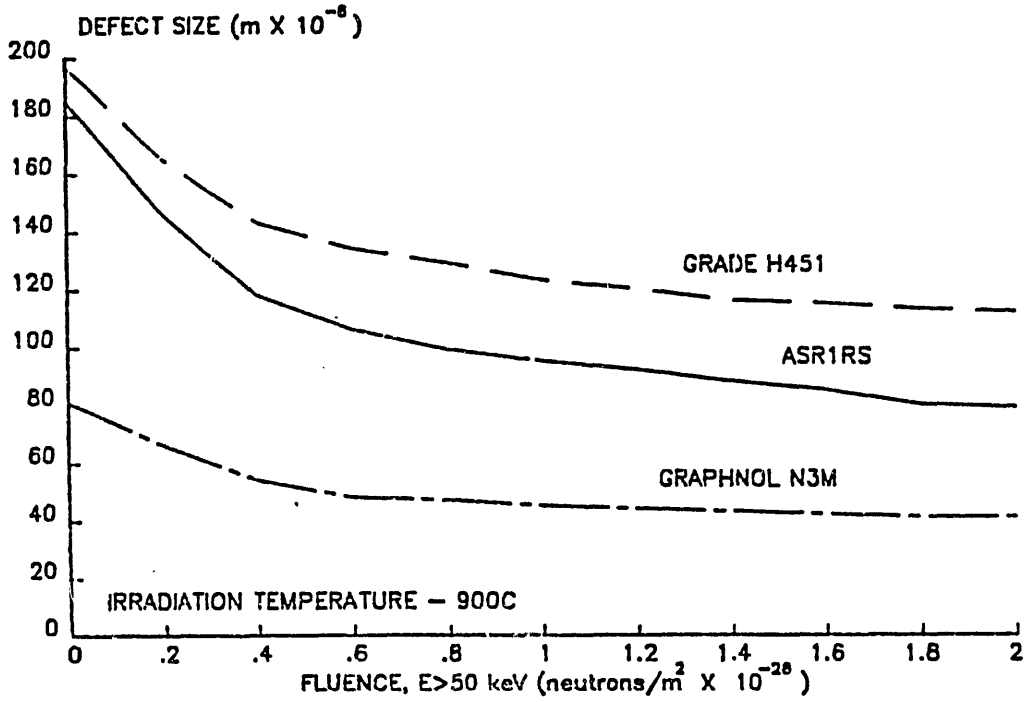

STRAIN ENERGY RELEASE RATE DECREASES WITH FLUENCE

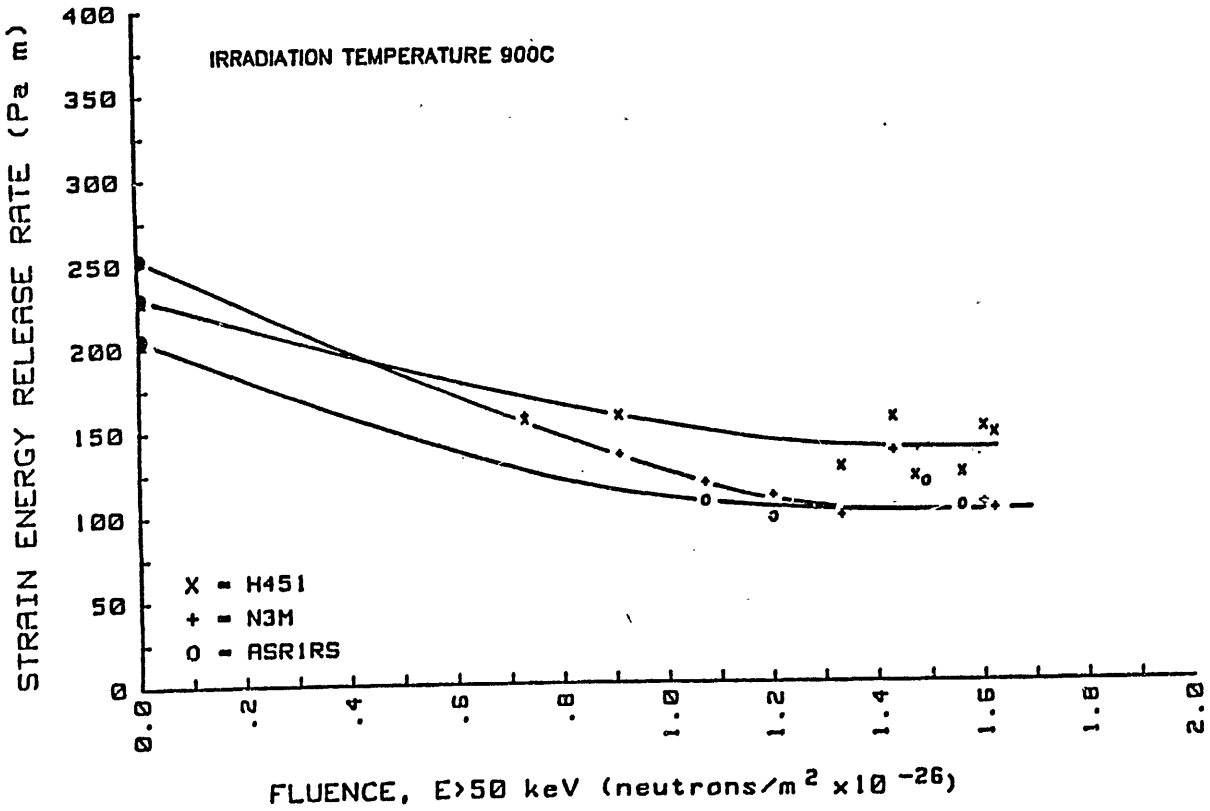

FUTURE WORK INDICATED

- SEPERATION OF G_{IC} AND G_P
- REASSESMENT OF PAST STUDIES
- APPLICATION OF FRACTURE TOUGHNESS TO DESIGN
  - SECTION SIZE
  - STRESS GRADIENTS
  - IMPACT LOADING

Neutron irradiation tests for graphite and Low-Z-ceramics

Jochen Linke

K F A

Abstract

A short report is given on the irradiation test which are planned on have already started in the frame of the KFA programme. These include neutron irradiation tests on graphites and low-Z ceramics in a fission neutron environment(HFR-Petten) and in a spallation neutron flux(LAMPF-Los Alamos), respectively.

Irradiation Tests for Graphites and Ceramics

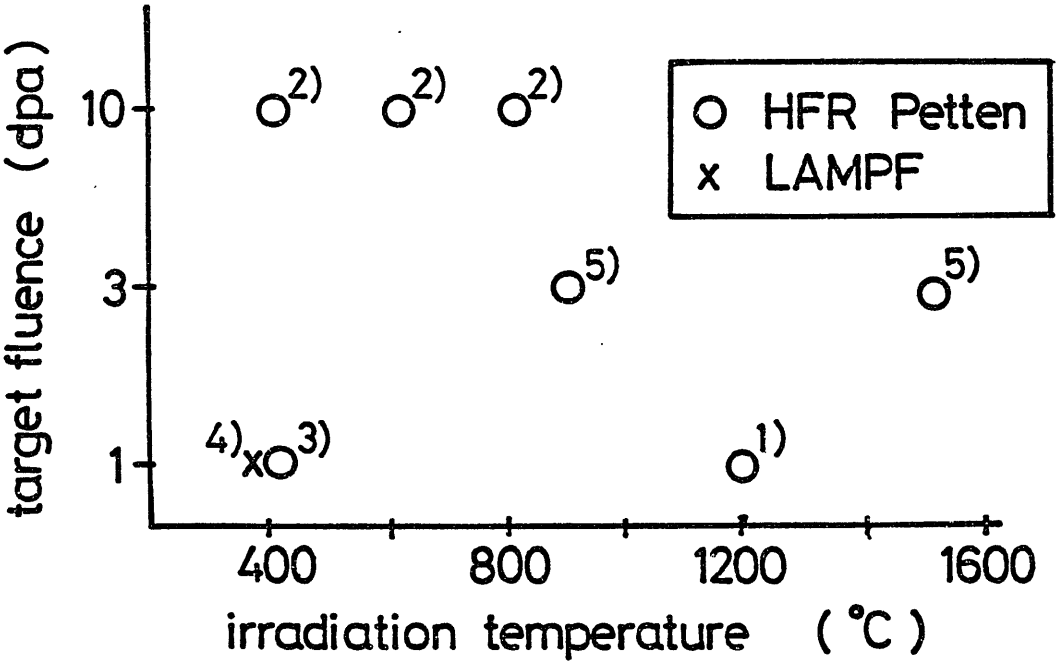

	post irradiation testing	typ of materials	partners	beginning of irradiation
1)	-bending test	graphites + ceramics	KfK,CER	09/86
2)	-thermal conductivity			06/87
3)				beginning of 88
4)			JAERI	06/86
5)	-thermal shock	graphites C-C comp. SiC	KfK	11/87

Ran Away Electron Analysis for TORE SUPRA

R.T. McGrath

Sandia National Laboratories

Abstract

The localized energy deposition of runaway electrons can have discontinous effects for tokamak interior components, especially there operating with active cooling. Experience on JET implies that as much as 40kJ can be deposited over small surface areas, $\sim 5cm^2$, per runaway event. Presented here is the analysis of electron slowing down in graphite armor and coolant lines for the actively cooled limiters to be used on TORE SUPRA. We find that significant energy is deposited outside the projected beam aria due to large angle scattering events and that 2.0 cm or more of graphite armor is required to reduce localized heating of the coolant lines to a manageable level.

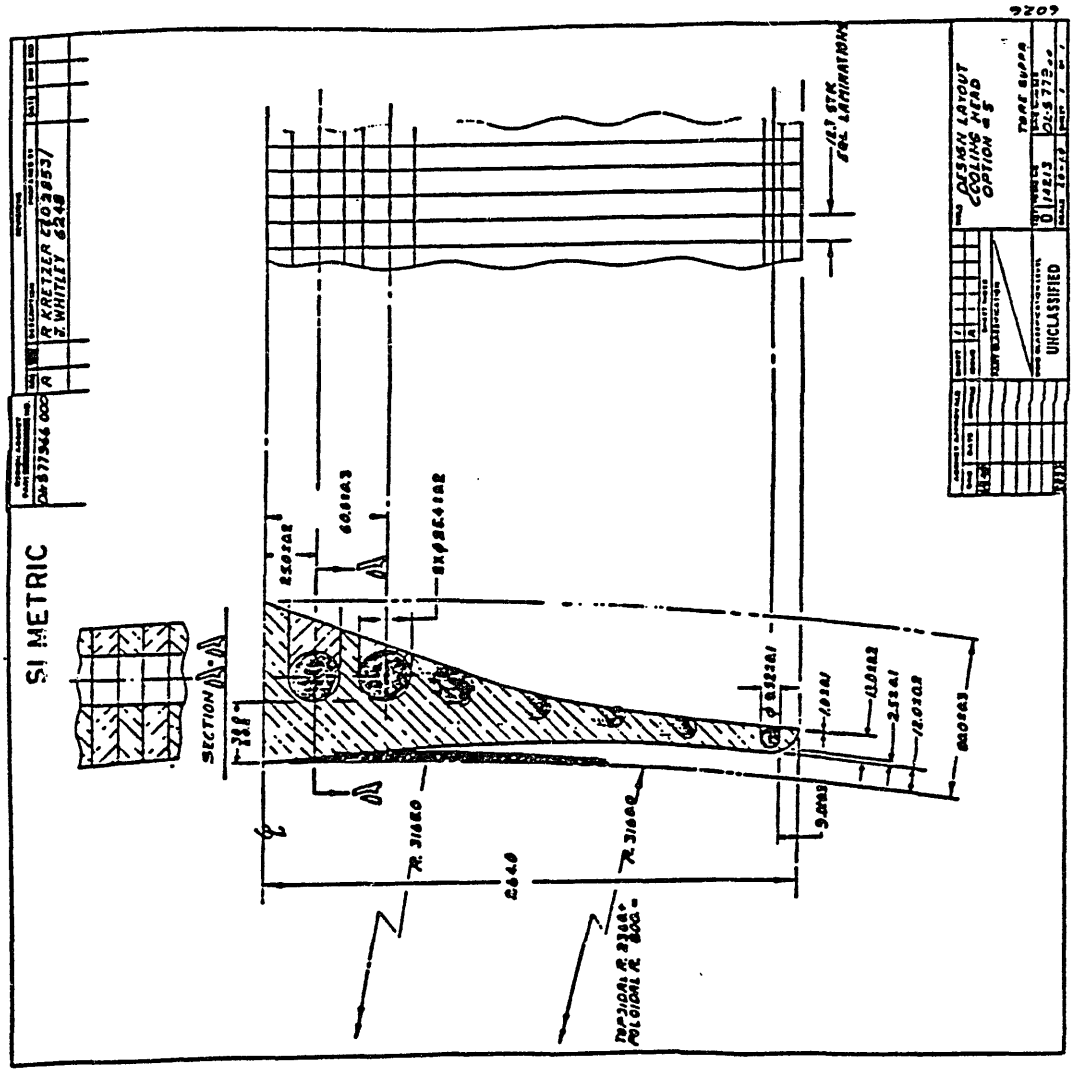

TIGER SUMMARY

* Tiger has proven to be a powerful tool for analyzing runaway electron energy deposition.

* Dispersion of the incident electrons results in substantial energy depostion outside the projected beam area.

* A better understanding of the flux and energy distribution of the runaways is needed.

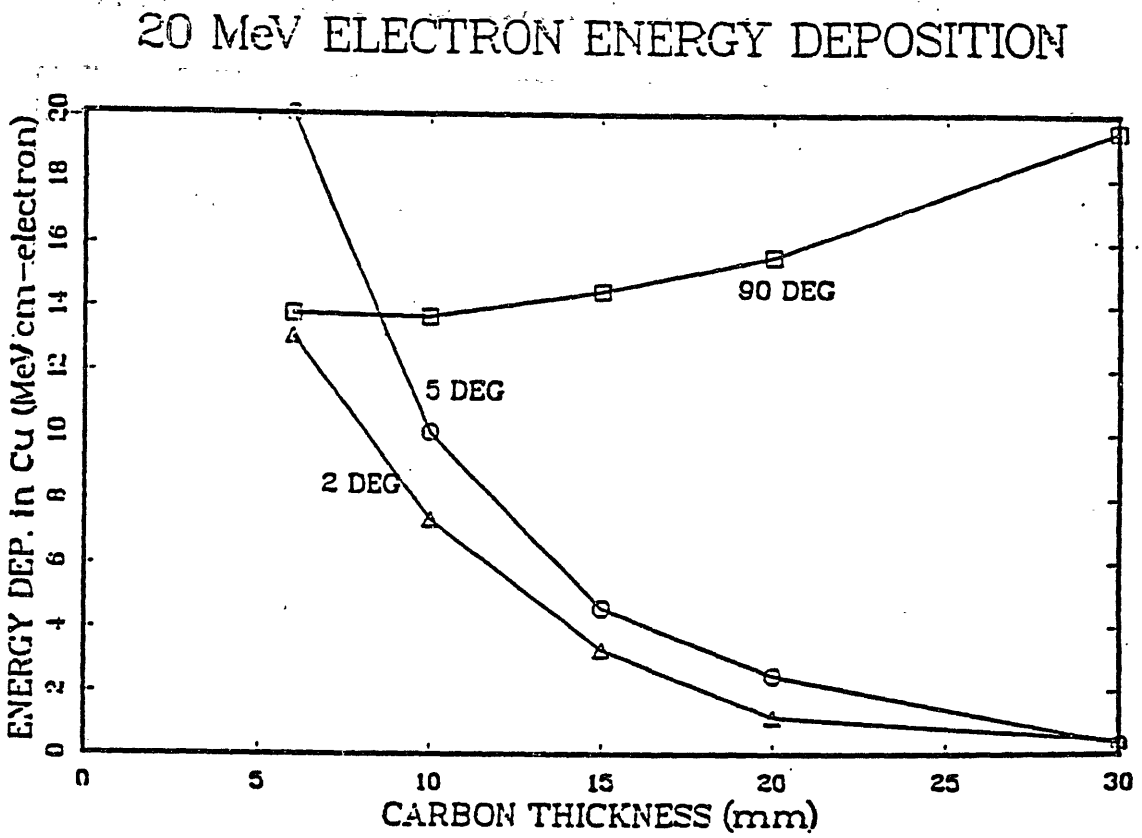
20 MeV ELECTRON ENERGY DEPOSITION
ENERGY DEP. in Cu (MeV/cm-electron)
0
2
4
6
8
10
12
14
16
18
20
90 DEG
5 DEG
2 DEG
0
5
10
15
20
25
30
CARBON THICKNESS (mm)

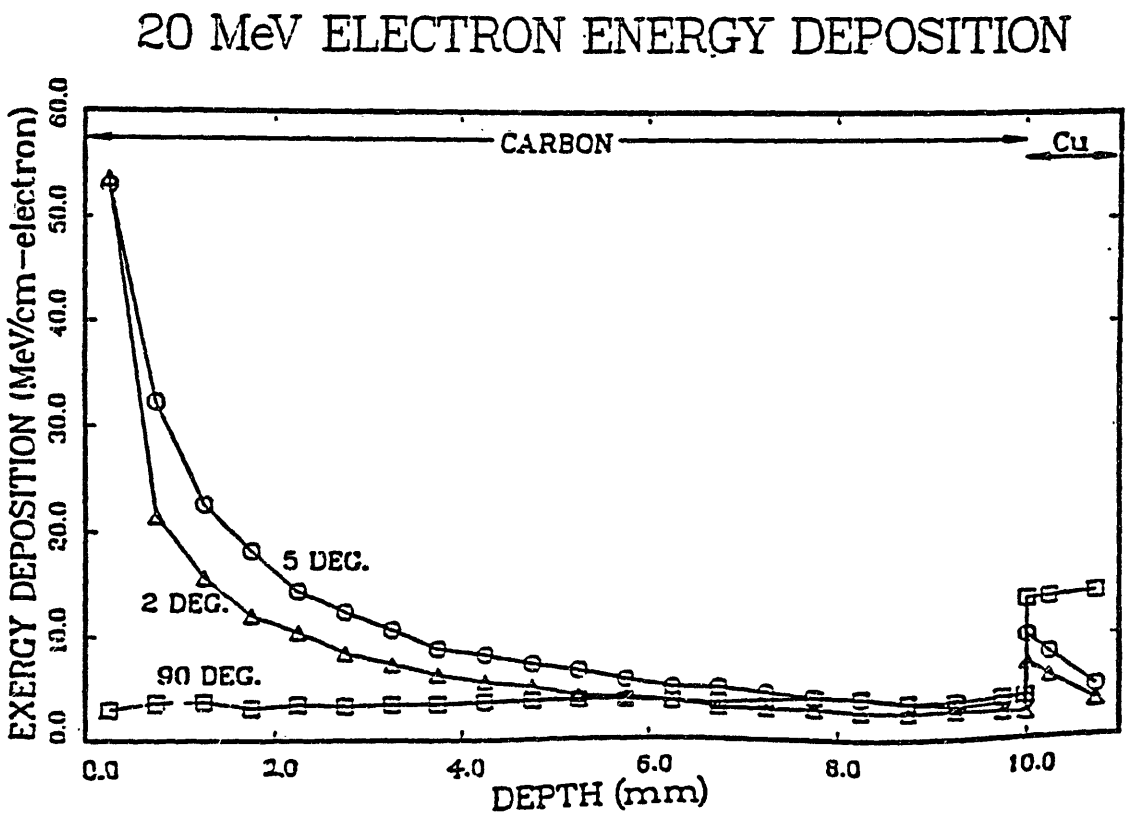
20 MeV ELECTRON ENERGY DEPOSITION
EXERGY DEPOSITION (MeV/cm-electron)
0.0
10.0
20.0
30.0
40.0
50.0
60.0
CARBON
Cu
5 DEG.
2 DEG.
90 DEG.
0.0
2.0
4.0
6.0
8.0
10.0
DEPTH (mm)

20 MeV ELECTRON ENERGY DEPOSITION

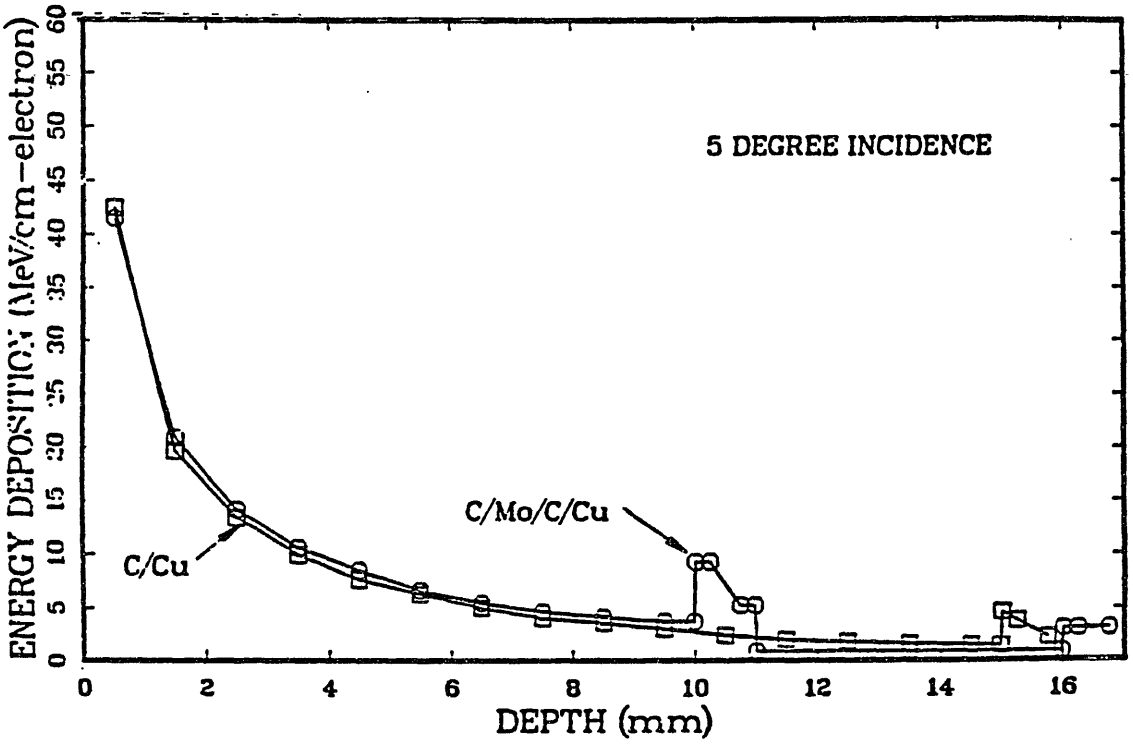

20 MeV ELECTRON ENERGY DEPOSITION

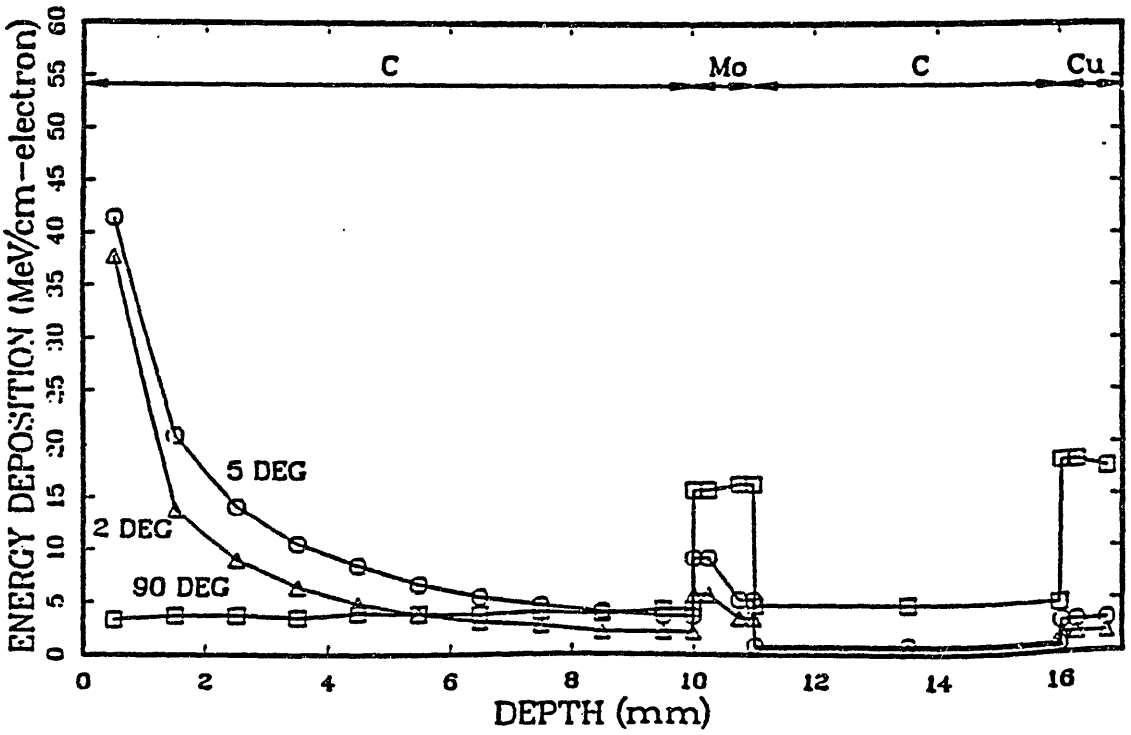

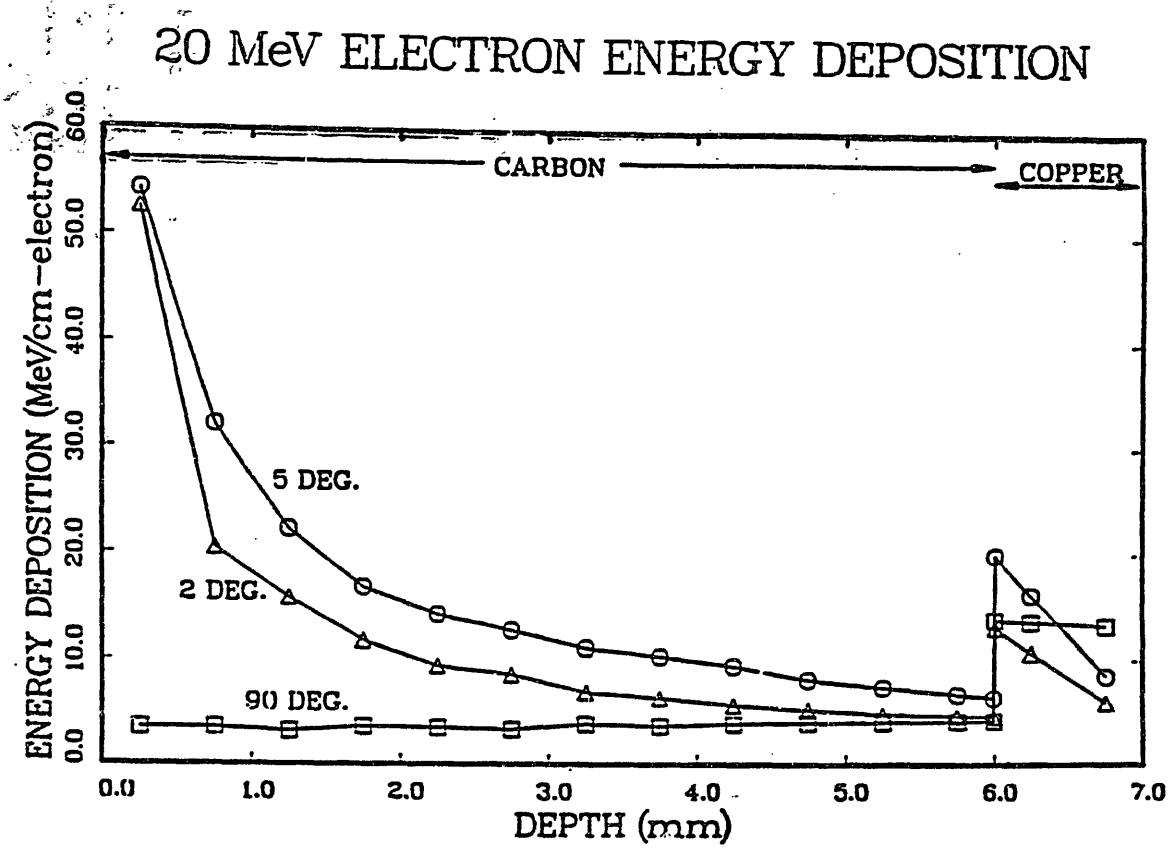

Model for 1-D runaway analysis

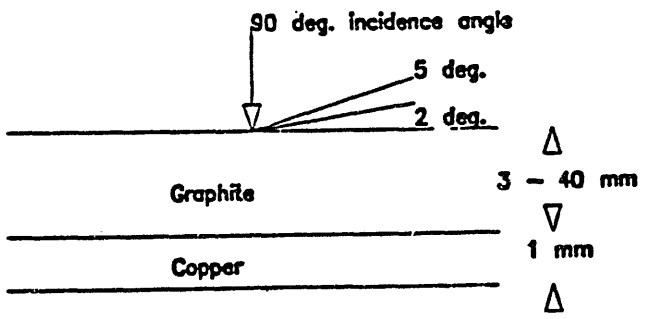

For Cu, 1 MeV/cm·e⁻ ⇒ ~ 100 °C temp rise.

RUNAWAY ELECTRON ANALYSIS

Tiger: A time-independent, coupled electron/photon

Monte Carlo transport code.

- multimaterial
- multidimensional
- based on ETRAN model which combines microscopic photon transport with macroscopic random walk for electron transport.
- can include arbitrary macroscopic electric and magnetic fields.
- includes cross-section data from 1 keV to 1 GeV.

Runaway electron flux estimates:

From JET results;

4 – 40 msec deposition time

6 – 40 kJ per event

crater size about 5 cm^2

gives about 8 kJ/cm^2 maximum

For 20. MeV particles, this gives fluence of about 2.5×10^{15} electrons/cm^2

or, in 20 msec, a flux of about 1.2×10^{17} electron/sec.-cm^2

Outline

1) Run-Away Electron Analysis

2) Global Model for Recycling and Isotope Exchange

see – Heifetz, et al., 7th PSI (see Wilson's talk in section 2.5 or the references to the left)
– Bruce, et al.; " "
– McGrath, et al.; " "

Fusion application of C-C composites

Takashi Uchikawa

Mitsubishi Heavy Industries

Abstract

C-C composites have high potentialies for fusion applications, although limitation on fabricability and long time needed for production, etc. are engineering subjects at present.

As one step to realize a large C-C composite fusion component, advanced ALT-II limiter blades of C-C composite are now being developed.

C-C composites should be characterized considering the factors such as fiber properties, composite production methods, weave configuration, treatment conditions, etc.

US-Japan Workshop on Material Data Needs for
the Next Step and Steady State Devices
January 26-30, 1987

FUSION APPLICATION OF C-C COMPOSITES

T. Uchikawa, Mitsubishi Heavy Industries, Ltd.

1. Genral Description

Carbon-carbon composites have high potentialites as high heat flux material for fusion applications. The advantages of c-c composites are :

1) High strength and stiffness

2) High thermalshock resistance, mainly due to large strength and small thermal expansion coefficient.

3) Larger electrical resistivity which leads to smaller electromagnetic forces induced on compared with metal structure

The above features would be attractive in order to supply high heat flux components which are exposed to severe heat load conditions.

On the other hand, the c-c composites at present also suffer disadvantages as follows:

A) Limitation on fabricability: In general it is rather difficult to supply large, three dimensionally shaped product.

B) Long period of time needed for material production: 4-8 months

C) High cost: $350-5000/kg

Faster and more inexpensive production, as well as appropriate design application, of c-c composites is a crucial engineering subject.

2. Development of c-c composite limiter blade for ALT-II advancement

As one step to realize a large three dimensional c-c composite fusion-component, ALT-II advanced limiter blade made of c-c composite is now being developed. The development stage at this point is going into an actual fabrication of the blade material based on the sample plate production and properties evaluation.

Typical characteristics of C-C composite

Final heat treatment temperature	2000 °C
Density	~1.6 g/cm³
Porosity	~10 %
Flexural strength	~150 MPa
Tensile strength	~120 MPa
Thermal expansion coefficient	// $< 1\times10^{-6}$ (°C⁻¹) ⊥ $\sim 6\times10^{-6}$ (°C⁻¹)
Thermal conductivity	// ~100 W/m·°C

C-C composite characteristics depend upon:

1) Fiber properties
2) Composite production method
3) Weave configuration
4) Treatment conditions

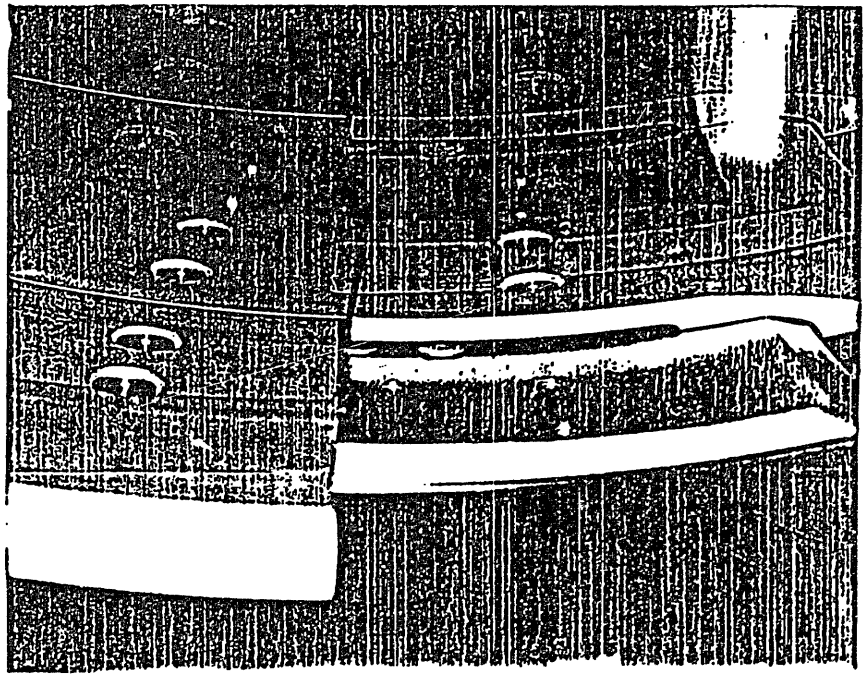

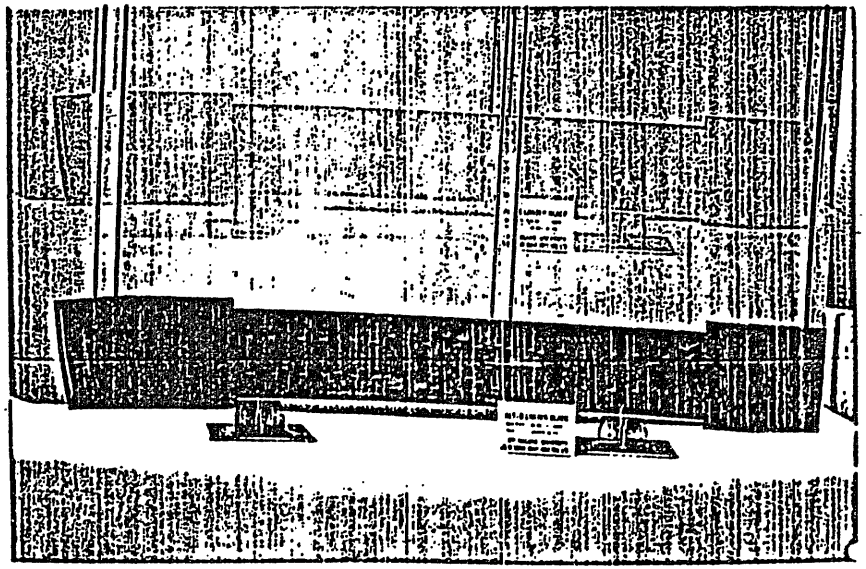

Problems with Criteria for Material Selection and Failure Assessment

Masanao Shibui

Toshiba Corporation

Abstract

Criteria for material selection and failure assessment have been discussed and reviewed with particular emphasis on the localized erosion due to intense pulsed energy deposition and failure mode of graphite under biaxial stress state.

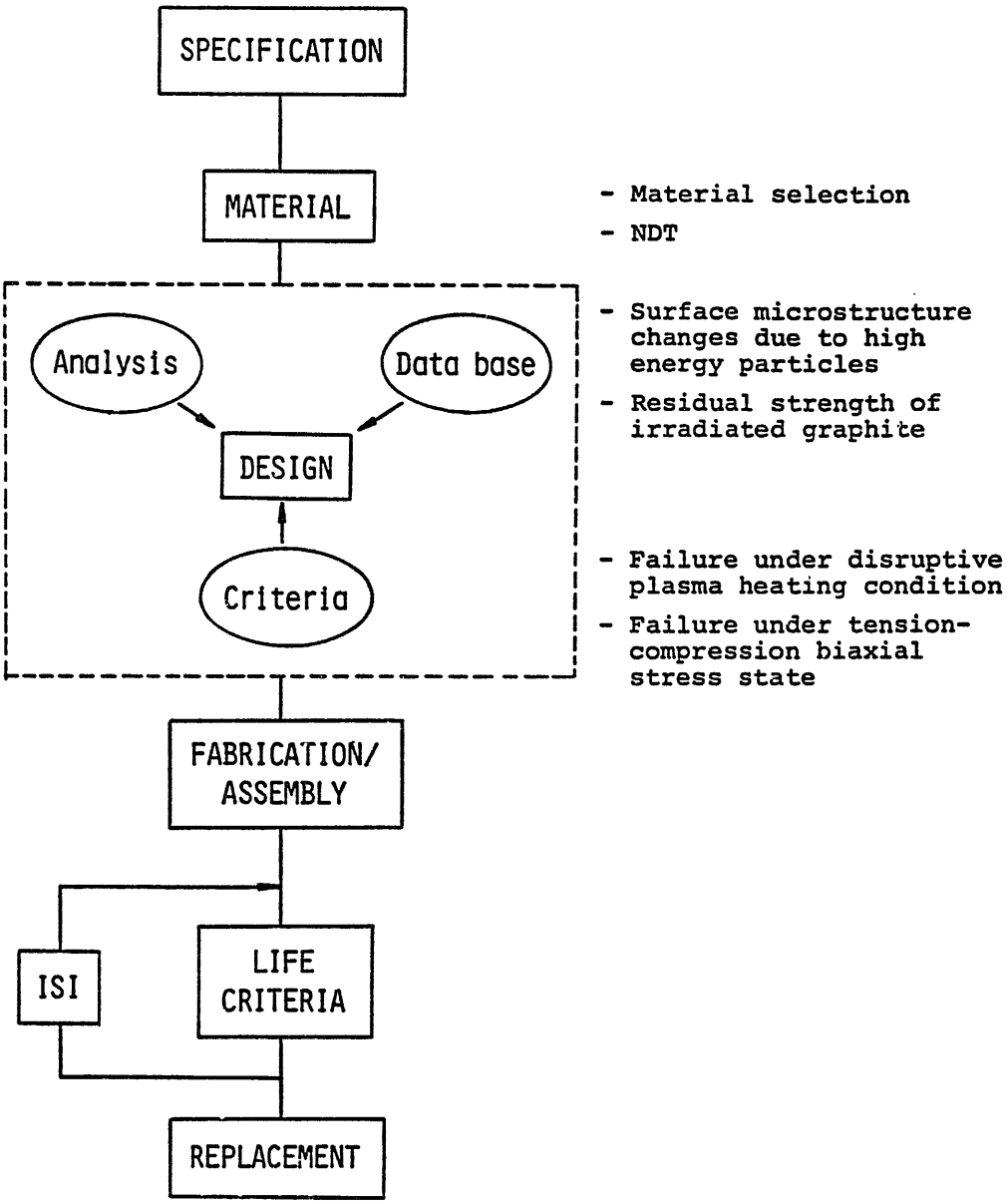
SPECIFICATION
MATERIAL
Analysis
Data base
DESIGN
Criteria
FABRICATION/
ASSEMBLY
ISI
LIFE
CRITERIA
REPLACEMENT
- Material selection
- NDT
- Surface microstructure changes due to high energy particles
- Residual strength of irradiated graphite
- Failure under disruptive plasma heating condition
- Failure under tension-compression biaxial stress state

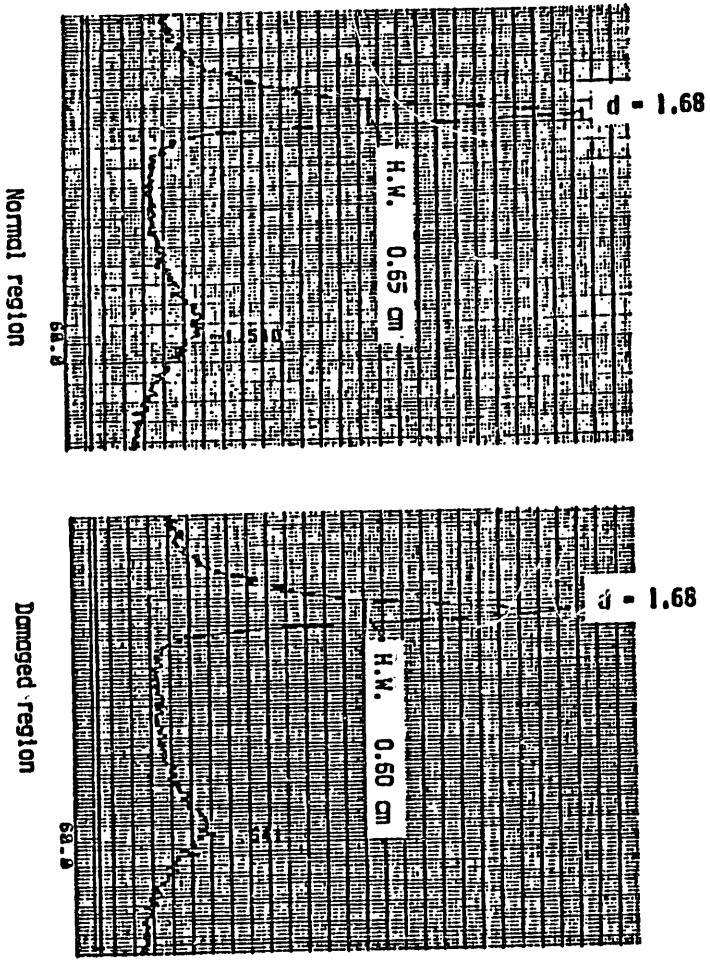

Normal region

Damaged region

Fig. Example results of XRD

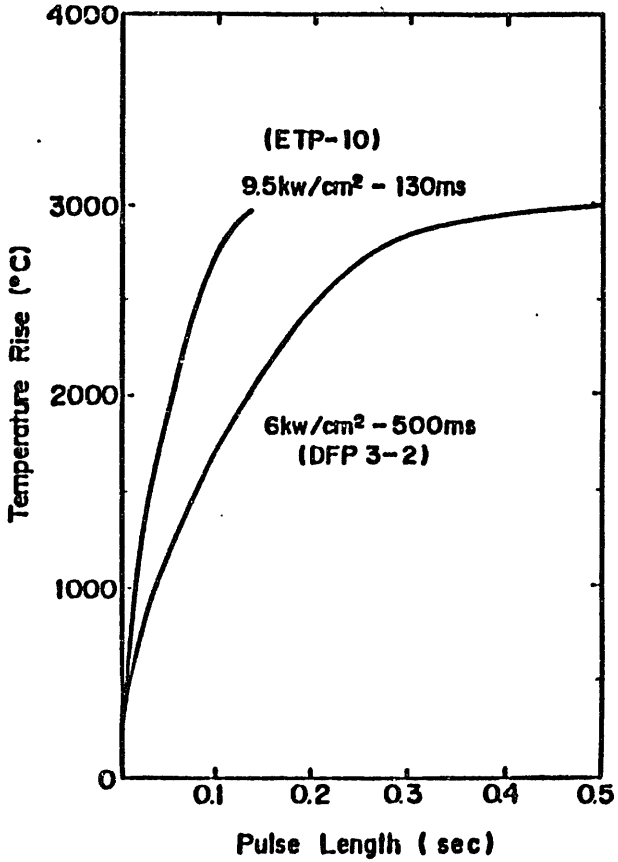

Fig. Thermal analyses including sublimation effects

9.5 kW/cm²

7.4 kW/cm²

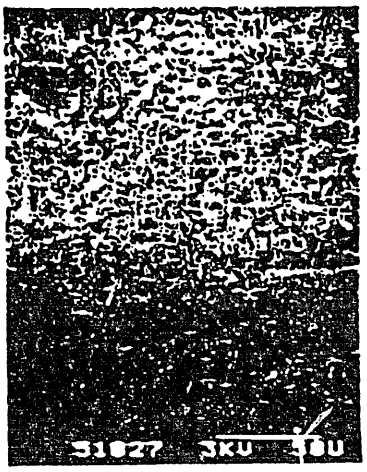

6.0 kW/cm²

After 130ms - 4 shots (ET-10)

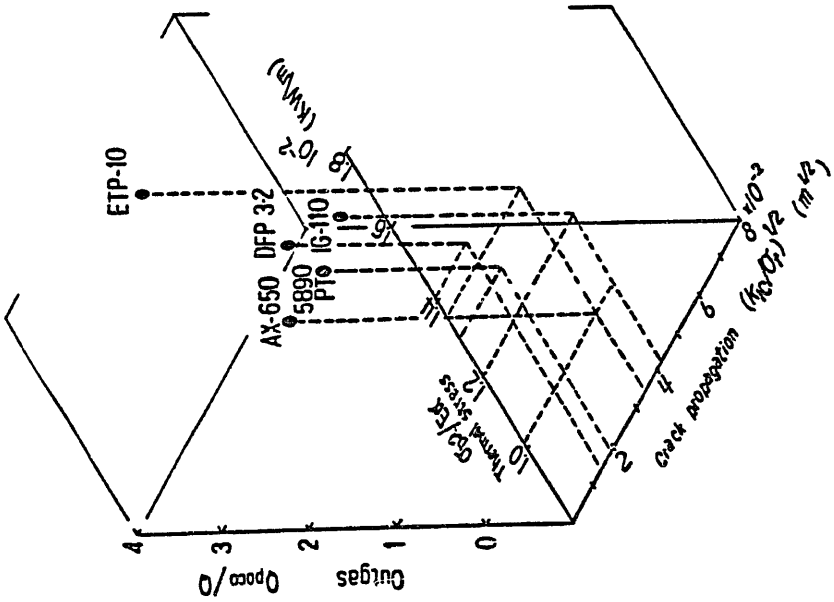

Fig. Assessment of graphite by three parameters

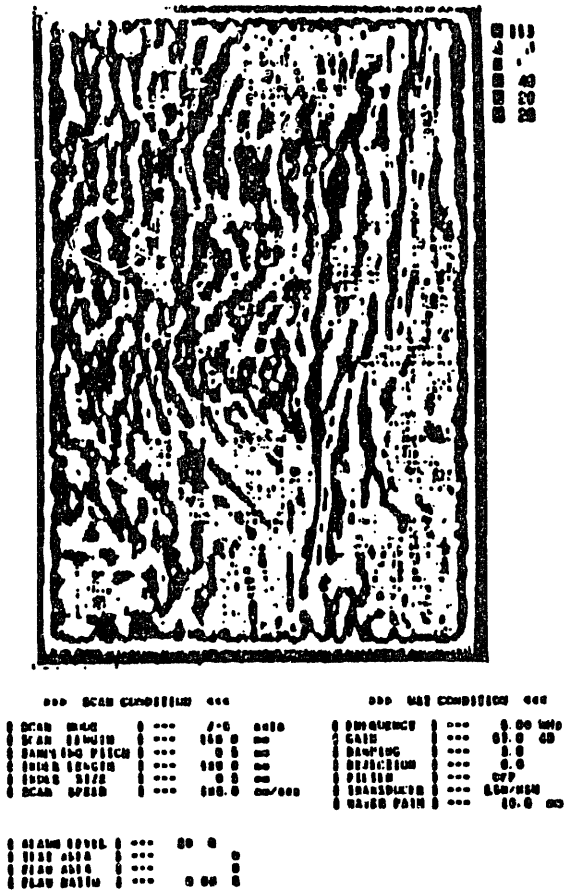

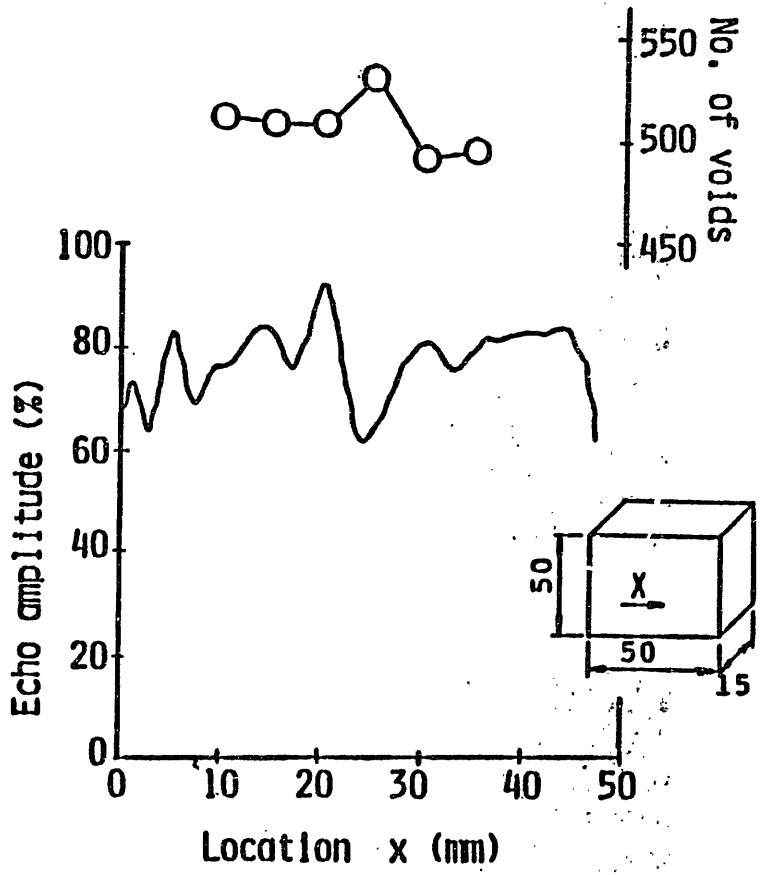

Fig. Example results of UT

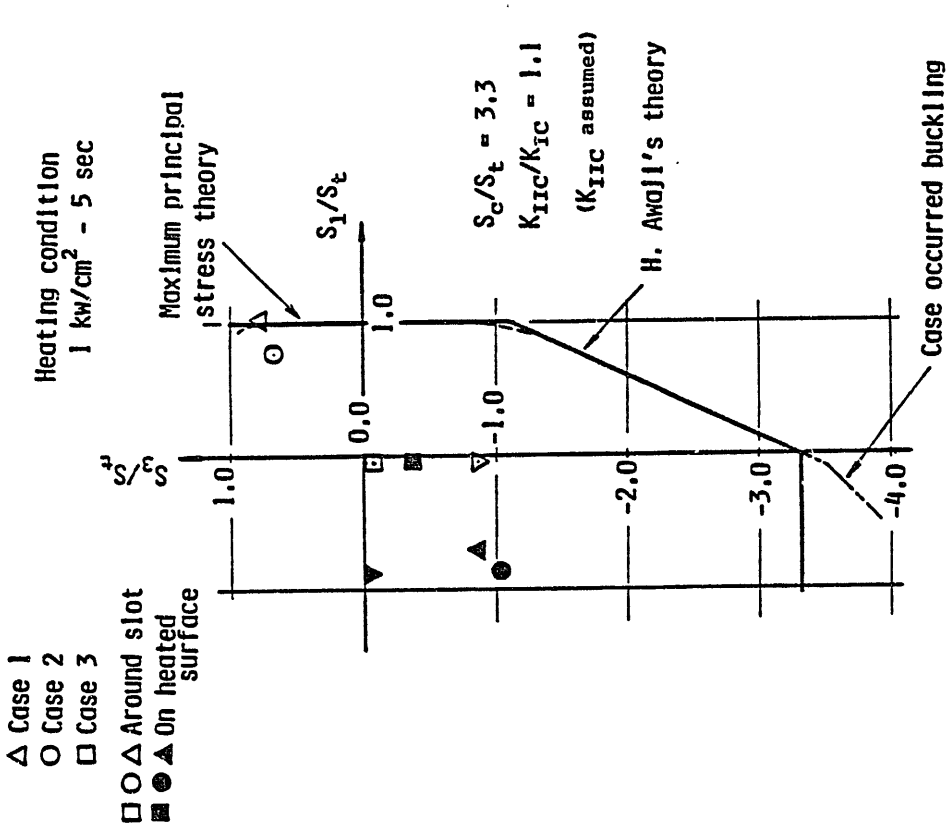

Fig. Fracture criterion under tension-compression biaxial stress state.

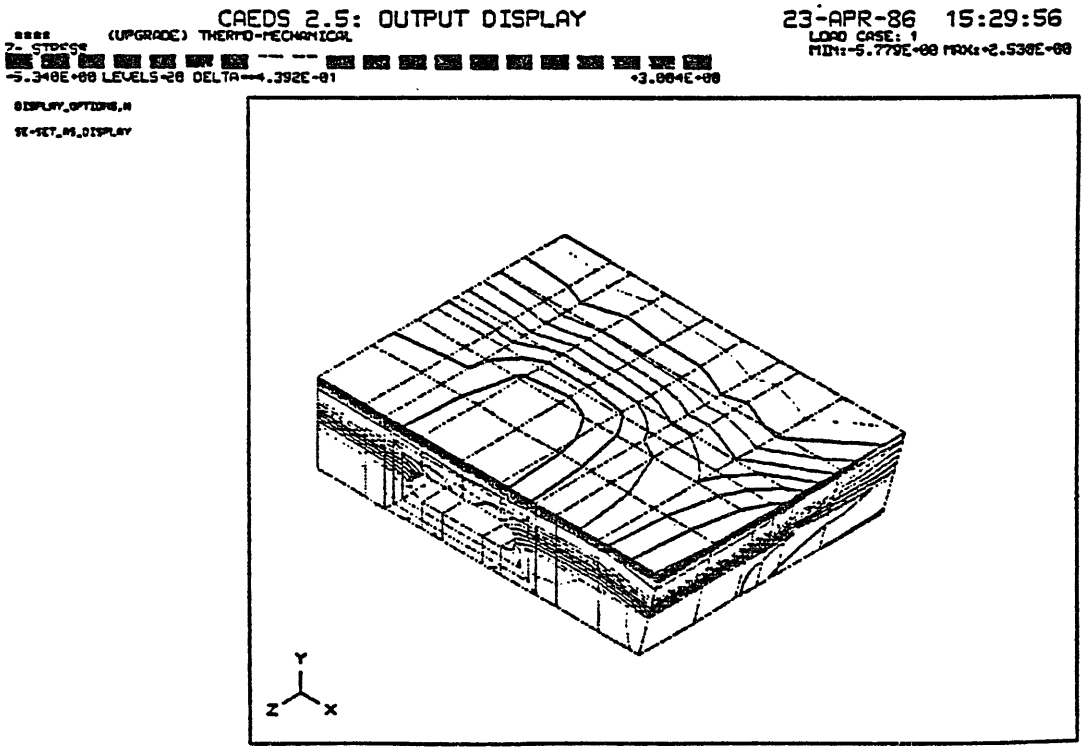

Fig. Principal stress distribution

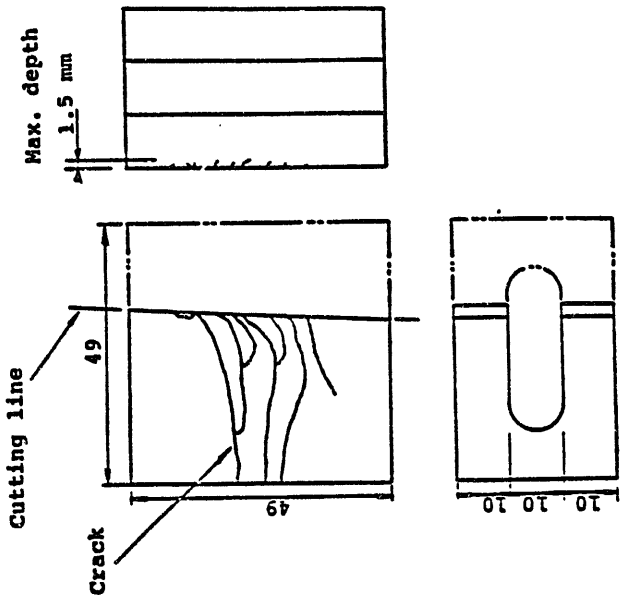

Fig. Cracks created after cutting

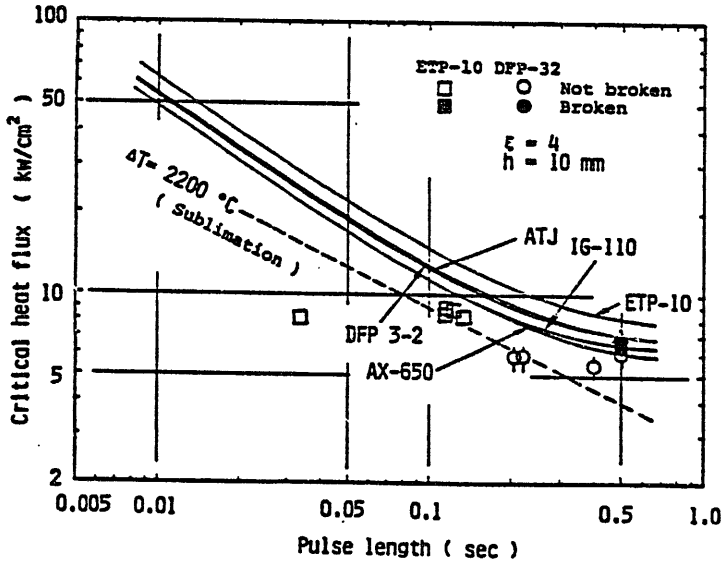

$$q_c = \frac{1}{3}\frac{(1-\ )^{1/2}}{E\alpha}\frac{\lambda}{h}S_b\left(\frac{\xi}{\phi}\right)^{1/2}$$

q_c = Critical heat flux
E = Young's modulus
α = Coefficient of thermal expansion
S_b = Bending strength
ξ = Thermal stress factor ($S_{thermal}/S_{mechanical}$)
φ = φ(a,h,τ)
a = Thermal diffusion
h = Thickness of plate
λ = Thermal conductivity
τ = Pulse length

Fig. Critical heat flux for thermal shocks

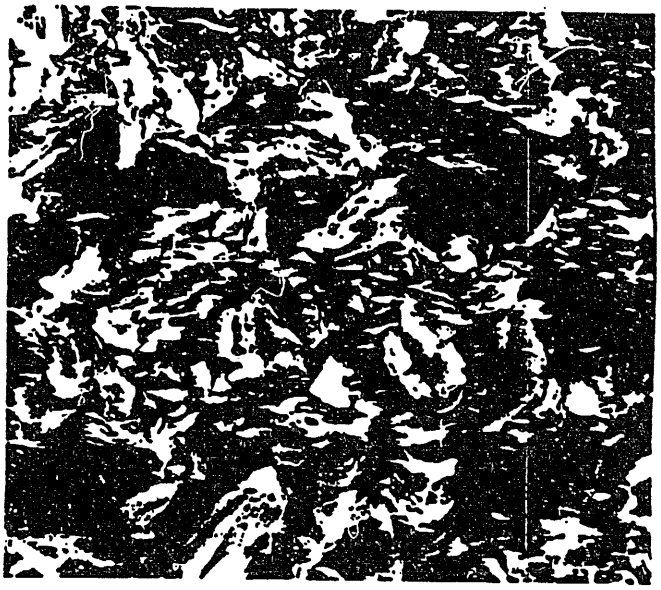

9.5 kW/cm²

7.4 kW/cm²

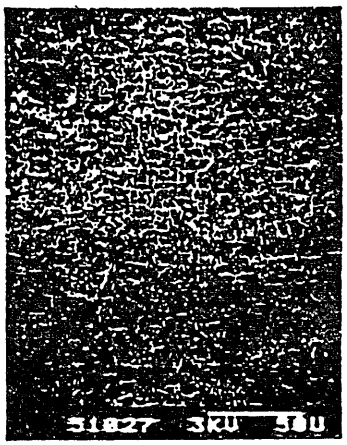

6.0 kW/cm²

After 130ms - 4 shots (ET-10)

Active Cooling with Swirl Tube Enhancement with Application to the Tore Supra Modular Limiter Design

R.T. McGrath
Sandia National Laboratories

Abstract

Tokamaks operating with pulse length greater than 10 seconds will require active cooling of plasma contacting surfaces. For limiter leading edges heat fluxes as high as 3-5kW/cm^2 are to be expected. Testing at the electron beam test facility at Sandia shows that these limits can be achieved using high flow velocity, subcooled water with enhancement of the heat transfer with twisted tapes. In addition, surface temperatures of graphite armor tiles can be kept below 1200°C using pyrolytic graphite.

CREEP RUPTURE

why GlidCop ? Al-15

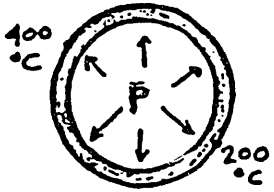

$\sigma_\theta = \frac{PR}{t}$ "HOOP" STRESS

$\sigma_\theta = \frac{(700\ \text{psi})(4.76)}{(0.794)}$

$\sigma_\theta = 4200$ psi (29 MPa)

P = 4.8 MPa

→ OFHC COPPER TOO WEAK.

ELEVATED TEMPERATURE STRESS RUPTURE PROPERTIES OF GLIDCOP AL-15

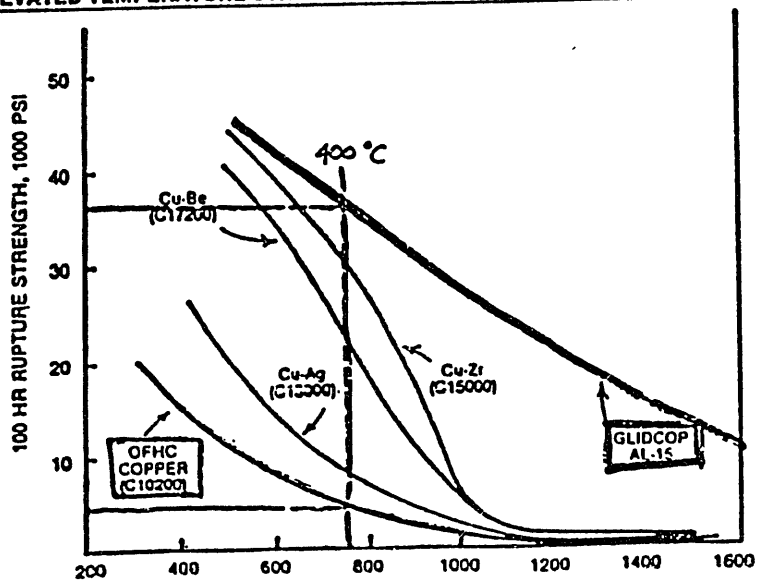

PYROLYTIC GRAPHITE

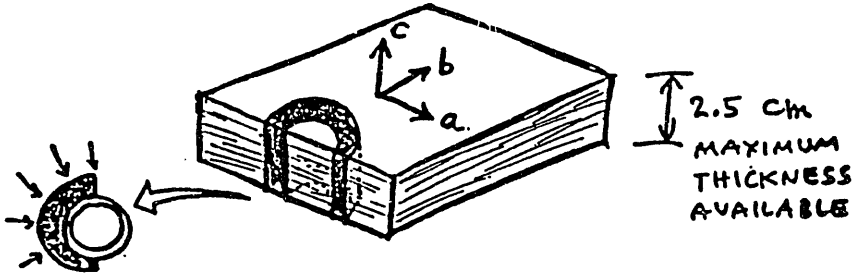

THERMAL CONDUCTIVITY (a-b PLANE)

PYROLYTIC	3.5	(W/cmK)
POCO AXF-5Q	1.0	
OFHC COPPER	4.0	
MOLYBDENUM	1.4	

THERMAL EXPANSION COEFFICIENT ($°C^{-1}$)

PYROLYTIC (a-direction)	2	E-6
PYROLYTIC (c-direction)	23	E-6
POCO AXF-5Q	5	E-6
OFHC COPPER	21	E-6
MOLYBDENUM	6	E-6

POCO AXF-5Q GRAPHITE

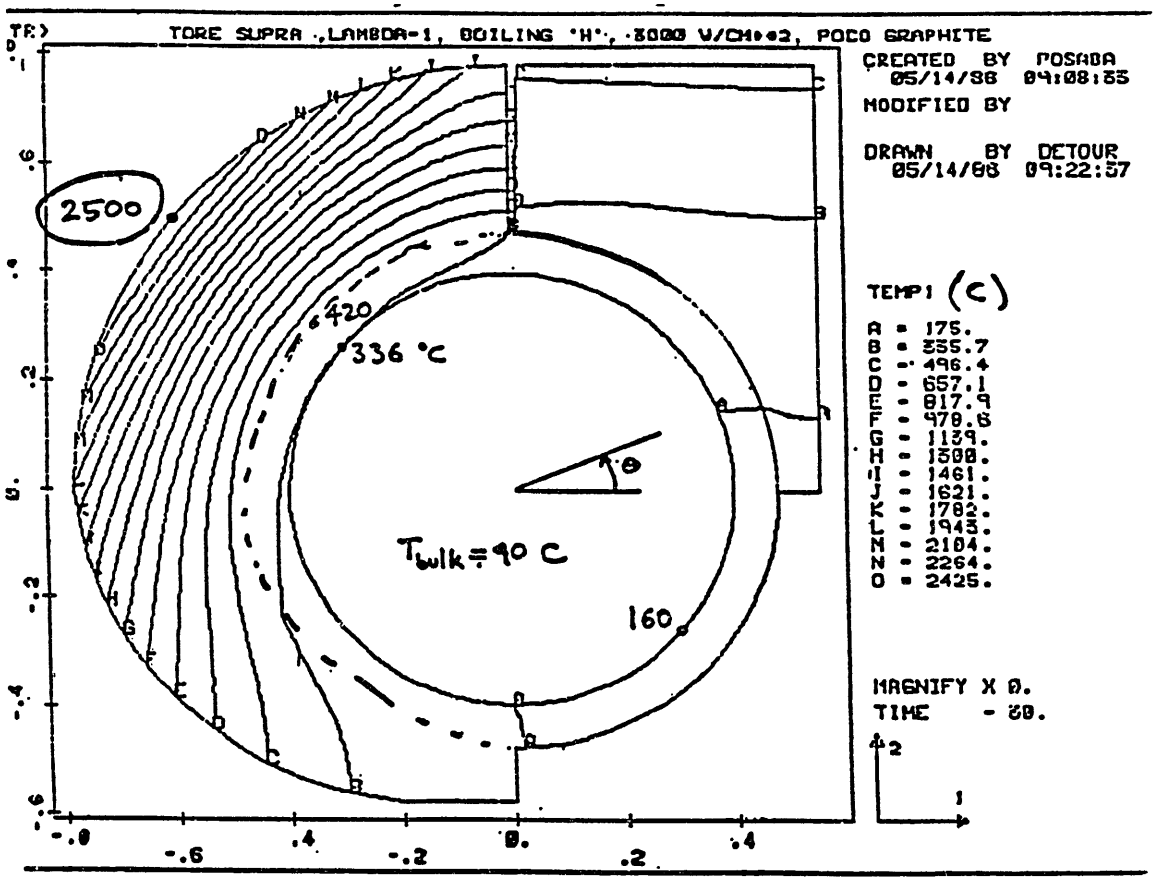

PYROLYTIC GRAPHITE

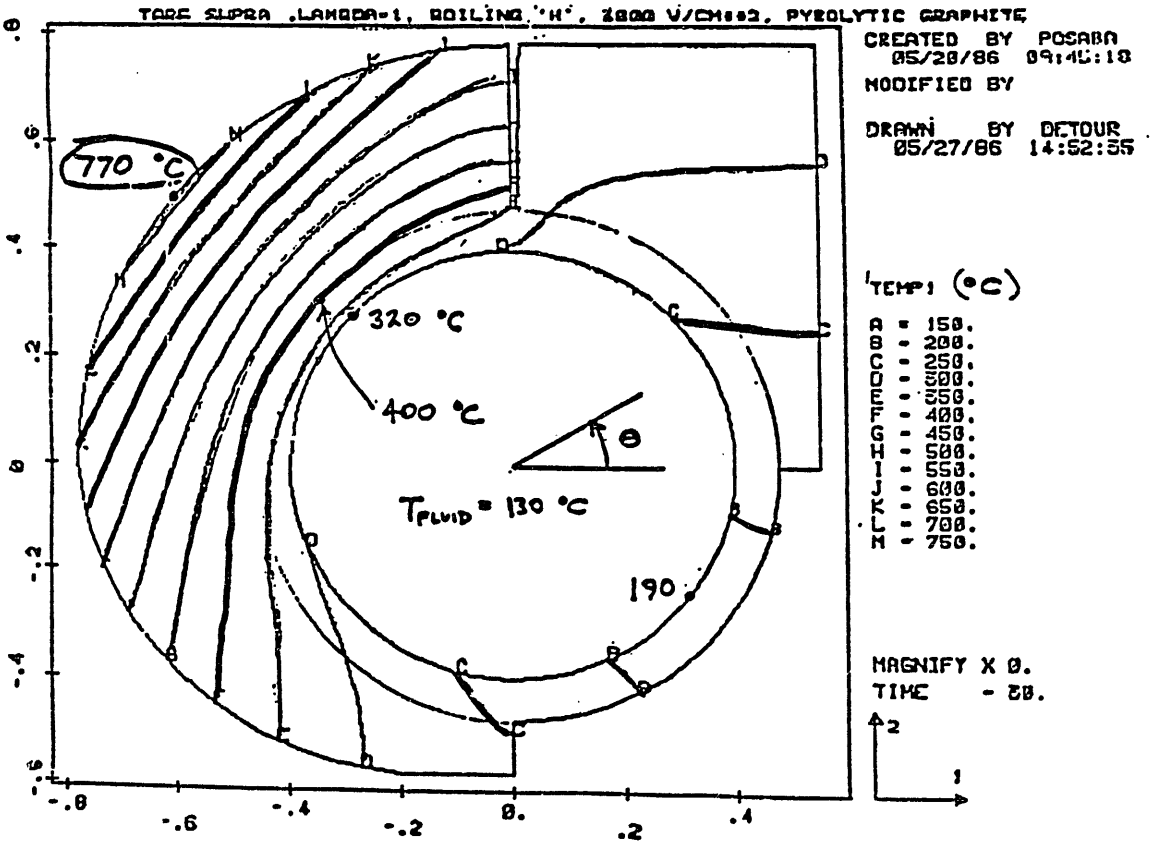

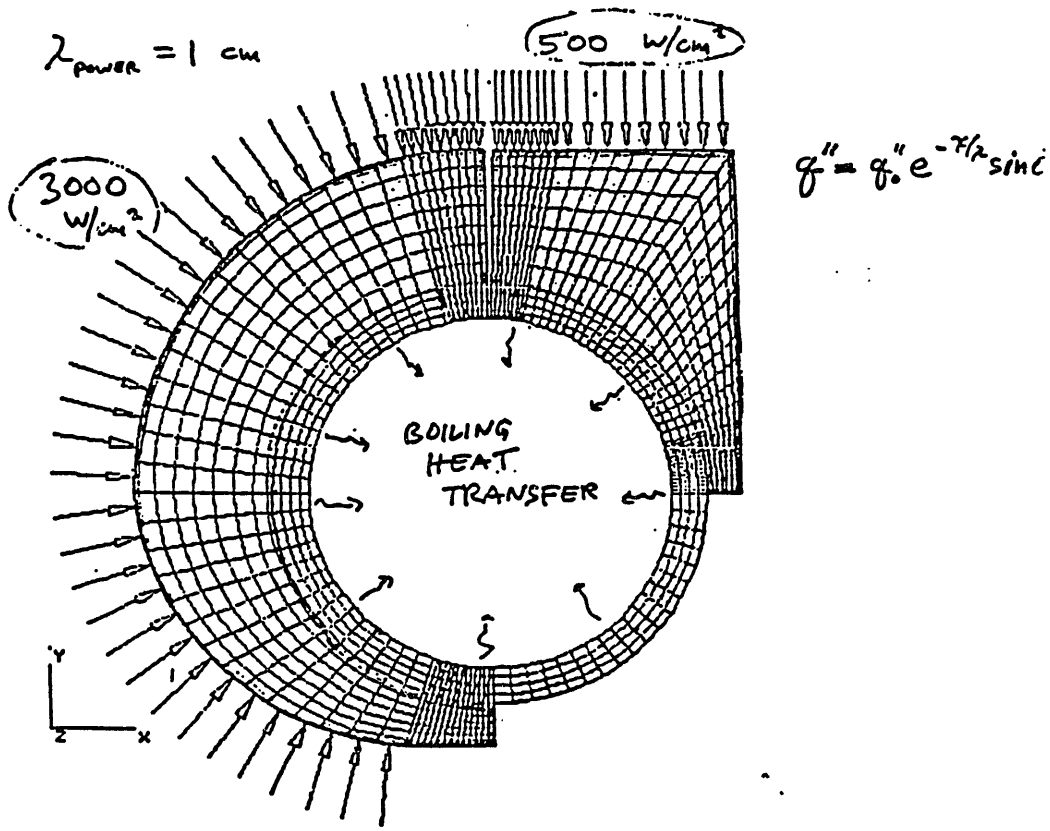

MODE? 1.GEOMETRY 2.ANALYSIS MODEL 3.ANALYZE 4.RESULTS 5.INTERFACE 6.STOP

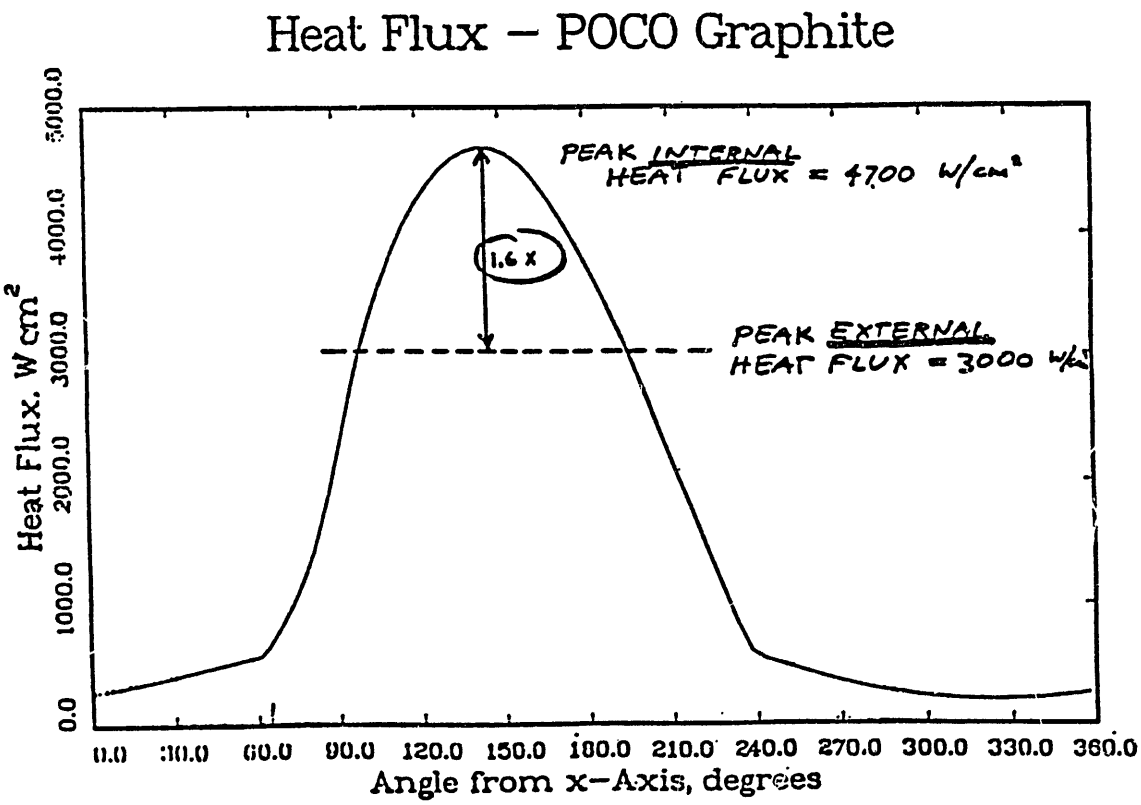

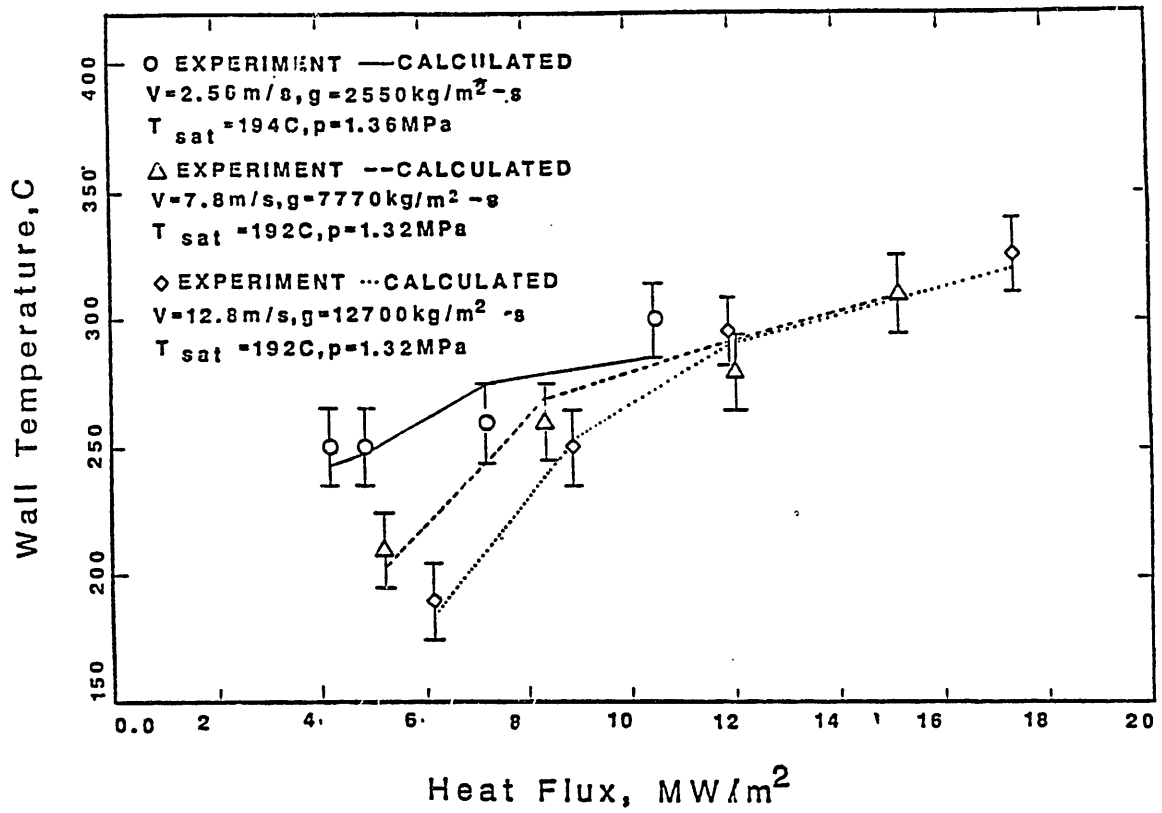
O EXPERIMENT —CALCULATED
V=2.56m/s, g=2550kg/m²-s
T sat =194C, p=1.36MPa
△ EXPERIMENT --CALCULATED
V=7.8m/s, g=7770kg/m²-s
T sat =192C, p=1.32MPa
◇ EXPERIMENT ···CALCULATED
V=12.8m/s, g=12700kg/m²-s
T sat =192C, p=1.32MPa
Wall Temperature, C
Heat Flux, MW/m²
150
200
250
300
350
400
0.0
2
4
6
8
10
12
14
16
18
20

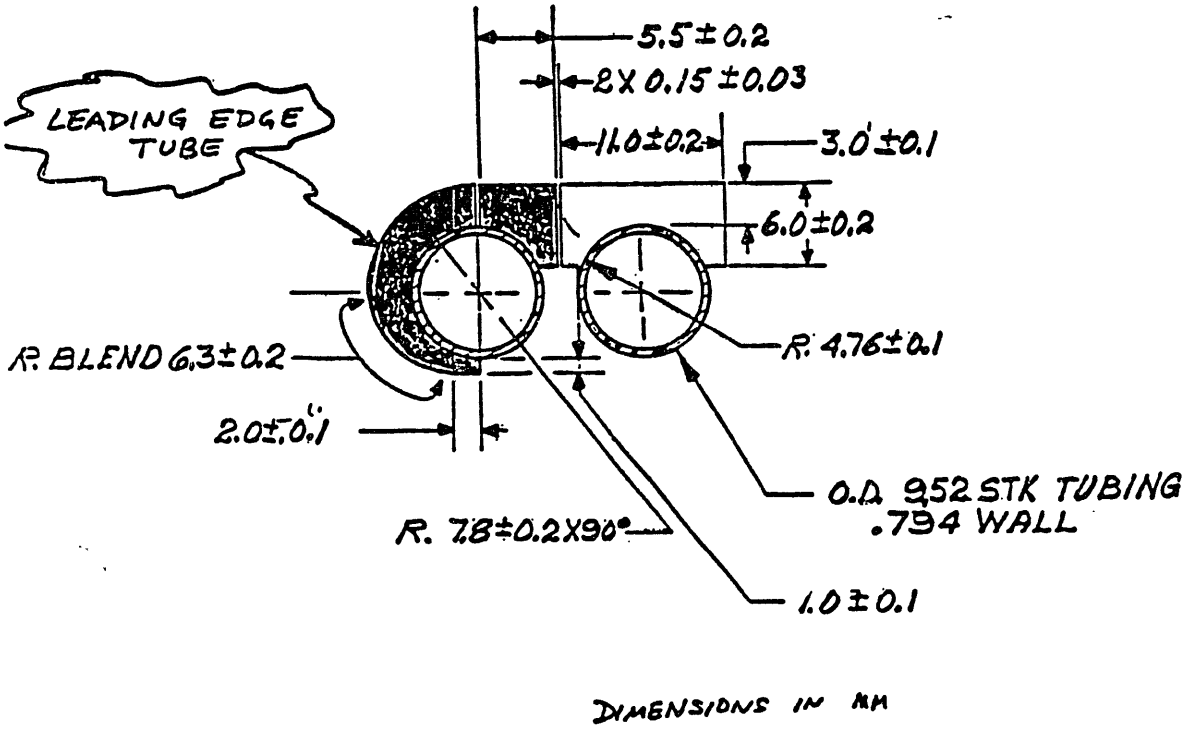
LEADING EDGE TUBE
5.5±0.2
2X 0.15±0.03
11.0±0.2
3.0±0.1
6.0±0.2
R. BLEND 6.3±0.2
R. 4.76±0.1
2.0±0.1
O.D. 9.52 STK TUBING
.794 WALL
R. 7.8±0.2X90°
1.0±0.1
DIMENSIONS IN MM

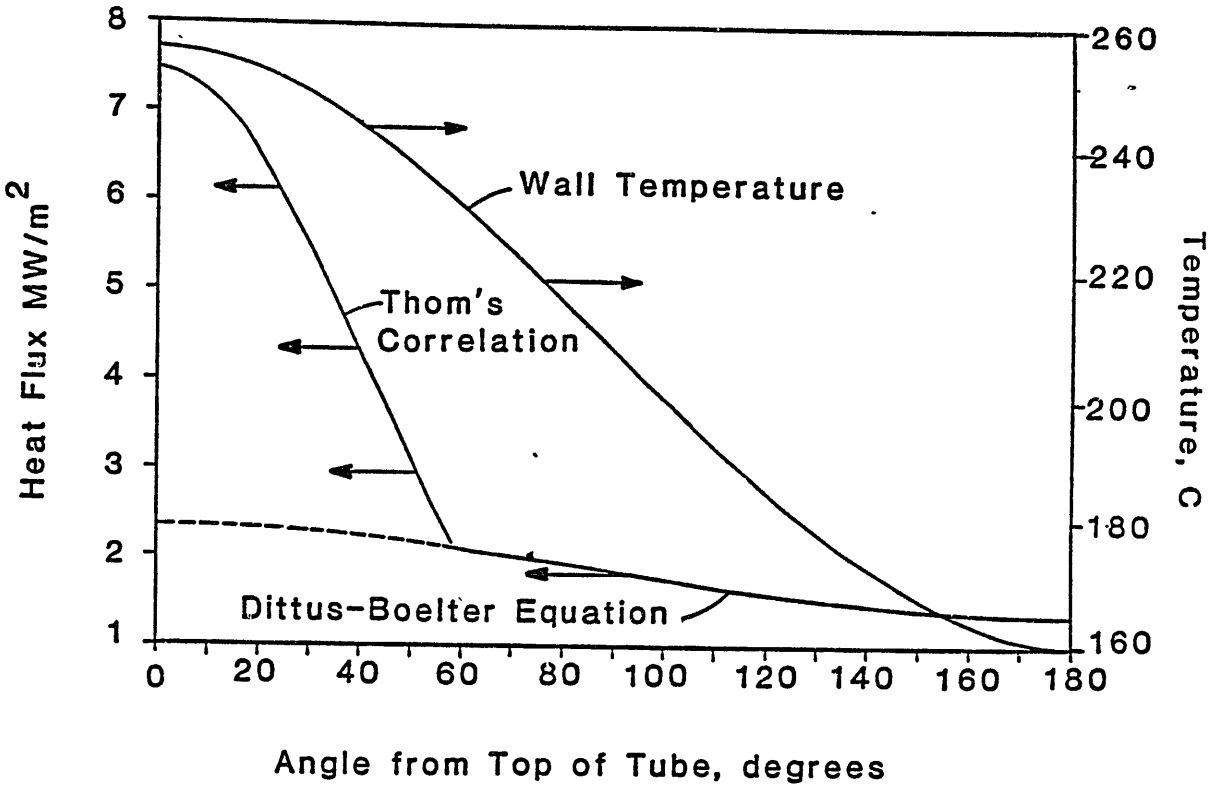
Heat Flux MW/m2
Temperature, C
Wall Temperature
Thom's Correlation
Dittus-Boelter Equation
Angle from Top of Tube, degrees
0
20
40
60
80
100
120
140
160
180
1
2
3
4
5
6
7
8
160
180
200
220
240
260

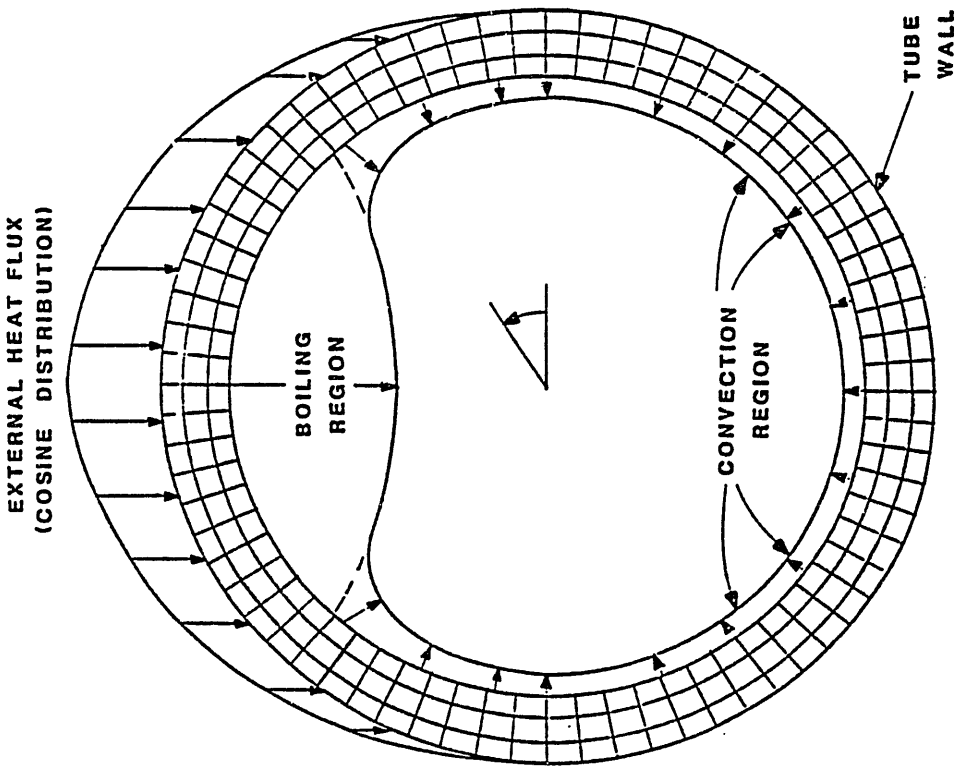
EXTERNAL HEAT FLUX
(COSINE DISTRIBUTION)
BOILING
REGION
CONVECTION
REGION
TUBE
WALL

DITTUS-BOELTER CORRELATION

$$Nu = 0.023\ Re^{0.8}\ Pr^{0.4}\ (\mu_w/\mu_b)^{0.18}$$

where,

Nu = Nusselt Number, hD/k
Re = Reynolds Number, $\rho vD/\mu$
Pr = Prandtl Number, $\mu c_p/k$
μ_w = Viscosity at wall temperature
μ_b = Viscosity at fluid bulk temperature

#60924JAK-8

BOILING MODEL (Finite element calcs.)

* Assumes correlations can be applied locally around tube wall
* Thom's correlation used for subcooled boiling
* Dittus - Boelter correlation used for convection
* Program chooses boiling if better than convection and $T_{wall} > T_{sat}$
* Approach experimentally verified in Sandia e-beam

#60924JAK-6

CHF Correlations – Tore Supra Conditions

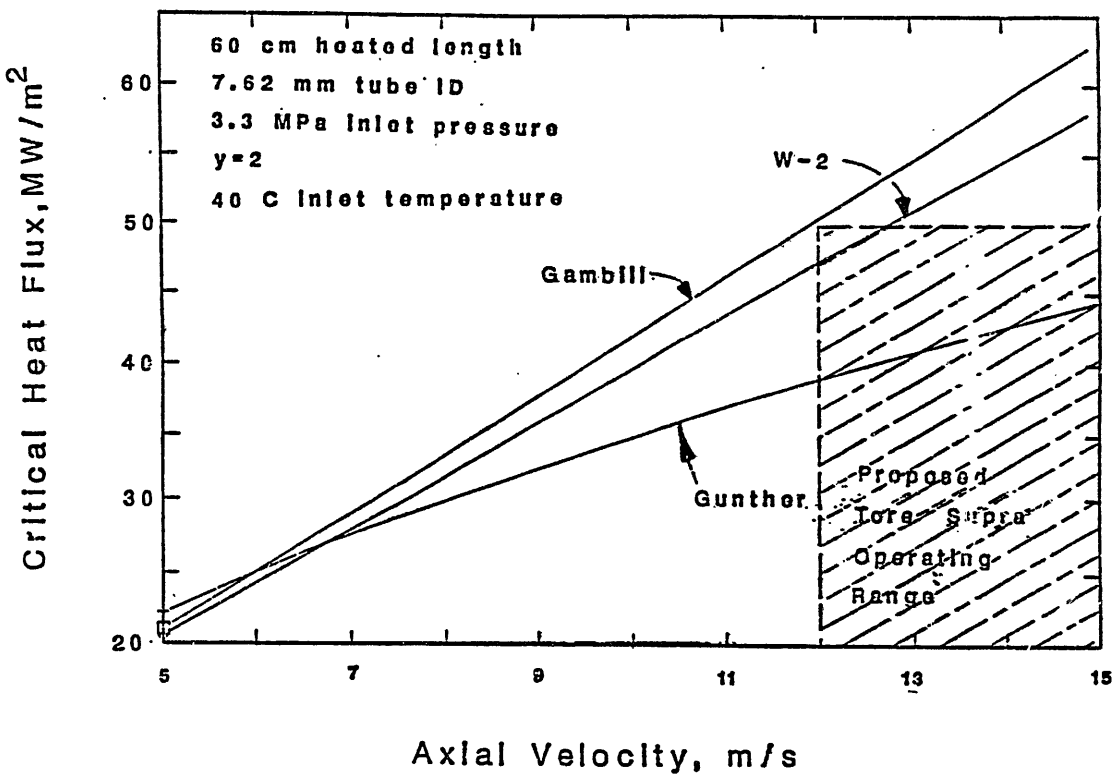

THOM'S CORRELATION

For fully developed subcooled flow:

$$\Delta T_{sat} = 22.65\ q^{0.5} \exp(-p/87)$$

where,

$$\Delta T_{sat} = T_{wall} - T_{sat}$$

#SCSAJAK-7

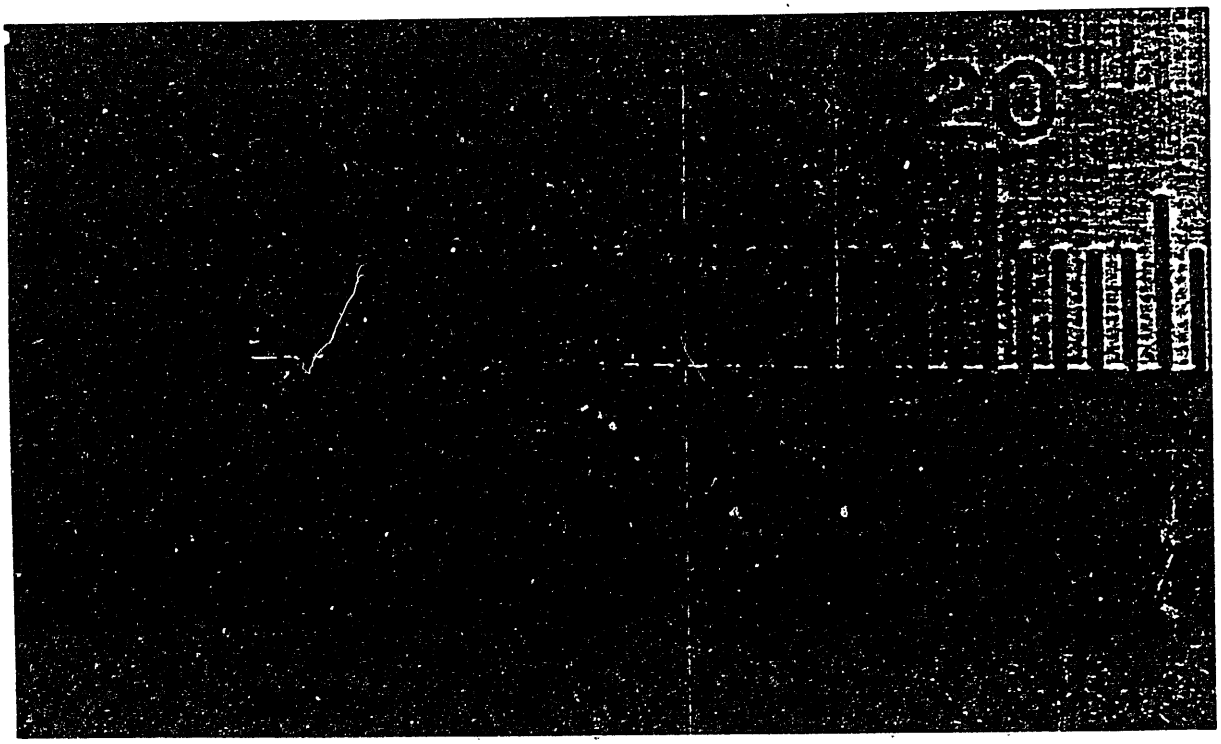

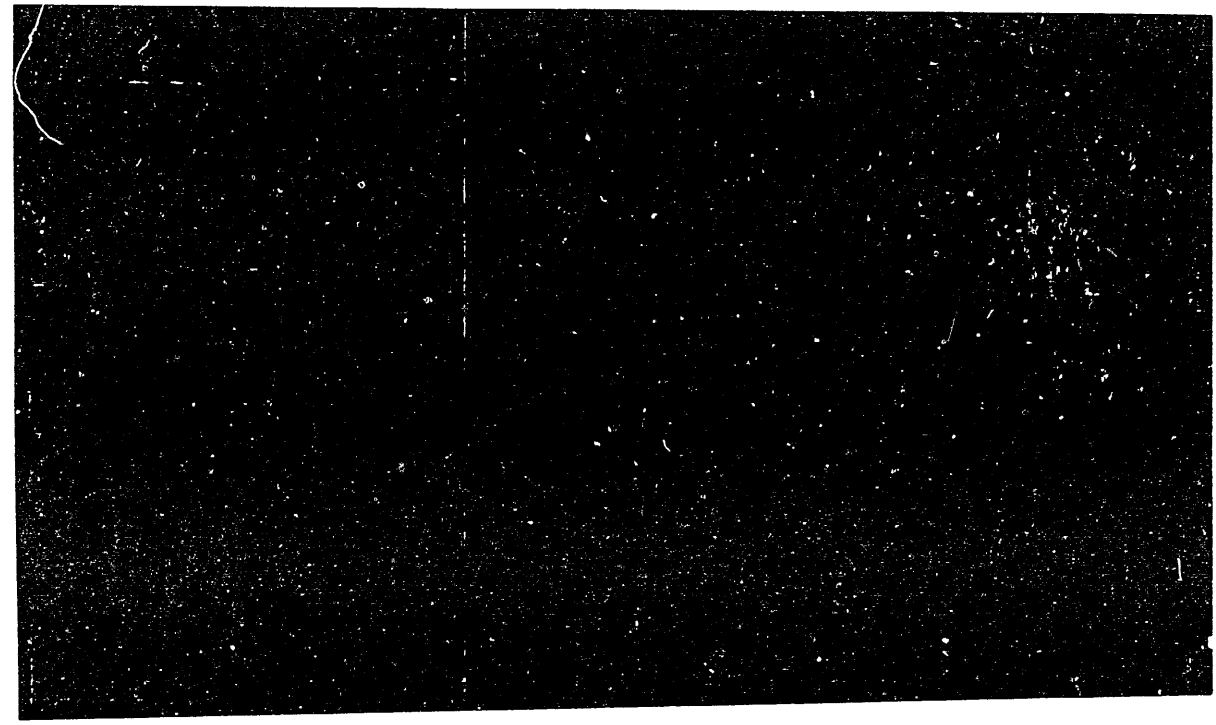

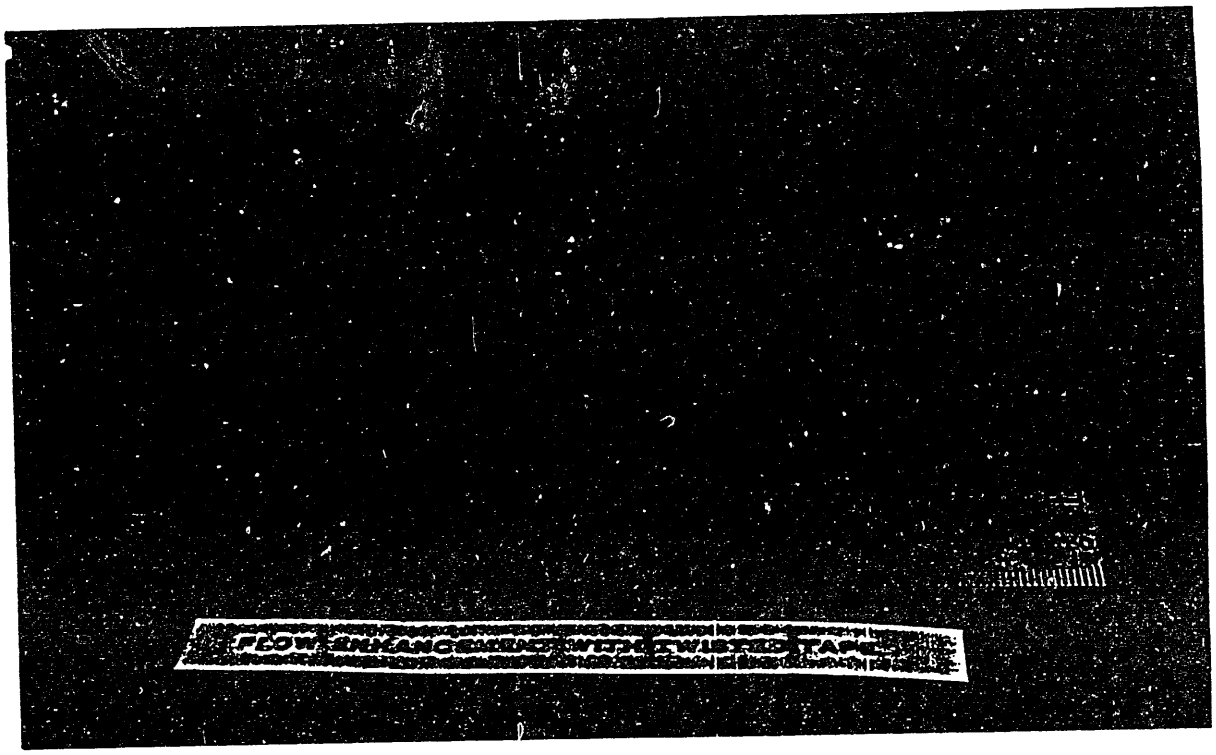

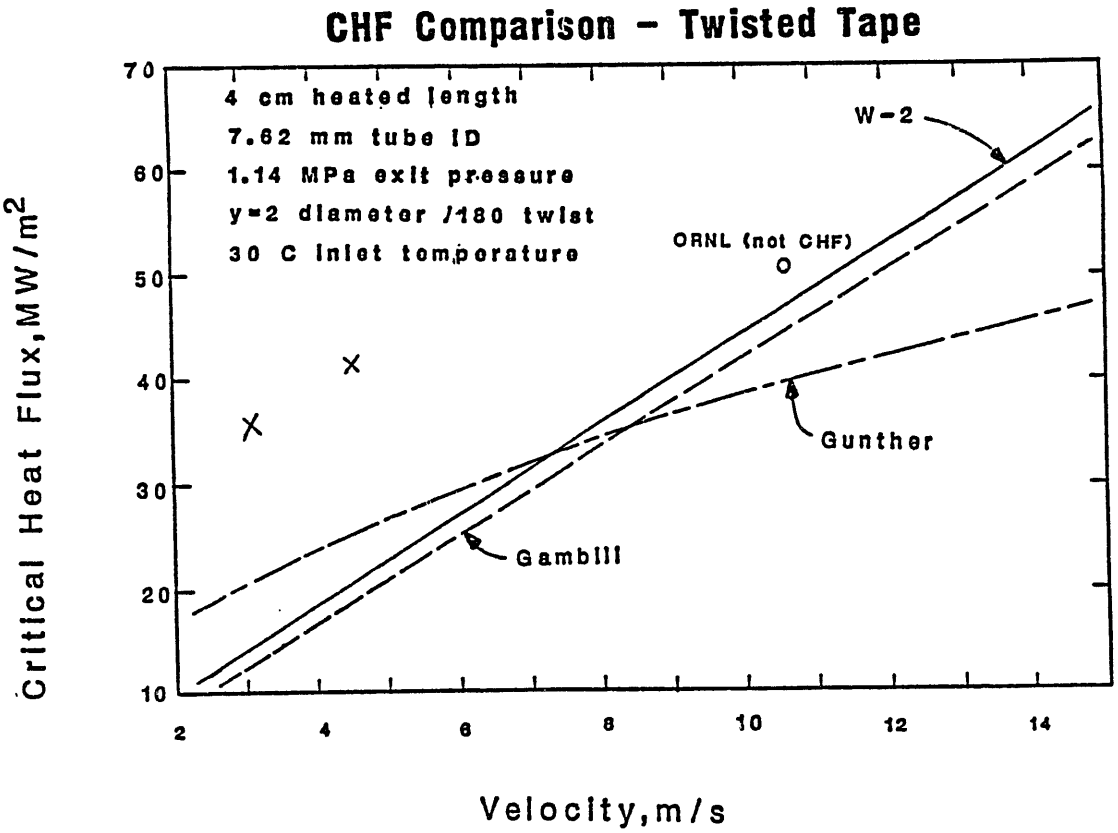
CHF Comparison - Twisted Tape
4 cm heated length
7.62 mm tube ID
1.14 MPa exit pressure
y=2 diameter /180 twist
30 C inlet temperature
W-2
ORNL (not CHF)
Gunther
Gambill
Critical Heat Flux, MW/m2
Velocity, m/s
70
60
50
40
30
20
10
2
4
6
8
10
12
14

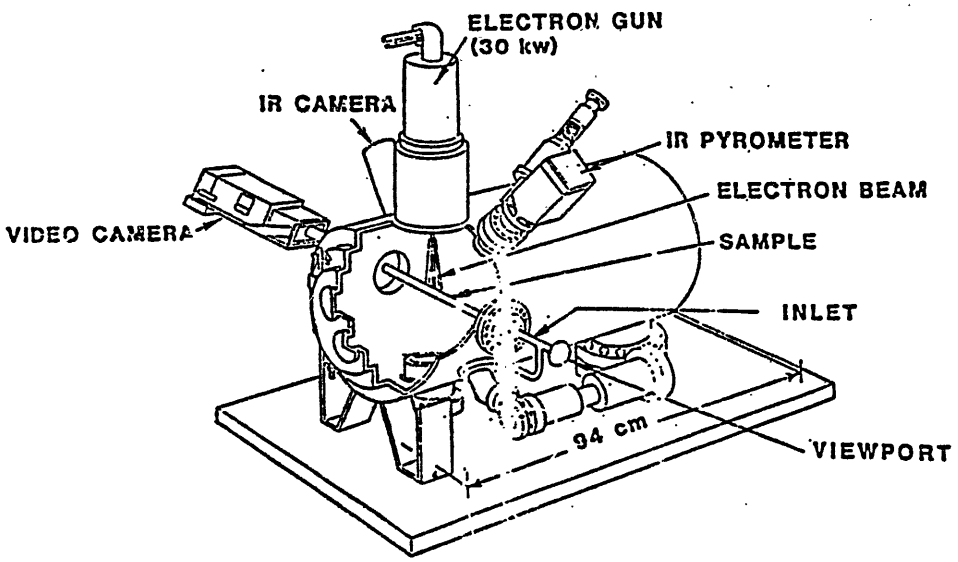

Sandia National Laboratories

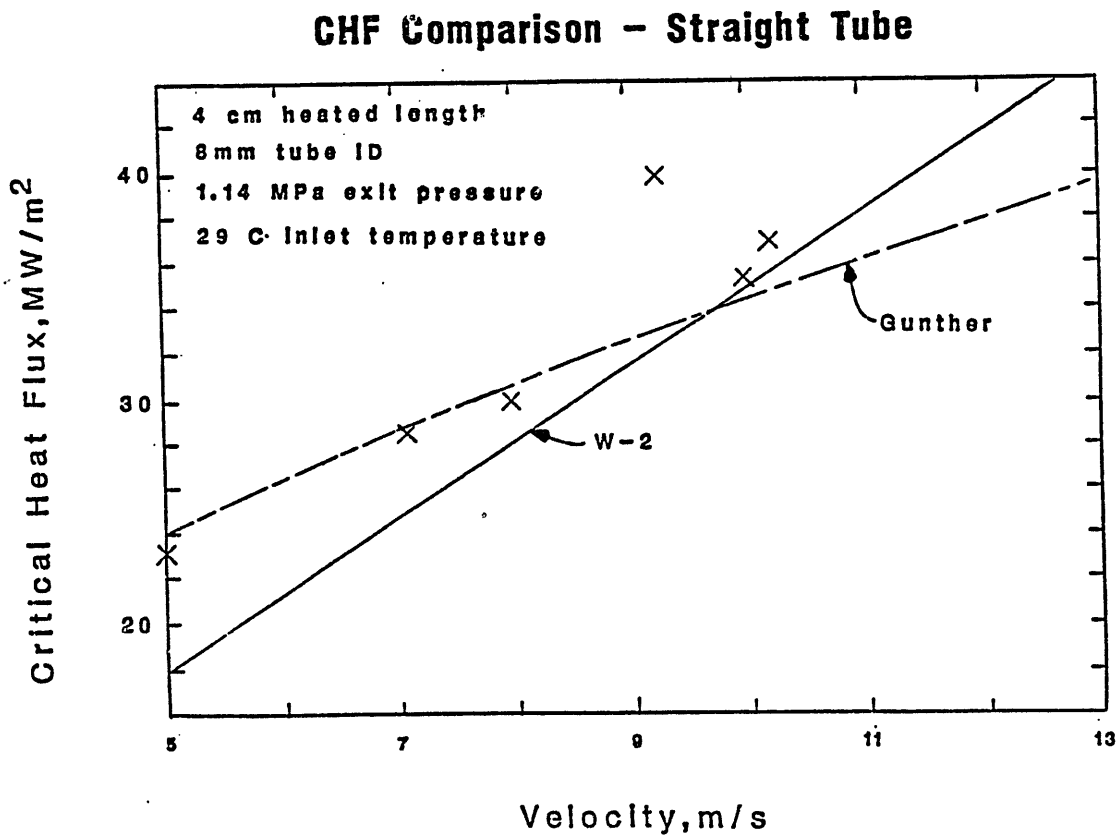

CRITICAL HEAT FLUX CORRELATIONS

* Most existing CHF correlations:
  - uniform circumferential heat flux
  - vertical tubes
  - saturated boiling conditions
  - aimed at predicting DNB for nuclear power applications

* Subcooled boiling correlations:
  -Gunther (1951)
  -Westinghouse (1963,1968)

* Peak heat flux suggested as best correlation parameter for subcooled flows by Leontiev (1981) (confirmed experimentally with Sandia e-beam)

#60924.JAK-4

EXPERIMENTAL ARRANGEMENT

* Sandia e-beam apparatus
  - 30 kV, 30 kW electron beam
  - beam rastered over 8 cm length
  - 15 kW max. delivered to water
* Water at 0.3-2 MPa (50-300 psi)
* Flow velocities 2 -. 20 m/s
* Glidcop copper tube targets 9.5 mm OD

#60924.JAK-9

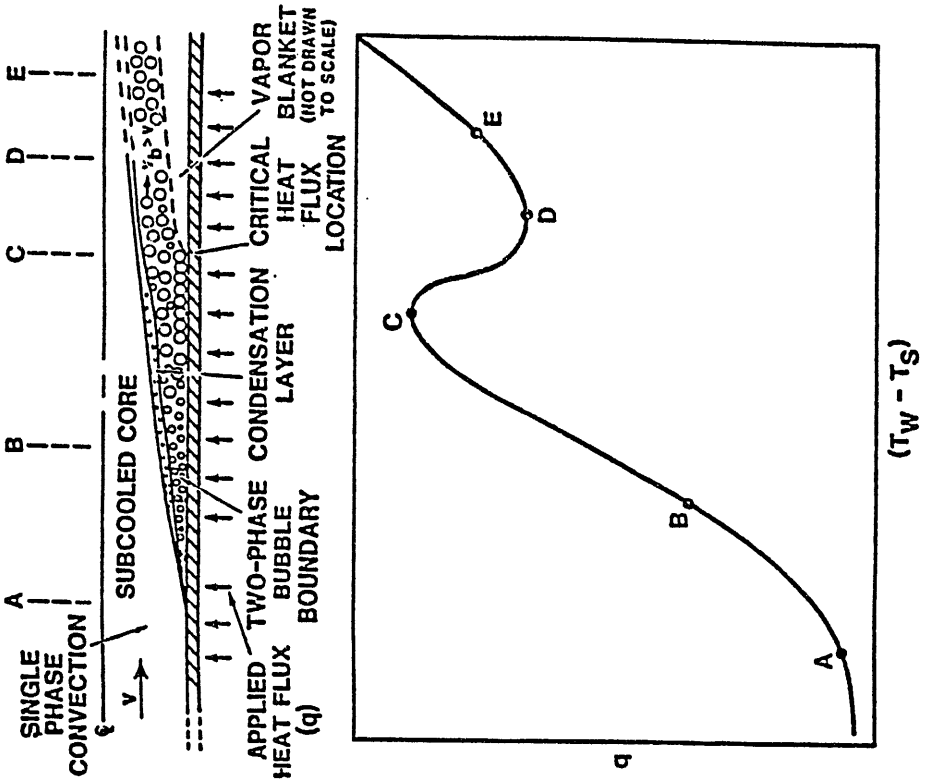

CRITICAL HEAT FLUX

* Vapor blanket forms at wall
* Limits heat transfer
* Wall superheats preventing further liquid contact

* Prevention:
  - -increase flow
  - -increase subcooling
  - -increase pressure

* Major problem: burnout of tube

#6092UAK-3

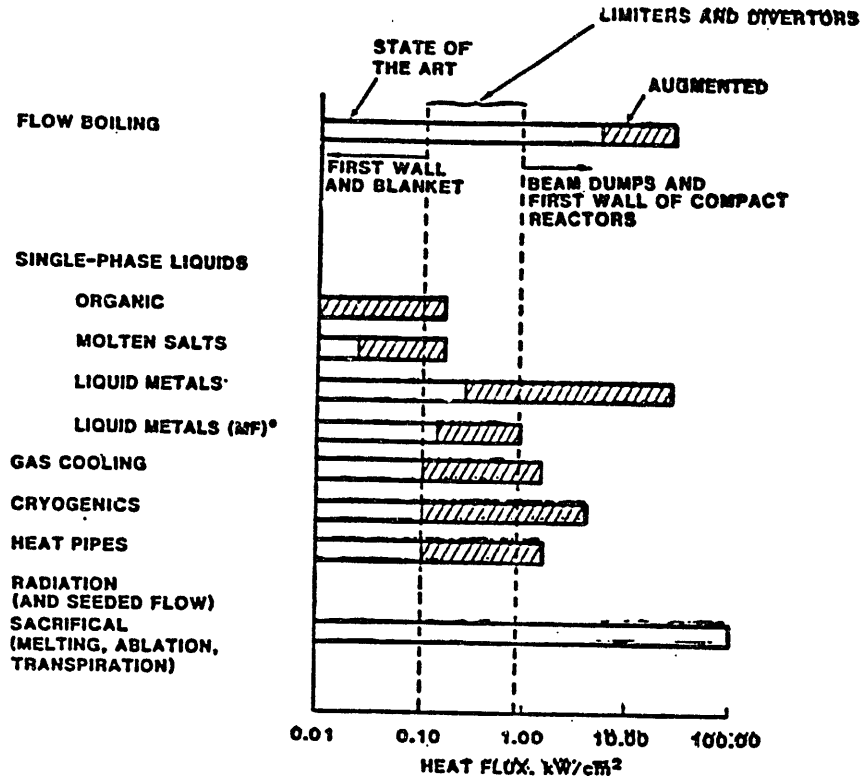

*MF - IN THE PRESENCE OF A TRANSVERSE MAGNETIC FIELD

USE OF SUBCOOLED FLOW BOILING

Advantages:
* Higher heat fluxes
* Lower fluid pressure
* Lower flow rates

Potential Disadvantages:
* Cavitation, erosion
* Vibration, noise
* Burn-out (critical heat flux)
* Flow instabilities, surges
* High pressure drop

#5092JAY-2

Glidcop Tube Subcooled Boiling Experiments

Glidcop copper tubing in being considered for the tube bank in the US pumped limiter for the Tore Supra machine. A total of 8–10 tubes (4 ft each) will be subjected to heat fluxes of 1000 – 4400 W/cm2.

Purpose

Since this is the first application of this tubing heat transfer data must be obtained experimentally. This would include heat transfer coefficents, critical heat flux values, and the effect of twisted tape inserts.

Test Parameters

Sample size: 9.5mm o.d. x 15 cm
Power density: 1000 4400 W/cm2
Pulse length: 30 seconds
Heated area: 4 cm2
Coolant flow: 0.3 – 1.0 l/s
Coolant pressure: 0.5 – 1.5 MPa

Results

Twisted tape roughly doubles observed CHF.

Tore Supra Pump Limiter

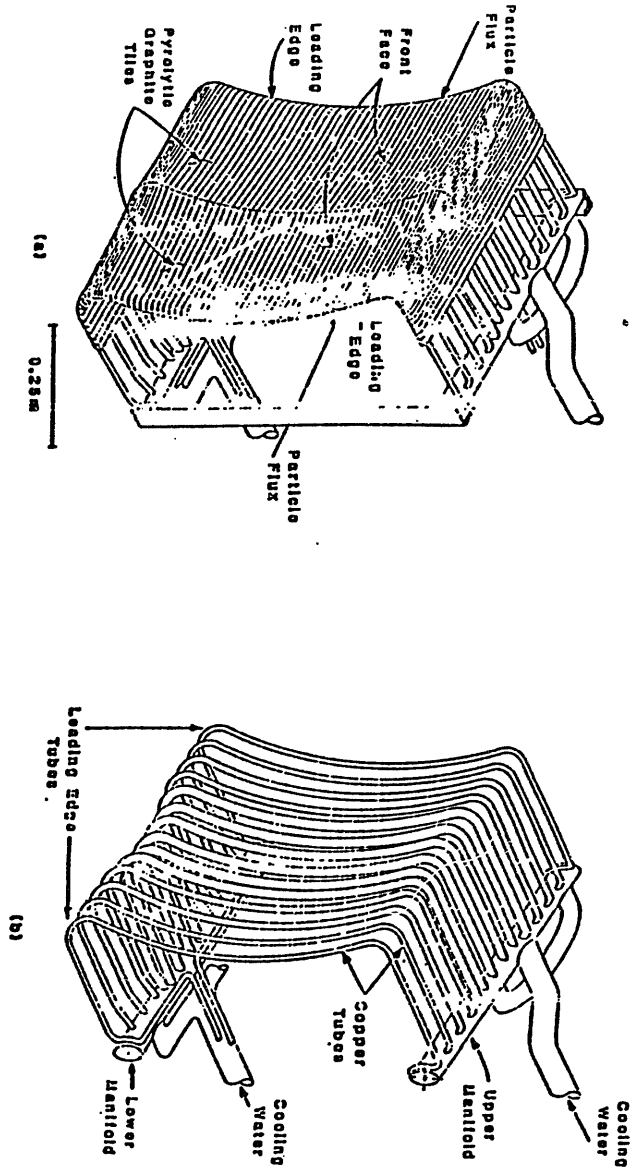

TORE SUPRA PARAMETERS

MAJOR RADIUS	2.25 - 2.4M
MINOR RADIUS	0.70 - 0.85M
PLASMA CURRENT	1.7 MA
TOROIDAL FIELD	
ON AXIS	4.5T
MAXIMUM	9.0T
PULSE LENGTH	≥30S
PLASMA HEATING (PHASE I)	
NEUTRAL BEAMS	4
TOTAL NEUTRAL BEAM POWER	7MW
ICRH	
AT 35-65 MHZ	9MW
AT 120 MHZ	6MW
LOWER HYBRID (16 KLYSTRONS)	8MW
TOTAL PLASMA HEATING - PHASE I	15MW

POWER HANDLING FOR TORE SUPRA

MODULAR LIMITER SYSTEM

1 HORIZONTAL MODULE

2MW - TOTAL POWER DEPOSITION

3.0kW/cm^2 - LEADING EDGE HEAT FLUX

0.5m^2 - SURFACE AREA

6 VERTICAL MODULES

1.0 MW TOTAL POWER DEPOSITION

1.0 - 2.0 kW/cm^2 LEADING EDGE HEAT FLUX

0.2m^2 - SURFACE AREA

SYSTEM OPERATING PARAMETERS

7.0 MW TOTAL POWER HANDLING

3 - 12% EXHAUST EFFICIENCY

CO_2 Laser Beam Test of an Actively Cooled First-wall Element with a Graphite-clad SiC Armor Tile

Yoshitake Gotoh
Hitachi Research Laboratory

Abstract

A graphite-clad SiC tile of 29mm dia and 15mm thickness is bonded to a base metal (Cu or 316 SS) with insertion of Cu-35 vol%C composite sheet. The elements are tested under active cooling condition by using 3.5kW CO_2 laser beam at heat flux condition of 0.3 ∿ 1.7kW/cm^2 and a pulse length of 40s.

CO_2 Laser Beam Test of an Actively Cooled First-wall Element with a Graphite-clad SiC Armor Tile

Yoshitaka Gotoh, Hisanori Okamura, Shinnichi Itoh
Hitachi Research Laboratory; Hitachi Works, Hitachi Ltd.

Graphite is a hopeful candidate material for first wall of the next machine, because it has high thermal-shock resistivity and low vapor pressure. Silicon carbide is another candidate with high thermal conductivity below several hundreds ℃ and good UHV compatibility. However, those candidates have some drawbacks: with respect to UHV compatibility for graphite, and thermal-shock resistivity for silicon carbide. In the present study, an attempt is made to develope a graphite/SiC-layered structure tile for actively cooled first-wall element with both high thermal-shock resistivity and high cooling efficiency.

Graphite-clad SiC tiles are fabricated through hot pressing. High thermal conductivity SiC layer (HITACERAM SC101) of 2, 5 or 10 mm thickness and 20 mm diam. is hot pressed in isotropic graphite dies at 2100℃ under pressure of 300 kg/cm². Hot-pressed graphite/SiC-bilayer plate is cut into a hexagonal tile (graphite-clad SiC tile) as shown in Fig. 1. SiC face of each tile is bonded to a Cu or 316SS base plate with insertion of a Cu-35vol.%C composite sheet. Two thermo-couple elements are attached to each tile at different depths from tile front surface as shown in Fig. 1.

Wall elements, mounted on a water-cooled test bed, are irradiated with CO_2 laser beam of total power from 1.5 to 3.5 kW, with duration time of 40 s. Fig. 2 compares temperature change on same type graphite-clad SiC tiles but bonded to different base plate materials: Cu and 316SS. T_s and T_{10} are tile temperatures at thermo-couple positions just below and at a 10 mm depth from the surface, respectively. Heat flux on the tile front, at thermocouple position (J_s) is estimated to be 300 W/cm², while that at center of the tile (J_0) is 1300 W/cm² for beam power of 2.5 kW. At the end of a 40 s laser irradiation, tile temperatures of the Cu-base element are found to reach almost equilibrium values which are by 350 ℃ lower than those for a 316SS base plate element.

The equilibrium temperature T_s and T_{10} at the end of each 40 s laser pulse for the Cu base plate element are plotted against laser power from 1.5 to 3.5 kW in Fig. 3. Open points are measured T_s values, while solid points are T_{10} values. Relatively good agreement is found between measured values and calculated results (dashed lines) for laser power of up to 3.5 kW. Therefore, it is concluded that the element has worked under heat loading condition of up to 420 W/cm² at the thermocouple element on the tile surface with a maximum heat flux of 1700 W/cm² at the center part of the tile at repetetion time of 10 cycles. No cracks are found in the graphite layer, but fairy amount of vaporization/particle emission has been observed at the graphite surface, especially at the center part of the front face.

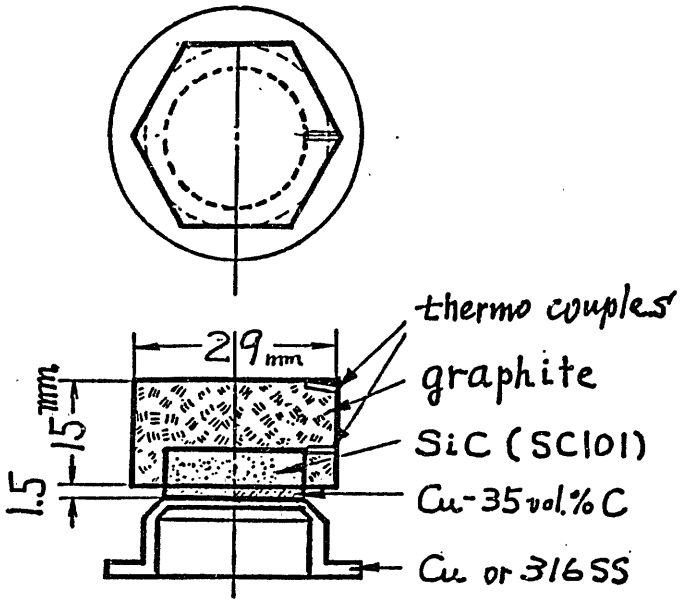

Fig. 1 Structure of first wall element

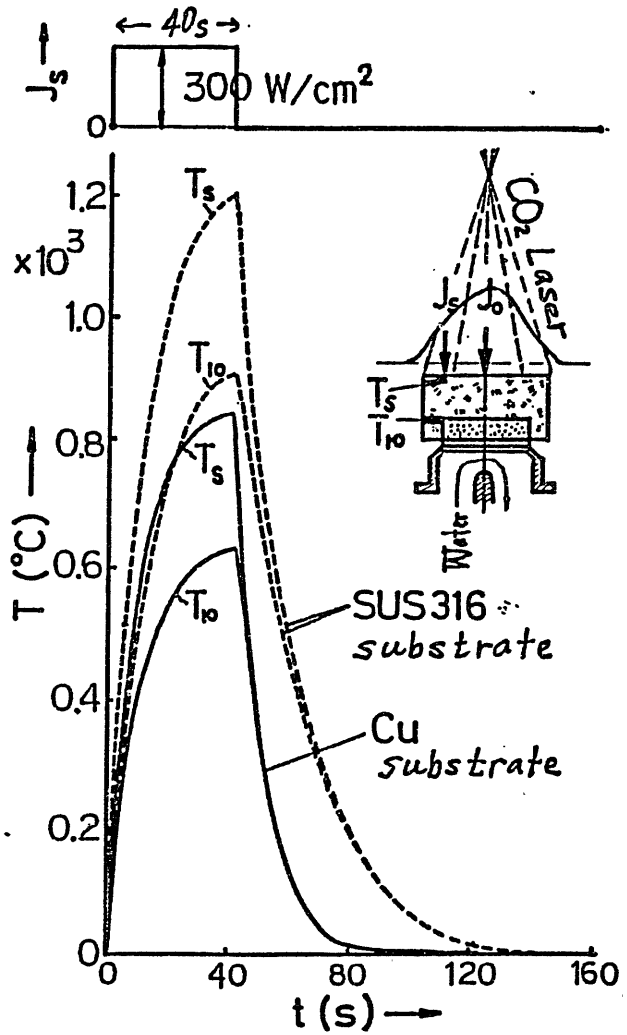

Fig. 2 Temperature changes of an armor tile

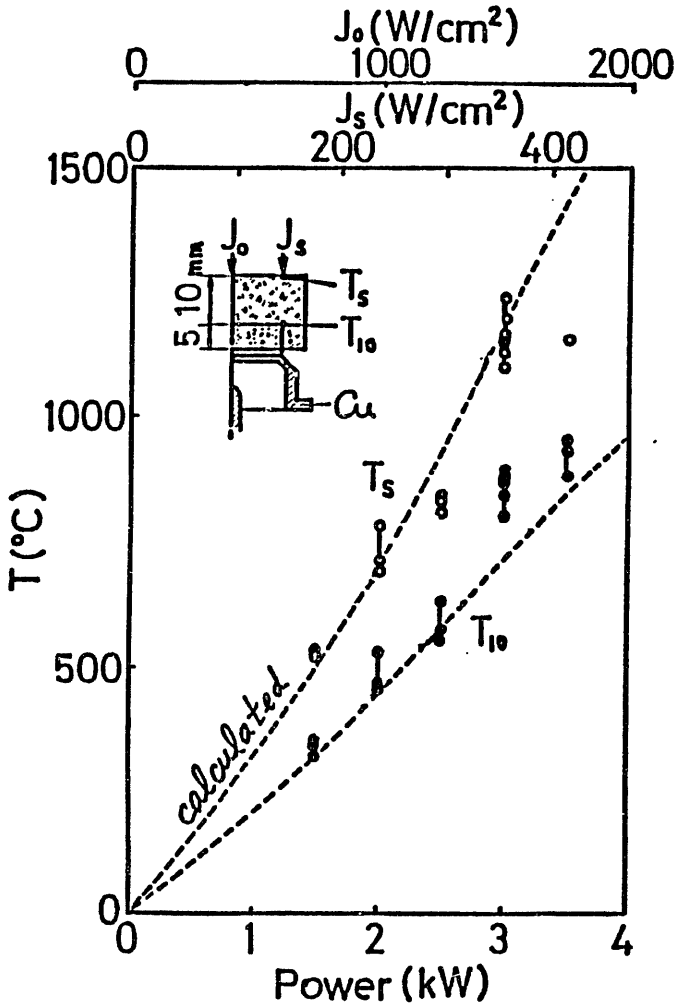

Fig. 3 Laser power dependence of T_s, T_{10} at 40s.

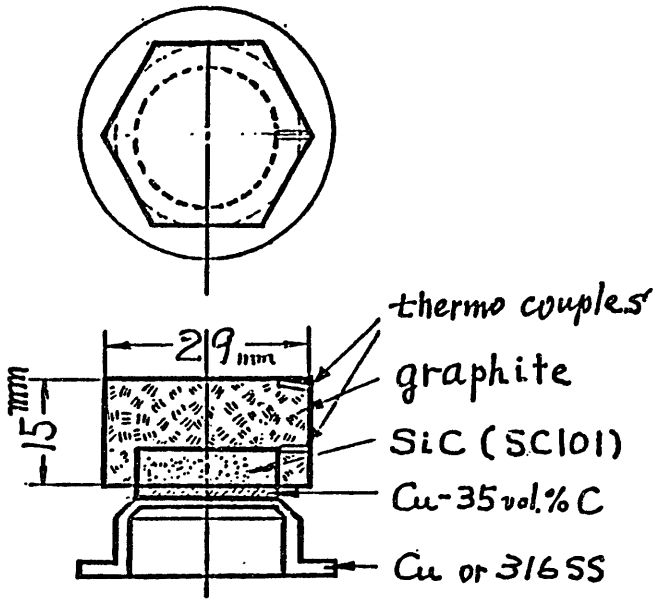

Fig. 1 Structure of first wall element

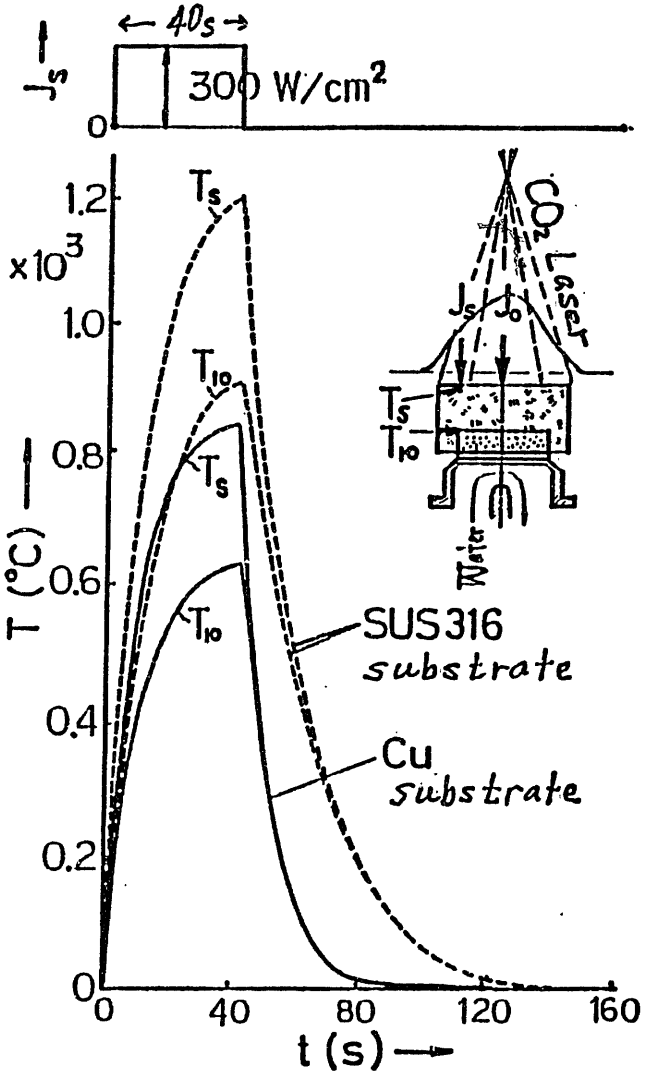

Fig. 2 Temperature changes of an armor tile

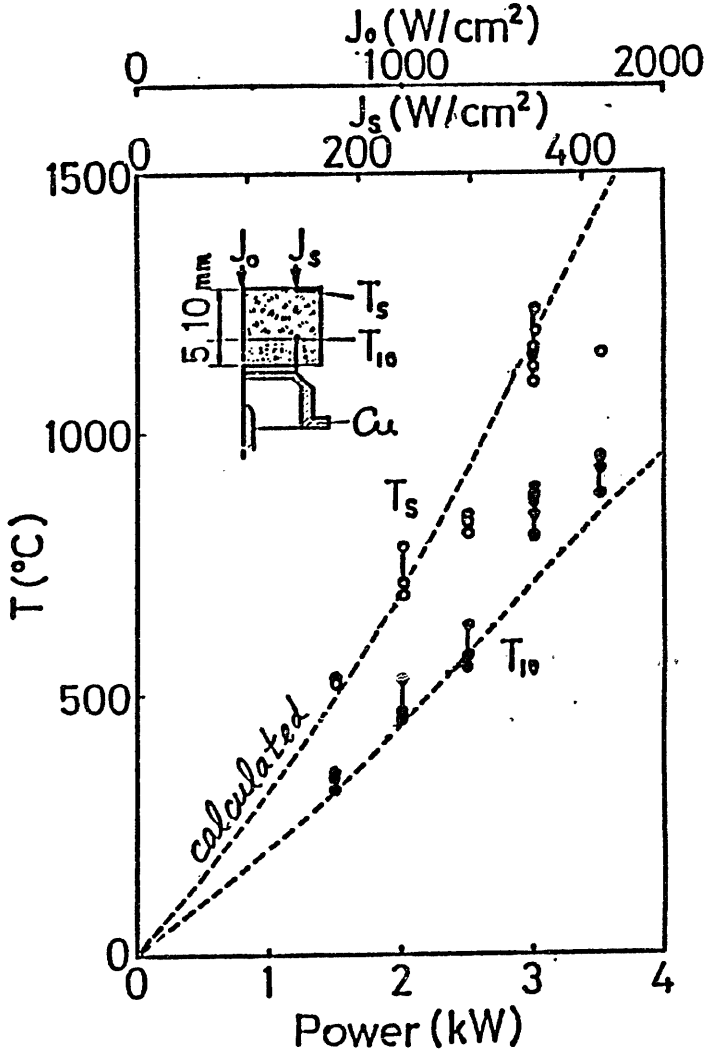

Fig. 3 Laser power dependence of T_s, T_{10} at 40s.

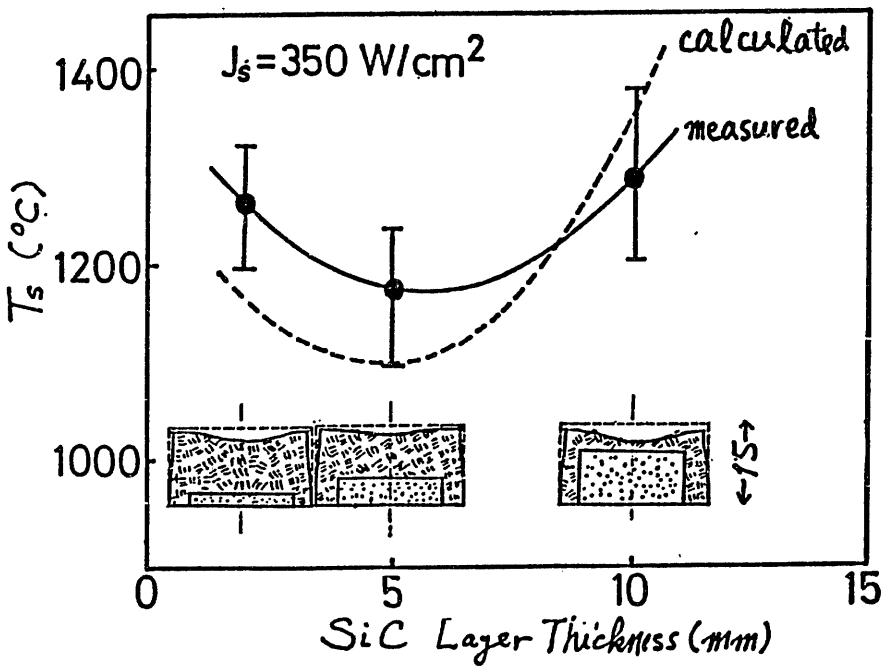

Fig.4

SiC Layer Thickness Dependence of T_s at 40s

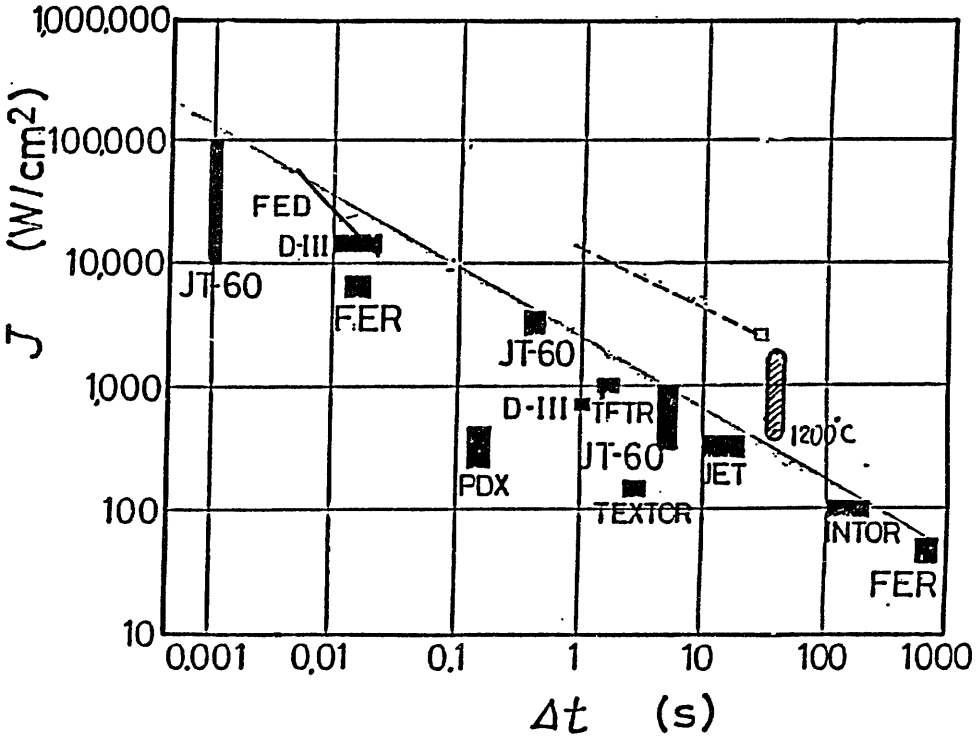

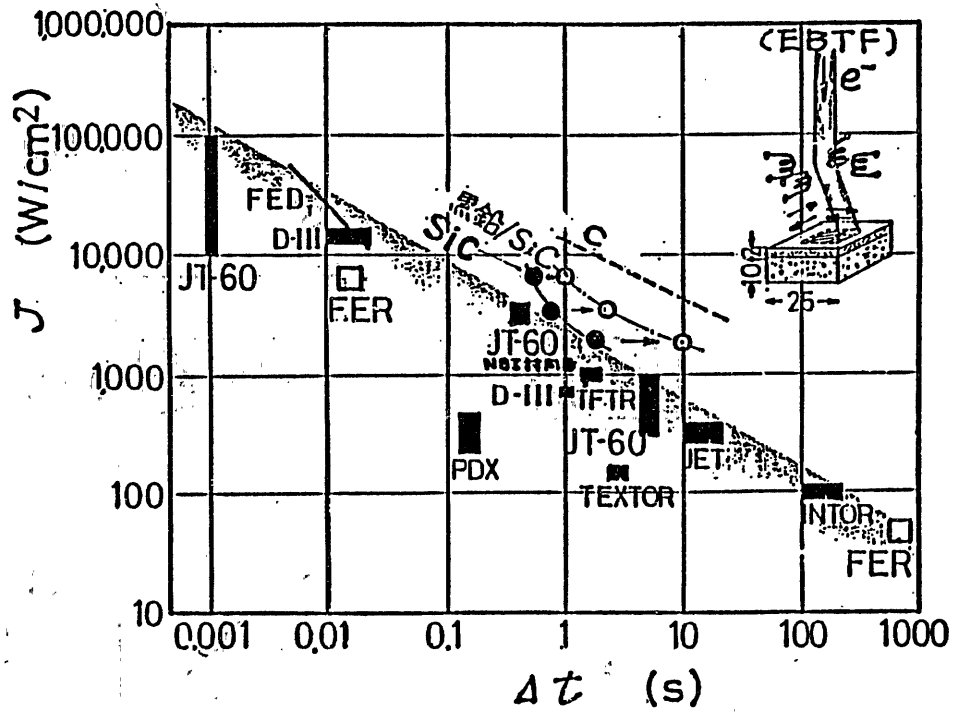

HEAT FLUX LEVEL FOR FIRST WALL : J
/MAXIMUM ENDURABLE HEAT LOADING

Limiter Heat Loads in TFTR Due to Disruptions

M. Ulrickson

Princeton University
Princeton, New Jersey USA

Abstract

A fast infrared thermometer was constructed to measure the temperature of the TFTR Bumper Limiter during disruptions with 10μsec time resolution. The results indicate peak surface temperatures of 1800C at 10MJ of NB heating. The rise time of the temperature is as short as 20μsec. The heat flux is found to be up to 40kW/cm^2. The energy deposition is up to 200J/cm^2. Extrapolation to CIT is made.

Disruptions on TFTR

Dr. Ulrickson
PPPL

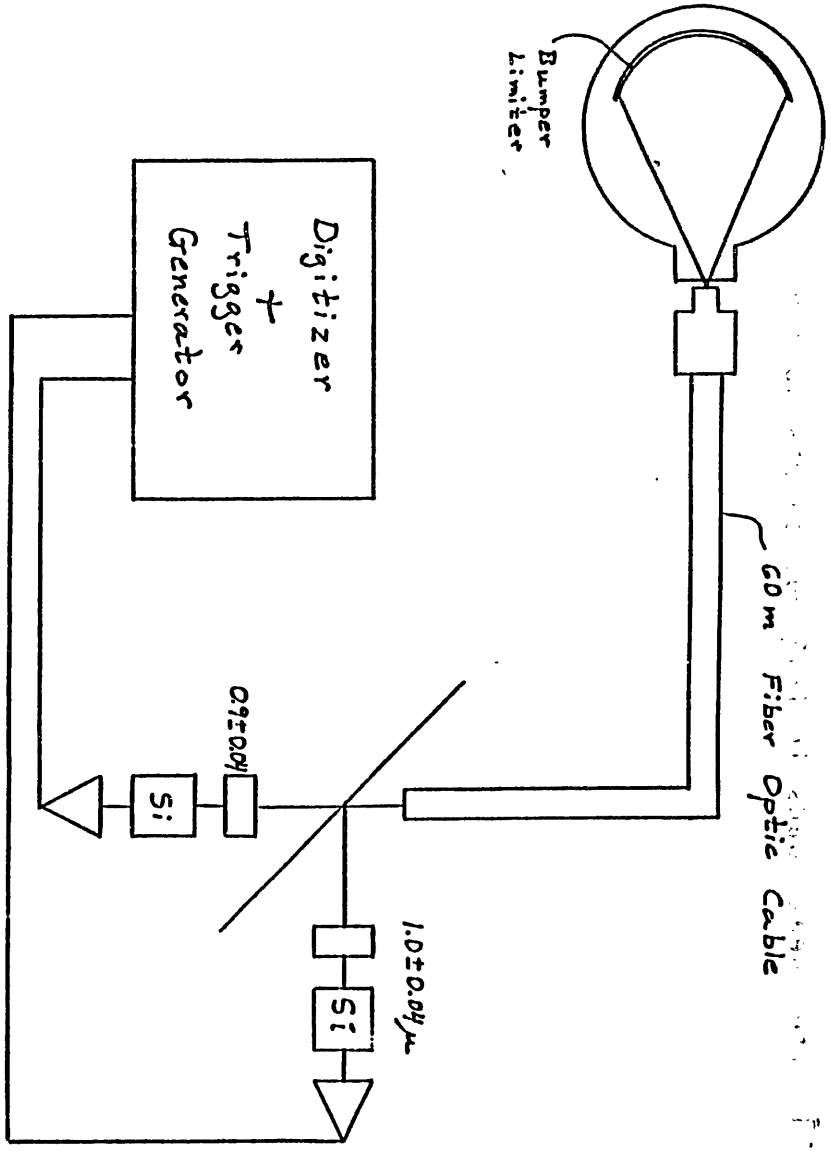

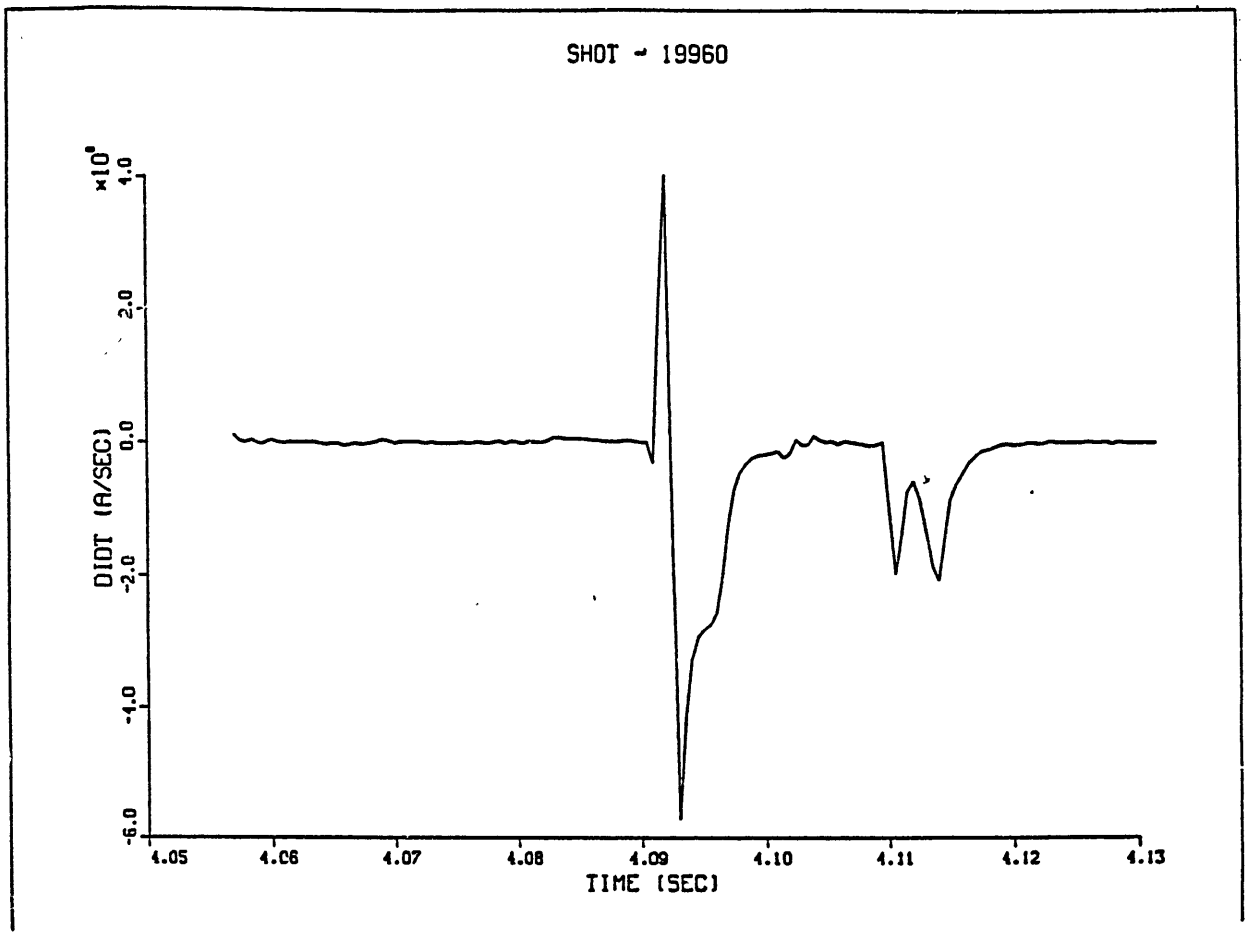
SHOT - 19960
DIDT (A/SEC)
×10⁵
4.0
2.0
0.0
-2.0
-4.0
-6.0
4.05
4.06
4.07
4.08
4.09
4.10
4.11
4.12
4.13
TIME (SEC)

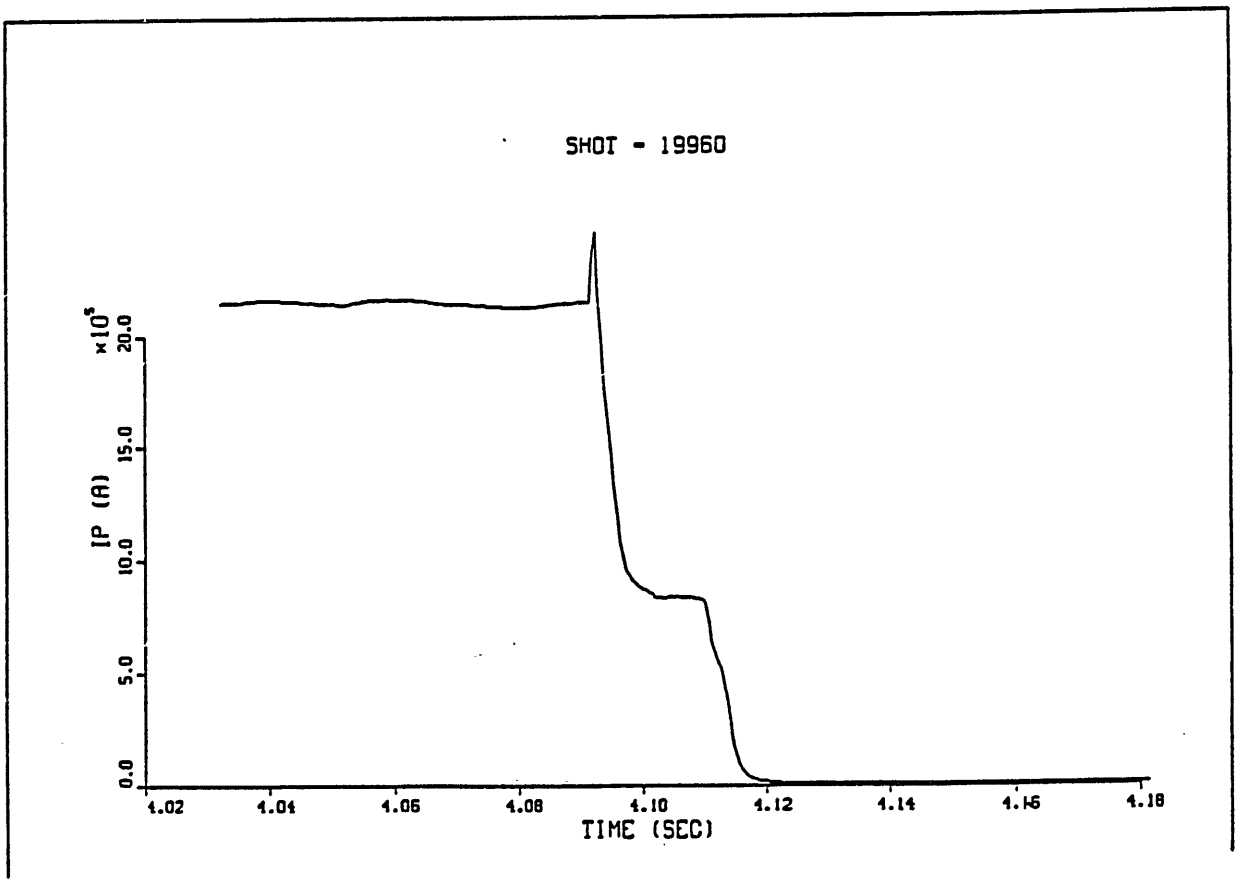
SHOT - 19960
IP (A)
×10⁵
20.0
15.0
10.0
5.0
0.0
4.02
4.04
4.06
4.08
4.10
4.12
4.14
4.16
4.18
TIME (SEC)

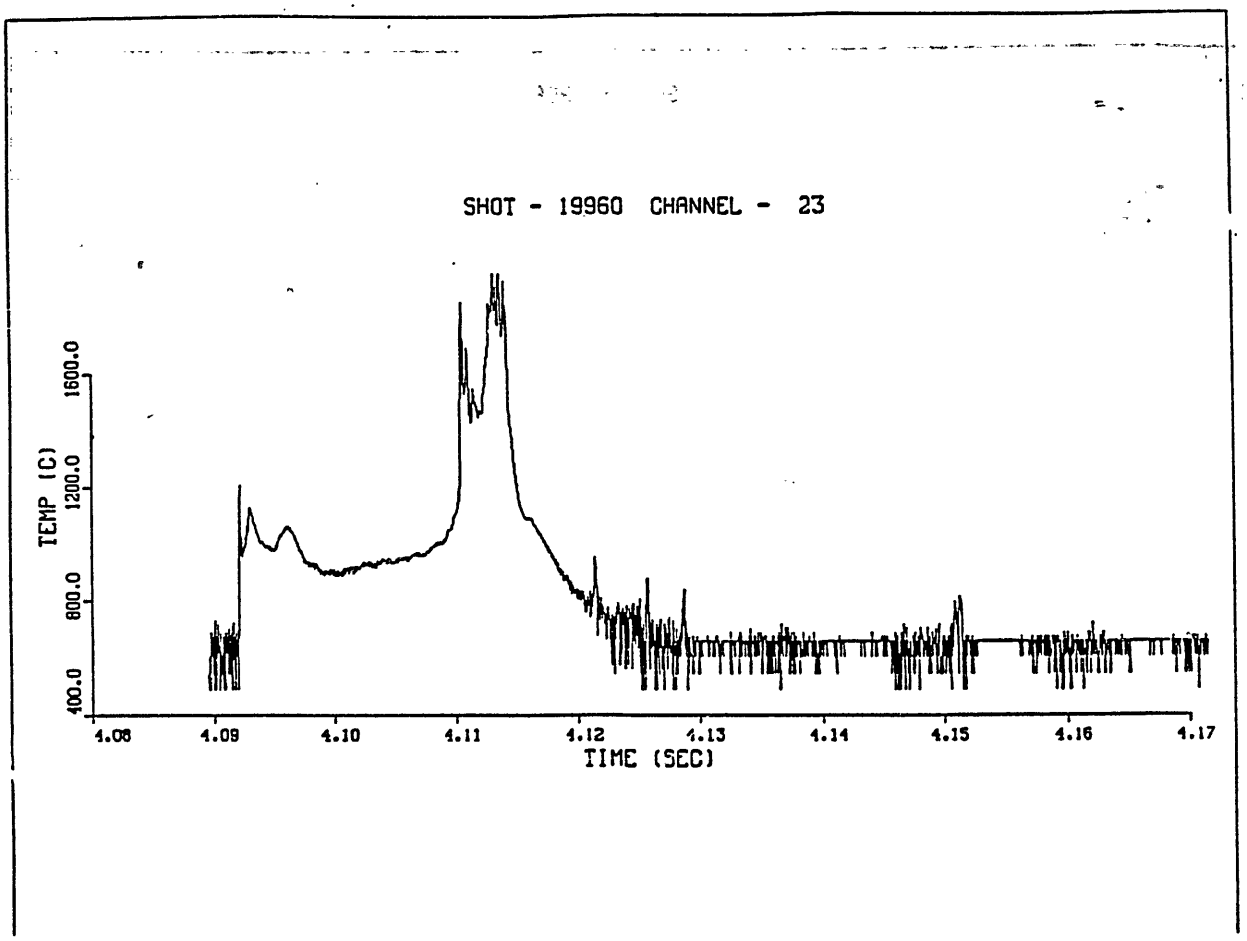
SHOT - 19960 CHANNEL - 23
TEMP (C)
400.0
800.0
1200.0
1600.0
4.08
4.09
4.10
4.11
4.12
4.13
4.14
4.15
4.16
4.17
TIME (SEC)

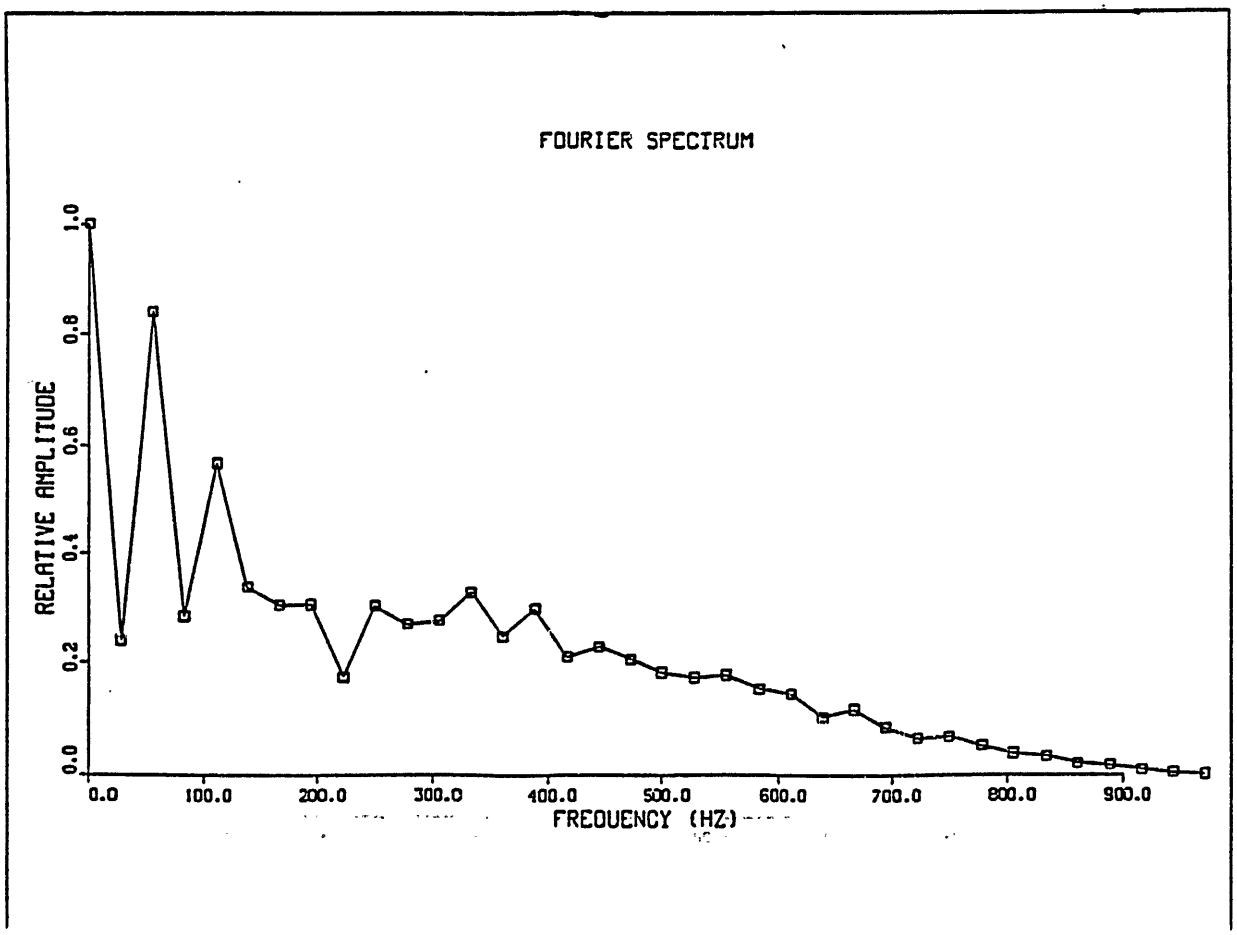
FOURIER SPECTRUM
RELATIVE AMPLITUDE
0.0
0.2
0.4
0.6
0.8
1.0
0.0
100.0
200.0
300.0
400.0
500.0
600.0
700.0
800.0
900.0
FREQUENCY (HZ)

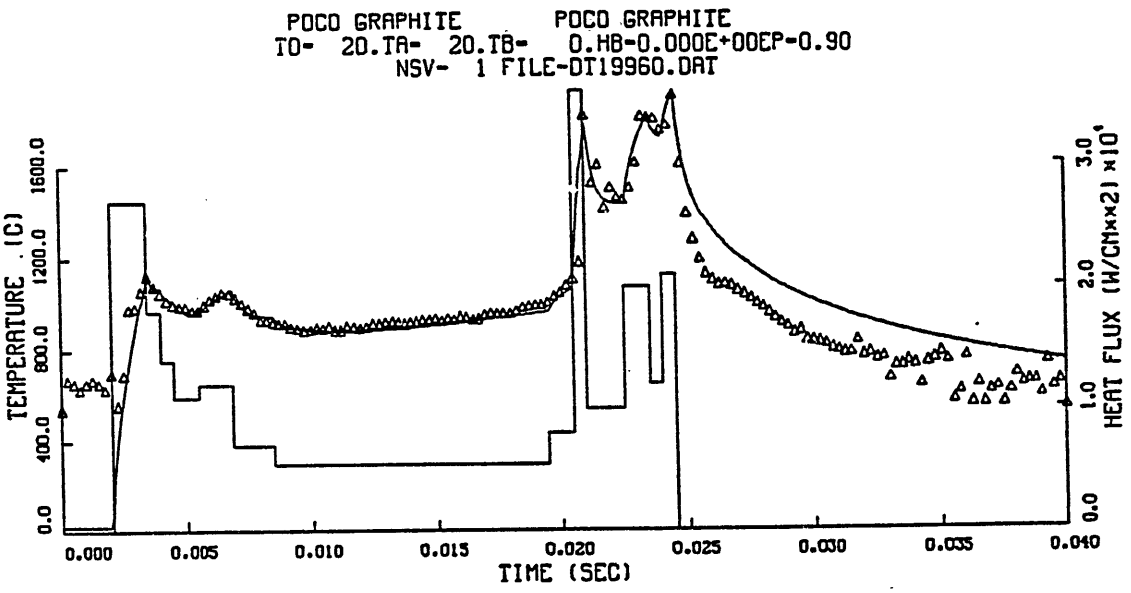
POCO GRAPHITE POCO GRAPHITE
TO- 20.TA- 20.TB- 0.HB-0.000E+00EP-0.90
NSV- 1 FILE-DT19960.DAT
TEMPERATURE (C)
HEAT FLUX (W/CM**2) *10⁴
TIME (SEC)

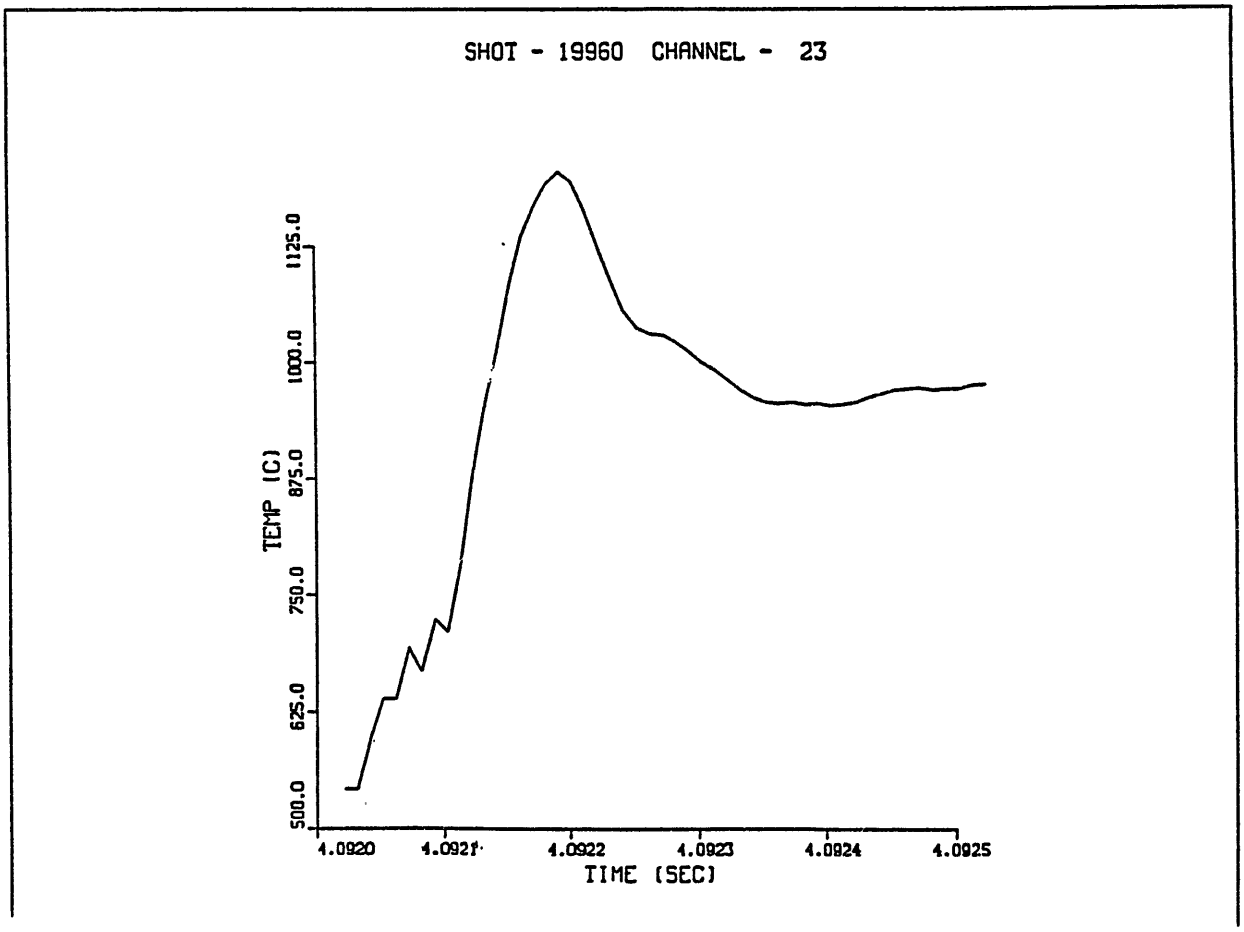
SHOT - 19960 CHANNEL - 23
TEMP (C)
TIME (SEC)

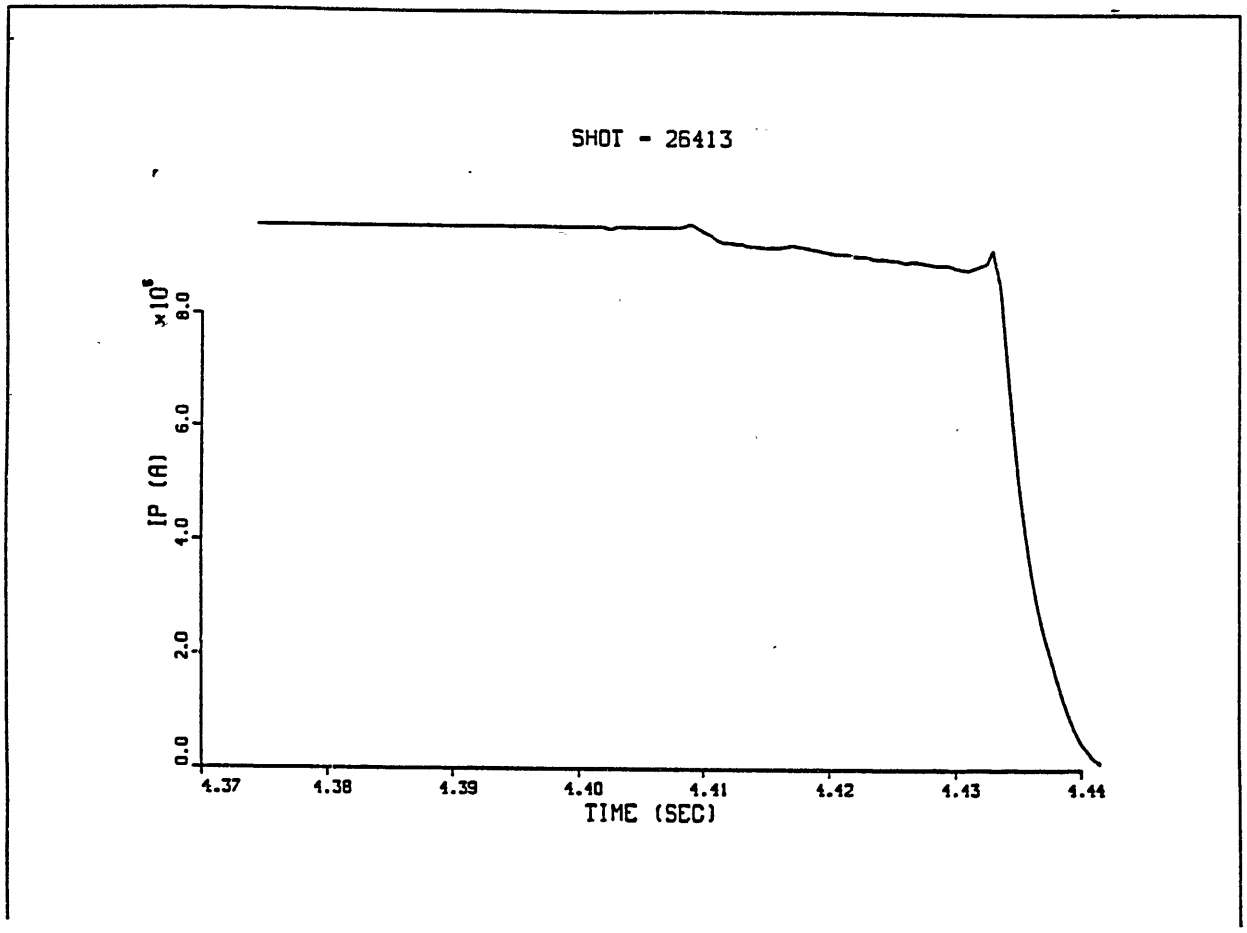
SHOT - 26413
IP (A)
×10⁵
0.0
2.0
4.0
6.0
8.0
4.37
4.38
4.39
4.40
4.41
4.42
4.43
4.44
TIME (SEC)

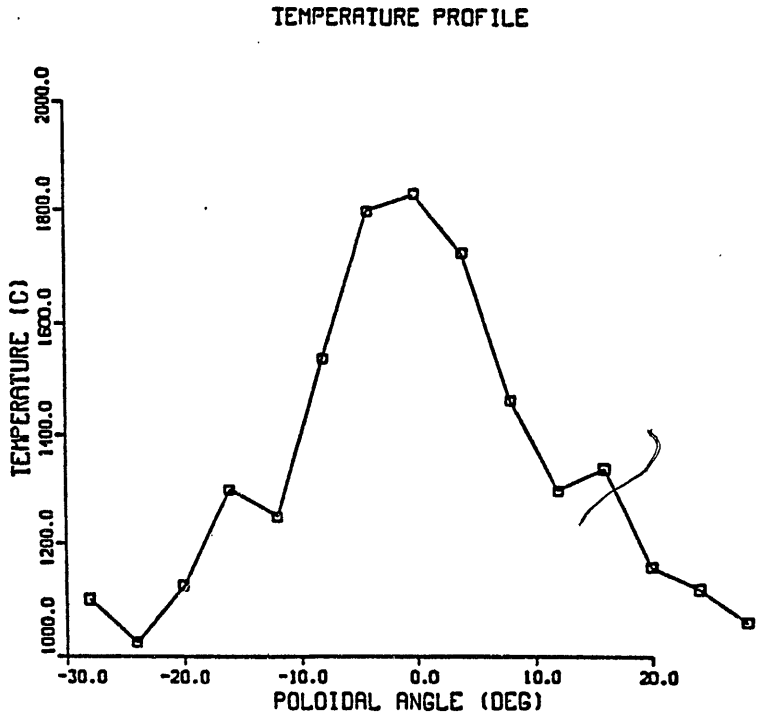
TEMPERATURE PROFILE
TEMPERATURE (C)
1000.0
1200.0
1400.0
1600.0
1800.0
2000.0
-30.0
-20.0
-10.0
0.0
10.0
20.0
POLOIDAL ANGLE (DEG)

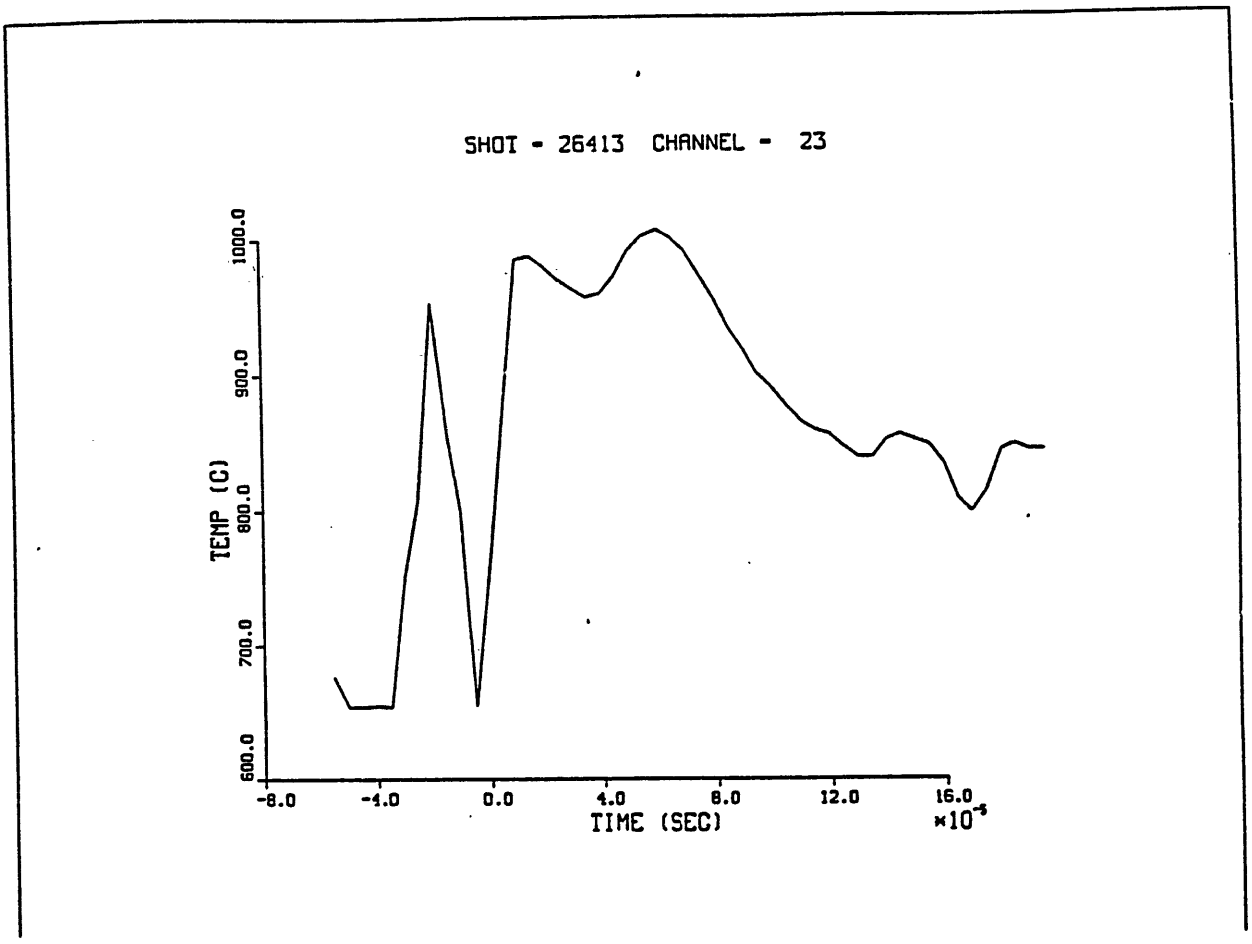
SHOT - 26413 CHANNEL - 23
TEMP (C)
1000.0
900.0
800.0
700.0
600.0
-8.0
-4.0
0.0
4.0
8.0
12.0
16.0
TIME (SEC)
×10⁻⁵

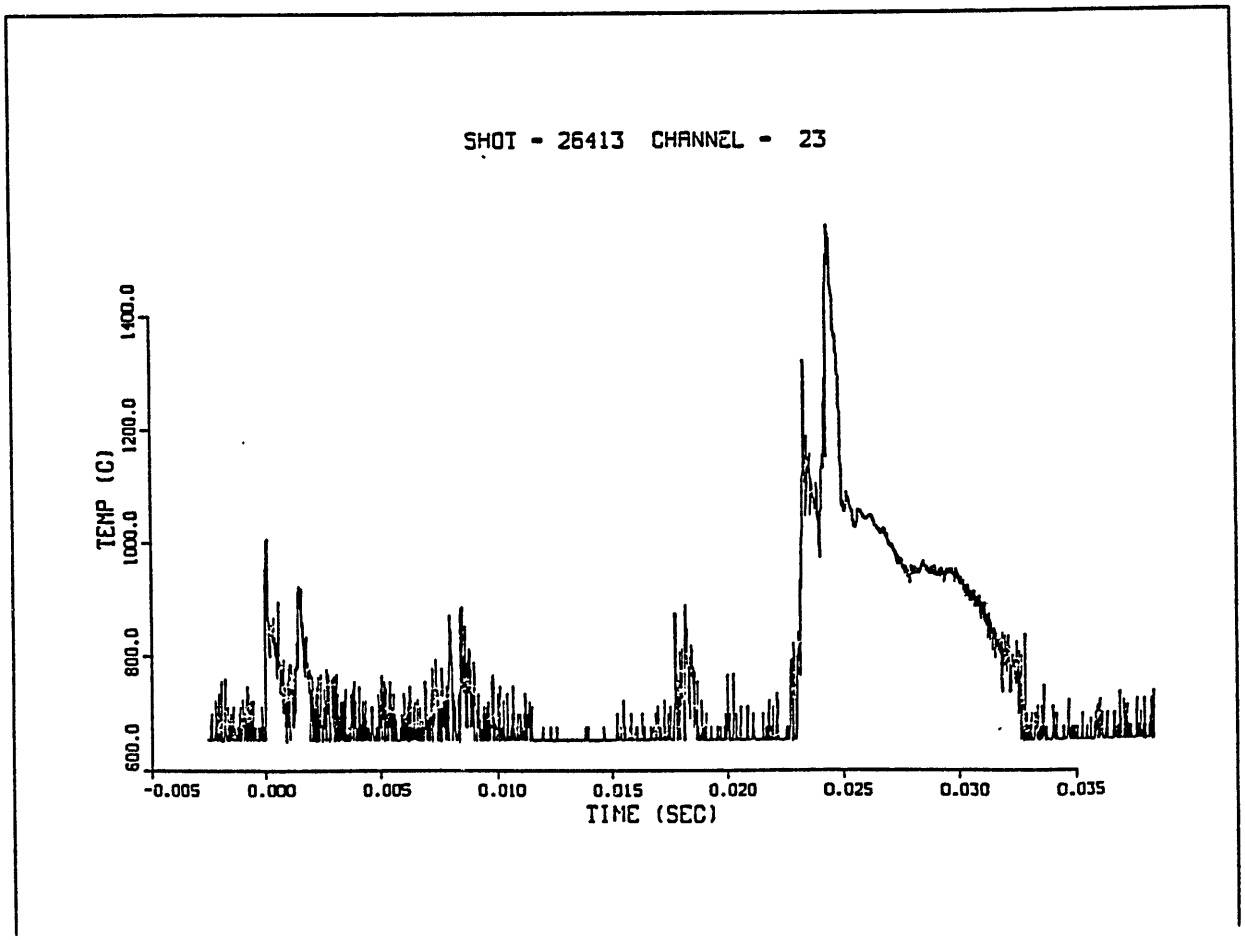
SHOT - 26413 CHANNEL - 23
TEMP (C)
1400.0
1200.0
1000.0
800.0
600.0
-0.005
0.000
0.005
0.010
0.015
0.020
0.025
0.030
0.035
TIME (SEC)

CONCLUSIONS

I. Plasma current decay rates of up to 600 kA/msec have been observed.

II. The fastest disruptions occur at low q.

III. Thermal energy decay times are between 20 and 100 μsec with the fastest for high β disruptions.

IV. Up to 50 % of the plasma stored energy (magnetic plus thermal) is deposited on the limiter.

V. Up to 200 J/cm^2 has been deposited.

TFTR Disruptions

Stored energy
Thermal energy = 1.1 MJ
Magnetic energy = 5.3 MJ

Energy to the bumper limiter = 3.4±1.4 MJ

Energy radiated = 3.0±1.0 MJ

Disruptions on Compact Devices

Stored energy
Thermal energy = 36 MJ
Magnetic energy = 42 MJ

Peak heat flux in 100 μsec thermal dump = 45 GW/m^2

Peak heat flux in 10 msec current decay = 470 MW/m^2

Total energy deposited 920 J/cm^2

LIMITER PUMPING AND RECYCLING IN TFTR

Review evidence seen during low density (He,D) conditioning sequences:

1) low density limit decreases

2) D_α emission falls in He conditioning discharges

3) edge neutral pressure (P_o) decreases

Recycling changes in 800 kA OH target plasmas as a result of the conditioning

1) low density limit decreases (lowest = $\bar{n}_e = 5.5 \times 10^{18}$)

2) D_α, P_o decrease (by approx. a factor of 10)

3) τ_p^* decreases (to a minimum value of 0.15s)

4) inferred value of the global recycling coefficient, R, decreases from R ~ 1 to R < 0.5

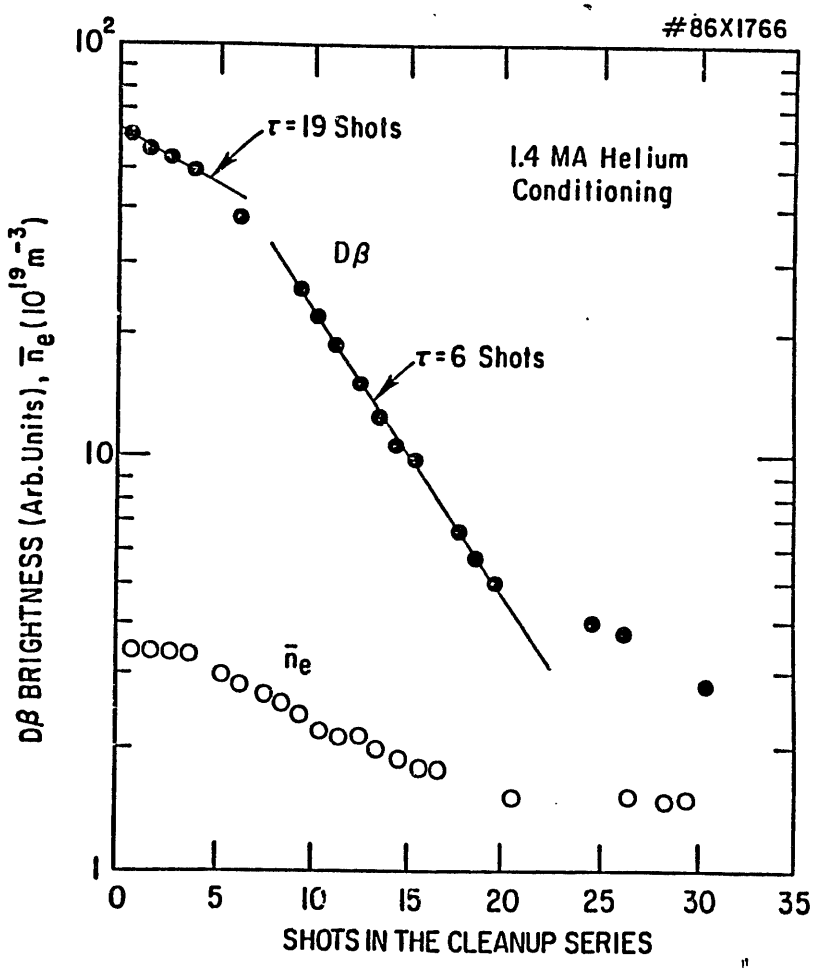

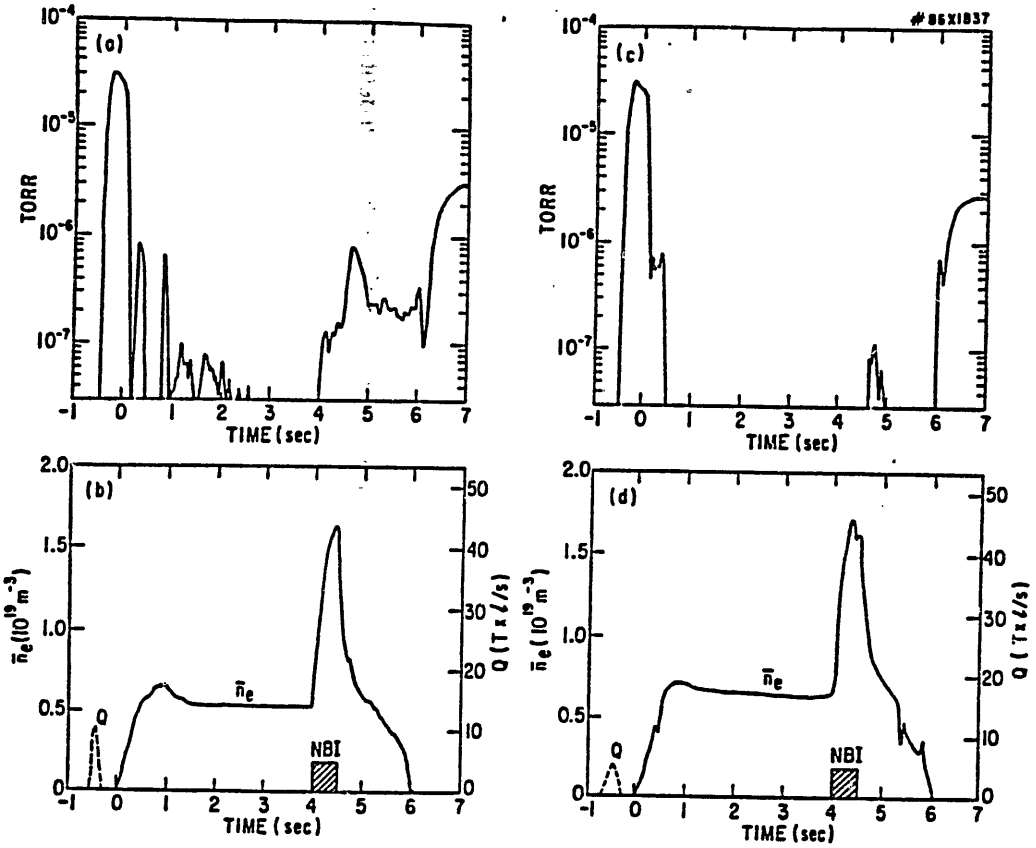
#86X1837
(a)
(b)
(c)
(d)
TORR
TIME (sec)
$\bar{n}_e$
Q
NBI
$\bar{n}_e(10^{19}m^{-3})$
Q (Tx ℓ/s)

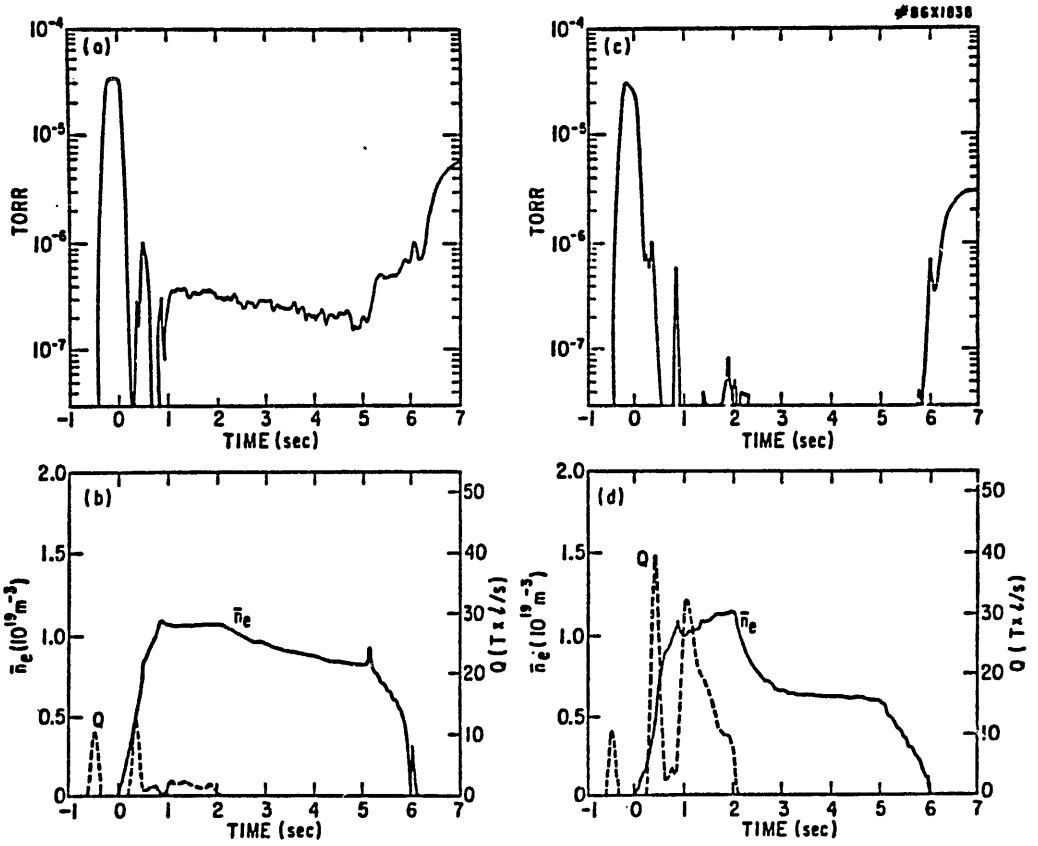
#86X1838
(a)
(b)
(c)
(d)
TORR
TIME (sec)
$\bar{n}_e$
Q
$\bar{n}_e(10^{19}m^{-3})$
Q (Tx ℓ/s)

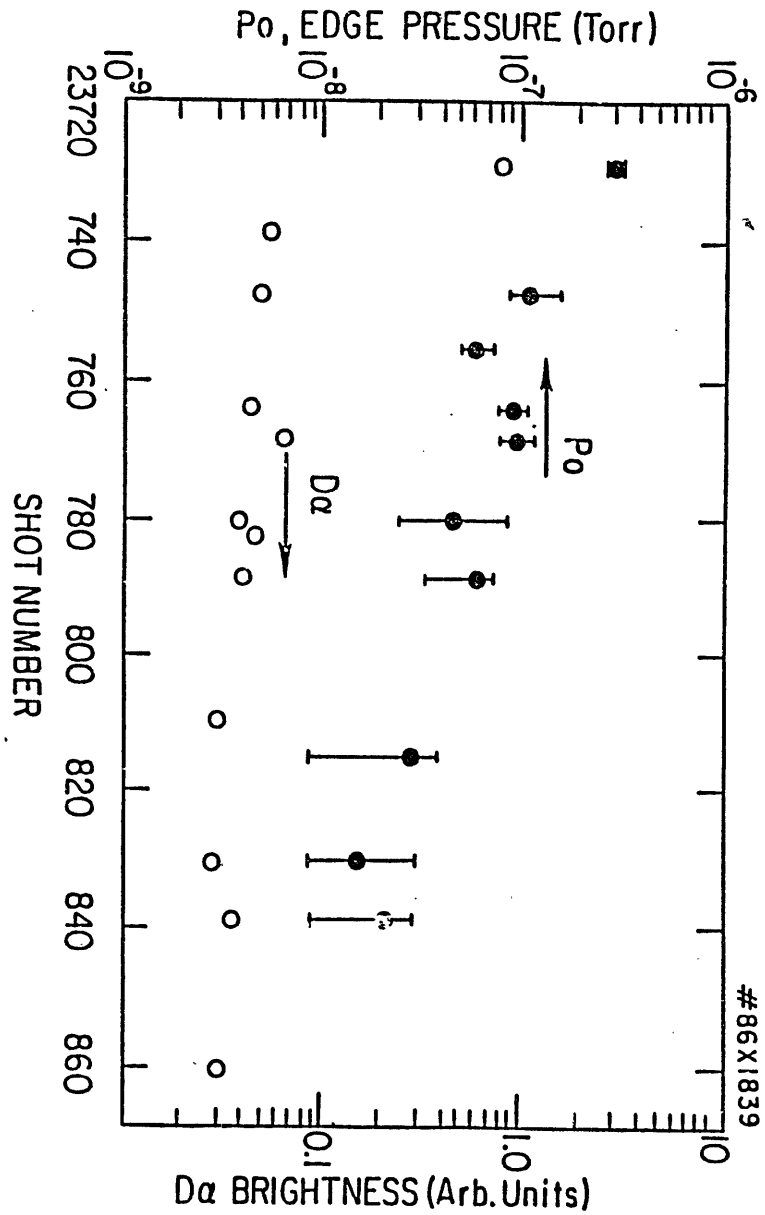

τ_p^* Measurements:

- τ_p^* extracted from the density decay to a baseline value after termination of D_2 gas feed

"C2 Fiducials"

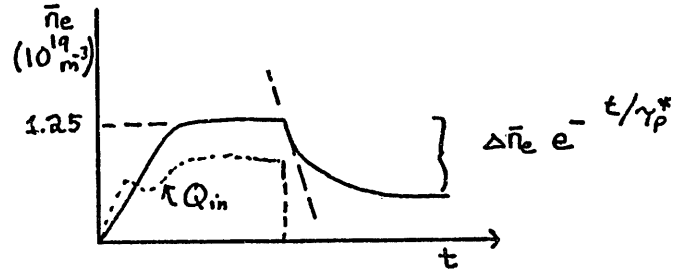

- assumes τ_p^* is representative of the decay in deuteron density

γ_p Measurement:

- from Dα measurements during " gassed-up" limiter sequence (shots 24836-856)

- calculated total number of deuterons in plasma from line-averaged density (assumed parabolic profile), and corrected for dilution using PHA Z_{eff} (K.Hill)

- used Dα emission measurements from 4 poloidal channels viewing bumper limiter (A.Ramsey)

- assumed Dα emission comes only from bumper limiter (ie, $\Delta\phi = \pm 60^0$); and that emission is toroidally symmetric (needed correction-toroidal modulation seen on plasma TV)

- corrected for emission outside last closed flux surface ($r > 0.80$m), and molecular emission (Heifetz, McNeill)

$$\gamma_p = \frac{\text{tot. \# of deuterons } (r<a)}{D^+ \text{ ionizations /s } (r<a)} = \frac{\int \bar{n}_e \cdot dV \times \left(\frac{\bar{n}_D}{\bar{n}_e}\right)}{4\pi B \cdot \frac{A p l}{3} \times S'}$$

$$R = 1 - \frac{\gamma_p}{\gamma_p^*}$$

$S' = D^+ / D\alpha$ photon

- errors: ± 15% in deuteron density

± 30% in absolute calibration

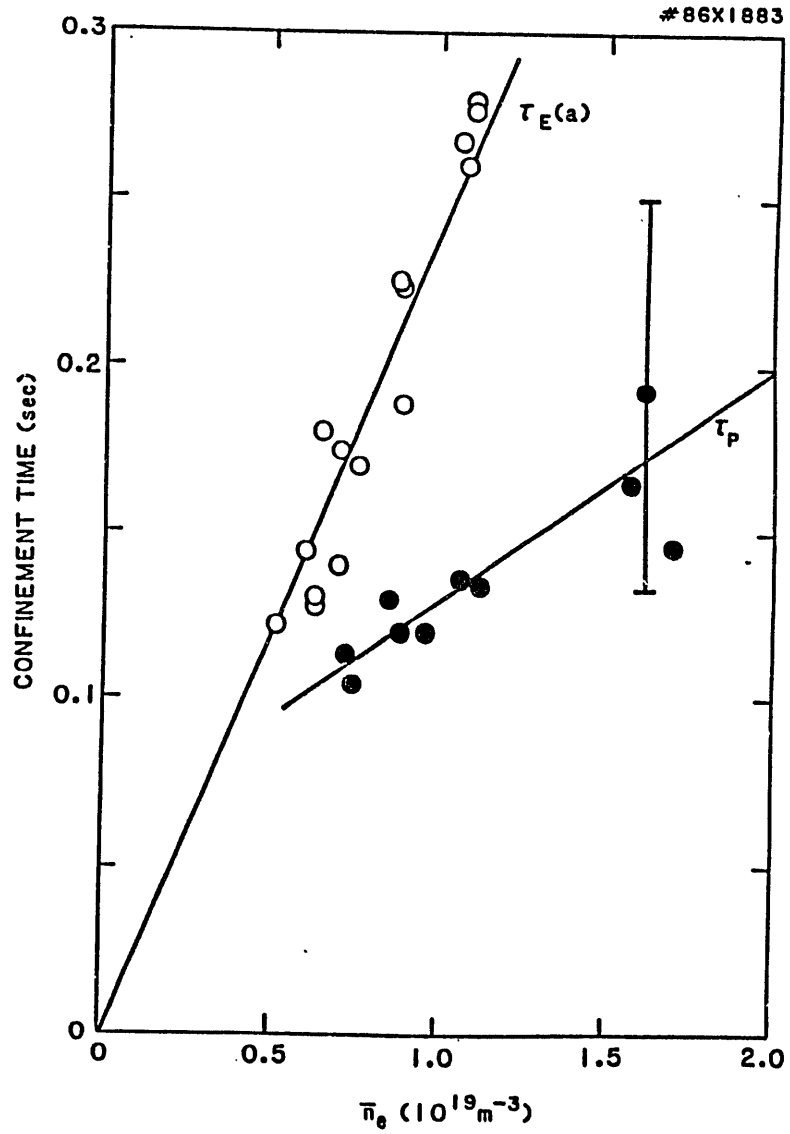

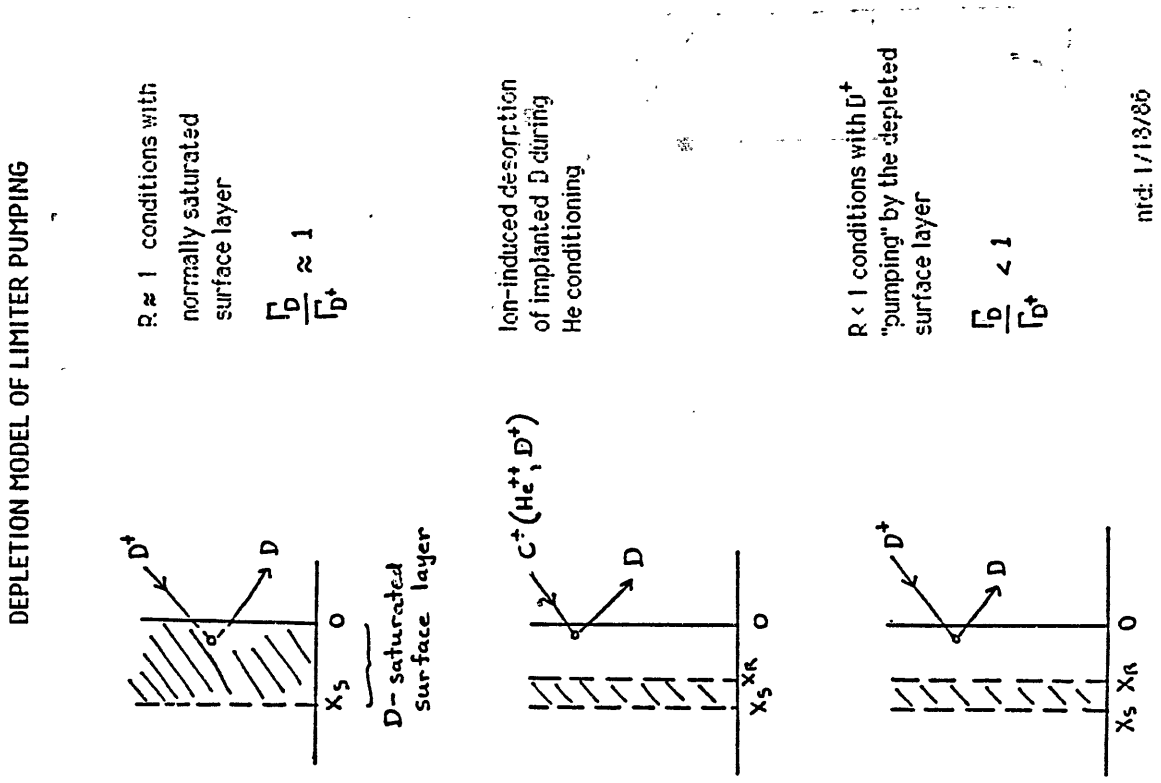
DEPLETION MODEL OF LIMITER PUMPING
R ≈ 1 conditions with normally saturated surface layer
$\frac{\Gamma_D}{\Gamma_{D^+}} \approx 1$
D^+
D
x_s
0
D- saturated surface layer
Ion-induced desorption of implanted D during He conditioning
$C^+(He^{++}, D^+)$
D
x_s
x_R
0
R < 1 conditions with D^+ "pumping" by the depleted surface layer
$\frac{\Gamma_D}{\Gamma_{D^+}} < 1$
D^+
D
x_s
x_R
0
nrd: 1/13/86

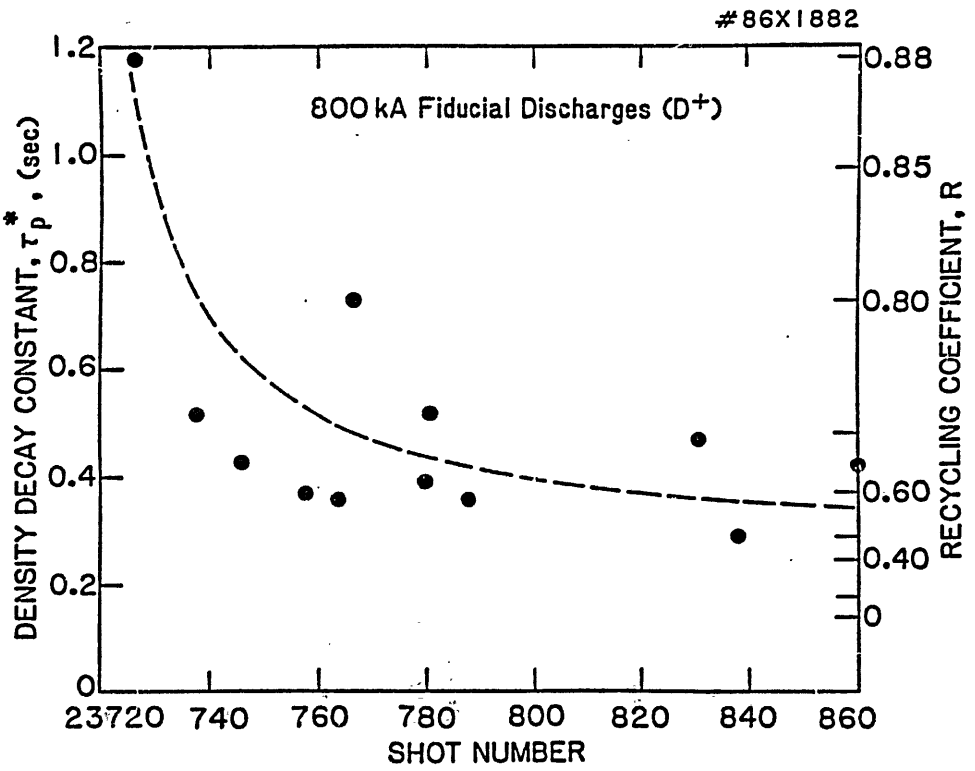
#86X1882
800 kA Fiducial Discharges (D^+)
DENSITY DECAY CONSTANT, τ_p^*, (sec)
RECYCLING COEFFICIENT, R
SHOT NUMBER
0
0.2
0.4
0.6
0.8
1.0
1.2
0
0.40
0.60
0.80
0.85
0.88
23720
740
760
780
800
820
840
860

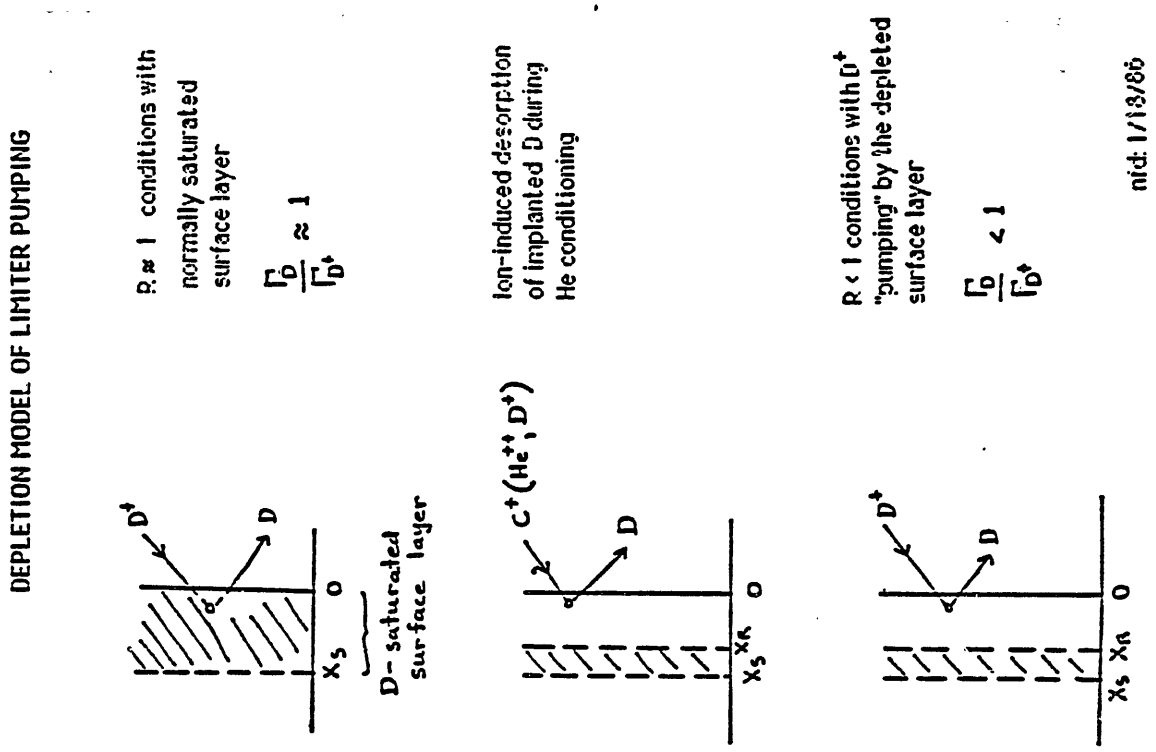
DEPLETION MODEL OF LIMITER PUMPING
R ≈ 1 conditions with normally saturated surface layer
$\frac{\Gamma_D}{\Gamma_{D^+}} \approx 1$
D^+
D
X_S
0
D- saturated surface layer
Ion-induced desorption of implanted D during He conditioning
$C^+(He^{++}, D^+)$
D
X_S X_R
0
R < 1 conditions with D^+ "pumping" by the depleted surface layer
$\frac{\Gamma_D}{\Gamma_{D^+}} < 1$
D^+
D
X_S X_R
0
nfd: 1/13/86

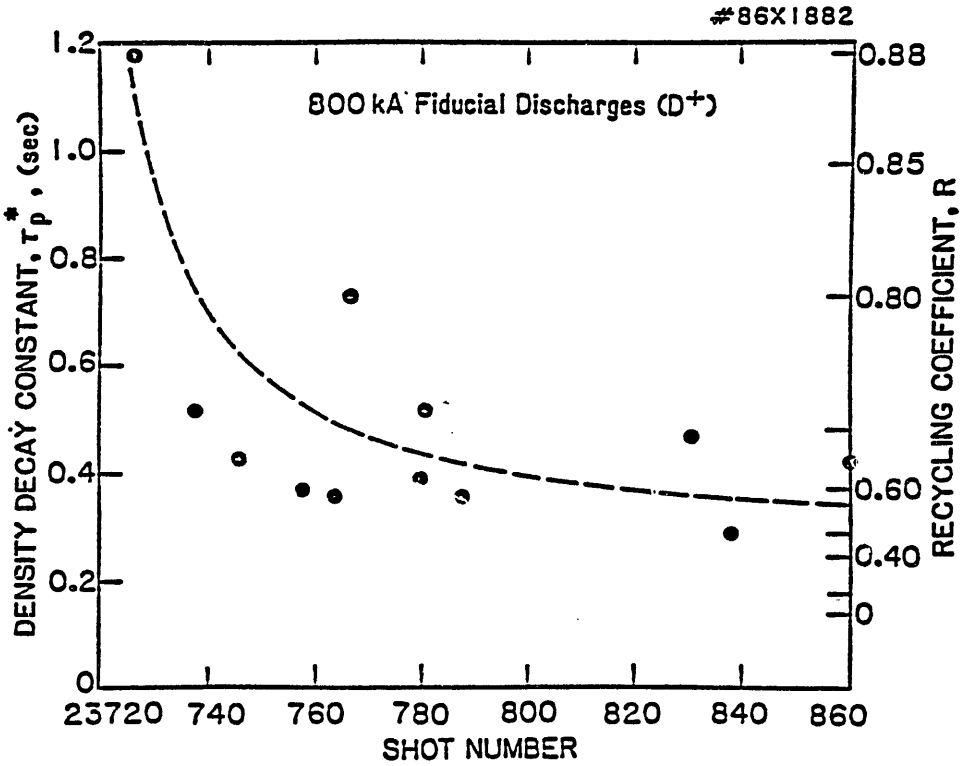
#86X1882
800 kA Fiducial Discharges (D^+)
DENSITY DECAY CONSTANT, τ_p^*, (sec)
RECYCLING COEFFICIENT, R
SHOT NUMBER
0
0.2
0.4
0.6
0.8
1.0
1.2
0
0.40
0.60
0.80
0.85
0.88
23720
740
760
780
800
820
840
860

Ion-Induced Release Process during Limiter Conditioning

- Conditioning discharges are dominated by carbon ($Z_{eff} = 6$)

- Measurements of ion-induced release of D from D-saturated graphite show that the C-ion induced release is the dominant process

C^+/C self sputtering coefficient $\doteq 0.6$

$C^+/D(C)$ Ion induced desorption coefficient = 5 @ 3keV

$He^+/D(C)$ " =2 @ 0.6 keV

$H^+/D(C)$ " = 1 @ 0.3 keV

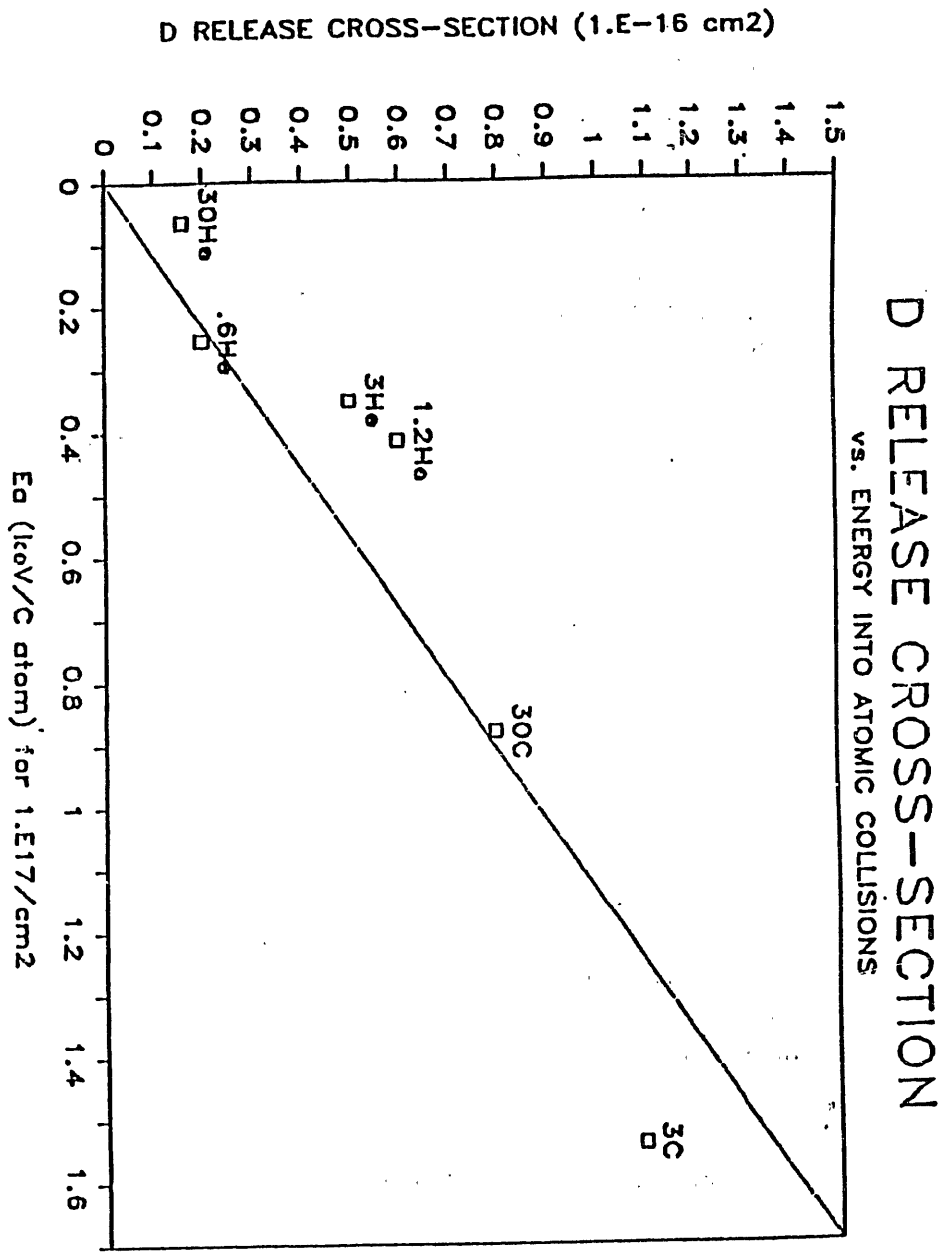

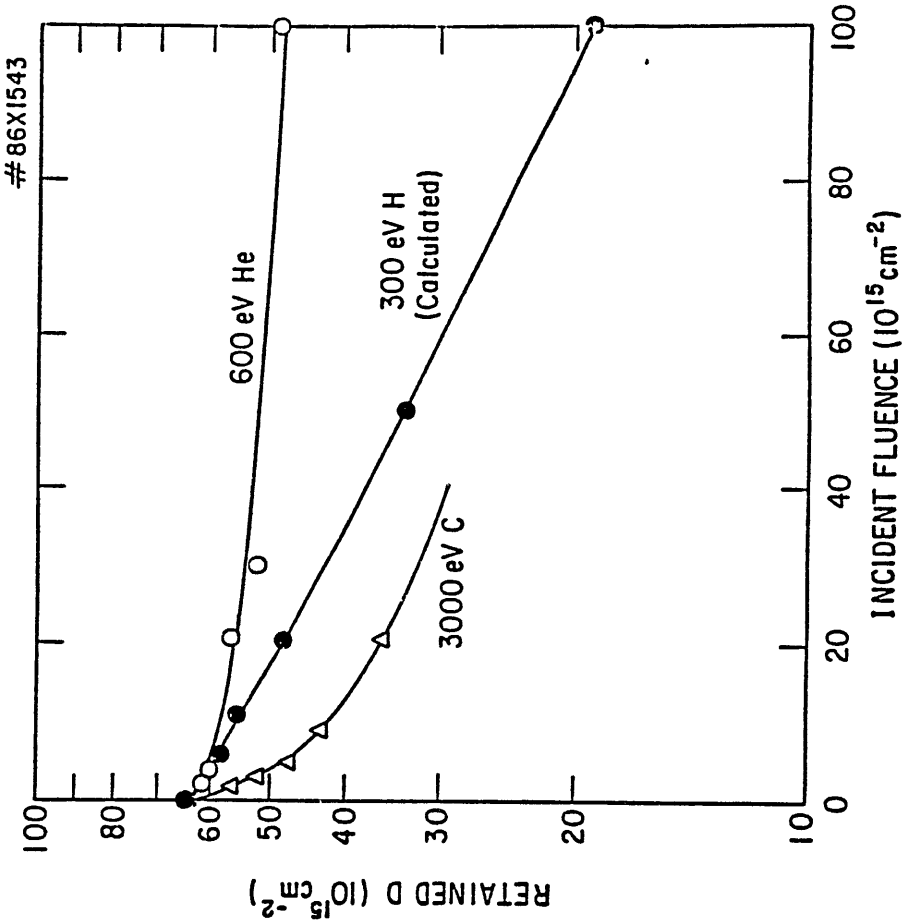
#86X1543
600 eV He
300 eV H
(Calculated)
3000 eV C
INCIDENT FLUENCE (10^{15}cm^{-2})
RETAINED D (10^{15}cm^{-2})
0
20
40
60
80
100
10
20
30
40
50
60
80
100

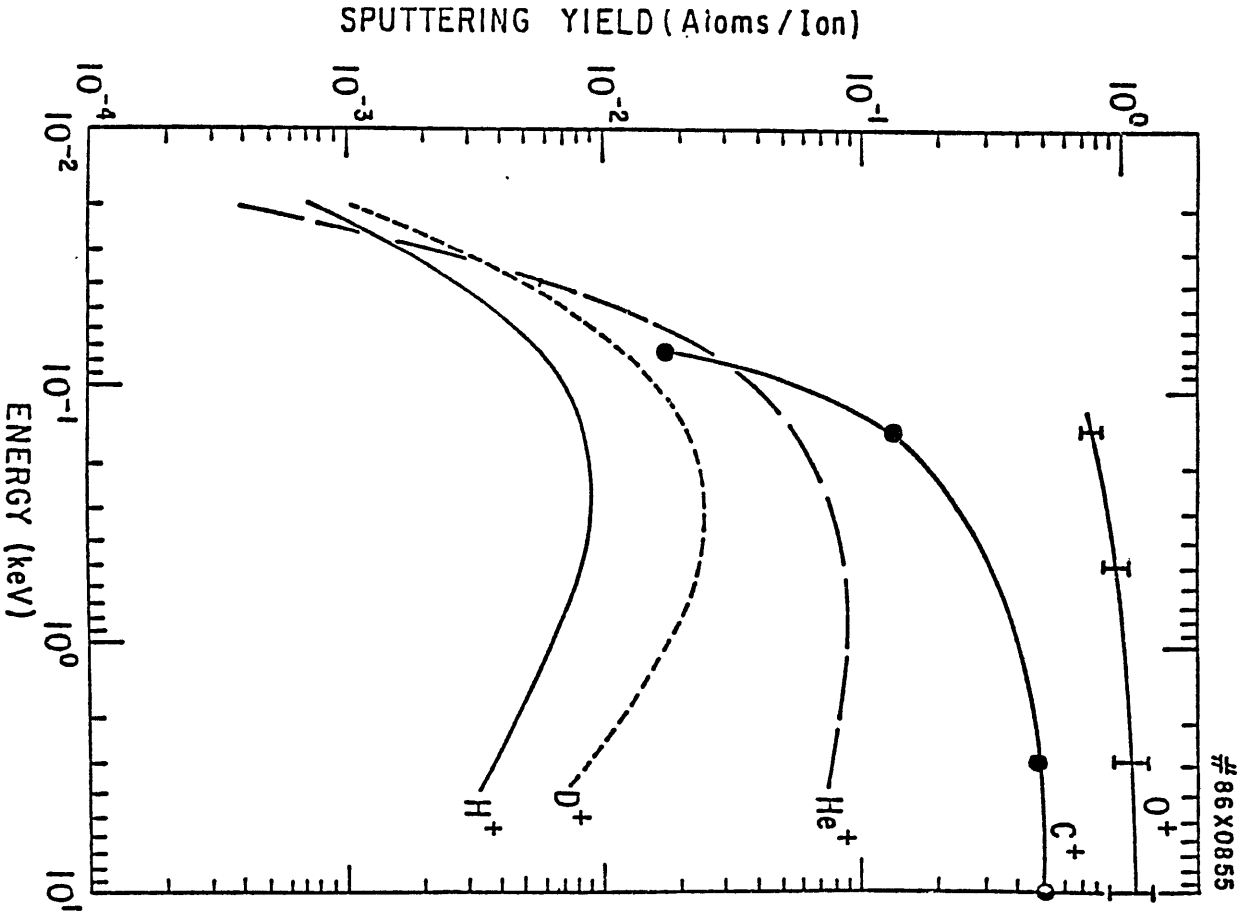
SPUTTERING YIELD (Atoms / Ion)
ENERGY (keV)
H^+
D^+
He^+
C^+
O^+
#86X0855
10^{-4}
10^{-3}
10^{-2}
10^{-1}
10^{0}
10^{-2}
10^{-1}
10^{0}
10^{1}

CODEPOSITION MODEL OF LIMITER PUMPING

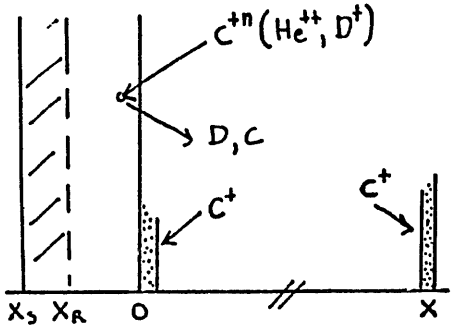

Deposition of C-film on low flux areas of the limiter and wall from C sputtered from high flux areas of the limiter

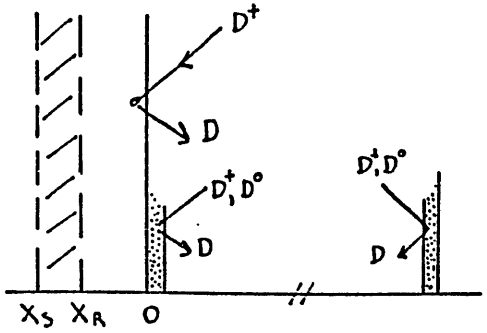

Codeposition of D^{+} (D^{o}) in wall and limiter C-films

$R < 1$

$$\frac{\Gamma_{D^{\cdot}}}{\Gamma_{D^{+}}} < 1$$

SUMMARY: LIMITER PUMPING EFFECTS

Depletion model is consistent with TFTR observations:

1) pumping capacity is of the order of 100 torr-liters which equals the capacity of the saturated area of the bumper limiter

2) strong pumping effects (ie, small values of γ_p^*) have been seen only on the bumper limiter which operates at low temperature (< 60C)

3) saturation concentration falls rapidly with temperature; very little bulk absorption capacity at moveable limiter temepratures (>1000C)

4) C films observed on TFTR wall (March,1986) have only 1-6% deuterium

5) calculated D flux at wall is a small fraction (1-5%) of the total particle flux (Heifetz)

6) pumping effect is observed when plasma is moved from moveable limiter to bumper limiter

Codeposition model is more relevant to JET and TEXTOR

1) with limiter base temperature at 300C, C sputtering by D is increased

2) pumping capacity in JET is larger (>1000 torr-liters,Cohen)

hfd

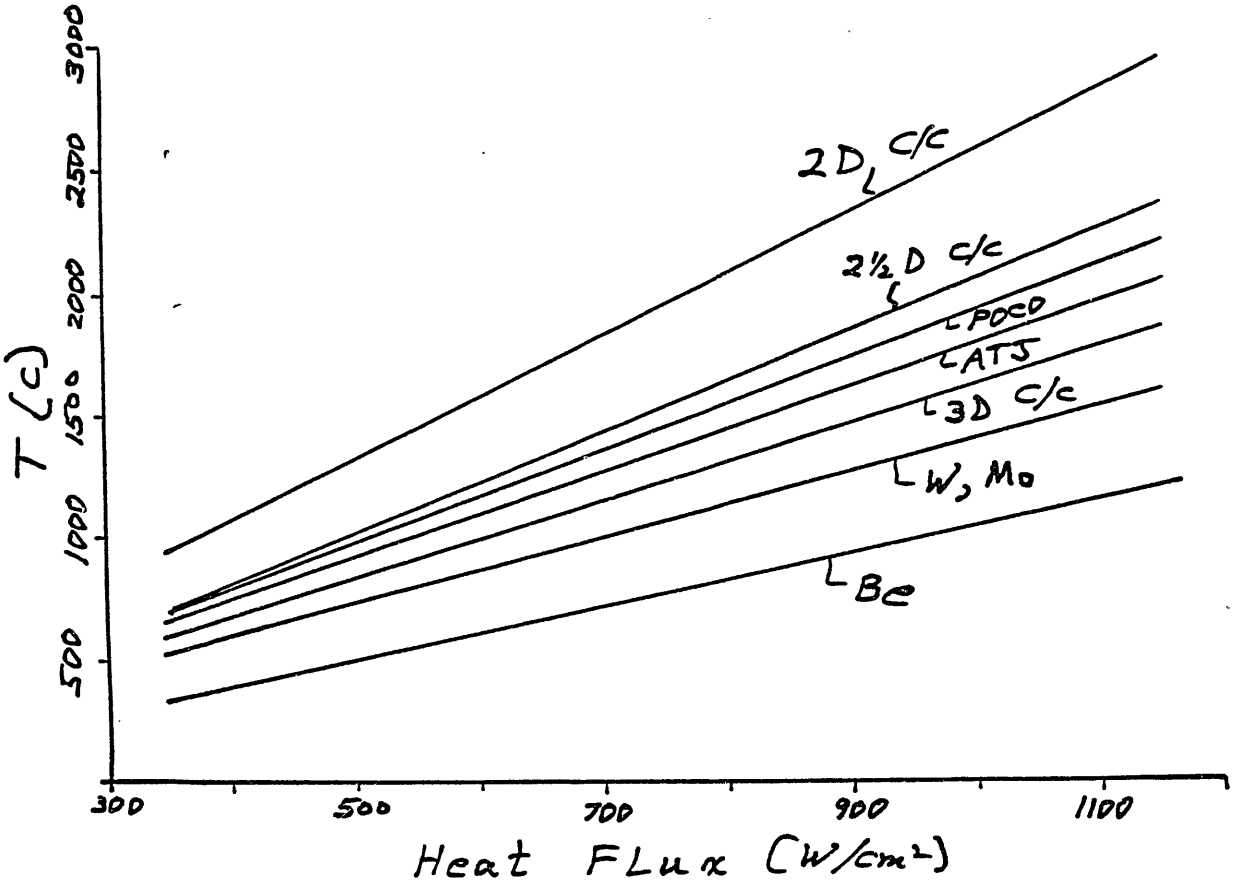

PURPOSE

1. Shield the ICRF antenna from plasma loads.
2. Serve as the limiter for plasma startup.
3. Pump limiter test module.

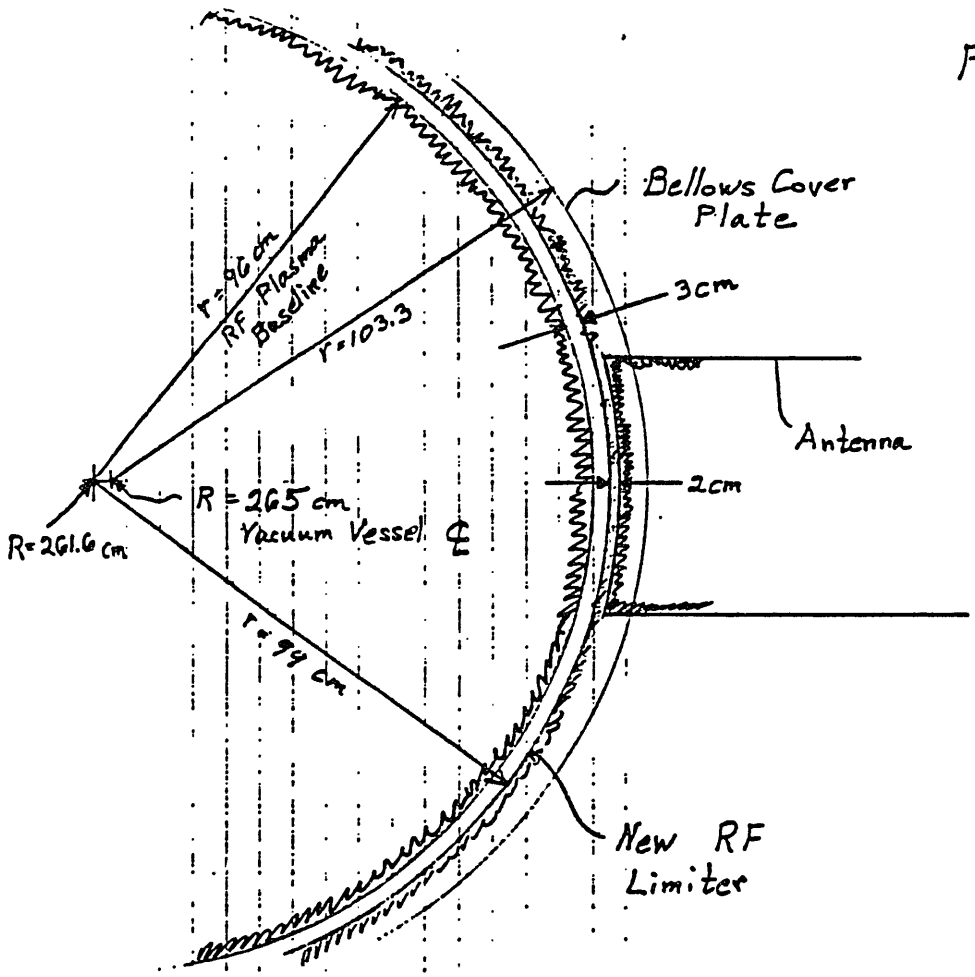

Dimensions of the shield limiters

1. Major radius of the ICRF plasma = 261.6 cm.
2. Minor radius of ICRF plasma = 96. cm.
3. Major radius of shield limiter at mid–plane = 360.6 cm.
4. Poloidal radius of curvature of shield lim. = 99. cm.
5. Toroidal radius of curvature of shield lim. = 155. cm.
   (Away from the plasma).

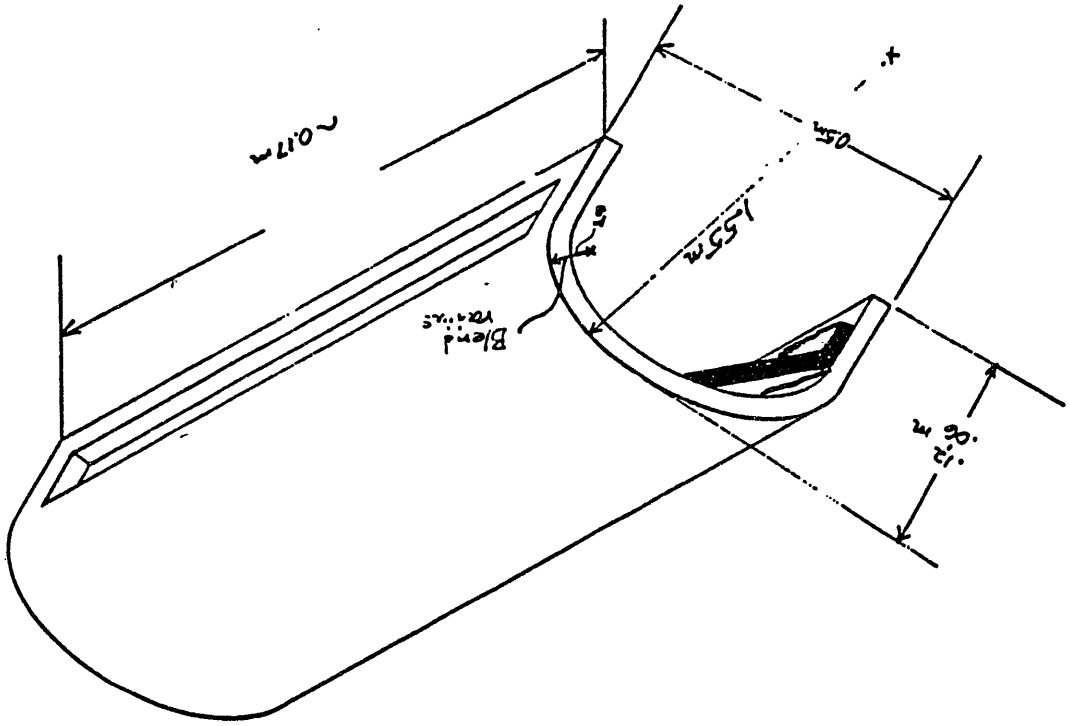

Figure 3

Figure 2

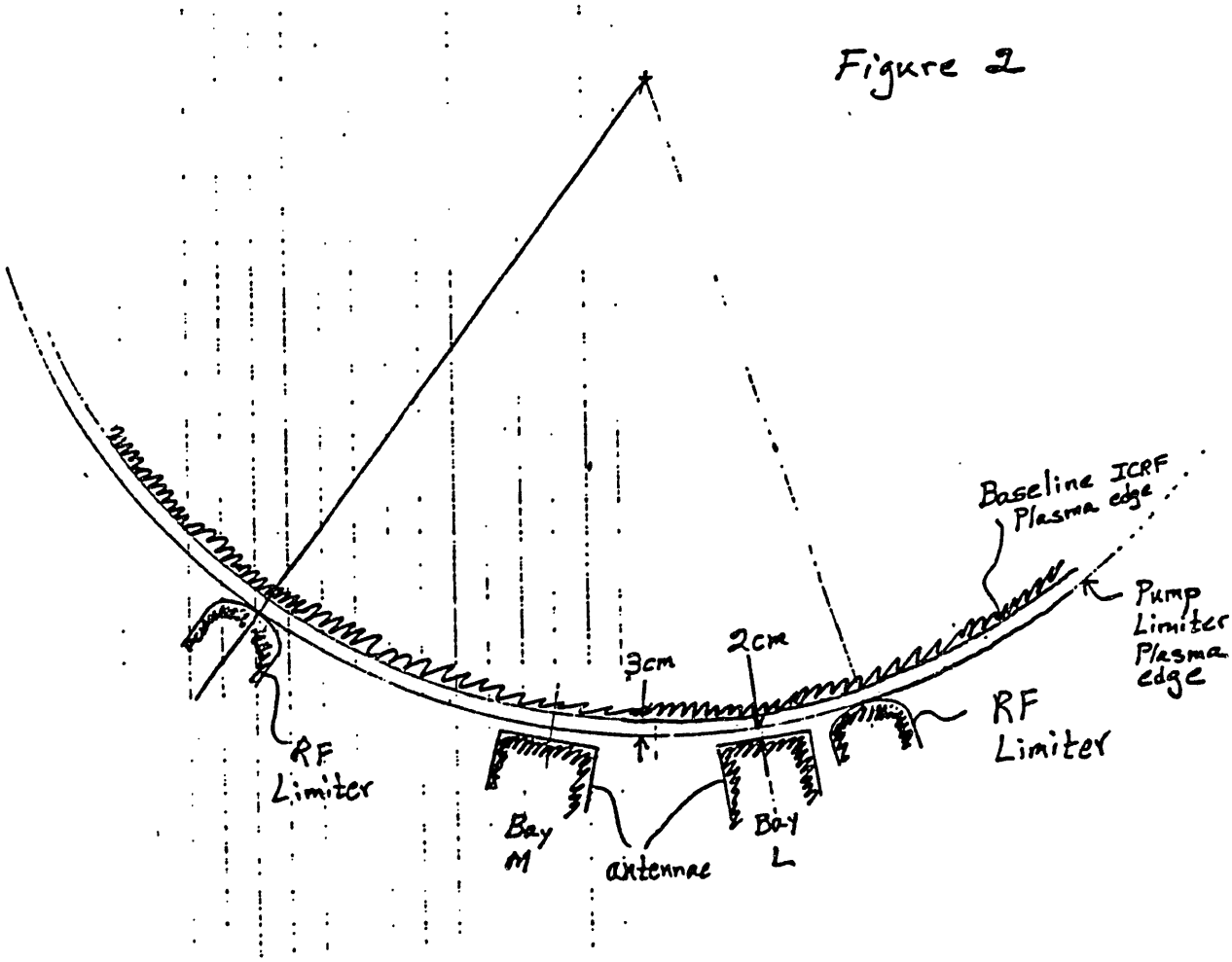

T F T R Needs

1. Improved estimates of tritium retention for graphite.
2. Estimates for new materials related to Tritium Neutral Beam and Tritium Pellet Injection.
3. Properties of Carbon/Carbon Composites.
   a) Fatigue
   b) Outgassing
   c) Tritium

Design Aspects of in Vessel Components

K.J. Dietz

J E T

Abstract

The process leading from the design idea to the procurement of in vessel components is shown, starting from the physics input the iterative process of the design is demonstrated in form of functional blocs.

DESIGN · ASPECTS

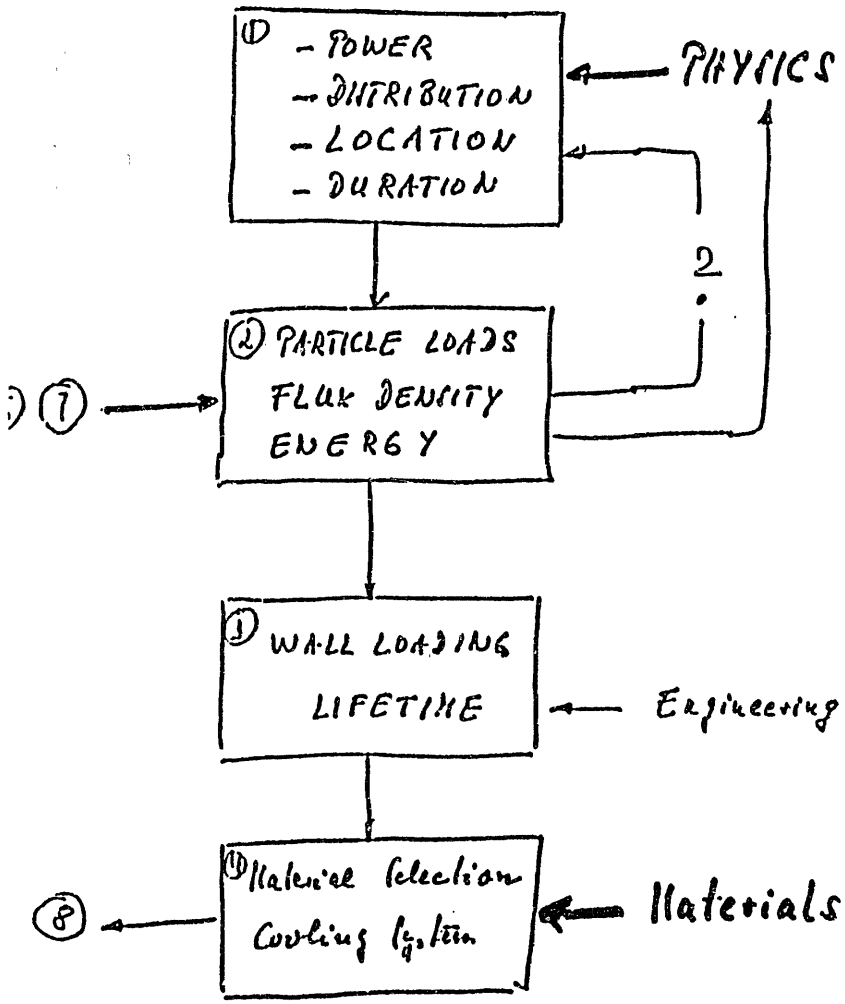

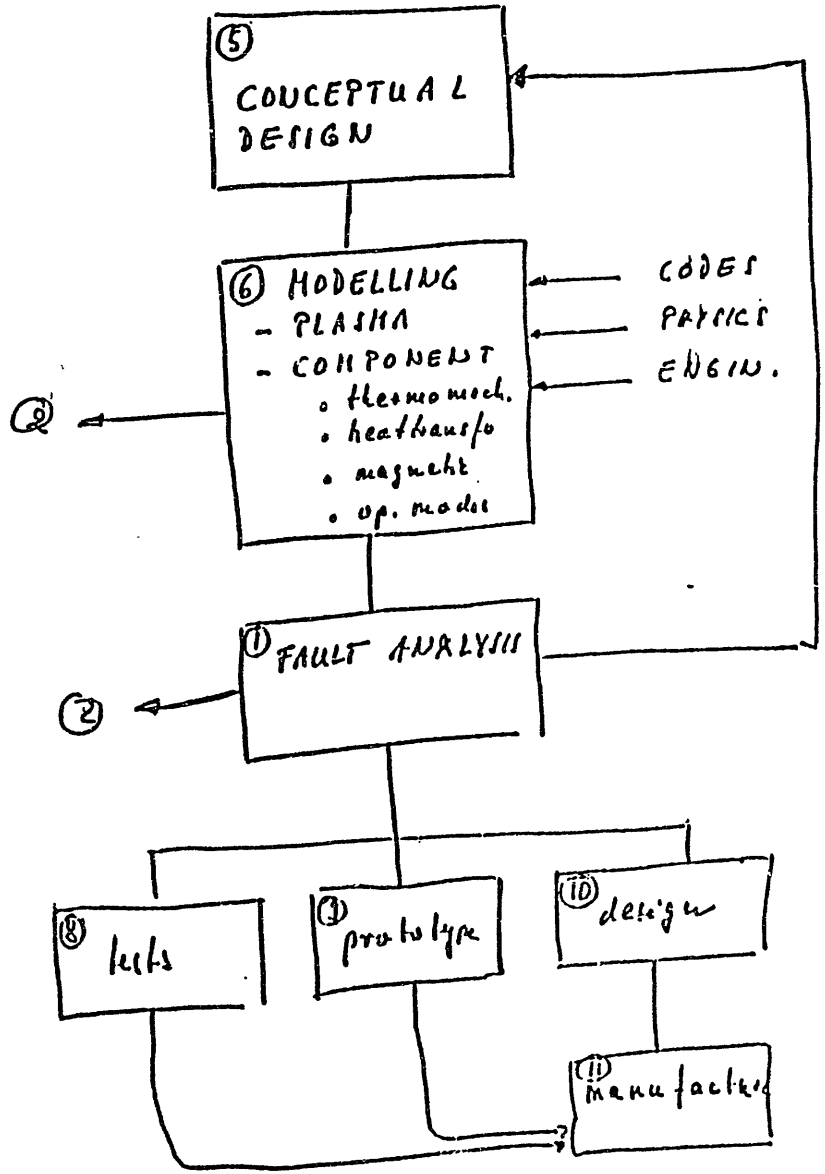

I: GRAPHITE COMPONENTS IN JET :

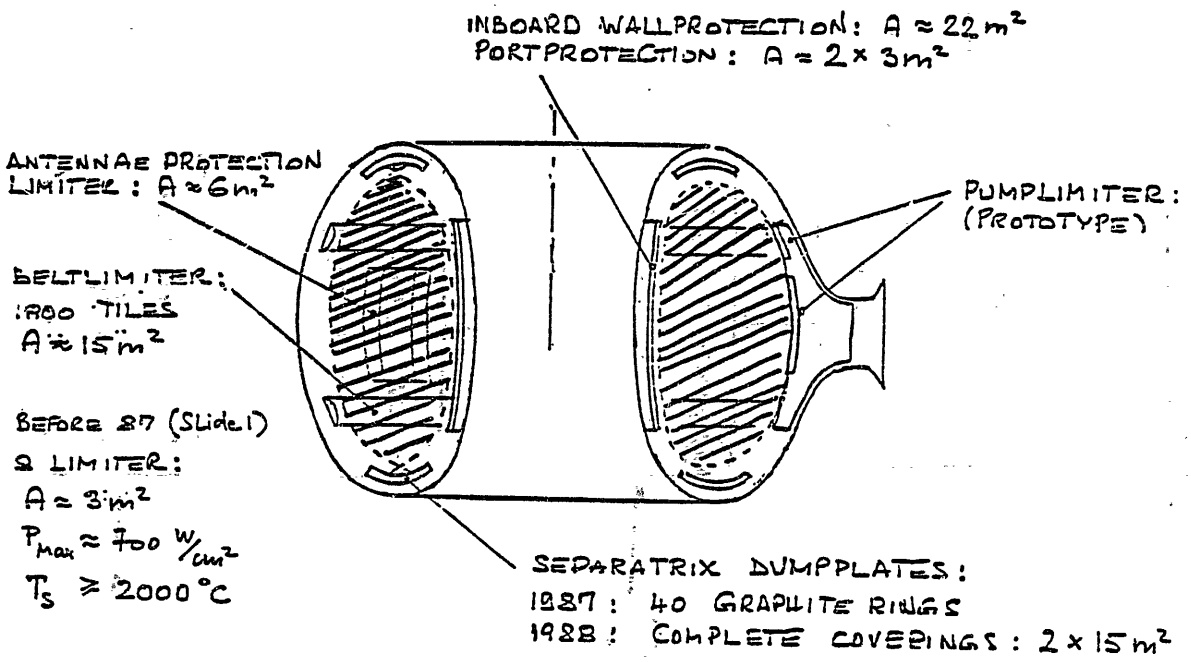

Experiment on First Wall Carbon Coating-Focusing Hydrogen Concentration

Yuichi Sakamoto

Institute of Physical and Chemical Research

Abstract

A simulation experiment on the first wall carbon coating has been carried out by the use of RIKEN ECR-2 device. Main results are as follows,

1) we have hard, high density and amorphous carbon films on SUS 304 samples by ECR discharge in CH_4/H_2(1/1) mixture gas,

2) high energy ion bombardment seems to be effective to decrease in H/C value,

3) we can clean up harmful carbon films deposited on observation windows and so on, by a local pure hydrogen plasma.

EXPERIMENT ON FIRST WALL CARBON COATING -FOCUSING HYDROGEN CONCENTRATION

Y. SAKAMOTO
and coworkers

1. Introduction
2. RIKEN ECR-2 Device
3. Experimental Results
   3.1 Plasma Behavior
   3.2 Characteristics of Carbon Films
   3.3 Cleaning of Harmful Carbon Films
4. Conclusion

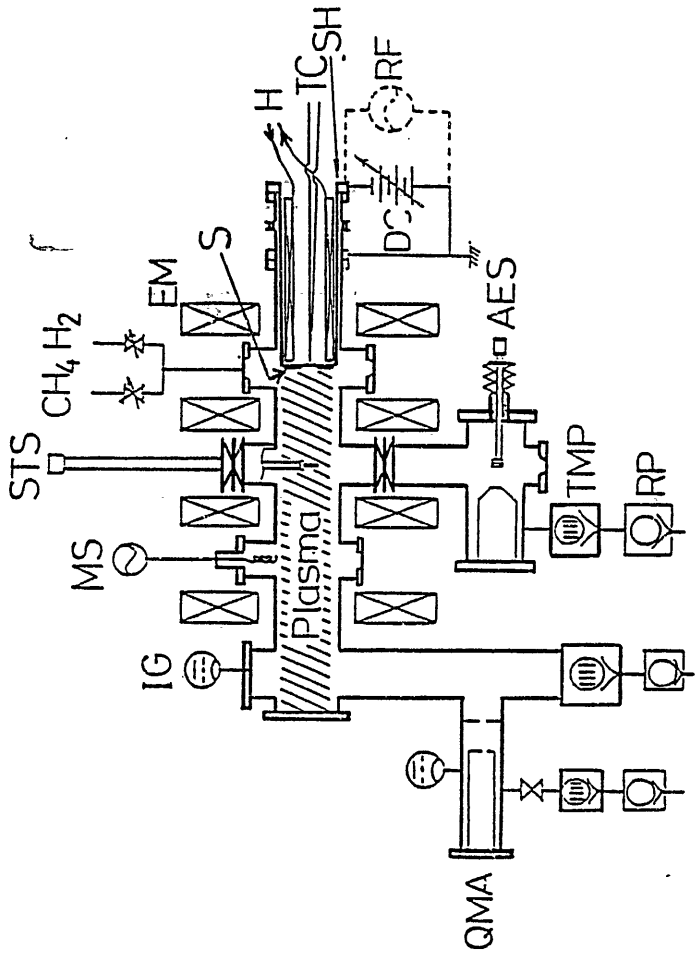

Introduction

Carbonization of

DIVA
TEXTOR
JIPPT-II U
ASDEX
JET
HELIOTRON

Decrease of Metal and Oxygen

Aim of RIKEN-ECR 2 Experiment

Decrease of Hydrogen Concentration in Carbon Film

Typical Plasma Parameters

Gas: CH_4/H_2 : 1/1 and 10^{-2} Pa

Microwave : freq 2.45 GHz

power 200 W

Electron Density : 2 - 4 x 10^{10} cm^{-3}

Electron Temperature : 4 - 9 eV

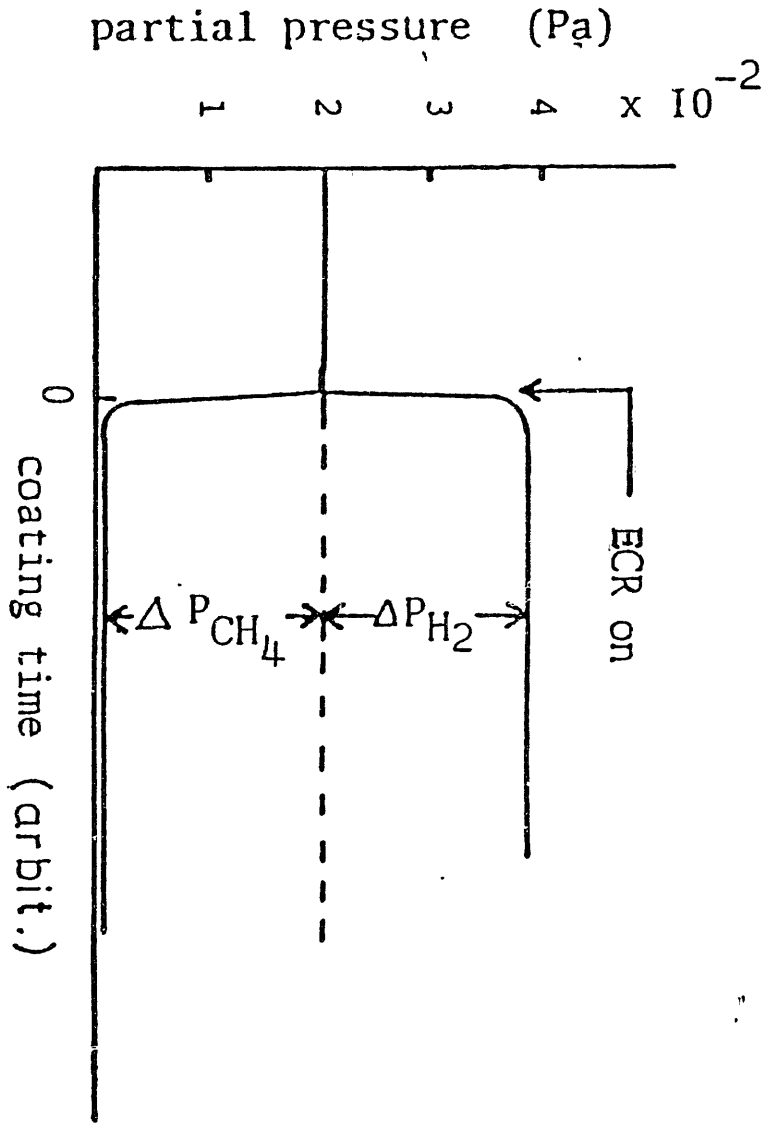

Table 2. Characteristics of carbon films

Items	Condition	Estimation
structure	CH_4/H_2 = 1/1 P_{total} = 0.01-0.1 Pa P_{micro} = 200 W V_{bias} = 0 -100 V	RHEED amorphous FTIR amorphous
hardness	V_{bias} = 0 V	870 kg mm^{-2}
specific weight	perpendicular	~ 3 g cm^{-3}
hydrogen H/C	V_{bias} = 0 V (V_{sheath} = +30 V)	NRA 0.28

Table 1. Comparison of H/C evaluation methods

methods / sample NO.	NRA*	ERDA**	TDSA	Partial Pressure Measurement
NO. 147	0.22	0.24	0.12	0.42
NO. 156	0.23	0.30	0.26	0.42
NO. 193	0.16	0.24	0.12	—

* $^{1}H(^{15}N,\alpha\gamma)^{12}C$, $^{12}C(d,p)^{13}C$

** by Ar^{4+} 64MeV

CONCLUSION

Simulation experiments have been carried out and the main results are

1) we have hard high density and amorphous carbon films on SUS 304 samples by ECR discharge in CH_4/H_2 (1/1) mixture gas,
2) high energy ion bombardment seems to be effective to decrease H/C value,
3) we can clean up harmful carbon films deposited on observation windows and so on by a local pure hydrogen plasma.

Table 3. Relation between the H/C value and the bias voltage

V_{bias}	H/C by NRA	conditions
0 V	0.26	$P_T = 5.3 \times 10^{-3}$ Pa
-100 dc	0.22	
-150 dc	0.19	CH_4/H_2 = 1/1
175 rf (20 MHz)	0.16	P_m = 200 W

Properties of Carbon Coating Films Produced by Glow, RF and ECR Discharges

Tomoaki Hino

Hokkaido University

Abstract

Carbonization experiments have been sucessfully performed in Heliotron E, JIPP-IIU, TEXTOR and ECR-II(RIKEN). We have investigated the properties of C-films produced in above devices; film thickness, depth composition profile, hydrogen content, chemical binding state and crystal structure. The film deposition rates are ∿10Å/min in glow discharge and ∿50Å in ECR discharge. The dense/hard carbon film can be obtained by ECR plasmas.
The hydrogen content of C-films due to ECR plasmas is lower.

In Heliotron E, the erosion rate of the carbon film due to hydrogen plasmas is estimated as 20Å/hr, which is much smaller than the film deposition rate. In addition, the TiC ceramics is formed at the wall both with carbonization and Ti-flashing.

Radiation Rate from Plasma

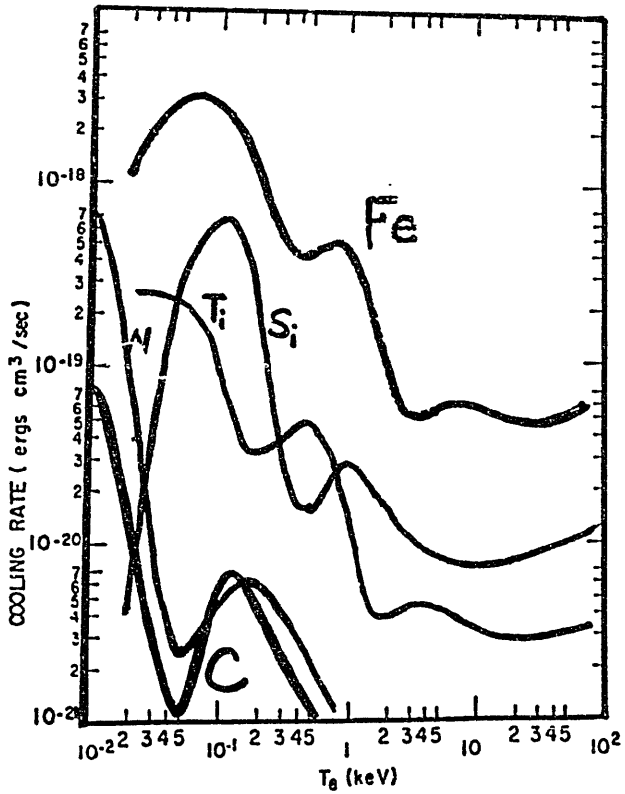

plasma temperature

Carbonization Experiments

TEXTOR
RG discharge $CH_4 + H_2$
$CD_4 + D_2$

JIPP T - IIU
Glow discharge $CH_4 + H_2$

Heliotron E
Glow discharge $CH_4 + H_2$

ECR II (RIKEN)
ECR discharge $CH_4 + H_2$

RIKEN ECR-II

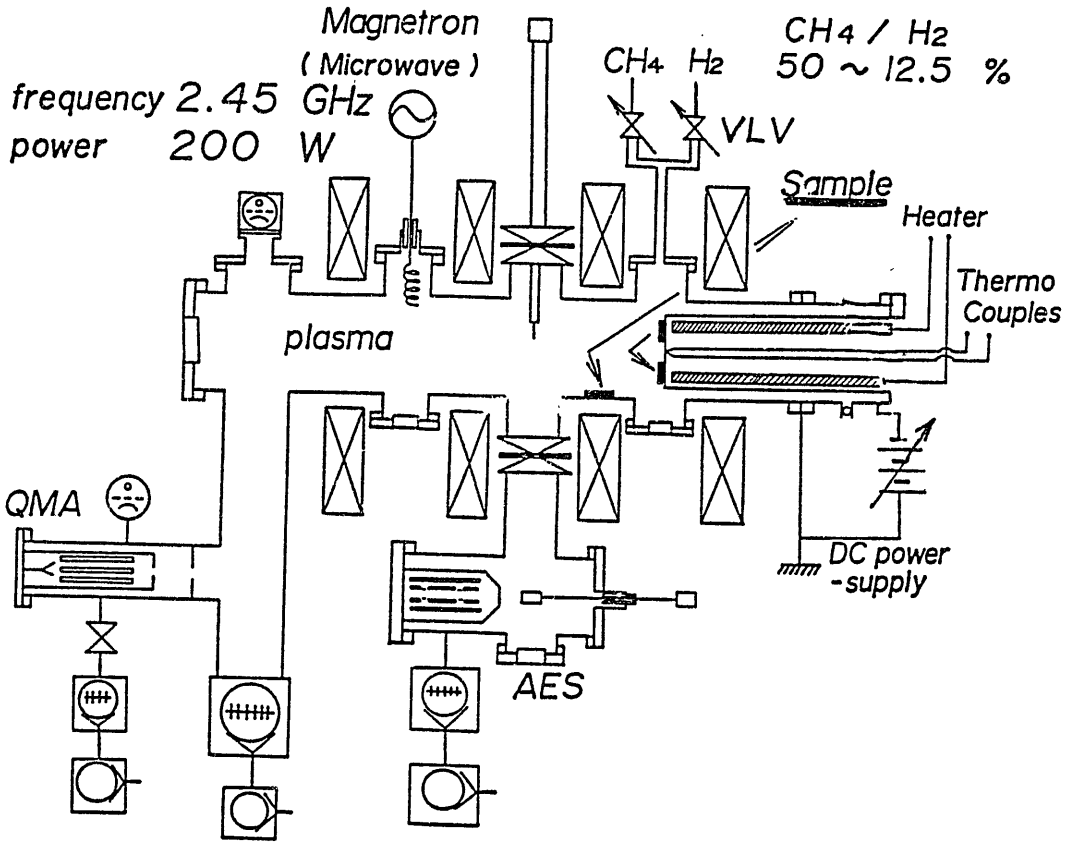

Carbon film analysis

(1) crystal structure
XRD: X-ray diffraction

(2) film thickness
Interferometer: Transky method

(3) depth composition profile
AES: Auger electron spectroscopy

(4) hydrogen concentration
TDS: thermal desorption spectroscopy

Standard Case

discharge gas	$H_2 + CH_4$
total pressure	1.1×10^{-1} Pa
CH_4 / H_2	50 %
substrate temperature	R.T.
sample biased potential	0 V (ground potential)
sample position	edge wall (perpendicular to magnetic field)

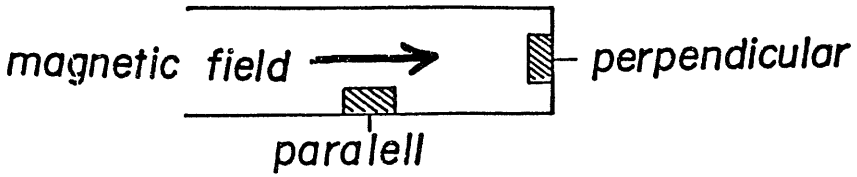

Variable Parameters

(1) sample biased potential
(2) substrate temperature
(3) CH_4 / H_2
(4) total pressure

Hydrogen concentration 20~30 %

Negatively biased sample

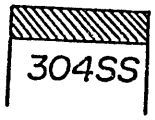

impurities : Fe, Cr, Ni, etc
deposition rate → lower
$\frac{H}{C+H}$ → lower 20.5 %

sample position

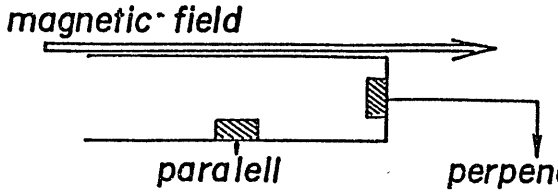

Deposition rate	1	:	2
$\frac{H}{C+H}$	24.9 %	~	30.9 %

Lower total pressure ($CH_4 + H_2$)

lower $\frac{H}{C+H}$

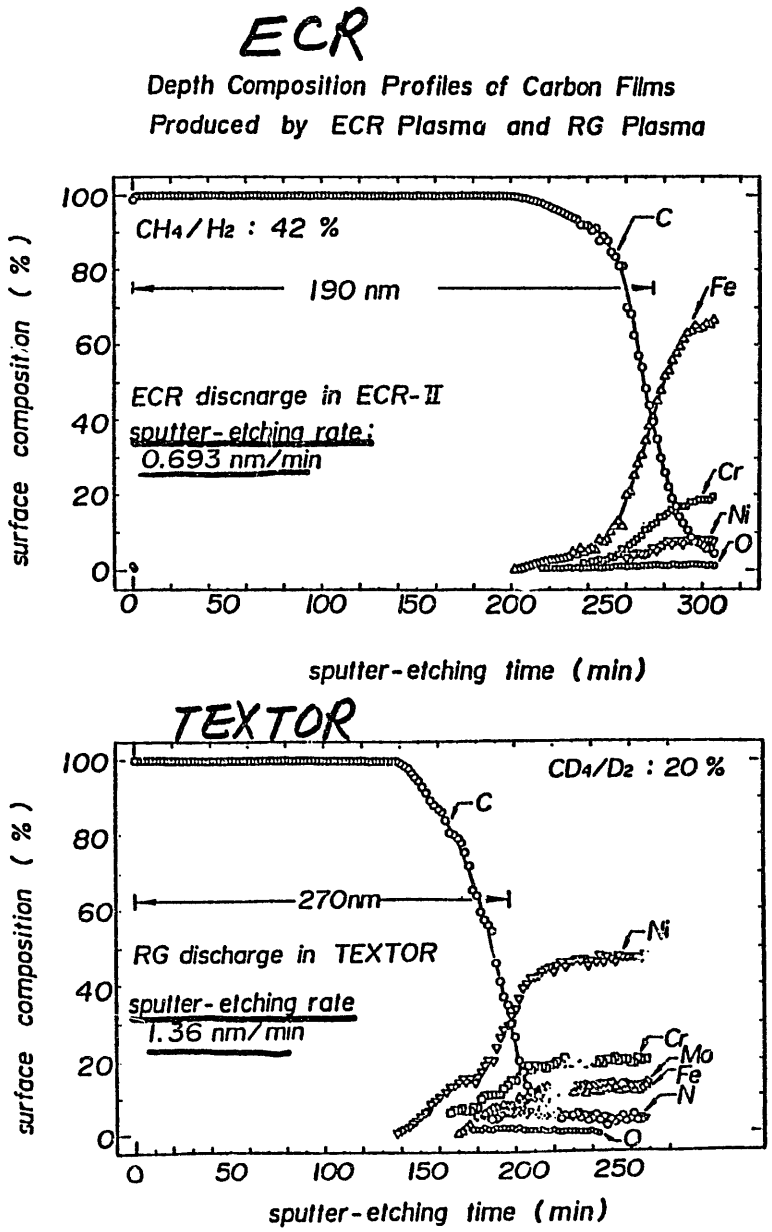
ECR
Depth Composition Profiles of Carbon Films
Produced by ECR Plasma and RG Plasma
CH4/H2 : 42 %
190 nm
ECR discnarge in ECR-II
sputter-etching rate:
0.693 nm/min
C
Fe
Cr
Ni
O
surface composition (%)
sputter-etching time (min)
TEXTOR
CD4/D2 : 20 %
270nm
RG discharge in TEXTOR
sputter-etching rate
1.36 nm/min
C
Ni
Cr
Mo
Fe
N
O
surface composition (%)
sputter-etching time (min)

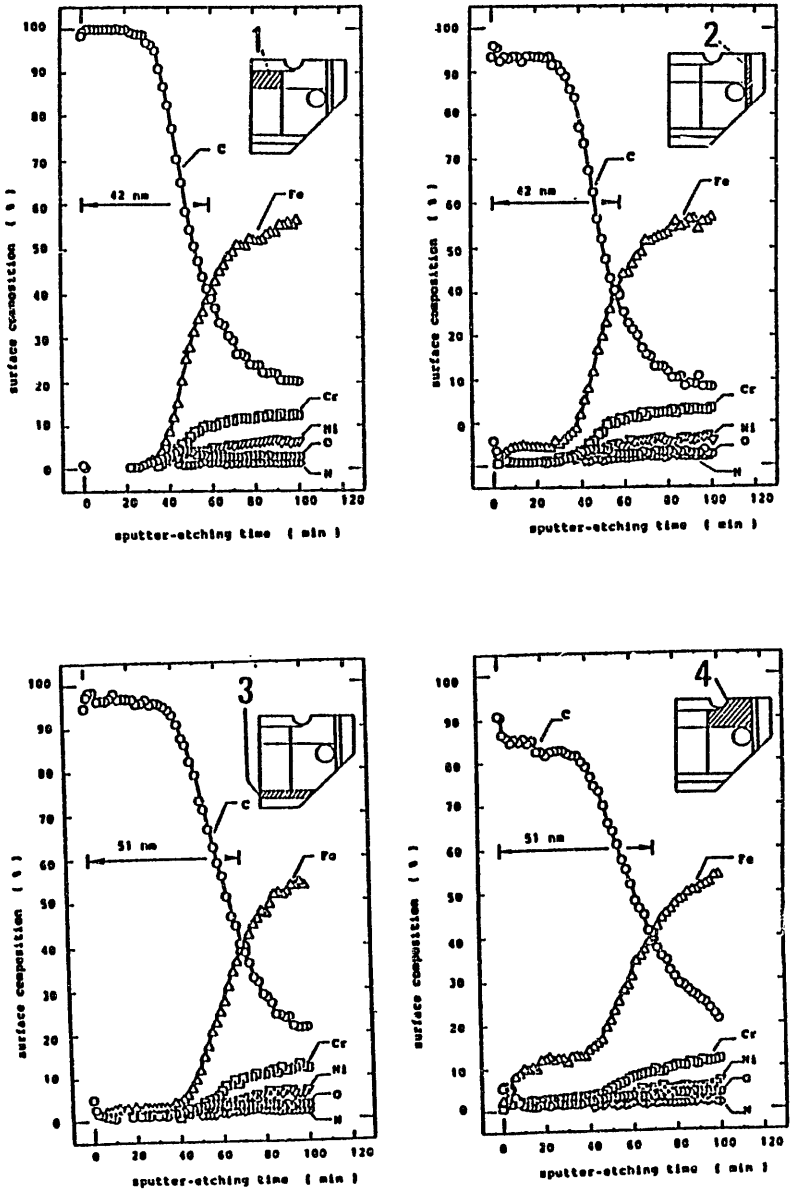
1
2
3
4
42 nm
51 nm
C
Fe
Cr
Ni
O
N
surface composition (%)
sputter-etching time (min)

fig. 2

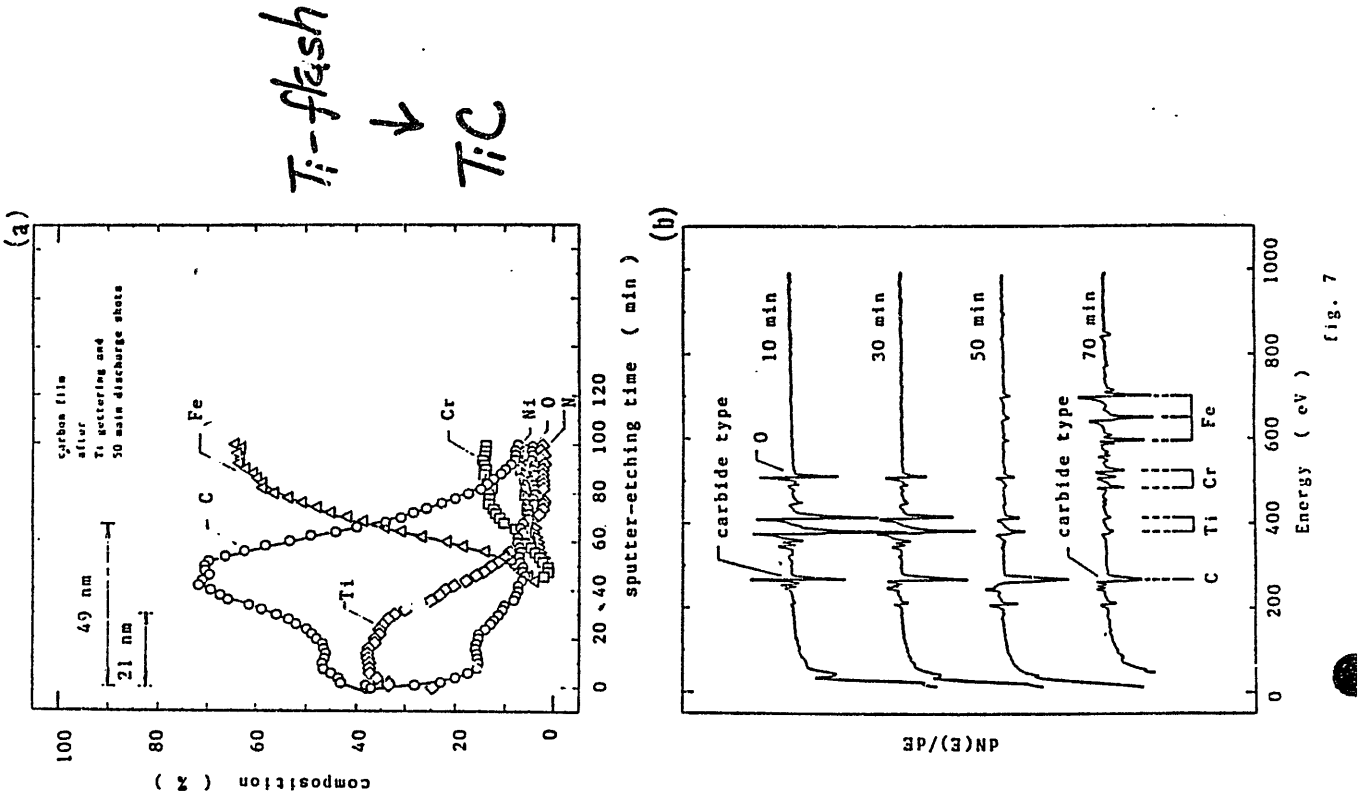

fig. 7

Heliotron E

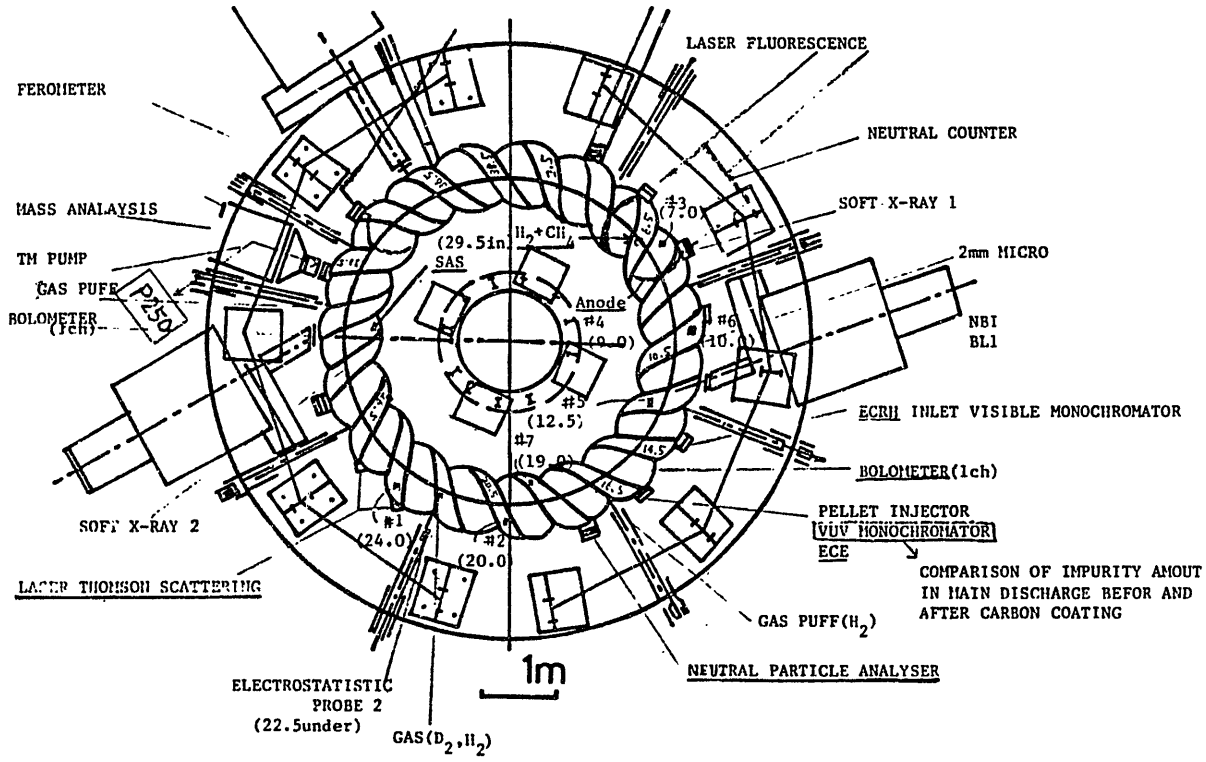

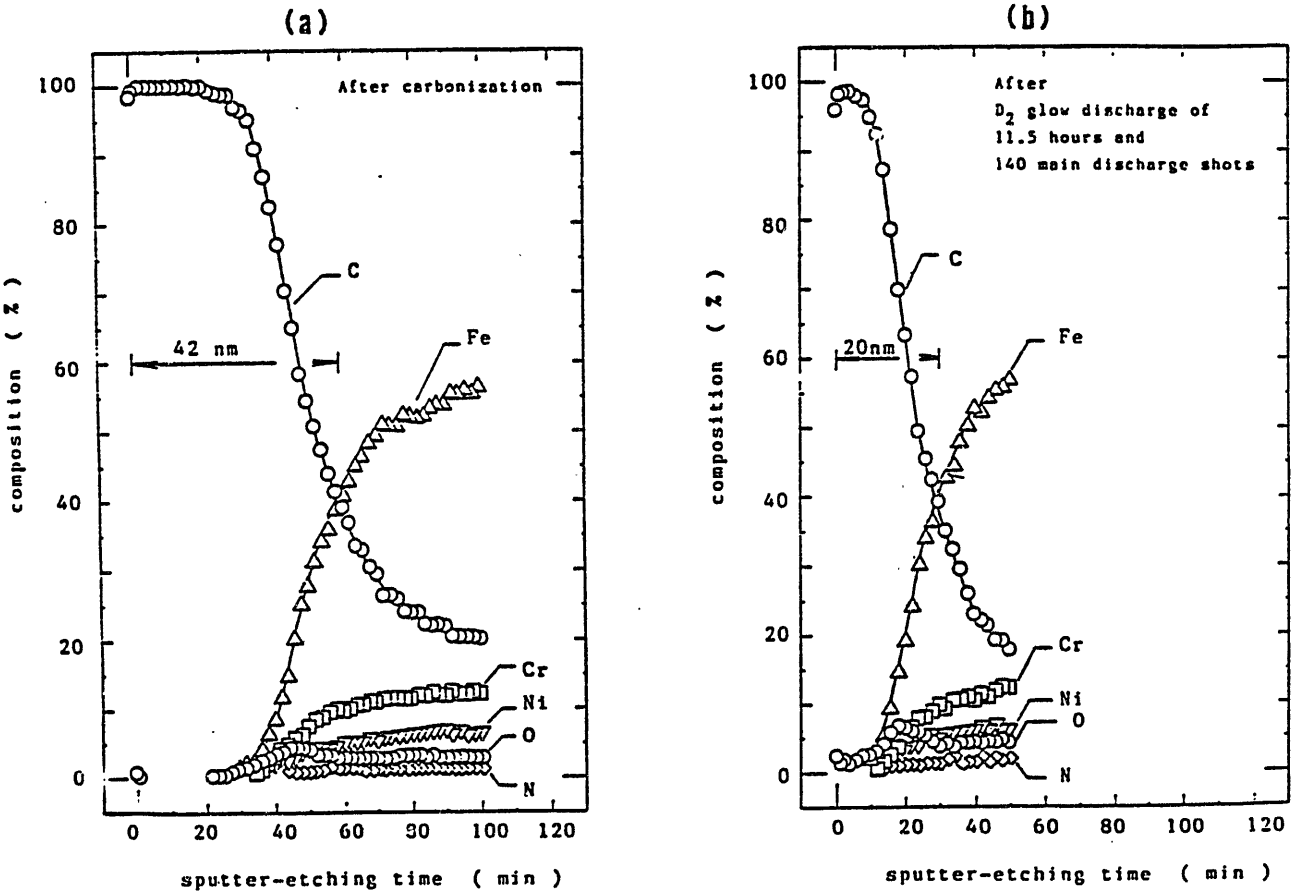

fig. 5

Erosion Rate ≃ 2 nm/hr

LIST OF IPPJ-AM REPORTS

IPPJ-AM-1* "Cross Sections for Charge Transfer of Hydrogen Beams in Gases and Vapors in the Energy Range 10 eV–10 keV"
H. Tawara (1977) [Published in Atomic Data and Nuclear Data Tables 22, 491 (1978)]

IPPJ-AM-2* "Ionization and Excitation of Ions by Electron Impact –Review of Empirical Formulae–"
T. Kato (1977)

IPPJ-AM-3 "Grotrian Diagrams of Highly Ionized Iron FeVIII-FeXXVI"
K. Mori, M. Otsuka and T. Kato (1977) [Published in Atomic Data and Nuclear Data Tables 23, 196 (1979)]

IPPJ-AM-4 "Atomic Processes in Hot Plasmas and X-Ray Emission"
T. Kato (1978)

IPPJ-AM-5* "Charge Transfer between a Proton and a Heavy Metal Atom"
S. Hiraide, Y. Kigoshi and M. Matsuzawa (1978)

IPPJ-AM-6* "Free-Free Transition in a Plasma –Review of Cross Sections and Spectra–"
T. Kato and H. Narumi (1978)

IPPJ-AM-7* "Bibliography on Electron Collisions with Atomic Positive Ions: 1940 Through 1977"
K. Takayanagi and T. Iwai (1978)

IPPJ-AM-8 "Semi-Empirical Cross Sections and Rate Coefficients for Excitation and Ionization by Electron Collision and Photoionization of Helium"
T. Fujimoto (1978)

IPPJ-AM-9 "Charge Changing Cross Sections for Heavy-Particle Collisions in the Energy Range from 0.1 eV to 10 MeV I. Incidence of He, Li, Be, B and Their Ions"
Kazuhiko Okuno (1978)

IPPJ-AM-10 "Charge Changing Cross Sections for Heavy-Particle Collisions in the Energy Range from 0.1 eV to 10 MeV II. Incidence of C, N, O and Their Ions"
Kazuhiko Okuno (1978)

IPPJ-AM-11 "Charge Changing Cross Sections for Heavy-Particle Collisions in the Energy Range from 0.1 eV to 10 MeV III. Incidence of F, Ne, Na and Their Ions"
Kazuhiko Okuno (1978)

IPPJ-AM-12* "Electron Impact Excitation of Positive Ions Calculated in the Coulomb-Born Approximation –A Data List and Comparative Survey–"
S. Nakazaki and T. Hashino (1979)

IPPJ-AM-13 "Atomic Processes in Fusion Plasmas – Proceedings of the Nagoya Seminar on Atomic Processes in Fusion Plasmas Sept. 5-7, 1979"
Ed. by Y. Itikawa and T. Kato (1979)

IPPJ-AM-14 "Energy Dependence of Sputtering Yields of Monatomic Solids"
N. Matsunami, Y. Yamamura, Y. Itikawa, N. Itoh, Y. Kazumata, S. Miyagawa, K. Morita and R. Shimizu (1980)

IPPJ-AM-15 "Cross Sections for Charge Transfer Collisions Involving Hydrogen Atoms"
Y. Kaneko, T. Arikawa, Y. Itikawa, T. Iwai, T. Kato, M. Matsuzawa, Y. Nakai, K. Okubo, H. Ryufuku, H. Tawara and T. Watanabe (1980)

IPPJ-AM-16 "Two-Centre Coulomb Phaseshifts and Radial Functions"
H. Nakamura and H. Takagi (1980)

IPPJ-AM-17 "Empirical Formulas for Ionization Cross Section of Atomic Ions for Electron Collisions –Critical Review with Compilation of Experimental Data–"
Y. Itikawa and T. Kato (1981)

IPPJ-AM-18 "Data on the Backscattering Coefficients of Light Ions from Solids"
T. Tabata, R. Ito, Y. Itikawa, N. Itoh and K. Morita (1981) [Published in Atomic Data and Nuclear Data Tables 28, 493 (1983)]

IPPJ-AM-19 "Recommended Values of Transport Cross Sections for Elastic Collision and Total Collision Cross Section for Electrons in Atomic and Molecular Gases"
M. Hayashi (1981)

IPPJ-AM-20 "Electron Capture and Loss Cross Sections for Collisions between Heavy Ions and Hydrogen Molecules"
Y. Kaneko, Y. Itikawa, T. Iwai, T. Kato, Y. Nakai, K. Okuno and H. Tawara (1981)

IPPJ-AM-21 "Surface Data for Fusion Devices – Proceedings of the U.S–Japan Workshop on Surface Data Review Dec. 14-18, 1981"
Ed. by N. Itoh and E.W. Thomas (1982)

IPPJ-AM-22 "Desorption and Related Phenomena Relevant to Fusion Devices"
Ed. by A. Koma (1982)

IPPJ-AM-23 "Dielectronic Recombination of Hydrogenic Ions"
T. Fujimoto, T. Kato and Y. Nakamura (1982)

IPPJ-AM-24 "Bibliography on Electron Collisions with Atomic Positive Ions: 1978 Through 1982 (Supplement to IPPJ-AM-7)"
Y. Itikawa (1982) [Published in Atomic Data and Nuclear Data Tables 31, 215 (1984)]

IPPJ-AM-25 "Bibliography on Ionization and Charge Transfer Processes in Ion-Ion Collision"
H. Tawara (1983)

IPPJ-AM-26 "Angular Dependence of Sputtering Yields of Monatomic Solids"
Y. Yamamura, Y. Itikawa and N. Itoh (1983)

IPPJ-AM-27 "Recommended Data on Excitation of Carbon and Oxygen Ions by Electron Collisions"
Y. Itikawa, S. Hara, T. Kato, S. Nakazaki, M.S. Pindzola and D.H. Crandall (1983) [Published in Atomic Data and Nuclear Data Tables 33, 149 (1985)]

IPPJ-AM-28 "Electron Capture and Loss Cross Sections for Collisions Between Heavy Ions and Hydrogen Molecules (Up-dated version of IPPJ-AM-20)
H. Tawara, T. Kato and Y. Nakai (1983) [Published in Atomic Data and Nuclear Data Tables 32, 235 (1985)]

IPPJ-AM-29 "Bibliography on Atomic Processes in Hot Dense Plasmas"
T. Kato, J. Hama, T. Kagawa, S. Karashima, N. Miyanaga, H. Tawara, N. Yamaguchi, K. Yamamoto and K. Yonei (1983)

IPPJ-AM-30 "Cross Sections for Charge Transfers of Highly Ionized Ions in Hydrogen Atoms (Up-dated version of IPPJ-AM-15)"
H. Tawara, T. Kato and Y. Nakai (1983) [Published in Atomic Data and Nuclear Data Tables 32, 235 (1985)]

IPPJ-AM-31 "Atomic Processes in Hot Dense Plasmas"
T. Kagawa, T. Kato, T. Watanabe and S. Karashima (1983)

IPPJ-AM-32 "Energy Dependence of the Yields of Ion-Induced Sputtering of Monatomic Solids"
N. Matsunami, Y. Yamamura, Y. Itikawa, N. Itoh, Y. Kazumata, S. Miyagawa, K. Morita, R. Shimizu and H. Tawara (1983) [Published in Atomic Data and Nuclear Data Tables 31, 1 (1984)]

IPPJ-AM-33 "Proceedings on Symposium on Atomic Collision Data for Diagnostics and Modelling of Fusion Plasmas, Aug. 29 – 30, 1983"
Ed. by H. Tawara (1983)

IPPJ-AM-34 "Dependence of the Backscattering Coefficients of Light Ions upon Angle of Incidence"
T. Tabata, R. Ito, Y. Itikawa, N. Itoh, K. Morita and H. Tawara (1984)

IPPJ-AM-35 "Proceedings of Workshop on Synergistic Effects in Surface Phenomena Related to Plasma-Wall Interactions, May 21 – 23, 1984"
Ed. by N. Itoh, K. Kamada and H. Tawara (1984) [Published in Radiation Effects 89, 1 (1985)]

IPPJ-AM-36 "Equilibrium Charge State Distributions of Ions ($Z_1 \geqq 4$) after Passage through Foils -- Compilation of Data after 1972"
K. Shima, T. Mikumo and H. Tawara (1985) [Published in Atomic Data and Nuclear Data Tables 34, 357 (1986)]

IPPJ-AM-37 "Ionization Cross Sections of Atoms and Ions by Electron Impact"
H. Tawara, T. Kato and M. Ohnishi (1985)

IPPJ-AM-38 "Rate Coefficients for the Electron-Impact Excitations of C-like Ions"
Y. Itikawa (1985)

IPPJ-AM-39 "Proceedings of the Japan-U.S. Workshop on Impurity and Particle Control, Theory and Modeling, Mar. 12 – 16, 1984"
Ed. by T. Kawamura (1985)

IPPJ-AM-40 "Low-Energy Sputterings with the Monte Carlo Program ACAT"
Y. Yamamura and Y. Mizuno (1985)

IPPJ-AM-41 "Data on the Backscattering Coefficients of Light Ions from Solids (a Revision)"
R. Ito, T. Tabata, N. Itoh, K. Morita, T. Kato and H. Tawara (1985)

IPPJ-AM-42 "Stopping Power Theories for Charged Particles in Inertial Confinement Fusion Plasmas (Emphasis on Hot and Dense Matters)"
S. Karashima, T. Watanabe, T. Kato and H. Tawara (1985)

IPPJ-AM-43 "The Collected Papers of Nice Project/IPP, Nagoya"
Ed. by H. Tawara (1985)

IPPJ-AM-44 "Tokamak Plasma Modelling and Atomic Processes"
Ed. by T. Kawamura (1986)

IPPJ-AM-45 Bibliography of Electron Transfer in Ion-Atom Collisions
H. Tawara, N. Shimakura, N. Toshima and T. Watanabe (1986)

IPPJ-AM-46 "Atomic Data Involving Hydrogens Relevant to Edge Plasmas"
H. Tawara, Y. Itikawa, Y. Itoh, T. Kato, H. Nishimura, S. Ohtani, H. Takagi, K. Takayanagi and M. Yoshino (1986)

IPPJ-AM-47 "Resonance Effects in Electron-Ion Collisions"
Ed. by H. Tawara and G. H. Dunn (1986)

IPPJ-AM-48 "Dynamic Processes of Highly Charged Ions (Proceedings)"
Ed. by Y. Kanai and S. Ohtani (1986)

IPPJ-AM-49 "Wavelengths of K X-Rays of Iron Ions"
T. Kato, S. Morita and H. Tawara (1987)

IPPJ-AM-50 "Proceedings of the Japan-U.S Workshop P-92 on Plasma Material Interaction/High Heat Flux Data Needs for the Next Step Ignition and Steady State Devices, Jan. 26 – 30, 1987"
Ed. by A. Miyahara and K. L. Wilson (1987)

Available upon request to Research Information Center, Institute of Plasma Physics, Nagoya University, Nagoya 464, Japan, except for the reports noted with*.